In vivo neuroimaging of synaptic density in Lewy body diseases and its relationship to structural, functional, and molecular markers

Yousaf, Tayyabah

Awarding institution:
King's College London

King's College London
Institute of Psychiatry, Psychology & Neuroscience
Department of Neuroimaging

In vivo neuroimaging of synaptic density in Lewy body diseases and its relationship to structural, functional, and molecular markers

Tayyabah Rahimah Yousaf

A thesis submitted to King's College London for the degree of Doctor of Philosophy in Neuroimaging

2022

Statement of work

This thesis used data from three independent studies.

All chapters utilised data from studies "The role of SV2A in PD and PD with cognitive impairment" funded by Invicro Ltd, "MIND-MAPS-PD", funded by Invicro Ltd and "Molecular Pathology and Neuronal Networks in LRRK2 PD" funded by GlaxoSmithKline. A portion of the healthy control data was shared from the "MIND-MAPS Consortium", funded by Invicro Ltd. Patient recruitment and/or collection of clinical and imaging data was performed by Dr George Dervenoulas, Dr Silvia Rota, Dr Lucia Batzu, Dr Marcello Esposito, Dr Chloe Farrell, Mr Sotirios Polychronis, Dr Gennaro Pagano, and Dr Edoardo De Natale. I was responsible for generating the ideas and research questions with guidance from my supervisors Professor Mitul Mehta and Dr Owen O'Daly, with input also from Dr Mattia Veronese. I was responsible for devising and implementing the analysis strategy, for interpretation of the findings and writing up of the thesis with feedback from my supervisors.

I declare that this thesis was composed by myself, and the research presented is my original own.

Acknowledgements

I would firstly like to express deep gratitude to my supervisors: Professor Mitul Mehta and Dr Owen O'Daly. Thank you both for taking me under your wings when things became difficult and for your unwavering support, patience, and guidance over the last couple of years. Mitul, your knowledge, and insightfulness is truly astounding, and I am sincerely grateful for having had the opportunity to finish this PhD under your supervision. Owen, your knowledge in all things neuroimaging and your technical expertise is mind-blowing. Thank you for going above and beyond in your role as my supervisor and for being a key source of encouragement.

I also owe much gratitude to Professor Sarah Byford. You stepped in when things were at their worst and found new homes for each of us. You've been a shining light in the darkness, and I will forever be grateful for your unflinching encouragement, support, and compassion.

A huge thanks goes out to Dr Mattia Veronese. You are truly a role model scientist; your expertise in PET imaging and neuroscience is staggering and your passion for research is inspiring. Thank you for your unwavering willingness to help and for giving me a peek into your brilliant mind.

Thank you to Dr George Dervenoulas, Dr Silvia Rota, Dr Lucia Batzu, Dr Marcello Esposito, Dr Chloe Farrell, Mr Sotirios Polychronis, Dr Gennaro Pagano, and Dr Edoardo De Natale for their momentous role in patient recruitment and/or collection of clinical and imaging data. Thank you to Professor Steve Williams and Professor Kallol Ray Chaudhuri for sharing a portion of their data from the study "Molecular Pathology and Neuronal Networks in LRRK2 PD" (18/LO/1915; IRAS ID: 249061) and to Professor Illan Rabiner for providing a proportion

of data from the MIND-MAPS consortium. A final thanks to Alessio Giacomel for sharing his python coding expertise.

I would also like to offer my thanks to the Medical Research Council Doctoral Training Partnership for funding my PhD studies, Invicro Ltd for funding the study "The role of SV2A in PD and PD with cognitive impairment" (16/LO/1129; IRAS ID: 20584) and "MIND-MAPS-PD" (17/LO/0042; IRAS ID: 213442) and GlaxoSmithKline for funding the study "Molecular Pathology and Neuronal Networks in LRRK2 PD" (18/LO/1915; IRAS ID: 249061). Finally, I would like to thank the participants of the study for making this research project possible.

To my amazing friends: Arifa, Dipesh, Chloe, Supreet, and Kanvil. Arifa, thank you for believing in me when I didn't believe in myself, for never failing to offer advice and for keeping me sane. I don't think I would have made it to the end without you. Dipesh, thank you for keeping me company daily, for always making sure I was well-fed and hydrated and for keeping me motivated. My trauma buddy Chloe, thank you for providing a safe space for pig-outs, rubbish movies and endless laughs. Supreet, you've been a source of encouragement and kindness, and for that, I thank you. Kanvil, thank you for always checking in and for the many walks we took together.

To my wonderful family: my parents Marium and Mohammed, and siblings Nafisa, Ansa, Shaziah and Mohmin. Thank you all for your continual du'as, for your unshakable belief in me and for surviving my wrath during periods of heightened stress. I'm really blessed to be part of this family and I wouldn't be who I am today if it wasn't for you all.

To my husband Oufa, for your patience, love, ceaseless support, and advice throughout. Your faith in me kept me going in moments of doubt and for that, I will forever be grateful. Thank

you for the countless sacrifices you have made to help me get to this point. And most of all, thank you for being my best friend.

Finally, grace and gratitude to Allah, for giving me the strength and courage to complete this thesis and for always showing me the light at the end of the tunnel.

Abstract

Lewy body diseases refers collectively to are a highly heterogenous group of neurodegenerative disorders that include Parkinson's disease (PD), Parkinson's disease dementia (PDD) and dementia with Lewy bodies (DLB). The pathological hallmark of such diseases are intracellular proteinaceous inclusions formed primarily of misfolded and aggregated forms of α-synuclein, thus these diseases are primarily classified as synucleiopathies. Progress over the last two decades has disclosed compelling evidence that synapse loss and dysfunction is a key feature in Lewy body diseases, thus they have also been termed 'synaptopathies'. However, until relatively recently, all approaches for synapse quantification in the human brain have relied heavily on the examination of brain tissue from autopsy or surgical resection. The recent development of the novel positron emission tomography (PET) radioligand [^{11}C]UCB-J has now made it feasible to quantify synaptic density *in vivo* since [^{11}C]UCB-J is a synapse-specific radioligand that binds to ubiquitously expressed synaptic vesicle glycoprotein 2A (SV2A).

Recent studies have demonstrated that both PD and Lewy body dementia exhibit a reduction of SV2A as measured by [^{11}C]UCB-J PET. However, further investigation is required to determine whether SV2A is sensitive to disease chronicity and whether this marker of synaptic density is related to alterations in grey matter volume and brain perfusion. Furthermore, whilst localised alterations of SV2A provides useful information about the spatial location of such alterations, the potential neurophysiological mechanisms underlying these observations is currently unexplored in Lewy body disease.

In this thesis, a series of cross-sectional studies were performed in modestly sized cohorts of drug-naïve PD patients, medicated PD patients and healthy controls (Chapter 3) and medicated PD, PDD and DLB patients and healthy controls (Chapter 4). [^{11}C]UCB-J PET was employed

with high resolution PET to evaluate localised alterations of synaptic density in these subjects. Quantitative measures of T1-weighted Magnetic Resonance Imaging (MRI) and Arterial Spin Labelling (ASL) within the same participants allowed for an assessment of grey matter volume and perfusion alterations and how these measures relate to synaptic density. The clinical relevance of [^{11}C]UCB-J was evaluated by delineating its associations with motor and non-motor symptoms, as well as cognitive performance. To gain an insight into the potential biological mechanisms contributing to alterations in SV2A, spatial correlation analyses were conducted between the spatial distribution pattern of group-level alterations in SV2A expression and the canonical distribution of neuromodulatory neuroreceptors and transporters derived from healthy control PET and SPECT maps. The spatial distribution patterns of group-level grey matter volume and perfusion alterations were also integrated in these analyses.

Here, synaptic density was clearly reduced in early, symptomatic stages of PD, concomitant with negligible reductions in grey matter volume. On the other hand, and consistent with the notion that dopamine replacement therapies may promote neuroplasticity, medicated PD patients exhibited comparable SV2A concentrations to healthy controls and increased compared to drug-naïve PD patients. In Lewy body dementia, more extensive reductions of SV2A were present in PDD, characterised predominately by frontal and parietal involvement, whilst DLB exhibited a more widespread reduction of SV2A across the cortex and subcortex. Notably, synaptic density reductions were not simply explained by volumetric reductions as demonstrated in the dementia cohorts, although volumetric alterations exhibited limited confounding effects. Across all Lewy body disease cohorts, there was a general discordance between hypoperfusion and synaptic density reductions. Finally, the spatial distribution pattern of SV2A alterations were explained, in part, by discrete neurophysiological markers at each stage of the disease, with the dopaminergic system predominately most consonant at early stages but becoming less consistent with SV2A

distribution as the disease progressed to dementia where instead grey matter volume was more closely associated.

Overall, this thesis provides some preliminary insight regarding synaptic density alterations across Lewy body diseases, and the potential neurophysiological properties that may be contributing to these alterations at different stages of the disease. These findings also contribute, albeit in an indirect manner, to the utility of [^{11}C]UCB-J as a specific marker of synaptic protein SV2A.

Table of Contents

Table of Tables

Table of Figures

List of Abbreviations

Abbreviation	Meaning
1TC	1 Tissue Compartmental Model
6-OHDA	6-hydroxydopamine
AADC	Aromatic L-Amino Acid Decarboxylase
AD	Alzheimer's Disease
AMPA	2-Amino-3-(5-Methyl-3-Oxo-1,2-Oxacol-4-Y1) Propanoic acid
ASL	Arterial Spin Labelling
BBB	Blood Brain Barrier
BDI	Beck Depression Inventory
BP_{ND}	Nondisplaceable Binding Potential
CBF	Cerebral Blood Flow
CSF	Cerebrospinal Fluid
CT	Computed Tomography
DAT	Dopamine Transporter
DBS	Deep Brain Stimulation
DJ-1	Deglicase 1 Gene
DLB	Dementia with Lewy bodies
DNA	Deoxyribonucleic Acid
EDS	Excessive Daytime Sleepiness
ESS	Epworth Sleepiness Scale
GABA	Gamma-Aminubutyric acid
DARTEL	Diffeomorphic Anatomical Registration Through Exponentiated Lie Algebra
GDS	Geriatric Depression Scale
H&Y	Hoehn & Yahr
IY	Iterative Yang
L-DOPA	Levodopa
LBD	Lewy body dementia
LIDs	Levodopa-induced dyskinesias
LRRK2	Leucine-rich Repeat Kinase 2
LTD	Long Term Depression
LTP	Long Term Potentiation
MAO-B	Monoamine oxidase B
MBq	Megabecquerel
MCI	Mild Cognitive Impairment
MDS-UPDRS	Movement Disorder Society Unified Parkinson's Disease Rating Scale
MG	Müller-Gartner
MMSE	Mini Mental State Examination
MoCA	Montreal Cognitive Assessment
MPRAGE	Magnetisation Prepared Rapid Acquisition Gradient Echo

MR	Magnetic Resonance
MRI	Magnetic Resonance Imaging
mRNA	Messenger RNA
mSv	Millisievert
NET	Noradrenaline transporter
NMDA	N-Methyl-D-Aspartate
NVC	Neurovascular Coupling
NVU	Neurovascular Unit
PARK2	Parkin Gene
PD	Parkinson's disease
PDD	Parkinson's disease dementia
PDQ-39	Parkinson's Disease Questionnaire
PDSS	Parkinson's Disease Sleep Scale
PE2I	Selective dopamine transporter ligand
PET	Positron Emission Tomography
PVC	Partial Volume Correction
RBD	REM Sleep Behaviour Disorder
RBDQ	REM Sleep Behaviour Disorder Questionnaire
ROI	Region-of-interest
SCOPA-AUT	Scales for Outcomes in PD – Autonomic Dysfunction
SERT	Serotonin Transporter
SN	Substantia igra
SNpc	Substantia nigra *pars compacta*
SNCA	Synuclein Gene
SPECT	Single Photon Emission Computed Tomography
SRTM	Simplified Reference Tissue Model
SV2	Synaptic Vesicle Glycoprotein
T1	Longitudinal Relaxation Time
T2	Transverse Relaxation Time
TE	Time Echo
TR	Time Repetition
UCB-J	Selective SV2A ligand
UPSIT	University of Pennysylvania Smell Identification Test
VBM	Voxel-based Morphometry
VMAT2	Vesicular Monoamine Transporter 2
VaChT	Vesicular Acetylecholine Transporter
WM	White Matter
UKPDSBB	The United Kingdom PD Society Brain Bank

1 Introduction

1.1 Overview

This introduction provides context for this work. Here, I summarise the epidemiology, core clinical features and diagnostic criteria of the disorders studied in this thesis. I then review the basic nervous system properties that are important to the pathophysiology of these diseases, including a summary of the research that is demonstrative of synaptic pathology and loss. Finally, I provide a brief overview of [^{11}C]UCB-J and its target protein. The aims and hypotheses are then presented.

1.2 Synucleinopathies

Amongst proteinopathies are a heterogenous group of neurodegenerative disorders, termed synucleinopathies, that are characterised by intra- and extracellular accumulation of abnormal protein filaments, with the aggregation of pathologic, insoluble α-synuclein within proteinaceous inclusions representing the key histopathological hallmark. Primary synucleinopathies including Lewy body disorders such as Parkinson's disease (PD), Parkinson's disease dementia (PDD) and dementia with Lewy bodies (DLB), among other less common disorders, share a range of clinical, genetic, and biochemical signatures, and are pathologically characterised by intracytoplasmic and intraneuritic inclusions termed Lewy bodies and Lewy neurites, respectively. Most idiopathic synucleinopathies are age-related, thus their prevalence is rising in parallel with the global increase in life expectancy (Van Den Eeden et al., 2003). The classification of these disorders typically centres around clinical presentation and the spatiotemporal progression of aberrant α-synuclein pathology.

1.3 Parkinson's disease

Just over two hundred years ago, James Parkinson meticulously detailed the pathognomonic symptoms of six patients in his seminal monograph '*An Essay on the Shaking Palsy*', which until then had only partially been described in some ancient manuscripts (Parkinson, 2002). A great proportion of his clinical descriptions have withstood the test of time reflected in the fact that to the present day, PD is clinically characterised by cardinal motor symptoms. However, despite James Parkinson including significant details on several key non-motor symptoms, including fatigue, sleepiness and dysautonomia, the traditional notion of PD has been predominated by the key misconception that it is synonymous with a dopamine deficiency motor syndrome. This view has been strongly reinforced by the drastic effect that dopamine replacement therapy has in relieving motor symptomology attached to PD, which, whilst transforming patient care, has fallen short in tackling non-motor symptoms that considerably hinder quality of life (Chaudhuri et al., 2006). However, tremendous progress has since been made in understanding the underlying molecular and neurophysiological mechanisms of the disease and its associated symptoms, alongside the neuropathology implicated in PD and its progression throughout the nervous system. Nowadays, PD is recognised as a multifaceted, multi-neurotransmitter disorder, manifesting as a heterogenous clinical syndrome with sizeable heterogeneity in disease progression and pathology; reflected in the fact that disease progression can span over a duration of 10-30 years, although in some individuals this can be accelerated (Sato et al., 2006).

Nevertheless, the quintessential pathological hallmark of PD is selective loss of neuromelanin-containing dopaminergic neurons within the substantia nigra *pars compacta* (SNpc), which leads to subsequent dopaminergic denervation of forebrain areas, principally the striatum (Marsden, 1982). This reduction in dopaminergic transmission in the motor aspect of the striatum is responsible for the classic parkinsonian features PD patients present with. In fact, motor symptoms do not manifest until approximately 30% of SNpc dopamine-producing neurons have

been lost, with a much more profound loss of striatal dopamine nerve terminals and concentration (Cheng et al., 2010). Highly efficacious treatment of PD remains to be anchored on the substitution of striatal dopamine through pharmacological intervention, though with important refinements and the addition of non-dopaminergic approaches to tackle both motor and non-motor features. In recent years, there have also been ground-breaking expansions for managing treatment-related motor complications such as the introduction of deep brain stimulation (DBS) and pump therapy. These advances in treatment strategies have undoubtedly made PD the first and still unparalleled exemplar of a neurodegenerative disease that can be efficaciously managed for up to decades after disease onset. However, the treatments available today are not curative and PD continues to be a progressive disease that eventually causes severe disability – notably by the growing severity of treatment-resistant motor complications and non-motor signs. Therefore, modifying disease progression and further delaying disability are key unmet needs to be tackled by future research efforts. Of great potential is the identification of early manifestations of the disease, ideally those that antedate the onset of defining motor symptoms.

1.3.1 Epidemiology

PD is now recognised to be the second most common neurodegenerative disease of the elderly, with approximately 6.1 million individuals affected by PD worldwide in 2016 (Collaborators, 2019). This chronic movement disorder typically clinically manifests insidiously after the fifth decade of life, with its incidence increasing five-to-ten-fold from the sixth to ninth decade (Twelves et al., 2003, Savica et al., 2013a, Van Den Eeden et al., 2003). The global prevalence also surges sharply with age, as informed by epidemiological studies that show that PD affects approximately 1.5-2.0% of the population over sixty years of age and 4.0% of those over eighty years (Pringsheim et al., 2014, de Rijk et al., 2000). Improvement in healthcare has led to longer life expectancy that is likely conducive to a longer disease duration, which is in turn associated

with the rising prevalence of PD over time (Lix et al., 2010). In fact, a recent global survey revealed that the number of people with PD has more than doubled over the past generation, with it found to be the fastest growing neurological disorder globally (Collaborators, 2019, Dorsey et al., 2018). Thus, as the world population continues to age, there is likely to be a progressive increase in future personal, societal, and economic burden associated with PD (Dorsey et al., 2007, Leibson et al., 2006).

1.3.2 Clinical features and diagnostic criteria

Whilst a definitive diagnosis of PD is still only possible at post-mortem, within the clinical setting PD diagnosis is based on clinical assessment, with several criteria and guidelines published over the last three decades. The United Kingdom PD Society Brain Bank (UKPDSBB) represented the first formal diagnostic clinical criteria proposed for PD and is the one that was employed in this study to make a diagnosis of PD (Box 1). The more recently published diagnostic criteria by the International Parkinson and Movement Disorder Society (MDS) task force (Postuma et al., 2015) encompasses two main previous sets of criteria (UKPDSBB and Gelb's criteria), with the incorporation of novel components such as the inclusion of non-motor symptoms as additional diagnostic features and the adoption of prodromal PD.

PD is typically characterised by a motor syndrome universally referred to as Parkinsonism (Massano and Bhatia, 2012, Armstrong and Okun, 2020). PD is clinically defined by the presence of bradykinesia in combination with at least one of the following cardinal motor symptoms: rest tremor (4-6 Hz) and muscle rigidity, as well as additional supporting and exclusionary criteria (Box 1) (Marsili et al., 2018, Gibb and Lees, 1988, Postuma et al., 2015). Onset of motor symptoms is typically unilateral, which become bilateral as the disease progresses. Whilst the age of PD onset ranges from <40 to >80 years of age, PD typically manifests in the late fifties.

Young-onset PD is ordinarily defined by an age of onset <45 years of age, with >10% of those cases having a genetic basis (Alcalay et al., 2010, Marder et al., 2010). If, on the other hand, the age of onset is below 30 years of age, the proportion of genetically defined cases can rise to >40% (Alcalay et al., 2010, Marder et al., 2010).

Although the classical signs of Parkinsonism remain to be the core features of the disease, it is now apparent that a multitude of non-motor symptoms including sleep disturbances, cognitive impairment, hyposmia, dysautonomia, depression and pain are a key component of the disease, often dominating its clinical presentation. In fact, some of these symptoms can antedate the onset of cardinal motor manifestations by years or even decades, becoming progressively prevalent over the course of PD and vastly impair quality of life, progression of overall disability and the need for nursing home placement (Bernal-Pacheco et al., 2012, Boersma et al., 2016).

Efforts towards clinical validation of PD have revealed variable diagnostic specificity, sensitivity, and accuracy. A meta-analysis, which incorporated the neuropathological examination as gold standard, reported a pooled diagnostic accuracy of 80.6% (Rizzo et al., 2016), while Jousta and colleagues reported a sensitivity close to 90%, but specificity below 60% for a clinical diagnosis of PD compared to a definitive diagnosis of PD using post-mortem analysis (Joutsa et al., 2014). For the UKPDSBB criteria specifically, (Rizzo et al., 2016) demonstrated that its overall accuracy was 82.7%, with sensitivity of 90.8% and specificity of 34% (Rizzo et al., 2016). Whilst there is a need for clinicopathologic validation studies of the MDS diagnostic criteria, they have been validated against expert clinical diagnosis, which revealed a sensitivity of 88.5%, specificity of 94.5%, and overall accuracy of 92.6% for a diagnosis of probable PD (Postuma et al., 2018), highlighting the improvement of the clinical diagnostic accuracy of PD over time.

Box 1. UK Parkinson's disease society brain bank clinical diagnostic criteria for Parkinson's disease (Gibb and Lees, 1988)

Step 1: Diagnosis of parkinsonian syndrome

- Presence of bradykinesia (as slowness of movement) in combination with one of the following:
    - Rigidity
    - 4-6 Hz rest tremor
    - Postural instability not caused by primary visual, proprioceptive, cerebellar, or vestibular dysfunction

Steps 2: Exclusion criteria for Parkinson's disease

- All secondary causes of parkinsonian syndrome should be excluded, including a history of repeated strokes or head injury with stepwise progression of parkinsonism, oculogyric crises, history of definite encephalitis, supranuclear gaze palsy, familial history, cerebellar signs, Babinski sign, negative response to L-DOPA, early severe autonomic involvement or dementia, neuroleptic treatment at symptom onset, presence of secondary cause on imaging, exposure to toxic agents, sustained remission, and unilateral features after 3 years.

Step 3: Supportive features

- A beneficial response (70-100%) to L-DOPA therapy, presence of classic rest tremor, unilateral onset, presence of levodopa-induced dyskinesia, progressive disorder, persistent asymmetry affecting the side of onset most, clinical course of at least 10 years and L-DOPA response for 5 years or more.

Diagnosis of **definitive PD** requires the fulfilment of the following criteria:

- Three or more supportive criteria in combination with those outlined in step 1.

1.3.3 Motor circuit pathophysiology

The basal ganglia are a key component of several parallel, but anatomically segregated thalamo-cortico-basal ganglia circuits, which function as complex, integrated networks with several feedback and feedforward loops that play a crucial role in the control of actions and goal-directed behaviour. Four circuits with functionally comparable, yet topographically discrete, organisation have been ascertained to subserve motor, limbic, prefrontal-associative and oculomotor function by connecting the corresponding frontal cortical regions, thalamic subregions and basal ganglia (Alexander et al., 1990, Alexander et al., 1986)

The most basic circuit model of the basal ganglia involves the 'direct' and 'indirect' pathways (Albin et al., 1989). When a given motor pattern is computed by cortical motor areas, it conveys somatotopically organised glutamatergic signals to striatal GABAergic medium spinal neurons. These striatal medium spiny neurons project to output nuclei either indirectly, through the external segment of the globus pallidus and the subthalamic nucleus to further suppress thalamic activity (striatopallidal), or directly through the internal segment of the globus pallidus and substantia nigra *pars reticulata* to reduce their activity and thus release firing from thalamocortical neurons (striatonigral). Via both these pathways, striatal dopaminergic tone modulates the GABAergic output activity of the basal ganglia, where it ultimately promotes the direct pathway's net excitatory effect and weakens the indirect pathway's net inhibitory effect. In PD, dopamine depletion leads to an imbalance in the prokinetic direct striatonigral and inhibitory indirect striatopallidal pathways, due to a shift in dopamine-dependent firing rate modulation of striatal medium spiny neurons (Albin et al., 1989). Dopamine loss reduces D_1 receptor-dependent direct pathway medium spiny neuron activation and enhances D_2 receptor-dependent indirect pathway medium spiny neuron inhibition, thus leading to a net effect of a strong increase in the firing rate of basal ganglia GABAergic output neurons. This ultimately results in the over-inhibition of

thalamocortical projections and brainstem areas (Figure 1-1) (Wichmann and DeLong, 1996, Obeso et al., 2008).

It is important to add that the model has been amended with the inclusion of additional connections such as the 'hyperdirect pathway', whereby a monosynaptic connection directly between motor-related cortical regions and the subthalamic nucleus conveys powerful excitatory effects to the globus pallidus internus, bypassing the striatum, thus providing rapid inhibition as a second input structure of the basal ganglia (Figure 1.1) (Nambu et al., 2000). The hyperdirect pathway may play a role in deterring premature responses by bolstering the activity of the indirect pathway, ultimately permitting more time to select the most fitting response at the cortical level (Frank et al., 2007). Indeed, elevated cortical drive and subthalamic hyperactivity has been linked to akinesia, bradykinesia and rigidity in PD and related models (Galvan and Wichmann, 2008, Jenkinson and Brown, 2011). Moreover, whilst a single mechanism of action is unlikely to explain the efficacy of deep brain stimulation, studies utilising animal models have suggested that the anti-kinetic effect of subthalamic DBS may be driven by the antidromic activation of the hyperdirect pathway (Gradinaru et al., 2009, Li et al., 2012).

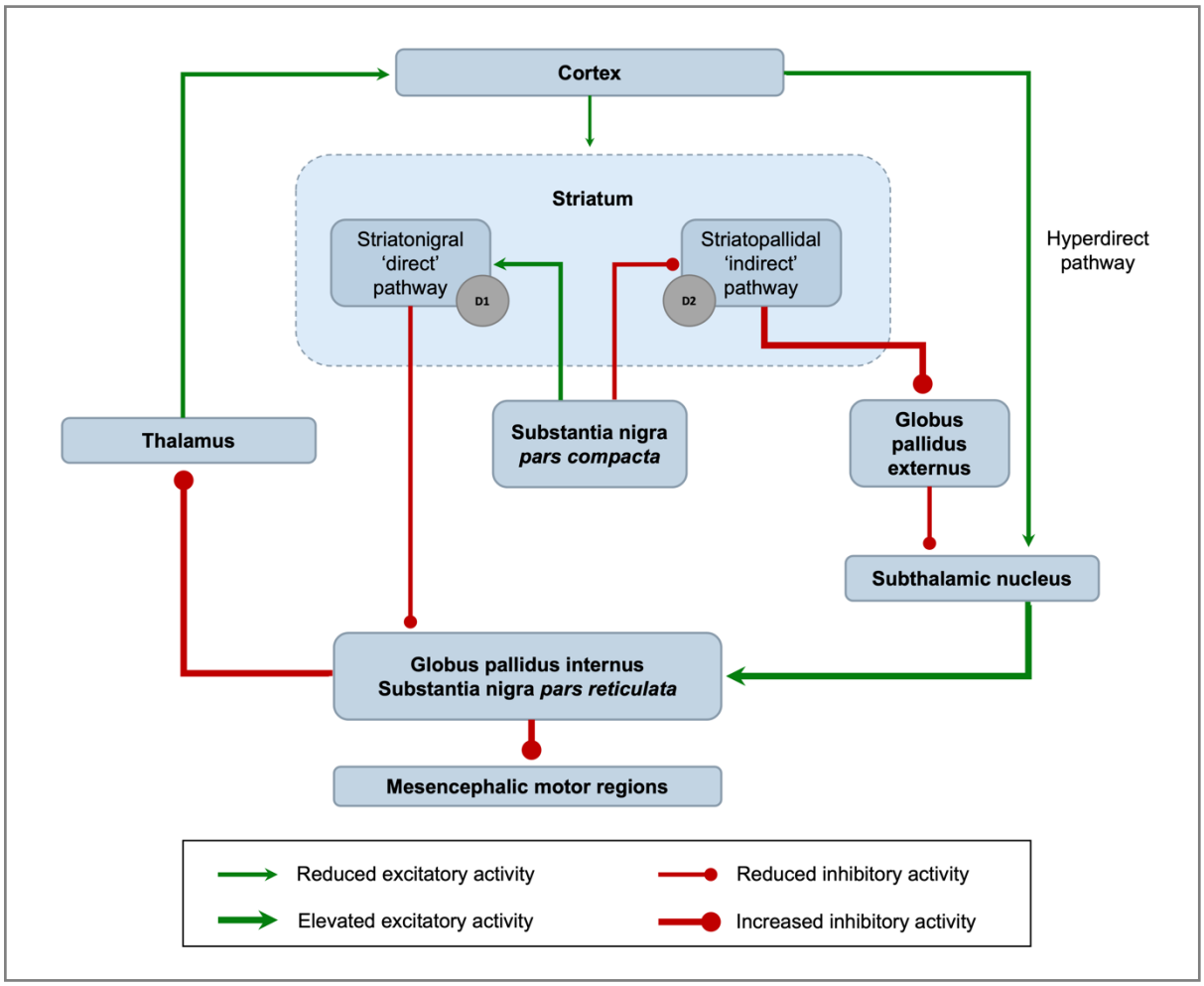

Figure 1.1. A simplified schematic of the altered direct, indirect and hyperdirect pathways in PD. Dysfunction in the basal ganglia motor circuit is a fundamental contributing factor to the pathophysiology of hypokinetic and hyperkinetic motor symptoms observed in PD

1.3.4 L-DOPA

L-DOPA is a metabolic precursor of dopamine and after more than 50 years of clinical use, it remains to be the gold standard for symptomatic treatment of PD, alleviating motor symptoms such as bradykinesia and rigidity, with mixed efficacy in improving tremor, posture and gait problems (Connolly and Lang, 2014). The imbalance between the basal ganglia and the cortical-cerebellar pathways due to maladaptive adjustments in neural circuits due to dopamine denervation (Kordower et al., 2013, Palmer et al., 2009, Kalaitzakis and Pearce, 2009) may be normalised following administration of dopamine replacement therapy. Chronic treatment with L-DOPA has been shown to restore physiological striatal synaptic plasticity potentially due to

maintaining a tonic dopamine level (Picconi et al., 2008). During the first few years of PD, it is highly efficacious at achieving stable symptomatic control, referred to as the 'honey-moon' period. However, the therapeutic window of L-DOPA narrows during disease progression, exerting fluctuations in efficacy, with reduced 'on' times and a surge in frequency of 'off' times. The diminished efficacy of L-DOPA over time is likely linked to the progressive loss of dopaminergic neurons.

L-DOPA can penetrate the blood-brain barrier and its therapeutic action relies on its enzymatic conversion to dopamine by aromatic L-amino acid decarboxylase (AADC). It has several unique physiological actions such as serving directly as a Ca^{2+}-dependent 'classic' neurotransmitter, as observed in several brain regions (Misu et al., 2003), and can act at various central nervous system sites with neuromodulatory properties divergent from those of dopamine. Among these is the dose-dependent down-regulation of AAAD (King et al., 2011). It has become evident, particularly from clinical phenomena associated with long-term use of L-DOPA such as drug-induced dyskinesias and dose-by-dose fluctuations, that L-DOPA is more than just a dopamine precursor, thus, its exact mechanism of action is still puzzling (Mercuri and Bernardi, 2005).

L-DOPA's ability to restore striatal dopaminergic neurotransmission has been demonstrated by several lines of preclinical and clinical evidence. Following the analysis of post-mortem brain tissue from L-DOPA-treated and untreated PD patients in 1975, Lloyd and colleagues determined that the efficacy of L-DOPA is associated with its metabolism to dopamine in the brain (Lloyd et al., 1975). Concentrations of dopamine were preferentially increased within the striatum, which was up to 15 times higher in treated than untreated PD patients and were within the range observed in healthy controls. It was also evident that patients who responded well to treatment exhibited higher striatal dopamine concentrations (Lloyd et al., 1975). Rodent and animal models of PD have revealed that L-DOPA enhances dopamine tissue content and

extracellular levels in the striatum (Navailles et al., 2013, Zetterstrom et al., 1986). L-DOPA also has the ability to increase the loading of dopamine into synaptic vesicles, which was confirmed in living animals using electrochemical cytometry (Omiatek et al., 2013). In healthy mice, L-DOPA was reported to increase vesicular dopamine storage by 240%, highlighting that, even in intact dopaminergic axons, L-DOPA can be transported into the cytosol and converted to dopamine that is packaged into synaptic vesicles. This increase in vesicular dopamine content has been noted to be accompanied by an increase in the volume of secretory vesicles (Colliver et al., 2000).

These findings raise the question of how L-DOPA corrects basal ganglia function when an extensive proportion of striatal dopaminergic axons die and only a small proportion of dopamine release sites remain, as demonstrated by drug-naïve PD patients who have been shown to have approximately 70% reduction in striatal dopamine content and more than 50% of striatal dopamine fibres (Burke and O'Malley, 2013). Firstly, it is important to recognise that the degenerating dopaminergic system is remarkable at maintaining sufficient dopamine transmission and preserving motor functions until relatively late stages of the disease through adaptive modifications in the presynaptic function of the spared dopaminergic terminals. First, depleted extracellular dopamine and a reduction in dopamine autoreceptor activation stimulates dopamine synthesis (Zigmond, 1997), which may enhance dopamine release from the terminals remaining. Second, dopaminergic axonal degeneration also elicits a comparable loss of dopamine transporter activity, ultimately leading to a larger volume of transmission and activation of extrasynaptic dopamine receptors that are distal from release sites (Venton et al., 2003). Finally, even in more advanced stages of the disease, where there is extensive loss of dopaminergic projections from the substantia nigra to the striatum, studies have found that there sufficient AAAD activity remaining to achieve rapid and thorough conversion of L-DOPA to dopamine. Although it remains to be elucidated where this enzymatic activity resides, in the absence of dopamine terminals, the conversion of L-DOPA to striatal dopamine may occur via AAAD

localised to striatal serotonergic nerve terminals (Tanaka et al., 1999), or alternatively, enzymatic activity in striatal interneurons or glia (Hefti et al., 1981).

In rodent models of PD, Picconi et al. (2004) demonstrated that a dose of L-DOPA reversed glutamatergic overactivity and hypersensitivity of presynaptic D_2 dopamine receptors governing glutamate release from corticostriatal terminals. Surprisingly, the sensitivity of presynaptic D_2 dopamine receptors modulating GABAergic transmission remained unchanged in both parkinsonian and L-DOPA-treated rodents (Picconi et al., 2004). These findings suggest that the reversal of glutamatergic overactivity in the striatum and the normalisation of hypersensitive D_2 dopamine receptors modulating excitatory transmission may be one of the mechanisms of action underlying the therapeutic actions of L-DOPA in PD.

Finally, amongst the various postulated mechanisms of action underlying the beneficial motor and cognitive effects of L-DOPA, is the restoration of physiological forms of synaptic plasticity such as long-term potentiation (LTP) and long-term depression (LTD), as well as synaptic depotentiation. As well as regulating the excitability of striatal D_1- and D_2-bearing neurons, dopamine also modulates glutamate-mediated LTD, LTP and synaptic depotentiation, thus is implicated in regulating the plasticity of striatal neurons. Activation of D_1 receptors is crucial to induce both LTP and depotentiation, whilst the coactivation of D_1 and D_2 receptors is necessary for the induction of LTD (Calabresi et al., 2000). It has been demonstrated that the complete depletion of striatal dopamine leads to the loss of LTP and LTD, though partial lesions selectively affect NMDA-dependent LTP, but not LTD. Furthermore, complete, or partial dopaminergic denervation alter the composition of the NMDA receptor subunit in the postsynaptic density in distinct manners signifying that different levels of striatal dopamine depletion have differential effects on corticostriatal synaptic plasticity (Paille et al., 2010). Using field-evoked potentials elicited with a nearby microelectrode in PD patients, Prescott et al. (2009)

demonstrated that following oral administration of L-DOPA, high frequency stimulation in the substantia nigra *pars reticulata* was able to induce lasting potentiation of the field-evoked potentials amplitudes, which was not the case in those who were not administered L-DOPA (Prescott et al., 2009). This clinical finding emphasises that L-DOPA, through increasing dopaminergic tone within the basal ganglia, modulates the activity-dependent synaptic plasticity causing LTP-like synaptic changes.

Whilst chronic treatment with L-DOPA has been shown to restore physiological striatal synaptic plasticity potentially due to maintaining a tonic dopamine level (Picconi et al., 2008), theoretically, chronic treatment may also stimulate the production of trophic factors that compensate for dendritic morphological changes induced by dopaminergic denervation (Zetterstrom et al., 1986, Deutch et al., 2007), although it is also possible that L-DOPA itself induces aberrant structural plasticity in the dendritic spines of striatal medium spiny neurons, causing additional short- and long-term alterations of glutamatergic and dopaminergic transmission (Nishijima et al., 2014, Zhang et al., 2013).

1.4 Lewy body dementias

PDD and DLB, referred to collectively as Lewy body dementia, are amongst the most common cause of dementia worldwide, second to Alzheimer's disease (AD), accounting for 15-20% of the global incidence of dementia (Aarsland et al., 2001a, Aarsland et al., 2005, Mueller et al., 2017, Vann Jones and O'Brien, 2014). Lewy body dementia is an umbrella term used for these two related neurocognitive syndromes that share a comparable phenotype of dementia combined with parkinsonism, and common underlying pathological substrates, which includes the coexistence of Lewy-related pathology with AD-type neuropathology. Clinically and neuropathologically, these disorders are difficult to differentiate (Irwin et al., 2017, Postuma et

al., 2016, Tsuboi et al., 2007), although the overall consensus is that DLB is generally a more severe condition than PDD, especially regarding cognitive and potentially neuropsychiatric domains (Bougea et al., 2018), and has a higher prevalence of AD-like pathology than PDD (Ballard et al., 2006, Hepp et al., 2016). Nevertheless, Lewy body dementias negatively affect activities of daily living, resulting in increased nursing home admission and longer and more frequent hospital admissions, which inevitably drive health-care costs (Lee et al., 2018, Bostrom et al., 2007, Mueller et al., 2018). Indicatively, although mortality rates do not differ between the two disorders, they are approximately three times higher than the general population (Larsson et al., 2018). Thus, the socioeconomic burden of Lewy body dementia is substantial, necessitating the development of diagnostic toolkits for accurate and timely diagnoses, as well as disease-modifying treatments and useful biomarkers to improve prognosis.

Clinically, both PDD and DLB are characterised by the presence of dementia accompanied by shared core clinical features of Lewy body dementias that include fluctuations in cognition and alertness, recurrent visual hallucinations and REM sleep behaviour disorder, alongside parkinsonism (although 25% of DLB patients will never go on to develop parkinsonian symptoms) (Emre et al., 2007, McKeith et al., 2017, Walker et al., 2015b, Kim et al., 2014). The cognitive domains are congruently affected in these syndromes, with progressive executive dysfunction, visuospatial deficits, and memory impairment (Lippa et al., 2007). Whilst there is considerable overlap in clinical, neurochemical, and morphological features, PDD and DLB are incorporated into DSM-5 as two distinct entities of major neurocognitive syndromes characterised by widespread cortical Lewy body deposition with unknown aetiology (Association, 2013, McKeith et al., 2017). These diseases are clinically differentiated based upon the time of onset of motor and cognitive symptoms, where cognitive impairment precedes, or occurs concurrently with, the onset of parkinsonism in DLB, but manifests in the context of well-established PD in PDD. This relatively arbitrary definition has been criticised but is nevertheless

useful within the clinical setting, particularly since it is unfeasible to differentiate a parkinsonian patient as PDD or DLB based on a single examination without considering the temporal sequence of events.

Despite the distinctive temporal sequence of emergent clinical symptoms, both diseases exhibit remarkably convergent clinical, neuropathological, and morphological features, albeit with some divergence (Jellinger, 2009b, Garcia-Esparcia et al., 2017, Hepp et al., 2016, Walker et al., 2015b), which has led to the ongoing debate around the nosological relationship between both syndromes. Controversy still exists as to whether PDD and DLB are the same disease (Friedman, 2018), are different phenotypic expressions of the same underlying process (i.e. two ends of the spectrum) (Galvin et al., 2006, Goldmann Gross et al., 2008, Jellinger and Korczyn, 2018, Aarsland et al., 2004) or dichotomous entities (Boeve et al., 2016, Postuma et al., 2015). In many ways, PDD and DLB are more likely to be considered as subtypes in a continuum of Lewy body disease, despite some pathological differences between DLB and PDD being noted, such as DLB patients exhibiting higher striatal amyloid plaque deposition, increased frequency of α-synuclein in hippocampal CA2/3 area, elevated 5-HT_{1A} receptor density in the frontal cortex, less discernible nigral cell loss and a relative lack of striatal D_2 receptor upregulation. Furthermore, with progression of the disease, the two conditions appear even more alike in terms of clinical features and underlying neuropathological features, although the complex neuropathophysiological mechanisms leading to phenotypic heterogeneity between both syndromes deserve further elucidation.

1.4.1 Epidemiology

Both PDD and DLB are age-related disorders, although onset prior to the sixth decade is not uncommon and both diseases are more prevalent in males than females.

Since PDD is a late complication of PD, the risk of dementia increases with disease duration, with a cumulative prevalence of 75-90% of patients with established PD going onto develop dementia after a disease duration of ten or more years (Buter et al., 2008, Hely et al., 2008, Aarsland and Kurz, 2010a), with an overall prevalence of 31.1% (Aarsland et al., 2005), highlighting that PD patients have a 4- to 6-fold increased risk of going onto develop dementia compared to the age-matched general population (Aarsland et al., 2010). The prevalence of PDD in the general population aged 65 and over has been estimated to be 0.3-0.5%, accounting for 3-4% of all dementia cases (Aarsland and Kurz, 2010b, Aarsland et al., 2005). Community-based studies have reported incidence rates of 95.3 – 112.5 per 1000 person-years, indicating that around 10% of the PD population go on to develop dementia per year. Since increasing age serves as a major risk factor for the manifestation of PDD in PD patients, the time to dementia onset declines with increasing age of PD onset (Aarsland et al., 2007).

Whilst there are fewer reports of prevalence and incidence rates for DLB, two systematic reviews estimated that the proportion of individuals with dementia accounted for by DLB ranges from 0.3% to 24.4% (Vann Jones and O'Brien, 2014, Hogan et al., 2016), with prevalence estimates increasing with age. In community-based studies, probable DLB accounted for 4.2% of all dementia diagnoses, whilst in clinic-based studies, the mean prevalence was 7.5% (Vann Jones and O'Brien, 2014). However, it is important to highlight that DLB appears to be under-diagnosed in clinical practice (Mok et al., 2004, Toledo et al., 2013), thus these values are likely underestimated. This is evidenced in the fact that the three studies that focused on identifying DLB cases and included a neurological examination reported higher prevalence of the disease ranging from 16-24% of those with diagnosed dementia (Vann Jones and O'Brien, 2014). Furthermore, studies that incorporated tools that increase diagnostic accuracy, such as dopamine transporter (DAT) imaging, screening for REM sleep behaviour disorder and employing standardised scales focussed on the core features of DLB, suggest that 10-15% of dementia cases

have DLB (Rahkonen et al., 2003, Stevens et al., 2002). In a population-based study, 7.6% of dementia cases were diagnosed with DLB (Tola-Arribas et al., 2013).

In a USA-based study, the incidence of probable DLB was 3.5 per 100,000 person-years, with incidence rates rising to 31.6 per 100,000 person-years in those over the age of 65 years (Savica et al., 2013b). On the other hand, in France the estimated incidence was 112 per 100,000 person-years in individuals ages 65 years and older (Perez et al., 2010). The inconsistency between these studies could be explained by the fact that in the USA study, the patients included were only those who had a diagnosis of parkinsonian syndrome in their medical record, thus individuals with mild or absent parkinsonism would have been excluded (Savica et al., 2013b). In the French study, all participants were screened for parkinsonian symptoms and cognitive impairment (Perez et al., 2010). However, in both studies, core features of DLB were sought retrospectively and the presence of REM sleep behaviour disorder, which is highly prevalent in DLB and now acknowledged as a core clinical feature, was not systematically assessed, thus both studies were probably impeded by underdiagnosis of DLB.

1.4.2 Clinical features and diagnostic criteria

The presenting features of Lewy body dementias can be divided into three categories: cognitive impairment, behaviour/psychiatric phenomena, and physical symptoms (Donaghy and McKeith, 2014). Boxes 2 and 3 shows the diagnostic criteria for DLB and PDD, respectively. Currently, the biggest diagnostic challenge for DLB is early diagnosis and differentiation from AD, whilst for PDD the primary challenge is prediction and timely identification of cognitive impairment.

The first consensus guidelines clinically classifying probable and possible DLB were defined and published by a group of experts, namely the International DLB Consortium, in 1996 which was then revised in 2005 and further refined in 2017 (McKeith et al., 1996, McKeith et al., 2005,

McKeith et al., 2017). Clinically, DLB is characterised by four core symptoms of fluctuating cognition, visual hallucinations, parkinsonism, and REM sleep behaviour disorder in the context of cognitive decline with moderate memory deterioration (McKeith et al., 2017). Visual hallucinations may transpire spontaneously, independent of perceptual and visuospatial impairments (Cagnin et al., 2013), whilst in PDD they typically arise following dopaminergic therapy (Lippa et al., 2007, McKeith et al., 2005). Language impairments tend to be mild, with deficits in verbal and semantic fluency. In earlier stages of dementia, DLB patients reportedly exhibit slightly worse performance on tests of attention-executive function compared to PDD, with more severe impairment in tests of visuospatial abilities, particularly the intersecting pentagon test (Petrova et al., 2015), suggesting that visuospatial function may be disproportionately affected in DLB. Although up to 85% of DLB patients experience parkinsonian motor symptoms (McKeith et al., 2017), classical rest tremor is considered to be uncommon in DLB (Onofrj et al., 2013). Naturally, parkinsonian features in PDD can be moderate-to-severe despite the higher use of antiparkinsonian medications. In fact, the long-term exposure to high-dose antiparkinsonian medications can induce commensurate complications such as motor fluctuations and psychosis (Factor et al., 2017, Ray Chaudhuri et al., 2018). Nevertheless, the rate of cognitive decline is reportedly faster in DLB than in PDD and AD (Blanc et al., 2017, Kramberger et al., 2017).

In PDD, the clinical and cognitive features present are in several respects like those observed in DLB. Whilst the cognitive domains impaired in PDD coincide with those impaired in DLB, the timing, profile and rate of cognitive decline show considerable heterogeneity in PDD depending on the neurotransmitter systems implicated along the trajectory of disease progression (Papagno and Trojano, 2018). Indeed, the average time to dementia onset following a diagnosis of PD is approximately ten years, but this could be extended to as long as twenty years (Aarsland et al., 2017). Attentional fluctuations that are characteristic of DLB are less prevalent in PDD (Goetz

et al., 2008), but are clinically indistinguishable between both syndromes (Varanese et al., 2010). Executive and visuospatial dysfunction are often described to dominate the cognitive profile in PDD, whilst language deficits are rare (Meireles and Massano, 2012, Postuma et al., 2015). Visual hallucinations, although less frequent in PDD (Eversfield and Orton, 2019), have a similar phenomenology of those occurring in DLB (Frei and Truong, 2017). REM sleep behaviour disorder has a high prevalence in both disorders, with up to 90% of patients affected after more than ten years (Iranzo et al., 2016). In fact, REM sleep behaviour disorder may even precede cognitive decline and parkinsonism by decades in DLB and PDD, respectively (Boeve, 2013, Ferman et al., 2011). A summary of the shared and distinct clinical features of PDD and DLB can be found in Table 1.

Once dementia insidiously develops in PD, there are no clinical or biological differences that can reliably distinguish PDD from DLB. Thus, the distinct initial clinical presentations of PDD and DLB, namely the temporal sequence of onset of dementia and parkinsonism, is fundamental to differentiating between the two syndromes. More specifically, on clinical grounds, the two conditions are discerned according to the 'one year rule' whereby if dementia manifests in the setting of established PD or at least one year after the onset of parkinsonism, then the diagnosis is deemed to be PDD. If, on the other hand, dementia precedes or occurs concomitantly with parkinsonian motor signs or within a year from its onset, then a diagnosis of DLB would be made.

Table 1.1. Clinical overlap and dissimilarities between PDD and DLB

Shared clinical features	**Divergent clinical features**
Rigidity, akinesia, similar cognitive profiles, frontal executive dysfunction, visuospatial impairment, mild language impairment, mood disturbances, visual hallucinations, delusions, REM sleep behaviour disorder, neuroleptic sensitivity	DLB have greater impairments in attention and episodic verbal memory, tremor is less frequent in DLB, delusions, attentional fluctuations and hallucinations are more frequent in DLB, poorer balance and slower walk in DLB, orthostatic hypotension is more frequent in DLB, frontal/temporal-associated cognitive subsets are more severe in DLB, cognitive decline is faster in DLB than in PDD, visual hallucinations are spontaneous in DLB, whereas in PDD they usually occur after L-DOPA therapy

Box 2. Diagnostic criteria for dementia with Lewy bodies (McKeith et al., 2017, McKeith et al., 2005, McKeith et al., 1996)

Essential feature (compulsory for probable or possible diagnosis)

- Progressive dementia of sufficient severity to interfere with normal social or occupational function
- Deficits on tests of executive function, attention and visuospatial ability may be particularly prominent

Core features

- Fluctuating cognition with marked variations in attention and alertness, recurrent visual hallucinations, REM sleep behaviour disorder, spontaneous parkinsonism

Supportive features (commonly present but not proven to have diagnostic specificity)

- Severe sensitivity to antipsychotic agents, repeated falls, postural instability, severe autonomic dysfunction, transient unexplained loss of consciousness, non-visual hallucinations, systematised delusions, depression. Relative perseveration of the medial temporal lobe structures, generalised low perfusion/metabolism with reduced occipital activity ± cingulate island sign, prominent posterior slow-wave activity on EEG with periodic fluctuations in the pre-alpha/theta range

Indicative biomarkers

- Reduced dopamine transporter uptake in the basal ganglia, abnormal metaiodobenzylguanidine myocardial scintigraphy, polysomnographic verification of REM sleep without atonia

Diagnosis of **probable DLB** requires the fulfilment of the following criteria:

- Two or more core clinical features, with or without the presence of indicative biomarkers, or
- Only one core clinical feature is present concurrently with one or more indicative biomarkers

Diagnosis of **possible DLB** requires the fulfilment of the following criteria:

- Only one core clinical feature is present, with no indicative biomarker evidence, or
- No core clinical features present, but there is one or more indicative biomarkers

Box 3. Diagnostic criteria for Parkinson's disease dementia (Emre et al., 2007)

Core features

- Diagnosis of PD according to Queen Square Brain Bank Criteria (Gibb and Lees, 1988)
- Dementia developing in the setting of established PD, with impairment in more than one cognitive domain and with sufficient severity to impair daily life

Associated clinical features (commonly present but not proven to have diagnostic specificity)

- Cognitive features include impairment in attention, executive function, visuospatial functions, and memory
- Behaviour features include apathy, depression, anxiety, hallucinations, delusions, and excessive daytime sleepiness

Diagnosis of **probable PDD** requires the fulfilment of the following criteria:

- Both core features must be present
- Typical cognitive profile includes impairment in at least two of the following domains: (1) attention, which may fluctuate; (2) executive function (3) visuospatial function; (4) free recall, which usually improves with cueing
- The presence of at least one behavioural symptom, although absence does not exclude diagnosis

Diagnosis of **possible PDD** requires the fulfilment of the following criteria:

- Both core features must be present
- Atypical cognitive profile in one or more domains, such as prominent or receptive-type aphasia, or pure storage-failure type amnesia with preserved attention

A diagnosis of **PDD cannot be made** if:

- Cognitive and behaviour symptoms appear solely in the setting of other conditions such as systemic diseases, drug intoxication, or major depression
- Patient meets criteria for probable vascular dementia

Despite the current consortium criteria for DLB having a relatively high specificity, it has been criticised for poor sensitivity, as demonstrated by several studies (Jellinger, 2008, Weisman et al., 2007), including the largest being in 2861 cases from the National Alzheimer's Coordinating Center registry, where the sensitivity of clinical diagnosis of pure DLB against autopsy-confirmed cases was 32.1%, whilst specificity was over 95% (Nelson et al., 2010). The revised diagnostic criteria of DLB (McKeith et al., 2005) boosted the proportion of cases fulfilling the criteria for probable DLB by 24% (Aarsland et al., 2008). A recent meta-analysis conducted by Rizzo et al. (2018) assessed the potential improvement of diagnostic criteria over time in 22 studies on 1584 patients. According to the McKeith 1996 consensus guidelines for a diagnosis of probable DLB, a pooled sensitivity, specificity, and accuracy of 48.6%, 88% and 79.2% was reported, whereas for the revised McKeith 2005 consensus guidelines, a pooled sensitivity, specificity, and accuracy of 88.3%, 80.8%, and 90.7% for probable DLB was reported (Rizzo et al., 2018). These findings demonstrate that these diagnostic criteria have become more sensitive and accurate over time, but detection rates in the clinical setting remain suboptimal with the main issue being that many cases are missed or misdiagnosed, usually as AD (Vann Jones and O'Brien, 2014). It is also important to highlight that diagnostic accuracy is superior when α-synuclein is extensive, but poorer with increasing neuritic plaque pathology, with no influence exerted by amyloid-β load (Tiraboschi et al., 2015). In fact, phenotype and diagnostic accuracy is highly influenced by neuritic AD pathology as opposed to cortical Lewy body distribution, where only 15% of autopsy-confirmed DLB cases with severe AD pathology were correctly diagnosed, compared to 52% in those with low AD Braak stage (Jellinger, 2008, Weisman et al., 2007).

Overall, the diagnostic accuracy remains to be moderate in research and poor in clinical settings, with DLB being most often misdiagnosed as AD. Whilst the inclusion of REM sleep behaviour disorder as a core feature has improved sensitivity without sacrificing specificity, the current diagnostic criteria remains to be limited in its ability to accurately identify DLB with high

specificity and sensitivity, indicating that further improvements are needed, perhaps with the incorporation of novel biomarkers, to improve diagnostic accuracy of DLB in the clinical and research setting.

1.5 The synapse

The synapse serves as a major information transfer unit in the nervous system that facilitate the flow of neural information between neurons. Synapses in the CNS are intercellular junctions between neurons that convey action-potential encoded information (Sudhof, 2012). They are primarily classified as either electrical, which enable charged ions and small molecules to directly transfer through pores known as gap junctions, or chemical, which transmit electrical activity unidirectionally from one neuron to another via chemical mediators, termed neurotransmitter (Rouach et al., 2002). Depending on the influence these molecules have on the recipient neuron, synapses are further subdivided into excitatory and inhibitory, with excitatory synapses primarily situated at the top of tiny dendritic protrusions termed dendritic spines and inhibitory synapses located on the shaft of dendrites or on neuron soma and axon initial segments (Bourne and Harris, 2008). Whilst the synapse has distinct morphology, molecular composition, and function, its general organisation comprises a presynaptic terminal loaded with neurotransmitter-containing vesicles, perfectly juxtaposed to the postsynaptic compartment, which is adorned with an assortment of surface-expressed protein complexes that are receptive to neurotransmitter release, so-called 'receptors'. The pre- and post-synaptic compartments are connected by synaptic cell adhesion molecules (Pinto and Almeida, 2016, Sheng and Kim, 2011, Missler et al., 2012). The homeostasis and sustained functionality of the synapse depends largely on numerous synaptic proteins residing in the presynaptic boutons, mitochondrial influx, and elevated bioenergetics in the presynaptic compartment that fuel effective and sustained

neurotransmission, as well as postsynaptic membrane-receptors that bind the neurotransmitter and convey the neural information to the postsynaptic neuron.

The presynaptic terminal is a specialised area of clustered synaptic vesicles, with each nerve terminal possessing around 100-200 synaptic vesicles. The synaptic vesicle is a tiny endosomal compartment, which has a diameter of approximately 40 nm, and contains the neurotransmitter associated directly and/or indirectly with over a hundred proteins for appropriate functioning. Synaptic vesicle exocytosis is tightly regulated by Ca^{2+}, whereby when an action potential arrives at the presynaptic terminal, presynaptic voltage-gated Ca^{2+} channels open and the influx of Ca^{2+} promotes the assembly of a molecular machinery predominately composed of Ca^{2+} sensor synaptotagmin and the soluble NSF-attachment protein receptor (SNARE) complex, including protein components such as SNAP-25, VAMP-2 and Syntaxin-1 (Sudhof, 2013). This ultimately triggers the trafficking of synaptic vesicles from the readily releasable pool to a small segment of the presynaptic plasma membrane at which synaptic vesicles cluster to be exocytosed, designated as the presynaptic active zone (Sudhof, 2012). This area forms an intrinsic component of the synaptic vesicle release machinery at which docking, priming and fusion of synaptic vesicles to the presynaptic plasma membrane occurs, leading to the release of neurotransmitters into the synaptic cleft, where they activate postsynaptic receptors. Following exocytosis, the synaptic vesicle membrane is retrieved from the synaptic cleft via endocytosis and locally loaded with neurotransmitter, thus are recycled for another round of exo-endocytotic membrane cycling (Gross and von Gersdorff, 2016). This mechanism enables neuronal sustainability of a high firing rate without depletion of pools of synaptic vesicles (Gross and von Gersdorff, 2016).

The molecular composition of the active zone and presynaptic terminal is extensive, with approximately 450 proteins identified to-date (Sudhof, 2012, Dieterich and Kreutz, 2016, Wilhelm et al., 2014, Boyken et al., 2013, Weingarten et al., 2014). Alongside the highly

conserved protein complex of Rab3-interacting molecules (RIMs), RIM-binding proteins, Munc13, α-liprin and ELKS that are highly enriched at the active zone, other presynaptic proteins include synapsin, synaptogyrin, synaptophysin, piccolo and bassoon, small GTPases, neurotransmitter transporters, axonal trafficking proteins, channel proteins and synaptic vesicle glycoprotein 2 (SV2), (Figure 1.2).

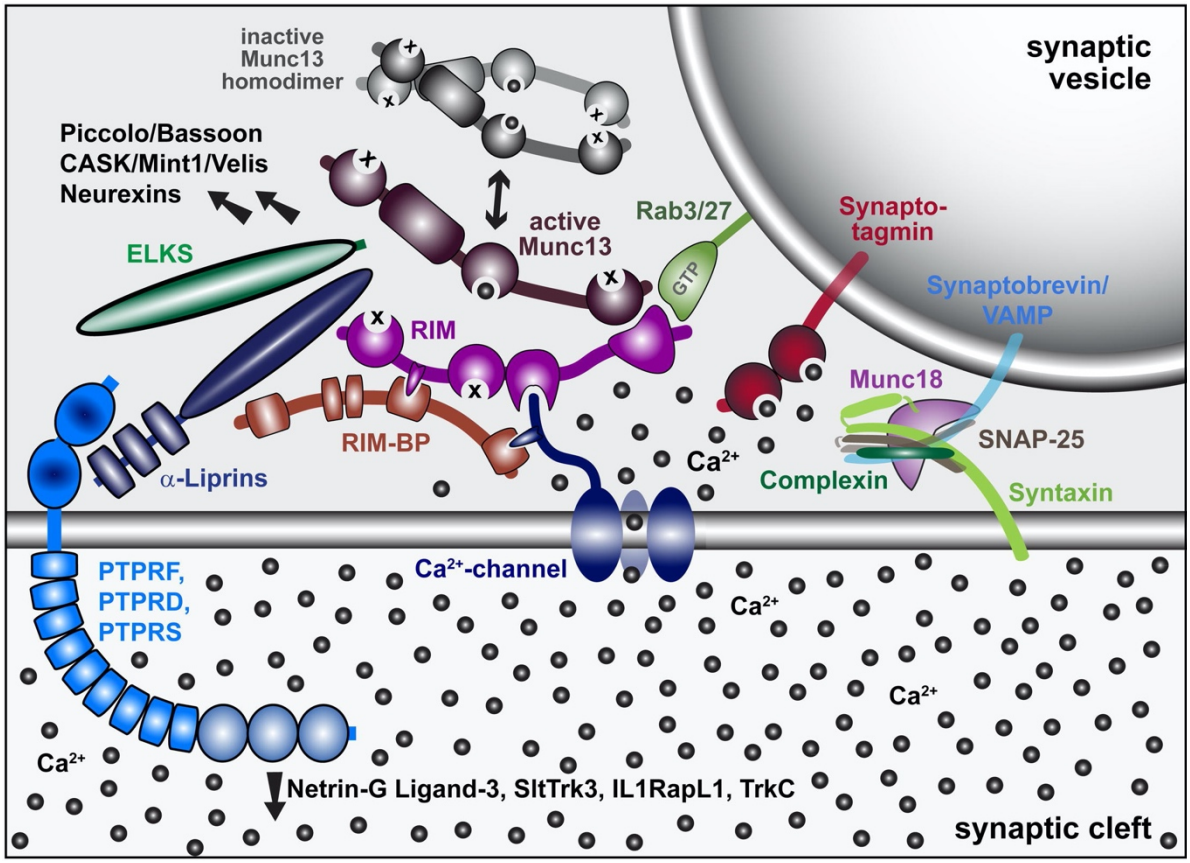

Figure 1.2. Illustration of the active zone protein complex and the main proteins involved in exocytosis. *Reprinted from Neuron, 75(1), Südhof T. C., The Presynaptic Active Zone, 11-25, Copyright © 2012, with permission from Elsevier*

Adjacent to the presynaptic terminal is the post-synaptic density. This disc-like structure is a specialised recipient of the neurotransmitter signal transmitted from the presynaptic terminal, which it then transduces into electrical and biochemical changes in the postsynaptic cell (Frank and Grant, 2017). The cardinal functional components of the postsynaptic compartment into excitatory or inhibitory synapses are ionotropic receptors for glutamate and γ-aminobutyric acid

(GABA), respectively. These ligand-gated ion channels are localised at the postsynaptic membrane, embedded in a dense protein rich network comprised of anchoring and scaffolding molecules, cytoskeletal components, signalling enzymes and other membrane proteins. In fact, over four hundred protein components have been described thus far (Sheng and Kim, 2011).

Synapses are reliably distinct from one another in their properties, not only in terms of neurotransmitter type, but also in terms of basic synaptic parameters such as the release probability and post-synaptic receptor composition (Sudhof, 2018). The mammalian brain encompasses hundreds of different neuronal populations, which form and receive synapses that exhibit unique characteristics that depend on both the pre- and postsynaptic neuron (Koester and Johnston, 2005). Consequently, there are probably hundreds of different types of synapses that function via the same fundamental mechanism but exhibit discrete computational properties.

1.6 Neuromodulation of synapses

An array of substances including small molecule transmitters, biogenic amines, and neuropeptides, can be released in ways divergent from classical fast synaptic transmission, modifying neural circuit output to generate extensive adaptability in behaviours (Bucher and Marder, 2013). Their modulatory action is exerted by altering the properties of a neural circuit's integral neurons, their synaptic connections, or the inputs to the circuit. Such functional reconfiguration of hard-wired neural circuits is fundamental for the nervous system's adaptability.

Synaptic transmission is modified by neuromodulators via several mechanisms that can be broadly categorised into actions that directly target synapses and those that indirectly alter synaptic interactions by modifying the excitability of neurons. Both direct and indirect effects on

synaptic interactions can be divided into pre- and post-synaptic mechanisms. Indirect influences include presynaptic modulation that induces changes in the shape of the action potential (Rosen et al., 1989, Sakurai et al., 2006, Sasaki et al., 2011), and postsynaptic modulation that could, for example, result in an increase of voltage-gated inward currents that enhance excitatory postsynaptic potentials (Heckman et al., 2009, Murray et al., 2011, Rank et al., 2011). Direct effects include neuromodulators influencing the probability of vesicular release presynaptically by modifying Ca^{2+} influx into the presynaptic terminal, the size of the reserve pool, or proteins in the active zone (McKay et al., 2007, Higley and Sabatini, 2010, Regehr et al., 2009, Logsdon et al., 2006). Postsynaptically, the surface expression and properties of neurotransmitter receptors can be adjusted to modify the postsynaptic response, independent of neurotransmitter release (Sun et al., 2005, Feng et al., 2001). Neurotransmitter release can also be modulated through local feedback via retrograde messengers (Kano et al., 2009) or autoreceptors (Fu et al., 1998, Langer, 2008). Finally, a broader category of neuromodulation, referred to as meta-modulation, is where neuromodulator release itself can be moderated, with an example being nitric oxide altering the modulatory actions of serotonin or glutamate (Pinard and Robitaille, 2008, Straub et al., 2007, Ribeiro and Sebastiao, 2010).

Overall, synaptic transmission involves a large array of molecules that exert a complex, tight regulation, and intricate localisation properties. There is a growing appreciation that disruption of these fundamental synaptic processes can have profound implications, with impaired synapse function being recognised as a key feature across multiple neurological disorders. Therefore, it is tempting to speculate that molecular elements of synapses are pivotal candidates that contribute to, or even cause, brain malfunction. In the next section, I will present the evidence that Lewy body diseases are disorders of synaptic function.

1.7 Signs of synaptopathy in Lewy body disease

Until recent years, much of the focus in the field of neurodegeneration has been on neuronal death, with neuroprotection equating to the rescue of the neuron soma. In this concept, that has prevailed in the design of clinical trials, there is a tacit assumption that the death of neuron soma either precedes or occurs concomitantly with axonal degeneration, and so strategies that protect the neuron perikaryon would be expected to protect axons too. Whilst much of the debate around the origins of PD has been centred around regional studies of α-synuclein pathology in the post-mortem brain (Braak et al., 2003), an imperative question to address is where the diseases commences on a cellular level. Just over twenty years ago, Dr. Oleh Hornykieweicz postulated, based on the cellular localisation of the DAT that is enriched in striatal terminals rather than on nigral cell bodies, that the manifestation of PD starts by first affecting axons in the dorsal striatum prior to the loss of dopaminergic neurons in the substantia nigra (Hornykiewicz, 1998). However, it was not until recently that this notion gained strong support through a plethora of pathological and molecular data that have demonstrated that the earliest detectable pathology is at the level of the synapse and axon, not the neuron soma. In fact, several studies have indicated that dysfunction of various neurotransmitter systems ensues even prior to the presence of Lewy pathology and consequent neuronal loss. This has led to the hypothesis that neurodegeneration in PD and Lewy body dementia is a dying back-like phenomenon, which initiates at the synaptic terminals and progresses proximally along the axon towards neural cell bodies leading to the subsequent death of neuronal perikaryal.

Altered structural and functional phenotype of the presynaptic terminal is now recognised to be a common denominator of several neurological diseases; thus, they may be collectively deemed as diseases of the synapse, or synaptopathies. In late-onset degenerative diseases, synaptic defects have been considered as an inevitable endpoint incident of an ongoing pathophysiological cascade, with a number of these diseases exhibiting early impairment of synaptic function (Bae

and Kim, 2017). Synaptic dysfunction often occurs concomitantly with the development of cognitive impairments, with neuronal loss emerging at later stages of the disease (Schulz-Schaeffer, 2010, Milnerwood and Raymond, 2010, Picconi et al., 2012).

According to the current diagnostic criteria, PD is clinically diagnosed when disease progression is already advanced. There have been numerous studies that have focussed on assessing the magnitude of nigral neuron loss, and that of striatal terminal loss, at PD onset which have made it possible to compare the degree of early pathology in these two cellular compartments. Whilst a majority of reviews have reported that motor signs first become evident when about 50% of nigral dopamine neurons are atrophied (Marsden, 1990, Ross et al., 2004), with estimates of up to 70% also being proposed (Lang and Lozano, 1998, Dauer and Przedborski, 2003), subsequent comprehensive clinico-neuropathological studies performing regression analysis more accurately ascertained a ~30% loss of dopamine-producing neurons in the substantia nigra by the time motor symptoms manifest (Fearnley and Lees, 1991, Ma et al., 1997, Greffard et al., 2006), with a much more profound deterioration of dopaminergic terminals, particularly within the putamen (Kurowska et al., 2016, Kordower et al., 2013). Thus, the pathological processes underlying PD likely commence prior to the onset of detectable motor symptoms, which is the period at which a variety of non-motor symptoms, such as hyposmia, constipation and rapid eye movement (REM) sleep behaviour disorder, are often observed (Hawkes et al., 2010, Kalia and Lang, 2015, Mahlknecht et al., 2015). This period is referred to as the prodromal phase, which can last anywhere between 5-20 years and represents a stage in which there is little to no degenerative cell loss, thus interventions at this point could halt disease progression. Imaging studies of striatal dopaminergic terminals using single photon emission tomography (SPECT) with ligands specific for the DAT have revealed significant striatal terminal loss during this prodromal stage (Jennings et al., 2017, Fazio et al., 2018, Barber et al., 2017, Sierra et al., 2013). In fact, during the prodromal phase of PD and PD-related syndromes, the expression levels of a range of proteins

implicated in synaptic transmission have been found to be altered in the cingulate and prefrontal cortices, alongside the substantia nigra (Dijkstra et al., 2015, Bereczki et al., 2016), indicating that non-motor and motor symptoms are associated with impaired synaptic communication.

Whilst a majority of cases in PD are sporadic, about two dozen genes including *SNCA*, *LRRK2*, *PARKIN*, *DJ-1*, *PINK1*, and *GBA* contribute to the heritable cases of the disease (Ferreira and Massano, 2017, Klein and Westenberger, 2012) and have been instrumental in providing compelling insight into the key pathogenic mechanisms implicated in PD (Keane et al., 2011, Kalia and Lang, 2015), including the establishment of mitochondrial dysfunction, lysosomal storage dysfunction and inflammation as major pathogenic pathways contributing to PD aetiology (Exner et al., 2012, Pickrell and Youle, 2015, Gan-Or et al., 2015). Nevertheless, accumulating evidence has revealed that several PD-related genetic factors play a critical role in synaptic function (Picconi et al., 2012) (Table 1-2).

Table 1.2. Brief summary of presynaptic phenotypes induced by PD-related genes

Gene	Protein and function	Presynaptic terminal phenotype	Reference
SNCA	α-synuclein: regulates synaptic vesicle trafficking, SNARE complex formations and subsequent neurotransmitter release.	- Impaired dopamine release in SNpc - Impaired synaptic vesicle endocytosis and reclustering - Decline in synaptic vesicle recycling pool	(Lundblad et al., 2012, Xu et al., 2016, Nemani et al., 2010, Scott and Roy, 2012)
LRRK2	LRRK2: multidomain protein including kinase, GTPase and protein-protein interaction domains.	- Impaired dopamine release in SNpc and reduced dopamine uptake - Impaired presynaptic endocytosis	(Li et al., 2010a, Matta et al., 2012)

PINK1	PINK1: putative mitochondrial serine/threonine kinase	- Impaired synaptic plasticity and release of dopamine	(Morais et al., 2009)
PARKIN	Parkin: E3 ubiquitin ligase; regulates mitophagy and protein degradation	- Reduced dopamine release - Impaired striatal synaptic plasticity	(Cortese et al., 2016, Kitada et al., 2009)
DJ-1	DJ-1: Multifunctional protein that generally acts as a sensor for cellular redox homeostasis.	- Defective LTD through inhibitory D_2 receptor effects	(Goldberg et al., 2005)

1.7.1 Synaptic and axonal deficits in Lewy body disease

1.7.1.1 Dopaminergic neurons: Pathological evidence of synaptic and axonal deficits

Whilst there is a consensus that there is about a 30% loss of total neurons in the substantia nigra when motor signs appear (Fearnley and Lees, 1991, Ma et al., 1997, Greffard et al., 2006), the extent of striatal dopaminergic terminal loss at motor symptom onset is more difficult to determine with post-mortem neurochemical studies. The most often cited work supporting the statement that Parkinsonian motor symptoms manifest when approximately 80% of striatal or putaminal dopamine is lost is that of Bernheimer and colleagues (Bernheimer et al., 1973), although there are several major drawbacks to this study such as the fact that dopamine was measured in only a small proportion of PD patients and no regression analysis was conducted. A subsequent neurochemical study by Riederer and Wuketich (1976), which focused on dopamine levels in the caudate in post-mortem tissue in two cohorts defined by their age of disease onset (~60 years of age vs ~73 years of age), reported an extrapolation to time of symptom onset ranging from 68% to 82% of dopamine reduction, respectively (Riederer and Wuketich, 1976). To circumvent the concerns about post-mortem delay, Scherman et al. (1989) quantified binding of vesicular monoamine transporter (VMAT2) with tritiated alpha-dihydrotetrabenazine

([^{3}H]TBZOH) in post-mortem caudate tissue and concluded that motor symptoms become apparent when there is a loss of 49% of binding sites. Since there is a greater degree of dopamine terminal loss in the putamen compared to the caudate (Kish et al., 1988), it can be assumed that the loss of dopamine terminals in the putamen ranges even higher than 50% by the time motor symptoms appear.

A post-mortem study, using quantitative immunohistochemistry to tyrosine hydroxylase and DAT in PD patients at different intervals post-diagnosis, was able to track the progression of nigrostriatal degeneration (Kordower et al., 2013). In PD, dopamine terminals in the dorsal putamen were severely and rapidly reduced, leading to a virtually complete loss of neurites by year five after the clinical diagnosis, compared to healthy controls. Contrastingly, in the substantia nigra, TH-positive cell bodies were less severely affected from the earliest time points, with minimal further loss over time, resulting in a residual population of dopaminergic neurons, even decades after diagnosis (Kordower et al., 2013). The same group of researchers observed an early reduction of kinesin protein (an anterograde transport motor protein) within the putamen of PD patients early in their disease course, whilst decreases of typical cytoplasmic proteins such as dynein light chain Tctex 3 and TH expression levels were only detected at later stages of PD (Chu et al., 2012). A subsequent meta-analysis concluded that by the time a diagnosis of PD is made, dopamine terminal loss in the striatum exceeds cell body loss in the substantia nigra that continues to persist in later stages (Cheng et al., 2010).

1.7.1.2 Dopaminergic neurons: Neuroimaging evidence of synaptic and axonal deficits

Since there are concerns about the reliability of neuropathological and neurochemical measures due to post-mortem delay, numerous *in vivo* molecular imaging studies have examined dopaminergic terminal loss by measuring VMAT2 and DAT and their consequent relationship with motor symptom onset. It has consistently been demonstrated within the literature that there

is a profound loss of striatal and putaminal dopaminergic terminals when motor symptoms appear, with an estimate of up to 56% (Schwartz et al., 2004). PD patients with early unilateral motor symptoms provide a unique opportunity to assess the extent of dopamine terminal loss within the 'window' of motor symptom onset. Using [^{123}I]β-CIT SPECT to label presynaptic DAT expression in early, drug-naïve PD patients, Tissingh et al. (1998) reported a reduction of dopaminergic terminals contralateral to the most affected side by 39% to 51% in the striatum and 51% to 64% in the putamen. In a larger study that employed [^{11}C]MP and [^{11}C]DTBZ PET for DAT and VMAT2, respectively, the loss of putaminal dopaminergic innervation was between 51% and 71% for both tracers (Lee et al., 2000). A recent [^{123}I]β-CIT SPECT study demonstrated that 67% of individuals with both hyposmia and low baseline levels of DAT converted to PD over 4 years (Jennings et al., 2017), with a combination of hyposmia and initial DAT deficit placing the relative risk of conversion to PD at 17.47 (i.e., those with a combination of hyposmia and DAT deficits were 17.47 times more likely to convert to PD). The subsequent development of a superior radioligand [^{18}F]FE-PE2I has facilitated high resolution, selective imaging of dopaminergic presynaptic terminals *in vivo,* with its employment in early PD patients revealing an approximate reduction of 75.6% of putaminal dopamine terminals and 30% in the cell bodies (Fazio et al., 2018, Delva et al., 2020).

In conclusion, assessment of the available data suggests that there is a greater loss of striatal terminals relative to the loss of nigral soma. In fact, the evidence presented here support the hypothesis that the onset and evolution of PD progresses in a dying back-like manner, from initial synaptic dysfunction and deconstruction of axons to eventual death of the neuron perikarya, with progressive loss of terminals likely to better coincide with progressive worsening of symptoms.

1.7.1.3 Serotonergic neurons: Pathological evidence of synaptic and axonal deficits

Serotonergic neurotransmission is widely distributed throughout the brain and mediated by serotonergic neurons in the raphe nuclei of the brainstem. Clusters of neurons in the rostral raphe nuclei primarily project to the forebrain, providing serotonergic innervation to brain areas such as the basal ganglia, hippocampus, amygdala, hypothalamus, and several cortical areas (Parent et al., 2011, Wallman et al., 2011). Several important functions have been attributed to the serotonergic system in the brain including cognition, mood, and motor function. In PD, dysfunction of serotonin neurotransmission contributes to typical non-motor symptoms, such as apathy, depression, anxiety, and anhedonia (Ballanger et al., 2012, Pavese et al., 2010, Pagano and Politis, 2018, Maillet et al., 2016), as well as resting tremor and levodopa-induced dyskinesias (LIDs) (Doder et al., 2003, Rylander et al., 2010, Politis et al., 2014, Pagano et al., 2018).

Neuropathological investigations have illustrated the early involvement of serotonergic neurons in PD (Halliday et al., 1990, Paulus and Jellinger, 1991), related to the presence of Lewy pathology within the raphe nuclei at early stages of the PD, as well as in DLB (Braak et al., 2003, Seidel et al., 2015). More specifically, Halliday et al. (1990) detailed an approximate 56% loss of serotonergic neurons in the median raphe nucleus in PD patients, with a subsequent study observing a relationship between serotonergic cell loss and depression where patients with depression exhibited increased neuronal cell loss in the dorsal raphe nucleus (Paulus and Jellinger, 1991). Classic non-motor symptoms that are likely associated with the serotonergic system such as anxiety or depression are often present prior to motor symptom onset in PD (Weintraub et al., 2015), which is also in line with the proposed gradual ascending progression of pathology where brainstem pathology predominates in the earlier years of the disease and is consequently established by the time the motor system is affected (Braak et al., 2003, Kingsbury et al., 2010). Furthermore, several target areas of the raphe nuclei, such as the basal ganglia, hippocampus, hypothalamus, and prefrontal cortex, have been shown to exhibit a depletion of

serotonin (Fahn et al., 1971, Shannak et al., 1994), with a preferential reduction of serotonin transporter (SERT) immunoreactivity, tryptophan hydroxylase, serotonin and its metabolites in the caudate nucleus relative to the putamen in post-mortem tissue from PD patients (Kish et al., 2008).

1.7.1.4 Serotonergic neurons: Neuroimaging evidence of synaptic and axonal deficits

Radioligands with specificity for various markers of the serotonergic system, such as serotonin receptors and SERT, have permitted novel insights into PD-related alterations of the serotonergic system *in vivo*. However, the quantification of SERT specifically with [^{11}C]DASB PET has enabled tracing of serotonergic terminals and a surfeit of studies have employed this imaging technique to assess the role serotonergic dysfunction plays in the development of an array of symptoms (Politis and Niccolini, 2015, Pagano and Politis, 2018). The earliest studies detected a reduction of SERT binding consistently in the caudate and putamen (Guttman et al., 2007, Kerenyi et al., 2003). However, few studies have been conducted from which we can infer that the degeneration of serotonergic nerve terminals is an early event. In an effort to stage serotonergic dysfunction, Politis et al. (2010a) stratified PD patients according to their disease duration and found that patients early in their course exhibited a loss of serotonergic terminals in the caudate nucleus, thalamus, hypothalamus and anterior cingulate cortex, followed by further deficits in the putamen, insula, posterior cingulate and prefrontal cortex in patients with established PD (Politis et al., 2010a). Interestingly, a loss of SERT binding within the caudal and rostral raphe nuclei was only evident in patients with advanced disease, which indicates that serotonergic projections are affected earlier compared to serotonergic neurons. This notion is corroborated by findings reported by Albin et al. (2008) whereby SERT was reduced in the forebrain but preserved in the brainstem in 5 early-stage PD patients (H&Y 1 - 2.5). Whilst these imaging studies point to an early loss of serotonergic nerve terminals, a temporal dissociation of

the loss of serotonergic terminals in the forebrain and the number of raphe nuclei neurons has not been well-established.

1.7.1.5 Cholinergic neurons: Pathological evidence of synaptic and axonal deficits

The three dominant sources of cholinergic projections in the brain include the basal forebrain that provides the principal cholinergic innervation to the entire cortical mantle (Mesulam and Geula, 1988), the PPN which is a brainstem centre that provides cholinergic inputs to the thalamus, several brainstem nuclei, cerebellum, some striatal fibres, and the spinal cord (Heckers et al., 1992) and finally, there is a population of interneurons in the striatum that constitute a small fraction (1-2%) of striatal neurons. The cholinergic system is involved in several important processes, with the nucleus basalis of Meynert cholinergic network strongly implicated in regulating attention, memory, visual processing and motor plasticity (Gratwicke et al., 2013), whilst the PPN appears to be a key player in motor coordination and the maintenance of arousal (MacLaren et al., 2014). In PD, cholinergic dysfunction has been found to be associated with gait disturbances and falls (Morris et al., 2019), visual hallucinations (Russo et al., 2019) and sleep disturbances (Yousaf et al., 2018), with cortical cholinergic deficits closely associated with worsening cognitive decline, thus is prominently impaired in PDD and DLB (Perez-Lloret and Barrantes, 2016, Gratwicke et al., 2015). In fact, degeneration of the nucleus basalis of Meynert has been shown to be predictive of cognitive impairments in both PDD and DLB. Furthermore, predictive clinical features such as REM sleep behaviour disorder and pentagon copying (Cagnin et al., 2015, Postuma et al., 2019, Sadiq et al., 2017) have a strong putative cholinergic basis, thus the predominance of cholinergic dysfunction underlying the clinical predictors of Lewy body dementia highlights the relative importance of damage to this network above others in their pathogenesis.

Early human neuropathological studies reported neuronal loss and Lewy bodies in the PPN (Jellinger, 1988) and nucleus basalis of Meynert in PD patients (Candy et al., 1983, Ruberg et al., 1982), with additional post-mortem investigations estimating a loss of cholinergic neurons in the nucleus basalis of Meynert to be in the range of 30-70% (Arendt et al., 1983, Nakano and Hirano, 1984, Tagliavini et al., 1984). Moreover, a severe loss of cholinergic basal forebrain neurons has been found to differentiate demented patients from those who are non-demented, as reflected by a 32% cell loss in non-demented PD patients rising to 54-70% in PDD (Whitehouse et al., 1983, Gaspar and Gray, 1984, Perry et al., 1985, Hall et al., 2014). Furthermore, a decline in expression levels of choline acetyltransferase (ChAT), an enzyme localised to cholinergic axon terminals responsible for acetylation of choline, in the cortex has also been reported to be related to cognitive decline (Candy et al., 1983, Mattila et al., 2001). A more recent study by Hall et al. (2014) assessed cholinergic dysfunction in post-mortem brains of sixteen patients with 'pure' Lewy body PD, of which half had dementia. In line with previous studies, there was an estimated 55% loss of cholinergic neurons in the nucleus basalis of Meynert (Ch4) in PDD patients. Notably, whilst there was a relative sparing of Ch1 and Ch2 septal cholinergic neurons projecting to the hippocampus, their terminals were significantly reduced only in those patients with dementia, who also had a higher burden of Lewy pathology in the basal forebrain. These findings strongly indicate that cholinergic terminal dysfunction, perhaps together with widespread Lewy body pathology, contribute to the development of dementia and demonstrate that an early synaptic phenotype preceding the degeneration of perikaryal is also present in cholinergic neurons in Lewy body disease.

1.7.1.6 Cholinergic neurons: Imaging evidence of synaptic and axonal deficits

Molecular neuroimaging of various markers of the cholinergic system, including muscarinic (mAChRs) and nicotinic (nAChRs) receptor, ChAT, acetylcholine esterase (AChE) and vesicular acetylcholine transporter (VaChT), have enhanced our understanding of the clinical correlates of

cholinergic dysfunction in PD with cognitive decline, with the latter three markers serving as indicators of cholinergic axon terminals. Indeed, a series of *in vivo* studies conducted with various radioligands have detailed aspects of the association between cholinergic dysfunction and cognitive impairment, with significant reductions of presynaptic cholinergic markers AChE and VAChT in approximately 30% of non-demented patients with mild-to-moderate PD (Bohnen et al., 2012, Bohnen et al., 2013). In cognitively unimpaired PD patients, this reduced uptake was quantified at approximately 10%, whilst in PDD patients it was between 20-30%, with cholinergic denervation spreading from parieto-occipital brain areas in non-demented cases to the frontal and temporal cortices in more cognitively affected cases, which was comparable to what is observed in DLB (Kuhl et al., 1996, Bohnen et al., 2003, Bohnen et al., 2006b, Hilker et al., 2005b, Shimada et al., 2009). Furthermore, a loss of cortical cholinergic terminals was shown to correlate with impaired cognitive performance in cognitively-sound PD patients (Bohnen et al., 2015), with other findings revealing that cortical and subcortical cholinergic denervation is associated with deficits in attention and executive dysfunction, as well as impaired visual perception (Bohnen et al., 2006b, Lorenz et al., 2014). Importantly, cholinergic dysfunction can be present early in the disease course as demonstrated by drug-naïve PD patients who exhibited reduced occipital AChE activity (Shimada et al., 2009). These findings demonstrate that synaptic and axonal deficits are also present in non-dopaminergic neuronal populations, occurring early in the disease course and likely contribute to the underlying pathophysiology of several symptoms, most prominently cognitive symptoms in Lewy body disease.

1.7.1.7 Noradrenergic neurons: Pathological evidence of synaptic and axonal deficits

The locus coeruleus is a neuromelanin-pigmented, bilateral nucleus located in the upper dorsolateral pontine tegmentum, serving as the principal source of noradrenaline in the central nervous system with an extensive projecting network, sending descending projections to the spinal cord and densely innervating almost the entire forebrain including limbic structures such

as the amygdala and hippocampus, thalamus, pallidum, cerebellum, and cortex, as well as other neuromodulatory nuclei such as the SNpc and dorsal raphe nucleus (Fallon et al., 1978, Loughlin et al., 1986, Kim et al., 2004, Chandler et al., 2014, Kempadoo et al., 2016, McCall et al., 2017, Beas et al., 2018, Baldo et al., 2003). Contrastingly, areas that are richly innervated by the dopaminergic system such as the nucleus accumbens and striatum have discrete, but scarce noradrenergic innervation (Mason and Fibiger, 1979, Berridge et al., 1997, Delfs et al., 1998, Fitoussi et al., 2013). The degeneration of the noradrenergic system in PD is associated with a broad spectrum of non-motor symptoms that encompass cognitive, behavioural, and autonomic parameters, such constipation, orthostatic hypotension, urogenital dysfunction, sleep disturbances, depression, and cognitive flexibility, with the severity of dementia also being linked to a loss of noradrenergic neurons in the locus coeruleus.

Over several decades that, numerous post-mortem studies in PD brains have reported a moderate to severe cell loss of 30%-90% in the locus coeruleus, accompanied by more than 80% depletion of noradrenaline concentration (Chan-Palay and Asan, 1989, German et al., 1992, Bertrand et al., 1997, Zarow et al., 2003, Taquet et al., 1982, Jenner et al., 1983, Gaspar et al., 1991), with neuronal loss in the locus coeruleus exceeding that of the SNpc (83% vs 78%) (Zarow et al., 2003). More specifically, neuromelanin-containing medium-size locus coeruleus neurons exhibit somatic and dendritic alterations, whereas smaller non-noradrenergic cells in the locus coeruleus do not display severe pathological changes (Patt and Gerhard, 1993).

Forebrain noradrenaline depletion, as well as morphological alterations in noradrenergic fibres, synapses and mitochondria have been dependably observed in PD (Rommelfanger and Weinshenker, 2007, Delaville et al., 2011, Fornai et al., 2007, Espay et al., 2014), with Baloyannis et al. (2006) revealing alterations in noradrenergic synapses in terms of size and shape of the pre- and postsynaptic components, polymorphisms of the synaptic vesicles and notable

morphological alterations of the mitochondria (Chan-Palay and Asan, 1989, Baloyannis et al., 2006). In fact, whilst A53T α-synuclein transgenic mice exhibited no cell loss in the locus coeruleus, an age-dependant loss of noradrenergic terminals and tissue levels was shown (Sotiriou et al., 2010), which suggestive of axon terminal loss occurring prior to frank cell body degeneration, indicative of noradrenergic neurons also undergoing a 'dying-back' phenotype, similar to that of the dopaminergic system.

1.7.1.8 Noradrenergic neurons: Imaging evidence of synaptic and axonal deficits

Whilst *in vivo* PET studies using non-specific ligands failed to detect noradrenergic damage, more recent studies using neuromelanin-sensitive MRI identified a progressive loss of signal in the locus coeruleus in PD patients (Sasaki et al., 2006, Castellanos et al., 2015, Schwarz et al., 2017, O'Callaghan et al., 2021), which was also notable in drug-naïve PD (Wang et al., 2018). A recent study employing ultra-high field 7T imaging reported that the caudal portion of the locus coeruleus exhibited the greatest reduction of neuromelanin signal in PD patients compared to healthy controls (O'Callaghan et al., 2021). Using [^{18}F]DOPA PET as an index of monoaminergic nerve terminal function, Pavese et al. (2011) revealed reduced uptake in the locus coeruleus which was indicative of a progressive loss of noradrenergic terminal function.

Efferent noradrenergic projections have also been reported to degenerate in PD, as reflected by reduced noradrenergic innervation of its target structures, including the thalamus, striatum, hypothalamus, and prefrontal and motor cortex (Shannak et al., 1994, Pavese et al., 2011, Pifl et al., 2012, Sommerauer et al., 2018b, Sommerauer et al., 2018a, Nahimi et al., 2018).

A recent multi-modal imaging study utilising PET with [^{11}C]MeNER for visualising noradrenaline transporters (NET) located at terminal sites, and neuromelanin-sensitive MRI for measuring locus coeruleus cell bodies, demonstrated that terminal deterioration exceeded cell

body degeneration by 10-20%, suggesting principal terminal damage of the noradrenergic system in PD (Doppler et al., 2021). Furthermore, the authors did not observe a correlation between locus coeruleus MRI contrast and noradrenaline transporter density, which pointed to uncoupled disintegration of terminals and cell bodies in PD, further emphasising that axonal and synaptic deficits serve as a central part of PD pathology, which is differentially regulated from cell body death (Doppler et al., 2021).

1.8 Neuropathological and pathophysiological considerations

1.8.1 α-synuclein: the pathological hallmark of Lewy body disease

α-synuclein is a small soluble cytoplasmic protein of 140 amino acid encoded by the *SNCA* gene, and together with β-synuclein and γ-synuclein, belongs to the synuclein protein family (Goedert, 2001, Marques and Outeiro, 2012). This family of proteins are identical in 55-62% of their sequence, with similar domain organisation and are highly expressed in the human brain (Goedert, 2001), although α-synuclein and β-synuclein share the same subcellular distribution at presynaptic terminals in neurons (Goedert, 2001, Jakes et al., 1994). In its native form, wildtype α-synuclein functions as a soluble monomer, whereas under cellular stress and pathological conditions, these monomers can interact to form oligomers that buffer the formation of protofibrils that eventually lead to the formation of β-sheet-rich fibrils that aggregate into Lewy bodies (Goedert et al., 2017, Spillantini et al., 1997, Serpell et al., 2000). Thus, α-synuclein is the only protein of the synuclein family that is found in Lewy bodies and implicated in the pathogenesis of PD and DLB.

Amongst the PD-related genes identified, *SNCA* is the most potent culprit underlying PD, with several point mutations in *SNCA* and multiplications of the gene locus found to be causally related to severe forms of PD (Satake et al., 2009, Simon-Sanchez et al., 2009, Singleton et al.,

2003), although given that patients present with severe cognitive and psychiatric symptoms, describing them as DLB may be a more accurate representation rather than PD. Nevertheless, increased gene dosage caused by duplication or triplication of the gene locus is directly correlated with motor and non-motor symptoms, cognitive decline, and phenotypic severity (Venda et al., 2010, Kalia and Lang, 2015). These findings strongly evidence the key pathogenic role α-synuclein dysfunction and accumulation plays in both familial and sporadic forms of PD.

1.8.2 Not solely Lewy bodies

The neuropathological signatures of PD, PDD and DLB were originally described by Fritz Jacob Heinrich Lewy in 1912, who identified sizeable eosinophilic spherical or kidney-shaped inclusions in neuronal cell bodies that were subsequently termed Lewy bodies. He also described structures that morphologically varied between short and thick or long and thread-like, which were later termed Lewy neurites. Subsequently, Lewy bodies were found to be highly enriched with ubiquitin (Kuzuhara et al., 1988, Lowe et al., 1988), although not strictly a requirement, and contained aggregates of α-synuclein that is the major component of Lewy bodies and Lewy neurites (Goedert et al., 2017, Spillantini et al., 1997, Serpell et al., 2000).

There are currently three major staging systems used for the assessment of the progressive regional distribution of α-synuclein in PD (Braak et al., 2003, Braak et al., 2006), DLB (McKeith et al., 2005) and revised guidelines for Lewy body disease (McKeith et al., 2017, Beach et al., 2009, Zaccai et al., 2008). Based on semiquantitative assessment of Lewy bodies, a hypothetic staging system of the chronological spread of Lewy-related pathology was proposed by Braak, denoting a predictable sequence with accumulative severity throughout the brain and ascending progression was proposed. This was founded on the idea that Lewy body pathology serves as a crucial pathogenic feature and toxic α-synuclein species propagate from the peripheral nervous system and olfactory bulb to the subcortical regions in a uniform, bottom-up caudo-rostral

fashion; reaching the neocortex in later stages (Braak et al., 2003, Braak et al., 2006, Del Tredici and Braak, 2016, Braak et al., 2004, Del Tredici et al., 2002). These findings are paralleled by deficits in several neurotransmitter systems, with many studies establishing that cholinergic neurons in the pedunculopontine nucleus (PPN), noradrenergic neurons of the locus coeruleus, cholinergic neurons of the nucleus basalis of Meynert and of the dorsal motor nucleus of the vagus (DMV), and serotonergic neurons of the raphe nuclei undergo degeneration in Lewy body disease (Giguere et al., 2018).

The topographical distribution of α-synuclein is thus thought to be intimately linked to the clinical symptoms observed in Lewy body disorders, whereby α-synuclein lesions in the brainstem is predominantly responsible for the manifestation of extrapyramidal motor symptoms and a plethora of non-motor symptoms, whereas cognitive impairment transpires as a result of limbic and neocortical spread of Lewy-related pathology (Braak and Del Tredici, 2008). Therefore, PD, PDD and DLB are widely considered to represent distinct phenotypic expressions in a continuum within the spectrum of a single disease, wherein the clinical manifestations are primarily dependant on the anatomical distribution and load of α-synuclein pathology.

Whilst Lewy-related pathology is paramount for the diagnosis of PD, PDD and DLB, mounting evidence has revealed that α-synuclein in Lewy bodies and neurites often coexists with the presence of Alzheimer's-type pathology, such as amyloid-β senile plaques and tau neurofibrillary tangles, which have been shown to be important contributing factors for cognitive impairment and dementia; so much so, that a combination of these pathologies is far superior at predicting dementia in PD than any single pathology (Compta et al., 2014, Compta et al., 2011), as well as being associated with a more aggressive disease course, shorter survival times and higher incidence of cognitive dysfunction compared to 'pure' Lewy body disease (Hansen et al., 1990,

Kraybill et al., 2005, Howlett et al., 2015, Jellinger et al., 2007, Sabbagh et al., 2009). These proteins are considered to mutually promote the aggregation of each other, with synergistic effects demonstrated by the strong association observed between the extent of neurofibrillary tangles, neuritic plaques and α-synuclein (Irwin et al., 2017) and PDD/DLB patients who have more cortical amyloid-β plaques also having more cortical α-synuclein (Lashley et al., 2008, Dickson et al., 2009). Whilst AD-related pathologies are a common feature of Lewy body disease, there is now an increasing recognition of a spectrum of overlapping pathobiology, as reflected by the gradient of increasing amyloid-β and tau burden: PD < PDD < DLB (Gomperts et al., 2016a, Hansen et al., 2017, Ruffmann et al., 2016, Bohnen et al., 2017).

1.8.3 How relevant are Lewy bodies?

Given the co-incidence of both Lewy bodies and neuronal loss, it was considered that Lewy bodies were pathophysiologically relevant form of α-synuclein and, in conjunction with cell death, were responsible for the disease. However, it is now fairly evident that Lewy pathology and nigral neuronal death are, at best, an indirect marker for idiopathic PD. Studies have demonstrated that the presence of Lewy bodies does not predispose nigral neurons to undergo apoptotic cell death to a greater degree than the general population of nigral neurons, with the majority of neurons absent of Lewy body pathology undergoing degeneration (Tompkins and Hill, 1997, Milber et al., 2012). Nigral neurons, regardless of whether they contain Lewy bodies or not, are similarly affected by biochemical changes or morphological dendritic abnormalities, suggesting that neurons as a whole are implicated in the disease process (Bergeron et al., 1996, Javoy-Agid et al., 1990, Patt et al., 1991). In fact, consequent attempts to assess the association between the density of either cortical or brainstem Lewy bodies with clinical symptoms in PD and DLB have been unsuccessful, with a majority of studies failing to observe a relationship between Lewy body density and early disease onset, disease duration, severity of parkinsonism and cognitive decline (Gomez-Isla et al., 1999, Gomez-Tortosa et al., 2000, Gomez-Tortosa et

al., 1999, Weisman et al., 2007). Furthermore, a percentage of PD patients who go onto develop dementia exhibit an absence of cortical or brainstem Lewy body pathology (Galvin et al., 2006, Libow et al., 2009), raising serious questions about Lewy body pathogenicity. Thus, the biological significance and clinical consequence of Lewy bodies remains unclear. Like other fibrillary proteinaceous inclusions, such as amyloid-β plaques or Pick bodies, Lewy bodies could simply be an epiphenomenon, or scars of unknown neuronal degenerative processes, thus serving as indirect indicators of disease, but not reflecting the full extent of neurodegenerative pathology (Jellinger, 2009a).

In fact, biophysical studies have demonstrated that oligomers and protofibrils, as opposed to the fibrillary form of α-synuclein, are cytotoxic (Ingelsson, 2016, Caughey and Lansbury, 2003, Volles and Lansbury, 2003, Tofaris and Spillantini, 2005), whilst Lewy-related pathology composed of insoluble fibrillary α-synuclein typically seen at autopsy may be a cytoprotective response devised to confine and degrade cytotoxic proteins or abnormal cytoskeletal elements (Kuusisto et al., 2003, Tanaka et al., 2004, Pan et al., 2008, Olanow et al., 2004). This notion is in line with genetic and post-mortem studies that revealed Lewy bodies are formed in a way similar to aggresomes, which are proteinaceous inclusions formed at the centrosome in response to proteolytic stress (Ardley et al., 2003, Kopito, 2000, McNaught et al., 2002).

1.8.4 Synaptic pathology

Under normal physiological conditions, wild type α-synuclein monomers function in a dynamic equilibrium between a soluble and membrane-bound state and are particularly enriched in presynaptic terminals (Burre, 2015). Progress over the last couple of decades has provided compelling evidence that a major site of α-synuclein-mediated toxicity is the presynaptic terminal.

Braak and colleagues were the first to provide evidence in support of this notion where, in their pioneering study, demonstrated that extensive and thin α-synuclein inclusions were not only a major component of Lewy body inclusions in the neuron cell body but were also present in axonal processes (Braak et al., 1999). This was corroborated by further studies that reported the localisation of α-synuclein within presynaptic axon terminals and perhaps more strikingly, in dystrophic axonal neurites in patients with neurodegenerative diseases including PD and DLB (Duda et al., 2002, Galvin et al., 1999); indicative of synaptic dysfunction arising as a result of these lesions. The subsequent development of a technique called paraffin-embedded tissue enabled the localisation of α-synuclein to be studied in further detail (Kramer and Schulz-Schaeffer, 2007). Here, the authors were able to detect an abundance of α-synuclein micro-aggregates in the neuropil as opposed to the neuron soma in brains of DLB patients, with this abundance of synaptic α-synuclein micro-aggregates far exceeding the quantity of aggregated α-synuclein in Lewy bodies or Lewy neurites by one to two orders of magnitude (Kramer and Schulz-Schaeffer, 2007). Their filtration technique revealed that up to 92% of α-synuclein micro-aggregates were entrapped within the presynaptic terminal, which correlated with the striking downregulation of presynaptic proteins such as synaptophysin and syntaxin, and was paralleled with an almost complete loss of dendritic spines at the postsynaptic level (Kramer and Schulz-Schaeffer, 2007). This novel mechanistic insight into synaptic deficits serving as a starting point in α-synuclein-mediated toxicity is in line with previous reports, where aggregates of α-synuclein species were found in axon terminals and preceded the formation of Lewy bodies in DLB, with associations observed between axonal pathology and cognitive impairment (Marui et al., 2002). Similar reports of a selective decline in dendritic spines in PD indicate that equivalent pathophysiological alterations at the synapse level underlie PD (Ingham et al., 1989, Solis et al., 2007, Deutch, 2006, Patt et al., 1991), as was shown for DLB. In fact, a depletion of dendritic spines has also been observed in animal models overexpressing α-synuclein and in neurons with fibril-induced inclusion formation (Blumenstock et al., 2017, Wu et al., 2019, Froula et al., 2018).

Taken together, these data provide strong evidence for the implication of α-synuclein that the presynaptic accumulation of α-synuclein pathologically impinges on synaptic function, leading to retrograde axonal damage and terminating in the soma, inducing neuronal death in a dying-back fashion. Thus, synaptic dysfunction may be a central event in the initiation of neurodegeneration in Lewy body disease.

Whilst the physiological functions of α-synuclein remain poorly understood, deficiencies in synaptic transmission are seen in response to both overexpression and knockdown of α-synuclein, indicating that α-synuclein plays a role in regulating neurotransmitter release, synaptic function, and homeostasis (Kahle et al., 2000, Zhang et al., 2008, Lee et al., 2008, Vargas et al., 2017), with several steps of neurotransmitter release being affected by α-synuclein accumulation. Elevated concentrations of α-synuclein have been shown to alter the size of synaptic vesicle pools and impair their trafficking in the presynaptic terminal (Cabin et al., 2002, Larsen et al., 2006, Nemani et al., 2010, Scott and Roy, 2012, Dalfo et al., 2004). Its overexpression can also misgovern or redistribute protein components of the presynaptic SNARE complex, which induces deficiencies in tethering, docking, priming and fusion of synaptic vesicles at the active zone (Choi et al., 2013, Scott et al., 2010, Lai et al., 2014, Garcia-Reitbock et al., 2010). Furthermore, inclusions of α-synuclein are localised within the presynaptic active zone (Martin et al., 2006), which is concomitant with reduced levels of active zone proteins such as Piccolo (Scott et al., 2010), although the evidence for such an association is scarce. α-synuclein overexpression also causes a decline in the endocytic retrieval of synaptic vesicle membranes during vesicle recycling (Busch et al., 2014, Xu et al., 2016). These presynaptic alterations mediated by α-synuclein accumulation together impair neurotransmitter release and neuronal communication.

A recent study that employed a *Drosophila* model of synucleinopathy demonstrated that α-synuclein accumulation in the presynaptic terminal induced a downregulation of key synaptic proteins, synapsin and syntaxin 1A, as well as Bruchpilot puncta, a fundamental component of the presynaptic active zone that is critical for its structural integrity and function (Bridi et al., 2021). This led to an impairment in neuronal function that ultimately instigated behavioural deficits prior to the progressive loss of dopamine-producing neurons (Bridi et al., 2021). Interestingly, post-mortem brain samples of DLB patients exhibited comparable alterations in presynaptic active zone protein (Bridi et al., 2021). This interesting and comprehensive study highlights the key role of α-synuclein-mediated synaptopathy in initiating neurodegeneration in Lewy body disease.

Whilst α-synuclein is enriched at presynaptic terminals across several neuronal populations, its role in directly regulating dopamine levels may contribute to the heightened vulnerability of dopaminergic neurons to α-synuclein accumulation in PD (Venda et al., 2010). Indeed, evidence suggests that α-synuclein is a negative modulator of dopamine by inhibiting enzymes responsible for its synthesis, such as tyrosine hydroxylase and AADC (Perez et al., 2002, Kirik et al., 2002, Tehranian et al., 2006), as well as impairing dopamine transport and uptake by interacting with VMAT2 and DAT, reducing their activity (Guo et al., 2008, Wersinger and Sidhu, 2003, Wersinger et al., 2003). The subsequent dysregulation of dopamine concentrations directly promotes the formation of toxic α-synuclein oligomers (Mor et al., 2017). Together, these findings are suggestive of a vicious cycle of α-synuclein accumulation and unregulated dopamine levels that provoke synaptic dysfunction and compromised neuronal communication, ultimately inducing synaptopathy and progressive degeneration.

1.8.5 "Prion-like" transmission

Braak and colleagues postulated that Lewy pathology could spread from cell-to-cell in a manner comparable to the suggested spread of prion proteins. This notion was derived from the fact that Lewy pathology was confined to the lower brainstem in PD patients who succumbed early in their disease course, whilst those who died at later stages of the disease exhibited a greater abundance of Lewy pathology in the upper brainstem and cortex. It is worth noting that the progression of symptoms generally correlates with the topographical distribution of α-synuclein pathology between anatomically interconnected brain regions (Braak et al., 2003, Del Tredici and Braak, 2016), suggestive of trans-synaptic spread of pathology. Whilst this 'spreading' of α-synuclein is not testable without a validated biomarker that permits longitudinal tracking of PD over the course of the disease, this model gathered support when foetal tissue grafts transplanted into the striatum of PD patients developed α-synuclein-positive Lewy body-like inclusions, a decade after transplantation, suggesting a direct transfer of pathogenic α-synuclein from host-to-grafted tissue (Kordower et al., 2008a, Li et al., 2008).

A series of investigations aiming to demonstrate α-synuclein transmission between cells followed, with experimental evidence illustrating that α-synuclein pathology can be spread trans-synaptically, with neighbouring neurons taking up the endogenous protein, ultimately leading to the seeding of α-synuclein in recipient neurons (Desplats et al., 2009, Hansen et al., 2011, Angot et al., 2012, Luk et al., 2012). In mice, synthetic α-synuclein fibrils spread from the site of inoculation to synaptically connected structures, creating Lewy-like pathology (Luk et al., 2012, Masuda-Suzukake et al., 2013). This cell-to-cell transmission of α-synuclein may be the process by which the pathology spreads, as initially observed in PD brains (Kordower et al., 2008a, Li et al., 2008).

However, unequivocal evidence of α-synuclein inducing pathology or its ability to propagate between cells is yet to be provided, as studies have also reported an absence of Lewy-like inclusions in transplanted tissue (Mendez et al., 2008), whilst others have observed them only in a minority of grafted cells (Kordower et al., 2008b). It is also important to highlight that in animal models of PD, factors other than α-synuclein could be promoting the aggregation of α-synuclein, including damage from injection sites or local inflammation, and in cellular models, the concentrations of α-synuclein precursors are typically higher than physiological levels of α-synuclein (Uchihara and Giasson, 2016). Finally, the precise mechanism(s) of α-synuclein exocytosis, the aggregation state of extracellular α-synuclein and its potential association with other molecules such as a lipids and chaperones, remain unresolved issues that require elucidation.

For a mechanism involving cell-to-cell transmission of α-synuclein, it would be expected that cells with the greatest synaptic connectivity to brain areas affected early in the course of PD would be at utmost risk of developing Lewy-related pathology. However, this is not the case as demonstrated by rodent studies whereby regions with strong connectivity to the substantia nigra did not exhibit the most abundant Lewy pathology (Watabe-Uchida et al., 2012, Surmeier et al., 2017). Furthermore, the distribution pattern of Lewy pathology, as reported by Braak and colleagues, is not consistent with a simple prion model in which the spread of Lewy pathology is retrograde and determined solely by the brain connectome.

Instead, theories are emerging to suggest that the stereotypical distribution of Lewy body pathology in selective brain regions with disease severity reflects selective vulnerabilities of specific cells that tend to be affected first in PD, as opposed to the physical transmission of a pathological agent. Having said this, if Lewy pathology does propagate in Lewy body disease, it is likely to be gated by cell- or region-autonomous mechanisms.

Indeed, many of the neurons that are vulnerable in PD are key neurons in the neuromodulatory control networks (i.e., networks with diffuse axonal projections; implicated in the regulation of other neurons primarily via neurotransmitter release such as dopamine), as opposed to those in brain networks that have topographically confined synaptic connectivity and are dependent on classical neurotransmitters that stimulate fast ionotropic receptors. Neurons in the neuromodulatory networks share several notable traits and it is these common features that predispose specific neurons to early involvement in Lewy body disease.

1.8.6 Cell vulnerabilities

The most notable and well-characterised traits of vulnerable neurons in PD are long and highly branched axons with a large number of transmitter release sites. This diffuse axonal arborisation supports the coordination of activity in spatially distributed networks such as the basal ganglia. For example, nigral dopaminergic neurons in the rodent exhibit axons that branch copiously in the striatum and possess as many as 200,000 vesicular release sites (Matsuda et al., 2009). The vulnerability of thin, long axons to Lewy pathology is supported by the fact that other neurons that are preferentially affected in PD, PDD and DLB also display this anatomical confirmation. For example, cholinergic neurons of the nucleus basalis of Meynert are strongly implicated in the pathogenesis of dementia in PD (Perry et al., 1985, Gratwicke et al., 2013), which have been shown to be extremely long, with an average length of ~100 metres in humans, and a complex branching structure (Wu et al., 2014). Serotonergic neurons of the raphe nucleus also exhibit extensive axonal projections (Hale and Lowry, 2011), and the long, unmyelinated axons of the peripheral autonomic nervous system may explain the early and conspicuous implication of autonomic symptoms in Lewy body disease. Therefore, the anatomical configuration of neuronal cell types may reflect their specific vulnerability to PD progression, as well as the development of dementia.

There are several converging theories on selective vulnerability in PD related to dopamine toxicity, iron content, autonomous pace-making, and the extent of axonal arborisation. It is important to note that much of the literature that has focussed on determining features of neuronal vulnerability have primarily interrogated characteristics of nigral dopaminergic neurons that render them particularly vulnerable. It is likely that some of these functional or structural properties are shared between neurons that are selectively vulnerable in PD, as opposed to being truly unique to nigral dopaminergic neurons.

1.8.6.1 Other factors contributing to cell vulnerability

Dopamine toxicity is based on the fact that dopaminergic neurons are mostly at risk because dopamine can exert toxic effects in certain conditions because its oxidation generates reactive quinones (Segura-Aguilar et al., 2014). Such reactive by-products promote mitochondrial dysfunction, pathological aggregation of proteins such as α-synuclein and oxidative stress (Mosharov et al., 2009), as reflected by the deleterious influence these dopamine quinones have been shown to have on the function of mitochondrial protein complexes I, III, and V (Van Laar et al., 2009), as well as other proteins such as α-synuclein, DAT and tyrosine hydroxylase (Xu et al., 1998, Whitehead et al., 2001). Despite being highly relevant, this phenomenon alone does not provide an explanation for the differential vulnerability of different dopaminergic subgroups, for example nigral degeneration vs ventral tegmental area preservation. Therefore, although dopamine toxicity assuredly plays an instrumental role in nigral neuron degeneration, it is certainly not the sole factor driving neuronal death.

Iron content is another factor thought to play a part in the selective vulnerability of nigral dopamine neurons. It is well-known that iron can generate reactive oxygen species (ROS) via the Fenton reaction, with studies demonstrating its accumulation with age in the SNpc (Haacke et

al., 2010, Daugherty and Raz, 2013, Bilgic et al., 2012). Since the functionality of mitochondrial electron transport chain is dependent on iron sulphur clusters and considering the particularly high bioenergetic demands of dopamine-producing nigral neurons (Bolam and Pissadaki, 2012, Pacelli et al., 2015, Ren et al., 2005), elevated iron content could contribute to elevated and sustained mitochondrial activity.

A shared feature of vulnerable neurons in Lewy body disease is their distinctive physiology. *In vivo*, the neuromodulatory neurons that have been examined have slow, tonic activity (Surmeier et al., 2012). The most extensively studied member of this class is the dopamine-producing neuron of the SNpc. These neurons have broad action potentials (spikes) and demonstrate autonomous pace-making, i.e., they spike in the absence of an excitatory synaptic input. The combination of *all* features, namely broad spikes, pace-making, low intrinsic Ca^{2+} buffering and cytosolic Ca^{2+} oscillations, distinguish nigral dopaminergic neurons from those that are less vulnerable in the ventral tegmental area (Chan et al., 2007, Khaliq and Bean, 2010, Philippart et al., 2016). Despite the limited number of studies that have scrutinised these features in non-dopaminergic neurons that are particularly vulnerable, those that have investigated the locus coeruleus, DMV and PPN show that this phenotype is largely shared (Sanchez-Padilla et al., 2014, Goldberg et al., 2012, Kang and Kitai, 1990).

Another morphological feature common to dopaminergic, serotonergic, noradrenergic and cholinergic systems is the extensive axonal arborisation (Sulzer and Surmeier, 2013). The fundamental assertion of this notion is that highly branched axonal domains levy extraordinary metabolic costs on these cells and are almost at their maximum capacity to manage protein delivery, elevated energic demands, proteasomal systems and chronically high oxidative stress (Bolam and Pissadaki, 2012, Misgeld and Schwarz, 2017, Tao et al., 2017). Indeed, nigral dopamine-producing neurons have exuberant and highly arborized axonal branching with

estimates upwards of a million neurotransmitter release sites per neuron, which would make them some of the most highly arborized neurons within the central nervous system (Bolam and Pissadaki, 2012, Matsuda et al., 2009). This feature could potentially place considerable bioenergetic burden on these cells, leaving little margin for additional bioenergetic stress. Correspondingly, the energy cost for the propagation of one action potential rises exponentially with the level of branching (Pissadaki and Bolam, 2013). Interestingly, mitochondrial oxidant stress and vulnerability to toxins such as rotenone was shown to be sufficiently reduced following the reduction of axonal arbor size of nigral dopaminergic neurons by modulating axon guidance signals (Pacelli et al., 2015).

An obvious commonality between the four factors outlined above is that they suggest that vulnerable neurons are under intense mitochondrial/bioenergetic demand. Since areas of high energy consumption include presynaptic sites, as demonstrated by the fact that approximately half of the oxygen consumed by mitochondria in nigral dopamine-producing neurons seem to be used by activity-dependent cellular processes such as neuronal firing and neurotransmitter release (Sheng, 2014, Pacelli et al., 2015), it is perhaps unsurprising that synaptic failure may be an initial, central event in Lewy body disease pathogenesis. Indeed, studies have demonstrated a critical interplay between α-synuclein synaptic accumulation and mitochondrial dysfunction in Lewy body disease, which may explain why those neuronal populations with high metabolic demand are also those that exhibit α-synuclein synaptic pathology (Burbulla et al., 2017, Martinez-Vicente et al., 2008).

1.9 Neurovascular unit dysfunction

The brain is an energy-hungry organ; despite comprising only 2-3% of body's mass, it consumes approximately 20% of the body's resting energy, primarily to reverse ion fluxes that underlie

action potentials and synaptic potentials to maintain ionic electrochemical gradients (Howarth et al., 2012, Attwell and Laughlin, 2001). Since the brain lacks a reservoir to store energy for use when required, it relies on a constant supply of energy substrates to meet its high metabolic demands. Thus, if the energy supply to the brain is comprised, brain cells can become quickly injured or die.

Cerebral blood flow (CBF) refers to the rate of delivery of arterial blood to the capillary bed in brain tissue, quantified in millilitres of blood per 100g of brain tissue per minute. It is maintained by the coordinated action of interconnected blood vessels, which form a 400-mile-long vascular network in the human brain comprising of cerebral arteries, arterioles, and capillaries that supply oxygen, energy metabolites and nutrients to the brain (Zlokovic, 2011). Carbon dioxide and other metabolic waste products are removed from the brain via the cerebral venous return and enter the systemic circulation for clearance where carbon dioxide is cleared by the lungs and metabolic waste products by the liver and kidneys.

To meet the fluctuating activity-dependent energy requirements of neurons, the mammalian brain has evolved 'neurovascular coupling' mechanisms to regulate and fine-tune energy supply (Iadecola, 2004), thus CBF is proportional to the energy consumption of each brain region i.e. CBF is higher in regions with higher energy utilisation such as the inferior colliculus, and lower in regions with lower energy requirements, such as the white matter. Furthermore, blood flow is rapidly increased to regions where neurons are active – a response termed 'functional hyperaemia' (Attwell et al., 2010). Neurovascular coupling is a fundamental aspect of healthy brain function and a variety of cell types within the neurovascular unit (NVU) contribute to neurovascular coupling by maintaining the functional integrity of the blood-brain barrier (BBB) and regulating CBF volume (Sweeney et al., 2018). If the NVU is disrupted, it can cause dysfunction of the BBB and reduce CBF, which may contribute to the pathogenesis of

neurodegenerative disorders, such as Lewy body disease. However, whether deficits of the NVC drive pathology or if pathology drives NVC disruption remains largely unknown and requires more focused investigation. Whilst a decrease in CBF or disruption of the NVU could theoretically starve neurons of the energy they require as a result of reduced supply of oxygen and nutrients to the brain, a toxic environment can also be created due to the lack of clearance of neurotoxic substances such as α-synuclein from the brain parenchyma.

1.9.1 Neurovascular unit components

The NVU is an integrated and interactive entity, vital for autoregulation of CBF-based oxygen and nutrient delivery. It comprises of cerebral vascular cells (vascular smooth muscles, pericytes and endothelial cells), neurons and glia (astrocytes and microglia) (Zlokovic, 2011).

Whilst astrocytes are a crucial component of the NVU, they also play a fundamental role in maintaining healthy brain function by performing multiple specialised housekeeping tasks such as neurotransmitter clearance (Brew and Attwell, 1987), K^+ uptake (Kuffler et al., 1966, Olsen and Sontheimer, 2008), and recycling (Bak et al., 2006). Astrocytes can sense neuronal signals, and, in response, regulate synaptic function and plasticity (Bazargani and Attwell, 2016).

Astrocytes are ideally situated between the vasculature and neurons, which enables them to fulfil several key roles in regulating energy supply to neurons, including mediating neurovascular coupling (Nortley and Attwell, 2017). Astrocytes extend peri-synaptic processes that ensheath neuronal synapses, as well as more substantial 'endfeet' that wrap an estimated 99.7% of the surface of the brain vasculature (Mathiisen et al., 2010). The polarity of astrocytic structure permits astrocytes to convey signals between neurons and blood vessels in a bidirectional fashion (Presa et al., 2020). It is now well-established that synaptic neurotransmitter release can elicit an increase in internal astrocyte Ca^{2+} (Winship et al., 2007, Mishra et al., 2016), leading to

downstream release of vasoactive molecules onto the vasculature, thus driving NVC (Mishra et al., 2016). Astrocytes are also capable of receiving signals from blood vessels regarding the overall physiological state of the body, such as blood pressure or carbon dioxide levels. These signals are relayed to activate neurons to induce homeostatic neural control of peripheral organs (Wang and Parpura, 2018, Filosa et al., 2016). Certainly, astrocytes appear to have the capacity to change neuronal firing properties in response to alterations in vascular flow and pressure (Kim et al., 2016), which is termed vasculo-neuronal hypothesis (Presa et al., 2020). This novel concept may be the way in which the body state can dictate, or at least modulate, brain function.

Neurons are an integral component of the NVU, with neural activity driving increases in CBF during functional hyperaemia and, in fact, neurons consume most of the energy used by the brain (Howarth et al., 2021). Neuronal interactions with astrocytes, microglia, and blood vessels influences how the NVU responds to neural activity to induce NVC and mediate alterations in CBF (Attwell et al., 2010). The NVC is engaged in a feed-forward process wherein, irrespective of energy substrate availability, local blood supply is elevated following synaptic activity via intercellular signalling between NVU components (Mishra, 2017). This feed-forward control probably warrants an oversupply of oxygen and glucose to pre-emptively prohibit a state in which neural tissue may receive an insufficient energy supply (Buxton, 2021), although the reason for this oversupply remains unclear.

Neuronal activity can trigger local changes in blood supply directly via the release of vasoactive molecules onto arterioles to engage vascular smooth muscle cells or indirectly by signalling to astrocytes, which subsequently release vasoactive molecules onto capillary pericytes (Mishra, 2017). Neuron-derived vasoactive molecules include cyclooxygenase-2-derived prostanoids (Niwa et al., 2000) and nitric oxide (NO) (Dirnagl et al., 1993, Akgoren et al., 1994). Pharmacological receptor blocking studies have demonstrated the involvement of both

glutamate and GABA in neurovascular coupling, suggesting that haemodynamic responses are elicited by a combination of signals from both excitatory and inhibitory neurons, with evidence of a more prominent role for inhibitory interneurons (Lecrux et al., 2011, Han et al., 2019, Lee et al., 2020). Furthermore, stimulation of neuromodulatory systems leads to widespread increase in CBF across broad cortical areas, which holds true for the basal forebrain cholinergic pathway (Vaucher et al., 1995, Sato et al., 2001), the locus coeruleus noradrenergic pathway (Raichle et al., 1975, Toussay et al., 2013), the raphe nucleus serotonergic pathway (Underwood et al., 1995), and the dopaminergic pathways (Choi et al., 2006). Neurons of the neuromodulatory systems modulate local NVC response via their actions on most cells of the NVU, namely vascular smooth muscle and endothelial cells, perivascular astrocytes, pyramidal cells, and GABA interneurons. Since neuromodulatory neurons are particularly susceptible to degeneration in Lewy body disease, it is plausible that their loss could induce hypoperfusion in Lewy body disease. In fact, studies that have evaluated cerebral blood flow alterations in PD and Lewy body dementia have provided evidence of global and localised hypoperfusion. This will be discussed in further detail in the next section.

1.9.2 Reduced cerebral blood flow

Magnetic resonance imaging (MRI) arterial spin labelling (ASL) is a relatively new technique that is a non-invasive alternative for CBF quantification. It relies on electromagnetically labelled arterial blood water as an endogenous tracer, yielding absolute quantitative measures of CBF that directly reflect brain physiology and neural activity (Buxton et al., 2004, Wolk and Detre, 2012). Unlike molecular imaging techniques, ASL does not require the administration of any radioactive tracers, and it does not require long preparation times and scan times, or arterial blood sampling for perfusion measurements (Grade et al., 2015). This technique has been validated against other perfusion methods in both older and younger adults (Zhang et al., 2014), demonstrating a good

inter-rater reliability and reproducibility even in the geriatric population (Jiang et al., 2010, Sigurdsson et al., 2015).

Perfusion alterations have been widely investigated in Lewy body disease using PET, SPECT and now more recently, ASL (Melzer et al., 2011). The findings reported in the literature from historical PET and SPECT studies investigating perfusion alterations in PD were wildly inconsistent, which was largely a result of imaging modalities used and methodological approaches, with the most striking being whether global mean normalisation was performed. A detailed review that was restricted to PET and SPECT perfusion studies that conducted regions-of-interest or voxel-wise analyses and applied global mean normalisation is available elsewhere (Borghammer et al., 2008), but in summary, relative CBF reductions, as measured by PET and SPECT, were most frequently reported in parietal and frontal cortices, less frequently reported in the occipital cortex, and rarely reported in the temporal cortex. Relative increases of CBF were reported in the putamen, globus pallidus, thalamus, and motor cortex (Borghammer et al., 2008). On the other hand, the most robust findings from quantitative SPECT and PET studies were absolute decreases in the frontal and parietal cortices, with relative sparing of the temporal cortices. The occipital cortices are likely more affected than the temporal cortices, but less so than fronto-parietal cortices. CBF was unchanged or reduced in the striatum, thalamus and cerebellum (Borghammer, 2012).

Spatial covariance mapping disclosed specific metabolic brain networks related to the motor and cognitive manifestations of PD (Eidelberg, 2009). Ma and colleagues, through employing a network principal component strategy known as the scaled subprofile model (SSM) (Eidelberg et al., 1998, Moeller et al., 1999), identified disease-specific pattern of metabolism, known as the PD-related brain pattern (PDRP) (Ma et al., 2007). This pattern is characterised by relatively increased metabolism of the thalamus, lentiform nucleus, primary motor cortex, cerebellum, and

pons, with concomitant relative hypometabolism in the frontal, parietal, occipital, and temporal cortices. The test-retest reproducibility of the pattern is excellent and there is good correspondence between findings in CBF and glucose (Melzer et al., 2011, Teune et al., 2014). Contrastingly, the PD-related cognitive pattern is topographically distinct, characterised by a covariance structure distinct from PDRP: metabolic reductions predominately in the medial frontal and parietal association areas and relative increases in cerebellar cortex and dentate nuclei (Huang et al., 2007). Both patterns have been found to correlate with clinical rating of motor and cognitive disability across multiple patient populations (Eidelberg, 2009), as well as the PDRP being useful in discriminating between healthy controls, PD patients and patients with multiple systems atrophy (Tang et al., 2010, Tripathi et al., 2016).

However, since the conflicting patterns of perfusion reported could both not be physiologically sound, Borghammer and colleagues challenged the presence of such subcortical increases, arguing that they were simply an artifact introduced by global mean normalisation of the data as it is most likely biased (Borghammer et al., 2010, Borghammer et al., 2009a, Borghammer et al., 2009b). Normalisation is commonly used in PET and SPECT studies and is certainly necessary when absolute quantification is not feasible. Even when absolute quantification can be performed, perfusion measurements have great inter-individual variability with large coefficients of variation, making the small between-group differences difficult to detect (Borghammer et al., 2008). However, it is only appropriate when there is no difference in global mean perfusion between groups, which is an assumption that seems to be violated in PD when comparing to healthy controls, given that a meta-analysis revealed a significant global reduction of CBF in PD (Borghammer et al., 2010).

ASL MRI has been widely employed to assess CBF alterations in Lewy body diseases, with findings from resting-state studies that employed regions-of-interest and voxel-wise univariate

analyses consistently showing symmetrical cortical hypoperfusion in PD, involving predominately the parieto-occipital areas, with some studies observing hypoperfusion in additional areas such as the caudate nucleus, frontal regions and the cingulum (Wolf and Detre, 2007, Kamagata et al., 2011, Fernandez-Seara et al., 2012, Madhyastha et al., 2015, Syrimi et al., 2017, Barzgari et al., 2019), although Al-Bachari and colleagues reported no CBF alterations in PD (Al-Bachari et al., 2014). To the best of my knowledge, there have been no studies published to-date that have assessed perfusion alterations in drug-naïve PD patients specifically. In PDD, cortical hypoperfusion is much more widespread (Lin et al., 2016), with posterior perfusion deficits found to be more striking than in PD without dementia (Kamagata et al., 2011). In DLB, perfusion has been found to be reduced in frontal, parietal, occipital and cingulate cortices, with a relative preservation of the medial temporal lobe and posterior cingulate gyrus (Binnewijzend et al., 2014, Taylor et al., 2012, Fong et al., 2011, Nedelska et al., 2018). Whilst patterns of hypoperfusion largely overlap between PDD and DLB, with the same brain areas implicated, some studies have reported that DLB patients exhibit greater CBF reductions in frontal areas (Kasama et al., 2005). Nevertheless, these findings, along with those reported by perfusion PET and SPECT studies, highlight that hypoperfusion is common in Lewy body disease, although it is affected to different extents depending on how far along the disease has progressed or how severe the disease is.

The consequences of slow, progressive neuronal deterioration in Lewy body disease on the resting state brain perfusion and metabolism in Lewy body disease remains largely unknown. However, as discussed above, several studies have investigated the metabolic effects of acute or sub-chronic activation of neuromodulatory neurons, which revealed their role in contributing to NVC. Thus, it is plausible that the substantial neuron loss, in ascending systems in Lewy body dementia could result in spatially extensive hypoperfusion (Fernandez-Seara et al., 2012, Al-Bachari et al., 2014, Iadecola, 2017). Since synapses are the brain's major energy consumers, we

may expect there to be a linear association between CBF and synaptic density, particularly in healthy controls. However, since neuromodulatory neurons are most susceptible to injury in Lewy body disease, hypothetically, early synaptic dysfunction and/or loss could be associated with hypoperfusion. On the other hand, since the neurovascular unit is disrupted in Lewy body disease, the blood supply to synapses may not be appropriately regulated, potentially leading to neurovascular 'uncoupling'. Since CBF estimates within regions-of-interest may reflect differences in global perfusion, global CBF will be included in the statistical models as a nuisance covariate. This is to ensure that any relationship(s) observed between synaptic density and CBF is representative of region-specific CBF alterations.

1.10 Imaging synaptic density

The evidence presented thus far provides strong support for the implication of synaptic dysfunction in Lewy body disease aetiology and pathogenesis, with preclinical and clinical pathological and molecular imaging studies supporting the notion that presynaptic abnormalities are an early and distinct event in the disease process.

To date, approaches for synapse quantification in the human brain have typically relied on examination of brain tissue from autopsy or surgical re-section, thereby substantively limiting the utility of this approach for early diagnosis, monitoring disease progression, and evaluating treatment efficacy. In fact, quantification of synaptic density in the living human brain is also essential to further our understanding of brain disorders associated with synaptic pathology and attempts to develop therapeutic strategies aimed at correcting mechanisms underlying synaptic dysfunction, particularly at the presymptomatic stage, may be more effective. Thus, a minimally invasive approach to quantify synaptic density *in vivo* is desirable.

Traditional methods of synaptic density quantification in post-mortem brain tissue are associated with special challenges that are attributable to several confounding factors inherent to these tissues such as differences in the post-mortem interval, cause of death, complicated medical conditions, inconsistent pH and duration of storage and temperature of the tissues. These factors can disrupt the integrity of proteins, ultrastructures or microdomains (Crecelius et al., 2008, McCullumsmith et al., 2014).

Positron emission tomography (PET) is a powerful nuclear medicine imaging technique that allows for the three-dimensional mapping of functional dynamic processes in the body. When a positron-emitting radionuclide (radiotracer) is introduced into the body on a biologically active molecule, it indirectly emits pairs of gamma rays that are detected by the system. Therefore, depending on the characteristics of the injected compound, it is feasible to derive a vast range of biochemical and physiological parameters such as glucose metabolism, neuroreceptor binding and more recently, synaptic density. In contrast to structural imaging techniques such as MRI, PET can be employed to investigate dynamic alterations in specific functional processes, revealing not only the spatial location of these changes, but also measuring their magnitude.

In vivo quantification of proteins in the living brain has been achievable using PET, including an array for brain receptors, transporters, and enzymes, as well as other proteins (Jones et al., 2012). However, the currently available presynaptic markers tend to be specific to a subset of neurons, thus evidence of nerve terminal changes utilising these markers only permit researchers to draw conclusions about specific neuronal populations and so they cannot serve as general markers of synaptic density. Whilst there is strength in being able to evaluate pre- and postsynaptic molecular markers that are specific to neuronal populations, the annual radiation dose constraints render it impossible to investigate synaptic changes across all neuronal populations in the same group as a different PET scan would be required per marker of interest. Thus, *in vivo*

quantification of synapses across the entire brain is only possible when combining PET with a synapse-specific radioligand that binds to a protein ubiquitously expressed on all synaptic vessels. To this end, the most attractive markers of synaptic density are synaptic vesicle proteins, given the restricted localisation of vesicles to synaptic boutons and their ubiquitous distribution throughout the brain, and have previously been established as histologic markers of synaptic density (Goelz et al., 1981, De Camilli et al., 1983, Masliah et al., 1990).

1.10.1 Synaptic vesicle glycoprotein 2A

Discovered in the 1980s, the synaptic vesicle protein 2 (SV2) family are highly conserved 12-transmembrane glycoproteins comprising of three paralogs, SV2A, SV2B and SV2C, expressed in presynaptic vesicle membranes of neuronal and endocrine cells (Figure 1.3) (Buckley and Kelly, 1985). SV2 is vital for normal synaptic function and play a role in neurotransmitter release (Nowack et al., 2010). Despite all members of the SV2 family sharing approximately 60% of their sequences, they all have discrete patterns of expression across the brain (Bajjalieh et al., 1994) with SV2A being the only member that is ubiquitously and homogeneously expressed in all areas across the adult brain, irrespective of neurotransmitter type (Dong et al., 2006, Gronborg et al., 2010). SV2 is the most monodispersed synaptic vesicle protein, i.e., it has a consistent number of copies per vesicle. Over the last decade, SV2A has attracted much attention because it was identified as the molecular target of the antiepileptic drug levetiracetam (Lynch et al., 2004).

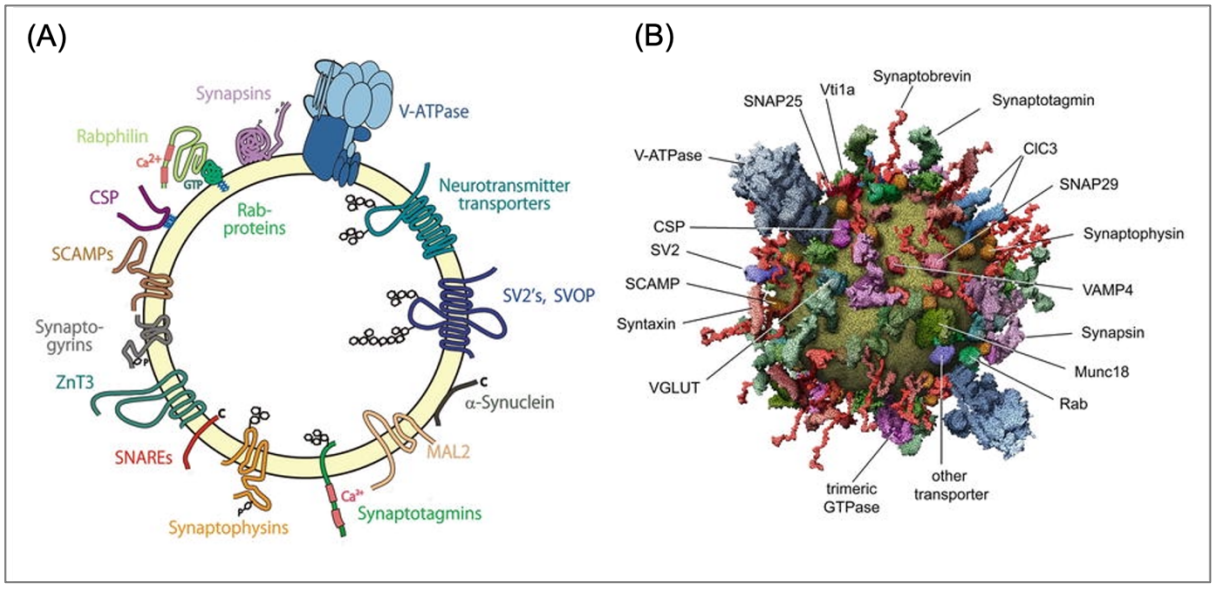

Figure 1.3. Molecular composition of synaptic vesicles. (A) Schematic representation of the structure of the major synaptic membrane proteins. (B) Molecular model of an average synaptic vesicle.*(A) Reprinted by permission from Springer Nature Customer Service Centre GmbH: Springer Nature, Springer eBook, Molecular Regulation of Synaptic Release, Jahn R. & Boyken J., Copyright © 2013. (B) Reprinted from Cell, 127(4), Takamori et al., 831-846, Copyright © 2006, with permission from Elsevier.*

Although the exact physiological role of SV2A remains unclear, SV2A appears to play a role in exocytosis mediated by Ca^{2+}. SV2A either regulates presynaptic Ca^{2+} levels during repetitive activity or serves as a target for residual Ca^{2+} (Mendoza-Torreblanca et al., 2013). In SV2A knockout models, malfunctioning SV2A leads to presynaptic accumulation of Ca^{2+}, which triggers abnormal neurotransmitter release, destabilises synaptic circuits and induces epilepsy (Janz et al., 1999). Knockdown of SV2A in neuronal cell cultures has been reported to cause a reduction of dendritic spine density of almost 30% (Cohen et al., 2011). SV2A has also been suggested to play a fundamental role in the endocytosis of synaptic vesicle protein synaptotagmin-1, thus is implicated in maintaining the readily releasable pool of synaptic vesicles (Yao et al., 2010). Indeed, it has been shown that reduced expression of SV2A leads to lower levels of synaptotagmin-1 in the synaptic vesicle, as well as the ratio of synaptotagmin-1 to synaptophysin being markedly reduced (Yao et al., 2010). Overall, whilst the exact function of SV2A, and the mechanism(s) by which it modulates neurotransmitter release remains elusive, the evidence indicates that this protein is involved in correct synaptic vesicle function, operating as a flexible protein that somehow interacts with Ca^{2+} and is thus important for synaptic function.

1.10.2 [^{11}C]UCB-J PET imaging

Given the widespread expression of SV2A in synapses throughout the brain (Bajjalieh et al., 1994), the highly consistent number of SV2 proteins per vesicle (Mutch et al., 2011, Takamori et al., 2006), and the fact that it correlates well with traditional markers of presynaptic terminals, such as synaptotagmin and synaptophysin (Finnema et al., 2016), a PET-derived brain measure of SV2A is a promising candidate for quantifying synaptic density *in vivo*, with it potentially providing an even more accurate measure of synaptic density owing to its greater uniformity in vesicles. A number of SV2A PET radioligands have been developed over the last few years including [^{11}C]levetiracetam (Cai et al., 2014), [^{11}C]UCB-A (Estrada et al., 2016), [^{18}F]UCB-H (Bretin et al., 2013) and [^{11}C]UCB-J (Nabulsi et al., 2016). Whilst radiolabelling of levetiracetam itself has been feasible, its affinity to SV2A is likely too low for optimal *in vivo* imaging with PET (Gillard et al., 2006), and an *in vivo* evaluation is yet to be reported for this candidate tracer. [^{11}C]UCB-A tracer binding in the brains of rats and pigs was reported to be specific for SV2A, but binding kinetics were slow in both species, potentially linked to slow metabolism and slow excretion of the tracer (Estrada et al., 2016). The uptake rate of [^{18}F]UCB-H was promising in rodents and nonhuman primates, but it has a lower binding affinity for SV2A, which led to low specific binding signals in nonhuman primates (Goutal et al., 2021). [^{11}C]UCB-J, on the other hand, has been shown to exhibit the best pharmacokinetic and imaging characteristics for quantifying SV2A, including high brain uptake, rapid and reversible tissue binding kinetics, high affinity and specificity for SV2A, moderately fast metabolism and high free fraction in the plasma (Nabulsi et al., 2016). Indeed, when the three UCB radioligands were translated to human studies, there was consistency with the preclinical data reports whereby [^{11}C]UCB-A presented slow binding kinetics in the human brain, making quantification analysis relatively challenging, [^{18}F]UCB-H displayed low specific binding signals and [^{11}C]UCB-J exhibited excellent imaging properties, as well as good test-retest reproducibility and high specificity (Finnema et al., 2016,

Finnema et al., 2018). Thus, whilst [^{11}C]UCB-A and [^{18}F]UCB-H have significant limitations as PET radiotracers for visualising and quantifying SV2A in the human brain, [^{11}C]UCB-J is the most extensively clinically validated of the SV2A tracers and has emerged as the superior radioligand for measuring synaptic density *in vivo*, which is also reflected in the fact that post-mortem quantification of SV2A is highly correlated with the commonly used synaptic density marker synaptophysin, with *in vivo* binding of [^{11}C]UCB-J excellently correlating with post-mortem SV2A density, and levetiracetam displacing [^{11}C]UCB-J binding in cortical regions confirming the specificity of its uptake (Finnema et al., 2016).

1.10.3 Applications of [^{11}C]UCB-J PET imaging in clinical research

Given the novelty of SV2A PET imaging, there are a limited number of studies that have employed [^{11}C]UCB-J PET to assess synaptic density in the context of neurological disorders, including but not limited to AD (Chen et al., 2018, Chen et al., 2021, Mecca et al., 2020), Huntington's disease (Delva et al., 2021), temporal lobe epilepsy (Finnema et al., 2016), primary tauopathies (Holland et al., 2021, Mak et al., 2021), major depressive and post-traumatic stress disorder (Holmes et al., 2019), and schizophrenia (Radhakrishnan et al., 2021, Onwordi et al., 2020).

To-date, three studies have employed [^{11}C]UCB-J PET to assess synaptic density *in vivo* in PD (Delva et al., 2020, Matuskey et al., 2020, Wilson et al., 2020) and two have been published in Lewy body dementia (Nicastro et al., 2020, Andersen et al., 2021), though one is a pilot case study of 2 DLB cases. Recently, Matuskey and colleagues published the first [^{11}C]UCB-J study in PD patients and found the largest reduction of [^{11}C]UCB-J binding in the substantia nigra, which was confirmed using postmortem ^{3}H-UCB-J autoradiography (Matuskey et al., 2020). This finding was confirmed by Delva et al. (2020), though they did not observe the additional significant reductions in the red nucleus, locus coeruleus and parahippocampal gyrus previously

reported. Furthermore, both studies reported an absence of significant SV2A loss in the striatum, as well as any associations between [^{11}C]UCB-J binding and clinical variables (Delva et al., 2020, Matuskey et al., 2020). Finally, within early PD patients, Wilson and colleagues reported widespread significant reductions of [^{11}C]UCB-J uptake in subcortical and brainstem nuclei, as well as across all cortical regions. Within Lewy body dementia, two studies reported a widespread decrease of cortical [^{11}C]UCB-J binding, particularly within parieto-occipital and frontal cortices (Nicastro et al., 2020, Andersen et al., 2021). Thus, there are a few recent publications that have investigated synaptic density alterations within PD groups, and reduced nigral [^{11}C]UCB-J uptake has transpired to be the most reproducible finding. However, whilst there is also need for replication studies to confirm these findings, what remains to be explored is whether dopamine replacement therapy influences synaptic density in PD patients.

Whilst L-DOPA does not prevent the inevitable loss of dopaminergic neurons, nor the continual formation of Lewy pathology throughout the brain (Olanow, 2019), its ability to restore motor activity, and in particular, induce motor complications like LIDs, is linked to its ability to impinge on the brain's 'plasticity potential', which conditions the capacity for functional recovery after injury and response to neuropsychiatric treatment interventions. This notion has been evidenced to be the case for antidepressant pharmacotherapies; there has been a recent study by Raval et al. (2021) where a single dose of psilocybin, a psychedelic and 5-HT$_{2A}$ receptor agonist, induced a localised increase of SV2A protein density in the hippocampus and prefrontal cortex, as determined by [^{3}H]UCB-J autoradiography, suggestive of psilocybin causing an increase in synaptogenesis (Raval et al., 2021). However, whilst the implications of neuroplasticity in response to antiparkinsonian medication is much less understood, there has been a surge of literature showing its pervasive, plasticity-promoting effects.

Studies have demonstrated that treatment with L-DOPA in PD rat models increases the expression of markers of dopaminergic nerve terminals in the striatum, suggesting that the remaining dopaminergic nerve fibres in these animals may be capable of sprouting (Murer et al., 1998, Datla et al., 2001). Gene array studies using rodents lesioned with 6-hydroxydopamine (6-OHDA) provided the first indications that treatment with chronic L-DOPA promotes structural plasticity in the brain, with Ferrario et al. (2004) demonstrating that 6 months of L-DOPA administration induced a prominent striatal upregulation of genes encoding growth factors, metalloproteinases and their inhibitors and myelin-related proteins (Ferrario et al., 2004).

In fact, L-DOPA has also been shown to exert long-lasting beneficial effects on symptom progression. This was demonstrated by Fahn et al. (2004) in their randomised, double-blind, placebo-controlled trial where patients either received L-DOPA or placebo for a duration of 42 weeks, followed by a 2-week wash-out. Here, patients who were administered L-DOPA did not display the same extent of deterioration of symptoms as those who were taking placebo, suggestive of L-DOPA inducing some long-lasting beneficial effect on symptom progression, which may be mediated by the plasticity of corticostriatal and nigrostriatal signalling (Surmeier et al., 2007, Calabresi et al., 2015, Albin and Leventhal, 2017). Thus, it is yet to be determined if the plasticity-promoting effects of L-DOPA can be visualised *in vivo* within PD patients and whether these effects are long-lasting or transient.

The confounding effects of atrophy to [^{11}C]UCB-J quantification has predominantly just been accounted for in the literature by applying partial volume correction techniques to the [^{11}C]UCB-J imaging data. However, insight into the influence that volume loss can have on [^{11}C]UCB-J outcome measures is less explored. Whilst there is a great deal of evidence that indicates that the mechanisms of neuron soma and axon degeneration are separate and distinct (Finn et al., 2000, Raff et al., 2002), with early involvement of synaptic/axonal deficits prior to neuronal loss

evidenced to be the case in Lewy body disease, it is important to determine whether [^{11}C]UCB-J is, in fact, a distinct marker of synaptic density, or if its loss simply reflects gross neuronal loss.

The contribution of atrophy to [^{11}C]UCB-J outcome measures has predominately been evaluated in AD (Chen et al., 2018, Mecca et al., 2020). Whilst there is also atrophy present in Lewy body dementia particularly, the influence of volume on measures of [^{11}C]UCB-J was not explicitly explored by Andersen et al. (2021), whereby partial volume correction (PVC) was applied to the [^{11}C]UCB-J data, but the authors simply reported that there were no major differences in data with or without PVC. In the small pilot case study of 2 DLB patients, however, Nicastro and colleagues assessed if there was regional associations between grey matter volume and [^{11}C]UCB-J binding, but reported no associations between these measures (Nicastro et al., 2020). Whilst there appears to be some influence of volume on measures of SV2A as indicated by Chen et. al. (2018) and Mecca et. al. (2020) in AD, in Lewy body dementias, this appears not to be the case. However, given the small sample size of 2 DLB patients, it is important to assess whether volumetric alterations can potentially confound [^{11}C]UCB-J measures, particularly in Lewy body dementia.

Whilst there have been some recent publications that have evaluated synaptic density alterations in Lewy body diseases, as measured with [^{11}C]UCB-J PET, what remains to unknown is whether such a marker of synaptic density is related to alterations in grey matter volume and cerebral blood flow within these disorders. Furthermore, L-DOPA medication has the potential to exert plasticity-promoting effects (Datla et al., 2001, Murer et al., 1998) and subsequently alter synaptic markers, but medicated and unmedicated PD patients have yet to be compared. In addition, in this introduction, I have argued that disease progression will have a major influence on markers of synaptic density (Tremblay et al., 2021) and associated grey matter volume (Rektorova et al., 2014) and blood flow (Kasama et al., 2005, Barzgari et al., 2019), but this is yet to be explored *in*

vivo across groups with varying disease severity who are at different stages of the disease. Finally, the biological underpinnings of synaptic density alterations in Lewy body disease are an uncharted area of research, and I have outlined in the introduction that synapse loss is likely to be influenced by an interplay between processes of degeneration and atrophy, as well as those involved in maintenance at the regional and network levels.

1.11 Aims and hypotheses

This thesis is cross-sectional in design and will explore *in vivo* synaptic density differences by employing [^{11}C]UCB-J PET in groups of HC, drug-naïve PD, mild-to-moderate PD, PDD and DLB. Quantitative measures of T1 will be collected, alongside quantitative ASL to allow for an assessment of grey matter volume and CBF, respectively within the same subjects. Please note that cross-sectional studies are often employed to make tentative inferences about what within-group changes may look like. In most cases, group differences are interpreted as alterations. Therefore, throughout the remainder of the thesis, I may refer to a between-group difference as an 'alteration' or 'change'; an 'increase', 'decrease', 'decline', 'loss' or 'atrophy'.

The first experimental chapter is dedicated to PD. Here, [^{11}C]UCB-J and high-resolution PET are employed to investigate synaptic integrity *in vivo* in PD patients at the early stages of the disease. This study extends previously published studies by including and directly comparing drug-naïve PD patients to those who are taking dopamine replacement therapy. The main aim of this study was to examine the degree to which synaptic density was reduced in PD patients prior to commencement of dopamine replacement therapy and how this may change following chronic administration of L-DOPA and disease progression. Regional volumes were also extracted to assess whether there was an association between grey matter volume and SV2A expression levels. Regional CBF values were extracted to assess whether reductions in CBF

qualitatively overlap with synaptic density reductions, and then assess if they are correlated. Finally, I wanted to determine the clinical relevance of [^{11}C]UCB-J binding in Lewy body disease by delineating its associations with motor symptoms and cognitive performance.

Since there is strong evidence illustrating that neurons undergo a dying-back phenotype, suggestive of synaptic dysfunction being an early event in PD, and with [^{11}C]UCB-J being considered as a selective marker of synaptic density, I expect [^{11}C]UCB-J will be sensitive to the early stages of PD. Therefore, I hypothesise that synaptic density reductions will be evident in drug-naïve PD patients compared to healthy controls, concomitant with negligible grey matter volumetric reductions. The early involvement and vulnerability of neuromodulatory systems in PD leads me to hypothesise that SV2A loss will be widespread in this sample. Due to the NVC, I hypothesise that there will be some qualitative overlap between regional reductions in SV2A expression and hypoperfusion in drug-naïve PD patients compared to healthy controls, with an observable linear association between these measures. I also hypothesise that there will a relationship between SV2A reductions and severity of motor and non-motor symptoms in drug-naïve PD patients. Whilst chronicity of disease would lead one to hypothesise that synaptic density would be further reduced in treated PD, given L-DOPA's known capacity to promote neuroplasticity, I hypothesise that in treated PD patients, SV2A expression will be comparable to that seen in healthy controls and elevated compared to drug-naïve PD. If SV2A levels are elevated in this group, I expect to observe correlations between SV2A binding and clinical measures whereby elevated SV2A would be associated with ameliorated clinical presentation.

The second chapter is dedicated to Lewy body dementia. Here, I aim to investigate synaptic integrity *in vivo* in PDD patients and DLB patients, compared to healthy controls, as well as volumetric alterations and CBF changes. Here, I hypothesise that synaptic density would be extensively reduced in Lewy body dementia, expanding predominately to cortical brain areas.

More specifically, I expect there to be more prominent SV2A reductions in parieto-occipital areas in Lewy body dementia. Compared to PD, I theorise that PDD patients will exhibit progressive deficits of synaptic density within posterior brain areas, as well as medial temporal lobe structures such as the hippocampus, that have previously been shown to be implicated in cognitive impairment and dementia in PD (Gratwicke et al., 2015). Similarly, I expect that both dementia groups will exhibit widespread cortical hypoperfusion predominately across parietal and occipital brain areas. Whilst I expect grey matter volume to be significantly reduced in this dementia group, I hypothesise that SV2A binding will not simply be a proxy measure of grey matter volume, but rather that grey matter volume will have some localised confounding effects on SV2A measures. Within Lewy body dementia, I hypothesise that SV2A expression will be related to cognitive performance in regions-of-interest relevant to cognition. These regions-of-interest have been selected because of their association with cognitive domains that are implicated in dementia, for example, I expect synaptic density alterations in regions implicated in the fronto-striatal network to be associated with executive function (Monchi et al., 2007) and parietal alterations to be linked to attentional deficits (Williams-Gray et al., 2008). Having said this, I may expect these domain-specific brain areas to also be associated with global measures of cognition given that, for example, frontal and parietal cortices have been shown to be implicated in overall cognitive deterioration in PDD (Liepelt et al., 2009) .

Since [^{11}C]UCB-J is a general marker of synaptic density, there is a lack of insight into the neurochemical, structural and functional pathology that could be associated with the patterns of synaptic density reductions in disease groups. Since neuromodulatory neurons are particularly vulnerable in PD, I was interested in assessing how the distribution pattern of group-level differences in synaptic density in patient groups is associated with the canonical distribution of neurotransmitter receptors and transporters that are markers of the dopaminergic, noradrenergic, serotonergic, and noradrenergic systems. I was also interested to assess whether the spatial

distribution of group-level SV2A alterations are related to the respective spatial distribution of group-level volumetric alterations and/or perfusion changes.

I hypothesise that there will be detectable, but variable, linear relationships between the spatial distribution of [^{11}C]UCB-J alterations and that of neurotransmitter-specific features, as well as the distribution of regional grey matter volume and perfusion differences in these patient groups. Following the mechanisms inducing synaptopathy in PD and eventual degeneration, I hypothesise that there will be a linear relationship between the regional distribution of grey matter volumetric alterations and the spatial distribution pattern of [^{11}C]UCB-J change, where a pattern of reduced [^{11}C]UCB-J V_T will be mirrored in lower grey matter volume. Furthermore, I expect grey matter volume to explain a larger proportion of [^{11}C]UCB-J variance in the dementia groups.

Given the established rich vascularisation required to support neuronal function, I expect to see a linear relationship between the spatial pattern of CBF change and the spatial pattern of [^{11}C]UCB-J change, whereby the regional distribution of areas illustrating higher [^{11}C]UCB-J uptake will be similar to the regional distribution of areas exhibiting higher perfusion.

The multi-system nature of PD and the early involvement of serotonergic, noradrenergic, and dopaminergic systems has led me to hypothesise that distribution patterns of [^{11}C]UCB-J alterations in drug naïve PD patients would be associated with the spatial distribution of these neurotransmitter system markers, though I expect it will have the strongest relationship with dopaminergic markers.

Since complex and diverse molecular and cellular pathologies contribute to patterns of dysfunction at the neural systems level, I expect that as the disease progresses, there will be a

consolidation of damage to different neurotransmitter systems, as well as atrophy and perfusion changes, contributing to the variance of the distribution patterns of [^{11}C]UCB-J change.

2 Methods

This section outlines the shared methods employed for chapters 3, 4 and 5. Any additional analyses conducted that are unique to each chapter can be found under the 'Methods' subheading within each chapter. This thesis involves measuring [^{11}C]UCB-J with high-resolution PET, grey matter volume with T1-weighted images and quantification of cerebral blood flow with ASL-MRI in groups of PD and dementia with Lewy bodies.

Before proceeding, it is important to mention that a proportion of the data, namely the [^{11}C]UCB-J PET and T1-weighted MRI data in drug-naïve PD patients, has previously been published (Wilson et al., 2020). This data was re-analysed to allow for the implementation of a semi-automated approach to explore further questions related to volumetric and partial volume effects that had not been previously considered, to conduct a cross-sectional comparison with a medicated PD group and to apply a novel approach that aids in furthering our understanding about the potential neurophysiological mechanisms underlying the regional variability in synaptic density.

2.1 Study design

2.1.1 Study participants

A total of 74 subjects were included in these cross-sectional studies: 21 non-demented patients with idiopathic Parkinson's disease, 18 subjects with Lewy body dementia and 35 healthy control subjects. All participants were screened for inclusion/exclusion criteria, underwent a clinical assessment, and had a blood sample taken for coagulopathies. Participants then underwent one [^{11}C]UCB-J PET scan and one 3-Tesla MRI scan.

Participants were divided into the following groups:

Group A: eleven drug-naïve PD patients (mean age ±SD: 58.8 ±9.0 years; 9M/2F)

Group B: ten PD patients on parkinsonian medication (mean age ±SD: 61.7 ±6.4 years; 7M/3F, mean LEDD ±SD: 467.6 ±227.62 mg)

Group C: nine PDD patients (mean age ±SD: 67.3 ±9.3 years; 6M/3F)

Group D: nine patients with probable DLB (mean age ±SD: 72.8 ±4.6 years; 8M/1F)

Group E: thirty-five healthy controls (mean age ±SD: 62.1 ±10.4 years, 22M/13F)

All patients were recruited from specialist Movement Disorder clinics at King's College Hospital NHS foundation, which is a national Foundation Centre of Excellence that delivers Movement Disorders services to 6 million people in south London and surrounding areas. The MINDMAPS Consortium provided eighteen healthy controls with [^{11}C]UCB-J PET and MRI data and the rest were recruited through advertisement.

Screening procedures and clinical assessments were conducted prior to the first imaging session and took place at the National Institute of Healthy Research (NIHR) Wellcome Trust King's College London Clinical Research Facility, where a blood sample was also taken for coagulopathies. Screening procedures included taking a detailed medical history, general screening questions, including an MRI safety questionnaire, physical and neurological examination, structured clinical interview for DSM-IV to exclude the presence of other neurological or psychiatric disorders, and the administration of Montreal Cognitive Assessment (MoCA) for assessment of cognitive status and Geriatric Depression Scale to determine the presence of depressive symptoms.

Inclusion criteria required the following:

For all groups:

- Male and female, 40-80 years of age
- No presence or history of other neurological or psychiatric disorders (Gibb and Lees, 1988)
- Adequate visual and auditory acuity to complete the psychological testing

Specific for Group A: drug-naïve PD

- Diagnosis of sporadic PD according to the UK Brain Bank Criteria (Gibb and Lees, 1988)
- Classified as Stage 1 on the modified Hoehn and Yahr (H&Y) scale for PD severity
- Disease duration of less than 24 months
- Never treated with dopamine agonists or L-DOPA
- No dementia

Specific for Group B: treated PD

- Diagnosis of sporadic PD according to the UK Brain Bank Criteria (Gibb and Lees, 1988)
- Classified as Stage 1 or 2 (in the ON state) on the modified H&Y scale for PD severity
- Disease duration of less than 96 months
- Treated with dopamine agonists or L-DOPA
- No motor complications
- No dementia

Specific for Group C: PDD

- A diagnosis of probable PDD according to the clinical diagnostic criteria for PDD established by the Movement Disorder Society's commissioned task force (Emre et al., 2007)

Specific for Group D: DLB

- A diagnosis of probable DLB according to the clinical diagnostic criteria for DLB established by the International DLB Consortium (McKeith et al., 2017).

Exclusion criteria included the following:

For all groups:

- Presence of other neurological disorders and/or known intracranial co-morbidities such as haemorrhage, stroke, or space-occupying lesions
- Current or recent history of drug or alcohol abuse/dependence
- Pregnancy or breastfeeding
- Contraindication to MRI, such as presence of metal devices or implants, metal deposited in the body (e.g., bullets or shells) or metal grains in the eyes
- History of cancer within the last 5 years except for skin or prostate cancer
- Claustrophobia and/or history of back pain that makes prolonged lying on the imaging scanner intolerable
- Use of medications with known actions on SV2A such as antiepileptics, for example levetiracetam or brivaracetam

All participants were successfully screened to undertake MRI and PET scanning procedures, under scanning safety criteria (http://www.mrisafety.com; https://www.gov.uk/government/publications/arsac-notes-for-guidance).

2.1.2 Ethical consideration

The study was approved by the institutional review boards and the research ethics committee (16/LO/1129; IRAS ID: 205849 and 18/LO/1915; IRAS ID: 249061). Written informed consent was obtained from all study participants in accordance with the Declaration of Helsinki.

2.1.3 Clinical assessments

Motor symptom severity was assessed with the Movement Disorder Society Unified Parkinson's Disease Rating Scale part-III (MDS-UPDRS-III) and Hoehn-Yahr (H&Y). Non-motor symptoms were assessed with the PD Non-Motor Symptom Questionnaire (PD NMS Questionnaire), Scales for Outcomes of Parkinson's disease - Autonomic dysfunction (SCOPA-AUT)). Sleep disturbances were assessed with the Epworth Sleepiness Scale (ESS), REM Behaviour Sleep Disorder Questionnaire (RBDQ) and the Parkinson's disease Sleepiness Scale (PDSS). Pain and olfactory dysfunction were assessed using the King's PD Pain Questionnaire and The University of Pennsylvania Smell Identification Test (UPSIT), respectively. The Mini Mental Status Examination (MMSE) and Montreal Cognitive Assessment (MoCA) were used to assess general cognitive status. Further cognitive and neuropsychiatric assessments for PDD and DLB were carried out using the Scales for Outcomes of Parkinson's disease – Cognition (SCOPA-COG) and the Parkinson's disease - Cognitive Rating Scale (PD-CRS).

2.2 Image Acquisition and Analysis

All participants underwent one [^{11}C]UCB-J PET scan (~90 minutes) and one 3T MRI scan (~90 minutes), which was performed at Invicro London Ltd, A Konica Minolta Company. Structural T1-weighted images were acquired for the quantification of grey matter volume, as well as for normalisation purposes and for providing partial volume estimates for partial volume correction.

ASL was used to obtain quantitative measures of CBF and [^{11}C]UCB-J PET scanning was performed for quantification of SV2A.

PET imaging was performed on a Siemens Biograph Hi-Rez 6 PET-CT scanner (Erlangen, Germany) and MRI scans were acquired with a 32-channel head coil on a Siemens Magnetom TrioTim syngo MR B17 (Erlangen, Germany), 3T MRI scanner.

2.2.1 MRI acquisition

2.2.1.1 Structural MRI

Participants underwent imaging with a Siemen's Magnetom TrioTim syngo MR B17 (Erlangen, Germany) equipped with a 32-channel head coil. A high-resolution, three-dimensional (3D) T1-weighted Magnetization Prepared Rapid Gradient Echo sequence (MPRAGE) was acquired with the following protocol: repetition time = 2300ms, echo time = 2.98ms, flip angle of 9°, time to inversion = 900ms, matrix = 240 x 256 x 160; voxel size = 1.0mm x 1.0mm x 1.0mm.

2.2.1.2 Arterial spin labelling (ASL)

Measurement of CBF was carried out using a pulsed-ASL (pASL) PICORE tagging scheme with QUIPSS II (PICORE Q2T) with multi-inversion times (5 TIs: 1200ms, 1500ms, 1800ms, 2100ms, and 2400ms). Distinct repetition times per TI was used, namely 2300ms, 2600ms, 2900ms, and 3500ms, such that imaging time was minimised. The general acquisition parameters were as follows: echo time = 11ms, field-of-view = 240x240mm, slice thickness = 5mm with a 30mm gap, flip angle of 90° and bolus length = 800ms. Sixteen control-label pairs were acquired per inversion time. The advantages of this multi-TI sequence is that it enables greater brain coverage and a kinetic model of the tracer arrival can be fit to the data, which can account for the variability in the time it takes for the tracer to cross the vasculature (Chappell et al., 2011). An unlabelled

(control) scan, namely M0, was acquired with fully relaxed magnetisation and no labelling with comparable acquisition parameters [repetition time = 10000ms, echo time = 11ms, field-of-view = 240x240mm, flip angle of 90°] to compute the CBF map in standard physiological units (ml blood/100g tissue/min).

2.2.2 [^{11}C]UCB-J PET acquisition

Prior to the PET scan, vital signs were measured, and pre-menopausal women also underwent a urine test to rule out pregnancy. Patients who were taking dopamine replacement therapy discontinued use of dopaminergic medications 24 hours prior to their PET scan.

A mean dose of 233.84 MBq (SD: ±46.58) of [^{11}C]UCB-J was administered intravenously as a slow bolus injection over 20s. Following administration of [^{11}C]UCB-J, dynamic emission data were acquired continuously for 90 minutes. The dynamic images were reconstructed into 26 frames (8 x 15s, 3 x 60s, 5 x 120s, 5 x 300s, and 5 x 600s), using a filtered back projection algorithm (direct inversion Fourier transform) with a 128 matrix, zoom of 2.6, producing images with isotropic voxel size of 2 mm^3, and smoothed with a transaxial Gaussian filter of 5 mm. Blood sampling was performed for [^{11}C]UCB-J through an arterial line, which was inserted in the radial artery to generate arterial plasma input data. During the first 15 minutes, radioactivity levels in blood were continuously measured through an automatic blood sampling system at 5ml/min, followed by samples at 5, 10, 20, 30, 50, 70 and 90 min during the scan. Parent fraction over the course of each PET scan was determined by high-performance liquid chromatography (HPLC) analysis using the Hilton column switching method (Hilton et al., 2000). Plasma input function of unmetabolised radioligand was generated using the continuous and discrete plasma samples. The plasma free fraction was measured by ultrafiltration in triplicate using an arterial blood sample taken prior to each tracer injection.

2.2.3 Structural MRI processing and analysis

Prior to any processing, the origin of the T1-weighted images was reset to the anterior commissure and the images were reoriented to the AC-PC line. Quantification of grey matter volume was done so in two ways: 1) morphometric measures derived from voxel-based morphometry (VBM) and 2) an atlas-based volume estimation corresponding to the regional estimates of [^{11}C]UCB-J V_T (see section 2.2.4.1 [MRI image processing and definition of regions-of-interest] for further detail).

2.2.3.1 Voxel-based morphometry

At its simplest, VBM comprises a voxel-wise comparison of the local grey matter concentrations between groups of subjects using the statistical approach of parametric mapping. Pre-processing and subsequent statistical analyses was performed in the open-source software package SPM12 (https://www.fil.ion.ucl.ac.uk/spm/), running in the MATLAB® (R2018b; MathWorks, Natick, MA, USA). T1-weighted images were first segmented using the segmentation tool into grey matter, white matter, and cerebrospinal fluid maps. This extension of Unified Segmentation (Ashburner and Friston, 2005) uses both the intensity value of each voxel in the images, alongside a priori tissue probability maps, to assign each voxel to a tissue class. Intensities are modelled using a mixture of Gaussians to permit non-Gaussian distributions to be modelled, which is especially useful for voxels with partial volume effects where signal may be impacted by more than one tissue type. There is also a bias correction step that corrects for inhomogeneity of the magnetic field that disrupts intensity values of voxels across the brain image. These were then imported for subsequent non-linear registration based on the algorithm referred to as 'Diffeomorphic Anatomical Registration Through Exponentiated Lie Algebra (DARTEL) (Ashburner, 2007). DARTEL is a normalisation method that utilises the segmented grey and white matter maps to generate a group-specific group template in standard space, to which the

segmented grey matter maps are then warped to. In brief, the first step involves the simultaneous formation of an initial template which is the mean of all segmented grey and white matter images together. Next, deformations from this initial template to each individual image are computed and, by applying the inverses of the deformations to the images and averaging, the template is subsequently re-created. This generates an increasingly crisp average template to which images are iteratively aligned. A final affine transformation warps the template into standard space. After 6 reiterations of this process, each subject will possess a unique set of *flow fields* that encode the deformations necessitated to move their data from native space into template space. Since DARTEL allows for improved characterisation of brain morphology, inter-subject alignment is more precise, there is an improvement in group analysis, localisation is more accurate and there is increased sensitivity. Whilst originally developed to enhance normalisation of structural data for morphological analyses, it has also been shown to serve as a superior normalisation method for PET data, compared to standard template techniques (Martino et al., 2013). Thus, DARTEL was used to build a study-specific template and a set of flow fields that were used for the normalisation of grey matter maps into standard space. Grey matter volumes in standard space also underwent modulation with Jacobian determinants, which involves scaling by the amount of contraction or expansion, to maintain the total amount of grey matter. Finally, the normalised grey matter maps were smoothed with an 8mm full width at half-maximum Gaussian kernel, which involves convolving the signal with a Gaussian function of a specific width that replaces a given voxel value with the spatially weighted average of its neighbours. There are several benefits to this, which include improving signal-to-noise ratio, increasing the normality of residuals, and reducing the effect of misregistration between images.

2.2.4 [^{11}C]UCB-J PET analysis pipeline

2.2.4.1 MRI image processing and definition of regions of interest

As part of the PET processing pipeline (Figure 2.1), skullstripping was first performed on individual MRIs using the FSL Brain Extraction Tool (bet) (Smith, 2002). The segmentation tool in SPM12 was employed to segment individual T1-weighted images into grey matter, white matter, and cerebrospinal fluid (CSF) maps. The skullstripped brain MRI was then rigidly registered with six degrees of freedom to a template MRI using normalised *mutual information* cost function moving the brain MRI into standard MNI space. The transformation matrix obtained from this registration step was applied to the brain tissue probability maps. Next, the deformations from the template MRI to the subject's rigidly registered brain MRI was computed and saved using the SPM normalisation tool. Regions-of-interest were anatomically delineated using the Clinical Imaging Centre (CIC) atlas. The CIC atlas was nonlinearly warped to the brain MRI in MNI space by applying the parameters determined in the earlier step. To tailor regions-of-interest to each subject's anatomy, the subject's segmented grey matter was used to mask the regions of interest. The atlas and MRI images, including the segmented tissues classes, were then resliced using the SPM reslice tool and ultimately downsampled to match the resolution of the PET images, with 2mm voxels. This was considered 'final space'. Finally, regional time activity curves (TACs) and corresponding grey matter volumes were extracted.

2.2.4.2 PET processing and quantification

PET data processing and kinetic modelling was performed using the Molecular Imaging and Kinetic Analysis Toolbox software package (MIAKAT™: www.miakat.org; version 4.3.24), implemented in MATLAB® (R2018b; The Mathworks, Natick, MA, USA). MIAKAT™ provides state-of-the-art functionality within a coherent analysis framework by combining in-house code with wrappers for FMRIB Software Library (FSL, http://fsl.fmrib.ox.ac.uk/fsl/fslwiki/) and Statistical Parametric Mapping (SPM, http://www.fil.ion.ucl.ac.uk/spm/) commands. The

MIAKAT™ processing pipeline was adhered to (Figure 2.1) and both parametric images and regional estimates of [^{11}C]UCB-J volume of distribution (V_T) were generated. Briefly, individual PET frames were corrected for head motion by employing a rigid body transformation to realign each frame to a single frame with high signal-to-noise ratio that was used as a reference. This approach minimises positional deviations between frames while maintaining the integrity of the original data as only linear transformations (i.e., rotations and translations along the x, y, and z axis) were applied. Within the same step, a frame-by-frame rigid registration was performed on the dynamic PET using the skullstripped MRI image already registered to MNI space as a reference image. TACs were next generated for all regions-of-interest (see regions-of-interest based analyses for further details). Next, the arterial input function was acquired to be implemented in subsequent kinetic modelling. Here, the continuous and discrete whole blood data were merged to form a whole blood TAC spanning the full duration of the dynamic PET scan. Plasma-to-whole blood ratios were fitted with a *constant fit* plasma-over-blood model, creating a plasma TAC with the same temporal resolution as the whole blood curve. A *sigmoid* parent fraction model was also fitted to the sparse parent fraction data for interpolation and extrapolation purposes prior to applying it the plasma TAC to produce a parent in plasma TAC (i.e., metabolite-corrected plasma TAC), which was used as the input function for kinetic modelling. Regional estimates of [^{11}C]UCB-J V_T were generated using the one-tissue compartmental model (1TC) with blood volume correction. [^{11}C]UCB-J parametric V_T maps were generated using 1TC model (Gunn et al., 2001). Kinetic analysis for [^{11}C]UCB-J has been evaluated in the literature, and studies have found that [^{11}C]UCB-J kinetics are best described by the 1TC model (Finnema et al., 2016, Finnema et al., 2018, Tuncel et al., 2021), thus it is the most widely used. Therefore, employing the 1TC model is in agreement with the literature.

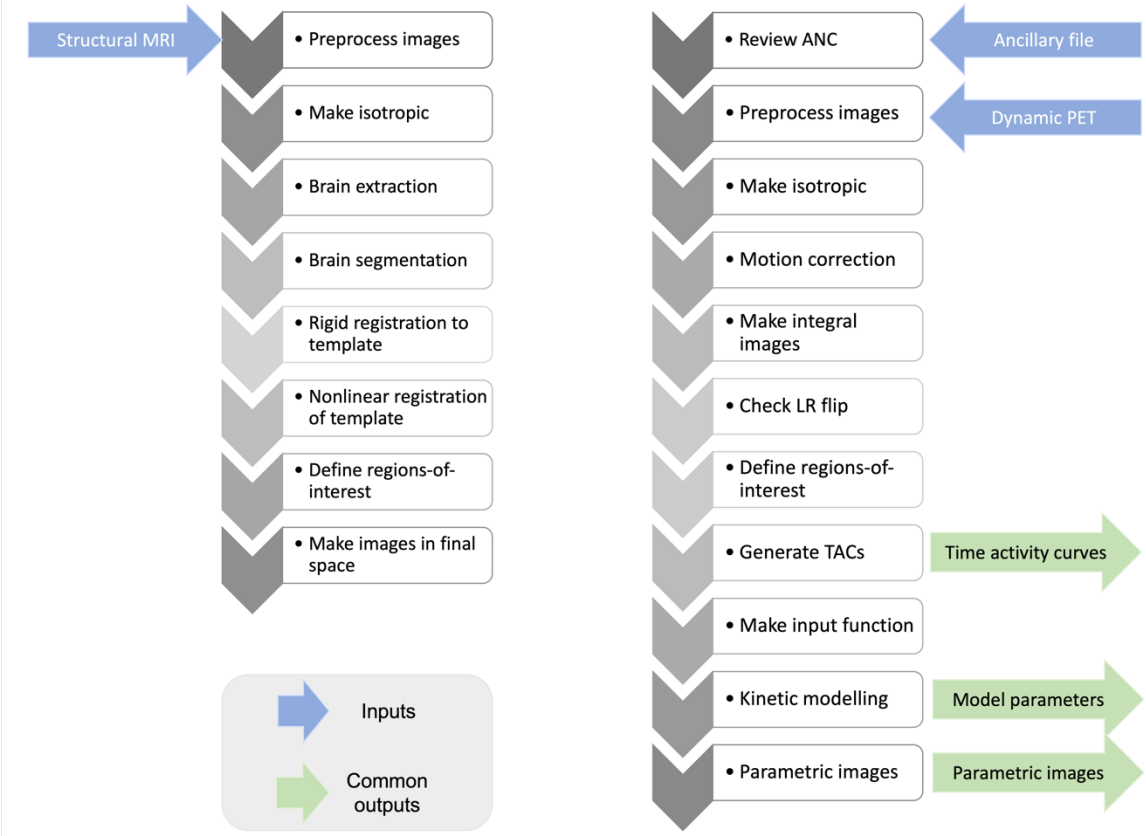

Figure 2.1. Schematic of the PET analysis pipeline. *Adapted from MIAKAT users' manual.*

2.2.4.3 Partial volume correction

Due to the relatively poor spatial resolution achievable with a PET scanner, the accuracy of quantification is limited. Spatial resolution-related effects are termed 'partial volume effects' (PVEs), which comprise two phenomena that diminish the quantitative accuracy of PET data. The primary PVE in emission tomography represents the spill-over of signal, or cross-contamination, between distinct regions due to the point-spread function (PSF) of the scanner. This effect is usually considered as two separate entities: spill-out and spill-in, whereby activity concentration within a target region can be underestimated due to spill-out of counts to neighbouring regions or activity concentration within a target region can be contaminated by spill-in from adjacent regions. The second effect corresponds to the voxel size of the images whereby any given voxel can in principle contain multiple tissue types, with the resultant voxel

signifying the mean signal from these fractional contributions. This mean signal intensity within a voxel is termed tissue-fraction effect and affects quantification since it does not accurately characterise the true distribution of the radiotracer. The magnitude of PVE is contingent on the regional contrast, alongside the size of each region whereby smaller regions typically suffer from greater PVE than those that are larger. Neurodegenerative disorders are more susceptible to PVEs due to the progressive atrophy that occurs across several brain areas. In this context, an observable reduction of apparent tracer uptake are often the result of a combination of atrophy and reduced tracer uptake. Therefore, to reveal true alterations in tracer uptake, PVE should be corrected.

Several partial volume correction (PVC) approaches have been proposed which reduce PVEs by compensating for spatial resolution-related effects on the PET image, thereby improving the quantitative accuracy of the data (for a detailed review, see Erlandsson et al., 2012). Most techniques can be divided into categories: PVC implemented during the PET reconstruction or applied as a post-reconstruction step. PVC implemented during reconstruction is often referred to as resolution recovery (RR) and must be supported by the scanner manufacturer. Since the latter method (i.e. post-reconstruction) is more feasible to implement, it is the most used to correct for PVEs.

Post-reconstruction image restoration techniques can be classified into those that are region-of-interest based and those that are image based. Region-of-interest based methods treat each region in its entirety, only attempting to recover its mean value. The primary disadvantage of a region-of-interest based method is that it only provides a PVC mean value for each target region but does not supply a PVC image. Contrastingly, an image-based method performs PVC for each voxel in the target regions, with examples including the Müller-Gärtner (MG) method (Muller-Gartner et al., 1992), 'iterative Yang' (Erlandsson et al., 2012) and Richardson-Lucy (RL).

Both MG and IY rely on parcellated MRI data, whereas RL is a deconvolution technique. The MG method targets only grey matter voxels, correcting them on a voxel-by-voxel basis, whilst white matter and cerebrospinal fluid are treated as background regions. MG requires a true mean estimate of white matter activity and assumes a uniform tracer uptake within the white matter, with the contribution from the cerebrospinal fluid considered to be zero. It also does not compensate for spill-in and spill-out between grey matter regions. IY, on the other hand, applies PVC to the whole image and corrects for PVE amongst grey matter regions. Here, the correction map is iteratively updated, with the final correction map being applied to the original PET image to conduct voxel-based PVC. RL assumes a Poisson noise model and is based on a multiplicative correction step, correcting for spillover from one region to another. The advantage of this technique is that it does not require segmentation, but the level of correction achievable is limited and it can lead to noise-amplification. MG and IY algorithms have been the most widely used within the [^{11}C]UCB-J PET literature to correct for PVEs.

A recent study by Lu et al. (2021) explicitly compared the effects of these two PVC algorithms in samples of AD and healthy controls and concluded that IY provides a theoretically more accurate PVC method than MG given the underlying assumptions of each method (Lu et al., 2021). Below is a summary of the assumptions made in these algorithms and how these may be violated, which could cause inaccurate corrections:

Assumption (1): MG assumes uniformity of tracer uptake in the white matter, whereas IY treats grey matter, white matter, and CSF equally. However, [^{11}C]UCB-J uptake in the entire white matter does not appear to be uniform, signified by the fact that the mean [^{11}C]UCB-J V_T after IY in the whole white matter was approximately two times higher than that of the centrum semiovale, which was used as a white matter value for MG PVC (Lu et al., 2021).

Assumption (2): MG assumes that the contribution from cerebrospinal fluid is null, thus correction for potential spill-in from this compartment is usually omitted. However, a lumbar

puncture performed on a rhesus macaque following injection with [^{18}F]SynVesT-1 revealed that activity in lumber cerebrospinal fluid was greater than zero (Lu et al., 2021). Since [^{18}F]SynVesT-1 has comparable kinetic properties with [^{11}C]UCB-J, it is likely that [^{11}C]UCB-J activity is also not absent in the CSF. In fact, activity in the brain ventricles is anticipated to be higher than that observed in lumbar cerebrospinal fluid. On the other hand, IY treats CSF (both in the ventricles and cortical surface) as separate regions.

Assumption (3): MG does not correct for inter-regional spill-over effects between discrete grey matter regions, with spill-in and spill-out between neighbouring grey matter regions potentially being an important component to correct for. Contrastingly, IY corrects for each parcellated region, including between grey matter regions.

Prior to proceeding with a PVC method, I conducted a small investigation to compare the effects of MG, IY and RL algorithms in my sample of subjects to determine which may be most suitable, particularly since I would be applying PVC directly onto the parametric [^{11}C]UCB-J V_T maps, as opposed to each dynamic frame as done by Lu et al. (2021). This comes with the advantage of greatly reducing the computational demand and potential errors of correcting noisy individual images. Here, I employed the PETPVC toolbox (Thomas et al., 2016), which an open-source, publicly available toolbox (https://github.com/UCL/PETPVC) that comprises a suite of PVC techniques that can be applied to PET data. To increase accuracy of PVC, it was performed in native T1 space. Here, [^{11}C]UCB-J parametric V_T maps and the CIC atlases generated at the end of the PET pipeline were linearly registered to respective T1-weighted MRIs using FSL's tool FLIRT (Jenkinson et al., 2002). First, a transformation matrix was generated by estimating the parameters of registering the 'final space' T1-weighted MRI to the T1-weighted MRI in native space using the correlation ratio cost function. This transformation matrix was then applied to the [^{11}C]UCB-J parametric V_T maps and the CIC atlases to coregister these images to the T1-weighted MR images in native space using the trilinear and nearest

neighbour interpolation methods, respectively. Finally, individual CIC atlases were masked with each subject's grey matter, white matter, and cerebrospinal fluid segmented tissue volume images. For the MG method, grey matter and white matter regions were merged to produce whole grey and white matter maps. All maps were converted into 4D volumes, where each 3D volume represented a segmented region for IY or a tissue class for MG. Regions that were being assessed were the frontal, temporal, parietal and occipital lobes, as well as the striatum, thalamus and substantia nigra.

Briefly, MG corrected for PVEs by estimating the average activity in the white matter and using it to scale the white matter estimates. These estimates were then convolved by the PSF of 8mm and subtracted from the original PET image, removing the spill-in activity from the white matter to the grey matter. The resultant image was then divided by the grey matter tissue mask, which had been convolved by the PSF on a voxel-by-voxel basis to correct for PVEs in the grey matter. The final image contained grey matter voxels only. For IY, a correction image was created iteratively. Using the PVC image from the previous iteration, regional means were computed, and a piecewise uniform image was built. The image was smoothed with a FWHM Gaussian PSF kernel of 8mm and the correction image was calculated as the ratio of the unsmoothed to smoothed images. RL assumes a multiplicative Poisson noise model and was performed without any priors with 10 deconvolution iterations. In each iterative step, the measured image was compared to the current version of the corrected image that was convolved with the PSF of 8mm.

To gain an insight into the effects of these PVC techniques, V_T comparisons were made for uncorrected data (No-PVC), and data corrected by MG, IY and RL for each group. For correlation analyses of regional V_T vs volume and percentage change due to PVC vs volume, all samples were pooled together and linear regression models with a bootstrapping approach were

employed, with 10, 000 iterations. Intuitively, we may expect a reduced associations between PVC-V_T and volume, and for percentage change vs volume, we may expect to observe negative correlations i.e., the larger the region, the smaller the correction factor. Finally, coefficients of Variation (CoV) across subjects were calculated per region per diagnostic group. The tables and figures can be found in the Appendix A.

These analyses enabled assessment of the most suitable PVC method and so are most appropriately presented here. In brief, the findings were largely similar to those reported by Lu et al. (2021) in that MG increased all grey matter values more than IY in both groups (which increased values more than RL), all PVC techniques induced a reduction in the association between V_T and volume, although RL had the least reduction, and MG was negatively associated with volume in the substantia nigra (which would be an argument against its use). Similarly, percentage change of MG was negatively associated with volume, but the association between volume and IY was non-significant, although still very similar to MG. Percentage change of RL had a weak negative association with volume. The CoVs for both MG and IY were comparable and in line with the uncorrected V_T values, highlighting that PVC was not artificially biasing the between-subject variability. Overall, both MG and IY appeared to be quite comparable in their performance, whereas RL appeared to be the most inferior technique out of the three. Thus, taken together with the assumptions behind each PVC method, I opted for IY algorithm for the [^{11}C]UCB-J PET data in this study following the same protocol outlined above with PETPVC toolbox. Since PVC was performed on the [^{11}C]UCB-J V_T parametric maps, [^{11}C]UCB-J parametric V_T maps uncorrected for PVC (no-PVC) were also analysed as a supplementary analysis and this can be found in Appendix B.

2.2.5 ASL MRI preprocessing

pASL data were processed by means of the Bayesian Inference for ASL MRI (BASIL) toolbox (Chappell et al., 2009), a collection of tools in FMRIB's Software Library (FSL) version 6.0.1. First, motion correction was applied to the timeseries of pASL images, corrected via a rigid body algorithm in MCFLIRT (Jenkinson et al., 2002). Next, a label-control subtraction was performed to remove the static tissue contribution. From the resulting time series, the relative CBF was calculated by inversion of the standard model for delivery of the ASL label using a Bayesian model inversion technique. Relative CBF (in scanner native units) was then converted to absolute physiological units (mL/100g/min) by estimating the equilibrium magnetisation of arterial blood. Absolute physiological measures were used as the metric of interest in this analysis as they provide the most meaningful comparison with volume and [^{11}C]UCB-J V_T from the same region.

The structural T1-weighted MR images were pre-processed using the fsl_anat tool according to the following pipeline: i) reorientation to the standard (MNI) orientation [fslreorient2std], ii) bias-field correction [FAST], brain-extraction [BET] and tissue segmentation [FAST].

The generated CBF images were corrected for the presence of partial volume effects using FSL BASIL's adaptive spatial prior approach (Chappell et al., 2011). This method exploits differences in the kinetics between grey and white matter signals, PV estimates of the tissue type and adaptive spatial regularisation. The correction of grey matter CBF has been shown to be comparable to a linear regression approach, whilst preserving spatial detail in the CBF image (Chappell et al., 2011). To proceed with partial volume correction, the T1-weighted images were coregistered to ASL image space using FSL's tool FLIRT. The same transformation matrix was applied to convert the high-resolution tissue probability maps (generated by FAST) to the low-resolution space of the ASL data. Spatial PVC was then performed as part of the FSL BASIL

toolbox, generating PVC CBF maps of grey matter perfusion. Next, the CBF maps were coregistered to the structural T1-weighted image in multiple steps, exploiting the Boundary-Based Registration (BBR) cost function and then normalised to MNI space using the DARTEL flow fields generated previously. Finally, normalised CBF maps were smoothed using an 8mm full width at half maximum (FWHM) kernel. Regional CBF values were extracted using the CIC atlas using fslstats.

2.2.6 Statistical analysis

Statistical analysis and graph illustration were performed with SPSS (version 20 Chicago, Illinois, USA) and GraphPad Prism (version 6.0c) for MAC OS X, respectively. Parametric statistical tests were employed. Whilst conventional statistical guidelines would recommend using nonparametric approaches for small sample sizes, this is not an equivocal consensus. In fact, the choice of a statistical test (parametric vs nonparametric), especially when sample sizes are small, should be predicated upon the distribution of the data. If a nonparametric test is chosen for data that follows a Gaussian distribution, it is likely that insignificant *p*-values will be returned, even when large differences are present in the data. Thus, using a nonparametric test on data that follows a Gaussian distribution can be misleading and have too little power to detect an effect. Given that the data roughly followed a Gaussian distribution, the most appropriate tests to perform in this instance were parametric tests. Details of individual statistical analyses performed can be found under the Methods section of each chapter.

3 Synaptic density changes in Parkinson's disease: An in vivo [^{11}C]UCB-J PET study

3.1 Introduction

Synapses are fundamental for neurotransmission, with a healthy human brain estimated to contain approximately 150-164 trillion synapses in the cerebral neocortex (Pakkenberg et al., 2003, Tang et al., 2001). Mounting evidence suggests that synaptic abnormalities in PD precede neuronal loss and Lewy body formation and that these synaptic deficits are closely related with clinical symptoms (Chung et al., 2009, Nikolaus et al., 2009, Calo et al., 2016, Henstridge et al., 2016, Bereczki et al., 2016, Vallortigara et al., 2014). Research into the continuum of genetic contributors have demonstrated that most DNA variants with high effect sizes in PD, such as *SNCA*, *LRRK2* and *PINK1* play a critical role in presynaptic function, with corresponding genetic models displaying a disruption of synaptic plasticity and neurotransmitter function (Belluzzi et al., 2012, Abeliovich and Gitler, 2016). In sporadic cases, evidence suggests that the pathological process of synucleinopathies may commence presynaptically, as post-mortem studies have revealed that at least 90% of aggregated α-synuclein is localised in presynaptic terminals that was accompanied by extensive loss of dendritic spines at the post-synaptic area (Kramer and Schulz-Schaeffer, 2007, Schulz-Schaeffer, 2010), with aggregation of α-synuclein and neurodegeneration potentially beginning within distal axons and propagating to neuronal somata (Orimo et al., 2008). Furthermore, the initial aggregation and misfolding of α-synuclein in presynaptic terminals has been shown to induce a loss of synaptic vesicle-associated proteins (Bajic et al., 2012, Orimo et al., 2008). Taken together, these findings not only illustrate that presynaptic α-synuclein aggregation impinges on synaptic function and axonal integrity, but that this pathology may initiate at the presynaptic level. Given that synaptic dysfunction is now

recognised to be heavily implicated in synucleinopathies, gaining insight into the disease pathogenesis and progression of synaptic loss and/or dysfunction has the potential to facilitate the characterisation of disease pathogenesis, monitor disease process and assess treatment efficacy.

However, the investigation of PD as a primary synaptopathy and the dynamic changes of synapses has been severely hampered by a technical inability to study synapses in the human brain, as regional synaptic density has traditionally been estimated via immunohistochemistry, stereology, and electron microscopy, which rely heavily on the examination of brain tissue from autopsy or surgical resection. The recently developed non-invasive imaging technique, [^{11}C]UCB-J PET, is proposed to make feasible the quantification of the density of presynaptic terminals *in vivo* given its high specificity for synaptic vesicle protein 2A (SV2A). SV2A belongs to a family of glycoproteins that are localised to synaptic vesicles of neuronal or endocrine cells and is one of three isoforms, amongst SV2B and SV2C. Each isoform is differentially expressed throughout the adult brain, with SV2A being the only member of the SV2 family that is ubiquitously expressed in virtually all presynaptic terminals, irrespective of neurotransmitter type, including both excitatory and inhibitory synapses (Bajjalieh et al., 1994, Bajjalieh et al., 1993, Buckley and Kelly, 1985, Dong et al., 2006, Gronborg et al., 2010). As SV2A has a relatively fixed number of copies per vesicle (Bajjalieh et al., 1993), a reduction in [^{11}C]UCB-J uptake will likely be reflective of a decrease in synaptic vesicles and be ascribable to synaptic density loss.

A limited number of studies employing [^{11}C]UCB-J PET have demonstrated it to be sensitive to lower synaptic density in AD (Chen et al., 2018), temporal lobe epilepsy (Finnema et al., 2018), primary tauopathies (Holland et al., 2020) and major depressive and post-traumatic stress disorder (Holmes et al., 2019). To date, three studies have employed [^{11}C]UCB-J PET to assess synaptic density *in vivo* in PD (Delva et al., 2020, Matuskey et al., 2020, Wilson et al., 2020). The

first [^{11}C]UCB-J study in PD patients found the largest reduction of [^{11}C]UCB-J binding in the substantia nigra, which was confirmed using postmortem ^{3}H-UCB-J autoradiography (Matuskey et al., 2020). This finding was replicated in an independent sample of patients with early PD by Delva et al. (2020), though they did not observe the additional significant reductions in the red nucleus, locus coeruleus and parahippocampal gyrus. Furthermore, both studies reported an absence of significant SV2A loss in the striatum, and did not find any associations between [^{11}C]UCB-J binding and clinical variables (Delva et al., 2020, Matuskey et al., 2020). Finally, within drug-naïve PD patients, Wilson and colleagues reported widespread significant reductions of [^{11}C]UCB-J uptake in subcortical and brainstem nuclei, as well as across all cortical lobes.

3.2 Aims and hypotheses

In this cross-sectional study, I employed [^{11}C]UCB-J and high-resolution PET, T1-weighted MRI and ASL-MRI to investigate synaptic density, grey matter volume and perfusion alterations, respectively, in two independent samples of PD patients (medicated and unmedicated) and healthy participants. This study extends previously published studies by employing a multimodal approach and including and directly comparing drug-naïve PD patients to those who are taking dopamine replacement therapy (treated PD). The aims of this study are the following:

1) To determine localised differences of synaptic density, grey matter volume and perfusion in drug-naïve PD patients and those on treatment compared to healthy controls and each other.
2) To explore the intra-regional linear relationship between [^{11}C]UCB-J binding for synaptic density and grey matter volume and perfusion within each patient group.
3) To evaluate the clinical relevance of SV2A binding by interrogating its association with motor and non-motor symptoms.

I hypothesised that drug-naïve PD patients would exhibit a widespread relative loss of synaptic density compared to healthy controls, concomitant with negligible grey matter volumetric reductions. I expected to observe the largest reductions in the substantia nigra and striatum, although given that dopaminergic denervation is not uniform across the striatum in PD, I expected to observe a larger magnitude of reduction in postcommissural putamen (sensorimotor) that is affected early in the disease course (Morrish et al., 1995). Whilst chronicity of disease would lead one to hypothesise that synaptic density would be further reduced in treated PD, if L-DOPA does in fact exert plasticity-promoting effects, then one could anticipate that that would be reflected by an increase of SV2A expression levels in treated PD patients, whereby they may exhibit comparable, if not higher, SV2A expression levels to healthy controls, which would likely be elevated when compared to drug-naïve PD. As mentioned in the introductory chapter, since synapses are the brain's major energy consumers, I may expect to observe a linear association between perfusion and synaptic density whereby early synaptic dysfunction and/or reduction would be associated with hypoperfusion. On the other hand, since the neurovascular unit is disrupted in PD, the blood supply to synapses may not be appropriately regulated, potentially leading to neurovascular 'uncoupling', thus there may be a discordance between brain areas exhibiting hypoperfusion and synaptic density reduction. Finally, I expected to observe associations between regional synaptic density alterations and motor and non-motor symptoms in both groups, whereby reduced synaptic density would be associated with worse symptom severity.

3.3 Methods

3.3.1 Participants

Details about participants have previously been described in detail in Chapter 2. Within this chapter, findings for eleven drug-naïve PD patients, ten medicated PD patients and thirty-five healthy controls are presented.

3.3.2 Clinical assessments

Details about clinical assessments have previously been described in detail in Chapter 2.

3.3.3 MRI acquisition and pre-processing.

Details regarding MRI acquisition parameters and pre-processing pipelines have previously been described in detail in Chapter 2, Section 2.2. In this chapter, I present grey matter volumetric measures estimated with an atlas-based approach corresponding to the regional estimates of [^{11}C]UCB-J V_T and partial volume corrected quantitative CBF estimates.

3.3.4 [^{11}C]UCB-J PET acquisition, processing and quantification

Details about PET acquisition parameters, PET processing and kinetic modelling have previously been described in detail in Chapter 2, Section 2.2. In this chapter, [^{11}C]UCB-J V_T estimates based on the mean time-activity curve of each region are presented as the main outcome measure. As a secondary outcome measure, regional estimates sampled from [^{11}C]UCB-J parametric V_T maps that had been corrected for partial volume effects following the iterative Yang (IY) approach (Erlandsson et al., 2012) are described in the results. Further detail of these results can be found in Appendix B.

3.3.5 Statistical analysis

Statistical analysis and graph illustration were performed with SPSS (version 20 Chicago, Illinois, USA) and GraphPad Prism (version 6.0c) for MAC OS X, respectively. For all variables, variance homogeneity and Gaussianity were tested with Shapiro-Wilk tests. Regional [^{11}C]UCB-J V_T, grey matter volumes and quantitative CBF measures were transformed using the natural logarithmic function (ln) to ensure they conformed to a normal distribution. Levene's test was employed to assess the equality of variances. Analysis of covariance (ANCOVA) was employed to assess

between-group differences in clinical variables, regional volumes, quantitative perfusion measures (including global CBF) and [^{11}C]UCB-J V_T, with age and gender included as covariates and global CBF included as an extra covariate when assessing between-group differences in regional absolute perfusion for both region-of-interest and voxel-wise analyses. It is important to note that in certain settings, a hierarchical approach is taken whereby one only proceeds with post-hoc tests if the omnibus F-test, which tests the null hypothesis of no mean differences across all groups, is significant. However, in this study, in the context where the omnibus F-test was not found to be significant, I proceeded with post hoc exploratory analyses. This is because there is a paucity of [^{11}C]UCB-J V_T studies comparing these groups of patients given that [^{11}C]UCB- PET is a relatively novel radioligand, and PET studies are expensive and challenging to orchestrate in these groups of patients. Therefore, it would be useful to provide findings that may be indicative of an effect as there is currently a gap in the literature for some of the group comparisons made. Furthermore, the data presented here is unique and the sample sizes are small, and so future studies wishing to investigate synaptic density in these groups will be well-informed about potential effect sizes. Therefore, by proceeding with post hoc analyses regardless of if the omnibus F-test is significant or not, the exploratory nature of many of the findings may facilitate hypothesis generation and inform power calculations for future studies. Throughout the thesis, I have endeavoured to provide sufficient information to support power calculations for future studies.

Within each group, linear regressions were employed to assess the relationship between regional grey matter volumes, quantitative perfusion measures and [^{11}C]UCB-J V_T and the relationship between regional [^{11}C]UCB-J V_T and clinical assessments were interrogated using Pearson's correlation.

p values for each variable were calculated following Benjamin-Hochberg correction to control the false discovery rate (FDR), with Q=0.1. Multiple comparison corrections were not performed on secondary analyses given their exploratory nature. All data are presented as mean ±SD and the α level for significance was set for all comparisons at p<0.05.

Subsequent voxel-level between-group comparisons of grey matter volume, absolute CBF and [^{11}C]UCB-J V_T, were performed in SPM12 in MATLAB 2015b mainly to illustrate the between-group differences unconstrained by the ROI definitions. These comparisons included a one-way ANOVA between healthy control subjects, drug-naïve PD, and treated PD patients with age and gender included as covariates and global CBF included as an extra covariate when assessing between-group differences in absolute perfusion. The cluster-defining threshold at the voxel-level analysis was set at p<0.005, uncorrected, with a minimum cluster size of 40 voxels. Voxels that survived the threshold were overlaid on a rendered brain of healthy control subjects from SPM12.

Here, both region-of-interest and voxel-wise analyses were performed because of their distinct assumptions and advantages. A region-of-interest approach is based on the assumption that an observed effect within a region is relatively homogenous, thus we assume that the mean response is a fair reflection of the region's activity. The advantages of a region-of-interest approach is that the SNR is improved, and the problem of multiple comparisons is minimised. However, it is possible that the spatial distribution of the effect is not homogenous across the anatomical structure and the process of averaging across the entire region may obscure a small, localised effect, as the signal from a small proportion of voxels may be grouped together with the remaining 'inactive' voxels, leading to lower mean measures. It could also be the case that the spatial patterns of a localised effect may cross anatomical boundaries, which would reduce the sensitivity of region-of-interest based approaches. Therefore, a voxel-wise approach could

potentially identify subtle, spatially discrete areas of the effect that may be 'washed away' by a region-of-interest approach. However, voxel-wise analyses have low SNR and being assured of control of false positives can result in potential type II errors without larger samples.

Please note it is not unusual that a region-of-interest and voxel-wise approach return different results. For example, if a significant effect is observed in the anatomically defined region without an effect detected on the voxel level, then this is most likely reflecting differences in SNR and/or issues with multiple comparisons correction. If a significant voxel-wise effect is observed without a mean effect observed in the region-of-interest, then this likely speaks to the fact that the localised effect is spatially restricted to a small proportion of voxels and/or is not sufficiently moderate in size whereby averaging the signal over an anatomically defined region results in a dilution of the effect.

3.4 Results

3.4.1 Demographic and clinical characteristics

Healthy controls did not differ from drug-naïve PD patients in terms of age (*MD*=3.24, 95% CI [-3.42, 9.9], p=0.33) and treated PD patients in terms of age (*MD*=0.36, 95% CI [-6.55, 7.26], p=0.92) and gender (X^2 (2, N=56)=1.41, p=0.50); drug-naïve PD patients and treated patients were also similar in age (*MD*=-2.88, 95% CI [-11.3, 5.53], p=0.36). Compared to drug-naïve PD patients, treated PD patients had longer disease duration (*MD*=31.13, 95% CI [11.22, 51.01]), worse motor symptom severity (MDS-UPDRS Part III: *MD*=10.28, 95% CI [4.62, 15.95]; H&Y: *MD*=0.48, 95% [0.13, 0.84]), higher burden of non-motor symptoms (MDS-UPDRS Part I: *MD*=3.03, 95% CI [0.49, 5.57]) and an overall greater disease burden (MDS-UPDRS Total: *MD*=14.09, 95% CI [3.89, 24.29]). Remarkably, treated patients had worse cognition (MoCA:

MD=-2.00, 95% CI [-3.56, -0.43]) when compared to drug-naïve PD patients. All *p* values, in addition to means and standard deviations can be found in Table 3.1.

Table 3.1. Clinical characteristics of drug naïve PD patients and treated PD patients

Characteristic (mean ±SD)	Drug naïve PD	Treated PD	P value
No. (M/F)	11 (9M/2F)	10 (7M/3F)	0.50
Age (years)	58.8 ± 9.0	61.7 ± 6.4	0.36
Disease duration (months)	16.5 ± 11.7	50.4 ± 31.4	**0.004***
Education (years)	16.9 ± 3.3	17.0 ± 2.5	0.92
LEDD (mg)	0.0 ± 0	467.6 ± 227.6	-
Patients treated with:			
L-DOPA	-	10	-
Dopamine agonist	-	5	-
MAO-B inhibitor	-	4	-
H&Y	1 ± 0	1.5 ± 0.5	**0.011***
MDS-UPDRS I	3.4 ± 2.1	6.3 ± 3.2	**0.022***
MDS-UPDRS II	6.0 ± 5.3	5.9 ± 3.3	0.93
MDS-UPDRS III	14.5 ± 6.4	24.8 ± 6.1	**0.001***
MDS-UPDRS Total	23.8 ± 11.0	37.6 ± 9.5	**0.010***
SCOPA-AUT	7.0 ± 4.4	6.6 ± 4.0	0.74
PD NMS Questionnaire	3.5 ± 2.3	6.1 ± 4.0	0.094
ESS	5.0 ± 2.97	5.7 ± 1.9	0.80
RBDQ	1.5 ± 0.8	3.2 ± 3.4	0.12
PDSS	130.7 ± 11.1	124.6 ± 18.1	0.29
King's PD Pain Questionnaire	0.5 ± 0.7	1.1 ± 1.3	0.19
UPSIT	23.3 ± 8.2	20.3 ± 6.7	0.48
MMSE	29.3 ± 1.0	29.3 ± 0.8	0.55
MoCA	29.6 ± 1.2	27.6 ± 1.9	**0.016***
GDS	4 .0 ± 4.8	4.0 ± 4.8	0.92

Abbreviations: H&Y=Hoehn and Yahr scale; MDS-UPDRS=Movement Disorder Society Unified Parkinson's Disease Rating Scale; MMSE=Mini Mental Status Examination; MoCA=Montreal Cognitive Assessment; PDSS: Parkinson's disease sleep scale; PD NMS Questionnaire=Parkinson's disease Non-Motor Symptom Questionnaire; ESS: Epworth Sleepiness Scale; RBDQ=REM Behaviour Sleep Disorder Questionnaire; SCOPA-AUT=Scales for Outcomes of Parkinson's disease–Autonomic; GDS=Geriatric Depression Scale

*p<0.05 between drug-naïve PD and treated PD, FDR-corrected

3.4.2 Grey matter volume

3.4.2.1 Regions-of-interest analyses

Statistically significant differences in GM volume between at least two groups were identified in the dorsolateral prefrontal cortex ($F(2,51)=5.23$, $p=0.009$), nucleus accumbens ($F(2,51)=3.88$, $p=0.027$), parahippocampal gyrus ($F(2,51)=4.41$, $p=0.017$), insula cortex ($F(2,51)=4.83$, $p=0.012$), and amygdala ($F(2,51)=3.47$, $p=0.038$). Whilst there was evidence of grey matter (GM) volume differences in treated PD compared to both healthy controls and drug-naïve PD patients, localised higher GM volume was more frequently observed. Pairwise comparisons showed that compared to healthy controls, treated PD patients exhibited significantly greater GM volume in the prefrontal dorsolateral cortex and structures of the limbic system, whereas significantly larger GM volume in the amygdala and nucleus accumbens was observed when these patients were compared to drug-naïve PD patients (Table 3.2; Figure 3.1). No differences in volume were observed between drug-naïve PD patients and healthy controls Table 3.2; Figure 3.1).

Table 3.2. Group comparison of GM volumes in healthy controls, drug-naïve PD patients and treated PD patients

Volume, mm^3 (mean ±SD)	HC n=35	Drug naïve PD n=11	Treated PD n=10	P value HC vs drug-naïve PD	P value HC vs treated PD	P value Drug-naïve PD vs treated PD
Brainstem	4288 ± 662	4560 ± 515	4623 ± 545	0.59 (+6%)	0.09 (+8%)	0.33 (+1%)
Substantia nigra	77 ± 34	76 ± 28	85 ± 27	0.83 (0%)	0.35 (+10%)	0.36 (+12%)
Caudate	4809 ± 694	4779 ± 640	5038 ± 511	0.30 (-1%)	0.27 (+5%)	0.088 (+5%)
Precommissural putamen	3600 ± 422	3621 ± 420	3645 ± 344	0.38 (+1%)	0.89 (+1%)	0.39 (+1%)
Postcommissural putamen	3133 ± 360	3045 ± 404	3044 ± 311	0.10 (-3%)	0.33 (-3%)	0.6 (0%)

Thalamus	7504 ± 1165	7853 ± 914	7936 ± 871	0.72 (+5%)	0.20 (+6%)	0.45 (+1%)
Precentral gyrus	29882 ± 4291	31682 ± 3357	30904 ± 2446	0.53 (+6%)	0.32 (+3%)	0.76 (-3%)
Postcentral gyrus	20152 ± 2603	21504 ± 2279	21006 ± 2038	0.33 (+7%)	0.25 (+4%)	0.86 (-2%)
Supplementary motor area	5440 ± 772	5681 ± 536	5615 ± 583	0.87 (+4%)	0.44 (+3%)	0.62 (-1%)
Dorsolateral prefrontal cortex	73204 ± 9223	78411 ± 5033	80798 ± 7074	0.26 (+7%)	**0.002*** **(+10%)**	0.094 (+3%)
Superior parietal lobe	96155 ± 13080	103820 ± 9520	100918 ± 9034	0.17 (+8%)	0.14 (+5%)	0.91 (-3%)
Temporal lobe	84041 ± 11606	88096 ± 7656	88671 ± 7900	0.90 (+5%)	0.065 (+6%)	0.16 (+1%)
Occipital lobe	72671 ± 9223	76421 ± 7379	76419 ± 8040	0.72 (+5%)	0.11 (+5%)	0.31 (0%)
Cerebellum	98563 ± 9695	102388 ± 8237	101827 ± 9446	0.71 (+4%)	0.29 (+4%)	0.56 (0%)
Exploratory regions-of-interest						
Nucleus accumbens	2973 ± 329	3007 ± 228	3144 ± 228	0.30 (+1%)	**0.028$** **(+6%)**	**0.010$** **(+5%)**
Parahippocampal gyrus	9158 ± 1171	9653 ± 754	9993 ± 822	0.54 (+5%)	**0.005$** **(+9%)**	0.059 (+4%)
Amygdala	3842 ± 453	3857 ± 344	4023 ± 266	0.14 (0%)	0.083 (+5%)	**0.011$** **(+4%)**
Insular cortex	12697 ± 1653	13530 ± 1283	13977 ± 1228	0.35 (+7%)	**0.003$** **(+10%)**	0.081 (+3%)
Anterior cingulate	29389 ± 4789	31320 ± 3970	32124 ± 3136	0.55 (+7%)	**0.026$^** (+9%)	0.17 (+3%)
Posterior cingulate	11198 ± 1912	12150 ± 1575	11805 ± 1288	0.33 (+9%)	0.19 (+5%)	0.76 (-3%)

**p<0.05, FDR-corrected; $p<0.05, uncorrected; ^ANCOVA omnibus test was not statistically significant*

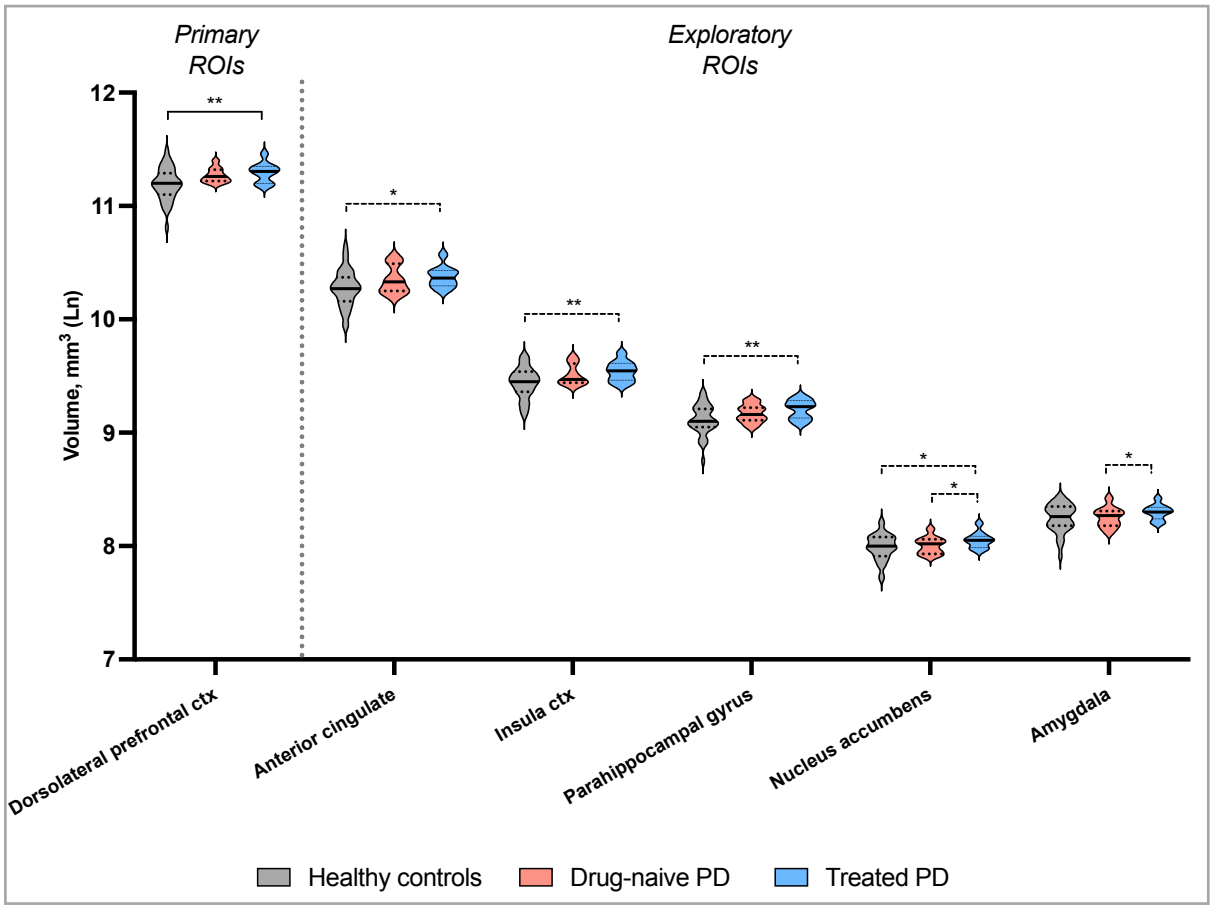

Figure 3.1. Violin plots illustrating cross-sectional differences in volume between healthy controls, drug-naïve and treated PD patients. Treated PD patients exhibited larger grey matter volume across these regions-of-interest compared to healthy controls. ***p<0.001; **p<0.01; *p<0.05; ---- uncorrected p value. ROIs=regions-of-interest; V_T=volume of distribution; Ln=natural log transformation. Exploratory regions-of-interest=additional brain areas that were analysed for exploratory purposes. Multiple comparison corrections were not performed on these secondary analyses.

3.4.3 Grey matter volume

3.4.3.1 Voxel-wise analyses

On the voxel-level, larger grey matter volume was observed in the bilateral dorsolateral prefrontal cortex, as well as the right insula and orbitofrontal cortex in treated PD patients compared to healthy controls (Table 3.3; Figure 3.2). No significant voxel-wise differences in grey matter volume were observed in drug-naïve PD patients compared to healthy controls or between medicated and unmedicated PD patients.

Table 3.3. Areas of higher grey matter volume in treated PD patients compared to healthy controls. Local maxima are shown in MNI coordinates (in mm).

Cluster size	Region	MNI coordinates			*T*	$P_{uncorrected}$
Treated PD > healthy controls						
4705	Dorsolateral prefrontal cortex R	32	66	8	6.17	<0.001*
579	Insula R	38	16	0	3.46	0.005
	Orbitofrontal cortex R	38	18	-14	3.38	
621	Dorsolateral prefrontal cortex L	-26	30	54	4.18	0.004

**Survived FWE cluster-level correction; p<0.005; Height threshold T = 2.68; Extent threshold = 40 voxel*

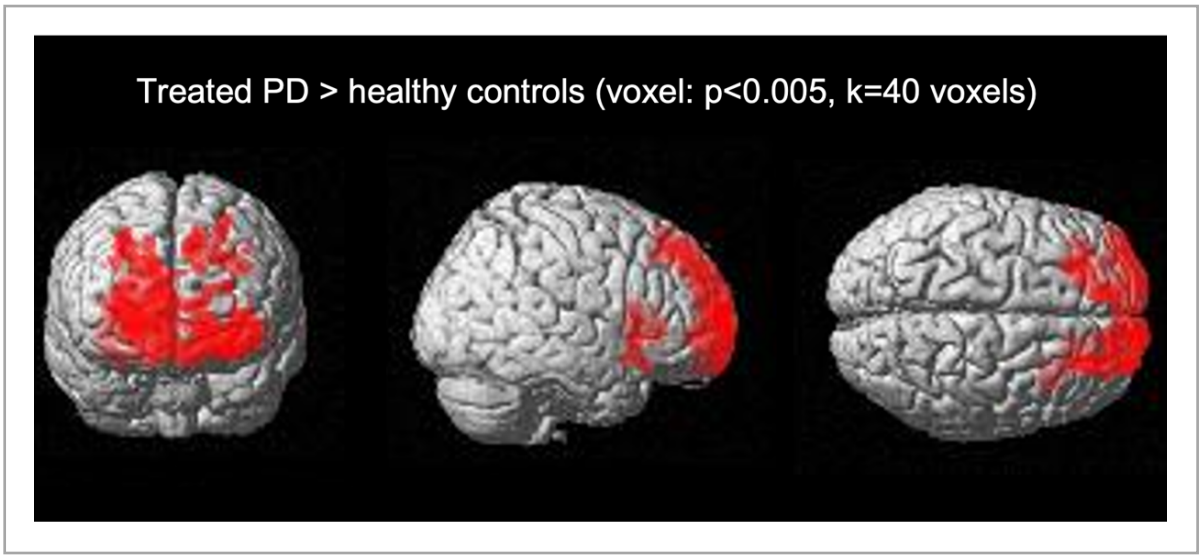

Figure 3.2. Voxel-wise grey matter differences in medicated PD patients compared to healthy controls. Treated PD patients exhibited larger grey matter volume in the bilateral dorsolateral prefrontal cortex, right insula, and right orbitofrontal cortex.

3.4.4 Cerebral blood flow

3.4.4.1 Regions-of-interest analysis

There was a statistically significant difference in global CBF between at least two groups ($F(2,51)=3.37$, $p=0.043$). Post-hoc analysis revealed that global CBF was reduced in drug-naïve PD patients with respect to the healthy controls (-16%, $p=0.021$; Table 3.4), whereas there was no significant reduction of global CBF in treated PD patients compared to healthy controls. No

regional differences in CBF were found between drug-naïve and treated PD compared to healthy controls, or between the two patient groups (Table 3.4).

Table 3.4. Group comparison of regional CBF (partial volume corrected) in healthy controls, drug-naïve PD patients and treated PD patients, after controlling for global CBF.

Cerebral blood flow ml/100g/min (mean ±SD)	HC n=31	Drug naïve PD n=10	Treated PD n=10	P value HC vs drug-naïve PD	P value HC vs treated PD	P value Drug-naïve PD vs treated PD
Global CBF	65.8 ± 9.8	55.5 ± 11.7	60.1 ± 13.7	**0.021 (-16%)**	0.12 (-9%)	0.50 (+8%)
Brainstem	43.5 ± 11	40.3 ± 11.1	44.5 ± 11.3	0.57 (-7%)	0.15 (+2%)	0.48 (+10%)
Substantia nigra	34.7 ± 12.4	30.7 ± 14	35.6 ± 10.1	0.62 (-11.5%)	0.43 (+2%)	0.28 (+16%)
Caudate	36.4 ± 7.9	33.3 ± 9.6	33.9 ± 9.7	0.34 (-8%)	0.77 (-7%)	0.56 (+2%)
Precommissural putamen	52.7 ± 10.5	45.7 ± 14.1	47.2 ± 12.7	0.99 (-13%)	0.64 (-10%)	0.71 (+3%)
Postcommissural putamen	60.8 ± 11.8	52.9 ± 16.6	54.6 ± 14.7	0.94 (-13%)	0.75 (-10%)	0.75 (+3%)
Thalamus	59.5 ± 16	53.2 ± 23.5	61.3 ± 21.1	0.96 (-11%)	0.27 (+3%)	0.34 (+15%)
Precentral gyrus	63 ± 13.2	51.7 ± 14.5	57.4 ± 18.6	0.91 (-18%)	0.89 (-9%)	0.99 (+11%)
Postcentral gyrus	58.4 ± 13.9	47.2 ± 15	52.2 ± 13.6	0.59 (-19%)	0.93 (-11%)	0.69 (+11%)
Supplementary motor area	58.2 ± 12.7	53.6 ± 13.6	51.9 ± 18.6	0.14 (-8%)	0.49 (-11%)	0.069 (-3%)
Dorsolateral prefrontal cortex	54.7 ± 10.4	45.3 ± 12.8	49.7 ± 14.7	0.96 (-17%)	0.92 (-9%)	0.98 (+10%)
Superior parietal lobe	58.7 ± 11.9	45.6 ± 14.1	52 ± 11.2	0.11 (-22%)	0.11 (-11%)	0.86 (+14%)
Temporal lobe	52.4 ± 8.9	42.3 ± 7.5	45.3 ± 11.3	0.19 (-19%)	0.76 (-14%)	0.27 (+7%)

Occipital lobe	59.6 ± 9.5	46.2 ± 15.8	54.2 ± 15	0.052 (-23%)	0.15 (-9%)	0.13 (+17%)
Cerebellum	56.5 ± 13.2	49.4 ± 13.8	59.9 ± 21.3	0.93 (-12%)	0.15 (+6%)	0.21 (+21%)
Exploratory regions-of-interest						
Nucleus accumbens	42.7 ± 8.9	39.9 ± 10.2	37.6 ± 11.5	0.15 (-7%)	0.43 (-12%)	0.063 (-6%)
Parahippocampal gyrus	69.5 ± 18.3	63.1 ± 11.1	71.9 ± 20	0.56 (-9%)	0.17 (+3%)	0.53 (+14%)
Amygdala	58.8 ± 17.7	52.8 ± 8.2	56.4 ± 20.6	0.29 (-10%)	0.74 (-4%)	0.52 (+7%)
Insular cortex	59.5 ± 13.1	52.3 ± 12.3	52.3 ± 15	0.67 (-12%)	0.4 (-12%)	0.29 (0%)
Anterior cingulate	55.9 ± 11.5	47.5 ± 10.1	49.8 ± 16.9	0.61 (-15%)	0.43 (-11%)	0.28 (+5%)
Posterior cingulate	70.0 ± 16.4	59.6 ± 14.2	69.2 ± 16.7	0.82 (-15%)	0.15 (-1%)	0.32 (+16%)

**p<0.05, FDR-corrected; $p<0.05, uncorrected.*

3.4.5 Cerebral blood flow

3.4.5.1 Voxel-wise analysis

On the voxel-level, in drug-naïve PD patients, CBF was significantly reduced in the left inferior parietal lobe compared to healthy controls (Table 3.5; Figure 3.3). Treated PD patients exhibited localised hyperperfusion in the left cerebellum, left superior parietal and left occipital lobe compared to drug-naïve PD patients (Table 3.5; Figure 3.3). No significant voxel-wise differences in CBF were observed in treated PD patients compared to healthy controls.

Table 3.5. Areas of localised hypo- and hyperperfusion (partial volume corrected) in drug-naïve patients compared to healthy controls and treated PD patients compared to drug-naïve PD. Local maxima are shown in MNI coordinates (in mm).

Cluster size	Region	MNI coordinates			*T*	$P_{uncorrected}$
Drug-naïve PD < healthy controls						
637	Angular gyrus L	-54	-62	28	4.05	0.029
	Supramarginal gyrus L	-62	-42	26	3.22	

Treated PD > drug-naïve PD						
	Lingual gyrus L	-10	-60	0	3.96	
682	Posterior cingulate gyrus	-2	-44	12	3.36	0.025
	Cerebellum L	-2	-68	-10	3.15	

p<0.005, uncorrected; Height threshold T = 2.68; Extent threshold = 40 voxels

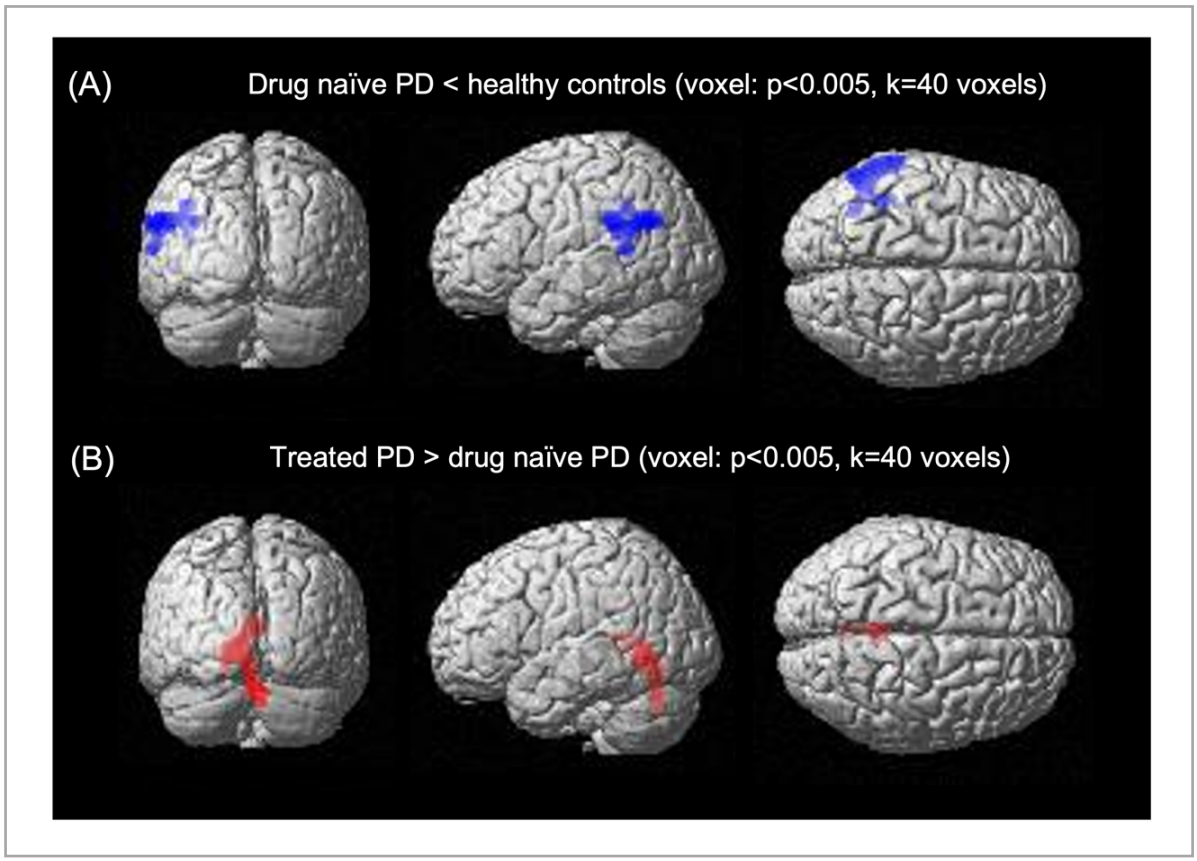

Figure 3.3. Voxel-wise CBF differences in unmedicated and medicated PD patients. (A) Comparison of drug-naïve PD patients versus healthy controls: localised hypoperfusion observed in the inferior parietal lobe (B) Comparison of treated PD patients versus drug-naïve PD patients: localised hyperperfusion observed in the cerebellum, lingual gyrus, and posterior cingulate gyrus.

3.4.6 [^{11}C]UCB-J V_T

3.4.6.1 Region-of-interest analysis

The results presented in this section are those using the regional TAC-based estimates (uncorrected for partial volume effects) and following PVC performed on the parametric [^{11}C]UCB-J V_T maps. There was high correspondence between regional TAC-based values and those obtained using the parametric maps as demonstrated by the strong correlations between

the two across all regions-of-interest (r=0.94 - >0.99), highlighting the strong agreement between TAC-based values and values obtained from parametric maps. Nevertheless, comparisons between groups using the [^{11}C]UCB-J V_T parametric map values can be found in Appendix B, although it's worth mentioning that these were largely analogous to those found using the TAC-based estimates. Please note: ANCOVA models including volume as an additional covariate were only performed for TAC-based [^{11}C]UCB-J V_T estimates that were uncorrected for partial volume effects.

One-way ANCOVA revealed that there were statistically significant differences in [^{11}C]UCB-J V_T between at least two groups in the brainstem (F(2,51)=4.44, p=0.017), substantia nigra (F(2,51)=5.29, p=0.008), caudate (F(2,51)=4.55, p=0.015), thalamus (F(2,51)=3.45, p=0.039), supplementary motor area (F(2,51)=3.44, p=0.04) and the dorsolateral prefrontal cortex (F(2,51)=3.22, p=0.048).

Post-hoc analysis revealed that compared to healthy controls, drug naïve PD patients had lower levels of [^{11}C]UCB-J V_T within subcortical and cortical regions, predominately in regions involved in the planning, control and execution of voluntary movement, as well as the parietal and temporal lobes (see Table 3.6 for a full list of regions; Figure 3.4). These findings survived after controlling for regional volume, aside from the amygdala. Following PVC of the drug-naïve PD maps, [^{11}C]UCB-J V_T persisted to be significantly lower in all regions, except the precentral gyrus, dorsolateral prefrontal cortex, temporal lobe, cerebellum, amygdala and posterior cingulate.

Treated PD patients, on the other hand, had negligible reductions in [^{11}C]UCB-J V_T when compared with healthy controls across cortical and subcortical regions-of-interest, with the largest reduction observed in the substantia nigra (-7%; Table 3.6; Figure 3.4). While this finding

remained after controlling for volume ($p_{uncorrected}$=0.028) and following PVC (-11%, $p_{uncorrected}$=0.003), it did not survive FDR-correction for multiple comparisons.

Compared to drug-naïve PD patients, treated PD patients exhibited generally higher estimates of [^{11}C]UCB-J V_T across the brain, with significantly greater [^{11}C]UCB-J V_T in the thalamus (+11%; Table 3.6; Figure 3.4), though this finding did not survive FDR-correction for multiple comparisons or after controlling for volume ($p_{uncorrected}$=0.062) or following PVC (+9%, p=0.08).

Table 3.6. Group comparison of regional [^{11}C]UCB-J V_T in healthy controls, drug-naïve PD patients and treated PD patients

[^{11}C]UCB-J V_T, ml/cm^3 (mean ±SD)	HC n=35	Drug naïve PD n=11	Treated PD n=10	P value HC vs drug-naïve PD	P value HC vs treated PD	P value Drug-naïve PD vs treated PD
Brainstem	8.6 ± 1	7.8 ± 0.8	8.3 ± 0.4	**0.004*** **(-9%)**	0.39 (-4%)	0.10 (+6%)
Substantia nigra	8.9 ± 1	8.2 ± 0.7	8.3 ± 0.7	**0.006*** **(-8%)**	**0.035$** **(-7%)**	0.60 (+1%)
Caudate	14.4 ± 2.6	12.6 ± 2.6	13.6 ± 1.4	**0.004*** **(-12%)**	0.45 (-5%)	0.08 (+8%)
Precommissural putamen	23.7 ± 2.9	21.8 ± 2.3	22.9 ± 2.4	**0.032*^** **(-8%)**	0.45 (-3%)	0.26 (+5%)
Postcommissural putamen	21.7 ± 2.6	20.2 ± 2	21 ± 2.2	**0.047*^** **(-7%)**	0.44 (-3%)	0.32 (+4%)
Thalamus	12.5 ± 1.9	11.4 ± 1.9	12.4 ± 1.1	**0.014*** **(-10%)**	0.96 (0%)	**0.043$** **(+11%)**
Precentral gyrus	15.9 ± 2.1	14.7 ± 1.9	15.7 ± 1.5	**0.021*^** **(-8%)**	0.71 (-2%)	0.12 (+6%)
Postcentral gyrus	17.8 ± 2.4	16.1 ± 2.4	17.4 ± 1.5	**0.035*^** **(-7%)**	0.91 (-1%)	0.12 (+7%)
Supplementary motor area	17.9 ± 2.3	16.4 ± 2.1	17.7 ± 1.5	**0.012*** **(-10%)**	0.66 (-2%)	0.089 (+8%)

Dorsolateral prefrontal cortex	19.6 ± 2.4	18.6 ± 2.1	19.7 ± 2	**0.015*** **(-8%)**	0.81 (-1%)	0.075 (+8%)
Superior parietal lobe	18.1 ± 2.4	16.8 ± 2.2	17.9 ± 1.5	**0.039*^** **(-7%)**	0.89 (-1%)	0.12 (+7%)
Temporal lobe	20.2 ± 2.6	18.9 ± 2	20.3 ± 1.9	**0.041*^** **(-6%)**	0.93 (0%)	0.086 (+7%)
Occipital lobe	18.2 ± 2.4	17.1 ± 1.9	17.9 ± 1.5	0.059 (-6%)	0.72 (-2%)	0.22 (+5%)
Cerebellum	16.3 ± 2	15 ± 1.4	15.9 ± 1.4	**0.019*^** **(-8%)**	0.58 (-2%)	0.15 (+6%)
Exploratory regions-of-interest						
Nucleus accumbens	22 ± 2.9	20.6 ± 2.2	21.7 ± 2.3	0.091 (-6%)	0.85 (-1%)	0.23 (+5%)
Parahippocampal gyrus	16.4 ± 2.1	15.1 ± 1.8	16 ± 1.4	0.051 (-6%)	0.96 (0%)	0.12 (+7%)
Amygdala	17.6 ± 2.1	16.4 ± 1.5	17.4 ± 2.1	**0.046$^** **(-7%)**	0.74 (-1%)	0.18 (+6%)
Insular cortex	21 ± 2.7	19.9 ± 2.1	21.3 ± 1.9	0.058 (-6%)	0.67 (+1%)	0.063 (+7%)
Anterior cingulate	20.7 ± 2.7	19.5 ± 2.3	20.8 ± 1.8	0.06 (-6%)	0.84 (0%)	0.095 (+7%)
Posterior cingulate	20.3 ± 2.9	18.9 ± 2.4	19.9 ± 1.6	**0.044$^** **(-7%)**	0.75 (-2%)	0.17 (+5%)

**p<0.05, FDR-corrected; $p<0.05, uncorrected. ^ANCOVA omnibus test was not statistically significant*

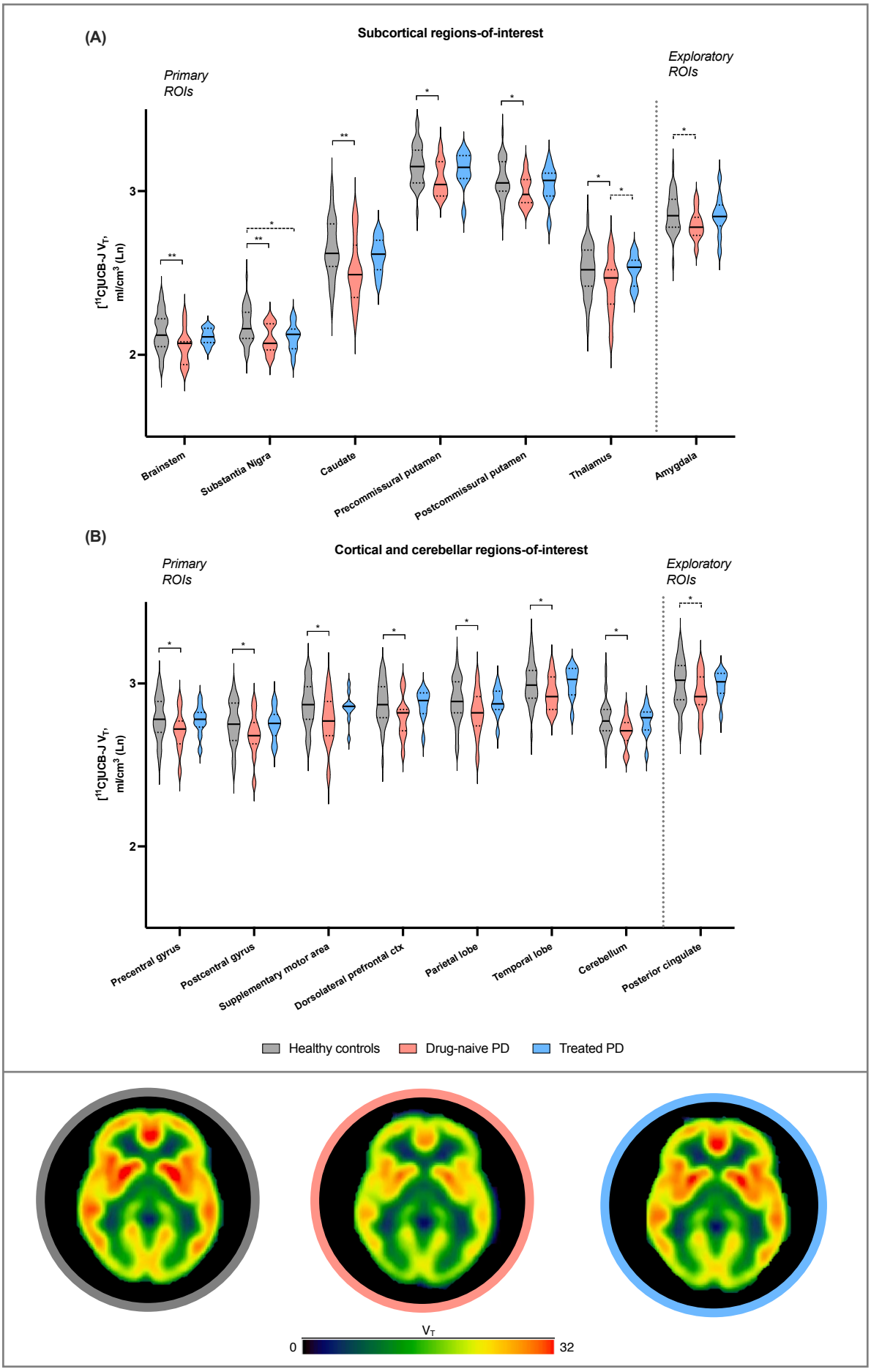
(A)
Subcortical regions-of-interest
Primary ROIs
Exploratory ROIs
[11C]UCB-J VT, ml/cm3 (Ln)
3
2
Brainstem
Substantia Nigra
Caudate
Precommissural putamen
Postcommissural putamen
Thalamus
Amygdala
(B)
Cortical and cerebellar regions-of-interest
Primary ROIs
Exploratory ROIs
[11C]UCB-J VT, ml/cm3 (Ln)
3
2
Precentral gyrus
Postcentral gyrus
Supplementary motor area
Dorsolateral prefrontal ctx
Parietal lobe
Temporal lobe
Cerebellum
Posterior cingulate
Healthy controls
Drug-naive PD
Treated PD
VT
0
32

Figure 3.4. Violin plots showing regional [^{11}C]UCB-J V_T for healthy controls, drug-naïve PD and treated PD patients. Data presented here were natural log transformed. (A) Subcortical brain areas exhibiting significant differences in [^{11}C]UCB-J V_T between groups; (B) Cortical brain areas exhibiting differences in [^{11}C]UCB-J V_T between groups. The bottom panel displays mean axial [^{11}C]UCB-J maps for controls (grey, n=35), drug-naïve PD patients (peach, n=11) and treated PD patients (light blue, n=10). ***p<0.001; **p<0.01; *p<0.05; ---- uncorrected p value. ROIs=regions-of-interest; V_T=volume of distribution; Ln=natural log transformation. Exploratory regions-of-interest=additional brain areas that were analysed for exploratory purposes. Multiple comparison corrections were not performed on these secondary analyses.

3.4.7 [^{11}C]UCB-J V_T

3.4.7.1 Voxel-wise analysis

Whole-brain voxel-wise analysis of the partial volume-corrected [^{11}C]UCB-J V_T parametric maps was largely in accordance with region-of-interest analyses, whereby small, localised clusters of [^{11}C]UCB-J V_T reduction were identified across frontal, temporal and parietal cortices, as well as larger clusters of reduction found in subcortical and brainstem brain areas in drug-naïve PD patients compared to healthy controls (Figure 3.5). The largest cluster of [^{11}C]UCB-J V_T reduction was observed in the bilateral cerebellum. For a further details, please refer to Table 3.7.

In line with the regional analyses, voxel-wise analyses revealed a cluster of higher [^{11}C]UCB-J V_T in the left thalamus in treated PD patients compared to those who were unmedicated. Additional brain areas such as the bilateral cerebellum, right medial temporal lobe, midbrain and left lentiform nucleus also exhibited small clusters of elevated [^{11}C]UCB-J V_T in treated PD patients compared to drug-naïve PD patients (See Table 3.7 for further details; Figure 3.5). There were no differences in [^{11}C]UCB-J V_T between treated PD patients and healthy controls.

Table 3.7. Areas of reduced [^{11}C]UCB-J V_T (partial volume corrected) in drug-naïve PD patients compared to healthy controls. Local maxima are shown in MNI coordinates (in mm).

Cluster size	Region	MNI coordinates			*T*	$p_{uncorrected}$
Drug-naïve PD < healthy controls						
1939	Cerebellum L	-6	-62	-38	5.68	<0.001*
	Cerebellum R	26	-40	-48	5.38	
304	Dorsal putamen L	-26	-14	4	4.48	<0.001*
	Globus pallidus L	-18	-6	-2	4.22	
178	Nucleus accumbens R	12	16	-6	3.60	<0.001
153	Midbrain	0	-22	-18	4.28	0.001
125	Thalamus L	-18	-20	16	3.95	0.002
117	Caudate L	-16	22	0	3.26	0.003
98	Insula L	-36	-6	12	3.86	0.005
	Parietal operculum L	-34	-28	20	3.81	
90	Parahippocampal gyrus L	-20	-40	-16	4.21	0.007
86	Inferior temporal gyrus L	-46	-16	-40	3.96	0.008
78	Midbrain	-4	-38	-16	4.29	0.011
	Pons	-10	-38	-26	3.96	
71	Cerebellum R	24	-50	-18	4.24	0.014
70	Cerebellum L	-14	-52	-12	3.81	0.015
67	Cerebellum L	-42	-62	-38	4.01	0.016
61	Temporal fusiform gyrus R	40	-12	-28	4.09	0.021
	Inferior temporal gyrus R	46	-18	-30	3.28	
57	Dorsolateral prefrontal cortex L	-38	46	22	3.92	0.025
51	Supramarginal gyrus L	60	-22	24	3.75	0.033
50	Supplementary motor area L	-4	2	68	3.82	0.034

49	Cerebellum L	-4	-64	-20	4.66	0.036
	Cerebellum R	4	-68	-14	4.00	
47	Cerebellum R	40	-48	-32	3.88	0.039
45	Parahippocampal gyrus L	-18	2	-28	4.58	0.043
44	Cerebellum L	-10	-82	-28	4.24	0.045
44	Precentral gyrus R	36	-14	66	3.66	0.045
43	Cerebellum R	32	-78	-38	3.82	0.047
Treated PD > drug-naïve PD						
92	Thalamus L	-2	-3	2	5.13	0.006
	Hypothalamus L	-2	-4	-8	3.72	
91	Cerebellum R	26	-40	-48	4.99	0.007
83	Midbrain	10	-32	-4	4.46	0.009
	Hippocampus R	20	-30	-6	4.22	
	Parahippocampal gyrus R	18	-28	-16	3.68	
46	Cerebellum R	8	-62	-42	4.59	0.041
74	Cerebellum L	-34	-60	-48	4.12	0.012
74	Cerebellum L	-16	-40	-48	3.90	0.012
63	Anterior cingulate gyrus	-2	12	-4	4.44	0.019
49	Insula L	-38	-8	12	4.24	0.036
	Central operculum L	-48	0	0	3.16	
49	Dorsal putamen L	-26	-16	2	3.85	0.036
	Globus pallidus L	-18	-4	0		

**Survived FWE cluster-level correction; p<0.005; Height threshold T = 2.68; Extent threshold = 40 voxels*

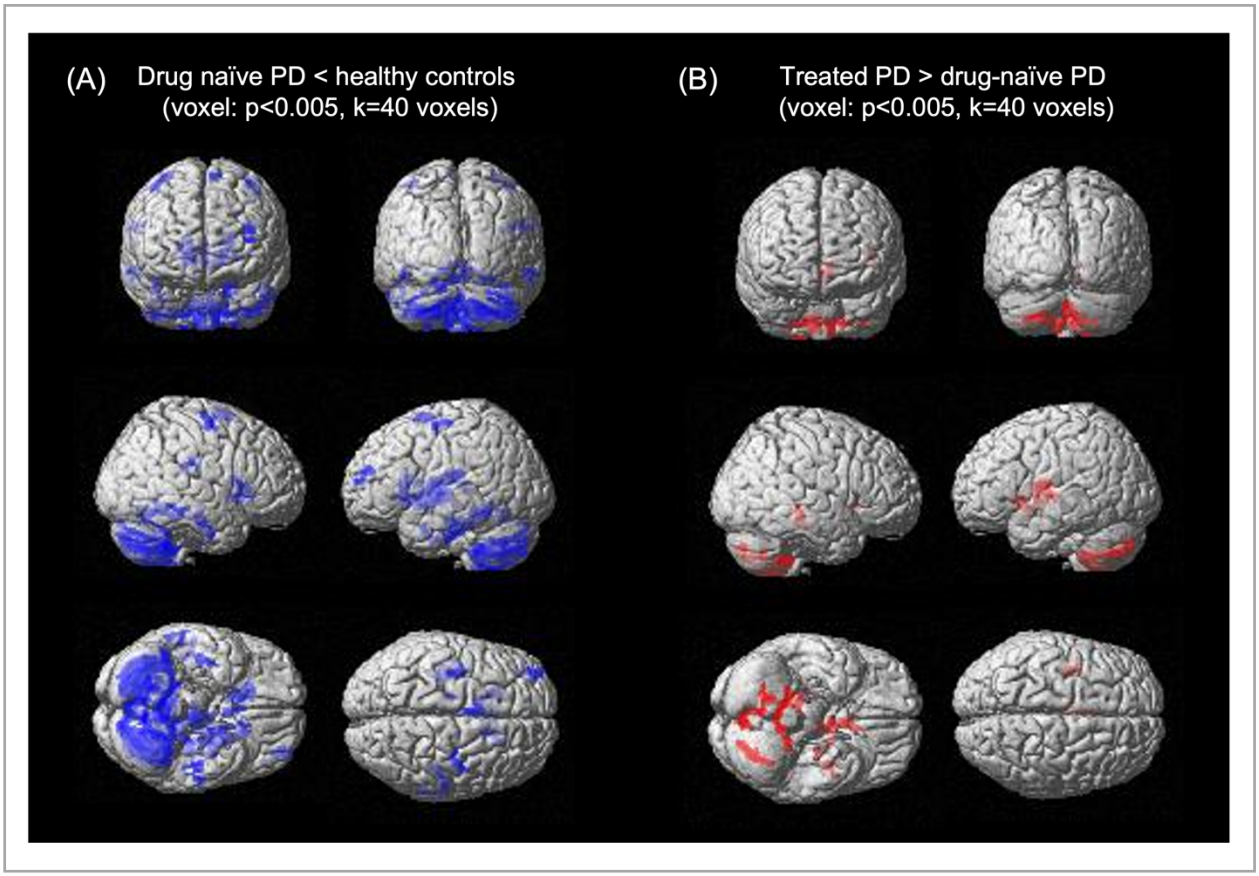

Figure 3.5. Voxel-wise [^{11}C]UCB-J V_T differences in unmedicated and medicated PD patients. (A) Comparison of drug-naïve PD patients versus healthy controls: widespread reductions of [^{11}C]UCB-J V_T across the frontal, temporal, and parietal lobe, brainstem, subcortical structures and cerebellum, (B) Comparison of treated PD patients versus drug-naïve PD patients: higher [^{11}C]UCB-J V_T was localised to the thalamus, medial temporal lobe and cerebellum.

3.4.8 Simple linear regression: regional volumes and [^{11}C]UCB-J V_T

Since some regional [^{11}C]UCB-J V_T differences did not survive after controlling for volume, which is suggestive of specific regional [^{11}C]UCB-J V_T differences actually reflecting volumetric differences, a confirmatory simple linear regression analysis was conducted between regional [^{11}C]UCB-J V_T (dependent variable) and volumetric estimates (independent variable) in those specific brain areas. Within drug-naïve PD patients, GM volume in the amygdala did not explain a significant amount of the variance in amygdala [^{11}C]UCB-J V_T ($F(1,9)=0.12$, $R^2=0.013$, $p=0.074$) and did not significantly correlate ($r=+0.11$) or predict amygdala [^{11}C]UCB-J V_T ($\beta=0.12$, $p=0.074$). Within treated PD patients, regional volume in the thalamus explained 40% of the variance of [^{11}C]UCB-J V_T in the thalamus, although the overall regression was not

statistically significant ($F(1, 8)=5.27$, $R^2=0.40$, $p=0.051$), and it was not a significant predictor ($\beta=0.58$, $p=0.051$), although there appeared to be a non-significant modest association ($r=+0.63$).

Given that treated PD patients exhibited greater grey matter volumes generally, I wanted to determine whether synaptic density levels could be contributing to these volumetric differences by assessing their association through a simple linear regression model where regional volume served as the dependent variable and [^{11}C]UCB-J V_T estimates served as the independent variable. The overall regression models for the dorsolateral prefrontal cortex ($F(1,8)=2.56$, $R^2=0.24$, $r=+0.49$, $p=0.148$), nucleus accumbens ($F(1,8)=2.80$, $R^2=0.26$, $r=+0.51$, $p=0.13$), amygdala ($F(1,8)=4.71$, $R^2=0.37$, $r=+0.61$, $p=0.062$), anterior cingulate ($F(1,8)=3.19$, $R^2=0.29$, $r=+0.53$, $p=0.11$) or insula ($F(1,8)=4.40$, $R^2=0.36$, $r=+0.60$, $p=0.069$) were not statistically significant and [^{11}C]UCB-J V_T in these regions did not predict respective regional GM volumes (dorsolateral prefrontal cortex: $\beta=0.52$, $p=0.148$; nucleus accumbens: $\beta=0.79$, $p=0.13$; amygdala: $\beta=1.13$, $p=0.062$; anterior cingulate: $\beta=0.52$, $p=0.11$; insula: $\beta=0.62$, $p=0.069$).

3.4.9 Simple linear regression: regional [^{11}C]UCB-J V_T and CBF

In order to assess the intra-regional associations between [^{11}C]UCB-J V_T and CBF; more specifically whether SV2A estimates predict CBF measures, a simple linear regression analysis was performed between [^{11}C]UCB-J V_T (independent variable) and CBF (dependent variable) within each region. Both measures included here were partial volume corrected in an attempt to minimise the potential influence volume could have on their association.

Within drug-naïve PD patients, healthy controls and treated PD patients, regional [^{11}C]UCB-J V_T was not a predictor of CBF within any regions-of-interest.

3.4.10 Simple linear regression: [^{11}C]UCB-J V_T and disease severity and duration

To gain an insight into whether disease severity and duration were driving the effects observed, a simple linear regression was performed between nigral [^{11}C]UCB-J V_T and disease duration and severity in drug-naïve and treated PD. The substantia nigra was chosen given it was a significant finding in both patient groups.

Across both drug-naïve and treated PD patients, disease duration explained 0.04% of the nigral [^{11}C]UCB-J V_T variance ($F(1,19)=0.008$; $R^2=0.00042$; $p=0.93$), whilst disease severity (as measured by MDS-UPDRS total score) explained ~6% of the variance ($F(1,19)=1.27$; $R^2=0.063$; $p=0.27$; Figure 3.6).

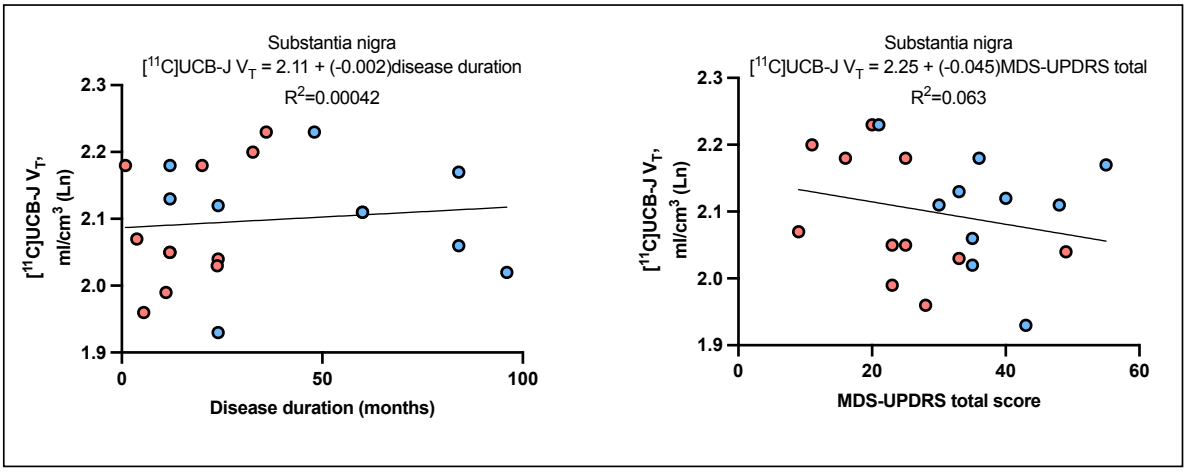

Figure 3.6. Linear regression between nigral [^{11}C]UCB-J V_T and disease duration and severity in drug-naïve and treated PD patients. Disease duration and severity did not explain a significant proportion of nigral [^{11}C]UCB-J V_T variance across these groups.

3.4.11 Correlations: [^{11}C]UCB-J V_T and clinical measures

Within the group of drug-naïve PD patients, lower [^{11}C]UCB-J V_T in the brainstem was associated with higher MDS-UPDRS Part III (r=-0.71, p=0.015) and higher MDS-UPDRS total score (r=-0.62, p=0.044; Figure 3.7). I did not find any associations between clinical measures, including the MoCA, and [^{11}C]UCB-J V_T in treated PD patients.

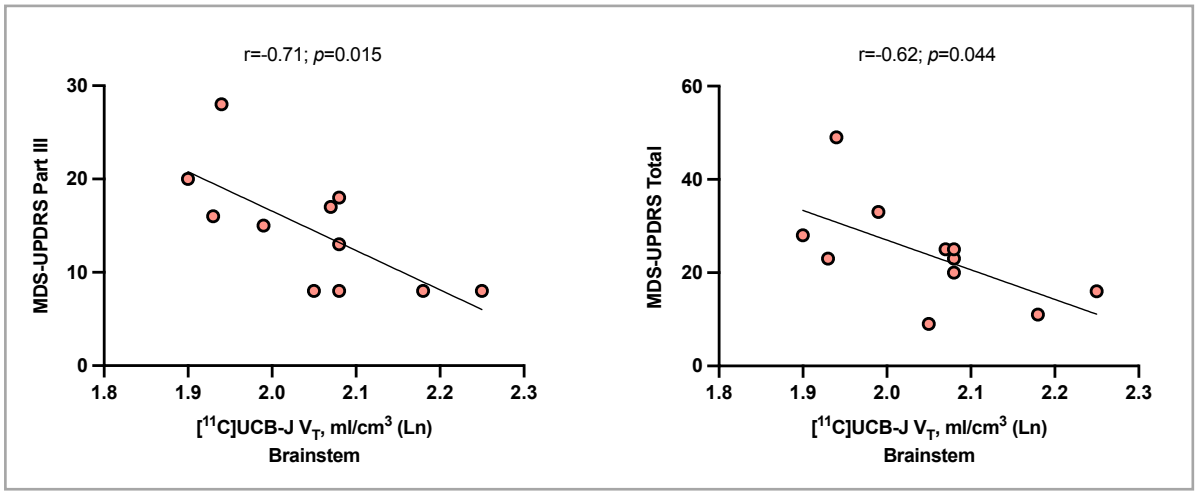

Figure 3.7. Correlations between [^{11}C]UCB-J V_T and measures of disease burden in drug-naïve PD patients. Reduced [^{11}C]UCB-J V_T in the brainstem was associated with worse motor symptom severity.

3.5 Discussion

This cross-sectional study evaluated [^{11}C]UCB-J V_T, perfusion and grey matter volume differences in small samples of medicated and unmedicated PD patients, both at the regional and voxel level, with the help of a healthy control group. The most important findings from this study are the distinct [^{11}C]UCB-J V_T differences between the two PD groups, whereby synaptic density was reduced across the brain in drug-naïve PD compared to healthy controls, but 'normalised' in treated PD. In fact, when unmedicated and medicated PD patients were compared directly to each other, the treated PD group exhibited generally higher measures of synaptic density.

More specifically, I found that drug-naïve PD patients exhibited a widespread loss of synaptic density across the brainstem, subcortical and cortical brain areas, including key frontal regions implicated in PD, with no volumetric reductions or associations observed between synaptic density and grey matter volume. At this early symptomatic stage of the disease, reduced SV2A in the brainstem was found to be associated with motor symptom severity and overall disease burden. Interestingly, in PD patients on dopamine replacement therapy, this initial widespread loss of SV2A was no longer evident, with a modest reduction confined to the substantia nigra. Although these patients exhibited a generally higher GM volume across brain areas, SV2A measures were not identified as statistically significant predictors, despite the linear regression analyses and associated correlation coefficients being indicative of a relationship, with some regional SV2A estimates accounting for 37% of the variance. This was likely due to the small sample sizes, as demonstrated by a sensitivity power analysis (G*Power, version 3.1.9.6, Faul et al., 2009) that showed that 11 participants would make a linear regression model with 1 predictor sensitive to effects of an R^2 of at least 0.47 with 80% power (α=0.05). This means that the linear regression analyses would not be able to reliably detect effects smaller than R^2=0.47. There was also evidence of discordance between brain areas exhibiting synaptic density loss and hypoperfusion in drug-naïve PD. Similarly, in treated PD, regional hyperperfusion and synaptic density alterations were not found to be associated.

Although disease duration and disease severity were significantly different between medicated and unmedicated PD patients, these variables did not explain a significant proportion of the variance of nigral synaptic density as demonstrated by disease duration explaining less than 1% of the variance and disease severity explaining ~6%. Furthermore, there did not appear to be an association between these parameters, as illustrated in Figure 3.6. These findings suggest that disease duration or severity are not underlying the differences observed in synaptic density. Nonetheless, it is worth noting that it can be challenging to match medicated and unmedicated

PD patients for parameters such as disease duration and/or disease severity. Furthermore, ANCOVA is designed to control for confounders when groups are randomly assigned, but not to control for naturally occurring group differences, as this can result in ANCOVA yielding bias results (Jamieson, 2004). Since these PD groups were stratified according to medication status, disease duration and severity, and because there were significant between-group differences in these parameters, it was inappropriate to control for them in the statistical model.

The loss of synaptic density observed in drug-naïve PD patients is in corroboration with those previously reported by Wilson et al. (2020) who also explored regional differences in synaptic density within the same group of patients compared to healthy controls. By including the same group of drug-naïve patients within this study, I was able to not only independently reproduce the general findings reported in that study, but also implement a semi-automated approach to explore further questions related to volumetric and partial volume effects, as well as include additional patient groups to assess the impact of dopaminergic medication and disease chronicity at a cross-sectional level by comparing drug-naïve PD patients to those on treatment (discussed in detail below). Furthermore, within our study, I had a larger sample of healthy controls (sixteen vs thirty-five), who were equally well-matched for age with drug-naïve PD patients (62.1 ±10.45 years of age vs 61.0 ±12.5 years of age). Strengths of Wilson's paper include assessing the longitudinal changes of SV2A over a mean follow-up period of eleven months. This permitted Wilson et al. (2020) to investigate temporal disease aspects and examine the relationship between synaptic density alterations and subsequent morbidity, thus providing insights into potential cause-and-effect relationships. The longitudinal design also had the advantage of reducing the risk for unobserved heterogeneity or confounding. However, seven out of eight patients remained to be drug-naïve at follow-up, thus the potential role of medication could not be investigated. Furthermore, the authors assessed synaptic density within distinct brainstem nuclei, which I did not include in this study, although I included the brainstem as whole as a region-of-

interest. Additionally, Wilson et al. (2020) assessed cortical thickness and volumes, though the association between these measures and synaptic density were not investigated. Finally, volumetric changes of the substantia nigra were evaluated by manually delineating the substantia nigra on the Fast Gray Matter Acquisition T1 Inversion Recovery (FGATIR) MRI sequence, which resulted in the authors observing a volumetric reduction in the substantia nigra in drug-naïve PD patients that I was unable to reproduce with an automated atlas-based approach. Both methods come with their advantages and disadvantages, whilst manual delineation can lead to biases from inter- and intra-operator variability, whereas automated methods have the advantage of completely removing the operator's subjectivity. On the other hand, automated approaches are susceptible to misalignment, particularly for small, subcortical structures. Nevertheless, I observed a similar reduction of synaptic density within the substantia nigra of drug-naïve PD patients (-6.9% vs -8.3%), although it is important to emphasise that whilst I observed this difference, further studies with a larger sample are required to confirm these findings. Finally, within this study, I explored specific cortical areas in the frontal lobe that are closely related to PD and its progression, whereas Wilson et al. assessed SV2A changes within the entire frontal lobe. I also investigated functional subdivisions of the striatum that were divided based on known contributions to fronto-striatal loops to explore whether these subdivisions were differentially affected as the disease progresses, while Wilson et al. considered a more classical anatomical definition of the striatum.

Given the uneven gradient of dopamine loss across the striatum, with the sensorimotor putamen being particularly susceptible in PD as it receives dopaminergic innervation from neurons in the SNpc that are selectively vulnerable and profoundly lost (Nakano et al., 2000, Bruck et al., 2006, Kish et al., 1988), I hypothesised that in early, drug-naïve PD patients, the postcommisurral putamen would have the steepest reduction of SV2A as opposed to the precommissural putamen or caudate. However, there was a comparable loss of SV2A in the pre- and

postcommissural putamen, with the caudate showing the largest loss (-8% vs -7% vs -12%, respectively). This may seem unexpected, particularly as a profound depletion of striatal dopamine concentration and marked loss of presynaptic dopaminergic markers is well-reported within the PD literature (Fazio et al., 2018, Kordower et al., 2013, Delva et al., 2020). However, there could be several reasons for this. Firstly, among the total population of striatal presynaptic terminals, dopaminergic terminals only constitute a small fraction; it has been shown that neurons expressing tyrosine hydroxylase, though typically assumed to be dopaminergic within the striatum, operate as GABAergic neurons, exerting widespread inhibition (Xenias et al., 2015, Huot and Parent, 2007). Given the non-specificity of [^{11}C]UCB-J PET to any one neuronal type, the radiotracer signal may be reflecting non-dopaminergic synapses that are differentially affected within PD. For example, nigrostriatal lesioning has been shown to lead to an up-regulation of synaptic input to GABAergic interneurons in the striatum (Unal et al., 2015). Secondly, although SV2A is expressed ubiquitously across the entire brain, including in nigrostriatal neurons (Bajjalieh et al., 1994), SV2C has a preferential localisation to dopaminergic neurons (Janz and Sudhof, 1999). Provided that each synaptic vesicle encompasses a relatively consistent number of SV2 molecules (five SV2 copies per vesicle) (Mutch et al., 2011, Dunn et al., 2017), the abundance of SV2A within nigrostriatal synaptic vesicles is perhaps lower than that in non-dopaminergic terminals, thus the sensitivity of [^{11}C]UCB-J binding to dopaminergic terminal loss would be further diminished. Finally, studies have demonstrated that SV2C is a genetic modifier of sensitivity to L-DOPA (Altmann et al., 2016), with its role in the striatum being demonstrated by Dunn et al. (2017) who, after genetically deleting SV2C, observed reduced dopamine release in the dorsal striatum, thus establishing that SV2C serves as a mediator of dopaminergic function, with its disruption contributing to dopaminergic dysfunction. SV2C may, therefore, serve as a more appropriate target to explore dopaminergic synaptic function with PD, particularly given its restricted expression within the basal ganglia, as well as its expression in PD post-mortem brain tissue being dramatically altered (Dunn et al., 2017).

Given that drug-naïve PD patients exhibited reduced SV2A expression in the brainstem, which also correlated with motor symptom severity and overall disease burden, or findings appear to be in line with the Braak hypothesis, particularly given the fact that early in the disease, multiple neurotransmitter systems and pathways, of which the cell bodies are situated in the brainstem and project diffusively throughout the entire brain, are implicated in the disease process. Having said this, the group of early, drug-naïve PD patients exhibited widespread loss of SV2A, particularly within corticostriatal circuits, indicates that synaptic dysfunction may occur without the presence of proteinaceous intraneuronal Lewy bodies *per se*, as according to the proposed Braak staging scheme, lesions appear in the neocortex in the final stages 5 to 6, with components of previously affected systems becoming progressively involved (Braak et al., 2003, Braak et al., 2006, Del Tredici and Braak, 2016). As such, if Lewy bodies are in fact the toxic species responsible for cell death, and if cell death was tightly coupled to synaptic loss, I may have expected to see the largest reduction of synaptic density within the brainstem, with less cortical involvement. However, within our group of drug-naïve PD patients, I observed a comparable loss of SV2A within cortical (up to -10%) and subcortical regions (up to -12%), as well as the brainstem (-9%), with no volumetric changes, indicating that synaptopathy is a distinct phenomenon from neuronal death with PD being caused by processes other than Lewy bodies. Furthermore, PD patients on treatment did not exhibit a continual loss of SV2A as one would expect if the temporal evolution of PD was primarily mediated by the prion-like spread of Lewy bodies. Instead, they had higher estimates of SV2A compared to drug-naïve PD patients, with no significant differences found when compared to healthy controls.

Growing evidence now suggests that synaptic and axonal abnormalities occur prior to the degenerative loss of neuronal cell bodies, with synaptic dysfunction potentially commencing decades before symptom onset. In fact, it is postulated that the onset and evolution of PD

progresses in a dying back-like manner, initiating from dysfunction at the synapse and disrupted axonal connections, to subsequent neuronal cell body death (Bridi and Hirth, 2018). My findings are in line with this notion as our group of drug-naïve PD patients, who had a disease duration of less than two years, exhibited synaptic dysfunction that was more widespread than hypothesised, with basal ganglia-cortical-cerebellar involvement, with no evidence of atrophy. Studies have shown that accumulation of α-synuclein at synapses is a crucial event in the pathogenesis of synucleinopathies, with α-synuclein predominately localising to presynaptic terminals of mature neurons and playing a role in synaptic plasticity and function (Calo et al., 2016). Interestingly, α-synuclein has been demonstrated to colocalize with presynaptic proteins such as synapsin 1 (Withers et al., 1997), synapsin III (Zaltieri et al., 2015), synaptotagmin, and the "gold standard" marker of synaptic density: synaptophysin (Murphy et al., 2000, Iwai et al., 1995). This evidence indicates that aggregation of pathological α-synuclein at synapses may be the primary effector of the disease leading to synaptic dysfunction and loss. Perhaps more relevant to this study, α-synuclein and SV2C have been shown to interact, with knock-out of SV2C leading to altered expression of α-synuclein highlighting that SV2C protein expression is closely associated with levels of α-synuclein. Disruptions in either SV2C or α-synuclein could modify this interaction, essentially contributing to the pathogenesis of PD (Dunn et al., 2017). Given that SV2C and SV2A share a majority of their sequences, they may have some overlap in functions. It's possible that SV2A may also interact, directly or indirectly, with α-synuclein, although studies are required to investigate the potential interaction between SV2A and α-synuclein.

In drug-naïve PD, there was a global reduction in CBF, which is in line with the notion proposed by Borghammer et al. (2010) who stated that global perfusion was likely reduced in PD, even at the earliest stages. In fact, based on the meta-analyses of PET and SPECT perfusion literature, Borghammer concluded that PD patients likely display decreases in regional and hence global

values, regardless of whether this is detected in each individual study due to the large inherent variance in the measured physiological values. Whilst, to the best of my knowledge, there have not been any studies published in drug-naïve PD that have employed ASL-MRI to assess CBF alterations in this group, previous SPECT and PET perfusion studies within this group have demonstrated region-specific hypoperfusion across cortical areas of the brain in PD, particularly in parieto-occipital brain areas (Nobili et al., 2011, Pelizzari et al., 2020). In line with these previous CBF reports in PD, on a voxel-level, there was localised hypoperfusion within the inferior parietal lobe. However, on a regional level, despite the relatively large degree of hypoperfusion found within parietal (-22%) and occipital lobes (-23%), they did not reach the threshold of significance. This is likely due to the inclusion of global CBF as a covariate of no interest within the ANCOVA model, which may have led to an increase of type II errors where I failed to reject the null hypothesis and successfully observe focal differences in CBF between drug-naïve PD patients and healthy controls.

PD patients treated with dopamine replacement therapy had comparable synaptic density levels to healthy controls, although perhaps unsurprisingly, there was a modest reduction of synaptic density confined to the substantia nigra. This finding agrees with the two previously published [^{11}C]UCB-J PET studies that assessed synaptic density alterations in groups of treated PD patients, whereby a reduction of nigral synaptic density was corroboratively reported (Matuskey et al., 2020, Delva et al., 2020). This finding is somewhat unsurprising given that the pathognomonic hallmark of PD is the degeneration of dopamine-producing neurons within the SNpc, with post-mortem studies estimating that 30-80% of dopaminergic neurons in the substantia nigra are lost when motor symptoms arise (Cheng et al., 2010). However, Matuskey et al. (2020) and Delva et al. (2020) observed a larger reduction of SV2A within the substantia nigra at -45% and -15.2%, respectively, compared to -7% in the group included in this study; there are several factors that may account for the variability in the extent of these reductions. Firstly, the

patient group assessed by Delva et al. (2020) were less advanced with a shorter disease duration (2 years vs 4 years in this study) and milder motor symptoms (H&Y stage 1 vs H&Y stage 1.5 in this study). On the other hand, whilst the patient group included in the study conducted by Matuskey et al. (2020) had a comparable disease duration to the PD sample in this study (approximately 4 years), they were slightly more advanced in that they all had bilateral disease and had worse motor symptoms. Our sample size of treated PD patients was also smaller than the two previously published studies, with Delva et al. (2020) having the largest sample size of 30 PD patients. Regarding differences in image analysis methods, both previously published studies reported BP_{ND} values using the centrum semiovale as a white matter reference region, whereas in this study V_T were estimated with an arterial plasma input function, which is a superior approach for quantifying radioligands (see limitations for further details). Finally, whilst it may appear that the approaches employed for the delineation of the substantia nigra was vastly different between this study and the two that were previously published, the approaches were, in fact, somewhat comparable. Matuskey and colleagues' hand-drew the substantia nigra on a dopamine tracer template, whereas Delva and colleagues, also using a dopamine tracer template, delineated the substantia nigra based on a set threshold. In this study, the substantia nigra was defined by the CIC atlas which based its delineation of the substantia nigra on [^{11}C]-(+)-PHNO PET signal that is a mixture of D_3 and D_2 receptor signal using a fixed sized region-of-interest (Tziortzi et al., 2011). In this study, each non-linearly transformed atlas was thoroughly checked per subject to ensure that the substantia nigra region-of-interest was appropriately defined for each subject. Nevertheless, despite the difference in the magnitude of nigral synaptic density reduction in treated PD and the differences in study design and analysis methods, the fact that this finding has now been reported by three independent [^{11}C]UCB-J PET studies is a strong indicator that synaptic density is reduced within the substantia nigra in PD patients early in their disease course. Furthermore, as I did not observe a significant volumetric change within the substantia nigra, or the significant reduction of SV2A in this region after controlling for volume and

following PVC indicates that PD does not solely cause a depletion of nigrostriatal neurons, but also reduces presynaptic terminal density within the substantia nigra. This may accord with previous PET studies that have employed other presynaptic monoamine imaging biomarkers, reporting a 30% reduction of dopamine transporter (DAT), with vesicular monoamine transporter 2 (VMAT2) being reduced by approximately 20-45% (Hsiao et al., 2014).

Since striatal SV2A was significantly reduced early in the disease course, particularly in structures implicated in the basal ganglia-cortico-cerebellar pathways, which was then somewhat restored in treated PD patients points to i) a potential medication effect or ii) spontaneous disease-related regeneration of neuronal fibres as part of a compensatory mechanism. Whilst it is not possible to tease apart which of these is contributing to the 'normalisation' of SV2A within the treated PD group, medication is likely to be playing a role, and I will outline the evidence below. Please note that I will largely focus on the potential therapeutic effects of L-DOPA, as this was the therapy that was universally taken by all patients in the treated PD group, a proportion of subjects were also taking other pharmacological agents in combination with L-DOPA (See Table 3.1 for more details), which may also be contributing to the change of SV2A levels and increased volume observed. Thus, whilst it is not plausible to disentangle their specific effects, given that most therapeutic approaches in PD involve the stimulation of dopaminergic transmission, there is a large overlap in their therapeutic actions.

Several rodent studies have investigated the impact of L-DOPA on the expression patterns of a range of presynaptic proteins, predominately in the context of levodopa-induced dyskinesias (LIDs), and have shown increased levels of presynaptic proteins, including those that serve as structural components of the synaptic vesicle such as synaptophysin and synapsin (Cakmakli et al., 2018, Valastro et al., 2007) and those that play a regulatory role in membrane trafficking such as synaptotagmin (Cakmakli et al., 2018), which has been suggested to be related to new synapse

formation, axonal sprouting and synaptic plasticity alterations (Cakmakli et al., 2018). Although these changes are not directly applicable or reflective of any potential alterations in SV2A expression levels, it is important to acknowledge that L-DOPA administration holds the potential to induce changes in the expression levels of presynaptic protein.

Whilst L-DOPA is not considered to be a disease-modifying therapy, theoretically, it could exert some neuroprotective and neurorescuing properties by providing trophic support, reversing metabolic abnormalities and/or bolstering failing compensatory mechanisms. Evidence has shown that in the presence of glia and in low concentrations, L-DOPA protects cultured dopamine-producing neurons (Mena et al., 1997a, Mena et al., 1997b) and upregulates antioxidant and antiapoptotic proteins (Mytilineou et al., 1993, Han et al., 1996). L-DOPA has also been shown to promote the survival of dopaminergic neurons and enhance sprouting of striatal dopaminergic terminals in rodent PD models (Murer et al., 1998, Datla et al., 2001).

The neurotrophin family is a group of small, basic, secreted proteins that play a major role in adult neuronal survival, maintenance, and regeneration. This family comprises of several neurotrophic factors including brain-derived neurotrophic factor (BDNF) and glial cell-line derived neurotrophic factor (GDNF). BDNF has been well characterised with respect to its interaction with dopaminergic neurons, supporting their survival, differentiation and proliferation, as well as serving as a potent inhibitor of apoptosis-mediated cell death (Scalzo et al., 2010). Preclinical and clinical evidence has revealed that PD patients show a marked reduction in nigrostriatal and cortical BDNF levels (Mogi et al., 1999, Parain et al., 1999, Howells et al., 2000, Nagatsu et al., 2000, Fumagalli et al., 2003), thus may be implicated in the aetiology and pathogenesis of PD. L-DOPA (along with other effective therapies in PD such as selective monoamine oxidase inhibitors and dopamine agonists), may contribute to the preservation of integrity and vitality of dopaminergic neurons through regulating neurotrophic biosynthesis,

which is in fact a common step in the pro-regenerative properties elicited by such drugs. Specifically, L-DOPA has been found to enhance the expression of BDNF in the striatum of healthy mice (Okazawa et al., 1992) and rodent PD models. It is important to note that BDNF mRNA is not synthesised in the striatum, but is instead transported from the cortex (Altar et al., 1997); in accordance with the fact that L-DOPA in PD enhances BDNF expression in the frontal cortex following either acute or chronic administration (Guillin et al., 2001). Several lines of research have highlighted the potential therapeutic roles of BDNF that not only includes increased cell survival (Ding et al., 2011, Massa et al., 2010, Monteggia, 2011), but also neuronal cell proliferation (Pencea et al., 2001), neurorecovery by neuritogenesis in early PD (Somoza et al., 2010) and axonal regeneration (Frim et al., 1994). Since BDNF plays a role in regulating synaptogenesis, it is plausible that the normalised expression levels of SV2A and the increase in volume are, at least partially, reflecting axonal sprouting in treated PD patients taking dopamine replacement therapy.

GDNF is a neurotrophic factor that promotes the development, differentiation and survival of dopaminergic neurons (Airaksinen et al., 1999). Several studies in animal models of PD (Soderstrom et al., 2006), as well as some in PD patients, have revealed that GDNF delivery can exert trophic effects, protect dopaminergic neurons and restore motor function (Gill et al., 2003, Slevin et al., 2007, Slevin et al., 2005). Thus, GDNF it has been highlighted as a potential therapeutic target for the treatment of several neurodegenerative disorders.

Afferent activity regulates the expression of neurotrophic factors, thus implicating dopamine as a likely candidate to control GDNF and BDNF expression in the nigrostriatal system (Hughes et al., 1999, Williams and Undieh, 2009). Several lines of evidence have demonstrated that dopaminergic activity is able to promote GDNF expression, whereby D_1 and D_2 receptor agonist have been shown to increase the synthesis of GDNF in mesencephalic and striatal neuronal

cultures (Guo et al., 2002), as well as in astroglial cultures (Ohta et al., 2000, Ohta et al., 2003, Ohta et al., 2004), and mice lacking D_2 receptors exhibit a reduction of striatal GDNF expression (Bozzi and Borrelli, 1999).

Given the role of dopamine in promoting GDNF expression, therapeutic approaches involving the stimulation of dopaminergic transmission induce GDNF expression in the nigrostriatal circuitry. Whilst dopamine agonists such as apomorphine have been shown to upregulate the expression of several neurotrophic factors including GDNF (Guo et al., 2002), the role of L-DOPA on GDNF expression in nigrostriatal system has not been extensively addressed. However, there is some evidence indicating that L-DOPA induces the upregulation of GDNF at the mRNA and protein level in nigral neuron-glia cell cultures via a process involving meditators that signal astrocytes to increase the expression of GDNF (Saavedra et al., 2005). Thus, it is plausible that synaptic density restitution is due to this pharmacological agent, through replenishing dopamine concentrations, boosting the expression of neurotrophic factors, including GDNF.

However, self-repairing systems may also be at work, as Saavedra et al. showed that L-DOPA did not affect astrocytic GDNF expression, suggesting that GDNF up-regulation was a result of neuronal factors instead (Saavedra et al., 2006). This led the authors to suggest that the upregulation of GDNF is triggered by the failing dopaminergic neurons that send signals to astrocytes to increase GDNF expression and not L-DOPA induced (Saavedra et al., 2006).

Although I cannot definitively conclude that the 'normalisation' of SV2A expression levels is due to medication because of the study design, the administration of dopamine replacement therapy is a key characteristic that holds the potential to influence SV2A measures, particularly given the 'social' nature of dopamine transmission and L-DOPA's ability, particularly in initial stages, to

correct dopaminergic signalling and exert neurotrophic effects. Even though there had been decades-long debate regarding L-DOPA toxicity, with the development of motor fluctuations and dyskinesias after chronic L-DOPA treatment being assigned to a 'toxic' effect, as opposed to a 'adverse' effect, we now know that even in those patients, there is evidence of maladaptive plasticity and anatomical modifications, including axonal regeneration, sprouting, neurogenesis and synaptogenesis, that are key contributors to the manifestation of this motor complication (Cerasa et al., 2014). Of course, the state of the PD brain is a fundamental determinant of the type of effects a medication has, but it appears from the evidence presented above that dopaminergic medication may contribute, at least in part, to the normalisation of SV2A that is observable in treated PD. Further research is required to determine if L-DOPA does in fact exert trophic effects that are reflected in SV2A measures.

I observed increased volume in treated PD patients in several structures of the limbic/paralimbic system. Whilst most volumetric studies assessing structural changes in PD have reported a general reduction in grey matter volume across multiple subcortical and cortical structures, studies have also reported region-specific increases (Li et al., 2017, Pitcher et al., 2012, Krabbe et al., 2005, Cui et al., 2020, Lee et al., 2011, Lewis et al., 2016, Fang et al., 2020). The increase of volume observed in the treated PD group is in line with several studies that reported PD-related brain volume increases in specific brain areas including those reported here, such as the frontal lobe, insula and anterior cingulate (Jubault et al., 2011, Cerasa et al., 2011). Few studies have assessed longitudinal alterations in volumetric measures in PD (Mak et al., 2015a, Jia et al., 2015, Charroud and Turella, 2021, Zarkali et al., 2021, Sarasso et al., 2021), and whilst the majority of these longitudinal studies have reported progressive atrophy in PD patients over time, our results are in line with Jia et al. (2015) who assessed drug-naïve PD patients over a 12-month follow-up period. Whilst these investigators observed a reduction in regional GM volume, they reported

that PD patients also exhibited increased volume in limbic/paralimbic structures when compared to controls (Jia et al., 2015), which was where volumetric increases were observed in this group.

The increased of volume in limbic/paralimbic structures, could be suggestive of a potential dopaminergic overstimulation in limbic structures receiving projections from the relatively spared ventral tegmental area in treated PD patients, subsequent to dopamine overdose from L-DOPA. L-DOPA has also been shown to induce morphological alterations such as hypertrophic axon terminals or dendrites (Tomiyama et al., 2004), potentially as a consequence of aberrant stimulation of D_1 receptors.

Studies have also demonstrated the vulnerability of the limbic system in PD, particularly in those with poor cognitive performance (Xia et al., 2013, Braak et al., 1994, Kamagata et al., 2012). This is especially noteworthy, as the group of treated PD patients had poorer cognition in comparison to drug-naïve PD patients, despite no difference in age. It is possible that increased volume manifests earlier in the disease process, prior to conceding to atrophic processes, following an inverted U-shape function. Such a rationale has been previously stipulated to explain increased cortical thickness and volumes in early PD with hallucinations (Pagonabarraga et al., 2014, Sawczak et al., 2019). An inverted U-shape function has also been seen in other neurodegenerative disorders such as prodromal Alzheimer's disease (Fortea et al., 2011, Sala-Llonch et al., 2015). It is yet to be established with longitudinal studies whether this increase of volume reflects the presence of pathological processes or rather indicates a brain reserve factor that safeguards vulnerable regions in cognitively unimpaired subjects.

Volumetric alterations can reflect a range of possible mechanisms including alterations in neuronal size, density and arrangement, changes in glial proliferation or glial size, neurogenesis, angiogenesis, modifications to dendritic density and spine size and remodelling of axonal

processes (Fischl and Dale, 2000, Ashburner and Friston, 2000, Keifer et al., 2015, Lerch et al., 2011, Asan et al., 2021). Furthermore, in PD, dopaminergic neuronal loss is accompanied by inflammatory changes in immune cells such as microglia and astrocytes. Both microglia and astrocytes proliferate and accumulate in response to neurodegeneration, which occurs early in the disease course prior neuronal death (Belloli et al., 2020), with reactive astrocytes also becoming hypertrophic (Jeong et al., 2014). Although we do not have data that speaks to these processes specifically, their potential contribution to the increase of volume observed cannot be excluded, particularly given the heterogeneity of the pathophysiological processes underlying PD.

Nevertheless, of the many potential mechanisms influencing volumetric measures this work proposes that synaptic density may make an important contribution the increase in regional volume. Although there was no qualitative overlap between the regions exhibiting a significant increase of volume and SV2A expression levels, I found that synaptic density was significantly associated with volume in parahippocampal gyrus in treated PD patients, with moderate associations also found between SV2A expression and volume in additional regions (non-significant, $r > 0.5$) suggesting that the 'restoration' of synaptic density from drug-naïve to treated PD may be, at least in part, contributing to the increase in volume observed in this group. It is important to mention that although the associations between regional [^{11}C]UCB-J V_T and regional volumes were not formally significant, the r values suggested a moderate association between these measures, but the sample size is likely too small for the association to be deemed significant. Further studies with larger sample sizes are required to allow for a definitive conclusion regarding the degree to which these measures may be related.

This study has several limitations. First, the sample sizes per patient group are modest, with different n numbers per group, which is likely to obscure possible between SV2A expression and volumetric or clinical measures within each group. However, future studies with larger samples

may permit a better understanding of how potential confounds interact with disease to alter synaptic density. Second, small structures of interest including brainstem nuclei such as dorsal raphe and the locus coeruleus, could not be resolved and accurately quantified given the low spatial resolution of the PET image, hence here I focused on using a whole-brainstem region of interest in our analyses. Third, I cannot be definitive about whether the reductions of SV2A uptake reflect loss of entire presynaptic boutons or a more selective loss of these proteins, though it is likely that the loss of SV2A is reflecting disease-related alterations in the presynaptic terminal. An obvious methodological drawback to the approach I have taken is that synaptic density, perfusion, and volumetric changes could only be investigated with the help of cross-sectional data gained from healthy controls and patient groups, thus the conclusions drawn from these data permit only assumptions of what changes in SV2A and volume reflect. For example, whilst I have speculated that the SV2A estimates in the medicated PD group points to a potential 'normalisation' of SV2A measures, it is possible that these higher estimates are reflecting inherent differences in the sample of medicated and unmedicated patients that may not actually be specific to the PD disease process. It is not feasible, for example, to rule out unobserved heterogeneity whereby there exists an unmeasured difference between these samples that is associated with SV2A estimates. For instance, the sample of drug-naïve PD patients that were enrolled into the study may have been relatively more seriously ill patients that felt more motivated to take part in research, or the medicated patients who self-selected to take part in research had higher synaptic density to begin with. Whilst I accounted for age and gender as potential confounders, it was not possible to eliminate other, unknown confounders which could include medication, lifestyle choices, and participant variability. Clearly, longitudinal follow-up data would inherently clarify if lower levels of [^{11}C]UCB-J V_T is reflective of a depletion of SV2A and volumetric reductions is reflective of atrophy within our patient groups, as well as if the higher levels of [^{11}C]UCB-J V_T in the medicated group is signifying 'restoration'. However, using these three datasets together permitted me, for the first time to my knowledge, to investigate

what between-group differences in synaptic density could reflect in the context of disease progression and currently, there are no longitudinal datasets available which have employed the novel radioligand [^{11}C]UCB-J, thus assessing disease progression cross-sectionally is a feasible approach to take in this instance. Nevertheless, longitudinal evaluation would be essential to draw conclusions about the progression of synaptic alterations, and in particular the role of treatment. Finally, I only evaluated synaptic changes perfusion alterations and atrophy, which are only two out of many mechanisms underlying the pathogenesis of disease. It is imperative to highlight that Lewy pathology is not present in all neuronal populations, but instead is typically localised to a subset of neurons within specific anatomical regions. Contingent on how far along the disease has progressed, affected neurons can encompass numerous neurotransmitter systems, including catecholaminergic, serotonergic, cholinergic, and glutamatergic neurons (Spillantini et al., 1997, Halliday et al., 2006, Beach et al., 2009). However, over the course of the disease, a considerable proportion of neurons that share these neurotransmitters do not feature α-synuclein inclusions, highlighting the contrasting susceptibilities neuronal subpopulations have to α-synuclein pathology. Since SV2A is not specific for anyone neuronal subtype, it would be of particular interest to gain insight into the neurochemical systems that may underlie or contribute to synaptic alterations observed in these groups.

In summary, I observed a prominent, widespread loss of presynaptic density during early stages of PD, though dopamine replacement therapy appeared to overcome this loss, as SV2A concentrations appeared to be restored to 'normal' levels in the treated PD patients. The normalisation of SV2A expression levels may be a contributing factor to the observed increased volume in this group, which may be a subsequent consequence of the therapeutic effects of dopamine replacement therapies. [^{11}C]UCB-J PET is likely to be a unique and specific marker of synaptic density, which is reflected in part by the fact that in early drug-naïve PD patients, there is a widespread reduction of SV2A, with no evident atrophy and no association between these

measures early in the disease course. Further evidence of this notion is demonstrated by the volumetric and synaptic density changes in treated PD, whereby although there seems to be an association between synaptic density and increased volume, there was no overlap in the brain areas where volume was increased and synaptic density was increase; in fact, synaptic density was not elevated, but instead comparable to the expression levels in healthy controls. This suggests that this method of measuring synapses *in vivo* is not simply reflecting volumetric alterations and is devoid of confounding factors such as glia that may be influencing estimates of volume in this group. My findings demonstrate that the processes underlying synaptic density loss is likely distinct from those underlying cell death, as synaptic density loss is observable in the absence of any atrophy in drug-naïve PD patients.

Overall, these results support the notion that synaptic impairments precede neuronal cell body loss, thus if synapses can be protected or restored, it may aid in the overall survival of neuronal cells. Finally, these findings indicate that [^{11}C]UCB-J PET may be a useful tool for not only monitoring disease progression, but for assessing the treatment effects of any future disease-modifying drugs. However, studies are essential to investigate the regulation of SV2A, as well as the potential impact L-DOPA has on its expression levels and whether this also occurs in residual synapses in PD. Furthermore, longitudinal studies assessing SV2A *in vivo* are warranted to not only confirm these findings but build upon them by shedding light on patterns of synaptic density changes throughout the natural time course of disease and the relationship between synaptic density and medication, as well as motor and non-motor symptom development.

4 Synaptic density changes in Lewy body dementia: An in vivo [^{11}C]UCB-J PET study

4.1 Introduction

Human life expectancy has been increasing at a rapid rate (Oeppen and Vaupel, 2002), but the resultant life extension is coupled to the growing prevalence of dementia worldwide, carrying serious implications for modern society (van der Flier and Scheltens, 2005). Whilst there have been tremendous strides in research and efforts towards developing new treatment strategies, the focus has largely been on AD. However, although PDD and DLB present with a particularly challenging symptom profile and together account for approximately 15% of dementia cases (Aarsland and Kurz, 2010b, Aarsland et al., 2005, Vann Jones and O'Brien, 2014), they have received far less attention. As is the case for AD, cholinesterase inhibitors provide symptomatic relief, but advancements towards developing disease-modifying therapies are at noticeably earlier stages.

The pathophysiology of Lewy body disease is complex as it involves far more than the selective depletion of striatal dopaminergic signalling, with several neurotransmitter systems undergoing progressive loss and altered functioning in the dementia brain. In stark contrast to the nigrostriatal pathology underlying the motor aspects of the disorder (Fahn et al., 1971, Hirsch et al., 1988), the pathophysiological processes underlying the dementing process remain obscure. A major hinderance in establishing the pathological mechanisms contributing to Lewy body dementia is that the underlying cellular-level pathology is heterogeneous, with Lewy bodies, senile plaques, neurofibrillary tangles, microvascular disease and argyophilic inclusions all implicated in the disease process (Irwin et al., 2012, Del Tredici and Braak, 2013, Horvath et al.,

2013, Halliday et al., 2014). Pathological studies have indicated that the burden of α-synuclein pathology is linked to cognitive decline, with concurrent AD-related pathology likely also contributing, although this only explains a small proportion of the variance. In fact, the anatomical distribution of such pathologies differs between cases (Colosimo et al., 2003, Galvin et al., 2006), and does not always correspond with clinical symptoms, as demonstrated by a large neuropathological study that revealed that 55% of PD cases who had limbic and neocortical Lewy bodies lacked clinical evidence of dementia (Parkkinen et al., 2008). Complicating the picture further, multiple genes are known to increase the risk of developing Lewy body dementia, including mutations in the α-synuclein (*SNCA*) and glucocerebrosidase (*GBA*) genes, as well as the microtubule-associated protein tau (*MAPT*) haplotype and apolipoprotein ε4 (*APOE4*) allele (Halliday et al., 2014), all of which are likely to be implicated in cognitive decline via discrete mechanisms. Further insight and understanding of disease substrates are required for targeted drug discovery and to permit better monitoring of disease progression.

Synapse loss and dysfunction is considered a key feature in most neurodegenerative disorders. In synucleinopathies like PD and DLB, growing evidence has demonstrated that aggregation of α-synuclein at the synapse is a major event in disease pathogenesis (Calo et al., 2016, Kramer and Schulz-Schaeffer, 2007). Small aggregates of α-synuclein have been identified to co-localise within synaptic terminals in post-mortem brain tissue from DLB patients (Colom-Cadena et al., 2017), and is likely implicated in altering synaptic function and integrity (Bridi et al., 2021). Altered synaptic function and/or loss is typically represented by changes in synaptic protein expression in the presynaptic or postsynaptic density (Gottschall et al., 2010). Indeed, studies have demonstrated that several proteins involved in synaptic transmission are affected in Lewy body disease, as illustrated by their altered expression levels in post-mortem brain tissue of Lewy body disease patients, with DLB exhibiting the most robust alterations, followed by PDD and AD cases (Mukaetova-Ladinska et al., 2013, Revuelta et al., 2008, Bereczki et al., 2016, Hansen et

al., 1998). Furthermore, Mukaetova-Ladinska et al. (2013) observed reduction of synaptophysin, syntaxin and SNAP25 in the visual cortex of DLB patients, a brain area where pathology is not usually pronounced (Taylor et al., 2012), suggestive of early synaptic involvement. In fact, synaptic dysfunction and/or loss may be particularly crucial in Lewy body dementia, given that structural imaging studies have demonstrated that brain atrophy is less pronounced in PDD and DLB compared to AD, despite the more severe disease course (Mak et al., 2015b). Therefore, synapse loss or dysfunction is likely to be an early and critical pathological event in Lewy body dementia and may be a final common biological mechanism linking protein pathologies to disease symptoms.

However, post-mortem tissue sample work is fraught with confounds, including selection bias, and only offer a snapshot of pathology, often at the end stages of the disease. With the development of novel radioligand [^{11}C]UCB-J, it is now possible to measure the expression levels of presynaptic protein SV2A in the living brain. To-date, *in vivo* evidence of synaptic alterations in Lewy body dementia is scarce, with only two studies published to-date employing [^{11}C]UCB-J PET: (1) Nicastro et al. (2020) conducted a case study of only 2 DLB patients and (2) Andersen et al. (2021) pooled DLB (n=9) and PDD (n=4) patients into one group. These studies reported widespread cortical reduction of [^{11}C]UCB-J binding, with more prominent reductions in parietal and occipital brain areas.

However, what remains unknown is whether, despite the shared clinical, neurobiological, and pathological features, DLB and PDD patients demonstrate differing synaptic density profiles. This could have implications for unravelling the clinical differences between PDD and DLB from underlying biological differences. As mentioned above, SV2A measures could potentially be affected by presynaptic accumulation of α-synuclein, but studies in AD have also demonstrated that AD-related pathology can have a toxic action on synaptic function (Shinohara

et al., 2013, Shinohara et al., 2014, Spillantini and Goedert, 2013). Thus, the varying degree of AD co-pathology present in Lewy body dementia, which represents an important source of clinically meaningful biological heterogeneity, could potentially be reflected in differing alterations in synaptic density between these disorders. Furthermore, alterations in synaptic markers according to the presence or absence of dementia in PD patients is currently unknown, thus non-demented PD and PDD patients are yet to be compared. This approach would provide preliminary insight into any localised alterations of SV2A expression levels that may be associated, specifically, with cognitive decline in PD as the disease progresses.

Additionally, the effects of tissue loss on measures of SV2A requires further investigation within Lewy body dementia, which is especially important given that these syndromes involve cortical and subcortical atrophy (Burton et al., 2004). Andersen et al. (2021) applied PVC to the [^{11}C]UCB-J data, and found that there were no major differences in data with or without PVC. In the small pilot case study, Nicastro and colleagues assessed if there was regional associations between grey matter volume and [^{11}C]UCB-J binding, but reported no associations between these measures (Nicastro et al., 2020). Contrastingly, in other neurodegenerative disorders like AD, there have been reports of some confounding effects of tissue volume on SV2A measures (Chen et al., 2018, Mecca et al., 2020). It is, therefore, important to clarify whether volumetric alterations can potentially confound [^{11}C]UCB-J measures in PDD and DLB.

Finally, the relationship between perfusion, which is considered an indirect measure of neuronal activity, and measures of putative synaptic density has not been explored in Lewy body dementia, which could provide a better understanding of the pathophysiology.

4.2 Aims and hypotheses

In this cross-sectional study, I employed [^{11}C]UCB-J PET, T1-weighted MRI and ASL-MRI to investigate synaptic density, grey matter volume and perfusion alterations, respectively, in PDD and DLB patients, along with a group of non-demented PD (previously referred to as 'treated PD') and healthy participants that served as 'control' groups, respectively. The aims of this study are the following:

1) To investigate localised alterations of synaptic density, grey matter volume and perfusion in PDD patients compared to non-demented PD and healthy controls, DLB compared to healthy controls and PDD compared directly to DLB.
2) To explore the intra-regional associations between [^{11}C]UCB-J binding for synaptic density and grey matter volume and perfusion within PDD and DLB patients.
3) To evaluate the clinical relevance of SV2A binding by interrogating its association with motor, non-motor, and cognitive symptoms.

I hypothesise that synaptic density would be extensively reduced in Lewy body dementia, expanding predominately to cortical brain areas. More specifically, relative to healthy controls I expect there to be more prominent SV2A reductions in parieto-occipital areas in Lewy body dementia. Compared to PD, I theorise that PDD patients will exhibit progressive deficits of putative synaptic density within posterior brain areas, as well as medial temporal lobe structures such as the hippocampus, that have previously been shown to be implicated in cognitive impairment and dementia in PD (Gratwicke et al., 2015). Since there is a tight coupling between neuronal activity and perfusion, the pattern of hypoperfusion may be similar to that of synaptic density in both dementia groups, with an observable linear relationship between the two measures. On the other hand, neurovascular uncoupling in these dementias could be represented by a discordance between synaptic density alterations and hypoperfusion. Whilst I expect grey

matter volume to be significantly reduced in this dementia group, I hypothesise that SV2A binding will not simply be a proxy measure of grey matter volume, but rather that grey matter volume will have some localised confounding effects on SV2A measures. Finally, within Lewy body dementia, I hypothesise that SV2A expression will be related to cognitive performance in regions-of-interest relevant to cognition. These regions-of-interest have been selected because of their association with cognitive domains that are implicated in dementia, for example, I expect synaptic density alterations in regions implicated in the fronto-striatal network to be associated with executive function (Monchi et al., 2007) and parietal alterations to be linked to attentional deficits (Williams-Gray et al., 2008). Having said this, I may expect these domain-specific brain areas to also be associated with global measures of cognition given that, for example, frontal and parietal cortices have been shown to be implicated in overall cognitive deterioration in PDD (Liepelt et al., 2009).

4.3 Methods

4.3.1 Participants

Details about participants have previously been described in detail in Chapter 2. Within this chapter, findings for ten non-demented (previously referred to as 'treated') PD patients, nine PDD patients, nine DLB patients and thirty-five healthy controls are presented.

4.3.2 Clinical assessments

Details about clinical assessments have previously been described in detail in Chapter 2.

4.3.3 MRI acquisition and pre-processing

Details regarding MRI acquisition parameters and the pre-processing pipelines have previously been described in detail in Chapter 2, Section 2.2. In this chapter, grey matter volumetric measures that were estimated with an atlas-based approach corresponding to the regional estimates of [^{11}C]UCB-J V_T are presented, as well as partial volume corrected quantitative CBF estimates.

4.3.4 [^{11}C]UCB-J PET acquisition, processing and quantification

Details about PET acquisition parameters, processing and kinetic modelling have previously been described in detail in Chapter 2, Section 2.2. In this chapter, [^{11}C]UCB-J V_T estimates based on the mean time-activity curve of each region are presented as the main outcome measure. As a secondary outcome measure, regional estimates sampled from [^{11}C]UCB-J parametric V_T maps that had been corrected for partial volume effects following the iterative Yang (IY) approach (Erlandsson et al., 2012) are described in the results. Further detail of these results can be found in Appendix B.

4.3.5 Statistical analysis

Statistical analysis and graph illustration were performed with SPSS (version 20 Chicago, Illinois, USA) and GraphPad Prism (version 6.0c) for MAC OS X, respectively. For all variables, variance homogeneity and Gaussianity were tested with Shapiro-Wilk tests. Regional [^{11}C]UCB-J V_T and volumes were transformed using the natural logarithmic function (ln) to ensure they conformed to a normal distribution. Analysis of covariance (ANCOVA) was employed to assess between-group differences in clinical variables, regional grey matter volumes, quantitative perfusion measures and [^{11}C]UCB-J V_T.

When assessing group differences in clinical measures, I conducted the following comparisons between groups with the following covariates:

- Non-demented PD vs PDD with age and gender included as covariates
- PDD vs DLB, with age and gender included as a covariates

When assessing differences in grey matter volume, perfusion and [^{11}C]UCB-J V_T, I conducted comparisons between the following groups with the following covariates:

- HC vs non-demented PD vs PDD, including age and gender as covariates. Global CBF was included as an extra covariate when assessing between-group differences in absolute perfusion.
- HC vs DLB, including gender as a covariate and global CBF when assessing between-group differences in absolute perfusion.
    - Here, age was not included as a covariate since the DLB patients were significantly older than the healthy controls. Since this covariate is related to the group variable, including it in the ANCOVA model means ANCOVA would control for both the effect of the group variable and the effect of the covariate, thereby it would bias the estimates of the group variable's effect, yielding biased conclusions (Miller and Chapman, 2001).
- PDD vs DLB, including age and gender as covariates, as well as global CBF when evaluating between-group differences in absolute perfusion.

It is important to note that in certain settings, a hierarchical approach is taken whereby one only proceeds with post-hoc tests if the omnibus F-test, which tests the null hypothesis of no mean differences across all groups, is significant. However, in this study, in the context where the omnibus F-test was not found to be significant, I proceeded with post hoc exploratory analyses. This is because there is a paucity of [^{11}C]UCB-J V_T studies comparing these groups of patients

given that [^{11}C]UCB- PET is a relatively novel radioligand, and PET studies are expensive and challenging to orchestrate in these groups of patients. Therefore, it would be useful to provide findings that may be indicative of an effect as there is currently a gap in the literature for some of the group comparisons made. Furthermore, the data presented here is unique and the sample sizes are small, and so future studies wishing to investigate synaptic density in these groups will be well-informed about potential effect sizes. Therefore, by proceeding with post hoc analyses regardless of if the omnibus F-test is significant or not, the exploratory nature of many of the findings may facilitate hypothesis generation and inform power calculations for future studies. Throughout the thesis, I have endeavoured to provide sufficient information to support power calculations for future studies.

Within each group, linear regressions were employed to assess the intra-regional relationship between grey matter volume, quantitative perfusion measures and [^{11}C]UCB-J V_T and the relationship between regional [^{11}C]UCB-J V_T and clinical assessments were interrogated using Pearson's correlation.

p values for each variable were calculated following Benjamin-Hochberg correction to control the false discovery rate (FDR), with Q=0.1. Multiple comparison corrections were not performed on secondary analyses given their exploratory nature. All data are presented as mean ±SD and the α level for significance was set for all comparisons at p<0.05.

4.3.6 Conjunction overlay

Conjunction analysis allows the identification of the common areas involved in two (or more) activation t-maps (Price and Friston, 1997). First, a one-way ANCOVA was performed in SPM12 where partial volume corrected [^{11}C]UCB-J V_T parametric maps of healthy controls, non-demented PD, PDD and DLB were populated and age and sex included as covariates. Next,

contrast maps were generated for HC > PDD, HC > DLB and non-demented PD > PDD. A conjunction analysis was performed between the contrast maps, namely [HC > PDD] & [HC > DLB] and [non-demented PD > PDD] & [HC > DLB]. The cluster-defining threshold at the voxel-level analysis was set at $p<0.005$. All results were cluster-level FDR-corrected ($p<0.05$), with an extent threshold of 200. Voxels that survived the threshold were overlaid on a canonical brain of healthy control subjects from SPM12.

4.4 Results

4.4.1 Healthy controls vs non-demented PD vs PDD

This group-level comparison was performed to assess alterations in neuroimaging measures in PDD in its entirety (PDD vs healthy controls) and those related specifically to the dementia component of the disease (PDD vs non-demented PD).

4.4.1.1 Demographic and clinical characteristics

PDD patients did not differ from healthy controls in terms of age (*MD*=5.28, 95% CI [-1.99, 12.54], p=0.15) and non-demented PD patients in terms of age (*MD*=5.63, 95% CI [-3.30, 14.56], p=0.21) and gender (X^2 (2, N=54)=0.19, p=0.91).

Compared to non-demented PD patients, those with PDD had lower educational attainment (*MD*=-3.74, 95% CI [-7.06, -0.42]), p=0.03) and a longer disease duration (*MD*=42.82, 95% CI [10.94, 74.69]). PDD patients also had worse motor symptom severity (H&Y, MDS-UPDRS Part II, MDS-UPDRS Part III), higher burden of non-motor symptoms (MDS-UPDRS Part I, PD NMS Questionnaire) and greater cognitive impairment (MMSE, MoCA). PDD patients also exhibited greater autonomic dysfunction (SCOPA-AUT), experienced more sleep disturbances (PDSS, ESS) and pain (King's PD Pain Questionnaire), were more depressed (GDS), and had an

overall greater disease burden (MDS-UPDRS Total, PDQ-39) compared to non-demented PD patients. All *p* values, in addition to means and standard deviations can be found in Table 4.1.

Table 4.1. Demographic and clinical characteristics of non-demented PD patients and PDD

Characteristic (mean ±SD)	Non-demented PD	PDD	P value
No. (M/F)	10 (7M/3F)	9 (6M/3F)	0.91
Age (years)	61.7 ± 6.4	67.3 ± 9.3	0.21
Disease duration (months)	50.4 ± 31.4	104.2 ± 44.0	**0.027***
Education (years)	17.0 ± 2.5	13.0 ± 3.6	**0.03***
LEDD (mg)	467.6 ± 227.6	721.1 ± 308.0	0.097
H&Y	1.5 ± 0.5	3.0 ± 0.0	**<0.001***
MDS-UPDRS I	6.3 ± 3.2	21.2 ± 3.2	**<0.001***
MDS-UPDRS II	5.9 ± 3.4	20.4 ± 4.3	**<0.001***
MDS-UPDRS III	24.8 ± 6.1	52.2 ± 13.0	**<0.001***
MDS-UPDRS Total	37.6 ± 9.5	93.9 ± 14.5	**<0.001***
SCOPA-AUT	6.6 ± 4.0	20.0 ± 5.7	**<0.001***
PD NMS Questionnaire	6.1 ± 4.0	13.3 ± 3.8	**0.001***
ESS	5.7 ± 1.9	9.0 ± 7.2	**0.024***
RBDQ	3.2 ± 3.4	4.0 ± 2.6	0.90
PDSS	124.6 ± 18.1	105.0 ± 8.9	**0.016***
King's PD Pain Questionnaire	1.1 ± 1.29	3.2 ± 1.9	**0.002***
UPSIT	20.3 ± 6.7	16.4 ± 4.9	0.41
MMSE	29.3 ± 0.8	23.3 ± 3.3	**<0.001***
MoCA	27.6 ± 1.9	20.6 ± 4.1	**0.001***
GDS	4.0 ± 4.8	13.2 ± 6.1	**0.001***

Abbreviations: H&Y=Hoehn and Yahr scale; MDS-UPDRS=Movement Disorder Society Unified Parkinson's Disease Rating Scale; MMSE=Mini Mental Status Examination; MoCA=Montreal Cognitive Assessment; PDSS: Parkinson's disease sleep scale; PD NMS Questionnaire=Parkinson's disease Non-Motor Symptom Questionnaire; ESS: Epworth Sleepiness Scale; RBDQ=REM Behaviour Sleep Disorder Questionnaire; SCOPA-AUT=Scales for Outcomes of Parkinson's disease–Autonomic; GDS=Geriatric Depression Scale

*p<0.05 between non-demented PD and PDD, FDR-corrected

4.4.1.2 Grey matter volume: Regions-of-interest analysis

There were statistically significant differences in GM volume between at least two groups in the amygdala ($F(2,49)=4.54$, $p=0.016$), dorsolateral prefrontal cortex ($F(2,49)=5.36$, $p=0.008$), orbitofrontal cortex ($F(2,49)=4.80$, $p=0.013$), postcentral gyrus ($F(2,49)=4.23$, $p=0.02$), insular cortex ($F(2,49)=4.44$, $p=0.017$), nucleus accumbens ($F(2,49)=3.63$, $p=0.034$), parahippocampal gyrus ($F(2,49)=4.68$, $p=0.014$), and temporal lobe ($F(2,49)=3.53$, $p=0.037$).

Post hoc analysis revealed that when compared to healthy controls, PDD patients exhibited reduced volume in the amygdala, although this did not survive FDR-correction for multiple comparisons (Table 4.2). Compared to non-demented PD patients, PDD patients had reduced volume in limbic structures such as the amygdala, insular cortex and anterior cingulate ($p_{FDR\text{-}corrected}<0.05$; Table 4.2; Figure 4.1), with further volume reductions observed in the frontal and parietal brain areas ($p_{FDR\text{-}corrected}<0.05$; Table 4.1). Within exploratory brain areas, lower volumes were found in limbic structures and the temporal lobe in PDD patients compared to non-demented PD patients ($p_{uncorrected}<0.05$; Table 4.2; Figure 4.1).

Table 4.2. Group comparison of regional volumes in healthy controls, non-demented PD patients and PDD patients

Volume, mm³ (mean ±SD)	HC n=35	Non-demented PD n=10	PDD n=9	P value HC vs PDD	P value Non-demented PD vs PDD
Caudate	4809 ± 694	5038 ± 511	4379 ± 1170	0.14 (-9%)	0.067 (-13%)
Putamen	6733 ± 730	6689 ± 489	6818 ± 1135	0.58 (+1%)	0.46 (+2%)
Thalamus	7504 ± 1165	7936 ± 871	6826 ± 1139	0.24 (-9%)	0.062 (-14%)
Amygdala	3842 ± 453	4023 ± 266	3524 ± 438	**0.04$^{\$\wedge}$ (-8%)**	**0.004* (-12%)**
Hippocampus	7801 ± 869	8265 ± 854	7470 ± 987	0.60 (-4%)	0.10 (-10%)
Precentral gyrus	29882 ± 4291	30904 ± 2446	27694 ± 3443	0.27 (-7%)	0.12 (-11%)

Supplementary motor area	5440 ± 772	5615 ± 583	5060 ± 454	0.29 (-7%)	0.14 (-10%)
Dorsolateral prefrontal cortex	73204 ± 9223	80798 ± 7074	67661 ± 9223	0.19 (-8%)	**0.003* (-16%)**
Orbitofrontal prefrontal cortex	28071 ± 3934	31152 ± 3022	26816 ± 3372	0.67 (-4%)	**0.013* (-14%)**
Postcentral gyrus	20152 ± 2603	21006 ± 2038	18227 ± 2152	**0.02$ (-10%)**	**0.007* (-13%)**
Superior parietal lobule	15042 ± 1998	15896 ± 1261	14391 ± 1699	0.57 (-6%)	0.12 (-10%)
Precuneus	23518 ± 3591	24590 ± 2641	22130 ± 2263	0.58 (-6%)	0.20 (-10%)
Inferior parietal lobe	32808 ± 4556	34492 ± 3461	30332 ± 4183	0.19 (-8%)	**0.046*^ (-12%)**
Insular cortex	12697 ± 1653	13977 ± 1228	12294 ± 1390	1.00 (-3%)	**0.03* (-12%)**
Occipital lobe	72671 ± 9223	76419 ± 8040	67791 ± 9223	0.28 (-7%)	0.052 (-11%)
Exploratory regions-of-interest					
Brainstem	4288 ± 662	4623 ± 545	4161 ± 745	0.62 (-3%)	0.11 (-10%)
Nucleus accumbens	2973 ± 329	3144 ± 228	2801 ± 397	0.18 (-6%)	**0.011$ (-11%)**
Parahippocampal gyrus	9158 ± 1171	9993 ± 822	8702 ± 1023	0.46 (-5%)	**0.009$ (-15%)**
Anterior cingulate	29389 ± 4789	32124 ± 3136	27577 ± 4264	0.53 (-6%)	**0.03$^ (-14%)**
Posterior cingulate	11198 ± 1912	11805 ± 1288	10643 ± 1318	0.98 (-5%)	0.29 (-10%)
Temporal lobe	84041 ± 11606	88671 ± 7900	77115 ± 10892	0.078 (-8%)	**0.011$ (-13%)**
Cerebellum	98563 ± 9695	101827 ± 9446	98229 ± 12684	0.76 (0%)	0.67 (-4%)

**p<0.05, FDR-corrected; $p<0.05, uncorrected. ^ANCOVA omnibus test was not statistically significant*

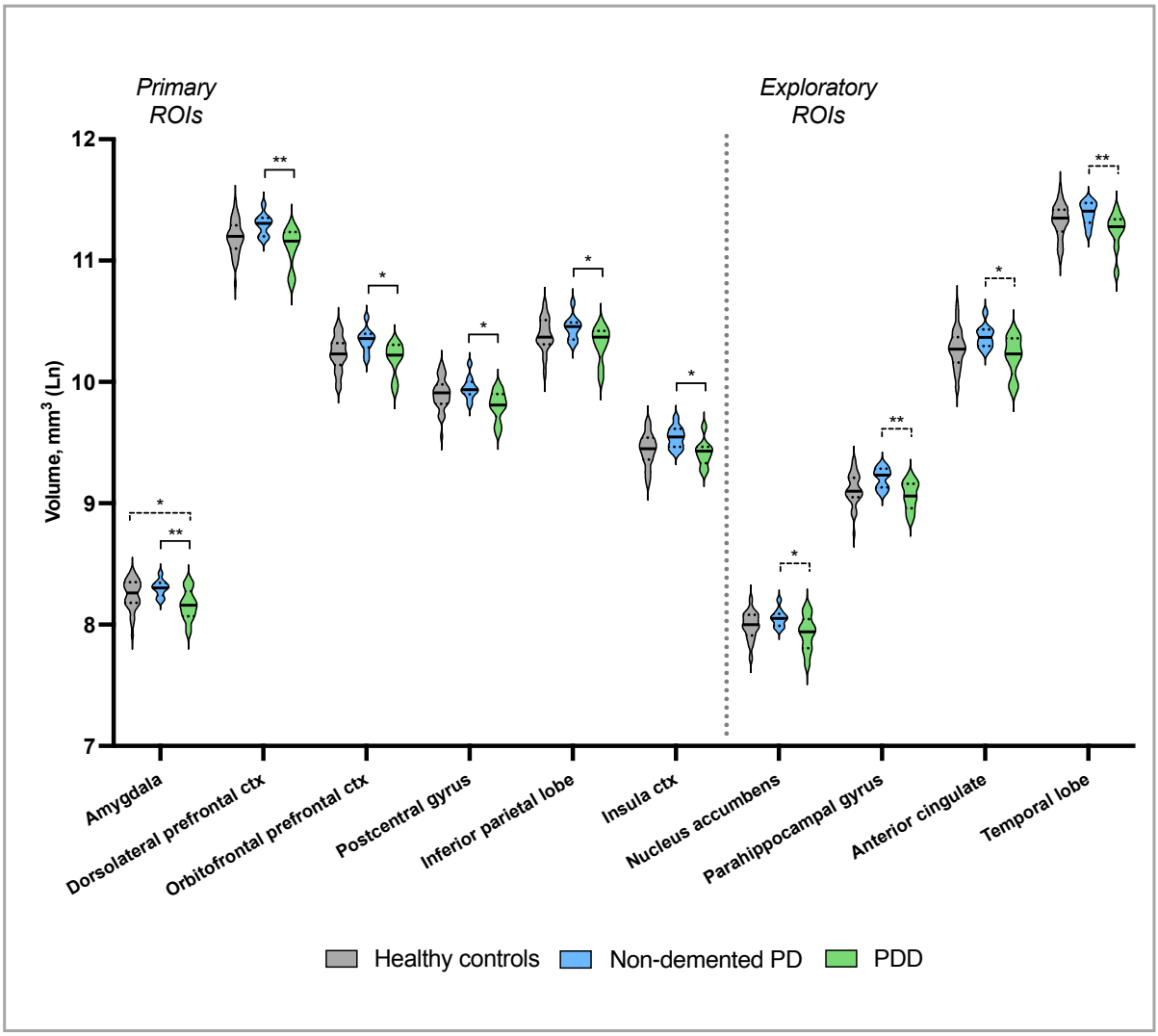

Figure 4.1. Violin plots illustrating cross-sectional differences in volume between healthy controls, non-demented PD and PDD groups. ***p<0.001; **p<0.01; *p<0.05, FDR-corrected; ---- uncorrected p value. ROIs=regions-of-interest; V_T=volume of distribution; Ln=natural log transformation. Exploratory regions-of-interest=additional brain areas that were analysed for exploratory purposes. Multiple comparison corrections were not performed on these secondary analyses.

4.4.1.3 Cerebral blood flow: Regions-of-interest analysis

There were statistically significant differences between at least two groups in global CBF ($F(2,49)=4.91$, $p=0.012$). After controlling for age, gender and global CBF, significant differences between at least two groups were identified in the precuneus ($F(2,49)=5.45$, $p=0.008$) and occipital lobe ($F(2,49)=8.89$, $p=0.001$).

Pairwise comparisons demonstrated that compared to healthy controls, PDD patients exhibited a global reduction of CBF, with region-specific reductions of up to 34% in areas of the parietal lobe and 37% in the occipital lobe (Table 4.3; Figure 4.2). In exploratory regions-of-interest, hypoperfusion was present in the anterior cingulate and temporal lobe.

Compared to non-demented PD, PDD patients exhibited hypoperfusion in parieto-occipital areas, with hyperperfusion observed in the supplementary motor area and anterior cingulate (Table 4.3; Figure 4.2).

Table 4.3. Group comparison of regional CBF (partial volume corrected) in healthy controls, non-demented PD patients and PDD patients.

Cerebral blood flow, ml/100g/min (mean ±SD)	**HC n=31**	**Non-demented PD n=10**	**PDD n=9**	**P value HC vs PDD**	**P value Non-demented PD vs PDD**
Global CBF	65.8 ± 9.8	60.1 ± 13.7	54.1 ± 8.3	**0.005 (-18%)**	0.21 (-10%)
Primary regions-of-interest					
Caudate	36.4 ± 7.9	33.9 ± 9.7	26.8 ± 9.4	0.16 (-26%)	0.15 (-21%)
Putamen	57.2 ± 11	51.3 ± 13.6	48 ± 16	0.87 (-16%)	0.87 (-7%)
Thalamus	59.5 ± 16	61.3 ± 21.1	47.9 ± 11.7	0.89 (-20%)	0.43 (-22%)
Amygdala	58.8 ± 17.7	56.4 ± 20.6	61.9 ± 26.6	0.062 (+5%)	0.17 (+10%)
Hippocampus	78.5 ± 18.9	80.8 ± 21.4	78.5 ± 21	0.25 (0%)	0.50 (-3%)
Precentral gyrus	63 ± 13.2	57.4 ± 18.6	59.3 ± 9.8	0.086 (-6%)	0.065 (+3%)
Supplementary motor area	58.2 ± 12.7	51.9 ± 18.6	61.2 ± 12.4	0.061 (+5%)	**0.017*^ (+18%)**
Dorsolateral prefrontal cortex	54.7 ± 10.4	49.7 ± 14.7	39.3 ± 9.4	0.06 (-28%)	0.072 (-21%)
Orbitofrontal prefrontal cortex	49.9 ± 9.8	42.1 ± 14.1	42.3 ± 18.8	0.93 (-15%)	0.68 (0%)
Postcentral gyrus	58.4 ± 13.9	52.2 ± 13.6	53.5 ± 8.2	0.34 (-9%)	0.22 (+2%)
Superior parietal lobule	49.8 ± 14	45.8 ± 8.3	36 ± 4.6	**0.003*^ (-28%)**	**0.035$^ (-21%)**

Precuneus	64 ± 11.9	60.5 ± 15.1	42.5 ± 10	**0.003*** **(-34%)**	**0.005*** **(-30%)**
Inferior Parietal lobe	59.1 ± 13	50.1 ± 10.1	43.5 ± 10.7	**0.05$^** **(-26%)**	0.32 (-13%)
Insular cortex	59.5 ± 13.1	52.3 ± 15	62.8 ± 12.6	0.67 (-3%)	0.27 (+6%)
Occipital lobe	59.6 ± 9.5	54.2 ± 15	37.7 ± 7.1	**<0.001*** **(-37%)**	**0.001*** **(-30%)**
Exploratory regions-of-interest					
Brainstem	43.5 ± 11	44.5 ± 11.3	40.4 ± 10.7	0.16 (-7%)	0.95 (-9%)
Nucleus accumbens	42.7 ± 8.9	37.6 ± 11.5	35.3 ± 15.3	0.67 (-17%)	0.68 (-6%)
Parahippocampal gyrus	69.5 ± 18.3	71.9 ± 20	72.3 ± 22.6	0.058 (+4%)	0.49 (1%)
Anterior cingulate	55.9 ± 11.5	49.8 ± 16.9	51.6 ± 11.9	**0.04$^** **(-8%)**	**0.024$^** **(+4%)**
Posterior cingulate	70 ± 16.4	69.2 ± 16.7	57.5 ± 5.7	0.93 (-18%)	0.23 (-17%)
Temporal lobe	52.4 ± 8.9	45.3 ± 11.3	46.7 ±10.2	0.37 (-11%)	0.06 (+3%)
Cerebellum	56.5 ± 13.2	59.9 ± 21.3	52 ± 11.1	0.37 (-8%)	0.98 (-13%)

**p<0.05, FDR-corrected; $p<0.05, uncorrected. ^ANCOVA omnibus test was not statistically significant*

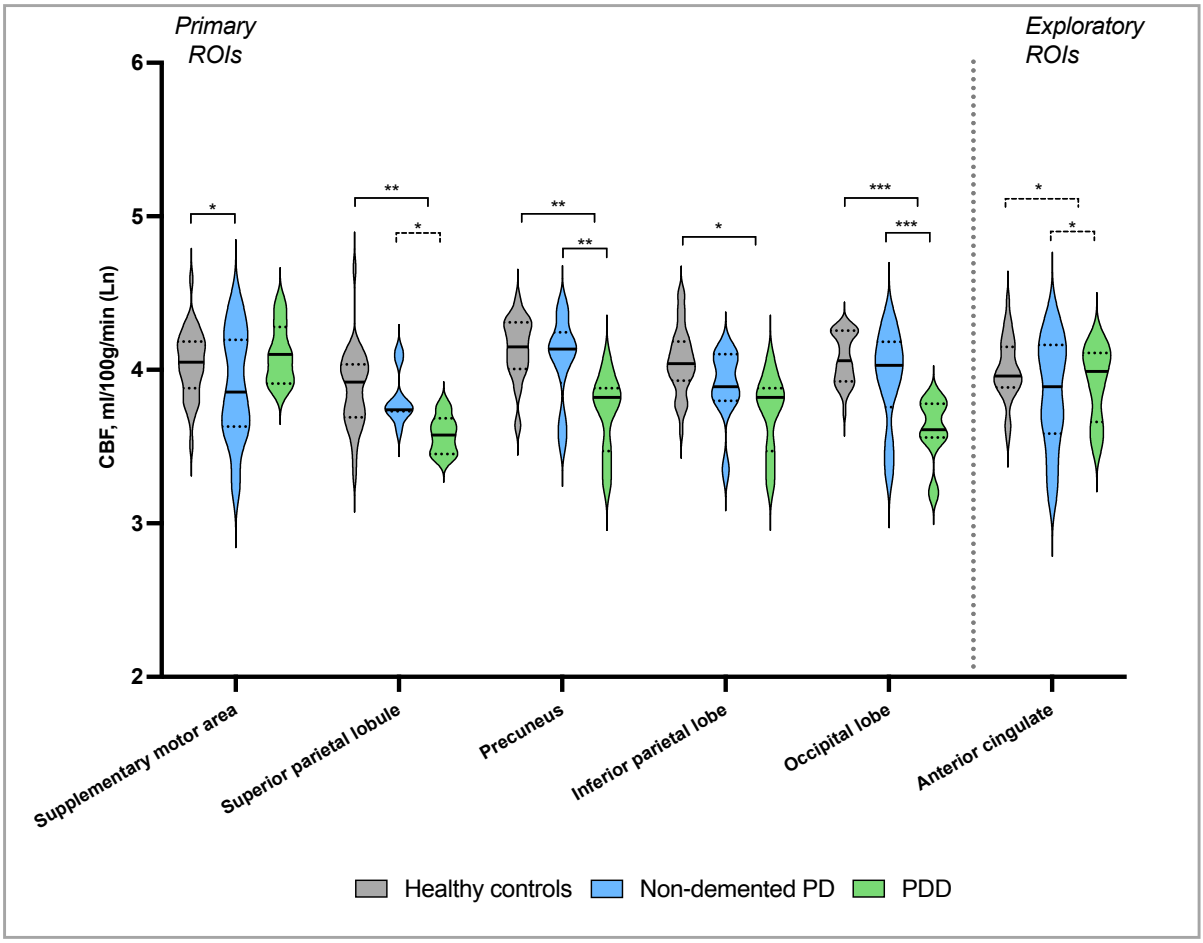

Figure 4.2. Violin plots illustrating cross-sectional differences in CBF between healthy controls, non-demented PD and PDD groups. ***p<0.001; **p<0.01; *p<0.05, FDR-corrected; ---- uncorrected p value. ROIs=regions-of-interest; V_T=volume of distribution; Ln=natural log transformation. Exploratory regions-of-interest=additional brain areas that were analysed for exploratory purposes. Multiple comparison corrections were not performed on these secondary analyses.

4.4.1.4 [^{11}C]UCB-J V_T: Regions-of-interest analysis

The results presented in this section are those using the regional TAC-based estimates (uncorrected for partial volume effects) and following PVC performed on the parametric [^{11}C]UCB-J V_T maps. There was high correspondence between regional TAC-based values and those obtained using the parametric maps as demonstrated by the strong correlations between the two across all regions-of-interest (r=0.94 - >0.99), highlighting the strong agreement between TAC-based values and values obtained from parametric maps. Comparisons between groups using the [^{11}C]UCB-J V_T parametric map were largely analogous to those found using the

TAC-based estimates and can be found in Appendix C. Please note: ANCOVA models including volume as an additional covariate were only performed for TAC-based [^{11}C]UCB-J V_T estimates that were uncorrected for partial volume effects.

One-way ANCOVA revealed that there were statistically significant differences in [^{11}C]UCB-J V_T between at least two groups in the caudate ($F(2,49)=3.52$, $p=0.037$), thalamus ($F(2,49)=4.04$, $p=0.024$) and superior parietal lobule ($F(2,49)=4.37$, $p=0.018$).

Although PDD patients generally exhibited lower levels of [^{11}C]UCB-J V_T across cortical and subcortical brain regions, post hoc analysis revealed principal reductions in parietal regions (of up to -17%), the caudate and thalamus, as well as the precentral and postcentral gyrus and supplementary motor area ($p_{FDR\text{-}corrected}<0.05$; Table 4.4; Figure 4.3) when compared to healthy controls. After controlling for volume, significant differences remained to be observed in the parietal lobule ($p_{FDR\text{-}corrected}=0.006$), alongside the caudate ($p_{uncorrected}=0.04$), thalamus ($p_{uncorrected}=0.017$), precuneus ($p_{uncorrected}=0.048$) and supplemental motor area ($p_{uncorrected}=0.044$), though the latter four findings did not survive FDR-correction for multiple comparisons. Following PVC, significant reductions persisted within the caudate, thalamus and parietal areas ($p<0.05$).

Pairwise comparisons showed that when PDD patients were compared to non-demented PD patients, lower level of [^{11}C]UCB-J V_T were observed in the thalamus and parietal lobule, though these findings did not survive after controlling for volume or following FDR-correction for multiple comparisons (Table 4.4; Figure 4.3). However, after PVC, differences remained significant in the thalamus and parietal lobule, with additional reductions seen in the caudate and precuneus ($p_{uncorrected}<0.05$), although this did not survive FDR-correction for multiple comparisons.

Table 4.4. Group comparison of [^{11}C]UCB-J V_T in healthy controls, non-demented PD patients and PDD patients.

[^{11}C]UCB-J V_T, ml/cm^3 (mean ±SD)	HC n=35	Non-demented PD n=10	PDD n=9	P value HC vs PDD	P value Non-demented PD vs PDD
Caudate	14.4 ± 2.6	13.6 ± 1.4	11.8 ± 3.5	**0.011*** **(-18%)**	0.12 (-14%)
Putamen	22.8 ± 2.8	22.1 ± 2.3	21.2 ± 4.2	0.26 (-7%)	0.65 (-4%)
Thalamus	12.5 ± 1.9	12.4 ± 1.1	10.4 ± 2.5	**0.008*** **(-17%)**	**0.027$** **(-16%)**
Amygdala	17.6 ± 2.1	17.4 ± 2.1	17.5 ± 2.8	0.82 (-1%)	0.65 (0%)
Hippocampus	14.5 ± 2	14.4 ± 1.2	13.5 ± 2.6	0.41 (-7%)	0.53 (-6%)
Precentral gyrus	16.4 ± 2.1	16 ± 1.4	14.5 ± 2.7	**0.042*^** **(-12%)**	0.12 (-10%)
Supplementary motor area	17.8 ± 2.4	17.4 ± 1.5	15.6 ± 3.1	**0.032*^** **(-13%)**	0.15 (-10%)
Dorsolateral prefrontal cortex	17.9 ± 2.3	17.7 ± 1.5	16.2 ± 3.7	0.12 (-9%)	0.28 (-8%)
Orbitofrontal prefrontal cortex	19.6 ± 2.4	19.7 ± 2	19.4 ± 3.9	0.93 (-1%)	0.99 (-2%)
Postcentral gyrus	15.9 ± 2.1	15.7 ± 1.5	13.9 ± 2.6	**0.038*^** **(-13%)**	0.11 (-12%)
Superior parietal lobule	17.3 ± 2.4	16.9 ± 1.8	14.4 ± 2.9	**0.005*** **(-17%)**	**0.043$** **(-15%)**
Precuneus	19.8 ± 2.7	19.5 ± 1.5	17.4 ± 3	**0.038*^** **(-12%)**	0.13 (-11%)
Inferior Parietal lobe	18.5 ± 2.5	18.4 ± 1.6	16.1 ± 2.9	**0.023*** **(-13%)**	0.07 (-12%)
Insular cortex	21 ± 2.7	21.3 ± 1.9	19.7 ± 4.1	0.43 (-6%)	0.37 (-8%)
Occipital lobe	18.2 ± 2.4	17.9 ± 1.5	16.6 ± 2.6	0.46 (-9%)	0.53 (-7%)
Exploratory regions-of-interest					
Brainstem	8.6 ± 1	8.3 ± 0.4	8.1 ± 1.1	0.49 (-5%)	0.90 (-2%)
Nucleus accumbens	22 ± 2.9	21.7 ± 2.3	20.2 ± 4.5	0.23 (-8%)	0.41 (-7%)
Parahippocampal gyrus	17 ± 2.2	16.9 ± 1.4	16.8 ± 3.1	0.79 (-1%)	0.83 (-1%)
Anterior cingulate	20.7 ± 2.7	20.8 ± 1.8	19.2 ± 4.2	0.29 (-7%)	0.34 (-8%)
Posterior cingulate	20.3 ± 2.9	19.9 ± 1.6	18.1 ± 3.4	0.091 (-11%)	0.26 (-9%)

Temporal lobe	20.2 ± 2.6	20.3 ± 1.9	19.1 ± 3.7	0.16 (-6%)	0.39 (-6%)
Cerebellum	16.3 ± 2	15.9 ± 1.4	15.1 ± 2	0.14 (-7%)	0.14 (-5%)

**p<0.05, FDR-corrected; $p<0.05, uncorrected. ^ANCOVA omnibus test was not statistically significant*

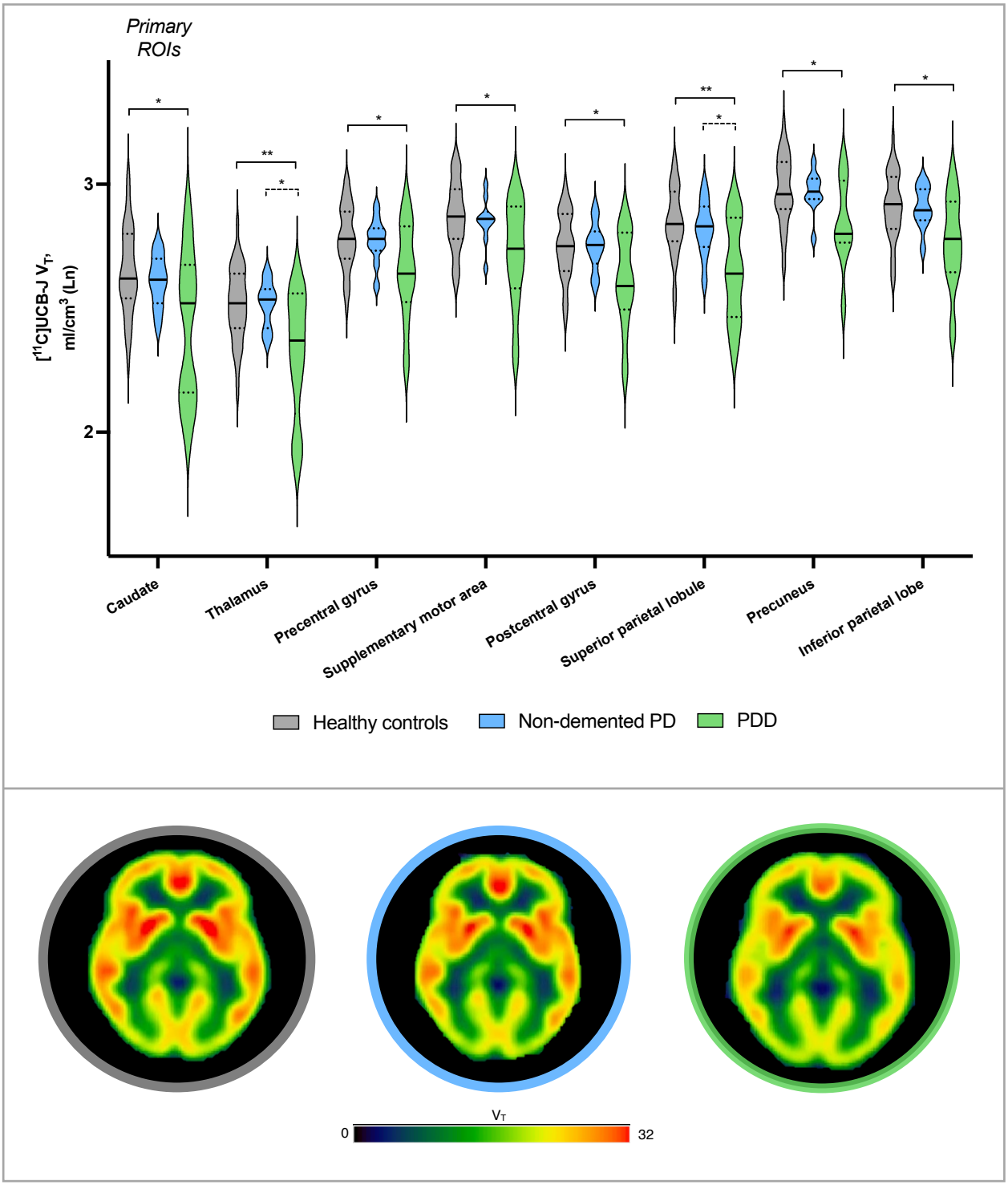

Figure 4.3. Violin plots showing regional [11C]UCB-J V_T for healthy controls, non-demented PD and PDD patients. The bottom panel displays mean axial [11C]UCB-J maps for controls (grey, n=35), non-demented PD patients (blue, n=11) and PDD patients (green, n=9). ***p<0.001; **p<0.01; *p<0.05, FDR-corrected; ----

uncorrected p value. ROIs=regions-of-interest; V_T=volume of distribution; Ln=natural log transformation. Exploratory regions-of-interest=additional brain areas that were analysed for exploratory purposes. Multiple comparison corrections were not performed on these secondary analyses.

4.4.1.5 Simple linear regression: regional GM volumes and [^{11}C]UCB-J V_T

Since some regional [^{11}C]UCB-J V_T differences did not survive after controlling for volume, which is suggestive of specific regional [^{11}C]UCB-J V_T differences actually reflecting volumetric differences, a confirmatory simple linear regression analysis was conducted between regional [^{11}C]UCB-J V_T (dependent variable) and volumetric estimates (independent variable) in those specific brain areas. In PDD patients, GM volume in the inferior parietal lobe explained 62% of [^{11}C]UCB-J V_T variance ($F(1,7)=11.48$, $R^2=0.62$, $p=0.012$) and was a significant predictor ($\beta=1.00$, $p=0.012$; Figure 4.4). Similarly, GM volume in the postcentral gyrus explained 62% of [^{11}C]UCB-J V_T variance ($F(1,7)=11.25$, $R^2=0.62$, $p=0.012$), which was identified as a significant predictor of [^{11}C]UCB-J V_T ($\beta=1.25$, $p=0.012$; Figure 4.4). Whilst GM volume in the precentral gyrus explained 43% of [^{11}C]UCB-J V_T variance, the model was not statistically significant ($F(1,7)=5.34$, $R^2=0.43$, $p=0.054$), and it was not a statistically significant predictor ($\beta=1.01$, $p=0.054$).

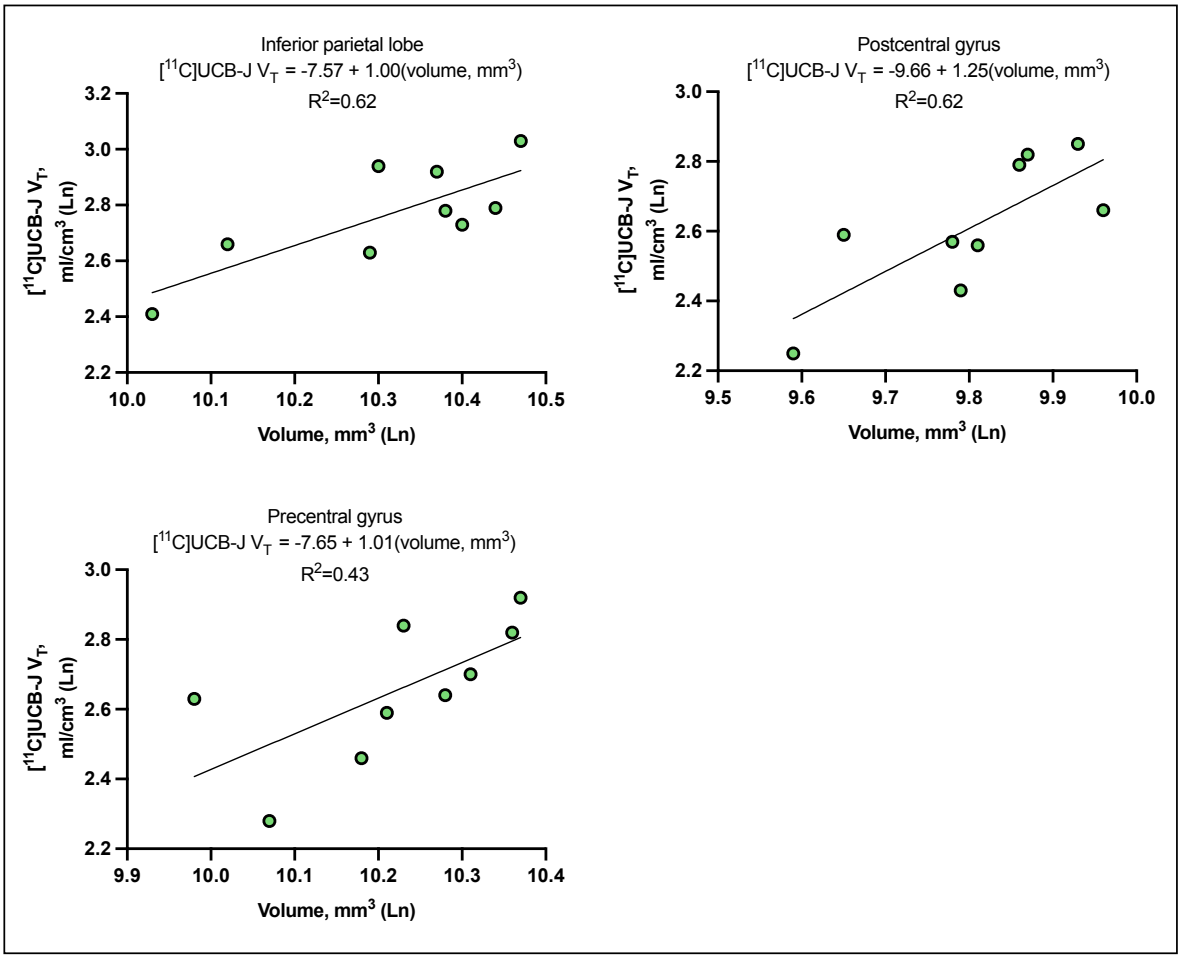

Figure 4.4. Linear regressions between regional [^{11}C]UCB-J V_T and volume in PDD patients. Higher volumetric estimates predicted higher [^{11}C]UCB-J V_T in parietal brain areas.

4.4.1.6 Simple linear regression: regional [^{11}C]UCB-J V_T and CBF

In order to assess the intra-regional associations between [^{11}C]UCB-J V_T and CBF; more specifically whether SV2A estimates influence CBF measures, a simple linear regression analysis was performed between [^{11}C]UCB-J V_T (independent variable) and CBF (dependent variable) within each region. Both measures included here were partial volume corrected in an attempt to minimise the potential amplificatory influence volumetric reductions could have on their association.

Within PDD patients, regional [^{11}C]UCB-J V_T was not a significant predictor of CBF in any regions-of-interest.

4.4.2 Healthy controls vs DLB

4.4.2.1 Demographic and clinical characteristics

DLB patients were significantly older than healthy controls (*MD*=10.72, 95% CI [3.47, 17.97], p=0.005), though there were no differences in gender (gender: X^2 (1, N=44)=2.24, p=0.14).

4.4.2.2 Grey matter volume: regions-of-interest analysis

Expectedly, DLB patients had extensive reductions in volume across all regions-of-interest compared to healthy controls (see Table 4.5 for a full list of regions). The largest reduction of volume was observed subcortically within the caudate (-27%) and thalamus (-24%) with comparable volume reductions across all cortical areas (Table 4.5; Figure 4.5). Further reductions were observed within all exploratory regions-of-interest, with the greatest reduction evident in the hippocampus (-20%, Table 4.5).

Table 4.5. Group comparison of regional volume across healthy controls and DLB patients

Volume, mm³ (mean ±SD)	HC n=35	DLB n=9	P value HC vs DLB
Nucleus accumbens	2973 ± 329	2455 ± 179	**<0.001* (-17%)**
Caudate	4809 ± 694	3495 ± 1036	**<0.001* (-27%)**
Thalamus	7504 ± 1165	5737 ± 699	**<0.001* (-24%)**
Amygdala	3842 ± 453	3142 ± 172	**<0.001* (-18%)**
Frontal lobe	157435 ± 21849	133181 ± 18373	**<0.001* (-15%)**
Temporal lobe	84041 ± 11606	70741 ± 7935	**<0.001* (-16%)**
Precuneus	23518 ± 3591	19114 ± 3668	**<0.001* (-19%)**
Inferior parietal lobe	32808 ± 4556	28121 ± 5577	**<0.001* (-14%)**
Superior parietal lobule	15042 ± 1998	13043 ± 2595	**0.001* (-13%)**
Lingual gyrus	12703 ± 1549	10865 ± 1051	**<0.001* (-14%)**
Cuneus	4212 ± 574	3526 ± 579	**<0.001***

			(-16%)
Calcarine sulcus	8178 ± 1540	6453 ± 978	**<0.001$ (-21%)**
Occipital pole	47578 ± 6242	41168 ± 6184	**<0.001$ (-13%)**
Insular cortex	12697 ± 1653	10683 ± 1191	**<0.001* (-16%)**
Anterior cingulate	29389 ± 4789	24172 ± 2821	**<0.001* (-18%)**
Posterior cingulate	11198 ± 1912	9161 ± 1546	**<0.001* (-18%)**
Exploratory regions-of-interest			
Brainstem	4288 ± 662	3764 ± 809	**<0.001$ (-12%)**
Putamen	6733 ± 730	5561 ± 907	**<0.001$ (-18%)**
Hippocampus	7801 ± 869	6276 ± 582	**<0.001* (-20%)**
Parahippocampal gyrus	9158 ± 1171	7965 ± 617	**<0.001* (-13%)**
Fusiform gyrus	25148 ± 3184	21203 ± 1796	**<0.001* (-16%)**
Cerebellum	98563 ± 9695	84741 ± 18122	**<0.001$ (-14%)**

**p<0.05, FDR-corrected; $p<0.05, uncorrected.*

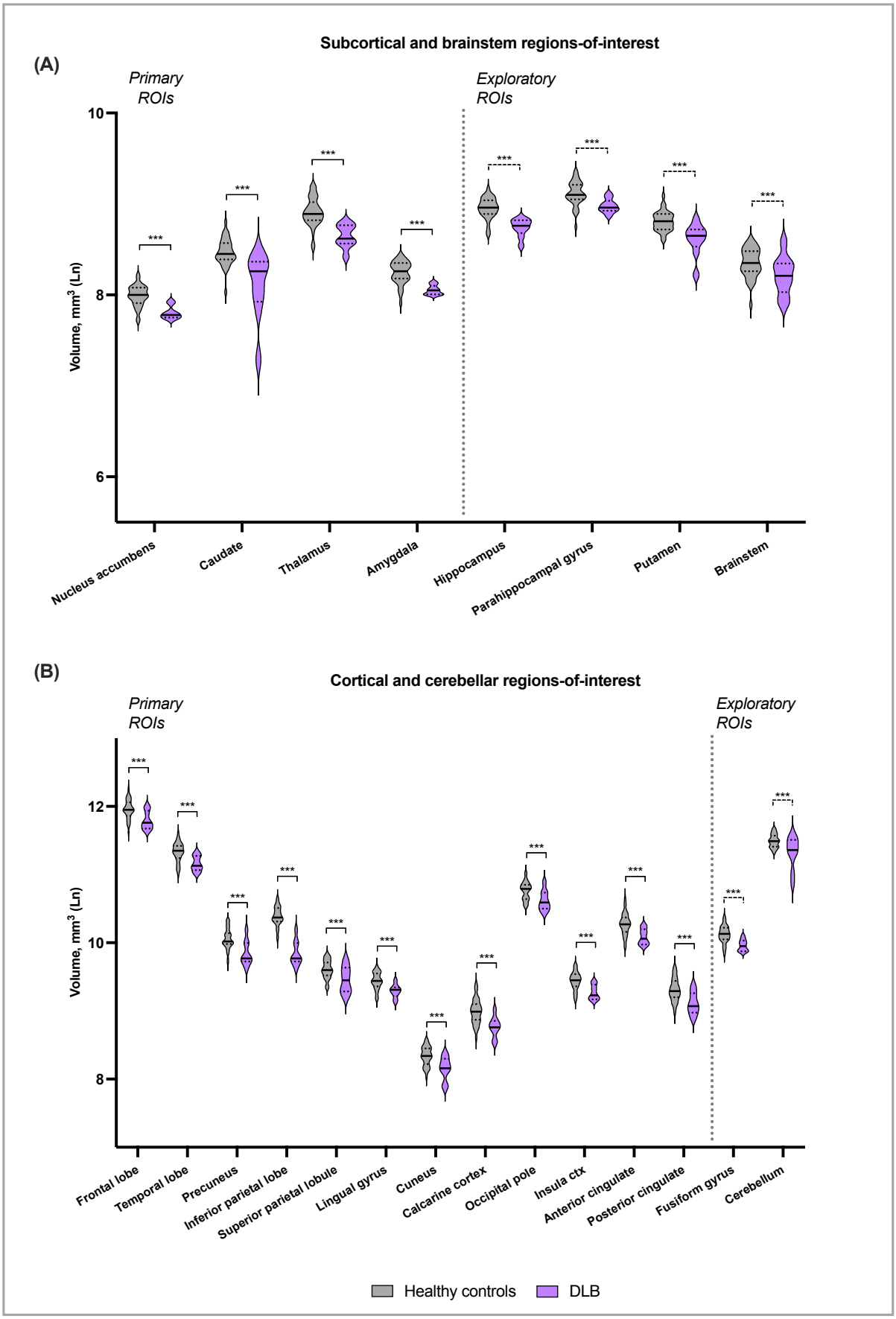

Figure 4.5. Violin plots illustrating cross-sectional differences in volume between healthy controls and DLB patients. (A) Subcortical and brainstem brain areas exhibiting significant alterations in GM volume between

groups; (B) Cortical brain areas exhibiting alterations in in GM volume between groups. ***p<0.001; **p<0.01; *p<0.05, FDR-corrected; ---- uncorrected p value. ROIs=regions-of-interest; V_T=volume of distribution; Ln=natural log transformation. Exploratory regions-of-interest=additional brain areas that were analysed for exploratory purposes. Multiple comparison corrections were not performed on these secondary analyses.

4.4.2.3 Cerebral blood flow: region-of-interest analysis

Global CBF was significantly reduced by 21% in DLB patients compared to healthy controls, with regional reductions observed in the frontal lobe, occipitoparietal areas and the anterior cingulate (For a full list of regions, see Table 4.6). Conversely, DLB patients exhibited CBF hyperperfusion in the amygdala relative to healthy controls (Table 4.6; Figure 4.6).

Table 4.6. Group comparison of CBF (partial volume corrected) in healthy controls and DLB patients.

Cerebral blood flow, ml/100g/min (mean ±SD)	HC n=31	DLB n=9	P value HC vs DLB
Global CBF	65.8 ± 9.8	52.3 ± 12.5	**<0.001 (-21%)**
Primary regions-of-interest			
Nucleus accumbens	42.7 ± 8.9	41.3 ± 14.5	0.28 (-3%)
Caudate	36.4 ± 7.9	27.5 ± 10.9	0.43 (-24%)
Thalamus	59.5 ± 16	45.4 ± 12.6	0.85 (-24%)
Amygdala	58.8 ± 17.7	67.1 ± 15.8	**0.009* (+14%)**
Frontal lobe	56.2 ± 10	42.7 ± 15.5	**0.011* (-24%)**
Temporal lobe	52.4 ± 8.9	45 ± 13	0.33 (-14%)
Precuneus	64 ± 11.9	39.8 ± 18.5	**<0.001* (-38%)**
Inferior parietal lobe	59.1 ± 13	41 ± 16.5	**0.031* (-31%)**
Superior parietal lobule	49.8 ± 14	29.4 ± 18	**<0.001* (-46%)**
Lingual gyrus	80 ± 17.2	61.3 ± 19.6	0.25 (-23%)
Cuneus	69.7 ± 17.4	50.4 ± 17.1	**0.002* (-28%)**
Calcarine cortex	80.9 ± 13.9	65.2 ± 14.5	**0.001* (-19%)**

Occipital pole	51 ± 9.3	27.6 ± 14.7	**<0.001* (-44%)**
Insular cortex	59.5 ± 13.1	58.6 ± 13.1	0.69 (-2%)
Anterior cingulate	55.9 ± 11.5	53.7 ± 14.9	**0.01* (-4%)**
Posterior cingulate	70 ± 16.4	59.4 ± 16.6	0.96 (-15%)
Exploratory regions-of-interest			
Brainstem	43.5 ± 11	31.7 ± 9.2	0.77 (-27%)
Putamen	57.2 ± 11	55.2 ± 9.3	0.061 (-4%)
Hippocampus	42.9 ± 9.9	39.3 ± 9	0.083 (-8%)
Parahippocampal gyrus	69.5 ± 18.3	69 ± 26.2	0.48 (-1%)
Fusiform gyrus	58.2 ± 12.5	47.7 ± 15.4	0.74 (-18%)
Cerebellum	56.5 ± 13.2	41.3 ± 14	0.68 (-27%)

**p<0.05, FDR-corrected; $p<0.05, uncorrected.*

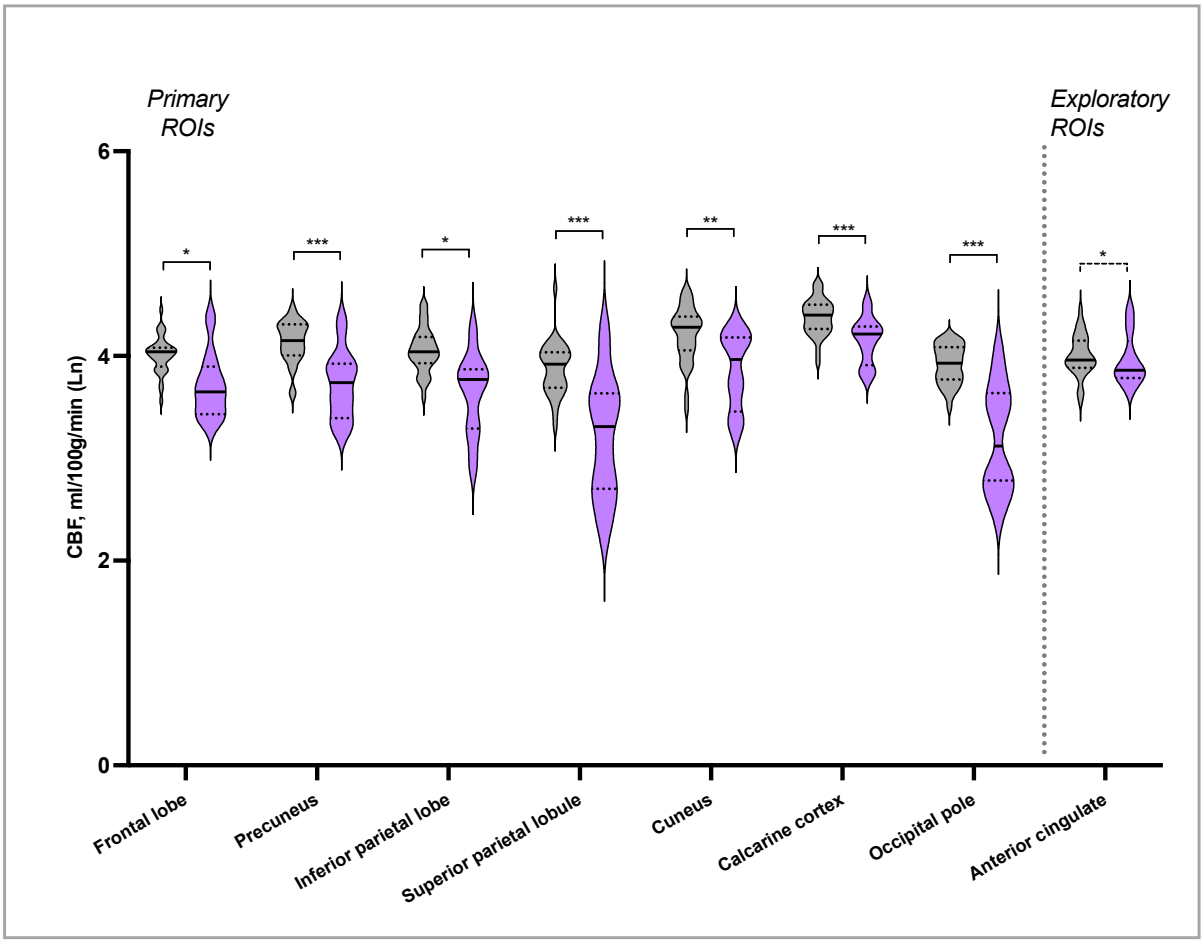

Figure 4.6. Violin plots illustrating cross-sectional differences in CBF between healthy controls and DLB patients. ***p<0.001; **p<0.01; *p<0.05, FDR-corrected; ---- uncorrected p value. CBF=cerebral blood flow; ROIs=regions-of-interest; V_T=volume of distribution; Ln=natural log transformation. Exploratory regions-of-interest=additional brain areas that were analysed for exploratory purposes. Multiple comparison corrections were not performed on these secondary analyses.

4.4.2.4 [^{11}C]UCB-J V_T: region-of-interest analysis

Compared to healthy controls, DLB patients exhibited a widespread reduction of [^{11}C]UCB-J V_T across all primary regions-of-interest (see Table 4.7 for a full list of regions), with more prominent reductions observed in the caudate and thalamus ($p_{FDR\text{-}corrected}$<0.001). DLB patients had reduced [^{11}C]UCB-J V_T within key limbic structures, as well as all lobes of the brain, with parietal and occipital areas appearing to be somewhat more affected in DLB as reflected by slightly lower levels of [^{11}C]UCB-J V_T (Table 4.7; Figure 4.7). After controlling for volume, DLB continued to exhibit a reduction in [^{11}C]UCB-J V_T in the parietal lobule ($p_{uncorrected}$=0.036) and the posterior cingulate, although the latter finding did not reach the threshold of significance ($p_{uncorrected}$=0.055). Following PVC, differences remained significant in key limbic structures and parieto-occipital regions.

Exploratory analyses revealed further reductions of [^{11}C]UCB-J V_T in the brainstem, hippocampus, parahippocampal gyrus, fusiform gyrus and cerebellum ($p_{uncorrected}$<0.05; Table 4.7). After controlling for volume, findings in the brainstem ($p_{uncorrected}$=0.004) and hypothalamus ($p_{uncorrected}$=0.017) survived. Following PVC, reductions in all regions survived, with [^{11}C]UCB-J V_T loss in the hypothalamus not quite reaching the threshold for significance ($p_{uncorrected}$=0.054).

Table 4.7. Group comparison of [^{11}C]UCB-J V_T in healthy controls and DLB patients.

[^{11}C]UCB-J V_T, ml/cm^3 (mean ±SD)	HC n=35	DLB n=9	P value HC vs DLB
Nucleus accumbens	22 ± 2.9	19.6 ± 2.3	**0.033* (-11%)**
Caudate	14.4 ± 2.6	11.1 ± 1.9	**0.001* (-23%)**
Thalamus	12.5 ± 1.9	9.8 ± 0.8	**<0.001* (-22%)**
Amygdala	17.6 ± 2.1	15.8 ± 1.3	**0.016* (-11%)**
Frontal lobe	18 ± 2.3	15.9 ± 2.1	**0.013* (-12%)**
Temporal lobe	20.2 ± 2.6	17.9 ± 2.2	**0.009* (-12%)**
Precuneus	19.8 ± 2.7	16.1 ± 1.8	**<0.001* (-19%)**
Inferior parietal lobe	18.5 ± 2.5	15.7 ± 1.7	**0.003* (-15%)**
Superior parietal lobule	17.3 ± 2.4	14.2 ± 1.6	**0.001* (-18%)**
Lingual gyrus	19.1 ± 2.6	16.2 ± 1.6	**0.002* (-15%)**
Cuneus	19 ± 2.8	16 ± 1.5	**0.005* (-16%)**
Calcarine cortex	19.8 ± 2.7	16.3 ± 1.3	**<0.001$ (-18%)**
Occipital pole	17.6 ± 2.3	15.4 ± 1.6	**0.008$ (-13%)**
Insular cortex	21 ± 2.7	17.9 ± 2.2	**0.002* (-15%)**
Anterior cingulate	20.7 ± 2.7	17.7 ± 2.3	**0.003* (-15%)**
Posterior cingulate	20.3 ± 2.9	16.3 ± 1.9	**<0.001* (-20%)**
Exploratory regions-of-interest			
Brainstem	8.6 ± 1	7.3 ± 0.5	**0.001$ (-15%)**
Putamen	22.8 ± 2.8	21 ± 2.6	0.076 (-8%)
Hippocampus	14.5 ± 2	11.8 ± 0.5	**<0.001$ (-18%)**
Parahippocampal gyrus	17 ± 2.2	14.7 ± 1.6	**0.005$ (-13%)**
Fusiform gyrus	20.4 ± 2.6	17.9 ± 2	**0.008$ (-12%)**
Cerebellum	16.3 ± 2	14.2 ± 1.4	**0.004$ (-13%)**

**p<0.05, FDR-corrected; $p<0.05, uncorrected. DFs: 1, 41*

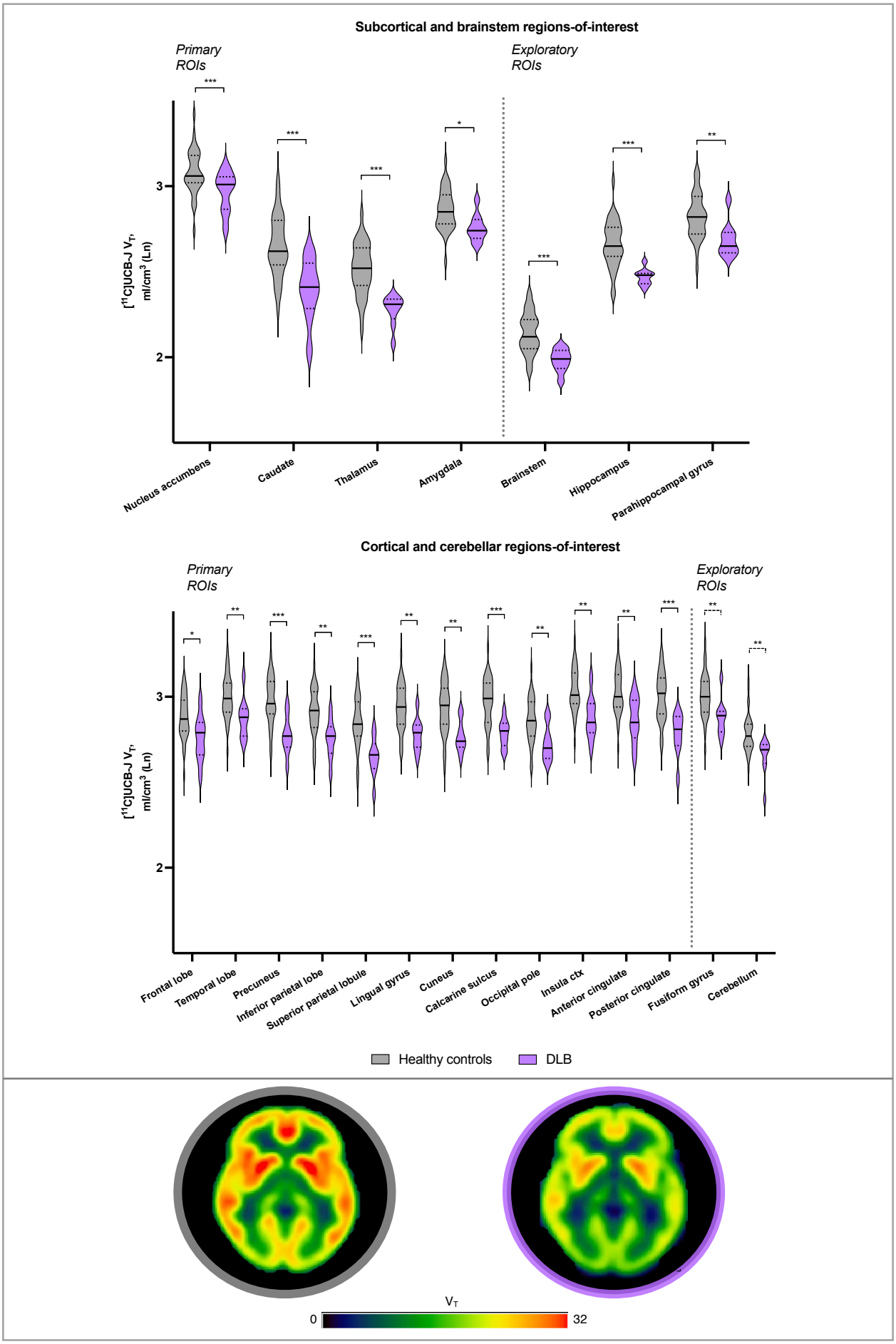
Subcortical and brainstem regions-of-interest
Primary ROIs
Exploratory ROIs
[11C]UCB-J VT, ml/cm3 (Ln)
3
2
Nucleus accumbens
Caudate
Thalamus
Amygdala
Brainstem
Hippocampus
Parahippocampal gyrus
Cortical and cerebellar regions-of-interest
Primary ROIs
Exploratory ROIs
[11C]UCB-J VT, ml/cm3 (Ln)
3
2
Frontal lobe
Temporal lobe
Precuneus
Inferior parietal lobe
Superior parietal lobule
Lingual gyrus
Cuneus
Calcarine sulcus
Occipital pole
Insula ctx
Anterior cingulate
Posterior cingulate
Fusiform gyrus
Cerebellum
Healthy controls
DLB
VT
0
32

Figure 4.7. Violin plots showing [^{11}C]UCB-J V_T in primary regions-of-interest for healthy controls and DLB patients. The bottom panel displays mean axial [^{11}C]UCB-J maps for controls (grey, n=35) and DLB patients (pink, n=9). ***p<0.001; **p<0.01; *p<0.05, FDR-corrected; ---- uncorrected p value. ROIs=regions-of-interest; V_T=volume of distribution; Ln=natural log transformation. Exploratory regions-of-interest=additional brain areas that were analysed for exploratory purposes. Multiple comparison corrections were not performed on these secondary analyses.

4.4.2.5 Simple linear regression: regional volumes and [^{11}C]UCB-J V_T

I next assessed whether regional volumetric was a predictor of [^{11}C]UCB-J V_T measures in regions that did not survive after controlling for volume. Interestingly, within DLB patients, GM volume in only two regions were identified as statistically significant predictors of [^{11}C]UCB-J V_T in the corresponding region: the caudate (β=0.43, p=0.002), which explained 77% of [^{11}C]UCB-J V_T variance ($F(1,7)$=23.50, R^2=0.77, p=0.002; Figure 4.8) and thalamus (β=0.50, p=0.035), which explained 49% of [^{11}C]UCB-J V_T variance ($F(1,7)$=6.77, R^2=0.49, p=0.035; Figure 4.8).

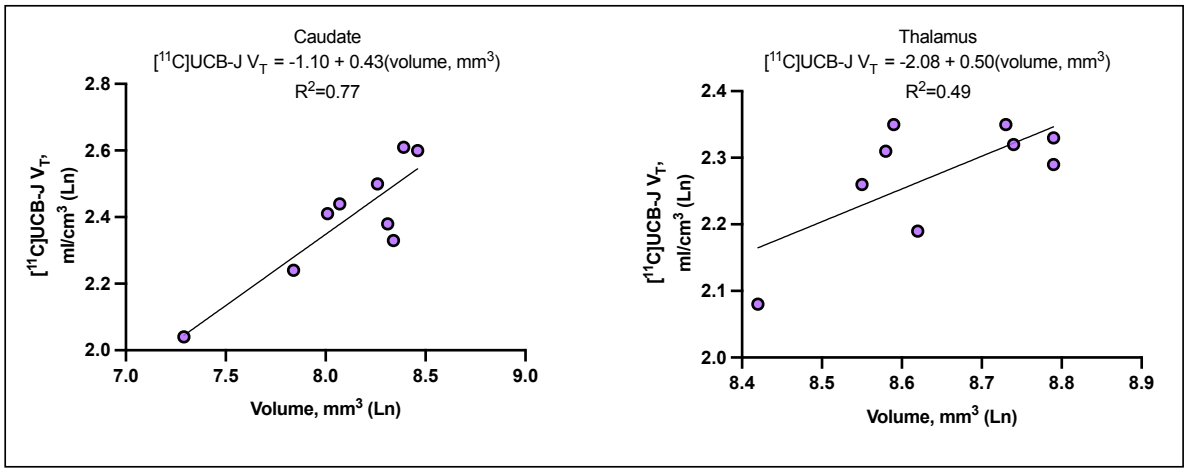

Figure 4.8. Linear regression between regional [^{11}C]UCB-J V_T and volume in DLB patients. Higher GM volumetric predicted higher [^{11}C]UCB-J V_T in DLB patients within the caudate and thalamus.

4.4.2.6 Simple linear regression: [^{11}C]UCB-J V_T and regional CBF

A simple linear regression analysis was performed between [^{11}C]UCB-J V_T (independent variable) and CBF (dependent variable) within each region explore the intra-regional associations between these measures. Both measures included were partial volume corrected in an attempt to minimise the potential amplificatory influence volumetric reductions could have on their association.

Within DLB patients, [^{11}C]UCB-J V_T in the caudate nucleus explained 54% of CBF variance ($F(1,7)=8.26$, $R^2=0.54$, $p=0.024$) and was found to be a predictor of CBF in the caudate ($\beta=1.15$, $p=0.024$).

4.4.3 PDD vs DLB

4.4.3.1 Demographic and clinical characteristics

PDD and DLB patients did not differ in terms of age (MD=-5.44, 95% CI [-12.80, 1.91], $p=0.14$) and gender (gender: X^2 (1, N=18)=1,29, $p=0.26$). PDD patients had a significantly longer disease duration ($p_{FDR\text{-}corrected}<0.001$) and higher total daily LED intake ($p_{uncorrected}=0.025$) compared to DLB patients, though the latter did not survive FDR-correction for multiple comparisons (Table 4.8). Compared to PDD, DLB patients exhibited greater cognitive impairment as demonstrated by their performance on domain-specific measures such as the SCOPA-COG memory and learning ($p_{uncorrected}=0.027$) and PD-CRS Immediate Free Recall Verbal Memory ($p_{uncorrected}=0.026$), though again, these findings did not survive FDR-correction for multiple comparisons (Table 4.8).

Table 4.8. Demographic and clinical characteristics of PDD and DLB patients

Characteristic (mean ±SD)	PDD	DLB	P value
No. (M/F)	9 (6M/3F)	9 (8M/1F)	0.26
Age (years)	67.33 ± 9.33	72.78 ± 4.6	0.14
Disease duration (months)	104.22 ± 43.98	34.54 ± 35.8	**0.002***
Education (years)	13. ± 3.6	12.1 ± 5	0.86
LEDD (mg)	721.06 ± 307.99	375.83 ± 316.83	**0.032§**
H&Y	3 ± 0	3.33 ± 1.23	0.40
MDS-UPDRS I	21.22 ± 3.19	20.11 ± 6.19	0.66
MDS-UPDRS II	20.44 ± 4.3	23.67 ± 13.48	0.76
MDS-UPDRS III	52.22 ± 13.01	48.44 ± 31.17	0.33

MDS-UPDRS Total	93.89 ± 14.49	92.22 ± 48.48	0.54
SCOPA-AUT	20 ± 5.66	22.75 ± 8.36	0.34
PD NMS Questionnaire	13.33 ± 3.84	12.44 ± 5.66	0.89
ESS	9 ± 7.23	10.67 ± 5.34	0.30
RBDQ	4 ± 2.55	4.44 ± 3.61	0.55
PDSS	105 ± 8.94	111.56 ± 17.53	0.54
King's PD Pain Questionnaire	3.22 ± 1.86	2.89 ± 3.18	0.64
UPSIT	16.44 ± 4.88	18.86 ± 9.91	0.69
MMSE	23.33 ± 3.32	17.89 ± 5.93	0.061
MoCA	20.56 ± 4.1	13.56 ± 6.11	0.08
GDS	13.22 ± 6.1	14.11 ± 5.82	0.13
SCOPA-COG Total	15.78 ± 5.45	8.5 ± 6.09	0.057
SCOPA-COG Memory & Learning	6.78 ± 2.22	3.5 ± 2.88	**0.025$**
SCOPA-COG Attention	2.11 ± 1.27	0.88 ± 0.99	0.087
SCOPA-COG Executive	4.56 ± 2.07	3.00 ± 1.85	0.29
SCOPA-COG Visuospatial	1.11 ± 0.93	1.00 ± 1.41	0.79
SCOPA-COG Memory	1.22 ± 1.64	0.13 ± 0.35	0.31
PD-CRS Total	48.33 ± 20.63	28 ± 15.37	0.10
PD-CRS Fronto-subcortical	32.67 ± 15.08	16.00 ± 9.81	0.061
PD-CRS Posterior-cortical	15.67 ± 6.67	12.00 ± 6.33	0.34
PD-CRS Immediate Free Recall Verbal Memory	**7.89 ± 2.8**	**4.75 ± 3.73**	**0.026$**
PD-CRS Confrontation Naming	10.67 ± 5.48	6.5 ± 5.18	0.14
PD-CRS Sustained Attention	3.11 ± 2.09	1.13 ± 1.46	0.11
PD-CRS Working Memory	4.11 ± 2.21	1.75 ± 1.75	0.092
PD-CRS Unpromoted Drawing of a Clock	4.33 ± 3.08	3.5 ± 2.73	0.80
PD-CRS Copy Drawing of a Clock	5.00 ± 2.69	5.5 ± 3.96	0.55

PD-CRS Delayed Free Recall Verbal Memory	2.78 ± 1.86	1.88 ± 1.89	0.31
PD-CRS Alternating Verbal Fluency	4.56 ± 3.84	1.13 ± 1.64	0.23
PD-CRS Action Verbal Fluency	5.89 ± 6.15	1.88 ± 2.85	0.31

Abbreviations: H&Y=Hoehn and Yahr scale; MDS-UPDRS=Movement Disorder Society Unified Parkinson's Disease Rating Scale; MMSE=Mini Mental Status Examination; MoCA=Montreal Cognitive Assessment; PDSS: Parkinson's disease sleep scale; PD NMS Questionnaire=Parkinson's disease Non-Motor Symptom Questionnaire; ESS: Epworth Sleepiness Scale; RBDQ=REM Behaviour Sleep Disorder Questionnaire; SCOPA-AUT=Scales for Outcomes of Parkinson's disease–Autonomic; GDS=Geriatric Depression Scale; SCOPA-COG=Scales for Outcomes of Parkinson's disease–Cognition; PD-CRS=Parkinson's Disease-Cognitive Rating scale
*P<0.05 between PDD and DLB, FDR-corrected; $^{\$}P$<0.05 between PDD and DLB, uncorrected

4.4.3.2 Grey matter volume: Regions-of-interest analysis

No volumetric differences were found between DLB and PDD patients.

4.4.3.3 Cerebral blood flow: region-of-interest analysis

There were no differences in CBF between PDD and DLB patients.

4.4.3.4 [^{11}C]UCB-J V_T: Regions-of-interest

Although DLB patients exhibited a widespread reduction of [^{11}C]UCB-J V_T across cortical and subcortical regions, there were no significant differences observed between PDD and DLB patients in any regions-of-interest (Table 4.9). No differences were identified after controlling for volume. This remained to be the case following PVC.

Table 4.9. Group comparison of [^{11}C]UCB-J V_T across PDD and DLB patients

[^{11}C]UCB-J V_T, ml/cm^3 (mean ±SD)	PDD n=9	DLB n=9	P value PDD vs DLB
Postcentral gyrus	13.9 ± 2.6	13.7 ± 1.2	0.36 (-12%)
Precuneus	17.4 ± 3	16.1 ± 1.8	0.23 (-14%)
Inferior parietal lobe	16.1 ± 2.9	15.7 ± 1.7	0.95 (-7%)

Inferior temporal lobe	19.7 ± 3.6	19.1 ± 2.6	0.46 (-7%)
Calcarine sulcus	18 ± 2.9	16.3 ± 1.3	0.24 (-9%)
Cuneus	17.4 ± 2.7	16 ± 1.5	0.28 (-10%)
Anterior cingulate	19.2 ± 4.2	17.7 ± 2.3	0.32 (-12%)
Posterior cingulate	18.1 ± 3.4	16.3 ± 1.9	0.11 (-14%)
Insular cortex	19.7 ± 4.1	17.9 ± 2.2	0.38 (-13%)
Fusiform gyrus	19.1 ± 3.2	17.9 ± 2	0.51 (-11%)
Nucleus accumbens	20.2 ± 4.5	19.6 ± 2.3	0.72 (-3%)
Caudate	11.8 ± 3.5	11.1 ± 1.9	0.90 (-6%)
Putamen	22 ± 4.3	21.9 ± 3	0.86 (-1%)
Amygdala	17.5 ± 2.8	15.8 ± 1.3	0.36 (-10%)
Hippocampus	13.5 ± 2.6	11.8 ± 0.5	0.21 (-13%)
Parahippocampal gyrus	16.8 ± 3.1	14.7 ± 1.6	0.43 (-12%)
Exploratory regions-of-interest			
Precentral gyrus	14.5 ± 2.7	14.1 ± 1.5	0.28 (-14%)
Supplementary motor area	15.6 ± 3.1	14.9 ± 1.8	0.18 (-13%)
Dorsolateral prefrontal cortex	16.2 ± 3.7	15.8 ± 2.2	0.56 (-7%)
Superior temporal lobe	18.3 ± 3.9	16.6 ± 2.2	0.56 (-7%)
Middle temporal lobe	19.5 ± 3.4	18.5 ± 2.2	0.56 (-9%)
Brainstem	8.1 ± 1.1	7.3 ± 0.5	0.21 (-10%)
Substantia nigra	8.8 ± 1.1	7.9 ± 0.9	0.095 (-10%)

**p<0.05, FDR-corrected; $p<0.05, uncorrected.*

4.4.3.5 Correlation: [^{11}C]UCB-J V_T and clinical measures

Within PDD patients, [^{11}C]UCB-J V_T in the thalamus was positively associated with MMSE scores (r=+0.70; p=0.035; Figure 4.9). No other associations were observed, including demographics like years of education and disease duration.

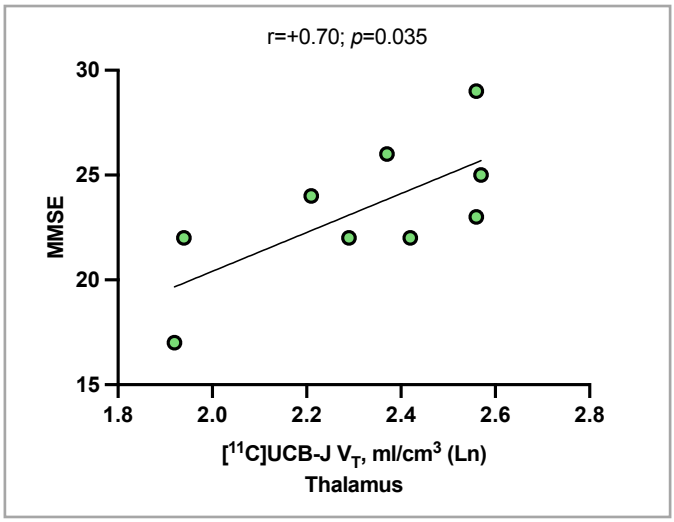

Figure 4.9. Positive correlation between thalamic [^{11}C]UCB-J V_T and MMSE scores in PDD patients

Within DLB patients, I found positive correlations between MMSE scores and [^{11}C]UCB-J V_T within the caudate (r=+0.70; p=0.034) and thalamus (r=+0.72; p=0.029). Associations were also observed between domain-specific measures such as the SCOPA-COG executive and [^{11}C]UCB-J V_T within the caudate (r=+0.75; p=0.032), as well as PD-CRS copy clock with [^{11}C]UCB-J V_T within the frontal lobe (r=+0.84; p=0.009; Figure 4.10). No other associations were observed, including with years of education and disease duration.

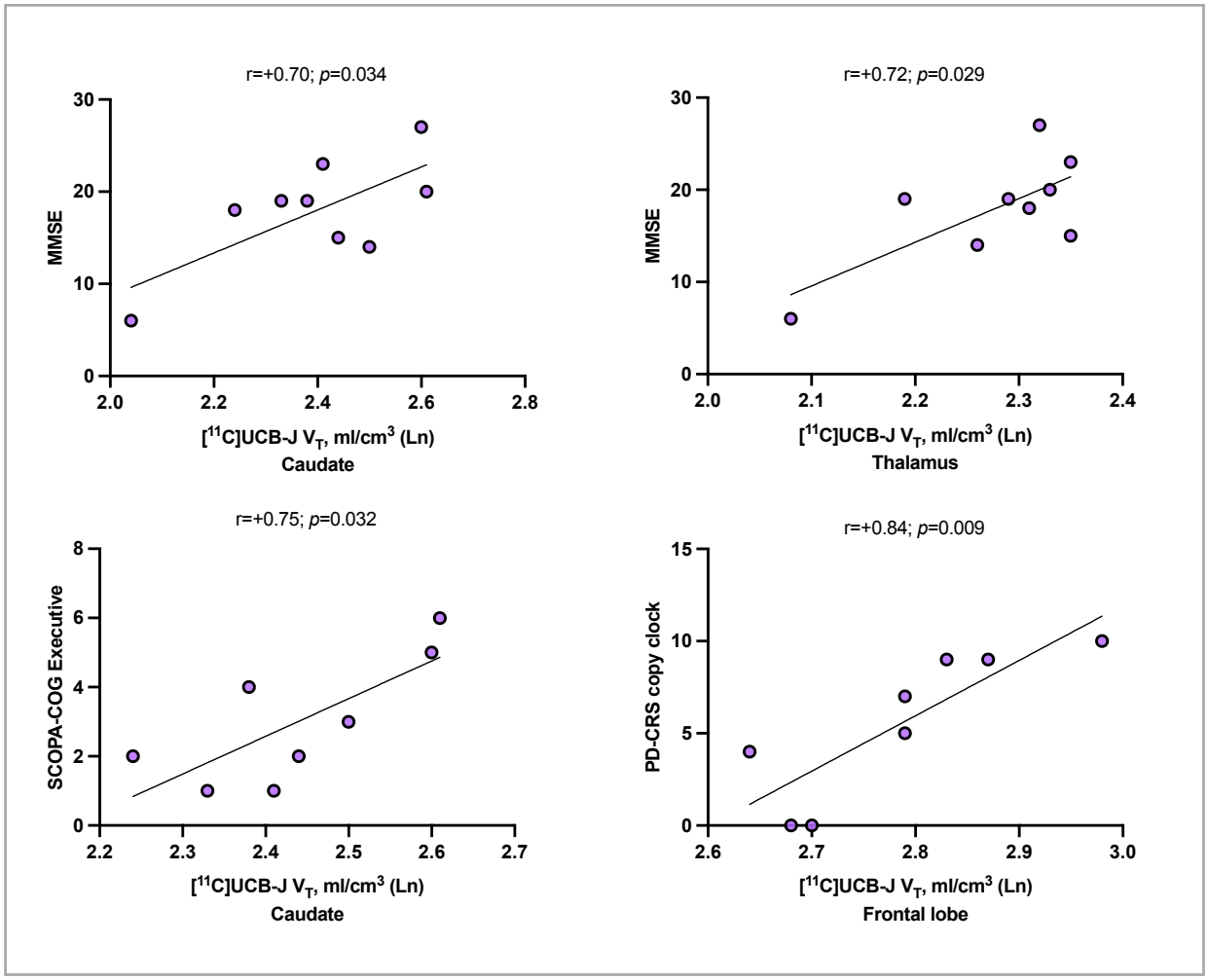

Figure 4.5. Correlations between regional [^{11}C]UCB-J V_T and clinical measures of cognitive function in DLB patients.

4.4.4 Conjunction overlay

4.4.4.1 (HC > PDD) vs (HC > DLB)

In order to determine where in the brain [^{11}C]UCB-J V_T was commonly reduced in PDD and DLB when compared to healthy controls, a conjunction analysis was performed. 2 clusters were observed where there was an overlap of reduced [^{11}C]UCB-J V_T in PDD and DLB (compared to healthy controls), which was localised to the bilateral thalamus (Table 4.10).

Table 4.10. Conjunction overlay for the overlapping reduction in [^{11}C]UCB-J V_T between (HC vs PDD) vs (HC vs DLB)

Cluster size	Region	MNI coordinates			*T*	$p_{FDR\text{-corrected}}$
	Thalamus L	-12	-32	6	4.17	
423	Thalamus L	-2	-4	2	3.99	0.001
	Thalamus L	-6	-12	14	3.92	
	Thalamus R	14	-30	8	3.84	
213	Thalamus R	20	-26	14	3.39	0.034
	Thalamus R	22	-34	2	3.38	

$p<0.005$, extent threshold=200

4.4.4.2 (Non-demented PD > PDD) vs (HC > DLB)

To gain an insight into the similarity of [^{11}C]UCB-J V_T alterations in DLB and PDD in the absence of PD, a conjunction analysis was performed between the non-demented PD > PDD contrast map and HC > DLB contrast map. A single cluster of overlap was identified, which corresponded to the left thalamus (Table 4.11).

Table 4.11. Conjunction overlay for the overlapping reduction in [^{11}C]UCB-J V_T between (non-demented PD vs PDD) vs (HC vs DLB)

Cluster size	Region	MNI coordinates			*T*	$p_{FDR\text{-corrected}}$
	Thalamus L	-12	-32	6	4.17	
323	Thalamus L	-4	-2	4	4.16	0.003
	Thalamus L	-12	-18	16	3.78	

$p<0.005$, extent threshold=200

4.5 Discussion

These preliminary findings indicate the presence of reduced synaptic density within cortical and subcortical brain areas in Lewy body dementia, as measured with [^{11}C]UCB-J PET imaging. Notably, DLB patients exhibited extensive synaptic density reductions across the entire brain compared to healthy controls, whereas PDD patients showed slightly more localised alterations of synaptic density. These findings are in line with the two previously published [^{11}C]UCB-J PET studies that reported reductions of synaptic density in cortical brain areas in Lewy body dementia (Andersen et al., 2021, Nicastro et al., 2020). Furthermore, regional patterns of synaptic density reductions and hypoperfusion were generally distinct, with few associations observed between these measures, suggestive of a certain level of discordance between synaptic density and hypoperfusion in Lewy body dementia. Furthermore, the confounding effects of grey matter volume on [^{11}C]UCB-J binding are limited, despite the magnitude of volumetric reductions.

More specifically, I found that PDD patients exhibited SV2A reductions predominately within the parietal areas of the brain, as well as frontal regions implicated in the planning and execution of movement and subcortically within the caudate and thalamus. These findings are in line with previous findings that have suggested that patients with early posterior cortical deficits have a higher risk of going on to develop dementia and that these changes are likely subtended by dysfunction of nondopaminergic circuitry (Williams-Gray et al., 2009, Biundo et al., 2013, Kehagia et al., 2013). Indeed, studies that employed [^{18}F]FDG-PET as an indirect marker of synaptic activity reported that PD patient with mild cognitive impairment, as well as those with dementia, showed extensive hypometabolism in frontal and parietal cortices compared to cognitively normal PD (Huang et al., 2008, Huang et al., 2007, Liepelt et al., 2009, Hosokai et al., 2009). Furthermore, compared to non-demented PD, PDD exhibited further reductions of [^{11}C]UCB-J binding in the superior parietal lobe, which may indicate that reductions of synaptic density within the superior parietal lobe may be implicated in cognitive decline and the

development of dementia in PD. The superior parietal lobule has close links with the occipital lobe and plays a role in aspects of attention and visuospatial perception. Indeed, PDD patients exhibited attentional and visuospatial deficits as measured with SCOPA-COG, although no associations were observed between these cognitive domains and synaptic density measures within the parietal lobe, which could potentially be due to the small sample size.

DLB patients, on the other hand, exhibited much more widespread reductions of synaptic density across the brain, both cortically and subcortically, with more prominent reductions observed replicating previous reports of changes in the parietal and occipital lobes, as well as key structures of the limbic system such as the hippocampus, amygdala, and cingulate gyrus. This study indicates that the presence of SV2A pathology is likely a widespread feature of DLB, with the highest degree of SV2A reductions corresponding to brain areas known to be affected by α-synuclein pathology. Indeed, α-synuclein has been suggested to play a synaptotoxic role, with microaggregates of α-synuclein being reported to be enriched in the presynaptic terminals of DLB patients (Kramer and Schulz-Schaeffer, 2007), and Colom-Cadena et al. (2017) illustrating that small aggregates of phosphyrlated α-synuclein disrupt synaptic structure and function. In line with this hypothesis, studies quantifying synaptic proteins in post-mortem brain tissue of DLB patients identified reductions of synaptic proteins such as synaptophysin, synaptosome-associated protein and syntaxin in the visual association cortex in DLB (Whitfield et al., 2014, Mukaetova-Ladinska et al., 2013), as well as the inferior parietal lobe (Bereczki et al., 2016), and hippocampus (Revuelta et al., 2008). A recent study by Bridi et al., (2021) provided evidence that bridged the gap between presynaptic α-synuclein accumulation and subsequent synaptopathy, whereby aggregation of α-synuclein in the presynaptic terminal induced a downregulation of presynaptic proteins, impairing neuronal function (Bridi et al., 2021). Therefore, reductions in SV2A expression may be reflecting the potential interaction between presynaptic aggregation of α-synuclein and SV2A, although future studies are needed to investigate their potential

interaction. Through this imaging technique, this study outlined in this chapter has demonstrated that synaptic protein alterations are a common, and likely widespread feature in DLB.

Although there were no significant differences in SV2A expression when DLB and PDD were compared directly, that could potentially be explained by the small sample sizes, there was a trend toward further reduction of synaptic density within DLB. Furthermore, when compared to healthy controls, these diseases exhibited a varying extent and pattern of SV2A alterations across the brain. This is in line with post-mortem DLB studies, whereby synaptic protein expression was reduced to a larger degree in DLB than PDD (Bereczki et al., 2016). Both PDD and DLB have been shown to exhibit an overlap of neuropathological features, with a variable mixture of α-synuclein and AD-related lesions. Whilst a common pathophysiological factor is synaptic dysfunction due to the initial aggregation of α-synuclein in presynaptic terminals (Uchihara, 2017), neuropathological and neuroimaging studies have illustrated that concomitant AD-related pathology is a more common feature of DLB than PDD, with 28% of DLB patients exhibiting sufficient pathology for a secondary neuropathological diagnosis of AD, compared to 10% of PDD cases. Furthermore, amyloid-β burden has been reported to be significantly higher in cortical and subcortical brain areas in DLB compared to PDD (Halliday et al., 2011, Hepp et al., 2016, Walker et al., 2015a). The presence of concomitant pathologies could be implicated in altering synaptic density. Studies in AD have shown that soluble forms of amyloid-β are toxic to synapses (Cline et al., 2018), with exposure to oligomers rapidly reducing synaptic protein expression (Lacor et al., 2007) and even correlating with frank synapse loss in rodent and cell models, as well as in AD brains (Shankar et al., 2008, Calabrese et al., 2007, Wang et al., 2017). Whilst future studies are required to investigate the potential influence various existing co-pathologies could have on synaptic function and integrity in DLB and PDD, it is possible that the AD-related pathology is having an additive effect, thus contributing to greater degree of synaptic density reductions in DLB, especially since the presence of such pathologies has been

shown to be associated with rapid cognitive decline, and shorter survival time from onset (Kraybill et al., 2005, Serby et al., 2003). Therefore, since synapse loss and/or dysfunction is considered a downstream effect of underlying disease mechanisms, including pathological protein aggregation, SV2A measures may be reflecting important sources of clinically meaningful biological heterogeneity that other imaging techniques are not sufficiently sensitive to capture (or reflect entirely different processes altogether). This could have important implications for further understanding disease pathogenesis and progression within these disorders and unravelling the contributions of such processes to their unique symptom profiles. Furthermore, such a biomarker could also aid in distinguishing between Lewy body dementias, as well as from other types of dementia like AD, through localisation of compromised synapses to distinct brain areas, although this would of course require investigation.

Furthermore, both PDD and DLB have previously been characterised as manifesting widespread lateral frontal, temporoparietal and occipital hypometabolism, with DLB demonstrating reduced glucose metabolism in the anterior cingulate compared to PDD (Yong et al., 2007). This is in line with our results, as DLB patients had reduced synaptic density in the anterior cingulate, whereas PDD patients did not. Additionally, [^{123}I]FP-CIT SPECT studies have demonstrated that DLB patients exhibit a greater loss of dopaminergic function within the caudate, whereas PDD patients have shown a loss of DAT within the putamen. This is in line with our study, as DLB patients had a greater loss of SV2A expression within the caudate when directly compared to PDD after controlling for volume (though this did not survive PVC, so should be taken with caution). Taken together, these findings speak to the fact that [^{11}C]UCB-J has high specificity for a protein that may be affected differentially by distinct underlying neurobiological mechanisms, that could be contributing to the distinct symptom profiles of these patients that are currently impossible to distinguish from each other with available imaging modalities.

Although there were varying degrees of SV2A alterations with DLB and PDD compared to healthy controls, both dementias also exhibited on overlap in regions of synaptic loss, including subcortical structures and the frontal and parietal cortices. These findings are supported by the fact that Lewy body dementia share many neurochemical and neuropathological features that deem these disorders indistinguishable from each other. Furthermore, conjunction overlay revealed that there was a significant overlap of SV2A reduction within the thalamus. The thalamus, though once perceived as a passive relay centre of sensory information to the cortical areas, has become increasingly recognised for its role in actively regulating and integrating signals transmitted to the cortex (Sampathkumar et al., 2021). Evidence suggest that first-order thalamic neurons are involved in modulating neural processing along sensory pathways to cortical brain areas according to behavioural context (McAlonan et al., 2008, O'Connor et al., 2002) and can strongly influence cortical activity (Saalmann et al., 2012, Purushothaman et al., 2012, Theyel et al., 2010). Lesions to higher-order thalamic areas have been shown to induce severe attention and memory deficits (Jankowski et al., 2013, Saalmann and Kastner, 2011), thus suggestive of the thalamus playing a key role in cognition. Furthermore, the thalamus is a key mediator of consciousness and is vulnerable to Lewy body-related pathology (Braak et al., 2003). Structural and functional abnormalities of the thalamus are a common feature in Lewy body dementia (Watson et al., 2017), with microstructural alterations and cholinergic imbalance proposed to play a role in the aetiology of cognitive fluctuations in DLB (Delli Pizzi et al., 2015a, Pimlott et al., 2006), which is also characteristic of PDD (Aarsland et al., 2001b, Emre et al., 2007). Fluctuating cognition affects up to 90% of patients, and it is often coupled with notable slowing of information processing and mental slowness (Vlagsma et al., 2016). Indeed, within both PDD and DLB, thalamic SV2A expression was found to be associated with global cognition, whereby lower SV2A levels were associated with poorer performance on cognitive tests of global cognition. A recent study demonstrated that a discernible and generalised slowing of microstate dynamics in Lewy body dementia (which may be indicative of less flexible, and ineffective, brain

functioning), was associated with the less dynamic connectivity of thalamic networks with large-scale cortical networks (Schumacher et al., 2019). Compounds that halt or reduce synapse damage or loss within the thalamus could potentially show benefit for treating cognitive impairment within both PDD and DLB, which would potentially have significant consequences for the functioning of the whole brain network. Future research assessing the integrity of synapses within selective thalamic nuclei may shed light on their role in specific cognitive domains in Lewy body dementia.

Although studies investigating volumetric changes in PDD have reported widespread grey matter atrophy across frontal, temporal and parietal cortices, as well as limbic and paralimbic brain structures (Beyer et al., 2007, Burton et al., 2004, Summerfield et al., 2005, Nagano-Saito et al., 2005), we did not observe these volumetric changes in PDD patients when compared to healthy controls. However, compared to non-demented PD patients, PDD patients exhibited reduced volume in parietal, limbic and paralimbic brain areas, as previously described (Aarsland et al., 2003, Santangelo et al., 2007, Song et al., 2011, Ramirez-Ruiz et al., 2007, Camicioli et al., 2009). A recent study investigating progressive cortical thinning and grey matter volume loss in PD patients over time found that cortical thinning accumulation was more prominent in the early stages of PD cognitive decline, with cognitively impaired PD and those with dementia accumulating the least damage over time (Filippi et al., 2020), suggesting that cortical volumetric alterations reach a plateau in early phases of cognitive impairment. There could be several reasons for the inconsistency of results, including high inter-subject variance, group size, clinical characteristics, and disease severity, alongside the methods used to assess volume. Most of these studies employed the voxel-based morphometry approach to measure grey matter volumes or cortical thickness, whereas I measured regional brain volumes with an atlas-based approach following segmentation of the T1-weighted MRI into grey matter. I opted for the atlas-based approach because these defined regions-of-interest were used to generate the TACs.

The reduction of SV2A in the absence of atrophy in PDD may speak to the fact that large cortical neurons may have hundreds, if not thousands, of axonal terminals and although a large proportion of those synapses may be lost that leads to clinical or physiological change, the perikaryon is likely to survive since it may still receive sufficient trophic factors from the terminals remaining. Of course, it is conceivable that in some circumstances, the major loss of presynaptic terminals is so heightened that it results in inadequate reception and retrograde flow of maintenance factors, with trophic deficiency inducing apoptosis and cell death, which may be reflected in the larger extent of atrophy observed within the DLB group.

Whilst [^{11}C]UCB-J can be confounded by grey matter volumetric alterations, the confounding effects of volume are limited and not widespread. This was illustrated by the fact that after applying PVC, the findings remained largely unchanged, with few correlations found between grey matter volume and [^{11}C]UCB-J V_T, particularly within the DLB group that exhibited extensive atrophy across the brain. However, it is important to note that the regions where SV2A loss did not survive were those in which there was an association between regional volume and [^{11}C]UCB-J V_T. For example, within PDD, synaptic density decline may have been influenced by volumetric measures within the inferior parietal lobe, precentral and postcentral gyrus as demonstrated by the association between these measures within these regions and the fact that the significant reduction of SV2A did not survive following the PVC or after controlling for volume. This highlights that volumetric change has the potential to influence [^{11}C]UCB-J V_T measures, thus it would be important to ensure that partial volume effects and/or atrophy are accounted for through subject-specific correction by applying PVC. Taken together, we demonstrate that [^{11}C]UCB-J PET provides an insight specifically into the distinct process of synaptic dysfunction and/or loss, highlighting that although synaptic density measures can be impacted by volumetric changes, [^{11}C]UCB-J PET is not just a proxy measure of gross

macroscopic atrophy and is highly specific for presynaptic protein SV2A. This is particularly important for those disorders classified as 'synaptopathies', where synaptic dysfunction precedes the death of the neuronal soma.

Both PDD and DLB exhibited widespread hypoperfusion as reflected by a global reduction in CBF compared to healthy controls, and in line with previous studies, had region-specific reductions in parietal and occipital brain areas (Fong et al., 2011, Firbank et al., 2003). In fact, PDD patients exhibited hypoperfusion within parieto-occipital areas when compared to non-demented PD patients, which is in line with a previous study that observed more posterior hypoperfusion in PDD patients (Kamagata et al., 2011, Fong et al., 2011), with parietal hypoperfusion being linked to overall cognitive decline (Sawada et al., 1992, Tachibana et al., 1995). Whilst there was an overlap in brain areas that exhibited synaptic density reductions and hypoperfusion, there appeared to be a discordance between these measures whereby the regional patterns of synaptic loss and hypoperfusion were not identical, the magnitude of hypoperfusion was significantly larger and there were limited associations found between the two measures. This is in line with a recent study in AD that reported a discordance between synaptic density and metabolism in less susceptible neocortical regions. If a relationship between CBF and synaptic density does in fact exist, then there could be several reasons for this divergence of synaptic density and hypoperfusion in these regions which is likely multifactorial and may include abnormal protein aggregation (Biju et al., 2020), altered vasculature (string vessels, shorter/loss of capillaries, tortuous vessels) (Guan et al., 2013), and/or astrocyte dysfunction: all of which can contribute to the disruption of neurovascular coupling and a larger magnitude of hypoperfusion compared to synaptic density loss.

However, it is also important to note that, although intuitively one may assume that the density of synapses would correspond to CBF alterations, particularly given that synapses are major

energy consumers of the brain, this may not necessarily be the case. Although further research is required to determine whether synaptic density is, in fact, associated with CBF, the lack of associations observed in healthy controls (data not shown) may be an indication that there may not be a relationship between CBF and synaptic density whereby an increase or decrease in synaptic density may not necessarily lead to elevated or decreased resting activity, as indexed by CBF. Further work is required to determine a (causal) link between changes in SV2A and a consequent change in local perfusion.

As mentioned in the previous chapter, the sample sizes of these groups were modest, although larger than the [^{11}C]UCB-J PET studies published to-date. The small sample sizes hampered the ability to include additional covariates, for example MDS-UPDRS III to control for motor symptom severity and assess alterations that may be more specifically related to cognitive impairment. When controlling for volume in the ANCOVA model assessing group-level difference in [^{11}C]UCB-J V_T between DLB and healthy controls, many of the significant [^{11}C]UCB-J V_T findings disappeared. Although outwardly this would be suggestive of grey matter volume confounding the SV2A measures within DLB, subsequent evaluation demonstrated that this was not the case whereby following PVC, the reductions in SV2A remained largely significant. ANCOVA combines the principles of ANOVA with those of regression, and works by decomposing the variance in the dependent variable ([^{11}C]UCB-J V_T) into variance explained by the covariate (grey matter volume), variance explained by the categorical independent variable (groups) and residual variance. In other words, ANCOVA allows the comparison of the 'adjusted mean' where the mean of the dependent variable for each independent group has been adjusted by the group means of the covariate. PVC techniques, on the other hand, are designed to correct PVEs, which become more important when investigating neurodegenerative disorders where grey matter atrophy confounds the interpretation of PET signals. Thus, PVC can be useful to separate atrophy from PET signal in the remaining tissue, particularly the IY method

which relied on parcellated MRI data to generate a PET map corrected for PVEs. Therefore, ANCOVA compensates for the confounding effects of volume by removing any shared variance between grey matter volume and synaptic density, whereas PVC accounts for volumetric effects by generating an image with recovered signal based on subject-specific tissue masks.

However, using ANCOVA becomes problematic when there is a relationship between the categorical independent variable and the covariate. As detailed by Miller and Chapman (2001), the right use of ANCOVA requires that the covariate and categorical independent variable are statistically independent, and so the groups should have equal mean scores on the covariate. If the covariate and grouping variable share variance, then removing the shared variance will alter the categorical independent variable itself. The remaining variance of the categorical independent variable may not be a good measure of the construct it is intended to measure (i.e., it will have poor construct validity). While the use of an ANCOVA is common practice to control for group differences in a confounding factor, the loss of significance for the DLB group is likely due to my effort to conform with this commonly used approach to aid comparison. In this case, atrophy is clearly and intuitively linked to the DLB group, thus including it as a covariate in the uncorrected data is problematic since the between-subject factor and grey matter volume share variance. It would, therefore, be suggested that in subjects that have extensive atrophy, volume should probably not be controlled for in the statistical model, but instead a PVC technique accounting for grey matter volumetric alterations should be applied to [^{11}C]UCB-J PET data.

For the same reason, age was not included as a covariate within the ANCOVA model, since there was a significant between-group difference in age. Although a 'normal age effect' could have been estimated from healthy controls to try and age-adjust patient data, this approach was not taken for a couple of reasons. First, implementation of this approach assumes that there is a linear relationship between age and any effect on brain measures. Numerous studies have

demonstrated that grey matter volume across several brain areas demonstrate distinct, non-linear age-related trajectories over the adult lifespan, which may be related to the preservation of volume in early adulthood, and a late acceleration of age-related decline (Ziegler et al., 2012). Second, the term 'brain age' has emerged in recent years to denote the predictive value of an individual's brain morphology in determining their chronological age. Using this framework, studies have illustrated that neurodegeneration exacerbates the normal trajectory of brain aging, whereby those suffering from neurodegenerative diseases have brain structures more analogous to a significantly older, healthy individual (Cole and Franke, 2017, Cole et al., 2019). Therefore, estimating normal age-related effects from this group of healthy controls may not necessarily be informative and may even lead to misleading interpretations, particularly since this group of healthy controls are younger and neurodegenerative disorders do not tend to follow the normal trajectory of aging.

This study extends previously published [^{11}C]UCB-J PET studies in Lewy body dementia by examining synaptic density alterations within groups of PDD and DLB. I found widespread reductions of SV2A within DLB, whilst in PDD, the reduction of SV2A was more restricted to parietal and frontal brain areas. SV2A binding was also associated with cognitive symptoms, indicating that [^{11}C]UCB-J PET may have some clinical relevance. Finally, the findings from this study support the uniqueness of [^{11}C]UCB-J PET imaging, whereby it is not merely a proxy measure of grey matter volume or perfusion, but could be employed in combination with these techniques to further understanding of the pathophysiology of these diseases. Future [^{11}C]UCB-J studies with larger sample sizes of PDD and DLB patients are needed to substantiate these preliminary findings.

5 The spatial distribution pattern of synaptic density alterations in Parkinson's disease and Lewy body dementia are associated with structural, functional and molecular markers

5.1 Introduction

The pathological processes leading to PD begins decades before the onset of typical motor symptoms. By the time a clinical diagnosis is made, between 70% - 80% of striatal dopamine (Bohnen et al., 2006a) and at least one-third of nigral neurons (Greffard et al., 2006) and striatal dopaminergic fibres (Hilker et al., 2005a) are already lost. However, the pathophysiology of PD is much more complex as it involves far more than the selective depletion of striatal dopaminergic signalling, with several neurotransmitter systems undergoing progressive functional alteration in the PD brain. In fact, PD involves degenerative alterations to numerous neurobiological processes spanning from molecular to macroscopic scales, including modified gene expression, proteinopathies, synaptic changes, hypometabolism, vascular dysregulation and neuronal atrophy (Poewe et al., 2017, Saeed et al., 2017).

Synapses are fundamental units for neural communication and are composed of the pre- and post-synapse. Presynaptic terminals are specifically essential for synaptic transmission upon neural activity. When an action potential arrives at a nerve terminal, voltage-gated Ca^{2+} channels open, leading to an influx of Ca^{2+} into the cytosol. Synaptic vesicles that store "classic" neurotransmitters for release are localised in an area near voltage-gated Ca^{2+} channels, along with synaptic proteins such as a Ca^{2+} sensor (synaptotagmin I) and vesicle fusion machinery (SNARE

complex) which are docked to the synaptic vesicle membrane. Subsequent to Ca^{2+} permeation, the neurotransmitter is released into the active zone via fusion of the synaptic vesicle where they bind to surface receptor sites on the postsynaptic cell that are responsive to neurotransmitter release. Thus, as a major information transfer unit in the brain, presynaptic physiology is critical for the initiation of neural communication; being responsible for evoking the downstream aspect of neural information flow. In PD, synaptic dysfunction is thought to be an early phenomenon in the disease process (Schirinzi et al., 2016, Phan et al., 2017), illustrated by the impairment of synaptic vesicle exocytosis, intracellular trafficking and vesicle fusion and recycling prior to neuronal degeneration (Nemani et al., 2010, Hunn et al., 2015, Vargas et al., 2014).

The accumulation and mislocalisation of α-synuclein in diseased neurons have been shown to lead to proteostasis imbalance that greatly affects synaptic terminal composition, organisation and function via numerous mechanisms, including local protein synthesis and clearance (Olivero et al., 2018, Klaips et al., 2018). The localisation of SV2A to synaptic vesicles and its role in maintaining a readily releasable pool of synaptic vesicles by regulating endocytosis means that its loss could result in altered synaptic vesicle release and impaired neural transmission.

Standard analyses of neuroimaging data typically focus on identifying region- or voxel-wise signal changes associated with specific disorders. This standard approach was taken in chapters 3 and 4, where I explored regional changes in [^{11}C]UCB-J uptake in groups of PD, PDD and DLB. Whilst this provided valuable information about the spatial location of synaptic density differences within these disease groups and provided tentative insight into effects possibly reflective of disease progression and volumetric effects on this measure, such analyses do not inform about the potential neurophysiological mechanisms underlying the observed alterations. For SV2A specifically, although the ubiquitous expression of SV2A is a characteristic that makes it an attractive target for assessing synaptic integrity *in vivo*, its lack of specificity to neuronal

subtypes and its lack of sensitivity to underlying cellular properties of the brain tissue makes its interpretation far more challenging; particularly with respect to understanding the neurochemical mechanisms underlying regional vulnerability to pathological changes in PD and related dementias. The focus on single disease factors, such as synaptic density in this case, provides limited comprehension into the pathophysiology of disease, as most biological mechanisms in PD are multi-factorial. There is also an incomplete multi-scale understanding of how molecular and macroscopic factors interact to cause disease progression, thus multi-modal neuroimaging models have the potential to unravel these limitations.

To overcome this biological limitation, the recent introduction of brain-wide gene expression atlases such as the Allen Human Brain Atlas (Shen et al., 2012, Hawrylycz et al., 2012) have enabled researchers to assess how spatial variations in mRNA expression patterns correlate with macroscopic neuroimaging phenotypes (Rizzo et al., 2014) and different neuroimaging features (Arnatkeviciute et al., 2019). The primary notion behind such analyses is that drug- or disease-induced alterations in neuroimaging markers arise due to their relationship with specific tissue properties (for example the expression of specific receptor subtypes) that are modulated by a drug or affected by a disease process. A growing body of literature has already started to provide insight into how regional variations in gene expression relate to diverse properties of brain structure (Patel et al., 2020, Patania et al., 2019, Romero-Garcia et al., 2018, Shin et al., 2018, Seidlitz et al., 2018, Liu et al., 2020) and function (Shen et al., 2021, Tang et al., 2021, Zhu et al., 2021, Hansen et al., 2021, Wen et al., 2018, Diez and Sepulcre, 2018), as well as disease-related brain alterations (Ji et al., 2021, Anderson et al., 2020, Keo et al., 2020, Morgan et al., 2019, Li et al., 2021, Jimenez-Marin et al., 2021, Seidlitz et al., 2020, Forsyth et al., 2021). However, whilst this is emerging as a promising approach, several concerns around the integration of the Allen Human Brain Atlas dataset with neuroimaging data have recently been discussed by Selvaggi et al. (2021), who highlighted that the lack of standardised pipelines for its integration can

ultimately lead to poor reproducibility. The lack of consensus is partially due to the limitations of the Allen Human Brain Atlas, which include a restricted number of donors (only 6 post-mortem brains), sampling primarily covering the left hemisphere only, with an inhomogeneous number of samples between brain regions and high between-donors variability (Selvaggi et al., 2021). Finally, it makes several assumptions that are ambiguous or unknown (Unterholzner et al., 2020). For example, associations with mRNA expression imply that there is transcription of the respective genes, and this leads to measurable changes of tissue structure and function. Furthermore, subtleties such as alternative splicing and post-translational modifications are not considered (Janusonis, 2017, Selvaggi et al., 2021).

A viable means of implementing this approach whilst avoiding these assumptions is via integration of benchmark molecular imaging markers derived from PET or SPECT maps, which also have considerably higher resolution than the Allen Human Brain Atlas. Recent advancements in molecular tracer development have led to a variety of novel tracers that can reliably quantify the availability of specific molecular targets, such as neuroreceptors subtypes and neurotransmitter transporters, alongside functional features such as synthesis capacity across a variety of neurotransmitters (Lehto et al., 2015, Beliveau et al., 2017, Mawlawi et al., 2001, McCann et al., 2005, Gjedde et al., 1991). Molecular measures derived from PET and SPECT provide a more direct quantification of specific tissue properties compared to mRNA expression. In line with this, Selvaggi et al. (2019) demonstrated that MRI-derived spatial activity patterns induced by antipsychotics correlated with PET-derived biomarkers implicated in the mechanism of action, with mRNA data explaining less variance than PET-derived maps.

One class of molecules that are especially relevant are neurotransmitter receptors and transporters that regulate an array of biological processes known to be dysfunctional in neurodegeneration. Given that neuroreceptors and transporters are mediators of several relevant

neurobiological factors, studying them is crucial for a comprehensive mechanistic understanding of brain disorders such as neurodegeneration (Hornykiewicz and Kish, 1984). Whilst the brain consumes a disproportionate amount of energy relative to its mass (Mink et al., 1981), a substantial proportion of this energy expenditure is attributable to synaptic transmission and molecular synthesis (Harris et al., 2012). The production and degradation of neurotransmitter receptors is a complex and dynamic process that is regulated in response to changes in numerous factors, such as receptor activation, gene expression and external stimuli (McCann et al., 2008).

PD is now widely recognised as a multisystemic syndrome, manifesting largely as a consequence of multi-neurotransmitter dysfunction. The multifaceted involvement of several neural systems, including the dopaminergic, cholinergic, serotonergic and noradrenergic systems, ultimately results in patients presenting with a range of non-motor symptoms, which are now recognised as an integral part of the symptom spectrum (Schrag et al., 2015). Non-motor symptoms in PD range from cognitive impairment and apathy to sleep dysfunctions such as rapid eye movement behaviour disorder (RBD) and excessive daytime sleepiness (EDS), which may transpire from varying density of Lewy body deposition and non-dopaminergic patterns of neurodegeneration in PD, as well as response to medication. Several neuroimaging studies have demonstrated that alongside dopamine, acetylcholine (ACh), noradrenaline (NA), serotonin (5-HT), glial pathology and neuroimmune responses may all play fundamental pathogenic roles in adding to the heterogeneity of PD, including the development and severity of a range of non-motor symptoms (Antonini et al., 1997, Thobois et al., 2004, Braak et al., 2003, Bohnen et al., 2009, Guttman et al., 2007, Politis et al., 2010b, Ballanger et al., 2010, Ouchi et al., 2005, Chaudhuri and Schapira, 2009). Thus, integrating neurotransmitter receptors and transporters with macroscopic neuroimaging data has the potential to uncover molecular pathways important to disease pathophysiology and progression.

5.2 Aims and hypotheses

In this chapter, I aimed to test whether changes in [^{11}C]UCB-J V_T covaries with *in vivo* measurements of a common set of receptor and transporter maps. In particular, I employed nine receptor and transporter template maps, each derived from the scanning of healthy volunteers, to evaluate the spatial correlation between [^{11}C]UCB-J V_T variation in patient groups against the canonical distribution of neurochemical markers including those of the serotonergic system: $5HT_{1A}$, $5HT_{1B}$ and $5HT_{2A}$ receptors and SERT, the dopaminergic system: D_1 and D_2 receptors and DAT, noradrenergic system: NAT and the cholinergic system: VaChT. Canonical in this context is referring to the fact that the spatial architecture of these molecular markers tends to be relatively consistent across individuals.

Furthermore, the concept that synaptic terminal loss is implicated as an early pathological event in PD, whereby α-synuclein accumulation is accompanied by neuronal abnormalities such as thread-like axons with irregularly spaced, densely labelled varicosities supports the "dying-back" pattern of neuronal degeneration in affected neurons (Ulusoy et al., 2013). Dying-back neuropathies are exemplified by a sequence that progresses from loss of synaptic function to distal axonopathy and eventually neuronal death (Bossy-Wetzel et al., 2004).

Whilst a major focus has been placed on the physiological, morphological, and neurochemical characteristics of nigral dopaminergic neurons that are linked to cell-autonomous pathways of vulnerability, these neuronal cells are not the only ones that are vulnerable in PD. In fact, neuronal populations implicated in the neuromodulatory control networks, including serotonergic, noradrenergic, and cholinergic neurons, share some of the functional and/or structural properties that render dopaminergic neurons vulnerable, such as long, poorly myelinated axons that are highly branched (Del Tredici and Braak, 2016). Although it is a relatively unexplored area of research of whether non-dopaminergic neuronal subtypes show

synaptic deficits, a recent study illustrated the selective vulnerability of neuronal subtypes after injecting α-synuclein fibrils into the pedunculopontine nucleus (Henrich et al., 2020). Whilst this brain region encompasses a range of neuronal phenotypes (GABAergic and glutamatergic), fibril-induced formation of α-synuclein inclusions were restricted to cholinergic neurons (Henrich et al., 2020). Therefore, neurons with extensive axonal arborisation and consequent increased metabolic burden may be particularly at risk and the first to undergo cellular dysfunction and exhibit synaptic toxicity (Uchihara and Giasson, 2016, Surmeier et al., 2017, Volpicelli-Daley, 2017).

Nevertheless, I also observed in previous chapters that although [^{11}C]UCB-J PET is not merely an index of volume loss, [^{11}C]UCB-J estimates could be confounded by volumetric changes, thus I am interested in assessing whether changes in [^{11}C]UCB-J V_T spatially relate to patterns of atrophy within our patient groups and how that differs at different stages of the disease.

Finally, the phenomenon referred to as neurovascular coupling refers to alterations in local perfusion that arise in response to changes in neuronal activity. This unique mechanism ensures that an adequate supply of both oxygen and glucose are delivered to activated brain structures by cerebral blood flow (CBF) to address their metabolic demands (Kisler et al., 2017). Astrocytes play a key role in regulating brain energy supply, which includes mediating neurovascular coupling. They are strategically positioned between the vasculature and neuronal synapses, allowing them to detect alterations in neuronal activity via their ability to sense neurotransmitter release (Nortley and Attwell, 2017). This information is relayed to the vasculature to alter the energy supply due to astrocytic control of vasodilation and vasoconstriction (Nortley and Attwell, 2017). As mentioned above, calculations of the brain energy budget have estimated that the largest proportion of brain energy expenditure is attributed to synaptic transmission, suggestive of synaptic transmission being preferentially impacted by reduced energy supply to

the brain. CBF measures are considered to reflect synaptic activity based on the tight coupling between synaptic activity and glucose metabolism and between glucose metabolism and CBF in rest conditions (Chen et al., 2011, Raichle, 1998, Nortley and Attwell, 2017). Whilst normal physiological ageing leads to progressive neurovascular dysfunction as a result of several pathophysiological changes linked with the neurovascular unit and a loss of key signalling pathways (Balbi et al., 2015, Toth et al., 2017), evidence of robust inflammatory response and vascular abnormalities, including increased permeability of the blood-brain barrier, is common in the spectrum of dementia disorders and shown to further exacerbate neuropathology seen in Lewy body dementias (Miners et al., 2014, Mackenzie, 2000, Maetzler et al., 2011, Raz et al., 2016, Janelidze et al., 2017). Evidence of injury to both neural innervations and capillaries, alongside BBB dysfunction, have also been reported in PD (Iadecola, 2017, Guan et al., 2013, Pisani et al., 2012, Kortekaas et al., 2005), suggestive of impaired neurovascular unit, with a limited number of *in vivo* imaging studies demonstrating altered neurovascular status (Lagana et al., 2020, Al-Bachari et al., 2017). However, the findings from these clinical studies are unequivocal, with studies also demonstrating preserved neurovascular coupling (Rosengarten et al., 2010). Therefore, the ASL data collected here, together with a marker of synaptic density, provides an opportunity to gain an insight into the spatial relationship between synaptic density and CBF by assessing how much variance of the group differences in regional [^{11}C]UCB-J V_T is explained by group differences in regional CBF and whether there is 'uncoupling' of any spatial relationship between these measures early in the course of PD patients and if this becomes more evident as patients progress from early stages of the disease to dementia.

Therefore, the overarching aim of the present work was to assess the spatial relationship between the mean between-group differences (denoted by Δ) in regional [^{11}C]UCB-J V_T (Δ[^{11}C]UCB-J V_T) and regional ΔGM volume and regional ΔCBF, as well as the neurotransmitter receptor and transporter distribution patterns in order to gain insight into which

neurotransmitter systems are most vulnerable in PD and dementia or whether Δ[^{11}C]UCB-J V_T is predominately reflective of atrophy or related to the pattern of perfusion. This approach permits the identification of neuroimaging markers with spatial profiles of regional estimates that track the anatomical variations in Δ[^{11}C]UCB-J V_T. I was also interested in evaluating the way in which the relationships between Δ[^{11}C]UCB-J V_T and structural, functional and molecular neuroimaging modalities differs at different disease stages, thus I assessed these associations in the following group comparisons: i) HC vs drug-naïve PD ii) drug-naïve PD vs treated PD iii) treated PD vs PDD. Finally, I assessed HC vs DLB and PDD vs DLB to investigate the way in which the same relationships differ specifically for dementia and whether the variance of Δ[^{11}C]UCB-J V_T in PDD and DLB can be understood by distinct or overlapping candidate mechanisms. Both CBF and [^{11}C]UCB-J PET maps were partial volume corrected in order to exclude partial volume effects and atrophy as confounding factors of synaptic density and CBF alterations.

I hypothesised that there will be detectable, but variable, linear relationships between the spatial distribution of Δ[^{11}C]UCB-J profiles and neurotransmitter-specific measures, as well as ΔGM volume and ΔCBF profiles in our patient groups. A post-hoc sensitivity power analysis (G*Power, version 3.1.9.6, Faul et al., 2009) revealed that a sample size of 115 (referring to the number of regions-of-interest) would make a linear regression model with one predictor sensitive enough to detect effects of an R^2 of at least 0.065 with a power of 80% (α=0.05, power=0.80) and Pearson's correlation coefficient would be sensitive to effects of an r of lease 0.26 with 80% power (α=0.05, two-tailed). The statistical power in this case is based on the number of regions-of-interest, which defined the degrees of freedom for the regression models.

More specifically, I hypothesised the following:

1. Following the mechanisms inducing synaptopathy in PD and eventual degeneration, I expect that the spatial distribution of ΔGM volume will track the anatomical distribution

of Δ[^{11}C]UCB-J. I hypothesise that there will be a linear relationship between the spatial profile of ΔGM volumetric patterns and the spatial profile of Δ[^{11}C]UCB-J across the brain, where a pattern of higher [^{11}C]UCB-J V_T will be similar to the regional volumetric distribution of areas characterised by higher volume. Furthermore, I expect ΔGM volume to explain a larger proportion of Δ[^{11}C]UCB-J variance in the dementia groups.

2. Given the neurovascular coupling model and the fact that the approach employed is evaluating whether ΔCBF can track the variations in Δ[^{11}C]UCB-J V_T, I expect to see a linear relationship between the spatial pattern of ΔCBF and the spatial pattern of Δ[^{11}C]UCB-J across the brain, whereby the regional distribution of areas illustrating higher [^{11}C]UCB-J V_T will be similar to the regional distribution of areas exhibiting higher perfusion. However, given the age- and disease-related pathophysiological mechanisms that underlie neurovascular dysfunction, I expect to see more striking evidence of neurovascular uncoupling in dementia patients.
3. Given the multi-system nature of PD and the early involvement of serotonergic, noradrenergic, dopaminergic systems, I hypothesised that Δ[^{11}C]UCB-J profiles in drug naïve PD patients compared to healthy controls would be associated with the spatial distribution of these neurotransmitter system markers, though I expect it will have the strongest relationship with dopaminergic markers.
4. Since complex and diverse molecular and cellular pathologies contribute to patterns of dysfunction at the neural systems level, I expect that as the disease progresses, there will be an mixture of different neurotransmitter systems, as well as atrophy and perfusion changes, contributing to the variance of Δ[^{11}C]UCB-J profiles.

5.3 Methods

5.3.1 Participants

Details about participants have previously been described in detail in Chapter 2. Briefly, eleven drug-naïve PD patients, ten PD patients on parkinsonian medication, nine PDD patients and nine patients with DLB were enrolled, along with thirty-five healthy controls with no history of neurological or psychiatric disorders.

5.3.2 MRI acquisition and pre-processing

Acquisition parameters and pre-processing steps have previously been described in Chapter 2, Section 2.2. In this chapter, VBM was employed to allow for a voxel-wise comparison of the local grey matter concentrations between groups of subjects based on statistical parametric mapping and partial volume corrected quantitative CBF estimates were integrated into the analyses.

5.3.3 [^{11}C]UCB-J PET acquisition, processing and quantification

Details about PET acquisition parameters, PET processing and kinetic modelling have previously been described in detail in Chapter 2, Section 2.2. In this chapter, regional [^{11}C]UCB-J V_T estimates were extracted from [^{11}C]UCB-J parametric V_T maps that had been corrected for partial volume effects following the iterative Yang (IY) approach (Erlandsson et al., 2012) using fslstats.

5.3.4 Neuroimaging PET templates

I gathered a pool of templates of various PET and SPECT tracers, including [^{11}C]WAY-100635, [^{11}C]P943, [^{18}F]altanserin, [^{11}C]DASB, [^{11}C]SCH23390, [^{18}F]Fallypride, [^{123}I]FP-CIT, [^{11}C]MRB

and [^{18}F]FEOBV (see Table 1 for a full list of tracers and their respective molecular targets). For each tracer, neuroimaging templates were produced as average maps from independent groups of healthy controls (sample size ranging from 6 to 36; Table 5.1). Data were acquired with different experimental design protocols and quantified according to the most appropriate imaging practice for each of these radioligands, as described in the respective original studies (Table 5.1). Each template was linearly rescaled to a minimum of 0 and a maximum of 1:

$$\text{Template}_{\text{rescaled}} = \frac{\text{Template} - \min(\text{Template})}{\max\left(Template - \min(Template)\right)}$$

Each neuroimaging template was segmented with the CIC atlas for each of the 125 regions-of-interest. The mean distribution within each region-of-interest was calculated by employing the *fslstats* function implemented in the FMRIB software library, version 6.0.1 (FSL, Oxford, UK). Given that conventional parametric modelling of regional binding potentials within a majority of the templates was performed by using the cerebellum as a reference region, I excluded both the left and right cerebellum regions-of-interest, thus a total of 115 regions-of-interest were included in all linear regression analyses. For the linear regression analyses with [^{123}I]FP-CIT and [^{11}C]MRB, I excluded both the left and right occipital regions-of-interest as the occipital lobe had been used as a suitable reference region for the quantification of DAT and NAT, respectively.

Table 5.1. PET tracers and their respective molecular targets

Tracer	Target	Modality	Quantification	Sample size	Mean age, years (range)	Gender (M/F)	Reference
[^{11}C]WAY-100635	$5HT_{1A}$	PET	BP_{ND}	36	26.3 (21-47)	18M/18F	(Savli et al., 2012)
[^{11}C]P943	$5HT_{1B}$	PET	BP_{ND}	22	28.7 (21-40)	14M/8F	(Savli et al., 2012)
[^{18}F]altanserin	$5HT_{2A}$	PET	BP_p	19	28.2 (18-44)	11M/8F	(Savli et al., 2012)
[^{11}C]DASB	SERT	PET	BP_{ND}	30	30.5 (19-54)	11M/19F	(Savli et al., 2012)
[^{11}C]SCH23390	D_1	PET	BP_{ND}	13	33.0	6M/7F	(Kaller et al., 2017)
[^{18}F]Fallypride	D_2	PET	BP_{ND}	6	29.8 (18-45)	5M/1F	(Dunn et al., 2009, Selvaggi et al., 2019)
[^{123}I]FP-CIT	DAT	SPECT	SUR	30	-	-	(Garcia-Gomez et al., 2013)
[^{11}C]MRB	NAT	PET	BP_{ND}	10	33.3 (22-50)	6M/4F	(Vettermann et al., 2018)
[^{18}F]FEOBV	VaChT	PET	SUVR	6	67.0	3M/3F	(Aghourian et al., 2017)

$5HT_{1A}$, $5HT_{1B}$ and $5HT_{2A}$: serotonin receptor subtypes, BP_{ND}: binding potential; SUR: specific uptake rate; BP_p: binding potential

5.3.5 Whole-brain analysis

[^{11}C]UCB-J, GM volume and CBF profiles were obtained from group-level contrast maps. Specifically, for each measure, two-sample *t*-tests were performed in SPM12 for the following group comparisons: i) healthy controls vs drug-naïve PD including age and gender as nuisance

variables ii) drug-naïve PD vs treated PD including age and gender as nuisance variables iii) treated PD vs PDD including age and gender as nuisance variables iv) HC vs DLB including gender as a nuisance variable v) PDD vs DLB including age, gender and MDS-UPDRS III scores as nuisance variables. For CBF profiles, whole brain total blood flow was added as a covariate in the model to account for between-subjects variability in global brain perfusion (Viviani et al., 2009), and GM volumes were proportionally scaled to the total intracranial volume and masked with a threshold of 0.2 to ensure only 'pure' GM voxels were included in the analyses. All subsequent contrast maps, namely healthy controls < drug-naïve PD, drug-naïve PD < treated PD, treated PD < PDD, HC < DLB, PDD < DLB for each neuroimaging modality were segmented using the CIC atlas with the same approach used for the extraction of receptor and transporter density profiles. This resulted in 115 regions-of-interest reflecting differences in [^{11}C]UCB-J, GM volume and CBF per group comparison, where positive beta-weights denote larger beta-weights in the latter group whereas negative beta-weights denote smaller beta-weights in the latter group compared to the former group. For consistency with the receptor and transporter density profile data, correlation analyses were conducted excluding the two cerebellum regions-of-interest, as well as the occipital lobe when correlating these profiles with DAT or NAT density profiles.

5.3.6 Spatial permutation test (spin test)

Given that the brain is a spatially-embedded system where neighbouring data points are not statistically independent, the assumptions of several common inferential frameworks are violated (Markello and Misic, 2021). Therefore, as a secondary analysis, the significance of the association between neuroimaging markers and Δ[^{11}C]UCB-J profiles were assessed using spatial permutation testing (spin test) to account for the inherent spatial autocorrelation of the imaging data, performed using the *Vasa* method as implemented in previously published studies (Alexander-Bloch et al., 2013a, Alexander-Bloch et al., 2013b, Vasa et al., 2018). Code used for

the spatial permutation test is freely available on GitHub (https://github.com/netneurolab/markello_spatialnulls) (Markello and Misic, 2021).

Prior to performing the spatial permutation testing, each contrast map and neuroimaging marker was segmented using the Desikan-Killiany Atlas (Desikan et al., 2006) and the mean distribution within each of the 83 regions-of-interest were calculated as detailed above. Again, the whole cerebellum was excluded. The Desikan-Killiany atlas was employed because it is fully integrated into the FreeSurfer routine, which was an essential requirement as the functions used in the code were only compatible with FreeSurfer parcellation atlas and related files. This prevented me from simply switching over and incorporating the CIC atlas into the spatial permutation test in this instance.

For this approach, the empirical correlation amongst two spatial maps were compared to a set of null correlations that were generated by randomly rotating the spherical projection of the spatial map that served as the dependent variable in the regression model (in this case, Δ[^{11}C]UCB-J profiles) before projecting back onto the brain parcel. Crucially, the rotated projection preserved the spatial contiguity of the empirical map, as well as the hemispheric symmetry. Given that subcortical regions could not be projected onto the inflated spherical pial surface, they were incorporated into the null models by shuffling the seven subcortical regions with respect to one another, whereas cortical regions were shuffled using the spin test. Therefore, the empirical correlations were assessed and compared to the set of null correlations across the entire brain i.e., cortical, and subcortical brain areas combined.

5.3.7 Statistical analyses

Statistical analysis and graph illustration were performed with SPSS (version 27; Chicago, IL) and GraphPad Prism (version 9.0.2), respectively. For all variables, Gaussianity was tested with the

Shapiro-Wilk test statistics and all data points were converted to Z-scores. Since most variables were not normally distributed, to test the association between Δ[^{11}C]UCB-J profiles (derived per group comparison) and neuroimaging markers, simple linear regression models with a bootstrapping approach was employed, with 10,000 iterations. For all linear regression models, Mahalanobis distance and Cook's distance were computed to determine the presence of multivariate outliers and highly influential data points. Mahalanobis distance values were compared to a chi-square distribution with degrees of freedom equal to the number of variables, with p=0.01. Any data point with Cook's distance higher than 1 was considered as a highly influential outlier and consequently excluded from the analysis. Stepwise linear regression, with the forward selection approach, was employed to determine which factors best contribute to Δ[^{11}C]UCB-J V_T and for this analysis, all data points were mean-centred in an attempt to alleviate multicollinearity. In addition, Fisher's r-to-z transformation was conducted to test the pairwise significance of the difference between correlation coefficients of Δ[^{11}C]UCB-J profiles and neuroimaging markers between different groups. Finally, pairwise Spearman correlations were computed between the regional distribution of neuroimaging markers derived from healthy control PET and SPECT templates to gain an insight into the interdependencies between them. All analyses were false discovery rate (FDR) corrected for the number of tests for each group comparison and the α level for significance was set at p<0.05.

5.4 Results

I investigated the association between the regional distribution of Δ[^{11}C]UCB-J V_T and a range of neuroreceptor and transporter maps in drug-naïve PD patients, those on treatment, PD patients with dementia and DLB patients. I also examined the relationship between the regional distribution of Δ[^{11}C]UCB-J V_T and group-level structural and blood flow differences in these groups. This is distinct from Chapters 2 and 3 since previously, intra-regional relationships were

investigated between the within-group means of [^{11}C]UCB-J V_T and GM volume and CBF across the sample, whereas this approach is assessing the spatial relationship between the mean between-group difference of [^{11}C]UCB-J V_T and GM volume and CBF across regions-of-interest. In all linear regression models, I did not identify any of the data points to be highly influential outliers (all Cook's distances <1) or multivariate outliers (all Mahalanobis distances (p>0.01).

Below, I present the results of linear regressions between Δ[^{11}C]UCB-J V_T and each map, organised into 3 main subsections to explore the progression of synaptic changes in PD over the course of the disease: i) Δ[^{11}C]UCB-J V_T in healthy controls vs drug naïve PD patients ii) Δ[^{11}C]UCB-J V_T in drug-naïve PD patients vs treated PD patients iii) and Δ[^{11}C]UCB-J V_T in treated PD patients vs PDD patients. The penultimate two subsections are dedicated to dementia, where I assessed the association between the regional distribution of Δ[^{11}C]UCB-J V_T and each map in healthy controls vs DLB patients, and then for PDD patients vs DLB patients. Finally, I present the results after incorporating the spatial autocorrelation structure of Δ[^{11}C]UCB-J V_T maps.

5.4.1 Correlations between PET and SPECT templates

A summary of the pairwise correlations between all maps can be found in Figure 5.1. Briefly, the strongest positive associations observed between DAT and VaChT (ρ=0.86), DAT and D_2 (ρ=0.81) and DAT and SERT (ρ=0.78). The strongest negative correlations were found between $5HT_{1A}$ and VaChT (ρ=-0.58), $5HT_{2A}$ and D_2 (ρ=-0.56) and $5HT_{2A}$ and VaChT (ρ=-0.55).

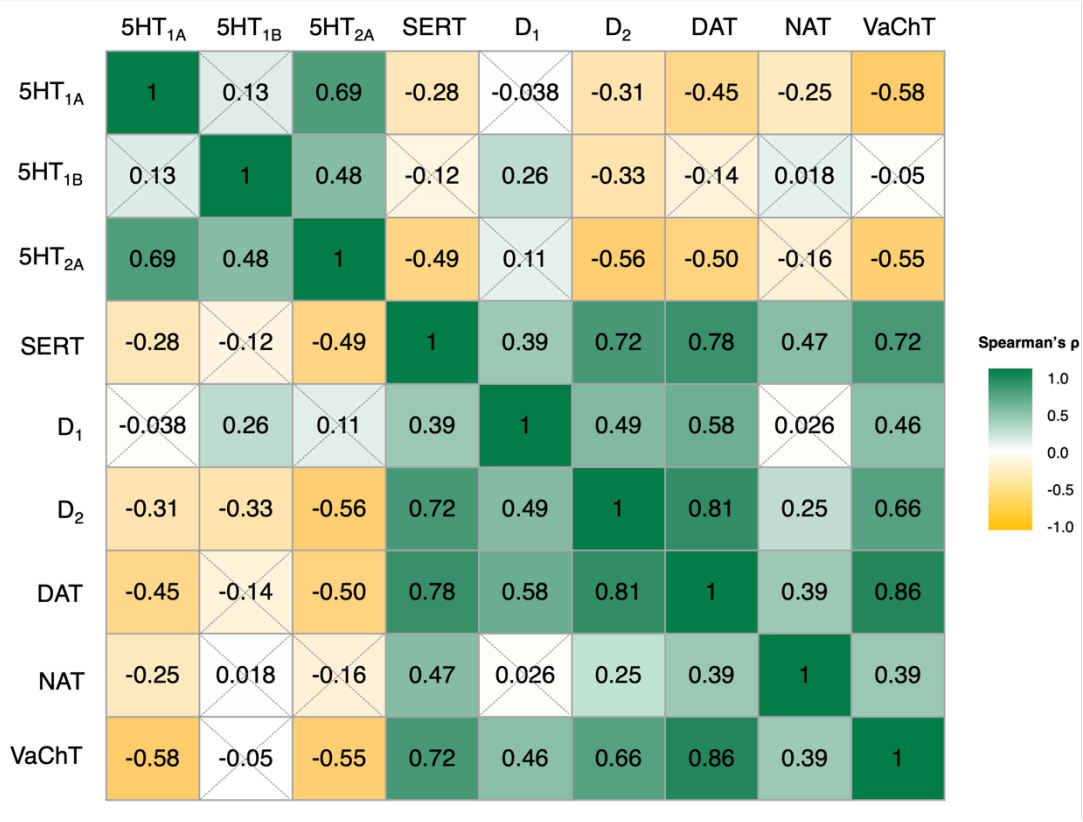

Figure 5.1. Pairwise Spearman correlations between the regional distribution of PET and SPECT templates. The crosses indicate correlations that did not reach the threshold for significance (p>0.05).

5.4.2 Healthy controls vs drug-naïve PD patients: Δ[^{11}C]UCB-J V_T

This contrast was employed to assess the early effects of PD. The distribution pattern of D_1R explained the largest amount of the variance (25%) of the regional distribution of Δ[^{11}C]UCB-J V_T in drug-naïve PD patients compared to healthy controls ($F(1, 113)=37.78$, $R^2=0.25$, $p<0.001$), followed by D_2R and DAT that explained 21% and 12% of the variance, respectively (D_2R: $F(1, 113)=30.37$, $R^2=0.21$, $p<0.001$; DAT: $F(1, 105)=14.02$, $R^2=0.12$, $p=0.005$; Table 5.2). These dopaminergic markers were negatively related to Δ[^{11}C]UCB-J V_T (D_1R: r=-0.50; D_2R: r=-0.46; DAT: r=-0.36; Figure 5.2). VaChT was found to explain 10% of Δ[^{11}C]UCB-J V_T variance ($F(1, 113)=0.32$, $R^2=0.10$, $p=0.005$), whilst $5HT_{2A}$ explained 6% ($F(1, 113)=7.54$, $R^2=0.063$, $p=0.016$). An increase in VaChT and $5HT_{2A}$ was associated with a reduction of Δ[^{11}C]UCB-J V_T (VaChT: r=-0.32, $5HT_{2A}$: r=-0.25). The distribution of NAT and ΔGM volume explained ~7% of the variance (NAT: $F(1, 105)=7.63$, $R^2=0.069$, $p=0.013$; ΔGM volume: ($F(1, 113)=9.05$, $R^2=0.074$,

p=0.021) and ΔCBF explained a negligible 4% of the variance of Δ[^{11}C]UCB-J V_T distribution (F(1, 113)=5.13, R^2=0.043, p=0.007). Higher estimates of NAT, ΔGM volume and ΔCBF were associated with higher Δ[^{11}C]UCB-J V_T (NAT: r=+0.26; ΔGM volume: r=+0.26; ΔCBF: r=+0.20).

Given the known pattern of receptor and transporter distribution across the brain, it was apparent that there was clustering of data points according to whether they belonged to cortical or subcortical brain areas. To determine if the relationship between Δ[^{11}C]UCB-J V_T and template maps were predominately driven by their subcortical distribution, I re-ran the linear regression models to only include subcortical regions-of-interest (Figure 5.2). I found that the subcortical distribution of receptor and transporter density profiles explained a larger proportion of the variance of subcortical Δ[^{11}C]UCB-J V_T. D_1R and D_2R each explained 52% of the variance (D_1R: F(1, 41)=43.56, R^2=0.52, β=-0.67, p<0.001; D_2R: F(1,41)=45.16, R^2=0.52, β=-0.71, p<0.001) and DAT explained 35% (F(1,41)=22.09, R^2=0.35, β=-0.62, p<0.001). Higher estimates of these dopaminergic markers were associated with reduced Δ[^{11}C]UCB-J V_T (D_1R: r=-0.72; D_2R: r=-0.72; DAT: r=-0.59). NAT explained 11% of the variance (F(1, 41)=5.12, R^2=0.11, β=0.31, p=0.035) and was positively associated with Δ[^{11}C]UCB-J V_T (r=+0.33), whilst $5HT_{2A}$ explained 26% (F(1, 41)=14.01, R^2=0.26, β=-1.50, p=0.023), and VaChT explained 38% of the variance (F(1, 41)=25.58, R^2=0.38, β=-0.70, p<0.001), both of which were negatively related to Δ[^{11}C]UCB-J V_T in drug naïve PD patients compared to healthy controls (5HT2A: r=-0.51; VaChT: r=-0.62).

Table 5.2. Variables that were predictive of the regional distribution of Δ[^{11}C]UCB-J V_T in drug-naïve PD patients compared to healthy controls following simple linear regressions.

Drug-naïve vs HC	**Δ[^{11}C]UCB-J V_T**			
Predictors	**β coefficient**	**r**	**R^2**	***p* value**
ΔGM volume	**0.26**	**+0.27**	**0.074**	**0.021**
ΔCBF	**0.20**	**+0.21**	**0.043**	**0.007**
$5HT_{1A}$	-0.12	-0.12	0.013	0.29
$5HT_{1B}$	-0.12	-0.11	0.013	0.22
$5HT_{2A}$	**-0.26**	**-0.25**	**0.063**	**0.016**
SERT	0.13	+0.13	0.018	0.29
D_1	**-0.50**	**-0.50**	**0.25**	**<0.001**
D_2	**-0.44**	**-0.46**	**0.21**	**<0.001**
DAT	**-0.33**	**-0.35**	**0.12**	**0.005**
NAT	**0.26**	**+0.26**	**0.069**	**0.013**
VaChT	**-0.31**	**-0.32**	**0.10**	**0.005**

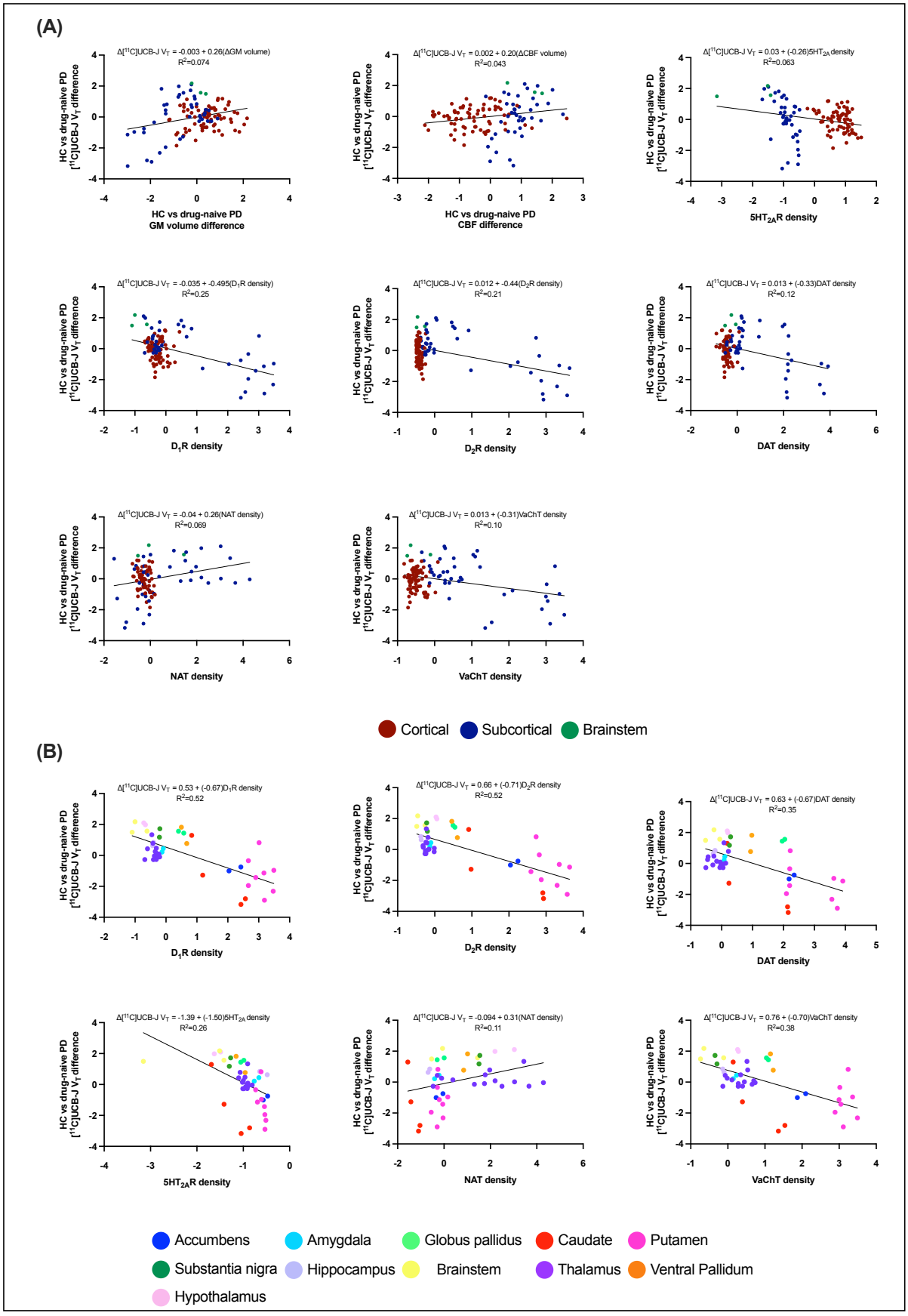

Figure 5.2. Simple linear regression analyses between Δ[^{11}C]UCB-J V_T and neuroimaging markers in drug-naïve PD patients vs healthy controls (A) Linear regression between Δ[^{11}C]UCB-J V_T and neuroimaging

markers in drug-naïve PD patients vs healthy controls contrast maps across the whole brain. (B) Linear regression between Δ[^{11}C]UCB-J V_T and receptor/transporter density profiles within the subcortex and brainstem in drug-naïve PD patients vs healthy controls. Negative [^{11}C]UCB-J V_T, GM volume and CBF values denote reductions in drug-naïve PD compared to healthy controls, whilst positive values reflect increases.

5.4.2.1 Stepwise linear regression

To determine which variables were the strongest predictors of the regional distribution of Δ[^{11}C]UCB-J V_T , I conducted a stepwise linear regression. D_1R density profile explained the largest proportion of variance of Δ[^{11}C]UCB-J V_T of 25% (F(1,113)=37.78, R^2=0.25, p<0.001), followed by $5HT_{2A}$, which contributed to explaining 14% of the variance (F(1,112)=26.21, R^2 change=0.14, p<0.001). D_2R further increased the variance explained by 6.4% (F(1,111)=12.99, R^2 change=0.064, p<0.001) and DAT explained a negligible amount of unique variance of 3.6% (F(1,110)=7.79, R^2 change=0.036, p=0.006; Table 5.3). Nevertheless, taken together, these molecular markers explained up to 49% of the variance of Δ[^{11}C]UCB-J V_T in drug naïve PD patients compared to healthy controls (F(4,110)=26.66, R^2=0.49, p<0.001).

When investigating these relationships subcortically, the strongest predictor of the subcortical distribution of Δ[^{11}C]UCB-J V_T was D_2R density profile, which explained 52% of Δ[^{11}C]UCB-J V_T variance (F(1,41)=45.16, R^2=0.52, p<0.001). DAT explained a further 6.4% of the variance (F(1,40)=6.23, R^2 change=0.064, p=0.017) and $5HT_{2A}$ contributed 6.5% of variance explained (F(1,39)=7.34, R^2 change=0.065, p=0.01; Table 5.3). Together, these molecular markers explained 65% of the variance of Δ[^{11}C]UCB-J V_T subcortically in drug-naïve PD patients compared to healthy controls (F(3,39)=24.52, R^2=0.65, p<0.001).

Table 5.3. Significant predictors of the regional distribution of Δ[^{11}C]UCB-J V_T in drug-naïve PD patients compared to healthy controls following a stepwise linear regression.

Drug-naïve PD vs HC	**Δ[^{11}C]UCB-J V_T**				
Whole-brain					
Predictors	**r**	**R^2**	**Change statistics**		
			R^2 change	***F* change**	***p* value**
D_1R	0.50	0.25	0.25	37.78	<0.001
D_1R and $5HT2_A$	0.63	0.39	0.14	26.21	<0.001
D_1R, $5HT2_A$ and D_2R	0.68	0.46	0.064	12.99	<0.001
D_1R, $5HT_{2A}$, D_2R and DAT	0.70	0.49	0.036	7.79	0.006
Subcortical					
Predictors	**r**	**R^2**	**Change statistics**		
			R^2 change	***F* change**	***p* value**
D_2R	0.72	0.52	0.52	45.16	<0.001
D_2R and DAT	0.77	0.59	0.064	6.23	0.017
D_2R, DAT and $5HT2_A$	0.81	0.65	0.065	7.34	0.01

5.4.3 Drug-naïve PD vs treated PD patients: Δ[^{11}C]UCB-J V_T

This contrast was employed to assess the effects of medication and PD chronicity. In treated PD patients compared to drug-naïve PD patients, the distribution of $5HT_{2A}$ explained ~8% of Δ[^{11}C]UCB-J V_T variance (F(1,113)=9.23, R^2=0.076, p=0.008), ΔGM volume explained 7% (F(1,113)=8.70, R^2=0.071, p=0.005) and D_1R explained ~5% (F(1,113)=5.76, R^2=0.048, p=0.032; Table 5.4). Higher estimates of $5HT_{2A}$, ΔGM volume and D_1R were associated with higher Δ[^{11}C]UCB-J V_T ($5HT_{2A}$: r=+0.28; ΔGM volume: r=+0.27; D_1R: r=+0.22; Figure 5.3). NAT explained 7% of the variance of Δ[^{11}C]UCB-J V_T distribution (F(1,103)=8.04, R^2=0.072, p=0.003) and SERT explained 5.6% (F(1,113)=6.67, R^2=0.056, p=0.015; Table 5.4). Higher NAT

and SERT were associated with higher Δ[^{11}C]UCB-J V_T across the brain (NAT: r=-0.27; SERT: r=-0.24; Figure 5.3)

Within subcortical regions-of-interest, SERT density profile explained 11% of the variance of Δ[^{11}C]UCB-J V_T distribution (F(1,41)=5.26, R^2=0.11, β=-0.35, p=0.043), D_1R explained 18% (F(1,41)=8.95, R^2=0.18, β=0.33 p=0.005) and NAT explained 14% (F(1,41)=6.46, R^2=0.14, β=-0.29, p=0.012).

Table 5.4. Predictor variables of the regional distribution of Δ[^{11}C]UCB-J V_T in treated PD patients compared to drug-naïve PD patients.

Treated PD vs drug-naïve PD	**Δ[^{11}C]UCB-J V_T**			
	β coefficient	**r**	**R^2**	***p* value**
ΔGM volume	**0.26**	**+0.27**	**0.071**	**0.005**
ΔCBF	-0.066	-0.066	0.004	0.54
$5HT_{1A}$	0.21	+0.21	0.043	0.053
$5HT_{1B}$	0.034	+0.032	0.001	0.74
$5HT_{2A}$	**0.29**	**+0.28**	**0.076**	**0.008**
SERT	**-0.24**	**-0.24**	**0.056**	**0.015**
D_1	**0.22**	**+0.22**	**0.048**	**0.032**
D_2	0.17	+0.17	0.03	0.092
DAT	0.063	+0.065	0.004	0.51
NAT	**-0.27**	**-0.27**	**0.072**	**0.003**
VaChT	0.074	+0.076	0.006	0.40

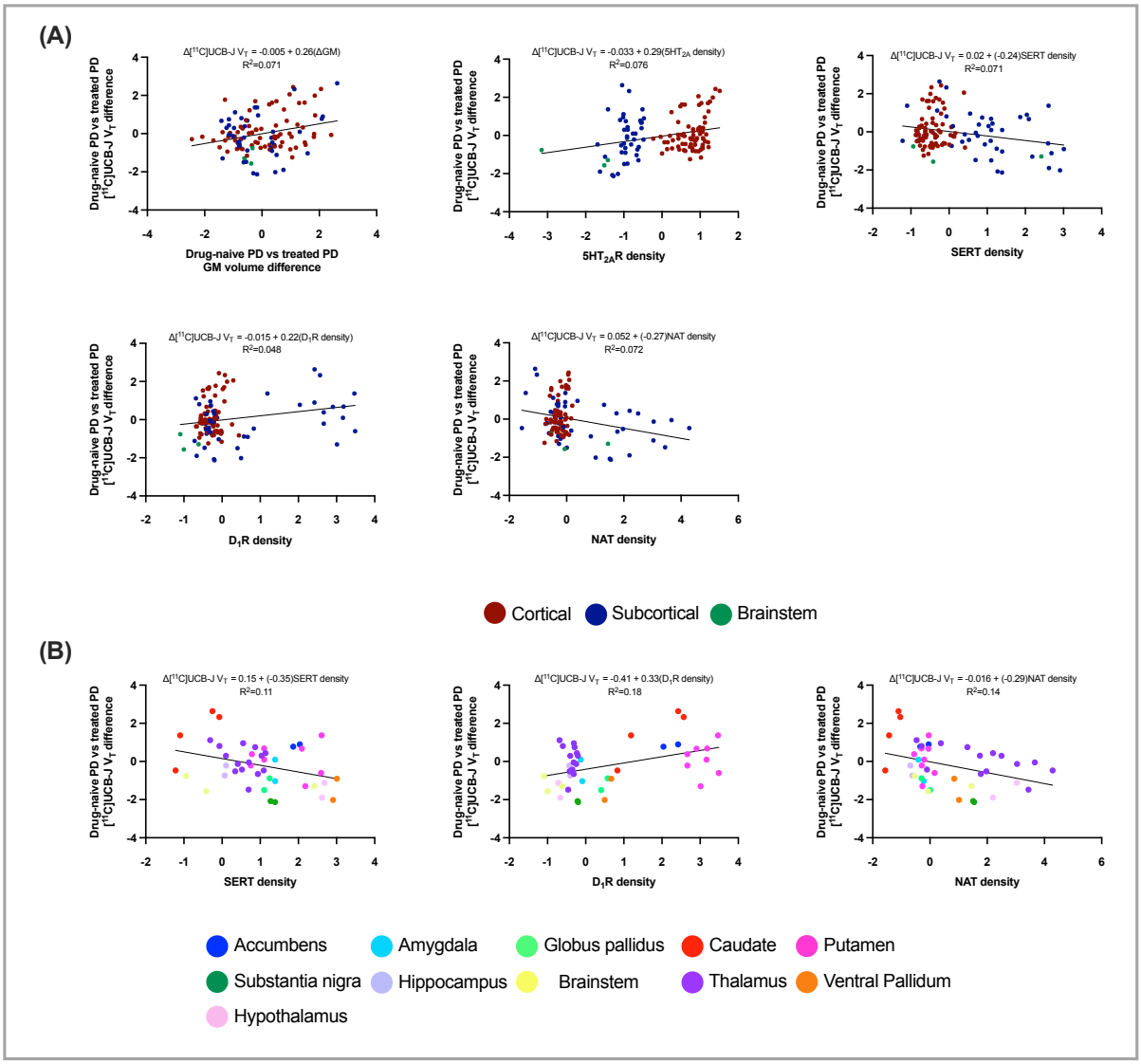

Figure 5.3. Linear regression between Δ[^{11}C]UCB-J V_T and neuroimaging markers in treated PD vs drug-naïve PD (A) Linear regressions between Δ[^{11}C]UCB-J V_T and neuroimaging markers in treated PD vs drug-naïve PD patients contrast maps across the whole brain. (B) Linear regressions between Δ[^{11}C]UCB-J V_T and receptor/transporter density profiles within the subcortex and brainstem in treated PD vs drug-naïve PD patients. Negative [^{11}C]UCB-J V_T, GM volume and CBF values denote reductions in treated PD compared to drug naïve PD, whilst positive values reflect increases.

5.4.3.1 Stepwise linear regression

Following a stepwise linear regression, the density profile of $5HT_{2A}$ explained 7.6% of the variance of Δ[^{11}C]UCB-J V_T of ($F(1,113)=9.23$, $R^2=0.076$, $p=0.003$), followed by D_1R, which explained a further 8.5% of the variance ($F(1,112)=11.39$, R^2 change=0.085, $p=0.001$). SERT explained an additional 6.4% ($F(1,111)=9.09$, R^2 change=0.064, $p=0.003$) and ΔGM volume contributed 4.3% of explained variance ($F(1,110)=6.51$, R^2 change=0.043, $p=0.012$; Table 5.5).

Taken together, this model explained 27% of Δ[^{11}C]UCB-J V_T variance (F(4,110)=10.06, R^2=0.27, p<0.001).

Predictors of the subcortical distribution of Δ[^{11}C]UCB-J V_T included D_1R density, which explained 18% of Δ[^{11}C]UCB-J V_T variance (F(1,41)=8.95, R^2=0.18, p=0.005) and SERT, which explained an additional 22% of variance (F(1,40)=14.40, R^2 change=0.22, p<0.001; Table 5.5). Taken together, these molecular markers explained 40% of the subcortical variance of Δ[^{11}C]UCB-J V_T in treated PD patients compared to drug-naïve PD patients (F(2,40)=13.14, R^2=0.40, p<0.001).

Table 5.5. Significant predictors of the regional distribution of Δ[^{11}C]UCB-J V_T in treated PD patients compared to those that were drug-naïve following a stepwise linear regression.

Treated PD vs drug-naïve PD	**Δ[^{11}C]UCB-J V_T**				
Whole-brain spatial correlations					
Predictor variables	**r**	**R^2**	**Change statistics**		
			R^2 change	***F* change**	***p* value**
$5HT_{2A}$	0.28	0.076	0.076	9.23	0.003
$5HT_{2A}$ and D_1R	0.40	0.16	0.085	11.39	0.001
$5HT_{2A}$, D_1R and SERT	0.47	0.22	0.064	9.09	0.003
$5HT_{2A}$, D_1R, SERT and ΔGM volume	0.52	0.27	0.043	6.51	0.012
Subcortical spatial correlations					
Predictor variables	**r**	**R^2**	**Change statistics**		
			R^2 change	***F* change**	***p* value**
D_1R	0.42	0.18	0.18	8.95	0.005
D_1R and SERT	0.63	0.40	0.22	14.40	<0.001

5.4.4 Treated PD vs PDD patients: Δ[^{11}C]UCB-J V_T

This contrast was employed to assess the effects of dementia in PD. ΔGM volumetric profile explained 14% of Δ[^{11}C]UCB-J V_T distribution (F(1,113)=18.61, R^2=0.14, p<0.001), alongside the density profile of NAT, which explained ~5% (F(1,103)=5.14, R^2=0.048, p=0.002), SERT and DAT each explained 7% (SERT: F(1,113)=8.65, R^2=0.071, p=0.003; DAT: (F(1,103)=7.8, R^2=0.07, p=0.006) and VaChT which explained 4.6% of Δ[^{11}C]UCB-J V_T in PDD compared to treated PD patients (F(1,113)=5.44, R^2=0.046, p=0.022; Table 5.6). Higher ΔGM volume, NAT, SERT, DAT and VaChT were related to higher Δ[^{11}C]UCB-J V_T (ΔGM volume: r=+0.38 ; NAT: r=+0.22; SERT: r=+0.27; DAT: r=+0.27; VaChT: r=+0.21; Figure 5.4). Finally, $5HT_{2A}$ explained 8.2% of Δ[^{11}C]UCB-J V_T variance (F(1,113)=10.13, R^2=0.082, p=0.004), and was negatively associated with Δ[^{11}C]UCB-J V_T (r=-0.29).

At the subcortical level, neuroreceptor or transporter density profiles did not predict the subcortical distribution of Δ[^{11}C]UCB-J V_T. However, cortical $5HT_{2A}$ explained 8.3% of the variance of the cortical distribution of Δ[^{11}C]UCB-J V_T (F(1,70)=6.37, R^2=0.083, β=-0.66, p=0.015).

Table 5.6. Variables that predicted the regional distribution of Δ[^{11}C]UCB-J V_T in PDD patients compared to PD patients on treatment

Treated PD vs PDD	**Δ[^{11}C]UCB-J V_T**			
	β coefficient	**r**	**R^2**	***p* value**
ΔGM volume	**0.38**	**+0.38**	**0.14**	**<0.001**
ΔCBF	-0.006	-0.006	0.00	0.96
$5HT_{1A}$	-0.15	-0.15	0.022	0.15
$5HT_{1B}$	-0.17	-0.17	0.027	0.07
$5HT_{2A}$	**-0.29**	**-0.29**	**0.082**	**0.004**
SERT	**0.27**	**+0.27**	**0.071**	**0.003**

D_1	0.13	+0.13	0.016	0.20
D_2	0.18	+0.18	0.031	0.079
DAT	**0.26**	**+0.27**	**0.07**	**0.006**
NAT	**0.22**	**+0.22**	**0.048**	**0.002**
VaChT	**0.21**	**+0.21**	**0.046**	**0.022**

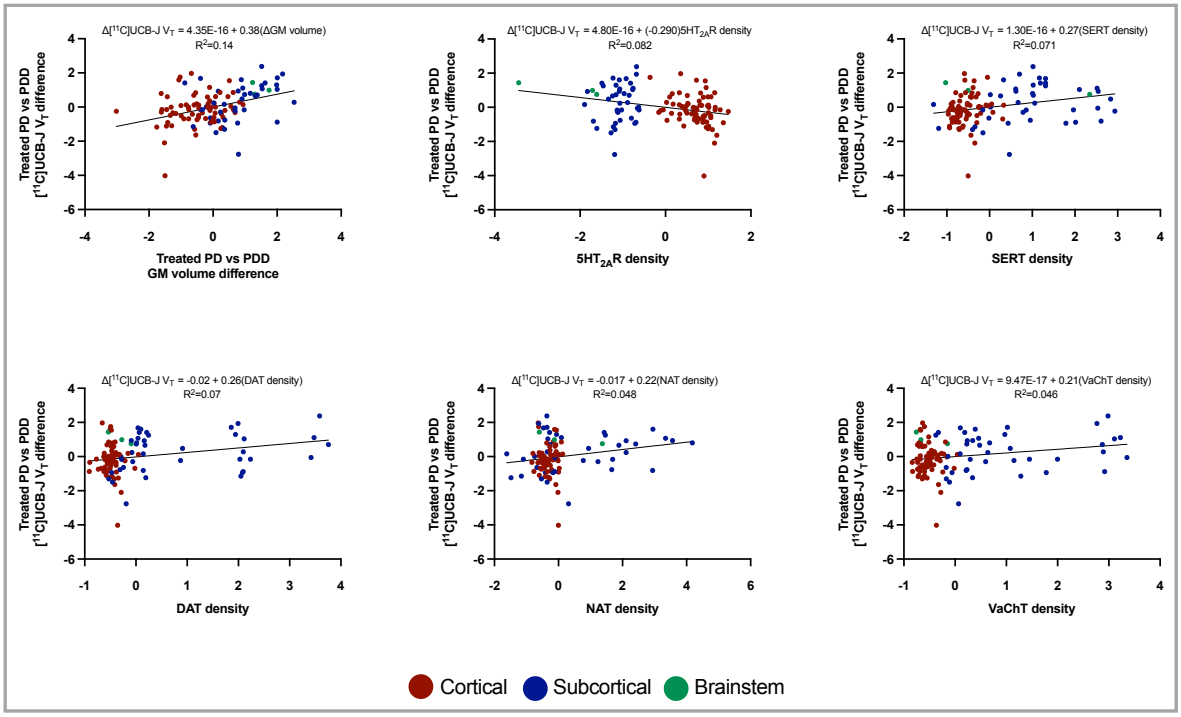

Figure 5.4. Linear regression between Δ[^{11}C]UCB-J V_T and neuroimaging markers in PDD vs treated PD patients contrast maps across the whole brain. Negative [^{11}C]UCB-J V_T, GM volume and CBF values denote reductions in PDD compared to treated PD, whilst positive values reflect increases.

5.4.4.1 Stepwise linear regression

Following a stepwise linear regression, ΔGM volume was the only variable that was a significant predictor of the regional distribution of Δ[^{11}C]UCB-J V_T, explaining 14% of its variance ($F(1,113)=18.61$, $R^2=0.14$, $p<0.001$; Table 5.7).

Table 5.7. Significant predictors of the regional distribution of Δ[^{11}C]UCB-J V_T in PDD patients compared to treated PD patients following a stepwise linear regression.

Treated PD vs PDD	**Δ[^{11}C]UCB-J V_T**				
Predictor variables	**r**	**R^2**	**Change statistics**		
			R^2 change	***F* change**	***p* value**
ΔGM volume	0.38	0.14	0.14	18.61	<0.001

5.4.5 Healthy controls vs DLB patients: Δ[^{11}C]UCB-J V_T

This contrast was employed to assess the effects of DLB. ΔGM volume explained 44% of the variance of the distribution of Δ[^{11}C]UCB-J V_T in DLB patients compared to controls (F(1,113)=87.45, R^2=0.44, p<0.001), whilst ΔCBF and SERT each explained ~9% (ΔCBF: F(1,113)=10.94, R^2=0.088, p<0.001; SERT: F(1,113)=11.74, R^2=0.094, p<0.001) and NAT explained 16% (F(1,103)=19.05, R^2=0.16, p<0.001; Table 5.8). Higher estimates of ΔGM volume, ΔCBF, SERT and NAT were related to higher estimates of Δ[^{11}C]UCB-J V_T (ΔGM volume: r=+0.66; ΔCBF: r=+0.30 SERT: r=+0.31; NAT: r=+0.40; Figure 5.5). Furthermore, receptor density profile $5HT_{2A}$ explained 11% of Δ[^{11}C]UCB-J V_T variance (F(1,113)=13.71, R^2=0.11, p=0.002) and $5HT_{1A}$ explained 6% (F(1,113)=7.25, R^2=0.06, p=0.02), with higher estimates of both serotonergic markers being related to lower estimates of Δ[^{11}C]UCB-J V_T ($5HT_{2A}$: r=-0.33; $5HT_{1A}$: r=-0.25; Figure 5.5).

Within the subcortex, $5HT_{2A}$ explained 6.4% of the variance of the subcortical distribution of Δ[^{11}C]UCB-J V_T (F(1,41)=2.83, R^2=0.064, β=-0.65, p=0.03). SERT explained 13% of the variance (F(1,41)=5.99, R^2=0.13, β=0.39, p=0.029) and NAT explained 25% (F(1,41)=13.82, R^2=0.25, β=0.40, p=0.002). No relationship was found between either the subcortical or cortical distribution of Δ[^{11}C]UCB-J V_T and $5HT_{1A}$, suggesting that that alleged relationship was likely a result of the distinction between cortical and subcortical distributions.

Table 5.8. Variables that were significantly associated with the regional distribution of Δ[^{11}C]UCB-J V_T in DLB patients compared to healthy controls.

HC vs DLB	**Δ[^{11}C]UCB-J V_T**			
	β coefficient	**r**	**R^2**	***p* value**
ΔGM volume	**0.68**	**+0.66**	**0.44**	**<0.001**
ΔCBF	**0.30**	**+0.30**	**0.088**	**<0.001**
$5HT_{1A}$	**-0.25**	**-0.25**	**0.06**	**0.02**
$5HT_{1B}$	-0.16	-0.15	0.021	0.15
$5HT_{2A}$	**-0.35**	**-0.33**	**0.11**	**0.002**
SERT	**0.31**	**+0.31**	**0.094**	**<0.001**
D_1	-0.11	-0.11	0.013	0.33
D_2	-0.063	-0.066	0.004	0.59
DAT	0.044	+0.045	0.002	0.68
NAT	**0.39**	**+0.40**	**0.16**	**<0.001**
VaChT	0.069	+0.071	0.005	0.40

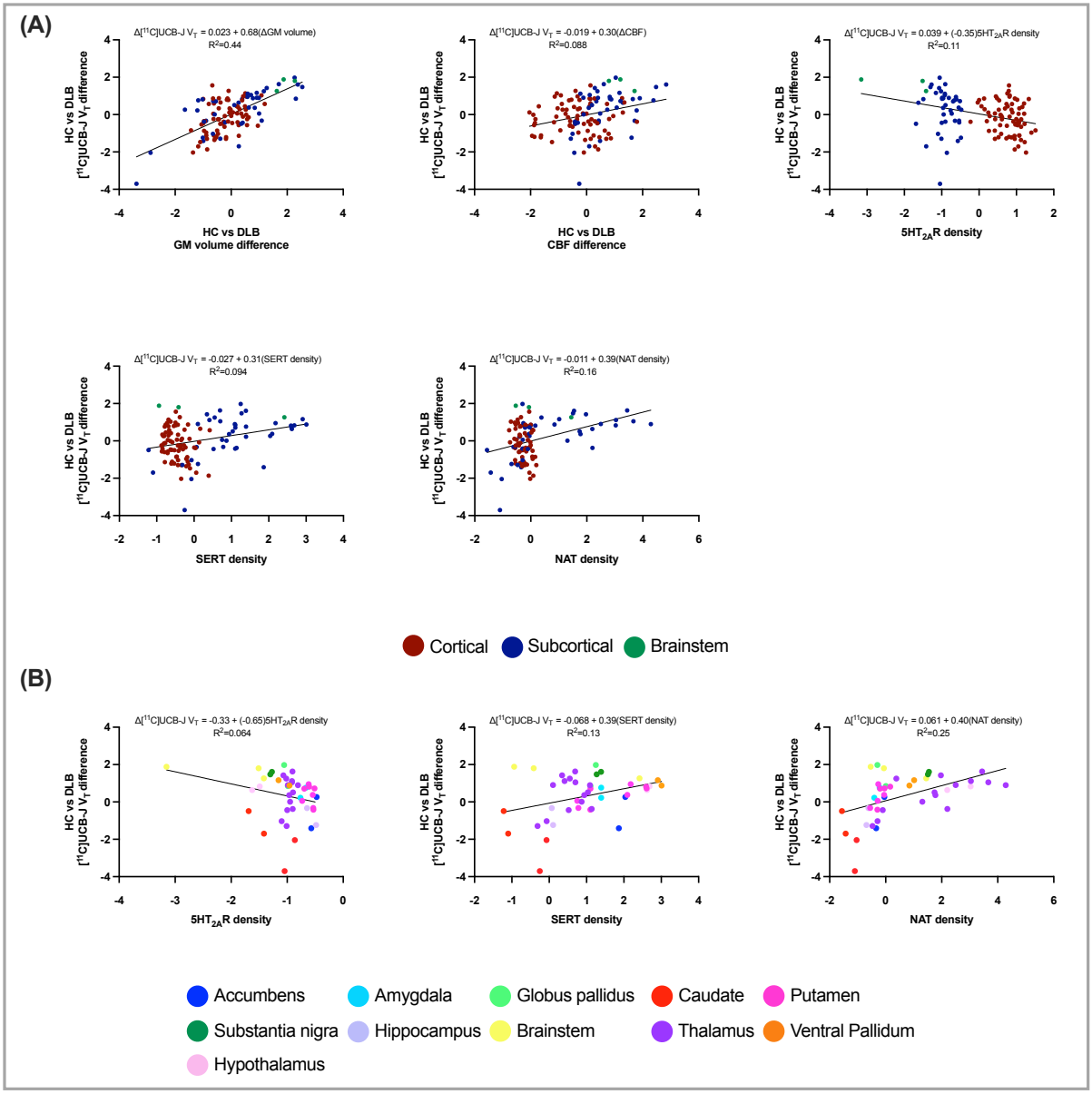

Figure 5.5. Linear regression between Δ[^{11}C]UCB-J V_T and neuroimaging markers in DLB vs healthy controls (A) Linear regressions between Δ[^{11}C]UCB-J V_T and neuroimaging markers in DLB vs healthy controls contrast maps across the whole brain. (B) Linear regressions between Δ[^{11}C]UCB-J V_T and receptor/transporter density profiles within the subcortex and brainstem. Negative [^{11}C]UCB-J V_T, GM volume and CBF values denote reductions in DLB compared to healthy controls, whilst positive values reflect increases.

5.4.5.1 Stepwise linear regression

Following a stepwise linear regression, Δ[^{11}C]UCB-J V_T spatial distribution was predominately explained by ΔGM volume profile where it explained 44% of [^{11}C]UCB-J V_T variance ($F(1,113)=87.45$, $R^2=0.44$, $p<0.001$), followed by SERT density profile which explained a further ~5% ($F(1,113)=10.73$, $R^2=0.049$, $p=0.001$;Table 5.9). Together, this model explained almost

50% of Δ[^{11}C]UCB-J V_T variance in DLB patients compared to healthy controls ($F(2,112)=52.86$, $R^2=0.49$, $p<0.001$; Table 5.9).

The subcortical distribution of Δ[^{11}C]UCB-J V_T remained largely explained by the ΔGM volume ($F(1,41)=56.4$, $R^2=0.58$, $p<0.001$, Table 5.9). Taken together with SERT, which explained a further 11% of Δ[^{11}C]UCB-J V_T variance ($F(1,40)=13.70$, R^2 change=0.11, $p=0.001$), these neuroimaging markers together explained nearly 70% of the subcortical variance of Δ[^{11}C]UCB-J V_T in PDD vs treated PD patients ($F(2,40)=43.79$, $R^2=0.69$, $p<0.001$).

Table 5.9. Significant predictors of the regional distribution of Δ[^{11}C]UCB-J V_T in DLB patients compared to healthy controls following a stepwise linear regression.

HC vs DLB	**Δ[^{11}C]UCB-J V_T**				
Whole-brain spatial correlations					
Predictor variables	**r**	**R^2**	**Change statistics**		
			R^2 change	***F* change**	***p* value**
ΔGM volume	0.66	0.44	0.44	87.45	<0.001
ΔGM volume and SERT	0.70	0.49	0.049	10.73	0.001
Subcortical spatial correlations					
Predictor variables	**r**	**R^2**	**Change statistics**		
			R^2 change	***F* change**	***p* value**
ΔGM volume	0.76	0.58	0.58	56.4	<0.001
ΔGM volume and SERT	0.83	0.69	0.11	13.70	0.001

5.4.6 PDD vs DLB patients: Δ[^{11}C]UCB-J V_T

This contrast was employed to assess the differential effects of PDD and DLB. 10% of the variance of Δ[^{11}C]UCB-J V_T distribution was explained by the respective ΔCBF profile

(F(1,113)=12.6, R^2=0.10, p=0.002), which was positively associated with Δ[^{11}C]UCB-J V_T (r=+0.32). D_1R and D_2R explained approximately 20% of Δ[^{11}C]UCB-J V_T variance (F(1,113)=25.58, R^2=0.19, p<0.001), D_2R (F(1,113)=27.38, R^2=0.20, p<0.001), and DAT explained 17% (F(1,103)=12.6, R^2=0.17, p<0.001; Table 5.10). Higher estimates of these dopaminergic markers were associated with higher estimates of Δ[^{11}C]UCB-J V_T (D_1R: r=+0.43; D_2R: r=+0.44; DAT: r=+0.41; Figure 5.6). $5HT_{1A}$ explained 10% of Δ[^{11}C]UCB-J V_T variance (F(1,113)=12.50, R^2=0.10, p=0.001) and $5HT_{2A}$ explained 3.1% (F(1,113)=3.63, R^2=0.031, p=0.033; Table 5.10). These serotonergic markers were negatively related to Δ[^{11}C]UCB-J V_T, where higher estimates of $5HT_{1A}$ and $5HT_{2A}$ were associated with lower Δ[^{11}C]UCB-J V_T ($5HT_{1A}$: r=-0.32; $5HT_{2A}$: r=-0.18). Finally VaChT explained 19% (F(1,113)=25.68, R^2=0.19, p<0.001; Table 5.10) of the variance of Δ[^{11}C]UCB-J V_T in DLB patients compared to PDD patients and was positively related to Δ[^{11}C]UCB-J V_T (r=+0.43; Figure 5.6).

Subcortically, $5HT_{1A}$ receptor density profile explained 18% of the variance of the distribution of Δ[^{11}C]UCB-J V_T (F(1,41)=9.20, R^2=0.18, β=-0.60, p=0.002), both D_1R and D_2R explained 35% of the variance (D_1R: F(1,41)=22.08, R^2=0.35, β=0.42, p<0.001; D_2R: F(1,41)=21.89, R^2=0.35, β=0.46, p<0.001), DAT explained 36% (F(1,41)=23.14, R^2=0.36, β=0.47, p=0.001), and VaChT explained 38% of the variance of Δ[^{11}C]UCB-J V_T (F(1,41)=25.57, R^2=0.38, β=0.53, p<0.001; Table 5.10; Figure 5.6).

Table 5.10. Variables that predicted the regional distribution of Δ[^{11}C]UCB-J V_T in DLB patients compared to PDD patients.

DLB vs PDD	**Δ[^{11}C]UCB-J V_T**			
	β coefficient	**R**	**R^2**	***p* value**
ΔGM volume	-0.015	+0.013	0.00	0.89
ΔCBF	**0.37**	**+0.32**	**0.10**	**0.002**
$5HT_{1A}$	**-0.32**	**-0.32**	**0.10**	**0.001**
$5HT_{1B}$	0.13	+0.12	0.014	0.25
$5HT_{2A}$	**-0.19**	**-0.18**	**0.031**	**0.033**
SERT	0.21	+0.21	0.043	0.061
D_1	**0.43**	**+0.43**	**0.19**	**<0.001**
D_2	**0.43**	**+0.44**	**0.20**	**<0.001**
DAT	**0.39**	**+0.41**	**0.17**	**<0.001**
NAT	0.11	+0.12	0.014	0.24
VaChT	**0.42**	**+0.43**	**0.19**	**<0.001**

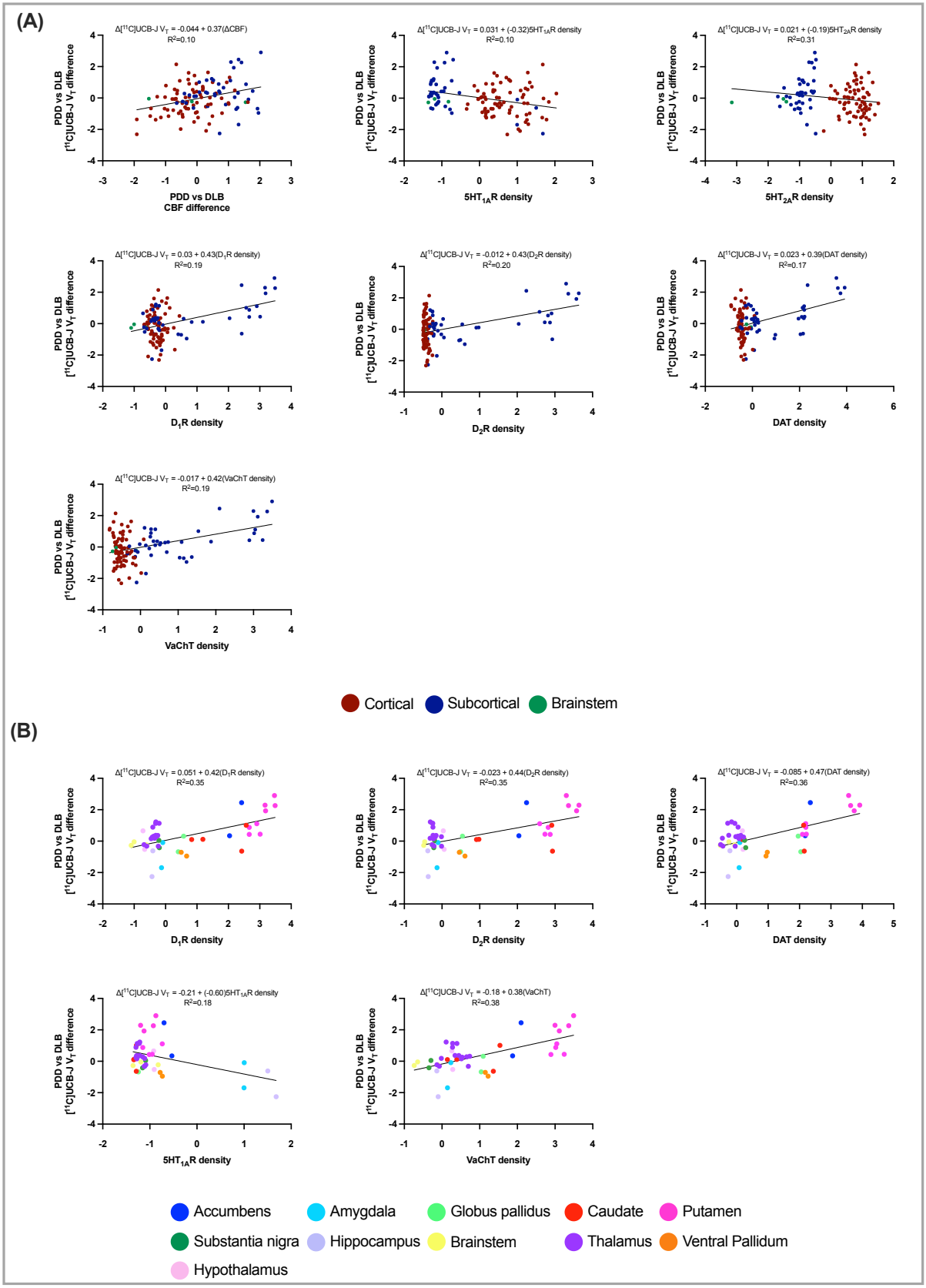

Figure 5.6. Linear regression between Δ[^{11}C]UCB-J V_T and neuroimaging markers in PDD vs DLB (A) Linear regression between Δ[^{11}C]UCB-J V_T and neuroimaging markers in DLB vs PDD contrast maps across the whole brain. (B) Linear regression between Δ[^{11}C]UCB-J V_T and receptor/transporter density profiles within

the subcortex and brainstem. Negative [^{11}C]UCB-J V_T, GM volume and CBF values denote reductions in DLB compared to PDD, whilst positive values reflect increases.

5.4.6.1 Stepwise linear regression

Following a stepwise linear regression incorporating all maps that were significant predictors of the regional distribution of Δ[^{11}C]UCB-J V_T, only D_2R density profile emerged as a significant predictor, explaining 20% of Δ[^{11}C]UCB-J V_T variance ($F(1,113)=27.38$, $R^2=0.20$, $p<0.001$; Table 5.11).

Within the subcortex, the VaChT density profile explained the largest proportion of Δ[^{11}C]UCB-J V_T variance of nearly 40% ($F(1,41)=25.57$, $R^2=0.38$, $p<0.001$), whilst $5HT_{1A}$ receptor density profile explained a further 12% of unique variance ($F(1,40)=10.11$, R^2 change=0.12, $p=0.003$; Table 5.11). Taken together, these molecular markers explained 51% of the overall variance of Δ[^{11}C]UCB-J V_T subcortical distribution ($F(2,40)=20.68$, $R^2=0.51$, $p<0.001$).

Table 5.11. Significant predictors of the regional distribution of Δ[^{11}C]UCB-J V_T in DLB patients compared to PDD patients following a stepwise linear regression.

PDD vs DLB	**Δ[^{11}C]UCB-J V_T**				
Whole-brain spatial correlations					
	r	**R^2**	**Change statistics**		
			R^2 change	***F* change**	***p* values**
D_2R	0.44	0.20	0.20	27.38	<0.001
Subcortical spatial correlations					
	r	**R^2**	**Change statistics**		
			R^2 change	***F* change**	***p* values**
VaChT	0.62	0.38	0.38	25.57	<0.001
VaChT and $5HT_{1A}$	0.71	0.51	0.12	10.11	0.003

Figure 5.7. An overview of the spatial linear regression analyses between Δ[^{11}C]UCB-J V_T in each group comparison and structural and functional differences, as well as receptor/transporter density profiles derived from PET and SPECT maps. The displayed numbers are the observed r correlation coefficients. Significant correlations are highlighted in bold and those that were not are denoted by crosses.

5.4.7 (HC vs drug-naïve PD) vs (treated PD vs drug-naive PD)

I next assessed the pairwise significance of difference between correlation coefficients of Δ[^{11}C]UCB-J V_T (r, acquired at the same time as the simple linear regression analyses) between HC vs drug-naïve PD and drug-naïve PD vs treated PD contrast maps. This was performed to evaluate whether the transmitter systems involved in explaining the spatial distribution of Δ[^{11}C]UCB-J V_T at one stage differs from those observed in another stage, ultimately providing insight into whether there was a significant difference in the spatial relationships at distinct disease stages of PD. This could be an indication of the evolution of synaptic density alterations in PD progression in relation to neurotransmitter systems. In the pairwise correlation comparisons, I found significant difference between contrast maps for the association between Δ[^{11}C]UCB-J V_T and ΔCBF ($z=3.6$, $p<0.001$), D_1R ($z=2.45$, $p=0.014$), D_2R ($z=2.42$, $p=0.016$), DAT ($z=2.11$, $p=0.035$), VaChT ($z=1.94$, $p=0.05$), whereby drug-naïve PD patients vs healthy controls exhibited stronger associations between these functional and molecular markers and

Δ[^{11}C]UCB-J V_T than those on treatment compared to drug-naïve PD patients. All other comparisons were not significantly different.

5.4.8 (Drug naïve PD vs treated PD) vs (treated PD vs PDD)

Here, I assessed the pairwise significance of difference between correlation coefficients of Δ[^{11}C]UCB-J V_T between drug-naïve PD vs treated PD and treated PD vs PDD contrast maps. This was performed to evaluate whether the transmitter systems involved in explaining the spatial distribution of Δ[^{11}C]UCB-J V_T significantly differed from those explaining the spatial distribution of Δ[^{11}C]UCB-J V_T related to dementia. Pairwise correlation comparisons revealed no significant differences between contrast maps for the association between Δ[^{11}C]UCB-J V_T and any of the structural, functional or molecular markers.

5.4.9 Spatial permutation testing

Given that this method was only available when using the Desikan-Killiany atlas, I firstly wanted to assess whether the atlas itself had an impact on the results to clarify whether a change of atlas or accounting for the spatial autocorrelation of the data was influencing the outcome of the results following the spatial permutation test. Therefore, as a safety check, I assessed the correlations between Δ[^{11}C]UCB-J profile in drug-naïve PD compared to healthy controls and neuroimaging markers that were parcellated with the Desikan-Killiany atlas before and after accounting for the inherent spatial autocorrelation of the data. I found that using the Desikan-Killiany atlas had a large impact on the results, where the correlation coefficients were generally lower and *p* values were higher than those observed with the CIC atlas (df=81; please see Appendix D for results including the Desikan-Killiany Atlas before and after accounting for spatial autocorrelation for HC vs drug-naïve PD as a case comparison). Nevertheless, the findings after accounting for the spatial autocorrelation of the neuroimaging data can be found

below (Figure 5.8), although any interpretation of these findings, along with the previously presented findings, must be tentative given the sensitivity to the atlas choice (for a more in-depth discussion on this, please refer to section 5.5).

5.4.9.1 Healthy controls vs drug-naïve PD: Δ[^{11}C]UCB-J V_T

After accounting for the inherent spatial autocorrelation of the imaging data, Δ[^{11}C]UCB-J V_T correlated with ΔGM volume (r=+0.26, p=0.04). After accounting for the inherent spatial autocorrelation of the subcortical imaging data only, Δ[^{11}C]UCB-J V_T appeared to be associated with D_1R, although this did not reach the threshold for significance (r=-0.44, p=0.06).

5.4.9.2 Drug-naïve PD vs treated PD patients: Δ[^{11}C]UCB-J V_T

After accounting for the inherent spatial autocorrelation of both cortical and subcortical imaging data, Δ[^{11}C]UCB-J V_T correlated with ΔGM volume (DK atlas: r=+0.37, p=0.003), whereas within subcortical regions-of-interest, no associations were observed (DK atlas, p>0.1)

5.4.9.3 Treated PD vs PDD patients: Δ[^{11}C]UCB-J V_T

After accounting for the inherent spatial autocorrelation of the imaging data, Δ[^{11}C]UCB-J V_T profile was only associated with the regional distribution of SERT (DK atlas: r=+0.29, p=0.04).

5.4.9.4 Healthy controls vs DLB patients: Δ[^{11}C]UCB-J V_T

After accounting for the inherent spatial autocorrelation of the imaging data, Δ[^{11}C]UCB-J V_T profile was significantly associated with ΔGM volumetric profile (DK atlas: r=+0.56, p<0.001) in DLB patients compared to healthy controls, whilst no correlations were observed when accounting for the spatial autocorrelation of the subcortex only (DK atlas, p>0.05).

5.4.9.5 PDD vs DLB patients: Δ[^{11}C]UCB-J V_T

After accounting for the inherent spatial autocorrelation of the imaging data, the regional distribution of Δ[^{11}C]UCB-J V_T was associated with $5HT_{1A}$ (DK atlas: r=-0.34, p=0.005), $5HT_{1B}$ (DK atlas: r=+0.29, p=0.03) and D_2 (DK atlas: r=+0.18, p=0.05) receptor density profiles. After accounting for the spatial autocorrelations of subcortical regions-of-interest alone, the distribution of Δ[^{11}C]UCB-J V_T was significantly associated with the density profiles of $5HT_{1A}$ receptor (DK atlas: r=-0.61, p=0.010), D_1R (DK atlas: r=+0.59, p=0.017), D_2R (DK atlas: r=+0.56, p=0.029) and VaChT (DK atlas: r=-0.61, p=0.010), with the correlation with DAT at the threshold of significance (DK atlas: r=+0.48, p=0.05).

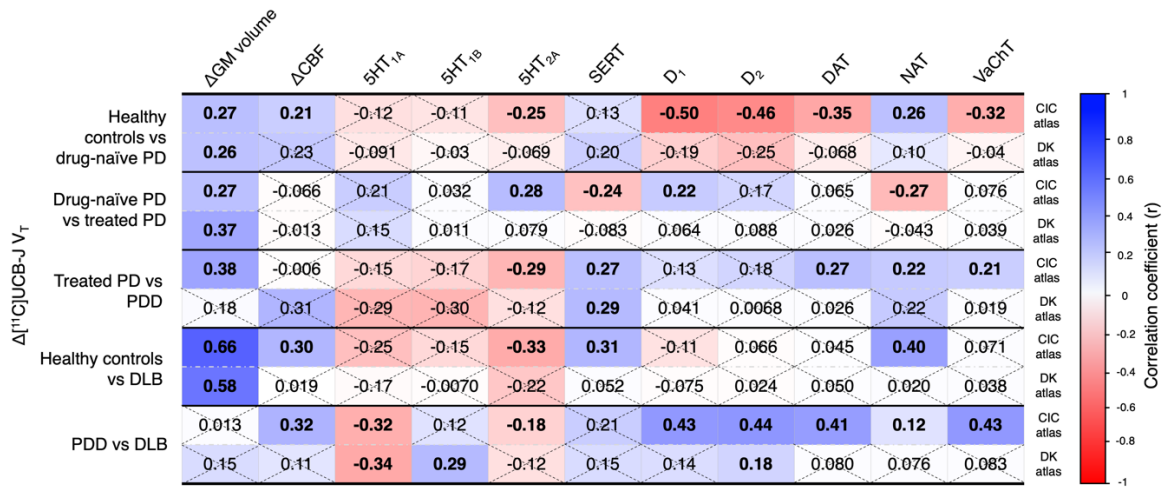

Figure 5.8. A comparison of the spatial correlation analyses following the parcellation of maps with the CIC atlas (without accounting for the spatial autocorrelation of the data) and the parcellation of maps with the DK atlas (accounting for the spatial autocorrelation of the data). The displayed numbers are the observed correlation coefficients (r). Significant correlations are highlighted in bold and those that were not are denoted by crosses. CIC atlas: Clinical Imaging atlas; DK atlas: Desikan-Killiany atlas.

5.5 Discussion

The aim of this work was to investigate the relationship between group-level Δ[^{11}C]UCB-J V_T in patient groups and receptor/transporter distribution profiles in the brain as indexed by the premorbid distribution patterns derived from healthy control PET and SPECT templates. I also assessed the association between Δ[^{11}C]UCB-J V_T and respective group-level differences in volume and perfusion to determine if these measures were better at explaining the spatial pattern of Δ[^{11}C]UCB-J V_T in patient groups. This exploratory analysis contributes to bridging the gap between the observable synaptic density alterations in Lewy body diseases and molecular, structural, and functional biomarkers. Specifically, this analysis can potentially contribute to understanding which neurotransmitter systems may be contributing to synaptic pathophysiology through their spatial relationships and how these may change and evolve throughout the progression of PD (Figure 5). Finally, I also assessed the differential pattern of [^{11}C]UCB-J V_T between DLB and PDD and how this maps onto neuroimaging markers, which was of particular interest given the pressing need to more clearly differentiate these syndromes and understand the receptor systems involved leading to either one.

Before proceeding with the interpretation of my findings, an important point must be addressed. The findings presented do not account for the inherent spatial autocorrelation of the data. Spatial autocorrelation is the ubiquitous phenomenon whereby neighbouring data points tend to be more similar than those that are spatially distant (Song et al., 2014, Wiedermann et al., 2016, Roberts et al., 2016, Burt et al., 2020, Markello and Misic, 2021). It is important to highlight that the assumptions built into conventional parametric and non-parametric nulls are typically violated by this characteristic property of brain maps known as spatial autocorrelation, thus null models that do not preserve spatial autocorrelation yield liberal statistical estimates and increased type 1 error rates. Whilst I appreciate that statistical claims about the topography of a specific brain map should be evaluated against a generative null model that explicitly preserves that target

map's spatial autocorrelation structure into the null hypothesis, the impact of spatial autocorrelation in the neuroimaging field has only recently been acknowledged, with the development of analysis frameworks accounting for spatial autocorrelation coming into fruition over the past few years.

Nevertheless, given the importance of accounting for the spatial properties of brain maps to yield more accurate statistical estimates, I implemented a null framework, but the implementation available to me only incorporated the Desikan-Killiany atlas. As mentioned above, the Desikan-Killiany atlas was found to influence the strength of the associations observed between Δ[^{11}C]UCB-J profiles and neuroimaging markers, which was likely due to the way in which regions were parcelled in the Desikan-Killiany atlas compared to the CIC atlas. The Desikan-Killiany atlas involved averaging the signal over structures that were particularly informative to the analysis, such as subcortical brain areas that were fractionated in a useful way by the CIC atlas. It may also have been because of reduced power as the Desikan-Killiany had fewer regions-of-interest compared to the CIC. Whilst this is a commonly used atlas within the neuroimaging field given its inclusion in FreeSurfer, I selected the CIC atlas for reasons of increased regional delineation and additional subcortical and brainstem regions (43 subcortical and brainstem regions-of-interest versus the 15 in the Desikan-Killiany atlas), which are of particular significance and importance in PD and related dementias since they are heavily implicated in the disease process. Whilst the method used to preserve the spatial autocorrelation of the target map worked appropriately, it has not been validated for the CIC atlas, and consequently the results accounting for the inherent spatial autocorrelation of the neuroimaging data does not hold much import with respect to the result derived from data parcellated with the CIC atlas since the atlas itself has been found to influence the outcome of the results. This ultimately makes the results accounting for the spatial autocorrelation of the neuroimaging data difficult to interpret in the context of the correlations observed after parcellating the brain maps

with the CIC atlas. A collaborative effort will be required to validate the use of the CIC atlas within the null framework employed in this work.

Therefore, whilst the findings are fascinating, it is important to highlight that these results are preliminary and must be interpretated with caution since I cannot be confident about the influence spatial autocorrelation has on these relationships observed. It's also important to note that the spatial distribution patterns observed were based on contrast maps generated from small samples sizes which means that the study risks having low statistical power to detect small effect sizes. Similarly, inferences made about the natural course of PD and disease progression must be moderated by the knowledge that longitudinal data was not included. Therefore, it will be necessary to not only replicate these findings in larger samples and account for the inherent spatial autocorrelation of the brain maps, but collect longitudinal data to properly extrapolate how the spatial distribution patterns change and evolve throughout the progression of PD.

Whilst there is now accumulating evidence that is indicative of synaptic impairments and axonal degeneration preceding neuronal cell body loss, it is also discernible that certain neuronal populations preferentially degenerate in PD and Lewy body dementias. [^{11}C]UCB-J is a PET-derived measure of SV2A levels, thus provides a unique opportunity to evaluate synaptic density *in vivo*, which is, of course, of particular value for the investigation of synaptopathies. However, its regional measurement alone provides information that is limited to the spatial location of synaptic density alterations; thus, we are unable to draw any conclusions about the potential neurophysiological mechanisms contributing to the observed variation in signal. On the one hand, the fact that SV2A is not specific to any one neuronal subtype, but is instead ubiquitously present in synaptic vesicles throughout the entire brain (Bartholome et al., 2017, Mendoza-Torreblanca et al., 2013, Shi et al., 2011, Heurling et al., 2019) deems it an ideal marker for measuring synaptic density *in vivo*, but on the other hand, the interpretability of region- or even

voxel-wise alterations in synaptic density is somewhat rudimentary, given the inability to evaluate what these changes mean in a biologically meaningful way. Therefore, integration of the [^{11}C]UCB-J PET data with PET-derived receptor and transporter maps that represent the state of neurotransmitter system functionality prior to the onset of any given disease, enables the investigation into the role of pre-exiting neurotransmitter systems and how their distribution may be mediating the spatial distribution of synaptic pathology, thus may also have a predictive value in understanding why synaptic density measures vary spatially.

Indeed, I observed a substantial variation across patient groups in the strength and direction of the observed correlations, with the differential pattern of [^{11}C]UCB-J V_T in drug-naïve PD being closely related to markers of the dopaminergic system, whilst in those on treatment, this association was no longer negative but became positively associated. Instead, a loss of [^{11}C]UCB-J V_T was associated with the distribution patterns of noradrenergic and serotonergic biomarkers in this sample of patients, though no one neurotransmitter was more associated with synaptic density than another. The [^{11}C]UCB-J V_T pattern of difference in PDD patients compared to treated PD was predominately explained by the respective pattern of difference of GM volume, with comparable involvement of serotonergic, dopaminergic, noradrenergic and cholinergic neurotransmitter systems. Similarly, the differential pattern of [^{11}C]UCB-J V_T in DLB patients compared to healthy controls was most strongly associated with the distribution patterns of GM volume difference. Finally, the findings for the pattern of difference in DLB patients compared to PDD were particularly remarkable, as the variance of Δ[^{11}C]UCB-J V_T was explained by the distribution patterns of all neurotransmitter systems investigated, as well as perfusion.

Since much of the pathology in Lewy body diseases predominately affect subcortical brain areas, I was interested in assessing the relationship between receptor and transporter maps and Δ[^{11}C]UCB-J V_T within the subcortex separately. I found that many of these relationships were

stronger, which is in line with the notion that pathology present subcortically could be impinging on the pattern of synaptic density within these brain areas that are particularly vulnerable.

5.5.1 Drug-naïve PD vs HC

Consistent with our hypothesis, the spatial distribution of Δ[^{11}C]UCB-J V_T in drug-naïve PD patients compared to healthy controls was predominately associated with the distribution patterns of dopaminergic markers including D_1R, D_2R and DAT, where reduced [^{11}C]UCB-J V_T was related to areas richest in these molecular markers, which is congruous with the predominant involvement of the dopaminergic system early in the course of the disease. These results are in accord with the well-established affectedness of the dopaminergic system in PD, although extending this knowledge to suggest that the distribution of synaptic dysfunction is related to the distribution of dopaminergic markers. Of note, these markers of the dopaminergic system do not reflect the current state of the PD system, as this would require individual PET scans for each molecular marker in each patient. Instead, it is the canonical distribution patterns that reflect the presumptive premorbid state of the patients. This concept is similar to that of integrating gene expression data, such as the Allen Human Brain Atlas dataset with neuroimaging data (Rizzo et al., 2014, Selvaggi et al., 2021), but with higher resolution markers for the proteins of interest. The close relationship observed between synaptic density loss and molecular markers of the dopaminergic system is likely because of the presynaptic accumulation of toxic α-synuclein, which is proposed to be the responsible species for synaptic dysfunction. Our findings align with a model whereby cells with α-synuclein aggregation are no longer able to regulate dopamine levels leading to a vicious cycle of accumulated α-synuclein and deregulated dopamine, thus triggering synaptic dysfunction and impaired neuronal communication (Bridi and Hirth, 2018); which manifests here as a relationship between the spatial distribution of dopaminergic markers and Δ[^{11}C]UCB-J V_T.

Given the early degeneration of the locus coeruleus that can occur as early as the prodromal phase of the disease, and the fact that this principal noradrenergic nucleus is one of the first nuclei to develop Lewy bodies, I expected to observe a negative association between the differential pattern of [^{11}C]UCB-J V_T in drug-naïve PD patients and NAT distribution profile. Evidence has shown a moderate to severe cell loss of 30%-90% in the locus coeruleus (Chan-Palay and Asan, 1989, German et al., 1992, Bertrand et al., 1997, Zarow et al., 2003), which has also been notable in drug-naïve PD (Wang et al., 2018), alongside reduced noradrenergic innervation of its target structures, including the thalamus, striatum, hypothalamus, and prefrontal and motor cortex (Shannak et al., 1994, Pavese et al., 2011, Pifl et al., 2012, Sommerauer et al., 2018b). However, in this study, I observed a positive association between the pattern of relative synaptic density in drug-naïve PD patients and the distribution patterns of NAT.

The pattern of Δ[^{11}C]UCB-J V_T in drug-naïve PD patients when compared to healthy controls followed a similar distribution to the NAT template. The direction of this association is particularly surprising, as it is in line with synaptic loss occurring in brain areas sparse of noradrenergic terminals whereas thalamic noradrenergic terminals have been shown to undergo significant degeneration in patients with PD (Pifl et al., 2012). This result suggests that synaptic density appears to be *somewhat* preserved within brain structures richly innervated by the noradrenergic system, with the lowest estimates of synaptic density in structures, namely the striatum, that have a low concentration of NAT. This is in keeping with the possibility that there is a perseveration of the noradrenergic system. Noradrenaline has been shown to have a neuroprotective effect on dopaminergic neurons from damage, thus its integrity may be crucial in determining the progression of the disease. Preclinical studies have revealed that destruction of the locus coeruleus exacerbates nigrostriatal dopamine neuronal loss (Yao et al., 2015, Li et al., 2018, Fornai et al., 1997, Mavridis et al., 1991), with a reduction of neurotoxicity induced by

neurotoxin MPTP following a boost of noradrenaline synthesis (Kilbourn et al., 1998, Archer, 2016), or genetic deletion of NAT (Rommelfanger et al., 2004). It is possible that in PD, a compensation for dopaminergic depletion could be through noradrenergic function. However, the association between the distribution of NAT and Δ[^{11}C]UCB-J V_T may be reflecting dopaminergic denervation in the striatum and have little to do with NAT specifically due to the spatial overlap between these markers, which highlights the challenge of treating each receptor and transporter map independently. In fact, the stepwise linear regression model illustrated the predominant role of dopaminergic markers serving as stronger predictors of the distribution patterns of synaptic loss in drug naïve PD and NAT did not contribute unique variance beyond that shared with dopaminergic markers.

Given the vulnerability of cholinergic neurons in PD, the observed negative association between Δ[^{11}C]UCB-J V_T in drug-naïve PD patients and VaChT distribution patterns was expected, which is consistent with synaptic density loss occurring in regions abundant in cholinergic terminals and cholinergic denervation manifesting early in the course of PD. The fact that the association between the pattern of synaptic density alterations and VaChT distribution was driven by the subcortical distribution of VaChT is suggestive of the involvement of striatal giant spiny cholinergic interneurons, which play a critical role in modulating striatal function (Martel and Apicella, 2021, Dautan et al., 2020, Mallet et al., 2019) and symptom manifestation in PD, with their stimulation reducing PD symptomatology (Lieberman et al., 2019, Chambers et al., 2019, Osada and Iwasaki, 2017, Kucinski and Sarter, 2015). However, the observed correlation with both neurotransmitter systems may be due to the coterminous projections of both systems, as also demonstrated by the strong positive correlation between VaChT and DAT distribution profiles (Figure 5.1), thus it is difficult to dissociate the specific effects of one of the two systems. Nevertheless, in addition to dopaminergic innervation, giant spiny cholinergic interneurons within the striatum have long been acknowledged to play a fundamental role in

balancing dopaminergic signalling and regulating movement. It could be possible that denervation of both systems is implicated in the pathogenesis of PD, but the data presented here cannot explicitly speak to the potential contribution of the cholinergic or dopaminergic system given their spatial overlap. Future studies employing that concurrent assessments of [^{11}C]UCB-J and a range of cholinergic molecular markers would be an important contribution.

The spatial distribution pattern of Δ[^{11}C]UCB-J V_T in drug-naïve PD was also found to be negatively associated with the regional distribution pattern of $5HT_{2A}$ receptors, which is congruous with the notion that synaptic density loss is present in regions that have an abundance of $5HT_{2A}$ receptors. It could be speculated that the distribution of these receptors may be contributing to synaptic density loss following diagnosis. This is distinct to the fate of $5HT_{2A}$ receptors in PD, which is unclear from the current literature as $5HT_{2A}$ receptor levels in PD have been reported to be decreased (Li et al., 2010b, Cheng et al., 1991, Maloteaux et al., 1988), increased (Zhang et al., 2007) or unchanged (Huot et al., 2012, Maloteaux et al., 1988), depending on the brain region under examination. Nevertheless, the findings here suggest that PD may be further understood in relation to the known distribution of serotonergic receptors and how they are related to synaptic density loss, as demonstrated by the pattern of synaptic density loss measured with [^{11}C]UCB-J aligning with the canonical distribution of $5HT_{2A}$ receptors across the brain in drug-naïve PD patients compared to healthy controls.

The regional pattern of [^{11}C]UCBJ V_T difference between drug-naïve PD and healthy controls was found to be associated with the respective regional pattern of GM volume difference, with brain areas exhibiting higher synaptic density being associated with higher GM volume. Although the mechanisms of α-synuclein-mediated synaptopathy are not fully understood, compelling evidence has demonstrated that the major sites of α-synuclein-mediated toxicity are presynaptic terminals. The subsequent neuronal dysfunction can cause cell-intrinsic toxicity,

whereby axonal deterioration progresses towards the cell body, eventually leading to a dying-back like neurodegeneration (Bridi and Hirth, 2018). Thus, it is foreseeable that there would be an association between synaptic loss and atrophy. However, it is important to note that the fact that molecular markers explained a higher proportion of Δ[^{11}C]UCBJ V_T variance than ΔGM volume reinforces the idea that, whilst GM volume shares a relationship with synaptic density, macroscopic atrophy is not the principal contributing factor to patterns of Δ[^{11}C]UCBJ V_T, at least in early stages of the disease.

Physiologically, the brain finely regulates its oxygen supply through neurovascular coupling, whereby active neurons signal to dilate local blood vessels, leading to the subsequent increase of blood flow and delivery of oxygen and glucose to localised areas of active neurons. Supported by this mechanism, and in line with our hypothesis, I found a positive association between patterns of [^{11}C]UCBJ V_T difference in drug-naïve compared to healthy controls and the respective pattern of difference in CBF, whereby brain areas with elevated synaptic density were similar to areas characterised by higher perfusion. This is in perhaps consistent with a recent study that reported high correlations between regional cerebral glucose metabolism and synaptic density in a group of healthy controls (van Aalst et al., 2021).

5.5.2 Treated PD vs drug-naïve PD

The spatial pattern of Δ[^{11}C]UCBJ V_T in treated PD patients compared to drug-naïve PD was found to be associated with markers of the serotonergic, dopaminergic and noradrenergic systems, but in opposite directions than those observed in drug-naïve PD patients compared to healthy controls. This is particularly intriguing, as this change in direction may be reflecting the way the pattern of synaptic dysfunction develops in PD and any potential medication effects.

The regional distribution of [^{11}C]UCB-J V_T difference in treated PD patients compared to drug-naïve PD was found to be positively associated with D_1 receptor density, whereby in regions where D_1 receptor density was generally higher in young healthy controls, synaptic density was relatively higher in treated than in untreated PD patients. Conversely, in regions where D_1 receptor density was generally lower in young healthy controls, synaptic density was relatively lower in treated than in untreated PD patients. This association between these measures became stronger when only the subcortex was considered. Taken together with our findings in drug-naïve PD patients, it is consistent with a 'normalisation' of synaptic density within dopamine-rich areas. This inverse correlation suggests that areas with higher D_1 receptor density may be neuroprotective. The fact that this association is observed in the treated group presents this as a possible mechanism of L-DOPA treatment. L-DOPA has been shown to affect spine morphology, mediated differentially by D_1 and D_2 receptors (Nishijima et al., 2018), and D_1 receptors have been shown to be essential for the maintenance of spine plasticity in striatal projection neurons (Suarez et al., 2020). Furthermore, L-DOPA has been shown to promote BDNF expression via the D_1-signalling pathway (Williams and Undieh, 2009). However, the spatially distribution of these changes is not well understood. The findings presented here suggests that potential neuroprotective or neuroplastic effects of L-DOPA may be mediated by the role of D_1 receptors across the brain in PD patients.

Neuromodulatory, divergent systems like the dopaminergic, noradrenergic, and serotonergic shape and regulate the activity of neurobiological networks. The interaction between these systems is important for understanding the pathophysiology of PD and play a crucial role in symptom manifestation. Since I have measured and assessed the spatial relationship between a marker that is expressed in all neuronal populations (SV2A) and the canonical distribution of a range of neurotransmitter systems, it is crucial to consider the intriguing interaction between these neurotransmitter systems in explaining the pattern of distribution of synaptic density.

Group-level [^{11}C]UCB-J V_T difference in treated PD patients was also associated with the distribution of NAT, whereby treated PD patients had relatively lower synaptic density than drug-naïve patients in areas with high concentrations of NAT in young healthy controls. This is consistent with relatively lower synaptic density occurring in treated patients in areas that normally have an abundance of noradrenergic terminals, whereby the presence of noradrenergic terminals in conjunction with dopaminergic treatment accelerates synapse loss. Furthermore, this finding is also congruous with the notion that, in drug-naïve PD patients, relatively higher synaptic density loss occurs in areas that are typically sparse in noradrenergic terminals. In fact, in unmedicated PD patients, these findings indicate that synaptic loss occurs away from noradrenergic terminals i.e., in dopaminergic terminals. Finally, these findings are compatible with the idea that in drug-naïve PD patients, noradrenergic terminals protect against synaptic loss more than in treated PD patients. Neuromodulators dopamine and noradrenaline have been shown to largely overlap in multiple domains, including convergent innervations, non-specificity of receptors and transporters and shared intracellular signalling pathways, suggesting that they may mediate similar physiological functions (Ranjbar-Slamloo and Fazlali, 2019). Indeed, analogous to the effects of dopamine (Seamans and Yang, 2004, Tritsch and Sabatini, 2012, Froemke, 2015), noradrenaline plays a prominent role in various forms of plasticity (Harley, 1987, Mouradian et al., 1991, Sara, 2009). Areas poorly innervated by dopaminergic fibres have dopamine concentrations as high as the medial prefrontal cortex that is densely innervated by noradrenergic fibres (Devoto et al., 2001) and adrenergic agonists and antagonists are more effective at modifying cortical dopamine levels (Kuroki et al., 1999, Devoto et al., 2001, Devoto et al., 2003, Devoto et al., 2004). Questions remain to be answered around whether the ratio of dopamine/noradrenaline is important, and how these two systems coordinate their actions to optimise function for appropriate behaviour. L-DOPA itself may alter the activity of noradrenergic neurons directly, though its potential effect is unclear. There have been conflicting

reports of whether levodopa has no effect, increases, or decreases noradrenaline tissue concentration (De Deurwaerdere et al., 2017, Engeln et al., 2015) and this requires further research. Nevertheless, these findings describe how the distribution of synaptic density alterations is associated with the distribution pattern of distinct neurotransmitter markers in PD, suggestive of synaptic density loss being coupled to the noradrenergic system in treated PD patients, as opposed to the dopaminergic system when patients are unmedicated. However, these results invite parallel investigation of both neurotransmitter systems in future longitudinal studies to track the evolution of the way in which these systems interact as drug-naive PD patients commence medication.

The distribution of markers of the serotonergic system, specifically SERT and $5HT_{2A}$ receptor densities, were also related to the regional pattern of [^{11}C]UCB-J V_T difference in treated PD patients, where regions with reduced synaptic density were associated with those rich in SERT, but scarce in $5HT_{2A}$ receptor. The negative association with SERT density profile is consistent with synaptic density loss occurring in brain areas that have an abundance of SERT, and could be reflecting the denervation of serotonergic pathways. Indeed, several *in vivo* PET studies have reported a reduction in striatal SERT levels, as well as in limbic and frontal regions (Albin et al., 2008, Brucke et al., 1993, Kerenyi et al., 2003, Politis et al., 2010a). A study evaluating the annual decline of SERT function in the raphe nuclei using a surrogate marker [^{18}F]DOPA observed a nearly 5% annual decline in early PD patients over a period of 3 years (Pavese et al., 2011), thus may explain why this association was seen in treated PD patients, but not in early stages. Whilst there are strong links between the serotonergic and dopaminergic systems, both structure and in function, it is important to highlight that the relative expression of dopaminergic markers is positively associated with SERT expression across the brain (Figure 1), thus there is some redundancy in the information provided by these molecular markers. This may be problematic in detecting the unique contributions of each of these markers to the spatial variability in [^{11}C]UCB-

J V_T measures. Nonetheless, the known interactions between these two systems, whereby an increase of dopamine with levodopa leads to a subsequent reduction of serotonergic neuronal connectivity to their target neurons, suggests that an increase of dopamine signalling via levodopa may acutely impact on serotonergic neuronal plasticity and negatively modulate the outgrowth of serotonin-producing neurons (Niens et al., 2017). Within this context, the negative association between the regional pattern of [^{11}C]UCB-J V_T and SERT distribution may be a result of the restoration of dopaminergic function following L-DOPA administration.

5.5.3 PDD vs treated PD and DLB vs HC

Both PDD and DLB patients, when compared to their respective 'control' groups, exhibited similar associations between the differential pattern of [^{11}C]UCB-J V_T and neuroimaging markers, with the overlap including a positive association with SERT and NAT density profiles and the pattern of ΔGM volume and a negative association with $5HT_{2A}$ receptor density profile. PDD patients had additional positive correlations between Δ[^{11}C]UCB-J V_T and DAT and VaChT distributions, whereas DLB had an association with ΔCBF that wasn't observed in PDD.

In PDD patients, the association between the differential pattern of [^{11}C]UCB-J V_T and neuroimaging markers are comparable to those seen early in the disease course, with the exception of SERT, DAT and VaChT, which all share a positive correlation. The direction of these associations is unexpected, as one would expect the opposite given the progressive nature of degeneration over the course of PD, the presentation of more severe motor and non-motor symptoms and the amplified dysfunction of these neurotransmitter systems at this stage of the disease. This is concordant with relative synaptic density loss, in PDD, occurring in brain areas away from serotonergic, dopaminergic, or cholinergic terminals. These findings are likely reflecting a complex interaction between these neurotransmitter systems, as well as between disease processes and medication. Given that the degenerative process continues over the course

of the disease to reach high rates of neuronal loss and there are progressive disease-related changes in neurotransmitter systems that are impacted to varying degrees, patient responses to medication often reflect both positive and deleterious mechanisms of action, which undoubtedly depend on the state of the PD brain.

Serotonergic terminals are a major locus for converting levodopa into dopamine, and although they have been extensively studied for their role in levodopa-induced dyskinesias, the "presynaptic serotonergic hypothesis" may also have some relevance in this context. According to this hypothesis, serotonin terminals correspond to the major presynaptic compartment releasing dopamine; possessing the ability to uptake levodopa, decarboxylate it to dopamine and package the dopamine into vesicles for exocytotic release (Arai et al., 1995, Ng et al., 1970, Tison et al., 1991, Yamada et al., 2007). Their contribution become proportionally greater with the gradual degeneration of nigrostriatal pathways in PD, with serotonergic neurons of the dorsal raphe nuclei shown to uptake levodopa-derived dopamine via SERT (Carta et al., 2007, Carta et al., 2008). Studies have showed that chronic administration of levodopa treatment impacts serotonergic neurons, modifying their morphology and synaptic plasticity, with these neurons exhibiting high receptiveness to growth-promoting properties of brain-derived neurotrophic factor (BDNF) (Berthet et al., 2009, Picconi et al., 2005, Picconi et al., 2010, Prescott et al., 2009, Rylander et al., 2010, Zeng et al., 2010). Such studies have also reported sprouting of serotonergic axon terminals and increased serotonergic innervation including hypertrophy of striatal serotonergic axonal varicosities, which was also linked to elevated BDNF mRNA levels and SERT density (Rylander et al., 2010, Zeng et al., 2010). Thus, together with our findings, the association between synaptic density and SERT in PDD and DLB may be reflective of the regional localisation of a compensatory mechanism due to the progressive loss of striatal dopamine. This brings us onto the positive association between the differential pattern of [^{11}C]UCB-J V_T in PDD compared to treated PD and DAT density profile, which may in fact be

reflecting the growth and hyperinnervation of serotonergic neurons within the striatum, which would ultimately lead to an increase of synaptic density within DAT-rich brain regions.

The cholinergic system has been found to be heavily implicated in Parkinsonian dementia, as evidenced by cholinergic deficits from atrophy of the nucleus basalis of Meynert (Gibb, 1989, Mattila et al., 1998, Whitehouse et al., 1983) and post-mortem studies observing a greater reduction of acetylcholine in frontal cortices of demented PD patients (-68%) compared to non-demented ones (-35%) (Ruberg et al., 1986). The denervation of the cholinergic system has also been corroborated with *in vivo* cholinergic studies that reported more extensive cholinergic deficits in PDD and DLB patients than those without dementia (Kuhl et al., 1996, Shinotoh et al., 1999, Hilker et al., 2005b, Shimada et al., 2009), highlighting a prominent and widespread cholinergic denervation in both PDD and DLB to a similar degree. Thus, the positive correlation between synaptic density and VaChT distribution in PDD is particularly surprising, as well as the fact that I did not observe an association in DLB. As mentioned previously, a potential explanation for the association in PDD could be the strong overlap between the distribution patterns of VaChT and DAT density, making it difficult to dissociate the specific effects of either one of these systems. Furthermore, it was only the pattern of group-level differences in GM volume that were predictive of the spatial distribution of [^{11}C]UCB-J V_T following the stepwise regression.

It is worth mentioning that the spatial pattern of group-level [^{11}C]UCB-J V_T difference in PDD and DLB patients compared to treated PD and healthy controls, respectively, was negatively associated with the distribution patterns of $5HT_{2A}$ receptors, whereby brain regions rich in $5HT_{2A}$ receptor density were those in which there was more relative synaptic density loss. Genetic evidence implicated $5HT_{2A}$ receptors as playing a role in both the emergence and treatment of dementia-related psychosis, with blockade of this receptor being a useful approach

at alleviating psychosis. Studies have demonstrated that PD patients with visual hallucinations have elevated expression levels of $5HT_{2A}$ receptors when compared to those without (Huot et al., 2010, Ballanger et al., 2010). Within the context of the existing literature, the associations I observed could indicate that a reduction of innervation to $5HT_{2A}$-rich brain areas results in an increase of their expression. Although our patients did not present with visual hallucinations at the time of enrolment, I cannot exclude the fact that there is a high probability of their manifestation, particularly in DLB in whom visual hallucinations are one of the most common feature that is present in 54%-70% of patients (Aarsland et al., 2001b). The fact that the negative association between synaptic density and $5HT_{2A}$ appeared stronger in the DLB group is an indication of this fact. Whether the increased expression of $5HT_{2A}$ receptors, as outlined in the existing literature, is in fact due to a reduction in synaptic innervation would obviously need to be confirmed in future studies.

Nevertheless, the pattern of group-level differences in GM volume explained the most variance of the regional pattern of [^{11}C]UCB-J V_T difference in PDD and DLB patients. This is foreseeable since impairment of synaptic function is thought to occur first, with neuronal degeneration emerging at later stages of the disease (Picconi et al., 2012, Schulz-Schaeffer, 2010). Thus, synaptic dysfunction is thought to occur prior to the active deconstruction of axons and loss of neuronal connectivity, which eventually leads to the death neuronal perikarya (Roy, 2017, Kouroupi et al., 2017, Fang et al., 2017, Bae and Kim, 2017, Schulz-Schaeffer, 2015). The succession of events indicates that neural death initiates at synaptic terminals and progresses proximally toward neural cell bodies in a dying back-like manner. Given the coupling of these two phenomena, I may expect to see a stronger relationship between synaptic density and GM volume given that Parkinsonian dementias are characterised by cerebral atrophy. Whilst I have discussed the role of α-synuclein accumulation at presynaptic terminals in facilitating synaptic dysfunction by affecting several steps of neurotransmitter release, it is also important to consider

the fact that α-synuclein pathology is often accompanied by amyloid-β and tau pathology, which, despite being heterogeneously deposited in PDD and DLB brains, contribute to cognitive impairment and a shorter lifespan (Irwin and Hurtig, 2018). In fact, these pathologies may synergistically interact to accelerate disease progression. A recent study exploring how amyloid-β and tau deposition are related to synaptic dysfunction and axonal structure over the course of AD concluded that amyloid-β and tau have toxic effects on synaptic function and axonal integrity, respectively (Pereira et al., 2021). This may be translatable to DLB and PDD, whereby accelerated synaptic dysfunction results in neuronal cell loss.

5.5.4 PDD vs DLB

Here, I assessed how the spatial pattern of group-level [^{11}C]UCB-J V_T difference in DLB patients compared to PDD was associated with neuroimaging markers to gain an insight into where differences lie. I found a positive association between [^{11}C]UCB-J V_T difference and dopaminergic markers, reflecting lower synaptic density in dopamine-rich regions in PDD than in DLB. Typically, studies have observed no difference between these groups in terms of DAT uptake (Marquie et al., 2014, Gomperts et al., 2016b), although striatal dopamine uptake has been reported to be significantly lower in PDD compared to DLB, which is consistent with the loss of nigral dopaminergic cells and the severity of parkinsonism (Colloby et al., 2012, O'Brien et al., 2004).

I also observed a negative association between [^{11}C]UCB-J V_T difference in DLB patients compared to PDD and $5HT_{1A}$ receptor density profile, which is in line with the notion that DLB patients exhibit a pattern of relative synaptic density loss in brain areas with high concentrations of $5HT_{1A}$ receptor. Studies have revealed a significantly higher $5HT_{1A}$ receptor binding density in DLB patients compared to PDD (Francis and Perry, 2007), which has been found to be associated with depression in both DLB and PDD patients (Sharp et al., 2008). Again, I could

speculate in the context of our findings that the increased expression of $5HT_{1A}$ receptors as reported in the literature is in response to a loss of innervation.

The differential pattern of [^{11}C]UCB-J V_T in DLB patients was associated with the pattern of difference of CBF. Studies have reported patterns of hypoperfusion in both PDD and DLB, with some studies revealing similar perfusion profiles (Firbank et al., 2003, Firbank et al., 2005, Kasama et al., 2005, Antonini et al., 2001, Rossi et al., 2009) and others reporting distinct patterns (Hung et al., 2018). Regardless of this, the question remains as to why the association between synaptic density and CBF exists only in the DLB group. The contribution of astrocytes to the blood-brain barrier (BBB) has been shown to be disrupted in patients in PD (Gray and Woulfe, 2015), with a recent study demonstrating that astrocytes exhibit increased expression of α-synuclein which led to altered metabolism (Sonninen et al., 2020). This may partially explain why the relationship between synaptic density and CBF was not observed in PD patients. Whilst aggregation of α-synuclein has also been observed in DLB patients (Fathy et al., 2019), given their physiological heterogeneity, further research is required to determine the role they play along the spectrum of synucleinopathies.

5.5.5 Limitations

These findings should be interpreted in light of several limitations of the study. The sample sizes were modest and unequal. It is important to note that semiquantitative estimates of all receptor and transporter densities were generated using a suitable reference region. This means that although the relative estimates of one receptor may appear to be higher than others in certain brain areas, it cannot be claimed that the absolute density of other receptors is lower, even if these other receptors have relatively higher densities in other brain areas. In other words, even if the density of one receptor is lowest in one particular region, this could still be higher than the highest density of another in the same region, because these estimates are contingent on the

non-specific binding in the reference region. Furthermore, I used receptor and transporter density profiles based on young healthy volunteers since the spatial architecture of these molecular markers tend to be relatively consistent across individuals. This has been useful to assess the way in which pre-existing receptor and transporter distribution patterns across the brain may explain the eventual spatial distribution of synaptic density alterations in disease, which can aid in explaining the variance of SV2A expression patterns. However, additional information about the relationship between synaptic density and disease-specific neurotransmitter changes would be useful to understand disease pathogenesis. Given that PD is associated with a unique combination of the brain regions involved and complex changes in various modulatory pathways. These alterations involve specific changes in the expression levels of neurotransmitter receptors and transporters that change over the course of the disease. Individualised receptor and transporter profiles mapping is likely to provide an insight into the relationship between synaptic density alterations and other brain changes, such as the expression of these molecular markers in the PD brain. A simple example is the alterations in D_1 and D_2 receptor densities observed in PD, whereby early in the disease course, there appears to be an upregulation of D_1 and D_2 receptor densities as part of a compensatory mechanism, which, after administration of dopamine replacement therapy, are downregulated to normal densities (Hassan and Thakar, 1988). With the current framework employed, I can only speculate that alterations in synaptic density are associated with up or downregulation of these receptors over the course of the disease, since assessing the relationship between the canonical distribution of neuroimaging markers and SV2A expression helps with interpreting the overall spatial pattern synaptic density loss, thus this would need to be confirmed using disease-specific receptor maps. This would be useful for understanding the interaction between these different systems and their relationship with synaptopathy and associated symptoms. This would also be particularly useful to assess the relationship between synaptic density and neurobiological processes such as tau and amyloid accumulation, which would be of particular significance for understanding the role of these

misfolded proteins and synaptic loss in PDD and DLB. Nevertheless, by assessing the relationship between the spatial patterns of [^{11}C]UCB-J V_T differences in patient groups and the premorbid distribution of a range of receptors and transporters has enabled us to explore which neurotransmitter systems are implicated in a specific synaptic marker of disease, to what extent and how that changes at different stages of disease, although the speculations put forward would need to be confirmed by future studies. Ultimately, I the first step was taken in making biologically meaningful interpretations of the spatial patterns of [^{11}C]UCB-J V_T alterations in PD and dementia. Furthermore, by using healthy control-derived PET and SPECT maps, I was also able to assess these spatial relationships in a holistic manner as I included a comprehensive number of molecular markers reflecting several neurotransmitter systems implicated in the disease, whereas this would not be feasible to do in patients. However, the drawback of including an extensive range of molecular markers is that if more than one is identified as a potential causal factor, the interpretation becomes complex and can lead to multiple, even contradictory, conclusions. In an attempt to mitigate this concern, a hypothesis-led stepwise linear regression model was performed to identify which maps with known relevance in these disorders were the most appropriate predictors.

In addition, the spatial overlap of receptor and transporter systems makes it difficult to dissociate the specific relationship each had with synaptic density; thus, caution is required when interpreting the observed single associations as being specific to a particular receptor or transporter. This could easily influence the interpretation of our results. However, I attempted to alleviate this issue by mean-centring the data and performing a stepwise multiple linear regression analysis which helped facilitate the interpretation of our findings.

When accounting for the inherent spatial autocorrelation of the imaging data, many correlations did not survive, which could potentially be due to the fact that the DK atlas was used instead of

the CIC atlas. Future work is required to include the CIC atlas into the null framework employed in order to increase the robustness of my findings.

5.5.6 Conclusions

Here, I had the opportunity to identify important pathways between the impairment of synaptic integrity and observable macroscopic and molecular neuroimaging in PD and dementia, which would not only advance our understanding of the individual susceptibility of specific neurotransmitter systems to the disease process, but also provide a holistic insight into its progression. In this work, I found that alterations in synaptic density in PD and dementia mirror the well-known spatial distribution patterns of several neurotransmitter systems, with the dopaminergic system predominately involved at early stages, which became less implicated as the disease progressed to dementia where instead GM volume was more closely associated. Essentially, I observed unique and variable associations between synaptic density and neuroimaging markers at different stages of the disease, which provides valuable insight into what synaptic alterations may reflect and the general pattern of their dysfunction.

6 Discussion

6.1 Overview

In this series of studies, a multimodal approach was employed to investigate the magnitude and anatomical distribution of alterations in measures of synaptic density, as measured by [^{11}C]UCB-J PET, grey matter volume measured using T1-weighted MRI and CBF, as measured by ASL-MRI, in the same Lewy body disease and healthy control participants, with intra-regional inter-tracer correlations interrogated within each patient group. I also evaluated the relationship between the spatial distribution of group-level synaptic density alterations and the spatial distribution of respective grey matter volume and CBF alterations, as well as the putative premorbid distribution of molecular neurotransmitter markers at a younger age.

In brief, I found that synaptic density was clearly reduced in early, symptomatic stages of PD. The group treated with dopamine replacement therapy (and/or disease chronicity) exhibited comparable SV2A concentrations to healthy controls, which was higher compared to drug-naïve PD, suggesting treatment may transiently restore the loss seen in the untreated group. In Lewy body dementia, however, a more extensive loss of SV2A was present in PDD, characterised predominately by frontal and parietal involvement, whilst DLB exhibited a widespread reduction of SV2A across the brain. Notably, synaptic density loss was not simply explained by volume loss as demonstrated in the dementia groups, emphasising that distinct processes underlie cell death and synaptic loss in neurodegenerative diseases. Furthermore, there was a discordance between hypoperfusion and synaptic density reductions across groups. The differential pattern suggests that areas of synaptic dysfunction indexed by [^{11}C]UCB-J binding do not lead to a loss of blood flow. One interpretation could be a disruption of neurovascular coupling and CBF autoregulation within Lewy body disease. Finally, the spatial distribution pattern of SV2A alterations were explained, in part, by discrete biological markers at different disease stages,

highlighting that synaptic levels are influenced by the complex interplay between processes of degeneration and atrophy and those of maintenance and compensation at regional and network levels.

6.2 Limitations

Prior to proceeding with the discussion, it is important to highlight and address some key limitations and caveats. The limitations outlined in this section apply generally to the findings from all chapters, which I will reiterate shortly, and consequently will not be revisited but should be borne in mind throughout.

First and foremost, the sample sizes of each group included within these studies are very modest, and unequal. Whilst unequal sample sizes can affect the robustness of the equal variance assumption of ANCOVA, which was employed in chapters 3 and 4, all data were log transformed which appeared to equalise the variances as confirmed by Levene's test. Nevertheless, the small and unequal sample sizes ultimately means that these studies risk being statistically underpowered, thus diminishing the likelihood of observing a statistically significant effects should it truly exist. However, they were sufficient to reveal significant differences in all patient groups. Thus, the results presented in the previous chapters and those that will be discussed below should be considered preliminary and interpreted with caution.

Of course, it is important to underscore that the cross-sectional nature of the data limits the interpretation of any findings, and ultimately provides a 'snapshot' of a disease process. However, cross-sectional study designs are often used in research as a proxy for longitudinal designs about developmental or disease processes given that longitudinal designs are expensive and time-consuming. To the best of my knowledge, this is the first study that can demonstrate

potential synaptic density alterations in the context of disease progression in PD, although conclusions regarding what differences in SV2A, volume and CBF reflect, require further research which goes beyond the scope of this thesis. However, by stratifying patients into meaningful groups based on their specific disease stage, I could explore how structural, functional, and synaptic density potentially change with chronicity and treatment, as well as with the manifestation of dementia. Since the disease duration of PD can stretch over decades, with an average of about ten years between time of PD onset and dementia manifestation, assessing disease progression cross-sectionally was a feasible approach to take in this instance.

A key caveat to the approach in this thesis is the fact that the disease trajectory is nonparallel, with Lewy body disease being well-known for the high heterogeneity between patients: not only in their clinical manifestation, but also the rate of disease progression and the underlying disease pathogenesis (Greenland et al., 2019). Thus, it is possible that the groups compared in these studies were inherently different to start with, with group differences potentially representing inter-individual variations as the small sample size means the estimates may not be representative of each illness stage. This could potentially impinge on the likelihood that the statistically significant differences reflect true disease effects. The most reliable information regarding progression would come from longitudinal follow-up studies that can account for the large interindividual variability that could mask more subtle changes and increase the statistical power (Locascio and Atri, 2011). Longitudinal studies would also be invaluable in capturing the natural progression of PD, as well as the contribution of such markers like synaptic density to characterise clinical manifestations and heterogeneity over time, as well as the multiple phenotypes. It is important to note, however, that the study findings when using a cross-sectional design are useful in providing informative preliminary evidence regarding possible brain alterations linked with disease stages. Such designs do permit tentative inferences to be made regarding progression, which provides the motivation and rationale for future researchers to

design subsequent efficient longitudinal studies. Therefore, whilst I acknowledge that a longitudinal design would be necessary to convincingly demonstrate a depletion/loss or increase of SV2A and whether lower and higher volumetric estimates reflect atrophy or increases, respectively, within our patient groups, I have utilised the cross-sectional findings to put forward a hypothetical model of disease trajectory, as informed by SV2A estimates at each stage, whereby in a longitudinal cohort, we may see reductions of SV2A in drug-naïve PD patients, which change towards the control groups following treatment. The terminology that has been used naturally arose from the framing of the groups as allowing some insight into the disease trajectory.

A fundamental consideration for this study was whether to combine PDD and DLB participants into one sample because this would have come with the advantage of boosting the sample size. However, I opted to analyse them separately because although they share many clinical, neurobiological, and pathological features, according to DSM-5, they are considered distinct diagnostic entities and *in vivo* neuroimaging of synaptic density within Lewy body dementia is an unexplored area of research, with only two studies published to-date. The first of these by Nicastro et al. (2020) assessed synaptic density in only 2 clinically diagnosed DLB patients and the second by Andersen et al. (2021) who pooled clinically diagnosed DLB (n=9) and PDD (n=4) into one group, an important question to address was whether PDD and DLB exhibit differing or comparable synaptic density profiles, and whether these could aid in separating the clinical differences between PDD and DLB. Of course, future studies with larger sample sizes will likely permit a better and more reliable insight into whether the synaptic density alterations are characteristic of these two disorders and provide a superior understanding of how potential confounds interact with disease processes to alter synaptic density.

It is also worth noting that diagnosis of DLB in this thesis was based on clinical diagnostic criteria and we did not have pathological confirmation of DLB pathology. Although past diagnostic criteria for DLB have had variable specificity and sensitivity, with AD being historically misdiagnosed for DLB (Jellinger, 2004, Merdes et al., 2003, Hohl et al., 2000), revisions made to the international consensus diagnostic criteria for DLB has improved specificity, but sensitivity remains considerably lower (McKeith et al., 2017). Whilst this may have implications within the clinical setting where the clinical misdiagnosis or under-detection of DLB patients can lead to significant delays in diagnosis (Galvin et al., 2010) or mismanagement of care which can have devastating consequences (McKeith et al., 1992), as well as present challenges for clinical trials/research studies regarding patient enrolment, a concern within this study is if those patients identified as DLB are not in fact DLB patients. However, the diagnostic criteria has high specificity (that is indicative of a low a false-positive rate), which can be up to 90% depending on the biomarkers used to make a diagnosis (McKeith et al., 2017). Furthermore, the fact that all DLB patients included within this study presented with Parkinsonian symptoms, and thus presented with at least one core feature, the probability of a correct diagnosis is largely increased. This notion was demonstrated by Savica et al. (2013b), who, by using parkinsonism as a selection criterion for patients to qualify for a diagnosis of DLB, reported very high clinical diagnostic accuracy as confirmed by autopsy results. Therefore, we can be fairly confident that the DLB patients included within this study were correctly diagnosed as DLB, rather than having AD, although that being said, it must be emphasised that their correct diagnosis is not guaranteed given that we were unable to confirm this at the pathological level and approximately 50% of all Lewy body dementia patients have sufficient AD-related pathology for a secondary neuropathologic diagnosis of AD, which could result in large heterogeneity amongst the DLB patients enrolled in the study. Given the small sample size of the DLB group, if there was a diagnostic error for even one or two DLB patients, this would inevitably largely impact the outcome measures; introducing a large proportion of variance to the data and the findings would

no longer be (at least preliminarily) representative of the pathophysiological alterations within this disease. Furthermore, brain areas characteristically affected in DLB rather than AD, such as the caudate and occipital lobe, exhibited the greatest alterations in the studies reported here, indicative that we can have confidence in our DLB diagnoses.

Another caveat to bear in mind is regarding confounder variables that were excluded from the statistical models employed due to their statistically significantly differing between groups, such as age when comparing DLB to healthy controls. Although it is common practice within the literature to include a covariate in the statistical model as a means to 'control' for the confounding effects of a covariate that is significantly different between groups, Miller and Chapman (2001) affirmed that it is imperative that the covariate for which is being controlled is *not* correlated with the grouping variable. This is because ANCOVA 'removes' the variance due to a covariate, thus if it is associated with the grouping variable, it can leave an under-characterised group-residual. Since the DLB group were significantly older than the healthy controls, age was not included as a covariate. Therefore, it was not possible to account for the potential confounding effects of age on the imaging outcome measures, since age was strongly correlated with the grouping variable in this case (Miller and Chapman, 2001). However, it is worth noting that a recent [^{11}C]UCB-J PET study demonstrated that, in healthy controls, age did not influence cortical synaptic density over the adult life span of up to 85 years (Michiels et al., 2021). Moreover, there is difficulty attributing variance to age, diagnosis, or disease duration, or even an interaction between these variables, because of the high collinearity between these variables. In other words, because there would be a high correlation between disease chronicity, disease duration and age, there would be difficulty attributing unique variance to each of these variables since there would be no way to partition the variance that these variables share, particularly given the small sample sizes. Therefore, by not including such confounder variables

within the multiple regression analyses ultimately means that the interpretations of findings would be notably confounded.

Furthermore, since a between-group difference in CBF values estimated within ROI may reflect difference in global perfusion, I included global CBF as a nuisance covariate within the ANCOVA model. However, the inclusion of global CBF may mean that true changes in local CBF in the same direction as the average change may not be detectable with small sample sizes. Such type II errors were more likely given the small size limitation. However, since the aim of these studies was to evaluate local differences in perfusion between groups and how these may be associated with brain areas exhibiting synaptic density alterations, excluding global CBF as a covariate within the statistical model would have introduced an obstacle to the interpretation of regional data given the probable confounding effect of global changes on regional measures.

The alternative approach would have been some sort of normalisation method. However, the most commonly employed normalisation method, termed ratio normalisation, has major limitations, especially since they require the absence of real group differences in the reference region of choice. For example, the most widely used reference region is whole brain volume of interest which is termed global mean normalisation or proportional scaling to the grey matter. However, the question of global CBF normalisation has caused some confusion within the literature of PD imaging, as Borghammer and colleagues advocated that ratio normalisation to global mean introduces bias into the analysis, particularly because there is likely a between-group difference in the global CBF that robustly biases subsequent statistical analyses (Borghammer et al., 2010). In fact, using simulated data, Borghammer and colleagues demonstrated that previous reports of PD-related relative subcortical hyperperfusion were in fact a result of artefactual inflation by this biased global mean normalisation (Borghammer et al., 2009b). Therefore, this approach was deemed invalid, particularly since there is likely a real reduction of global CBF

within PD patients. Central white matter structures have been suggested as a possible unbiased reference region to normalise CBF measures in PD (Borghammer, 2012), however, this approach has not been commonly employed within the PD literature, with the vast majority of published studies reporting absolute CBF values. Therefore, I opted for this approach to be consistent with the current literature on CBF alterations in PD.

Our primary [^{11}C]UCB-J outcome measure was volume of distribution, V_T, which is the concentration of the radioligand in the tissue target region relative to that in the plasma at equilibrium, thus is proportional to [^{11}C]UCB-J binding to the target in the region-of-interest, providing a direct estimation of physiology (Innis et al., 2007). It is important to highlight that V_T encompasses both the concentration of the radioligand specifically bound to SV2A and the non-specific uptake (referring to free radioligand concentrations and that which is non-specifically bound), which can be problematic when interpreting the findings since it is not possible to decipher whether a difference/change in V_T is representing a change in specific binding, nonspecific binding, or both. However, in nonhuman primates, approximately 80% of [^{11}C]UCB-J V_T in grey matter regions is accounted for by specific binding (Rabiner, 2018, Nabulsi et al., 2016). It is important to note that whilst we may have more confidence in specific binding driving large differences, it is possible that non-specific binding could drive small changes, although we may then expect those alterations to be more widespread. However, there was evidence of localised, small changes thus indicating that differences in SV2A uptake are likely mainly reflecting differences in specific binding. Although alternative approaches using a reference tissue model have several advantages such as eliminating the need to perform arterial cannulation to measure blood and metabolite concentrations, and readily enable clinical use of [^{11}C]UCB-J PET, I did not employ this approach as a secondary analysis. There are several reasons for this. First, estimating V_T with an arterial plasma input function is the gold standard for quantifying radioligands, including [^{11}C]UCB-J, and provides the opportunity to determine

individual rate parameters such as K_1 which may serve as a useful measure for blood flow when it is not feasible to acquire perfusion data. Second, the centrum semiovale has been reported in the literature to serve as a suitable pseudo-reference region as it is a white matter region that is largely devoid of presynaptic terminals and exhibits low [^{11}C]UCB-J uptake (Finnema et al., 2016, Finnema et al., 2018, Mansur et al., 2020). However, it has been shown to contain a small amount of specific binding (Rossano et al., 2020), with Finnema and colleagues observing some displacement of [^{11}C]UCB-J binding in the centrum semiovale following administration of levetiracetam, which is an antiepileptic drug that targets SV2A (Finnema et al., 2016). Blocking studies have showed that this is about 8% of the specific binding in grey matter, which would ultimately lead to (a slight) underestimation of specific binding in the grey matter. Finally, Mecca and colleagues found that, even after optimising the centrum semiovale to minimise spill-in, its V_T exceeded the grey matter non-displaceable binding by up to 40% (Mecca et al., 2020). This specific binding of SV2A in the centrum semiovale may represent several factors, principally axonal transport of synaptic vesicles (Rossano et al., 2020), which may be problematic for disorders such as Lewy body disease, where compromised axonal transport are implicated in the disease (Trimmer et al., 2009). The white matter tracts in the centrum semiovale comprise of corticocortical association fibres (Yeterian et al., 2012), which, just like their terminal endings in the grey matter of the neocortex, potentially have a decline of SV2A binding in neurodegenerative disorders such as PD and dementia. Thus, estimating binding potentials using the centrum semiovale as a reference region may not only result in an underestimation of binding potential, but lead to a small bias between diagnostic groups, with an underestimation of synaptic density reductions in neurodegenerative diseases. Given that the overarching aim of this study was to determine the pattern and progression of synaptic degeneration over the course of the disease, quantifying the V_T was the most appropriate approach in this instance as it is the superior measure. Further work is required to confirm the use of the centrum semiovale as a reference region for simplified analysis of [^{11}C]UCB-J PET data.

Notwithstanding these limitations, the studies do make useful contributions to the field that I will outline in more detail below.

6.3 Summary of findings

In Lewy body disease, I observed reduced [^{11}C]UCB-J V_T from early stages of the disease through to more advanced stages. Expectedly, there was a clear difference in the extent of [^{11}C]UCB-J V_T reduction in each group, with the dementia groups exhibiting more widespread reduction of cortical synaptic density. These *in vivo* findings support the notion that Lewy body diseases are in fact synaptopathies as illustrated principally by a range of post-mortem and rodent animal models (Dijkstra et al., 2015, Bereczki et al., 2016) and more recently by *in vivo* [^{11}C]UCB-J PET studies (Andersen et al., 2021, Delva et al., 2020, Matuskey et al., 2020, Nicastro et al., 2020, Wilson et al., 2020).

I hypothesised that drug-naïve PD patients would exhibit a widespread relative loss of synaptic density compared to healthy controls, concomitant with negligible grey matter volumetric reductions. In line with these hypotheses, synaptic density was observably reduced in drug-naive PD within key cortical and subcortical brain regions implicated in PD, with no evidence of grey matter volumetric reductions and no relationship observed between grey matter volume and synaptic density measures (see chapter 3 for further details). At this early symptomatic stage of the disease, reduced synaptic density in the brainstem was found to be associated with motor symptom severity and overall disease burden. The fact that there was a prominent, widespread reduction of presynaptic density in the absence of gross grey matter atrophy in PD patients with less than 2 years disease duration highlights that synaptic impairment is an early incident within the disease process, likely contributing to symptom manifestation. This is in line with *in vivo*

imaging and post-mortem studies demonstrating that dopaminergic cell body loss in the substantia nigra lags behind the loss of nigrostriatal axon terminals (Fazio et al., 2018, Kordower et al., 2013), thus these findings contribute to the notion that the pathological process of PD may be initiated at the presynaptic level and that synaptic density loss is an early phenomenon in PD.

Whilst chronicity of disease would lead one to hypothesise that synaptic density would be further reduced in treated PD, if L-DOPA does in fact exert plasticity-promoting effects, then one could anticipate that that would be reflected by an increase of SV2A expression levels in treated PD patients, whereby they may exhibit comparable, if not higher, SV2A expression levels to healthy controls and drug-naïve PD. Notably, as detailed in chapter 3, in PD patients receiving dopamine replacement therapy who were further along the disease course, the initial widespread loss of SV2A observed in drug-naïve PD was no longer evident, with a modest decline confined to the substantia nigra. In fact, when compared to drug-naïve PD patients, those receiving treatment exhibited elevated levels of SV2A, with the thalamus emerging as statistically significant. Animal models support the conclusion that this elevation of synaptic density may be a treatment effect as opposed to a disease effect, as demonstrated by increased expression of presynaptic proteins including those that serve as structural components of the synaptic vesicle such as synaptophysin and synapsin (Cakmakli et al., 2018, Valastro et al., 2007) and those that play a regulatory role in membrane trafficking such as synaptotagmin (Cakmakli et al., 2018). Although these changes are not directly applicable or reflective of any potential alterations in SV2A expression levels, L-DOPA administration holds the potential to induce changes in the expression levels of presynaptic proteins. Finally, treated PD patients also exhibited generally larger grey matter volumes across cortical brain areas compared with healthy controls, and although not found to be statistically significantly, Pearson's correlation coefficients indicated that there were strong positive relationships between grey matter volume and SV2A estimates

(r=0.4-0.69) and some regional estimates of SV2A accounted for just over 30% of the variance of GM volume. This may be indicative that the 'restitution' of synaptic density within this group is, at least in part, contributing to the increased grey matter volume within treated PD.

I hypothesised that synaptic density would be more extensively reduced in Lewy body dementia, expanding predominately to cortical brain areas, and would be associated with cognitive impairment. Indeed, as outlined in chapter 4, PDD was characterised by parietal and frontal involvement, specifically frontal cortices involved in motor planning and execution and parietal cortices that previous studies have shown to be involved in multiple cognitive domains that are impaired in PDD including executive dysfunction (Huang et al., 2007), attention deficits (Williams-Gray et al., 2008) and visuoperceptual deficits (Nombela et al., 2014, Pereira et al., 2009). Whilst I expected that, compared to PD, PDD patients would exhibit more widespread and progressive deficits of synaptic density within cognitive fronto-striatal loops, as well as supplementary involvement of medial temporal lobe structures, such as the hippocampus, I found that PDD patients exhibited reduced synaptic density within the thalamus and superior parietal lobule, although these findings did not survive correction for multiple comparisons. Nevertheless, these findings are in-line with the notion of posterior cortical involvement in PD being associated with rapid cognitive decline to dementia (Kehagia et al., 2013) and are suggestive of increased synaptic density loss in the thalamus and parietal brain areas being implicated in dementia development, although longitudinal studies would be required to confirm this hypothesis.

DLB patients, on the other hand, exhibited more widespread reductions of synaptic density across the entire brain, with more prominent loss observed in parietal and occipital lobes, as well as key structures of the limbic system. This is in line with two recent [^{11}C]UCB-J PET studies where reductions of SV2A were observed across cortical brain areas in 13 DLB/PDD patients

(DLB=9; PDD=4) with no differences observed in the putamen (Andersen et al., 2021) and a case control study of 2 DLB patients, also reporting a more prominent reduction of SV2A within parieto-occipital cortices (Nicastro et al., 2020).

In line with my hypothesis that *in vivo* [^{11}C]UCB-J binding will harbour some clinical relevance in Lewy body disease, I found that synaptic density within the thalamus (amongst others in DLB) was strongly associated with overall cognitive performance in PDD and DLB as measured by the MMSE ($r>0.7$), which was interestingly the region where synaptic density was commonly reduced in both groups as revealed by the conjunction analysis. This is in line with the notion that the thalamus plays a role in cognitive functioning, with previous studies pointing to the distinct role of the thalamus in attentional dysfunction and fluctuations in DLB (Delli Pizzi et al., 2015b, Watson et al., 2017, Chabran et al., 2020). The thalamus has also been identified as a predictor of dementia (de la Monte et al., 1989). Therefore, synaptic density loss in the thalamus appears to be a common feature in PDD and DLB, likely to be implicated in cognitive dysfunction within these patients.

The potential impact of atrophy on measures of synaptic density was assessed by interrogating correlations between grey matter volume and SV2A measures, as well as correcting the [^{11}C]UCB-J PET images for partial volume effects (chapters 3 and 4). Whilst I anticipated that grey matter volumetric reductions could potentially confound SV2A measures within Lewy body dementias, I expected this relationship to be localised, with SV2A emerging as a measure distinct from grey matter volume, despite the large extent of atrophy within these groups. Indeed, the effect of atrophy on SV2A measures was limited despite the more prevalent presence of atrophy in these groups, represented by the fact that most SV2A reductions survived following partial volume correction and associations between grey matter volumetric reductions and SV2A reductions were restricted to certain regions-of-interest within these groups. Furthermore, within

both groups, reductions of SV2A did not wholly coincide with volumetric reductions, which is indicative of [^{11}C]UCB-J uptake reflecting a distinct feature of the brain. Taken together, these findings highlight that although volumetric alterations/atrophy can have some localised confounding effects on synaptic density measures, [^{11}C]UCB-J PET is not just a proxy measure of gross macroscopic atrophy.

In chapters 3 and 4, I was also interested to better understand the relationship between CBF and synaptic density in Lewy body disease pathophysiology. Here, since perfusion measures are often utilised as a biomarker of neuronal and synaptic activity, I expected there to be a relationship between synaptic density and perfusion, whereby a loss of synaptic density would result in reduced energy demands, hence reduced blood flow. Therefore, I hypothesised that there would be some overlap in the regional patterns of synaptic loss and hypoperfusion within these groups, although these would likely not be identical, with correlations between [^{11}C]UCB-J binding and CBF within affected regions. In all groups, bar the treated PD group, there was evidence of global hypoperfusion, and whilst there were several brain areas in which synaptic density alterations and hypoperfusion overlapped, the magnitude of localised hypoperfusion was greater than synaptic density loss in all groups and across most regions-of-interest. I also found few intra-regional associations between CBF and SV2A measures, where drug naïve and PDD exhibited a positive correlation between these measures within the cerebellum and PDD and DLB exhibited positive correlations within the caudate, which is indicative of synaptic density loss holding the potential to contribute to hypoperfusion, although CBF and SV2A measures were not found to be associated in all regions reflecting a significant concomitant loss of synaptic density and hypoperfusion. This is in line with a recent study in AD that employed [^{18}F]FDG and [^{11}C]UCB-J PET that found a greater degree of hypometabolism within neocortical brain areas, but a comparable reduction in medial temporal regions (Chen et al., 2021), indicating that alterations in synaptic density and metabolism can be regionally divergent in the degenerating

brain. Reasons for this divergence are likely multifactorial but may be indicative of disrupted neurovascular coupling and CBF autoregulation in Lewy body disease. Taken together, these findings highlight that spatially variant decoupling of synaptic density and perfusion may be present in these disease states, although further investigation in a larger study is required for a better understanding of the relationships between CBF and synaptic density in Lewy body disease; especially since associations between these measures may have been masked by reduced power.

In chapter 5, when assessing the molecular, structural, and functional biomarkers that best explained the spatial distribution pattern of SV2A alterations within each patient group to understand which of these biological markers may be contributing to synaptic pathophysiology, I found that the spatial distribution pattern of SV2A within drug-naïve PD patients was predominately negatively associated with markers of the dopaminergic system, which together explained ~50% of the variance. This is in line with the well-established alterations of the dopaminergic system in PD. In treated PD patients, the spatial distribution of SV2A was predominately explained by the canonical distribution of dopaminergic and serotonergic markers, although it is worth noting that the association observed with the distribution pattern of D_1 receptors was positive in this group. This is consistent with the hypothesis that the normalisation of synaptic density in treated PD occurs in regions with higher D_1 receptor density in young healthy volunteers. In both PDD and DLB, the differential pattern of SV2A alterations was most strongly associated with the spatial distribution of grey matter volume alterations explaining 14% and 44% of the variance, respectively, highlighting a foreseeable relationship between synaptic density loss and neuronal cell loss, which is heightened in dementia. Finally, the differential pattern of SV2A alterations in DLB compared to PDD was explained principally by the premorbid distribution of D_2 receptor density, likely reflecting lower synaptic density in

dopamine-rich areas in the PDD group, which is in line with the long, progressive loss of nigral dopaminergic cells and the severity of parkinsonism (Colloby et al., 2012, O'Brien et al., 2004).

Overall, these findings demonstrate that there is a clear difference in the extent of synaptic density reduction at different stages of PD, where it becomes progressively reduced as the disease progresses. Having said that, according to these findings, synaptic density is unlikely to be lost uniformly or in a simple linear fashion, as there appeared to be a transient restitution of this loss in patients who initiated treatment. Furthermore, whilst atrophy may impinge on measures of synaptic density, SV2A does not appear to merely be an index of volume loss. Similarly, hypoperfusion does not appear to be as closely linked with synaptic density measures as one may have presumed, which may be reflecting a discordance between synaptic loss and neuronal function within these groups. Finally, we see here that, depending on where a patient is along the disease course, the spatial distribution of group differences in regional SV2A binding are found in areas with high specific receptor binding in young healthy controls, so may involve just these receptors with the proviso of the previous point made above. Taken together, these findings indicate that [^{11}C]UCB-J PET is measuring a unique component of the disease process and by combining it with other biological markers, we may be able to better understand disease pathogenesis.

6.4 Does PD medication promote synaptogenesis?

As mentioned in the summary, SV2A expression levels in treated PD patients was comparable to healthy controls and elevated when compared to drug-naïve PD, with the largest observable increase found in the thalamus. This is a particularly novel and interesting finding that may be reflecting a neuroplastic response of the basal ganglia-thalamocortical circuit in PD patients early in their disease course and who have been treated with dopamine replacement therapy. There are

two possible mechanisms that could explain the restitution of synaptic density in this group: (i) L-DOPA-induced plasticity or (ii) spontaneous disease-related regeneration of neuronal fibres as part of a compensatory mechanism. Given the small number of subjects and the study design, it has not been possible to firstly definitively conclude that synaptic density has been 'restored' within PD patients on treatment as a much larger sample size with a longitudinal design would be required to establish such a premise, and to secondly establish whether it is in fact the dopamine replacement therapy or simply the disease process itself that has contributed to this alteration. However, the positive association between the spatial distribution of SV2A expression levels and the canonical distribution pattern of D_1 receptors, whereby higher levels of SV2A are associated with D_1 receptor-rich brain areas, is an additional indicator of the normalisation of synaptic density towards healthy controls, which may be neurotransmitter dependent. Since L-DOPA is a precursor of dopamine, it is tempting to speculate that the normalisation of synaptic density in treated PD may be driven, or at least mediated by, the replenishment of dopamine concentrations, following pharmacologic dopamine replacement therapy, that are stimulating D_1 receptors and are mediating these changes.

Dopaminergic neurons originating from the SNpc and ventral tegmental area directly innervate well-defined neurogenic regions in the mammalian brain i.e., the subgranular zone in the hippocampal dentate gyrus and the subventricular zone. Evidence of dopamine receptor-mediated regulation of neurogenesis has highlighted the role of dopamine signalling in neuronal proliferation and differentiation in the adult central nervous system, where treatment with dopamine receptor agonists and L-DOPA have been shown to promote adult neurogenesis and increase neural progenitor cells, including within the substantia nigra which also possesses neurogenic potential (Mishra et al., 2019, Takamura et al., 2014, Hoglinger et al., 2004, Winner et al., 2009, Van Kampen and Eckman, 2006, Van Kampen and Robertson, 2005, Chiu et al., 2015). Indeed, chronic L-DOPA administration has been shown to alter several genes implicated

in synaptogenesis, neurite outgrowth and cell proliferation in 6-OHDA-lesioned rats (El Atifi-Borel et al., 2009, Ferrario et al., 2004).

Since D_1 receptors are preferentially responsive to phasic changes in dopamine levels (Dreyer et al., 2010), and D_1 receptors become hyperresponsive to dopamine in PD (Tong et al., 2004), physiological surges of dopamine as a result of L-DOPA administration may be contributing to the restitution of SV2A expression in treated PD via D_1-signalling. Furthermore, in a dose-dependent manner, dopamine has also been shown to induce an increase in neurotrophin BDNF protein expression in cortical, striatal, and hippocampal rat brain tissue slices via D_1-receptor signalling (Williams and Undieh, 2009) and L-DOPA has also been shown to enhance striatal expression of BDNF in healthy rodents (Okazawa et al., 1992). Clinical studies have also suggested that activation of D_1 receptors via agonists is beneficial in the management of PD (Braun et al., 1987, Reichmann, 2000). Taken together, in treated PD patients, it appears that neuroplastic effects of L-DOPA are being mediated by D_1 receptors.

To summarise, in drug-naïve PD, there is evidence of dopaminergic neurotransmitter dysfunction as reflected by the negative association between spatial distribution of dopaminergic markers and the distribution pattern of synaptic density. In treated PD patients where there is still the involvement of disease mechanisms, with the addition of L-DOPA mechanisms, this association is no longer evident. Instead, there appears to be a transient phase where the pattern of synaptic density changes so the initial association observed in the early phases is no longer present. Instead, the association between D_1 receptor distribution and synaptic density is in the opposite direction, which is consistent with a normalisation of synaptic density that is tracking the distribution of D_1 receptor density across the brain. I have outlined above that L-DOPA has been shown to induce neurotrophic and neuroplastic effects. My results allow me to put forward

the hypothesis that it is in fact D_1 receptors specifically that mediate the potential neuroplastic and neurotrophic effects of L-DOPA in PD.

Future studies are critical to tease apart which of these mechanisms are responsible for, or at least contributing to, the alteration of synaptic density in PD patients and if L-DOPA does in fact exert plasticity-promoting effects in human PD patients. Specific research questions would need to be outlined carefully, and in turn, a variety of conditions and factors would need to be taken into consideration and controlled for where possible when designing studies of this nature. For example, to address whether chronic L-DOPA administration does in fact hold the potential to induce alterations in synaptic density in patients with PD, studies performing a [^{11}C]UCB-J PET scan before and after active L-DOPA treatment would be valuable in determining what, if any, chronic effects L-DOPA has on synaptic density in PD. For example, animal studies where a subset of PD models are treated with L-DOPA and a subset are not would be ideal to assess the extent to which 1) synaptic density is reduced prior to commencement of dopamine replacement therapy and then 2) how this subsequently changes following L-DOPA treatment compared to when treatment is not initiated. This type of study would provide some clarity on whether L-DOPA exerts trophic effects and promotes the recovery of damaged neurons or whether this upregulation of SV2A is in fact some sort of compensatory disease mechanism. How this varies across the brain can be followed best in patients before and after treatment.

Similarly, to assess whether an acute dose of L-DOPA induces a change in SV2A expression, a double blind cross-over study in drug naïve PD is needed with [^{11}C]UCB-J PET scans performed pre- and post-administration of L-DOPA. This would provide insight into the effects of an acute stimulation of dopamine receptors following L-DOPA administration and its potential relationship with synaptic density alterations, as opposed to this acute effect being mixed with the effects of chronic stimulation of dopamine receptors if this study were performed in PD

patients already taking L-DOPA therapy. This study design would ultimately allow researchers to determine whether L-DOPA holds the potential to induce an alteration in synaptic density *in vivo* and if it is likely restored as a long duration response to L-DOPA therapy. It would also be particularly interesting and valuable to assess how these changes are related to the canonical distribution of receptor subtypes implicated in mediating the treatment effects.

Addressing the question of whether L-DOPA has the potential to influence SV2A uptake is important for future clinical trials that may eventually employ SV2A imaging as a biomarker or even as a surrogate endpoint (if future trials demonstrate that SV2A imaging is a meaningful endpoint that is a direct measure patient wellbeing or predicts the effect of a therapy). If the natural history of PD and the potential effects of L-DOPA are not taken into consideration, then it may conflate or confound the real effects of any future developed disease-modifying therapies since dopamine replacement therapy is part of standard care. Thus, whilst early intervention in drug-naïve PD patients would be ideal to demonstrate motor and nonmotor benefit of a new disease-modifying therapy, which are usually short-term trials, long-term trials would be likely to recruit patients who are already on medication or commence medication over the duration of the trial to observe effects of long-term therapies that modify disease progression. This may become problematic if it is under the assumption that L-DOPA does not exert any plasticity-promoting effects or have an influence on synaptic density measures. Whilst some previous preclinical studies in animals have demonstrated neurotrophic effects of L-DOPA, further work in animals and animal models, perhaps specifically assessing SV2A alterations, would be able to contribute to a deeper understanding of these changes. Since controlling for the effects of medication is virtually impossible in studies of progression in PD, as all patients would likely be medicated, it is important to clarify if L-DOPA does exert trophic effects, if that influences synaptic density and the way in which this evolves over the course of PD.

6.5 Progression of synaptic density loss

The inclusion of 4 patient datasets together provides some insight into the progression of synaptic density alterations over the course of PD, notwithstanding the limitations of this being a cross sectional study and statistical power, described earlier. Whilst synaptic density was reduced early in the disease, it does not appear to decline in a linear fashion during disease progression as demonstrated by the normalisation of synaptic density within treated PD and then subsequent greater magnitude of synaptic density loss in PDD, which was predominately in frontal and parietal brain areas, as well as the thalamus and caudate. Atrophy in these brain areas have previously been reported to be implicated in PDD or predictive of cognitive decline in PD (Mak et al., 2014, Hanganu et al., 2014, Monchi et al., 2016). This was similarly the case for grey matter volumetric and perfusion measures, whereby the alterations of these structural and functional markers deteriorated in a nonlinear fashion. As mentioned in the previous section, this is indicative of a combined effect of disease and medication. However, the continual decline in synaptic density illustrates that in more advanced stages of PD, the limitations of current pharmacological strategies emerge with the underlying pathological processes of the disease overwhelming the therapeutic (and potentially plasticity-promoting) benefits of dopamine replacement therapy. This is not particularly surprising, since L-DOPA is not a disease modifying therapy in that it does not slow down, halt or reverse the progression of PD. It seems likely that the efficacy of L-DOPA, or alternatively a synaptic therapy, would have the greatest impact if it was possible to administer it in combination with a disease-modifying agent. Furthermore, whilst some associations were observed between synaptic density loss and clinical symptom severity within drug-naïve and PDD patients, gaining an insight into the clinic-pathology would require a much larger sample size. In fact, large samples spanning more disease stages will be needed to provide a more comprehensive mapping of SV2A density in patients with PD using [^{11}C]UCB-J PET.

6.6 Are discrete transmitter-related patterns of synaptic loss a feature of PDD and DLB?

In PDD and DLB, the spatial pattern grey matter volume alterations best explained the distribution pattern of synaptic density alterations. This may simply be reflective of the progression of the disease to most areas of the brain, represented by a more extensive and widespread loss of SV2A and associated degeneration. The contribution of any one neurotransmitter system were smaller in magnitude. Nevertheless, relatively lower synaptic density in PDD occurred in regions with lower SERT, DAT and VaChT in healthy younger controls, which is consistent with relatively higher synaptic density loss arising in areas that are typically sparse of serotonergic, dopaminergic, and cholinergic transporters.

Perhaps more interestingly, the differential spatial pattern of SV2A in DLB compared to PDD followed the distribution pattern of dopaminergic markers, indicative of further reduced synaptic density within dopamine-rich areas in PDD. This may be reflecting the long-term progressive loss of dopaminergic neurons in PDD and are in line with previous studies that reported striatal dopamine uptake was reduced in PDD compared to DLB (Colloby et al., 2012, O'Brien et al., 2004). The implication of the dopaminergic system in explaining the differential spatial distribution of synaptic density between PDD and DLB highlights that this approach permits the incorporation of fundamental molecular properties of brain tissue that better inform the alterations of synaptic density of brain disease.

An alternative approach that would provide a more nuanced, cellular-level view of the mechanisms contributing to the spatial distribution of synaptic density alterations would be the use of brain-wide gene expression atlases such as the Allen Human Brain Atlas (Shen et al., 2012, Hawrylycz et al., 2012). The capacity to relate molecular pathways to macroscale brain organisation has open the door to the field of imaging transcriptomics, which is where gene

expression patterns are spatially correlated with a property of brain structure or function, as measured by neuroimaging (Arnatkeviciute et al., 2019). This approach enables researchers to identify genes (from several thousands of genes) with the spatial profiles of regional expression that most strongly track anatomical variations in a brain map of interest; ultimately allowing researchers to draw conclusions about the potential cellular or biological pathways that may underlie specific neuroimaging features (Arnatkeviciute et al., 2019). A growing body of literature has already started to provide insight into how regional variations in gene expression relate to diverse properties of brain structure (Patel et al., 2020, Patania et al., 2019, Romero-Garcia et al., 2018, Shin et al., 2018, Seidlitz et al., 2018, Liu et al., 2020) and function (Shen et al., 2021, Tang et al., 2021, Zhu et al., 2021, Hansen et al., 2021, Wen et al., 2018, Diez and Sepulcre, 2018), as well as disease-related brain alterations (Ji et al., 2021, Anderson et al., 2020, Keo et al., 2020, Morgan et al., 2019, Li et al., 2021, Jimenez-Marin et al., 2021, Seidlitz et al., 2020, Forsyth et al., 2021).

Recently, Martins et al. (2021) performed imaging transcriptomic analyses of the regional distribution of a plethora of molecular markers in the healthy human brain, including neuroreceptors, glia, metabolism, and synaptic proteins. The authors concluded that imaging transcriptomics can recover plausible cellular and transcriptomic correlates of the spatial distribution of molecular imaging markers. An approach like this holds the potential to improve our understanding of the biological pathways underlying the regional distribution of synaptic density alterations in Lewy body disease by providing additional mechanistic biological information and build upon the preliminary findings reported in this study.

In these studies, I was not able to stratify dementia patients according to whether co-pathologies such as β-amyloid and tau were present or not, which could potentially influence synaptic density measures. This is an important issue that should be taken into consideration in future studies

evaluating synaptic density alterations within Lewy body dementia, especially since approximately 50% of all Lewy body dementia patients have sufficient AD-related pathology for a secondary neuropathologic diagnosis of AD. Combining molecular imaging biomarkers of amyloid and tau pathologies along with synaptic density in Lewy body dementia could contribute to a greater understanding of how the different pathologies evolve and contribute to the clinical heterogeneity in Lewy body disease, especially since amyloid and tau can exert direct effects on synaptic integrity, as well as indirect effects on processes such as neuroinflammation and neuronal energetic that could contribute to synaptic deficits, as has been demonstrated in AD (Jackson et al., 2019). Understanding the underlying mechanisms of synaptic density loss that is related distinct pathologies could have treatment implications.

Currently, a primary challenge associated with clinical trials is the lack of established biologic, genetic or neuroimaging biomarkers that may inform study design. The development of biomarkers is an indispensable aspect of separating clinical differences between PDD and DLB from underlying biological differences, as well as distinguishing DLB from AD. Although I did not observe any direct, regional differences in synaptic density between PDD and DLB, the spatial correlation analyses revealed that the dopaminergic system may be more strongly implicated in PDD than in DLB. Whilst further research with larger sample sizes may be able to elucidate the clinical utility of [^{11}C]UCB-J in distinguishing between these disorders, the adoption of the spatial correlation approach and combining biomarkers, particularly if AD-related pathologies are incorporated into such analyses, could shed light on why synucleinopathy will present initially with cognitive decline or with extrapyramidal features. Furthermore, since there are likely to be multiple markers that will correlate with the spatial distribution of SV2A, identifying the underlying pathology(s) of these other markers may aid in the development of new and disease-specific preventative and curative treatments, as well as aid in monitoring

disease progression and treatment effects, but would likely require a multimodal approach such as the one employed here.

6.7 SV2A as a biomarker of synaptic density

Quantifying synaptic loss *in vivo* requires a molecular target with several suitable features. An appropriate and useful general marker of synaptic density will be one where the target is present on all synapses, as opposed to just a subset. There should also be a stable stoichiometric relationship between the target and the synapse, such that it should remain consistent in the presence of a disease process. Finally, treatment widely used in patient populations under investigation should not have substantial affinity for the molecular target. Considering that the cellular localisation of vesicles is restricted to synaptic boutons, that they are ubiquitously distributed throughout the brain and that they are highly phylogenetically conserved across vertebrate nervous systems, it is unsurprising that synaptic vesicle proteins now serve as prime markers of synaptic density (Goelz et al., 1981, Perdahl et al., 1984, Navone et al., 1986, De Camilli et al., 1983).

Given the widespread expression of SV2A in synapse throughout the brain (Bajjalieh et al., 1994), the highly consistent number of SV2 proteins per vesicle (Mutch et al., 2011, Takamori et al., 2006), and the fact that it correlates well with classic markers of presynaptic terminals, such as synaptotagmin and synaptophysin (Finnema et al., 2016), imaging of SV2A is an attractive tool for assessing synaptic integrity *in vivo*. However, it is critical to interpret a loss of SV2A with care, as to not conflate the loss of this presynaptic protein with the actual loss of functional synapses themselves. Further investigations are required to directly validate this notion.

The development and application of [^{11}C]UCB-J PET holds the potential to enhance our understanding of the role of synaptic dysfunction and/or degeneration, monitor disease progression, aid in clinical diagnoses and evaluate therapeutic effects. Given that [^{11}C]UCB-J ligand has high selectivity and affinity to SV2A, we are able to obtain regional estimates of the protein density, which can be assumed to reflect overall synaptic density. The pertinence of SV2A as a synaptic marker was illustrated by Kaufman et al. (2015) where AZD0530, a FYN tyrosine kinase inhibitor, rescued both memory and synapse (SV2A) loss in a rodent model of Alzheimer's disease. However, the future utility of [^{11}C]UCB-J radioligand as a marker of synaptic density will essentially depend on whether an association exists between signal change and disease progression. It remains unclear the degree to which this measurement is affected by dysfunctional SV2A, expression levels within vesicles (and the effects pathology has on the number of SV2A molecules per vesicle) or the number of vesicles per synapse. Evidence also indicates that whilst SV2A is expressed throughout the brain, its levels of expression vary between regions (Bajjalieh et al., 1994). It is also unknown whether SV2A is necessarily decreased in damaged neurons or whether a damaged neuron could, in fact, continue to contain the same density of SV2A proteins. Finally, there is need to understand whether acute changes in neuronal activity lead to alterations in [^{11}C]UCB-J uptake, since SV2A could potentially have variable physical conformations (Lynch et al., 2008), electrostatic properties (Correa-Basurto et al., 2015) or binding partners (Bartholome et al., 2017) at distinct stages of vesicle release, which could ultimately affect the affinity of [^{11}C]UCB-J radioligand to bind to the protein during synaptic activity. Thus, any activity-related alterations in binding would introduce a source of variance that would conflate the identification of true differences in synaptic density. Indeed, the binding stability of [^{11}C]UCB-J within the context of increased neuronal activity was recently investigated by Smart et al. (2021) who, by employing a multimodal approach, found that there was no apparent change in [^{11}C]UCB-J binding during the presentation of a visual stimulus, even though there was an evident surge in tracer delivery (K_1) to the primary visual cortex (Smart et

al., 2021). This finding is suggestive of [^{11}C]UCB-J serving as a stable and static marker of SV2A protein density that is unlikely to be influenced by dynamic processes related to protein function, local environment or synaptic activity during PET acquisition. Thus, whilst the relevance of SV2A as a biomarker of synaptopathies remains to be demonstrated, research addressing some of these concerns are emerging, which will inevitably help clarify whether SV2A imaging holds promise for investigating and monitoring brain pathology involving synaptic dysfunction.

Although a plethora of pre- and postsynaptic markers exist that are typically targeted by antibodies, synaptophysin is the most abundant synaptic vesicle protein (Takamori et al., 2006) and is a commonly used marker of synaptic density (Masliah et al., 1990, Knaus et al., 1986), because it was one of the first vesicle membrane proteins to be cloned and characterised (Navone et al., 1986, Wiedenmann and Franke, 1985, Leube et al., 1987). Accordingly, synaptophysin is renowned for being the gold standard. The high correlation between SV2A and synaptophysin in the nonhuman primate brain is suggestive of SV2A being a valid alternative marker of synaptic density (Finnema et al., 2016). Synaptophysin is polydispersed, potentially signifying its variable expression amongst vesicles of various neurotransmitter classes, whereas SV2A may even offer a more accurate measure of synaptic density, given that it is the most monodispersed synaptic vesicle protein (Mutch et al., 2011), thus has greater uniformity in vesicles.

Eventually, a panel of synaptic protein biomarkers may serve as a reliable readout for the various aspects of synapse loss (presynaptic, synaptic vesicle and dendritic), with more certainty being attained from quantifying the apparent overlap between pre- and postsynaptic markers. Given that there are no other PET markers of synaptic density on the market at this present time, this could potentially be investigated by combining imaging with CSF-proteomic techniques, perhaps with postsynaptic markers such as neurogranin.

6.8 Is SV2A imaging representing a unique component of disease?

In this series of studies, I found that [^{11}C]UCB-J PET was not simply an index of grey matter volume. This was evidenced by the fact that there was an observable reduction in SV2A in early, symptomatic PD who had less than two years disease duration and did not have any evidence of atrophy or volumetric reductions. These findings alone indicate that synaptic density is reduced in the likely absence of any volumetric change, thus not conditional on grey matter volumetric reductions. Furthermore, these findings highlight that whilst volumetric MRI offers a robust method to assess the progression of atrophy in the PD brain, it is clearly not sensitive enough to inform on subtle changes in synaptic dynamics and [^{11}C]UCB-J is a promising approach for this.

Yet, how relevant, and sensitive is SV2A binding when large-scale volumetric reductions are present? This was explored in Lewy body dementia who exhibited a sizeable degree of atrophy across cortical and subcortical brain areas. I found that some areas exhibiting reduced SV2A did not survive following PVC or after controlling for grey matter volume, and relatively strong positive associations were observed between SV2A and grey matter volume in a limited number of brain areas, indicating that atrophy could have a confounding effect on SV2A measures. However, this was not universally the case - particularly in DLB where atrophy was more widespread and extensive across the brain, but the influence of volumetric alterations on SV2A measures was limited to the caudate and thalamus. Furthermore, within both PDD and DLB, reductions of SV2A did not wholly coincide with volumetric reductions, which is indicative of [^{11}C]UCB-J uptake reflecting a distinct feature of the brain. Taken together, these findings highlight that although volumetric alterations/atrophy can have some localised confounding effects on synaptic density measures, [^{11}C]UCB-J PET is not just a proxy measure of gross macroscopic atrophy. This is particularly important for understanding the value of [^{11}C]UCB-J to serve as a biomarker for synaptic density and not simply be reflecting neuronal loss, as if atrophy

and synaptic density loss were concordantly reduced to the same magnitude with overlapping regional patterns of change, then [^{11}C]UCB-J PET would essentially be an expensive and invasive approach of quantifying volumetric alterations, which can be done using T1-weighted MRI. However, it is worth noting that since volumetric reductions have the potential to impinge on measures on synaptic density, it is important for future studies to ensure volumetric alterations are accounted for in neurodegenerative disorders, particularly those that exhibit extensive atrophy, with perhaps the most viable option being to perform partial volume correction on the PET images.

SV2A is also not simply a proxy measure of blood flow, as demonstrated by the discordant regional pattern of synaptic density reductions and hypoperfusion in Lewy body disease and the limited associations between these measures. Instead, employing these measures together could provide a useful insight into the relationship between local neural activity and synaptic integrity. As a side note, when performing full kinetic modelling, V_T is dependent on the ratio of K_1 (representative of the delivery rate of the tracer and dependent on perfusion) and K_2 (depictive of the transport of the tracer from the tissue back to the blood), thus the effect of blood flow is cancelled out, so there is no concern regarding a reduction of SV2A arising because of reduced blood flow/hypoperfusion.

[^{18}F]FDG is the most widely used PET ligand, which provides a measure of cellular glucose metabolism. In neurons, the demand for glucose is partially driven by synaptic terminals, which generate ATP for the synthesis, release, and recycling of neurotransmitter molecules, as well as for the maintenance of and recovering from action potentials. Thus, regional cerebral metabolic rate of glucose as measured with [^{18}F]FDG PET provides a direct measure of neuronal function and an indirect index of synaptic density (Attwell and Iadecola, 2002). Therefore, a disruption in glucose metabolism may be indicative of synaptic dysfunction. A decade of [^{18}F]FDG PET

research has provided evidence for this modality to serve as an effective and safe approach to identify diagnostic patterns of glucose hypometabolism in neurodegenerative disorders, where it has been shown to differentiate PDD and DLB from Alzheimer's disease (Minoshima et al., 2001). However, [^{18}F]FDG PET does not provide a direct marker of synaptic density and is often employed to assess brain activation, whereby its sensitivity to transient neural responses is exploited. Furthermore, metabolism measures can be confounded by medications, sensory stimulation, and blood glucose levels, with reports of intrasubject variability ranging between 10%-25% following test-retest comparisons, even in healthy individuals scanned at close time points and under well-controlled research conditions (Shiyam Sundar et al., 2020, Camargo et al., 1992). As a result, scanning conditions must be carefully controlled when acquiring metabolism measurements with [^{18}F]FDG PET (such as participant fasting) and its sensitivity is limited to detect only reasonably large alterations or group differences of ~25% or greater. Contrastingly, test-retest data with [^{11}C]UCB-J PET indicates that even small changes, as little as 10%, could be identified, which would be particularly useful for the detection of earlier and/or subtler disease effects. This has even been demonstrated in the findings presented here, where subtle reductions in SV2A binding were observable across all patient groups, including those with less than 2 years disease duration. Finally, [^{18}F]FDG has also been shown to accumulate at sites of infection and inflammation due to the enhanced glycolytic activity of activated neutrophils or macrophages and Jeong et al. (2017) suggested that [^{18}F]FDG PET could be employed to visualise neuroinflammation. Therefore, although [^{18}F]FDG PET has been exploited in the literature as an indirect measure of synaptic density, its measures can be confounded by several factors highlighting the need for a direct marker such as [^{11}C]UCB-J PET.

6.9 Could SV2A serve a valuable biological endpoint?

Whilst further studies with much larger sample sizes and superior study design are required to determine whether the rise in SV2A in treated PD is in fact indicative of L-DOPA exerting potential neuroprotective effects and/or promoting synaptogenesis, if this is deemed to be the case, it highlights that SV2A holds the potential to monitor therapeutic responses for future disease-modifying diseases, check the efficacy of drugs in clinical trials and could even potentially serve as a surrogate endpoint in clinical trials. Generally, drug effects on behaviour are evaluated by determining the relationship between dose and magnitude of behavioural response. Thus, for [^{11}C]UCB-J to be a valuable biological endpoint, it must represent the wellbeing of the patient and should predict the effect of therapy. In this study, I did not observe any associations between symptom severity and SV2A density, and in fact, patients on treatment had worse motor symptom severity and overall disease burden compared to drug-naïve PD patients, thus there appears to be a deviation between clinical and imaging markers of disease severity. This could be indicative that an increase of synaptic density is not necessarily resulting in an improvement of symptoms in PD. Having said that, with this cross-sectional data, I am not able to determine whether there has been an improvement in motor symptom severity in treated PD since medication commencement and given the large clinical heterogeneity and variability in disease progression, comparing to drug-naïve PD may not be a good indication of how effective L-DOPA has been on improving clinical symptoms. Therefore, future clinical trials will be critical to determine if a normalisation of SV2A expression levels is reflected in clinical improvement.

For example, there have been a handful of large clinical trials that have assessed the efficacy of L-DOPA, namely CALM-PD (Parkinson Study, 2002), REAL-PET (Whone et al., 2003) and ELLDOPA (Fahn et al., 2004) trials, that also employed neuroimaging techniques to quantify markers of intact nigrostriatal dopaminergic nerve terminals such as DAT, although these tracers

are not reflective of the number or density of dopaminergic neurons, axons or synapses. However, the reported findings are controversial regarding their meaning, since L-DOPA therapy resulted in superior motor improvement, but a more rapid decline in dopaminergic function as reflected by a reduction in these markers. This unanticipated divergence between clinical and imaging endpoints is not only puzzling but also an obstacle for the advancements of future therapeutic trials, since biological endpoints are mandatory to demonstrate a putative neuroprotective effect of a drug. Similarly, it is important for validation studies to determine whether [^{11}C]UCB-J would be a useful technique to monitor therapeutic responses, and L-DOPA may be a good candidate to determine whether clinical improvement is reflected in synaptic density restoration, although this is a prerequisite for any future disease-modifying therapies.

Whilst the validity of DAT imaging as a surrogate marker for clinical trials has been questioned (Morrish, 2003), the replication of this incongruity in three independent investigations using different neuroimaging markers is suggestive of factors other than the imaging technique influencing the outcomes. Amongst such possibilities is pharmacological interactions between radiotracers and L-DOPA and/or L-DOPA-induced reduction of DAT expression have been proposed (Ahlskog, 2003, Ravina et al., 2005), although Fernagut and colleagues later demonstrated in MPTP-treated monkeys that L-DOPA does not induce modifications of DAT expression (Fernagut et al., 2010). The administration of L-DOPA may also lead to competition between dopamine that is released into the synaptic cleft and the exogenous radioligand, leading to an apparent reduction of DAT binding (Nikolaus et al., 2013). Indeed, the discrepancy between PD symptom severity and DAT expression in L-DOPA treated PD patients has led to uncertainty regarding its usefulness as a biomarker of disease progression.

Therefore, the advantage of SV2A imaging over and above presynaptic terminal markers such as DAT is that it is (likely) a marker of synaptic density, whereas changes in DAT might reflect presynaptic dysfunction or altered DAT expression, as demonstrated by the fact that there may be a compensatory downregulation earlier in the disease course which is not entirely reflective of dopaminergic terminal loss *per se* (Nandhagopal et al., 2011). Furthermore, the DAT protein is distributed predominately in mesencephalic dopamine neurons and is particularly enriched in the striatum and nucleus accumbens, thus limiting its utility to assess disease-related or treatment effects to the striatum and associated motor symptom severity. On the other hand, since SV2A is expressed ubiquitously across all synapses in the brain, [^{11}C]UCB-J can be used as a cortical and subcortical marker, which has particular implications for Lewy body disease, since there is also cortical manifestation of the disease process as demonstrated in the findings presented here – including at very early stages of the disease. This would be especially valuable for research studies and clinical trials assessing both motor and non-motor symptoms, as SV2A is a broader, more generic marker of the disease.

6.10 Clinical implications of SV2A imaging

PET imaging of SV2A has shown great promise as a biomarker for synaptic density. The findings reported in this thesis contribute to the notion that SV2A is a unique biomarker whereby it is not simply a proxy measure of gross grey matter atrophy nor brain perfusion. Recently published [^{18}F]FDG PET studies, both in disease and healthy controls, have demonstrated a level of discordance between metabolism and synaptic density measures indicating that SV2A is also not simply a measure of metabolism. Therefore, we can be fairly confident that SV2A imaging is providing a unique insight into a biological phenomenon of the brain, namely synaptic density, for which existing neuroimaging techniques are not as well-equipped to measure.

Despite the biological insights SV2A can provide, the clinical utility of SV2A imaging is currently largely speculative for several reasons. First, whilst [^{11}C]UCB-J possesses ideal imaging and *in vivo* binding characteristics, carbon-11 has a short radioactive half-life of approximately 20 minutes, which ultimately limits its production and utility to PET centres that have onsite cyclotrons. Therefore, there is a prerequisite to develop ^{18}F-labelled SV2A radioligands to improve accessibility, facilitate large, multicentre clinical trials, and expedite their potential diagnostic applications within the clinical setting. Indeed, researchers from Yale University have predominately led the development of SV2A radiotracers and have successfully synthesised and evaluated the ^{18}F-labelled counterpart of a [^{11}C]UCB-J, namely [^{18}F]UCB-J (Li et al., 2019b), as well as a handful of ^{18}F-labelled analogues of UCB-J including [^{18}F]SDM-2 (Cai et al., 2017) and [^{18}F]SynVesT-1, also known as [^{18}F]SDM-8 (Li et al., 2019a), with the latter radiotracer also being successfully assessed in a group of healthy volunteers (Naganawa et al., 2021). Of the ^{18}F-labelled radiotracers evaluated to-date, [^{18}F]Syn-VesT-1 appears to hold the most promise as a radiotracer for SV2A and as a biomarker for synaptic density quantification across neurological disorders. Whilst both [^{18}F]UCB-J and [^{18}F]Syn-VesT-1 exert the same favourable properties as ^{11}C-labelled UCB-J such as high brain uptake, fast and reversible kinetics and high levels of specific binding, the radiosynthesis of [^{18}F]UCB-J had a low radiochemical yield (Li et al., 2019b), ultimately making its clinical translation especially challenging until alternative approaches to its radiosynthesis are discovered.

Whilst the development of ^{18}F-labelled radiotracers for SV2A is a step in the right direction when considering the translation of SV2A imaging into the clinical setting, given the longer half-life of ^{18}F at 110 minutes that makes central production and multisite distribution feasible, the gold standard for analysing dynamic SV2A PET acquisitions is with compartment models using a metabolite-corrected arterial input function (Finnema et al., 2018). This presents a problem for

its translation to the clinic since it requires blood sampling from an arterial line, which is an invasive procedure where a catheter is typically placed percutaneously into the radial artery at the wrist. Although placing an arterial line is feasible and reasonably safe (Everett et al., 2009), it is laborious, and tolerance for invasive research procedures can wane in ageing or ailing populations – especially in the case of repeated arterial cannulations. Additionally, since elderly patients are at higher risk of developing blood clots, they may require medications that influence the blood clotting cascade, which has notable implications for patients with age-related disorders i.e., neurodegeneration. As well as having implications for the clinical setting, procedures that are arduous for the participants can decelerate subject accrual for research purposes or contribute to dropout rates in longitudinal studies (Kang et al., 2018). Furthermore, concerns regarding the practicality of such arterial blood-based imaging techniques could potentially lead to drug developers to reconsider their utilisation in multicentre, longitudinal trials. Thus, to conveniently implement PET radiotracers in the clinical and research settings, it would be preferable to produce simple, clinically practical protocols that are patient-friendly and suitable for multicentre trials, highlighting the advantage of developing and applying non-invasive methods that eliminate the need for arterial blood sampling, such as those using reference regions, to obtain meaningful quantitative measurements of the target of interest. Reference region methods permit the quantification of the binding potential with respect to the nondisplaceable compartment, BP_{ND}. An archetypal reference region is one in which the total uptake in the reference region is equivalent to the nondisplaceable (i.e., free + non-specifically bound radiotracer) uptake in target brain areas. In short, an ideal reference region is one in which there should be no specific or displaceable uptake.

I have already mentioned the centrum semiovale as a potential reference region and the associated limitations (see Limitations section for further detail). An alternative reference region that has been investigated to-date is the pons (Rossano et al., 2020), although there has been

evidence of SV2A localisation within this brain region. Furthermore, blocking studies demonstrated a considerable amount of binding displacement upon drug administration which was twice the amount in the centrum semiovale and the uptake in the pons was higher than the nondisplaceable binding in the grey matter (Mecca et al., 2020). The cerebellum has also been employed as a reference region, although, since the cerebellum has SV2A-specific binding, it is unsuitable for computing BP_{ND} but could be useful to compute the distribution volume ratio (DVR) in diseases where the cerebellum is spared from intrinsic neuropathology, such as AD (Mecca et al., 2020). However, for any reference region employed for this tracer, it is important for researchers to be conscious of the projections to the reference region and whether those brain areas are affected by disease pathology, as this could theoretically lead to an underestimation of [^{11}C]UCB-J changes within disease states. In any case, the cerebellum would not be a useful reference region for Lewy body disease since it is implicated within the disease process, as also demonstrated by my findings.

Finally, an image-derived input function may be a useful alternative to employing a reference region (Schain et al., 2013). This method relies on identifying and extracting the time series of the voxels that belong to the carotid artery. It is based on calculating the Pearson correlation coefficient between time-activity curves of voxel pairs in the PET image to pinpoint voxels exhibiting blood-like behaviour (Schain et al., 2013). This method was employed by Bahri et al. (2017) who derived the input function from dynamic PET images and reported that it is highly efficacious in quantifying [^{18}F]UCB-H uptake, comparable to that of using manual arterial blood sampling as the input function. The authors then concluded that an image-derived input function is useful and obviates the need for arterial blood sampling. However, this is not entirely true as image-derived input functions require at least one arterial sample to provide good accuracy in the uptake estimates (Schain et al., 2013) and indeed, Bahri et al. (2017) scaled and corrected the image-derived input function to plasma radioactivity and mean unchanged plasma fractions,

respectively (Bahri et al., 2017). Whilst an approach like this could have been very promising if it substituted the need of frequent arterial sampling, it could help ease the burden of conventional arterial sampling, since few blood samples are required. An alternative that has been suggested is replacing arterial with venous samples when scaling the image-derived input function, although this is only feasible if the radioactivity level is comparable in arterial and venous plasma (Schain et al., 2013). One final consideration is the resolution and noise levels associated with the PET systems used, where low resolution scanners may not be able to implement such a method (Zanotti-Fregonara et al., 2009). Since identifying a reference region for [^{11}C]UCB-J is proving to be difficult, a method like this may merit further investigation.

Overall, the emergence of more readily available ^{18}F-labelled SV2A imaging probes is a promising indication that SV2A PET is anticipated to lead new insights into the aetiology of neuropsychiatric disorders, as well as aid the development of new treatment strategies. Further work is required concerning potential reference regions that would be optimal for SV2A quantification, not only concerning the region being devoid of SV2A binding, but also whether existing reference regions, like the centrum semiovale, are still appropriate to employ when investigating SV2A alterations within diseases where pathology impinges on SV2A binding within the reference region. Despite its limitations, presently, the centrum semiovale seems to be the most valuable reference region available for [^{11}C]UCB-J quantification.

6.11 Research potentials of SV2A imaging

Whilst the development of ^{18}F-labelled SV2A imaging probes opens doors for its potential translation into a clinical setting as well as providing a viable option for smaller PET centres and multicentre trials that would rely on radioligand distribution from central production sites, ^{11}C-labelled radioligands also have significant advantages over ^{18}F-labelled radioligands, which may

be more useful within a research setting. For example, with a radioligand labelled with ^{11}C, researchers have the capacity to acquire more than one scan a day on the same subject, which is particularly valuable when radial artery cannulation is a prerequisite or in studies involving behavioural or pharmacologic challenges. ^{11}C-labelled radioligands also have substantially lower dosimetry that permits multiple scanning of participants, which is particularly useful for multimodal imaging as employing PET with radioligands targeting specific molecular or pathological markers provide an avenue to elucidate processes at different levels of neurodegenerative pathology and explore any associations between these biological signatures. Mining this information could aid in a more precise stratification of patients, which could also help characterise treatment efficacy on an individual level.

Clarification is nevertheless required as to whether a loss of SV2A is, in fact, reflecting a loss of synapses or simply indicative of reduced SV2A expression levels within vesicles. This is vital for the interpretation of SV2A reduction/loss and its value as a marker of synaptic density. Perhaps animal models would be the most suitable approach to take to determine the degree to which SV2A loss is attributable to alterations in the number of synapses. For example, in SV2A knockout mice (-/-), whilst there was altered neurotransmission, there was no change observed in the number or morphology of synapses or synaptic vesicles, which was indicative that SV2 proteins are not structural components of the synapses (Crowder et al., 1999, Janz et al., 1999). However, a recent study in a Drosophila model of synucleinopathy demonstrated that the presynaptic accumulation human α-synuclein caused a downregulation of presynaptic proteins, impaired neuronal function and induced behavioural deficits, leading to progressive degeneration of dopaminergic neurons (Bridi et al., 2021). Therefore, the synapse is very likely to represent the critical substrate that links α-synuclein pathology to the devastating motor, non-motor, and cognitive symptoms across Lewy body diseases. Since there is a close relationship between presynaptic α-synuclein accumulation and presynaptic protein loss, an important avenue of

research would be to assess if its localisation to the presynaptic terminal also impinges on the expression of SV2A. To the best of my knowledge, there are no studies published to-date that have explored this relationship, although it would be important to clarify if pathogenic mechanisms affect SV2A expression, which would not only be important for a better understanding of the mechanisms that are inducing a reduction of SV2A within Lewy body disease, but if SV2A is part of the panel of proteins affected by α-synuclein aggregation, then perhaps we could assume that it is, in fact, reflecting an impairment of presynaptic integrity. A study addressing this question would likely have to be done preclinically or using post-mortem tissue due to the lack of reliable methods available to detect and track α-synuclein *in vivo*.

6.12 Perspectives and future directions

Prior to the development of SV2A-specific radioligands that permit *in vivo* imaging of synaptic density, methods evaluating synaptic loss in the human brain were limited to histology or electron microscopy of post-mortem tissue. Such examinations have discernible inadequacies for drug development, are inapt for evaluating patients early in their disease course and lack the ability to follow the longitudinal pathological changes within patients. Non-invasive molecular imaging technique provide an obvious means to address these drawbacks.

In order to build upon the preliminary findings that have been presented in this thesis, large samples spanning more disease stages will be needed to provide a more comprehensive mapping of SV2A density in patients with PD using [^{11}C]UCB-J PET. Having said that, whilst neuroimaging findings are generally derived from group-level analysis and have enriched our understanding about neurobiological differences, longitudinal studies would provide superior information about the trajectory of the disease and the underlying biological and physiological changes. Although longitudinal studies are more expensive and time-consuming, they would be

far more advantageous in gaining an insight into whether disease progression can be following by longitudinal [^{11}C]UCB-J PET imaging. Furthermore, despite a reasonably extensive panel of healthy control-derived neurotransmitter templates being employed to assess the relationship between the spatial distribution of synaptic density alterations and the canonical distribution of neurotransmitter markers, I focussed on neuromodulatory neurotransmitter systems, since these are heavily implicated in the pathogenesis of PD and Lewy body dementia, with previous neuroimaging studies indicating terminal damage of these subset of neurons. However, the relationship between synaptic density and markers of the major excitatory and inhibitory neurotransmitter systems, namely glutamate and GABA, respectively, should also be evaluated, since these systems are also implicated in Lewy body disease, though much less explored. These tweaks to study design would make for a higher quality, and likely more informative, version of the findings reported here, with sample size being a fundamental design issue to address.

In these studies, PD patients were stratified according to their medication status, which led to some interesting findings, but given the small sample sizes, I was unable to stratify PD patients in a more meaningful or extensive way. Heterogeneity in clinical presentations and disease progression of PD have provoked several attempts to cluster or subtype PD, which have imperative practical implications for clinicians and researchers, alike. Subtyping of PD patients at baseline would enable clinicians to predict prognosis and cultivate appropriate management plans, but it would also lead to more focused research into disease aetiology, pathophysiology, and development of curative therapies. There are several avenues that have been explored regarding PD subtyping, although the most popular concept has been motor subtypes (Zetusky et al., 1985, Jankovic et al., 1990) as there is a rich body of literature evidencing an association between these subtypes with other clinically relevant features, treatment response and distinction in the trajectory of the disease (Aleksovski et al., 2018, Xu et al., 2018, Huang et al., 2018). The two main subgroups are: 1) those that have tremor as the main feature (tremor-dominant) and 2)

those with postural instability and gait difficult (akinetic-rigid). The tremor-dominant cluster is linked with a more benign disease course and a slower rate of progression (Jankovic and Kapadia, 2001), whereas the akinetic-rigid subtype is associated with faster cognitive deterioration (Burn et al., 2003, Alves et al., 2006, Johnson et al., 2016), a greater prevalence of most non-motor symptoms (Ba et al., 2016), including a higher risk of apathy and depression (Reijnders et al., 2009), and generally a faster rate of progression (Jankovic et al., 1990, Lewis et al., 2005). However, the underlying biological contributions to the clinical heterogeneity of PD are currently unclear, with frontal lobe atrophy reported to be more prominent in akinetic-rigid subtypes (Rosenberg-Katz et al., 2013) and cerebellar atrophy being present in those that are classified as tremor-dominant (Benninger et al., 2009).

Whilst volumetric measures are robust, they are evidently not sensitive enough to inform on subtle changes in synaptic integrity that are observable at early stages of the disease. [^{11}C]UCB-J PET is a promising tool that has the potential to track early involvement of synaptic deficits (that is theorised to occur prior to neuronal loss), thus may be more informative about why the prognosis of these patients differs, which may be related to a differential pattern of synaptic density loss. As outlined in chapter 5, evaluating the spatial distribution pattern of [^{11}C]UCB-J with the pre-morbid distribution of neurochemical markers provides neurophysiological relevance to the observable pattern of synaptic density alterations. Therefore, this may further our understanding as to why these subtypes differ by assessing how the distribution of pre-existing neurotransmitter systems may be mediating the pattern of distribution of synaptic pathology within each of these subtypes. This has the potential to contribute to our understanding of which neurotransmitter systems are more implicated in one subtype than another, which could eventually lead to differential and more personalised management of these patients. Furthermore, by using healthy control-derived neurotransmitter templates, multiple neurochemical markers can be assessed, which would not be feasible to do in each participant

given the annual radiation dose constraint, which is 10mSv for healthy controls. Even if one was to design a longitudinal study, it would be feasible to do as only one [^{11}C]UCB-J PET scan would be needed (along with a T1-weighted MRI), which would be valuable in understanding the way in which the relationship between neurophysiological mechanisms and synaptic density evolves over the course of the disease that leads to the differential prognosis of these subtypes. This would also be particularly significant for patient stratification in clinical trials.

Of great potential is the objective identification of early manifestations of the disease, particularly those that predate the onset of defining motor symptoms. [^{11}C]UCB-J PET holds the potential to serve as such a biomarker, particularly since synaptic density was found to be reduced in at early stages of the disease and may be sensitive enough to capture synaptic deficits. Given that the onset of PD can commence decades before motor symptoms manifest, where patients experience a range of non-motor symptoms, performing [^{11}C]UCB-J PET imaging in patients with prodromal PD, for example those with hyposmia or RBD, may provide some insight into the synaptic deficits occurring early within the disease process, which may have predictive value for those who go onto develop PD. By assessing the relationship between the spatial distribution of SV2A and neurotransmitter systems, it may aid in the identification of the neurotransmitter systems implicated early within the disease, prior to the strong involvement of the dopaminergic system. Since not all individuals with the non-motor features typical of prodromal PD develop the disease, using a multimodal approach and identifying a spatial pattern of synaptic density alterations may have a superior predictor power of those who go onto develop the disease. Thus, this approach may aid in serving as a biomarker for the identification of individuals at risk for PD prior to symptom onset, which is an ideal group to trial disease-modifying therapies. This notion is also applicable to individuals with a highly penetrant genetic mutation, such as *SNCA* or *LRRK2*, especially since it is possible to identify these patients prior to the development of symptoms. This will also aid in our understanding about the potential differences and similarities

between the disease course of these patients, which could inevitably aid in the treatment strategies employed.

6.13 Summary

This thesis explored the extent of synaptic density reductions across Lewy body disease in conjunction with grey matter volumetric and perfusion alterations. The preliminary findings can be summarised as following:

1) Synaptic density was reduced in early, drug-naïve PD patients in the absence of grey matter volumetric reduction, providing an indication that [^{11}C]UCB-J PET can be employed as a marker of early synaptic deficits.
2) Synaptic density levels appeared to be 'normalised' in PD patients taking dopamine replacement therapy, indicative of a medication effect.
3) The magnitude of synaptic density loss was greater in Lewy body dementia, though the confounding effect of volume was limited. These findings are suggestive that [^{11}C]UCB-J PET may be a useful biomarker for disease progression.
4) The critical measures of synaptic loss, hypoperfusion and atrophy are sensitive to specific components of the disease process, thus combining them allows for a better understanding of the pathophysiology of PD and Lewy body dementia.
5) Assessing the relationship between the spatial distribution of synaptic density and the pre-morbid distribution of neurotransmitter markers provided insight into the neurophysiological mechanisms mediating synaptic density alterations in these groups. These were found to be distinct and specific for each stage of the disease, highlighting that the evolution of disease progression as reflected by synaptic density alterations is likely multifactorial, with distinct biological and physiological mechanisms involved at each stage.

This thesis provides some preliminary insight regarding synaptic density alterations in Lewy body diseases, and its relationship with atrophy and hypoperfusion. These findings also contribute, albeit in an indirect manner, to the utility of [^{11}C]UCB-J PET as a specific marker of synaptic density. Clinical validation studies of SV2A imaging are a necessity to pave the way for its utility in the clinical setting. Nonetheless, with the emergence of more readily available ^{18}F-labeled SV2A imaging probes, SV2A PET imaging may lead to new insights into the aetiology of neurodegenerative disorders, as well as treatment strategies. SV2A PET may also make important contributions to the drug discovery process by facilitating patient stratification, monitoring therapeutic responses, and monitoring the efficacy of drugs in clinical trials.

7 References

AARSLAND, D., ANDERSEN, K., LARSEN, J. P., LOLK, A. & KRAGH-SORENSEN, P. 2003. Prevalence and characteristics of dementia in Parkinson disease: an 8-year prospective study. *Arch Neurol,* 60**,** 387-92.

AARSLAND, D., ANDERSEN, K., LARSEN, J. P., LOLK, A., NIELSEN, H. & KRAGH-SORENSEN, P. 2001a. Risk of dementia in Parkinson's disease: a community-based, prospective study. *Neurology,* 56**,** 730-6.

AARSLAND, D., BALLARD, C., LARSEN, J. P. & MCKEITH, I. 2001b. A comparative study of psychiatric symptoms in dementia with Lewy bodies and Parkinson's disease with and without dementia. *Int J Geriatr Psychiatry,* 16**,** 528-36.

AARSLAND, D., BALLARD, C. G. & HALLIDAY, G. 2004. Are Parkinson's disease with dementia and dementia with Lewy bodies the same entity? *J Geriatr Psychiatry Neurol,* 17**,** 137-45.

AARSLAND, D., BRONNICK, K., WILLIAMS-GRAY, C., WEINTRAUB, D., MARDER, K., KULISEVSKY, J., BURN, D., BARONE, P., PAGONABARRAGA, J., ALLCOCK, L., SANTANGELO, G., FOLTYNIE, T., JANVIN, C., LARSEN, J. P., BARKER, R. A. & EMRE, M. 2010. Mild cognitive impairment in Parkinson disease: a multicenter pooled analysis. *Neurology,* 75**,** 1062-9.

AARSLAND, D., CREESE, B., POLITIS, M., CHAUDHURI, K. R., FFYTCHE, D. H., WEINTRAUB, D. & BALLARD, C. 2017. Cognitive decline in Parkinson disease. *Nat Rev Neurol,* 13**,** 217-231.

AARSLAND, D. & KURZ, M. W. 2010a. The epidemiology of dementia associated with Parkinson disease. *J Neurol Sci,* 289**,** 18-22.

AARSLAND, D. & KURZ, M. W. 2010b. The epidemiology of dementia associated with Parkinson's disease. *Brain Pathol,* 20**,** 633-9.

AARSLAND, D., KVALOY, J. T., ANDERSEN, K., LARSEN, J. P., TANG, M. X., LOLK, A., KRAGH-SORENSEN, P. & MARDER, K. 2007. The effect of age of onset of PD on risk of dementia. *J Neurol,* 254**,** 38-45.

AARSLAND, D., RONGVE, A., NORE, S. P., SKOGSETH, R., SKULSTAD, S., EHRT, U., HOPREKSTAD, D. & BALLARD, C. 2008. Frequency and case identification of dementia with Lewy bodies using the revised consensus criteria. *Dement Geriatr Cogn Disord,* 26**,** 445-52.

AARSLAND, D., ZACCAI, J. & BRAYNE, C. 2005. A systematic review of prevalence studies of dementia in Parkinson's disease. *Mov Disord,* 20**,** 1255-63.

ABELIOVICH, A. & GITLER, A. D. 2016. Defects in trafficking bridge Parkinson's disease pathology and genetics. *Nature,* 539**,** 207-216.

AGHOURIAN, M., LEGAULT-DENIS, C., SOUCY, J. P., ROSA-NETO, P., GAUTHIER, S., KOSTIKOV, A., GRAVEL, P. & BEDARD, M. A. 2017. Quantification of brain cholinergic denervation in Alzheimer's disease using PET imaging with [(18)F]-FEOBV. *Mol Psychiatry,* 22**,** 1531-1538.

AHLSKOG, J. E. 2003. Slowing Parkinson's disease progression: recent dopamine agonist trials. *Neurology,* 60**,** 381-9.

AIRAKSINEN, M. S., TITIEVSKY, A. & SAARMA, M. 1999. GDNF family neurotrophic factor signaling: four masters, one servant? *Mol Cell Neurosci,* 13**,** 313-25.

AKGOREN, N., FABRICIUS, M. & LAURITZEN, M. 1994. Importance of nitric oxide for local increases of blood flow in rat cerebellar cortex during electrical stimulation. *Proc Natl Acad Sci U S A,* 91**,** 5903-7.

AL-BACHARI, S., PARKES, L. M., VIDYASAGAR, R., HANBY, M. F., THARAKEN, V., LEROI, I. & EMSLEY, H. C. 2014. Arterial spin labelling reveals prolonged arterial arrival time in idiopathic Parkinson's disease. *Neuroimage Clin,* 6**,** 1-8.
AL-BACHARI, S., VIDYASAGAR, R., EMSLEY, H. C. & PARKES, L. M. 2017. Structural and physiological neurovascular changes in idiopathic Parkinson's disease and its clinical phenotypes. *J Cereb Blood Flow Metab,* 37**,** 3409-3421.
ALBIN, R. L., KOEPPE, R. A., BOHNEN, N. I., WERNETTE, K., KILBOURN, M. A. & FREY, K. A. 2008. Spared caudal brainstem SERT binding in early Parkinson's disease. *J Cereb Blood Flow Metab,* 28**,** 441-4.
ALBIN, R. L. & LEVENTHAL, D. K. 2017. The missing, the short, and the long: Levodopa responses and dopamine actions. *Ann Neurol,* 82**,** 4-19.
ALBIN, R. L., YOUNG, A. B. & PENNEY, J. B. 1989. The functional anatomy of basal ganglia disorders. *Trends Neurosci,* 12**,** 366-75.
ALCALAY, R. N., CACCAPPOLO, E., MEJIA-SANTANA, H., TANG, M. X., ROSADO, L., ROSS, B. M., VERBITSKY, M., KISSELEV, S., LOUIS, E. D., COMELLA, C., COLCHER, A., JENNINGS, D., NANCE, M. A., BRESSMAN, S. B., SCOTT, W. K., TANNER, C., MICKEL, S., ANDREWS, H., WATERS, C., FAHN, S., COTE, L., FRUCHT, S., FORD, B., REZAK, M., NOVAK, K., FRIEDMAN, J. H., PFEIFFER, R., MARSH, L., HINER, B., SIDEROWF, A., OTTMAN, R., MARDER, K. & CLARK, L. N. 2010. Frequency of known mutations in early-onset Parkinson disease: implication for genetic counseling: the consortium on risk for early onset Parkinson disease study. *Arch Neurol,* 67**,** 1116-22.
ALEKSOVSKI, D., MILJKOVIC, D., BRAVI, D. & ANTONINI, A. 2018. Disease progression in Parkinson subtypes: the PPMI dataset. *Neurol Sci,* 39**,** 1971-1976.
ALEXANDER, G. E., CRUTCHER, M. D. & DELONG, M. R. 1990. Basal ganglia-thalamocortical circuits: parallel substrates for motor, oculomotor, "prefrontal" and "limbic" functions. *Prog Brain Res,* 85**,** 119-46.
ALEXANDER, G. E., DELONG, M. R. & STRICK, P. L. 1986. Parallel organization of functionally segregated circuits linking basal ganglia and cortex. *Annu Rev Neurosci,* 9**,** 357-81.
ALEXANDER-BLOCH, A., GIEDD, J. N. & BULLMORE, E. 2013a. Imaging structural co-variance between human brain regions. *Nat Rev Neurosci,* 14**,** 322-36.
ALEXANDER-BLOCH, A., RAZNAHAN, A., BULLMORE, E. & GIEDD, J. 2013b. The convergence of maturational change and structural covariance in human cortical networks. *J Neurosci,* 33**,** 2889-99.
ALTAR, C. A., CAI, N., BLIVEN, T., JUHASZ, M., CONNER, J. M., ACHESON, A. L., LINDSAY, R. M. & WIEGAND, S. J. 1997. Anterograde transport of brain-derived neurotrophic factor and its role in the brain. *Nature,* 389**,** 856-60.
ALTMANN, V., SCHUMACHER-SCHUH, A. F., RIECK, M., CALLEGARI-JACQUES, S. M., RIEDER, C. R. & HUTZ, M. H. 2016. Influence of genetic, biological and pharmacological factors on levodopa dose in Parkinson's disease. *Pharmacogenomics,* 17**,** 481-8.
ALVES, G., LARSEN, J. P., EMRE, M., WENTZEL-LARSEN, T. & AARSLAND, D. 2006. Changes in motor subtype and risk for incident dementia in Parkinson's disease. *Mov Disord,* 21**,** 1123-30.
ANDERSEN, K. B., HANSEN, A. K., DAMHOLDT, M. F., HORSAGER, J., SKJAERBAEK, C., GOTTRUP, H., KLIT, H., SCHACHT, A. C., DANIELSEN, E. H., BROOKS, D. J. & BORGHAMMER, P. 2021. Reduced Synaptic Density in Patients with Lewy Body Dementia: An [(11) C]UCB-J PET Imaging Study. *Mov Disord.*
ANDERSON, K. M., COLLINS, M. A., KONG, R., FANG, K., LI, J., HE, T., CHEKROUD, A. M., YEO, B. T. T. & HOLMES, A. J. 2020. Convergent molecular, cellular, and

cortical neuroimaging signatures of major depressive disorder. *Proc Natl Acad Sci U S A,* 117**,** 25138-25149.
ANGOT, E., STEINER, J. A., LEMA TOME, C. M., EKSTROM, P., MATTSSON, B., BJORKLUND, A. & BRUNDIN, P. 2012. Alpha-synuclein cell-to-cell transfer and seeding in grafted dopaminergic neurons in vivo. *PLoS One,* 7**,** e39465.
ANTONINI, A., DE NOTARIS, R., BENTI, R., DE GASPARI, D. & PEZZOLI, G. 2001. Perfusion ECD/SPECT in the characterization of cognitive deficits in Parkinson's disease. *Neurol Sci,* 22**,** 45-6.
ANTONINI, A., SCHWARZ, J., OERTEL, W. H., POGARELL, O. & LEENDERS, K. L. 1997. Long-term changes of striatal dopamine D2 receptors in patients with Parkinson's disease: a study with positron emission tomography and [11C]raclopride. *Mov Disord,* 12**,** 33-8.
ARAI, R., KARASAWA, N., GEFFARD, M. & NAGATSU, I. 1995. L-DOPA is converted to dopamine in serotonergic fibers of the striatum of the rat: a double-labeling immunofluorescence study. *Neurosci Lett,* 195**,** 195-8.
ARCHER, T. 2016. Noradrenergic-Dopaminergic Interactions Due to DSP-4-MPTP Neurotoxin Treatments: Iron Connection. *Curr Top Behav Neurosci,* 29**,** 73-86.
ARDLEY, H. C., SCOTT, G. B., ROSE, S. A., TAN, N. G., MARKHAM, A. F. & ROBINSON, P. A. 2003. Inhibition of proteasomal activity causes inclusion formation in neuronal and non-neuronal cells overexpressing Parkin. *Mol Biol Cell,* 14**,** 4541-56.
ARENDT, T., BIGL, V., ARENDT, A. & TENNSTEDT, A. 1983. Loss of neurons in the nucleus basalis of Meynert in Alzheimer's disease, paralysis agitans and Korsakoff's Disease. *Acta Neuropathol,* 61**,** 101-8.
ARMSTRONG, M. J. & OKUN, M. S. 2020. Diagnosis and Treatment of Parkinson Disease: A Review. *JAMA,* 323**,** 548-560.
ARNATKEVICIUTE, A., FULCHER, B. D. & FORNITO, A. 2019. A practical guide to linking brain-wide gene expression and neuroimaging data. *Neuroimage,* 189**,** 353-367.
ASAN, L., FALFAN-MELGOZA, C., BERETTA, C. A., SACK, M., ZHENG, L., WEBER-FAHR, W., KUNER, T. & KNABBE, J. 2021. Cellular correlates of gray matter volume changes in magnetic resonance morphometry identified by two-photon microscopy. *Sci Rep,* 11**,** 4234.
ASHBURNER, J. 2007. A fast diffeomorphic image registration algorithm. *Neuroimage,* 38**,** 95-113.
ASHBURNER, J. & FRISTON, K. J. 2000. Voxel-based morphometry--the methods. *Neuroimage,* 11**,** 805-21.
ASHBURNER, J. & FRISTON, K. J. 2005. Unified segmentation. *Neuroimage,* 26**,** 839-51.
ASSOCIATION, A. P. 2013. *Diagnostic and statistical manual of mental disorders 5th Ed. (DSM-5)*, Arlington, VA: American Psychiatric Publishing.
ATTWELL, D., BUCHAN, A. M., CHARPAK, S., LAURITZEN, M., MACVICAR, B. A. & NEWMAN, E. A. 2010. Glial and neuronal control of brain blood flow. *Nature,* 468**,** 232-43.
ATTWELL, D. & IADECOLA, C. 2002. The neural basis of functional brain imaging signals. *Trends Neurosci,* 25**,** 621-5.
ATTWELL, D. & LAUGHLIN, S. B. 2001. An energy budget for signaling in the grey matter of the brain. *J Cereb Blood Flow Metab,* 21**,** 1133-45.
BA, F., OBAID, M., WIELER, M., CAMICIOLI, R. & MARTIN, W. R. 2016. Parkinson Disease: The Relationship Between Non-motor Symptoms and Motor Phenotype. *Can J Neurol Sci,* 43**,** 261-7.
BAE, J. R. & KIM, S. H. 2017. Synapses in neurodegenerative diseases. *BMB Rep,* 50**,** 237-246.
BAHRI, M. A., PLENEVAUX, A., AERTS, J., BASTIN, C., BECKER, G., MERCIER, J., VALADE, A., BUCHANAN, T., MESTDAGH, N., LEDOUX, D., SERET, A.,

LUXEN, A. & SALMON, E. 2017. Measuring brain synaptic vesicle protein 2A with positron emission tomography and [(18)F]UCB-H. *Alzheimers Dement (N Y),* 3**,** 481-486.
BAJIC, N., JENNER, P., BALLARD, C. G. & FRANCIS, P. T. 2012. Proteasome inhibition leads to early loss of synaptic proteins in neuronal culture. *J Neural Transm (Vienna),* 119**,** 1467-76.
BAJJALIEH, S. M., FRANTZ, G. D., WEIMANN, J. M., MCCONNELL, S. K. & SCHELLER, R. H. 1994. Differential expression of synaptic vesicle protein 2 (SV2) isoforms. *J Neurosci,* 14**,** 5223-35.
BAJJALIEH, S. M., PETERSON, K., LINIAL, M. & SCHELLER, R. H. 1993. Brain contains two forms of synaptic vesicle protein 2. *Proc Natl Acad Sci U S A,* 90**,** 2150-4.
BAK, L. K., SCHOUSBOE, A. & WAAGEPETERSEN, H. S. 2006. The glutamate/GABA-glutamine cycle: aspects of transport, neurotransmitter homeostasis and ammonia transfer. *J Neurochem,* 98**,** 641-53.
BALBI, M., GHOSH, M., LONGDEN, T. A., JATIVA VEGA, M., GESIERICH, B., HELLAL, F., LOURBOPOULOS, A., NELSON, M. T. & PLESNILA, N. 2015. Dysfunction of mouse cerebral arteries during early aging. *J Cereb Blood Flow Metab,* 35**,** 1445-53.
BALDO, B. A., DANIEL, R. A., BERRIDGE, C. W. & KELLEY, A. E. 2003. Overlapping distributions of orexin/hypocretin- and dopamine-beta-hydroxylase immunoreactive fibers in rat brain regions mediating arousal, motivation, and stress. *J Comp Neurol,* 464**,** 220-37.
BALLANGER, B., POISSON, A., BROUSSOLLE, E. & THOBOIS, S. 2012. Functional imaging of non-motor signs in Parkinson's disease. *J Neurol Sci,* 315**,** 9-14.
BALLANGER, B., STRAFELLA, A. P., VAN EIMEREN, T., ZUROWSKI, M., RUSJAN, P. M., HOULE, S. & FOX, S. H. 2010. Serotonin 2A receptors and visual hallucinations in Parkinson disease. *Arch Neurol,* 67**,** 416-21.
BALLARD, C., ZIABREVA, I., PERRY, R., LARSEN, J. P., O'BRIEN, J., MCKEITH, I., PERRY, E. & AARSLAND, D. 2006. Differences in neuropathologic characteristics across the Lewy body dementia spectrum. *Neurology,* 67**,** 1931-4.
BALOYANNIS, S. J., COSTA, V. & BALOYANNIS, I. S. 2006. Morphological alterations of the synapses in the locus coeruleus in Parkinson's disease. *J Neurol Sci,* 248**,** 35-41.
BARBER, T. R., KLEIN, J. C., MACKAY, C. E. & HU, M. T. M. 2017. Neuroimaging in pre-motor Parkinson's disease. *Neuroimage Clin,* 15**,** 215-227.
BARTHOLOME, O., VAN DEN ACKERVEKEN, P., SANCHEZ GIL, J., DE LA BRASSINNE BONARDEAUX, O., LEPRINCE, P., FRANZEN, R. & ROGISTER, B. 2017. Puzzling Out Synaptic Vesicle 2 Family Members Functions. *Front Mol Neurosci,* 10**,** 148.
BARZGARI, A., SOJKOVA, J., MARITZA DOWLING, N., POZORSKI, V., OKONKWO, O. C., STARKS, E. J., OH, J., THIESEN, F., WEY, A., NICHOLAS, C. R., JOHNSON, S. & GALLAGHER, C. L. 2019. Arterial spin labeling reveals relationships between resting cerebral perfusion and motor learning in Parkinson's disease. *Brain Imaging Behav,* 13**,** 577-587.
BAZARGANI, N. & ATTWELL, D. 2016. Astrocyte calcium signaling: the third wave. *Nat Neurosci,* 19**,** 182-9.
BEACH, T. G., ADLER, C. H., LUE, L., SUE, L. I., BACHALAKURI, J., HENRY-WATSON, J., SASSE, J., BOYER, S., SHIROHI, S., BROOKS, R., ESCHBACHER, J., WHITE, C. L., 3RD, AKIYAMA, H., CAVINESS, J., SHILL, H. A., CONNOR, D. J., SABBAGH, M. N., WALKER, D. G. & ARIZONA PARKINSON'S DISEASE, C. 2009. Unified staging system for Lewy body disorders: correlation with nigrostriatal degeneration, cognitive impairment and motor dysfunction. *Acta Neuropathol,* 117**,** 613-34.

BEAS, B. S., WRIGHT, B. J., SKIRZEWSKI, M., LENG, Y., HYUN, J. H., KOITA, O., RINGELBERG, N., KWON, H. B., BUONANNO, A. & PENZO, M. A. 2018. The locus coeruleus drives disinhibition in the midline thalamus via a dopaminergic mechanism. *Nat Neurosci,* 21**,** 963-973.

BELIVEAU, V., GANZ, M., FENG, L., OZENNE, B., HOJGAARD, L., FISHER, P. M., SVARER, C., GREVE, D. N. & KNUDSEN, G. M. 2017. A High-Resolution In Vivo Atlas of the Human Brain's Serotonin System. *J Neurosci,* 37**,** 120-128.

BELLOLI, S., MORARI, M., MURTAJ, V., VALTORTA, S., MORESCO, R. M. & GILARDI, M. C. 2020. Translation Imaging in Parkinson's Disease: Focus on Neuroinflammation. *Front Aging Neurosci,* 12**,** 152.

BELLUZZI, E., GREGGIO, E. & PICCOLI, G. 2012. Presynaptic dysfunction in Parkinson's disease: a focus on LRRK2. *Biochem Soc Trans,* 40**,** 1111-6.

BENNINGER, D. H., THEES, S., KOLLIAS, S. S., BASSETTI, C. L. & WALDVOGEL, D. 2009. Morphological differences in Parkinson's disease with and without rest tremor. *J Neurol,* 256**,** 256-63.

BERECZKI, E., FRANCIS, P. T., HOWLETT, D., PEREIRA, J. B., HOGLUND, K., BOGSTEDT, A., CEDAZO-MINGUEZ, A., BAEK, J. H., HORTOBAGYI, T., ATTEMS, J., BALLARD, C. & AARSLAND, D. 2016. Synaptic proteins predict cognitive decline in Alzheimer's disease and Lewy body dementia. *Alzheimers Dement,* 12**,** 1149-1158.

BERGERON, C., PETRUNKA, C., WEYER, L. & POLLANEN, M. S. 1996. Altered neurofilament expression does not contribute to Lewy body formation. *Am J Pathol,* 148**,** 267-72.

BERNAL-PACHECO, O., LIMOTAI, N., GO, C. L. & FERNANDEZ, H. H. 2012. Nonmotor manifestations in Parkinson disease. *Neurologist,* 18**,** 1-16.

BERNHEIMER, H., BIRKMAYER, W., HORNYKIEWICZ, O., JELLINGER, K. & SEITELBERGER, F. 1973. Brain dopamine and the syndromes of Parkinson and Huntington. Clinical, morphological and neurochemical correlations. *J Neurol Sci,* 20**,** 415-55.

BERRIDGE, C. W., STRATFORD, T. L., FOOTE, S. L. & KELLEY, A. E. 1997. Distribution of dopamine beta-hydroxylase-like immunoreactive fibers within the shell subregion of the nucleus accumbens. *Synapse,* 27**,** 230-41.

BERTHET, A., PORRAS, G., DOUDNIKOFF, E., STARK, H., CADOR, M., BEZARD, E. & BLOCH, B. 2009. Pharmacological analysis demonstrates dramatic alteration of D1 dopamine receptor neuronal distribution in the rat analog of L-DOPA-induced dyskinesia. *J Neurosci,* 29**,** 4829-35.

BERTRAND, E., LECHOWICZ, W., SZPAK, G. M. & DYMECKI, J. 1997. Qualitative and quantitative analysis of locus coeruleus neurons in Parkinson's disease. *Folia Neuropathol,* 35**,** 80-6.

BEYER, M. K., JANVIN, C. C., LARSEN, J. P. & AARSLAND, D. 2007. A magnetic resonance imaging study of patients with Parkinson's disease with mild cognitive impairment and dementia using voxel-based morphometry. *J Neurol Neurosurg Psychiatry,* 78**,** 254-9.

BIJU, K. C., SHEN, Q., HERNANDEZ, E. T., MADER, M. J. & CLARK, R. A. 2020. Reduced cerebral blood flow in an alpha-synuclein transgenic mouse model of Parkinson's disease. *J Cereb Blood Flow Metab,* 40**,** 2441-2453.

BILGIC, B., PFEFFERBAUM, A., ROHLFING, T., SULLIVAN, E. V. & ADALSTEINSSON, E. 2012. MRI estimates of brain iron concentration in normal aging using quantitative susceptibility mapping. *Neuroimage,* 59**,** 2625-35.

BINNEWIJZEND, M. A., KUIJER, J. P., VAN DER FLIER, W. M., BENEDICTUS, M. R., MOLLER, C. M., PIJNENBURG, Y. A., LEMSTRA, A. W., PRINS, N. D., WATTJES,

M. P., VAN BERCKEL, B. N., SCHELTENS, P. & BARKHOF, F. 2014. Distinct perfusion patterns in Alzheimer's disease, frontotemporal dementia and dementia with Lewy bodies. *Eur Radiol,* 24**,** 2326-33.

BIUNDO, R., CALABRESE, M., WEIS, L., FACCHINI, S., RICCHIERI, G., GALLO, P. & ANTONINI, A. 2013. Anatomical correlates of cognitive functions in early Parkinson's disease patients. *PLoS One,* 8**,** e64222.

BLANC, F., MAHMOUDI, R., JONVEAUX, T., GALMICHE, J., CHOPARD, G., CRETIN, B., DEMUYNCK, C., MARTIN-HUNYADI, C., PHILIPPI, N., SELLAL, F., MICHEL, J. M., TIO, G., STACKFLETH, M., VANDEL, P., MAGNIN, E., NOVELLA, J. L., KALTENBACH, G., BENETOS, A. & SAULEAU, E. A. 2017. Long-term cognitive outcome of Alzheimer's disease and dementia with Lewy bodies: dual disease is worse. *Alzheimers Res Ther,* 9**,** 47.

BLUMENSTOCK, S., RODRIGUES, E. F., PETERS, F., BLAZQUEZ-LLORCA, L., SCHMIDT, F., GIESE, A. & HERMS, J. 2017. Seeding and transgenic overexpression of alpha-synuclein triggers dendritic spine pathology in the neocortex. *EMBO Mol Med,* 9**,** 716-731.

BOERSMA, I., JONES, J., CARTER, J., BEKELMAN, D., MIYASAKI, J., KUTNER, J. & KLUGER, B. 2016. Parkinson disease patients' perspectives on palliative care needs: What are they telling us? *Neurol Clin Pract,* 6**,** 209-219.

BOEVE, B. F. 2013. Idiopathic REM sleep behaviour disorder in the development of Parkinson's disease. *Lancet Neurol,* 12**,** 469-82.

BOEVE, B. F., DICKSON, D. W., DUDA, J. E., FERMAN, T. J., GALASKO, D. R., GALVIN, J. E., GOLDMAN, J. G., GROWDON, J. H., HURTIG, H. I., KAUFER, D. I., KANTARCI, K., LEVERENZ, J. B., LIPPA, C. F., LOPEZ, O. L., MCKEITH, I. G., SINGLETON, A. B., TAYLOR, A., TSUANG, D., WEINTRAUB, D. & ZABETIAN, C. P. 2016. Arguing against the proposed definition changes of PD. *Mov Disord,* 31**,** 1619-1622.

BOHNEN, N. I., ALBIN, R. L., KOEPPE, R. A., WERNETTE, K. A., KILBOURN, M. R., MINOSHIMA, S. & FREY, K. A. 2006a. Positron emission tomography of monoaminergic vesicular binding in aging and Parkinson disease. *J Cereb Blood Flow Metab,* 26**,** 1198-212.

BOHNEN, N. I., ALBIN, R. L., MULLER, M. L., PETROU, M., KOTAGAL, V., KOEPPE, R. A., SCOTT, P. J. & FREY, K. A. 2015. Frequency of cholinergic and caudate nucleus dopaminergic deficits across the predemented cognitive spectrum of Parkinson disease and evidence of interaction effects. *JAMA Neurol,* 72**,** 194-200.

BOHNEN, N. I., FREY, K. A., STUDENSKI, S., KOTAGAL, V., KOEPPE, R. A., SCOTT, P. J., ALBIN, R. L. & MULLER, M. L. 2013. Gait speed in Parkinson disease correlates with cholinergic degeneration. *Neurology,* 81**,** 1611-6.

BOHNEN, N. I., KAUFER, D. I., HENDRICKSON, R., IVANCO, L. S., LOPRESTI, B. J., CONSTANTINE, G. M., MATHIS CH, A., DAVIS, J. G., MOORE, R. Y. & DEKOSKY, S. T. 2006b. Cognitive correlates of cortical cholinergic denervation in Parkinson's disease and parkinsonian dementia. *J Neurol,* 253**,** 242-7.

BOHNEN, N. I., KAUFER, D. I., IVANCO, L. S., LOPRESTI, B., KOEPPE, R. A., DAVIS, J. G., MATHIS, C. A., MOORE, R. Y. & DEKOSKY, S. T. 2003. Cortical cholinergic function is more severely affected in parkinsonian dementia than in Alzheimer disease: an in vivo positron emission tomographic study. *Arch Neurol,* 60**,** 1745-8.

BOHNEN, N. I., MULLER, M. & FREY, K. A. 2017. Molecular Imaging and Updated Diagnostic Criteria in Lewy Body Dementias. *Curr Neurol Neurosci Rep,* 17**,** 73.

BOHNEN, N. I., MULLER, M. L., KOEPPE, R. A., STUDENSKI, S. A., KILBOURN, M. A., FREY, K. A. & ALBIN, R. L. 2009. History of falls in Parkinson disease is associated with reduced cholinergic activity. *Neurology,* 73**,** 1670-6.

BOHNEN, N. I., MULLER, M. L., KOTAGAL, V., KOEPPE, R. A., KILBOURN, M. R., GILMAN, S., ALBIN, R. L. & FREY, K. A. 2012. Heterogeneity of cholinergic denervation in Parkinson's disease without dementia. *J Cereb Blood Flow Metab,* 32**,** 1609-17.

BOLAM, J. P. & PISSADAKI, E. K. 2012. Living on the edge with too many mouths to feed: why dopamine neurons die. *Mov Disord,* 27**,** 1478-83.

BORGHAMMER, P. 2012. Perfusion and metabolism imaging studies in Parkinson's disease. *Dan Med J,* 59**,** B4466.

BORGHAMMER, P., CHAKRAVARTY, M., JONSDOTTIR, K. Y., SATO, N., MATSUDA, H., ITO, K., ARAHATA, Y., KATO, T. & GJEDDE, A. 2010. Cortical hypometabolism and hypoperfusion in Parkinson's disease is extensive: probably even at early disease stages. *Brain Struct Funct,* 214**,** 303-17.

BORGHAMMER, P., CUMMING, P., AANERUD, J., FORSTER, S. & GJEDDE, A. 2009a. Subcortical elevation of metabolism in Parkinson's disease--a critical reappraisal in the context of global mean normalization. *Neuroimage,* 47**,** 1514-21.

BORGHAMMER, P., CUMMING, P., AANERUD, J. & GJEDDE, A. 2009b. Artefactual subcortical hyperperfusion in PET studies normalized to global mean: lessons from Parkinson's disease. *Neuroimage,* 45**,** 249-57.

BORGHAMMER, P., JONSDOTTIR, K. Y., CUMMING, P., OSTERGAARD, K., VANG, K., ASHKANIAN, M., VAFAEE, M., IVERSEN, P. & GJEDDE, A. 2008. Normalization in PET group comparison studies--the importance of a valid reference region. *Neuroimage,* 40**,** 529-540.

BOSSY-WETZEL, E., SCHWARZENBACHER, R. & LIPTON, S. A. 2004. Molecular pathways to neurodegeneration. *Nat Med,* 10 Suppl**,** S2-9.

BOSTROM, F., JONSSON, L., MINTHON, L. & LONDOS, E. 2007. Patients with dementia with lewy bodies have more impaired quality of life than patients with Alzheimer disease. *Alzheimer Dis Assoc Disord,* 21**,** 150-4.

BOUGEA, A., STEFANIS, L., PARASKEVAS, G. P., EMMANOUILIDOU, E., EFTHYMIOPOULOU, E., VEKRELIS, K. & KAPAKI, E. 2018. Neuropsychiatric symptoms and alpha-Synuclein profile of patients with Parkinson's disease dementia, dementia with Lewy bodies and Alzheimer's disease. *J Neurol,* 265**,** 2295-2301.

BOURNE, J. N. & HARRIS, K. M. 2008. Balancing structure and function at hippocampal dendritic spines. *Annu Rev Neurosci,* 31**,** 47-67.

BOYKEN, J., GRONBORG, M., RIEDEL, D., URLAUB, H., JAHN, R. & CHUA, J. J. 2013. Molecular profiling of synaptic vesicle docking sites reveals novel proteins but few differences between glutamatergic and GABAergic synapses. *Neuron,* 78**,** 285-97.

BOZZI, Y. & BORRELLI, E. 1999. Absence of the dopamine D2 receptor leads to a decreased expression of GDNF and NT-4 mRNAs in restricted brain areas. *Eur J Neurosci,* 11**,** 1275-84.

BRAAK, H., BOHL, J. R., MULLER, C. M., RUB, U., DE VOS, R. A. & DEL TREDICI, K. 2006. Stanley Fahn Lecture 2005: The staging procedure for the inclusion body pathology associated with sporadic Parkinson's disease reconsidered. *Mov Disord,* 21**,** 2042-51.

BRAAK, H., BRAAK, E., YILMAZER, D., DE VOS, R. A., JANSEN, E. N., BOHL, J. & JELLINGER, K. 1994. Amygdala pathology in Parkinson's disease. *Acta Neuropathol,* 88**,** 493-500.

BRAAK, H. & DEL TREDICI, K. 2008. Invited Article: Nervous system pathology in sporadic Parkinson disease. *Neurology,* 70**,** 1916-25.

BRAAK, H., DEL TREDICI, K., RUB, U., DE VOS, R. A., JANSEN STEUR, E. N. & BRAAK, E. 2003. Staging of brain pathology related to sporadic Parkinson's disease. *Neurobiol Aging,* 24**,** 197-211.

BRAAK, H., GHEBREMEDHIN, E., RUB, U., BRATZKE, H. & DEL TREDICI, K. 2004. Stages in the development of Parkinson's disease-related pathology. *Cell Tissue Res,* 318**,** 121-34.
BRAAK, H., SANDMANN-KEIL, D., GAI, W. & BRAAK, E. 1999. Extensive axonal Lewy neurites in Parkinson's disease: a novel pathological feature revealed by alpha-synuclein immunocytochemistry. *Neurosci Lett,* 265**,** 67-9.
BRAUN, A., FABBRINI, G., MOURADIAN, M. M., SERRATI, C., BARONE, P. & CHASE, T. N. 1987. Selective D-1 dopamine receptor agonist treatment of Parkinson's disease. *J Neural Transm,* 68**,** 41-50.
BRETIN, F., WARNOCK, G., BAHRI, M. A., AERTS, J., MESTDAGH, N., BUCHANAN, T., VALADE, A., MIEVIS, F., GIACOMELLI, F., LEMAIRE, C., LUXEN, A., SALMON, E., SERET, A. & PLENEVAUX, A. 2013. Preclinical radiation dosimetry for the novel SV2A radiotracer [18F]UCB-H. *EJNMMI Res,* 3**,** 35.
BREW, H. & ATTWELL, D. 1987. Electrogenic glutamate uptake is a major current carrier in the membrane of axolotl retinal glial cells. *Nature,* 327**,** 707-9.
BRIDI, J. C., BERECZKI, E., SMITH, S. K., POCAS, G. M., KOTTLER, B., DOMINGOS, P. M., ELLIOTT, C. J., AARSLAND, D. & HIRTH, F. 2021. Presynaptic accumulation of alpha-synuclein causes synaptopathy and progressive neurodegeneration in Drosophila. *Brain Commun,* 3**,** fcab049.
BRIDI, J. C. & HIRTH, F. 2018. Mechanisms of alpha-Synuclein Induced Synaptopathy in Parkinson's Disease. *Front Neurosci,* 12**,** 80.
BRUCK, A., AALTO, S., NURMI, E., VAHLBERG, T., BERGMAN, J. & RINNE, J. O. 2006. Striatal subregional 6-[18F]fluoro-L-dopa uptake in early Parkinson's disease: a two-year follow-up study. *Mov Disord,* 21**,** 958-63.
BRUCKE, T., KORNHUBER, J., ANGELBERGER, P., ASENBAUM, S., FRASSINE, H. & PODREKA, I. 1993. SPECT imaging of dopamine and serotonin transporters with [123I]beta-CIT. Binding kinetics in the human brain. *J Neural Transm Gen Sect,* 94**,** 137-46.
BUCHER, D. & MARDER, E. 2013. SnapShot: Neuromodulation. *Cell,* 155**,** 482-482 e1.
BUCKLEY, K. & KELLY, R. B. 1985. Identification of a transmembrane glycoprotein specific for secretory vesicles of neural and endocrine cells. *J Cell Biol,* 100**,** 1284-94.
BURBULLA, L. F., SONG, P., MAZZULLI, J. R., ZAMPESE, E., WONG, Y. C., JEON, S., SANTOS, D. P., BLANZ, J., OBERMAIER, C. D., STROJNY, C., SAVAS, J. N., KISKINIS, E., ZHUANG, X., KRUGER, R., SURMEIER, D. J. & KRAINC, D. 2017. Dopamine oxidation mediates mitochondrial and lysosomal dysfunction in Parkinson's disease. *Science,* 357**,** 1255-1261.
BURKE, R. E. & O'MALLEY, K. 2013. Axon degeneration in Parkinson's disease. *Exp Neurol,* 246**,** 72-83.
BURN, D. J., ROWAN, E. N., MINETT, T., SANDERS, J., MYINT, P., RICHARDSON, J., THOMAS, A., NEWBY, J., REID, J., O'BRIEN, J. T. & MCKEITH, I. G. 2003. Extrapyramidal features in Parkinson's disease with and without dementia and dementia with Lewy bodies: A cross-sectional comparative study. *Mov Disord,* 18**,** 884-9.
BURRE, J. 2015. The Synaptic Function of alpha-Synuclein. *J Parkinsons Dis,* 5**,** 699-713.
BURT, J. B., HELMER, M., SHINN, M., ANTICEVIC, A. & MURRAY, J. D. 2020. Generative modeling of brain maps with spatial autocorrelation. *Neuroimage,* 220**,** 117038.
BURTON, E. J., MCKEITH, I. G., BURN, D. J., WILLIAMS, E. D. & O'BRIEN, J. T. 2004. Cerebral atrophy in Parkinson's disease with and without dementia: a comparison with Alzheimer's disease, dementia with Lewy bodies and controls. *Brain,* 127**,** 791-800.
BUSCH, D. J., OLIPHINT, P. A., WALSH, R. B., BANKS, S. M., WOODS, W. S., GEORGE, J. M. & MORGAN, J. R. 2014. Acute increase of alpha-synuclein inhibits synaptic vesicle recycling evoked during intense stimulation. *Mol Biol Cell,* 25**,** 3926-41.

BUTER, T. C., VAN DEN HOUT, A., MATTHEWS, F. E., LARSEN, J. P., BRAYNE, C. & AARSLAND, D. 2008. Dementia and survival in Parkinson disease: a 12-year population study. *Neurology,* 70**,** 1017-22.
BUXTON, R. B. 2021. The thermodynamics of thinking: connections between neural activity, energy metabolism and blood flow. *Philos Trans R Soc Lond B Biol Sci,* 376**,** 20190624.
BUXTON, R. B., ULUDAG, K., DUBOWITZ, D. J. & LIU, T. T. 2004. Modeling the hemodynamic response to brain activation. *Neuroimage,* 23 Suppl 1**,** S220-33.
CABIN, D. E., SHIMAZU, K., MURPHY, D., COLE, N. B., GOTTSCHALK, W., MCILWAIN, K. L., ORRISON, B., CHEN, A., ELLIS, C. E., PAYLOR, R., LU, B. & NUSSBAUM, R. L. 2002. Synaptic vesicle depletion correlates with attenuated synaptic responses to prolonged repetitive stimulation in mice lacking alpha-synuclein. *J Neurosci,* 22**,** 8797-807.
CAGNIN, A., BUSSE, C., GARDINI, S., JELCIC, N., GUZZO, C., GNOATO, F., MITOLO, M., ERMANI, M. & CAFFARRA, P. 2015. Clinical and Cognitive Phenotype of Mild Cognitive Impairment Evolving to Dementia with Lewy Bodies. *Dement Geriatr Cogn Dis Extra,* 5**,** 442-9.
CAGNIN, A., GNOATO, F., JELCIC, N., FAVARETTO, S., ZARANTONELLO, G., ERMANI, M. & DAM, M. 2013. Clinical and cognitive correlates of visual hallucinations in dementia with Lewy bodies. *J Neurol Neurosurg Psychiatry,* 84**,** 505-10.
CAI, H., MANGNER, T. J., MUZIK, O., WANG, M. W., CHUGANI, D. C. & CHUGANI, H. T. 2014. Radiosynthesis of (11)C-Levetiracetam: A Potential Marker for PET Imaging of SV2A Expression. *ACS Med Chem Lett,* 5**,** 1152-5.
CAI, Z., LI, S., FINNEMA, S., LIN, S., ZHANG, W., HOLDEN, D., CARSON, R. E. & HUANG, Y. 2017. Imaging synaptic density with novel 18F-labeled radioligands for synaptic vesicle protein-2A (SV2A): synthesis and evaluation in nonhuman primates. *J Nucl Med,* 58.
CAKMAKLI, G. Y., VURAL, A., KOCAK, E. E., ELIBOL, B. & SAKA, E. 2018. Striatal Neurotransmitter Release-related Presynaptic Proteins in L-dopa Induced Dyskinesia in a Model of Parkinsonism. *Noro Psikiyatr Ars,* 55**,** 73-79.
CALABRESE, B., SHAKED, G. M., TABAREAN, I. V., BRAGA, J., KOO, E. H. & HALPAIN, S. 2007. Rapid, concurrent alterations in pre- and postsynaptic structure induced by naturally-secreted amyloid-beta protein. *Mol Cell Neurosci,* 35**,** 183-93.
CALABRESI, P., GHIGLIERI, V., MAZZOCCHETTI, P., CORBELLI, I. & PICCONI, B. 2015. Levodopa-induced plasticity: a double-edged sword in Parkinson's disease? *Philos Trans R Soc Lond B Biol Sci,* 370.
CALABRESI, P., GUBELLINI, P., CENTONZE, D., PICCONI, B., BERNARDI, G., CHERGUI, K., SVENNINGSSON, P., FIENBERG, A. A. & GREENGARD, P. 2000. Dopamine and cAMP-regulated phosphoprotein 32 kDa controls both striatal long-term depression and long-term potentiation, opposing forms of synaptic plasticity. *J Neurosci,* 20**,** 8443-51.
CALO, L., WEGRZYNOWICZ, M., SANTIVANEZ-PEREZ, J. & GRAZIA SPILLANTINI, M. 2016. Synaptic failure and alpha-synuclein. *Mov Disord,* 31**,** 169-77.
CAMARGO, E. E., SZABO, Z., LINKS, J. M., SOSTRE, S., DANNALS, R. F. & WAGNER, H. N., JR. 1992. The influence of biological and technical factors on the variability of global and regional brain metabolism of 2-[18F]fluoro-2-deoxy-D-glucose. *J Cereb Blood Flow Metab,* 12**,** 281-90.
CAMICIOLI, R., GEE, M., BOUCHARD, T. P., FISHER, N. J., HANSTOCK, C. C., EMERY, D. J. & MARTIN, W. R. 2009. Voxel-based morphometry reveals extra-nigral atrophy patterns associated with dopamine refractory cognitive and motor impairment in parkinsonism. *Parkinsonism Relat Disord,* 15**,** 187-95.

CANDY, J. M., PERRY, R. H., PERRY, E. K., IRVING, D., BLESSED, G., FAIRBAIRN, A. F. & TOMLINSON, B. E. 1983. Pathological changes in the nucleus of Meynert in Alzheimer's and Parkinson's diseases. *J Neurol Sci,* 59**,** 277-89.
CARTA, M., CARLSSON, T., KIRIK, D. & BJORKLUND, A. 2007. Dopamine released from 5-HT terminals is the cause of L-DOPA-induced dyskinesia in parkinsonian rats. *Brain,* 130**,** 1819-33.
CARTA, M., CARLSSON, T., MUNOZ, A., KIRIK, D. & BJORKLUND, A. 2008. Involvement of the serotonin system in L-dopa-induced dyskinesias. *Parkinsonism Relat Disord,* 14 Suppl 2**,** S154-8.
CASTELLANOS, G., FERNANDEZ-SEARA, M. A., LORENZO-BETANCOR, O., ORTEGA-CUBERO, S., PUIGVERT, M., URANGA, J., VIDORRETA, M., IRIGOYEN, J., LORENZO, E., MUNOZ-BARRUTIA, A., ORTIZ-DE-SOLORZANO, C., PASTOR, P. & PASTOR, M. A. 2015. Automated neuromelanin imaging as a diagnostic biomarker for Parkinson's disease. *Mov Disord,* 30**,** 945-52.
CAUGHEY, B. & LANSBURY, P. T. 2003. Protofibrils, pores, fibrils, and neurodegeneration: separating the responsible protein aggregates from the innocent bystanders. *Annu Rev Neurosci,* 26**,** 267-98.
CERASA, A., FASANO, A., MORGANTE, F., KOCH, G. & QUATTRONE, A. 2014. Maladaptive plasticity in levodopa-induced dyskinesias and tardive dyskinesias: old and new insights on the effects of dopamine receptor pharmacology. *Front Neurol,* 5**,** 49.
CERASA, A., MESSINA, D., PUGLIESE, P., MORELLI, M., LANZA, P., SALSONE, M., NOVELLINO, F., NICOLETTI, G., ARABIA, G. & QUATTRONE, A. 2011. Increased prefrontal volume in PD with levodopa-induced dyskinesias: a voxel-based morphometry study. *Mov Disord,* 26**,** 807-12.
CHABRAN, E., NOBLET, V., LOUREIRO DE SOUSA, P., DEMUYNCK, C., PHILIPPI, N., MUTTER, C., ANTHONY, P., MARTIN-HUNYADI, C., CRETIN, B. & BLANC, F. 2020. Changes in gray matter volume and functional connectivity in dementia with Lewy bodies compared to Alzheimer's disease and normal aging: implications for fluctuations. *Alzheimers Res Ther,* 12**,** 9.
CHAMBERS, N. E., MEADOWS, S. M., TAYLOR, A., SHEENA, E., LANZA, K., CONTI, M. M. & BISHOP, C. 2019. Effects of Muscarinic Acetylcholine m1 and m4 Receptor Blockade on Dyskinesia in the Hemi-Parkinsonian Rat. *Neuroscience,* 409**,** 180-194.
CHAN, C. S., GUZMAN, J. N., ILIJIC, E., MERCER, J. N., RICK, C., TKATCH, T., MEREDITH, G. E. & SURMEIER, D. J. 2007. 'Rejuvenation' protects neurons in mouse models of Parkinson's disease. *Nature,* 447**,** 1081-6.
CHAN-PALAY, V. & ASAN, E. 1989. Alterations in catecholamine neurons of the locus coeruleus in senile dementia of the Alzheimer type and in Parkinson's disease with and without dementia and depression. *J Comp Neurol,* 287**,** 373-92.
CHANDLER, D. J., GAO, W. J. & WATERHOUSE, B. D. 2014. Heterogeneous organization of the locus coeruleus projections to prefrontal and motor cortices. *Proc Natl Acad Sci U S A,* 111**,** 6816-21.
CHAPPELL, M. A., GROVES, A. R., MACINTOSH, B. J., DONAHUE, M. J., JEZZARD, P. & WOOLRICH, M. W. 2011. Partial volume correction of multiple inversion time arterial spin labeling MRI data. *Magn Reson Med,* 65**,** 1173-83.
CHAPPELL, M. A., GROVES, A. R., WHITCHER, B. & WOOLRICH, M. W. 2009. Variational Bayesian inference for a non-linear forward model. *IEEE Trans Signal Process,* 57**,** 223-236.
CHARROUD, C. & TURELLA, L. 2021. Subcortical grey matter changes associated with motor symptoms evaluated by the Unified Parkinson's disease Rating Scale (part III): A longitudinal study in Parkinson's disease. *Neuroimage Clin,* 31**,** 102745.

CHAUDHURI, K. R., HEALY, D. G., SCHAPIRA, A. H. & NATIONAL INSTITUTE FOR CLINICAL, E. 2006. Non-motor symptoms of Parkinson's disease: diagnosis and management. *Lancet Neurol,* 5**,** 235-45.

CHAUDHURI, K. R. & SCHAPIRA, A. H. 2009. Non-motor symptoms of Parkinson's disease: dopaminergic pathophysiology and treatment. *Lancet Neurol,* 8**,** 464-74.

CHEN, M. K., MECCA, A. P., NAGANAWA, M., FINNEMA, S. J., TOYONAGA, T., LIN, S. F., NAJAFZADEH, S., ROPCHAN, J., LU, Y., MCDONALD, J. W., MICHALAK, H. R., NABULSI, N. B., ARNSTEN, A. F. T., HUANG, Y., CARSON, R. E. & VAN DYCK, C. H. 2018. Assessing Synaptic Density in Alzheimer Disease With Synaptic Vesicle Glycoprotein 2A Positron Emission Tomographic Imaging. *JAMA Neurol,* 75**,** 1215-1224.

CHEN, M. K., MECCA, A. P., NAGANAWA, M., GALLEZOT, J. D., TOYONAGA, T., MONDAL, J., FINNEMA, S. J., LIN, S. F., O'DELL, R. S., MCDONALD, J. W., MICHALAK, H. R., VANDER WYK, B., NABULSI, N. B., HUANG, Y., ARNSTEN, A. F., VAN DYCK, C. H. & CARSON, R. E. 2021. Comparison of [(11)C]UCB-J and [(18)F]FDG PET in Alzheimer's disease: A tracer kinetic modeling study. *J Cereb Blood Flow Metab,* 41**,** 2395-2409.

CHEN, Y., WOLK, D. A., REDDIN, J. S., KORCZYKOWSKI, M., MARTINEZ, P. M., MUSIEK, E. S., NEWBERG, A. B., JULIN, P., ARNOLD, S. E., GREENBERG, J. H. & DETRE, J. A. 2011. Voxel-level comparison of arterial spin-labeled perfusion MRI and FDG-PET in Alzheimer disease. *Neurology,* 77**,** 1977-85.

CHENG, A. V., FERRIER, I. N., MORRIS, C. M., JABEEN, S., SAHGAL, A., MCKEITH, I. G., EDWARDSON, J. A., PERRY, R. H. & PERRY, E. K. 1991. Cortical serotonin-S2 receptor binding in Lewy body dementia, Alzheimer's and Parkinson's diseases. *J Neurol Sci,* 106**,** 50-5.

CHENG, H. C., ULANE, C. M. & BURKE, R. E. 2010. Clinical progression in Parkinson disease and the neurobiology of axons. *Ann Neurol,* 67**,** 715-25.

CHIU, W. H., DEPBOYLU, C., HERMANNS, G., MAURER, L., WINDOLPH, A., OERTEL, W. H., RIES, V. & HOGLINGER, G. U. 2015. Long-term treatment with L-DOPA or pramipexole affects adult neurogenesis and corresponding non-motor behavior in a mouse model of Parkinson's disease. *Neuropharmacology,* 95**,** 367-76.

CHOI, B. K., CHOI, M. G., KIM, J. Y., YANG, Y., LAI, Y., KWEON, D. H., LEE, N. K. & SHIN, Y. K. 2013. Large alpha-synuclein oligomers inhibit neuronal SNARE-mediated vesicle docking. *Proc Natl Acad Sci U S A,* 110**,** 4087-92.

CHOI, J. K., CHEN, Y. I., HAMEL, E. & JENKINS, B. G. 2006. Brain hemodynamic changes mediated by dopamine receptors: Role of the cerebral microvasculature in dopamine-mediated neurovascular coupling. *Neuroimage,* 30**,** 700-12.

CHU, Y., MORFINI, G. A., LANGHAMER, L. B., HE, Y., BRADY, S. T. & KORDOWER, J. H. 2012. Alterations in axonal transport motor proteins in sporadic and experimental Parkinson's disease. *Brain,* 135**,** 2058-73.

CHUNG, C. Y., KOPRICH, J. B., SIDDIQI, H. & ISACSON, O. 2009. Dynamic changes in presynaptic and axonal transport proteins combined with striatal neuroinflammation precede dopaminergic neuronal loss in a rat model of AAV alpha-synucleinopathy. *J Neurosci,* 29**,** 3365-73.

CLINE, E. N., BICCA, M. A., VIOLA, K. L. & KLEIN, W. L. 2018. The Amyloid-beta Oligomer Hypothesis: Beginning of the Third Decade. *J Alzheimers Dis,* 64**,** S567-S610.

COHEN, J. E., LEE, P. R., CHEN, S., LI, W. & FIELDS, R. D. 2011. MicroRNA regulation of homeostatic synaptic plasticity. *Proc Natl Acad Sci U S A,* 108**,** 11650-5.

COLE, J. H. & FRANKE, K. 2017. Predicting Age Using Neuroimaging: Innovative Brain Ageing Biomarkers. *Trends Neurosci,* 40**,** 681-690.

COLE, J. H., MARIONI, R. E., HARRIS, S. E. & DEARY, I. J. 2019. Brain age and other bodily 'ages': implications for neuropsychiatry. *Mol Psychiatry,* 24**,** 266-281.
COLLABORATORS, G. B. D. N. 2019. Global, regional, and national burden of neurological disorders, 1990-2016: a systematic analysis for the Global Burden of Disease Study 2016. *Lancet Neurol,* 18**,** 459-480.
COLLIVER, T. L., HESS, E. J., POTHOS, E. N., SULZER, D. & EWING, A. G. 2000. Quantitative and statistical analysis of the shape of amperometric spikes recorded from two populations of cells. *J Neurochem,* 74**,** 1086-97.
COLLOBY, S. J., MCPARLAND, S., O'BRIEN, J. T. & ATTEMS, J. 2012. Neuropathological correlates of dopaminergic imaging in Alzheimer's disease and Lewy body dementias. *Brain,* 135**,** 2798-808.
COLOM-CADENA, M., PEGUEROLES, J., HERRMANN, A. G., HENSTRIDGE, C. M., MUNOZ, L., QUEROL-VILASECA, M., MARTIN-PANIELLO, C. S., LUQUE-CABECERANS, J., CLARIMON, J., BELBIN, O., NUNEZ-LLAVES, R., BLESA, R., SMITH, C., MCKENZIE, C. A., FROSCH, M. P., ROE, A., FORTEA, J., ANDILLA, J., LOZA-ALVAREZ, P., GELPI, E., HYMAN, B. T., SPIRES-JONES, T. L. & LLEO, A. 2017. Synaptic phosphorylated alpha-synuclein in dementia with Lewy bodies. *Brain,* 140**,** 3204-3214.
COLOSIMO, C., HUGHES, A. J., KILFORD, L. & LEES, A. J. 2003. Lewy body cortical involvement may not always predict dementia in Parkinson's disease. *J Neurol Neurosurg Psychiatry,* 74**,** 852-6.
COMPTA, Y., PARKKINEN, L., KEMPSTER, P., SELIKHOVA, M., LASHLEY, T., HOLTON, J. L., LEES, A. J. & REVESZ, T. 2014. The significance of alpha-synuclein, amyloid-beta and tau pathologies in Parkinson's disease progression and related dementia. *Neurodegener Dis,* 13**,** 154-6.
COMPTA, Y., PARKKINEN, L., O'SULLIVAN, S. S., VANDROVCOVA, J., HOLTON, J. L., COLLINS, C., LASHLEY, T., KALLIS, C., WILLIAMS, D. R., DE SILVA, R., LEES, A. J. & REVESZ, T. 2011. Lewy- and Alzheimer-type pathologies in Parkinson's disease dementia: which is more important? *Brain,* 134**,** 1493-1505.
CONNOLLY, B. S. & LANG, A. E. 2014. Pharmacological treatment of Parkinson disease: a review. *JAMA,* 311**,** 1670-83.
CORREA-BASURTO, J., CUEVAS-HERNANDEZ, R. I., PHILLIPS-FARFAN, B. V., MARTINEZ-ARCHUNDIA, M., ROMO-MANCILLAS, A., RAMIREZ-SALINAS, G. L., PEREZ-GONZALEZ, O. A., TRUJILLO-FERRARA, J. & MENDOZA-TORREBLANCA, J. G. 2015. Identification of the antiepileptic racetam binding site in the synaptic vesicle protein 2A by molecular dynamics and docking simulations. *Front Cell Neurosci,* 9**,** 125.
CORTESE, G. P., ZHU, M., WILLIAMS, D., HEATH, S. & WAITES, C. L. 2016. Parkin Deficiency Reduces Hippocampal Glutamatergic Neurotransmission by Impairing AMPA Receptor Endocytosis. *J Neurosci,* 36**,** 12243-12258.
CRECELIUS, A., GOTZ, A., ARZBERGER, T., FROHLICH, T., ARNOLD, G. J., FERRER, I. & KRETZSCHMAR, H. A. 2008. Assessing quantitative post-mortem changes in the gray matter of the human frontal cortex proteome by 2-D DIGE. *Proteomics,* 8**,** 1276-91.
CROWDER, K. M., GUNTHER, J. M., JONES, T. A., HALE, B. D., ZHANG, H. Z., PETERSON, M. R., SCHELLER, R. H., CHAVKIN, C. & BAJJALIEH, S. M. 1999. Abnormal neurotransmission in mice lacking synaptic vesicle protein 2A (SV2A). *Proc Natl Acad Sci U S A,* 96**,** 15268-73.
CUI, X., LI, L., YU, L., XING, H., CHANG, H., ZHAO, L., QIAN, J., SONG, Q., ZHOU, S. & DONG, C. 2020. Gray Matter Atrophy in Parkinson's Disease and the Parkinsonian Variant of Multiple System Atrophy: A Combined ROI- and Voxel-Based Morphometric Study. *Clinics (Sao Paulo),* 75**,** e1505.

DALFO, E., BARRACHINA, M., ROSA, J. L., AMBROSIO, S. & FERRER, I. 2004. Abnormal alpha-synuclein interactions with rab3a and rabphilin in diffuse Lewy body disease. *Neurobiol Dis,* 16**,** 92-7.
DATLA, K. P., BLUNT, S. B. & DEXTER, D. T. 2001. Chronic L-DOPA administration is not toxic to the remaining dopaminergic nigrostriatal neurons, but instead may promote their functional recovery, in rats with partial 6-OHDA or FeCl(3) nigrostriatal lesions. *Mov Disord,* 16**,** 424-34.
DAUER, W. & PRZEDBORSKI, S. 2003. Parkinson's disease: mechanisms and models. *Neuron,* 39**,** 889-909.
DAUGHERTY, A. & RAZ, N. 2013. Age-related differences in iron content of subcortical nuclei observed in vivo: a meta-analysis. *Neuroimage,* 70**,** 113-21.
DAUTAN, D., HUERTA-OCAMPO, I., GUT, N. K., VALENCIA, M., KONDABOLU, K., KIM, Y., GERDJIKOV, T. V. & MENA-SEGOVIA, J. 2020. Cholinergic midbrain afferents modulate striatal circuits and shape encoding of action strategies. *Nat Commun,* 11**,** 1739.
DE CAMILLI, P., HARRIS, S. M., JR., HUTTNER, W. B. & GREENGARD, P. 1983. Synapsin I (Protein I), a nerve terminal-specific phosphoprotein. II. Its specific association with synaptic vesicles demonstrated by immunocytochemistry in agarose-embedded synaptosomes. *J Cell Biol,* 96**,** 1355-73.
DE DEURWAERDERE, P., DI GIOVANNI, G. & MILLAN, M. J. 2017. Expanding the repertoire of L-DOPA's actions: A comprehensive review of its functional neurochemistry. *Prog Neurobiol,* 151**,** 57-100.
DE LA MONTE, S. M., WELLS, S. E., HEDLEY-WHYTE, T. & GROWDON, J. H. 1989. Neuropathological distinction between Parkinson's dementia and Parkinson's plus Alzheimer's disease. *Ann Neurol,* 26**,** 309-20.
DE RIJK, M. C., LAUNER, L. J., BERGER, K., BRETELER, M. M., DARTIGUES, J. F., BALDERESCHI, M., FRATIGLIONI, L., LOBO, A., MARTINEZ-LAGE, J., TRENKWALDER, C. & HOFMAN, A. 2000. Prevalence of Parkinson's disease in Europe: A collaborative study of population-based cohorts. Neurologic Diseases in the Elderly Research Group. *Neurology,* 54**,** S21-3.
DEL TREDICI, K. & BRAAK, H. 2013. Dysfunction of the locus coeruleus-norepinephrine system and related circuitry in Parkinson's disease-related dementia. *J Neurol Neurosurg Psychiatry,* 84**,** 774-83.
DEL TREDICI, K. & BRAAK, H. 2016. Review: Sporadic Parkinson's disease: development and distribution of alpha-synuclein pathology. *Neuropathol Appl Neurobiol,* 42**,** 33-50.
DEL TREDICI, K., RUB, U., DE VOS, R. A., BOHL, J. R. & BRAAK, H. 2002. Where does parkinson disease pathology begin in the brain? *J Neuropathol Exp Neurol,* 61**,** 413-26.
DELAVILLE, C., DEURWAERDERE, P. D. & BENAZZOUZ, A. 2011. Noradrenaline and Parkinson's disease. *Front Syst Neurosci,* 5**,** 31.
DELFS, J. M., ZHU, Y., DRUHAN, J. P. & ASTON-JONES, G. S. 1998. Origin of noradrenergic afferents to the shell subregion of the nucleus accumbens: anterograde and retrograde tract-tracing studies in the rat. *Brain Res,* 806**,** 127-40.
DELLI PIZZI, S., FRANCIOTTI, R., TAYLOR, J. P., ESPOSITO, R., TARTARO, A., THOMAS, A., ONOFRJ, M. & BONANNI, L. 2015a. Structural Connectivity is Differently Altered in Dementia with Lewy Body and Alzheimer's Disease. *Front Aging Neurosci,* 7**,** 208.
DELLI PIZZI, S., FRANCIOTTI, R., TAYLOR, J. P., THOMAS, A., TARTARO, A., ONOFRJ, M. & BONANNI, L. 2015b. Thalamic Involvement in Fluctuating Cognition in Dementia with Lewy Bodies: Magnetic Resonance Evidences. *Cereb Cortex,* 25**,** 3682-9.

DELVA, A., MICHIELS, L., KOOLE, M., VAN LAERE, K. & VANDENBERGHE, W. 2021. Synaptic Damage and Its Clinical Correlates in People With Early Huntington Disease: A PET Study. *Neurology*.

DELVA, A., VAN WEEHAEGHE, D., KOOLE, M., VAN LAERE, K. & VANDENBERGHE, W. 2020. Loss of Presynaptic Terminal Integrity in the Substantia Nigra in Early Parkinson's Disease. *Mov Disord,* 35**,** 1977-1986.

DESIKAN, R. S., SEGONNE, F., FISCHL, B., QUINN, B. T., DICKERSON, B. C., BLACKER, D., BUCKNER, R. L., DALE, A. M., MAGUIRE, R. P., HYMAN, B. T., ALBERT, M. S. & KILLIANY, R. J. 2006. An automated labeling system for subdividing the human cerebral cortex on MRI scans into gyral based regions of interest. *Neuroimage,* 31**,** 968-80.

DESPLATS, P., LEE, H. J., BAE, E. J., PATRICK, C., ROCKENSTEIN, E., CREWS, L., SPENCER, B., MASLIAH, E. & LEE, S. J. 2009. Inclusion formation and neuronal cell death through neuron-to-neuron transmission of alpha-synuclein. *Proc Natl Acad Sci U S A,* 106**,** 13010-5.

DEUTCH, A. Y. 2006. Striatal plasticity in parkinsonism: dystrophic changes in medium spiny neurons and progression in Parkinson's disease. *J Neural Transm Suppl***,** 67-70.

DEUTCH, A. Y., COLBRAN, R. J. & WINDER, D. J. 2007. Striatal plasticity and medium spiny neuron dendritic remodeling in parkinsonism. *Parkinsonism Relat Disord,* 13 Suppl 3**,** S251-8.

DEVOTO, P., FLORE, G., PANI, L. & GESSA, G. L. 2001. Evidence for co-release of noradrenaline and dopamine from noradrenergic neurons in the cerebral cortex. *Mol Psychiatry,* 6**,** 657-64.

DEVOTO, P., FLORE, G., PIRA, L., LONGU, G. & GESSA, G. L. 2004. Alpha2-adrenoceptor mediated co-release of dopamine and noradrenaline from noradrenergic neurons in the cerebral cortex. *J Neurochem,* 88**,** 1003-9.

DEVOTO, P., FLORE, G., VACCA, G., PIRA, L., ARCA, A., CASU, M. A., PANI, L. & GESSA, G. L. 2003. Co-release of noradrenaline and dopamine from noradrenergic neurons in the cerebral cortex induced by clozapine, the prototype atypical antipsychotic. *Psychopharmacology (Berl),* 167**,** 79-84.

DICKSON, D. W., FUJISHIRO, H., ORR, C., DELLEDONNE, A., JOSEPHS, K. A., FRIGERIO, R., BURNETT, M., PARISI, J. E., KLOS, K. J. & AHLSKOG, J. E. 2009. Neuropathology of non-motor features of Parkinson disease. *Parkinsonism Relat Disord,* 15 Suppl 3**,** S1-5.

DIETERICH, D. C. & KREUTZ, M. R. 2016. Proteomics of the Synapse--A Quantitative Approach to Neuronal Plasticity. *Mol Cell Proteomics,* 15**,** 368-81.

DIEZ, I. & SEPULCRE, J. 2018. Neurogenetic profiles delineate large-scale connectivity dynamics of the human brain. *Nat Commun,* 9**,** 3876.

DIJKSTRA, A. A., INGRASSIA, A., DE MENEZES, R. X., VAN KESTEREN, R. E., ROZEMULLER, A. J., HEUTINK, P. & VAN DE BERG, W. D. 2015. Evidence for Immune Response, Axonal Dysfunction and Reduced Endocytosis in the Substantia Nigra in Early Stage Parkinson's Disease. *PLoS One,* 10**,** e0128651.

DING, Y. X., XIA, Y., JIAO, X. Y., DUAN, L., YU, J., WANG, X. & CHEN, L. W. 2011. The TrkB-positive dopaminergic neurons are less sensitive to MPTP insult in the substantia nigra of adult C57/BL mice. *Neurochem Res,* 36**,** 1759-66.

DIRNAGL, U., LINDAUER, U. & VILLRINGER, A. 1993. Role of nitric oxide in the coupling of cerebral blood flow to neuronal activation in rats. *Neurosci Lett,* 149**,** 43-6.

DODER, M., RABINER, E. A., TURJANSKI, N., LEES, A. J., BROOKS, D. J. & STUDY, C. W. P. 2003. Tremor in Parkinson's disease and serotonergic dysfunction: an 11C-WAY 100635 PET study. *Neurology,* 60**,** 601-5.

DONAGHY, P. C. & MCKEITH, I. G. 2014. The clinical characteristics of dementia with Lewy bodies and a consideration of prodromal diagnosis. *Alzheimers Res Ther,* 6**,** 46.
DONG, M., YEH, F., TEPP, W. H., DEAN, C., JOHNSON, E. A., JANZ, R. & CHAPMAN, E. R. 2006. SV2 is the protein receptor for botulinum neurotoxin A. *Science,* 312**,** 592-6.
DOPPLER, C. E. J., KINNERUP, M. B., BRUNE, C., FARRHER, E., BETTS, M., FEDOROVA, T. D., SCHALDEMOSE, J. L., KNUDSEN, K., ISMAIL, R., SEGER, A. D., HANSEN, A. K., STAER, K., FINK, G. R., BROOKS, D. J., NAHIMI, A., BORGHAMMER, P. & SOMMERAUER, M. 2021. Regional locus coeruleus degeneration is uncoupled from noradrenergic terminal loss in Parkinson's disease. *Brain,* 144**,** 2732-2744.
DORSEY, E. R., CONSTANTINESCU, R., THOMPSON, J. P., BIGLAN, K. M., HOLLOWAY, R. G., KIEBURTZ, K., MARSHALL, F. J., RAVINA, B. M., SCHIFITTO, G., SIDEROWF, A. & TANNER, C. M. 2007. Projected number of people with Parkinson disease in the most populous nations, 2005 through 2030. *Neurology,* 68**,** 384-6.
DORSEY, E. R., SHERER, T., OKUN, M. S. & BLOEM, B. R. 2018. The Emerging Evidence of the Parkinson Pandemic. *J Parkinsons Dis,* 8**,** S3-S8.
DREYER, J. K., HERRIK, K. F., BERG, R. W. & HOUNSGAARD, J. D. 2010. Influence of phasic and tonic dopamine release on receptor activation. *J Neurosci,* 30**,** 14273-83.
DUDA, J. E., GIASSON, B. I., MABON, M. E., LEE, V. M. & TROJANOWSKI, J. Q. 2002. Novel antibodies to synuclein show abundant striatal pathology in Lewy body diseases. *Ann Neurol,* 52**,** 205-10.
DUNN, A. R., STOUT, K. A., OZAWA, M., LOHR, K. M., HOFFMAN, C. A., BERNSTEIN, A. I., LI, Y., WANG, M., SGOBIO, C., SASTRY, N., CAI, H., CAUDLE, W. M. & MILLER, G. W. 2017. Synaptic vesicle glycoprotein 2C (SV2C) modulates dopamine release and is disrupted in Parkinson disease. *Proc Natl Acad Sci U S A,* 114**,** E2253-E2262.
DUNN, J. T., STONE, J., CLEIJ, M., MARSDEN, P. K., O'DOHERTY, M. & REED, L. J. 2009. Differential occupancy of striatal versus extrastriatal dopamine D2/D3 receptors by the typical antipsychotic Haloperidol in man measured using [18F]-Fallypride PET. *Neuroimage,* 47**,** S176.
EIDELBERG, D. 2009. Metabolic brain networks in neurodegenerative disorders: a functional imaging approach. *Trends Neurosci,* 32**,** 548-57.
EIDELBERG, D., MOELLER, J. R., ANTONINI, A., KAZUMATA, K., NAKAMURA, T., DHAWAN, V., SPETSIERIS, P., DELEON, D., BRESSMAN, S. B. & FAHN, S. 1998. Functional brain networks in DYT1 dystonia. *Ann Neurol,* 44**,** 303-12.
EL ATIFI-BOREL, M., BUGGIA-PREVOT, V., PLATET, N., BENABID, A. L., BERGER, F. & SGAMBATO-FAURE, V. 2009. De novo and long-term l-Dopa induce both common and distinct striatal gene profiles in the hemiparkinsonian rat. *Neurobiol Dis,* 34**,** 340-50.
EMRE, M., AARSLAND, D., BROWN, R., BURN, D. J., DUYCKAERTS, C., MIZUNO, Y., BROE, G. A., CUMMINGS, J., DICKSON, D. W., GAUTHIER, S., GOLDMAN, J., GOETZ, C., KORCZYN, A., LEES, A., LEVY, R., LITVAN, I., MCKEITH, I., OLANOW, W., POEWE, W., QUINN, N., SAMPAIO, C., TOLOSA, E. & DUBOIS, B. 2007. Clinical diagnostic criteria for dementia associated with Parkinson's disease. *Mov Disord,* 22**,** 1689-707; quiz 1837.
ENGELN, M., DE DEURWAERDERE, P., LI, Q., BEZARD, E. & FERNAGUT, P. O. 2015. Widespread Monoaminergic Dysregulation of Both Motor and Non-Motor Circuits in Parkinsonism and Dyskinesia. *Cereb Cortex,* 25**,** 2783-92.

ERLANDSSON, K., BUVAT, I., PRETORIUS, P. H., THOMAS, B. A. & HUTTON, B. F. 2012. A review of partial volume correction techniques for emission tomography and their applications in neurology, cardiology and oncology. *Phys Med Biol,* 57**,** R119-59.
ESPAY, A. J., LEWITT, P. A. & KAUFMANN, H. 2014. Norepinephrine deficiency in Parkinson's disease: the case for noradrenergic enhancement. *Mov Disord,* 29**,** 1710-9.
ESTRADA, S., LUBBERINK, M., THIBBLIN, A., SPRYCHA, M., BUCHANAN, T., MESTDAGH, N., KENDA, B., MERCIER, J., PROVINS, L., GILLARD, M., TYTGAT, D. & ANTONI, G. 2016. [(11)C]UCB-A, a novel PET tracer for synaptic vesicle protein 2A. *Nucl Med Biol,* 43**,** 325-32.
EVERETT, B. A., OQUENDO, M. A., ABI-DARGHAM, A., NOBLER, M. S., DEVANAND, D. P., LISANBY, S. H., MANN, J. J. & PARSEY, R. V. 2009. Safety of radial arterial catheterization in PET research subjects. *J Nucl Med,* 50**,** 1742.
EVERSFIELD, C. L. & ORTON, L. D. 2019. Auditory and visual hallucination prevalence in Parkinson's disease and dementia with Lewy bodies: a systematic review and meta-analysis. *Psychol Med,* 49**,** 2342-2353.
EXNER, N., LUTZ, A. K., HAASS, C. & WINKLHOFER, K. F. 2012. Mitochondrial dysfunction in Parkinson's disease: molecular mechanisms and pathophysiological consequences. *EMBO J,* 31**,** 3038-62.
FACTOR, S. A., MCDONALD, W. M. & GOLDSTEIN, F. C. 2017. The role of neurotransmitters in the development of Parkinson's disease-related psychosis. *Eur J Neurol,* 24**,** 1244-1254.
FAHN, S., LIBSCH, L. R. & CUTLER, R. W. 1971. Monoamines in the human neostriatum: topographic distribution in normals and in Parkinson's disease and their role in akinesia, rigidity, chorea, and tremor. *J Neurol Sci,* 14**,** 427-55.
FAHN, S., OAKES, D., SHOULSON, I., KIEBURTZ, K., RUDOLPH, A., LANG, A., OLANOW, C. W., TANNER, C., MAREK, K. & PARKINSON STUDY, G. 2004. Levodopa and the progression of Parkinson's disease. *N Engl J Med,* 351**,** 2498-508.
FALLON, J. H., KOZIELL, D. A. & MOORE, R. Y. 1978. Catecholamine innervation of the basal forebrain. II. Amygdala, suprarhinal cortex and entorhinal cortex. *J Comp Neurol,* 180**,** 509-32.
FANG, E., ANN, C. N., MARECHAL, B., LIM, J. X., TAN, S. Y. Z., LI, H., GAN, J., TAN, E. K. & CHAN, L. L. 2020. Differentiating Parkinson's disease motor subtypes using automated volume-based morphometry incorporating white matter and deep gray nuclear lesion load. *J Magn Reson Imaging,* 51**,** 748-756.
FANG, F., YANG, W., FLORIO, J. B., ROCKENSTEIN, E., SPENCER, B., ORAIN, X. M., DONG, S. X., LI, H., CHEN, X., SUNG, K., RISSMAN, R. A., MASLIAH, E., DING, J. & WU, C. 2017. Synuclein impairs trafficking and signaling of BDNF in a mouse model of Parkinson's disease. *Sci Rep,* 7**,** 3868.
FATHY, Y. Y., JONKER, A. J., OUDEJANS, E., DE JONG, F. J. J., VAN DAM, A. W., ROZEMULLER, A. J. M. & VAN DE BERG, W. D. J. 2019. Differential insular cortex subregional vulnerability to alpha-synuclein pathology in Parkinson's disease and dementia with Lewy bodies. *Neuropathol Appl Neurobiol,* 45**,** 262-277.
FAUL, F., ERDFELDER, E., BUCHNER, A. & LANG, A. G. 2009. Statistical power analyses using G*Power 3.1: tests for correlation and regression analyses. *Behav Res Methods,* 41**,** 1149-60.
FAZIO, P., SVENNINGSSON, P., CSELENYI, Z., HALLDIN, C., FARDE, L. & VARRONE, A. 2018. Nigrostriatal dopamine transporter availability in early Parkinson's disease. *Mov Disord,* 33**,** 592-599.
FEARNLEY, J. M. & LEES, A. J. 1991. Ageing and Parkinson's disease: substantia nigra regional selectivity. *Brain,* 114 (Pt 5)**,** 2283-301.

FENG, J., CAI, X., ZHAO, J. & YAN, Z. 2001. Serotonin receptors modulate GABA(A) receptor channels through activation of anchored protein kinase C in prefrontal cortical neurons. *J Neurosci,* 21**,** 6502-11.
FERMAN, T. J., BOEVE, B. F., SMITH, G. E., LIN, S. C., SILBER, M. H., PEDRAZA, O., WSZOLEK, Z., GRAFF-RADFORD, N. R., UITTI, R., VAN GERPEN, J., PAO, W., KNOPMAN, D., PANKRATZ, V. S., KANTARCI, K., BOOT, B., PARISI, J. E., DUGGER, B. N., FUJISHIRO, H., PETERSEN, R. C. & DICKSON, D. W. 2011. Inclusion of RBD improves the diagnostic classification of dementia with Lewy bodies. *Neurology,* 77**,** 875-82.
FERNAGUT, P. O., LI, Q., DOVERO, S., CHAN, P., WU, T., RAVENSCROFT, P., HILL, M., CHEN, Z. & BEZARD, E. 2010. Dopamine transporter binding is unaffected by L-DOPA administration in normal and MPTP-treated monkeys. *PLoS One,* 5**,** e14053.
FERNANDEZ-SEARA, M. A., MENGUAL, E., VIDORRETA, M., AZNAREZ-SANADO, M., LOAYZA, F. R., VILLAGRA, F., IRIGOYEN, J. & PASTOR, M. A. 2012. Cortical hypoperfusion in Parkinson's disease assessed using arterial spin labeled perfusion MRI. *Neuroimage,* 59**,** 2743-50.
FERRARIO, J. E., TARAVINI, I. R., MOURLEVAT, S., STEFANO, A., DELFINO, M. A., RAISMAN-VOZARI, R., MURER, M. G., RUBERG, M. & GERSHANIK, O. 2004. Differential gene expression induced by chronic levodopa treatment in the striatum of rats with lesions of the nigrostriatal system. *J Neurochem,* 90**,** 1348-58.
FERREIRA, M. & MASSANO, J. 2017. An updated review of Parkinson's disease genetics and clinicopathological correlations. *Acta Neurol Scand,* 135**,** 273-284.
FILIPPI, M., CANU, E., DONZUSO, G., STOJKOVIC, T., BASAIA, S., STANKOVIC, I., TOMIC, A., MARKOVIC, V., PETROVIC, I., STEFANOVA, E., KOSTIC, V. S. & AGOSTA, F. 2020. Tracking Cortical Changes Throughout Cognitive Decline in Parkinson's Disease. *Mov Disord,* 35**,** 1987-1998.
FILOSA, J. A., MORRISON, H. W., IDDINGS, J. A., DU, W. & KIM, K. J. 2016. Beyond neurovascular coupling, role of astrocytes in the regulation of vascular tone. *Neuroscience,* 323**,** 96-109.
FINN, J. T., WEIL, M., ARCHER, F., SIMAN, R., SRINIVASAN, A. & RAFF, M. C. 2000. Evidence that Wallerian degeneration and localized axon degeneration induced by local neurotrophin deprivation do not involve caspases. *J Neurosci,* 20**,** 1333-41.
FINNEMA, S. J., NABULSI, N. B., EID, T., DETYNIECKI, K., LIN, S. F., CHEN, M. K., DHAHER, R., MATUSKEY, D., BAUM, E., HOLDEN, D., SPENCER, D. D., MERCIER, J., HANNESTAD, J., HUANG, Y. & CARSON, R. E. 2016. Imaging synaptic density in the living human brain. *Sci Transl Med,* 8**,** 348ra96.
FINNEMA, S. J., NABULSI, N. B., MERCIER, J., LIN, S. F., CHEN, M. K., MATUSKEY, D., GALLEZOT, J. D., HENRY, S., HANNESTAD, J., HUANG, Y. & CARSON, R. E. 2018. Kinetic evaluation and test-retest reproducibility of [(11)C]UCB-J, a novel radioligand for positron emission tomography imaging of synaptic vesicle glycoprotein 2A in humans. *J Cereb Blood Flow Metab,* 38**,** 2041-2052.
FIRBANK, M. J., BURN, D. J., MCKEITH, I. G. & O'BRIEN, J. T. 2005. Longitudinal study of cerebral blood flow SPECT in Parkinson's disease with dementia, and dementia with Lewy bodies. *Int J Geriatr Psychiatry,* 20**,** 776-82.
FIRBANK, M. J., COLLOBY, S. J., BURN, D. J., MCKEITH, I. G. & O'BRIEN, J. T. 2003. Regional cerebral blood flow in Parkinson's disease with and without dementia. *Neuroimage,* 20**,** 1309-19.
FISCHL, B. & DALE, A. M. 2000. Measuring the thickness of the human cerebral cortex from magnetic resonance images. *Proc Natl Acad Sci U S A,* 97**,** 11050-5.

FITOUSSI, A., DELLU-HAGEDORN, F. & DE DEURWAERDERE, P. 2013. Monoamines tissue content analysis reveals restricted and site-specific correlations in brain regions involved in cognition. *Neuroscience,* 255**,** 233-45.
FONG, T. G., INOUYE, S. K., DAI, W., PRESS, D. Z. & ALSOP, D. C. 2011. Association cortex hypoperfusion in mild dementia with Lewy bodies: a potential indicator of cholinergic dysfunction? *Brain Imaging Behav,* 5**,** 25-35.
FORNAI, F., ALESSANDRI, M. G., TORRACCA, M. T., BASSI, L. & CORSINI, G. U. 1997. Effects of noradrenergic lesions on MPTP/MPP+ kinetics and MPTP-induced nigrostriatal dopamine depletions. *J Pharmacol Exp Ther,* 283**,** 100-7.
FORNAI, F., DI POGGIO, A. B., PELLEGRINI, A., RUGGIERI, S. & PAPARELLI, A. 2007. Noradrenaline in Parkinson's disease: from disease progression to current therapeutics. *Curr Med Chem,* 14**,** 2330-4.
FORSYTH, J. K., MENNIGEN, E., LIN, A., SUN, D., VAJDI, A., KUSHAN-WELLS, L., CHING, C. R. K., VILLALON-REINA, J. E., THOMPSON, P. M., Q, E. C. & BEARDEN, C. E. 2021. Prioritizing Genetic Contributors to Cortical Alterations in 22q11.2 Deletion Syndrome Using Imaging Transcriptomics. *Cereb Cortex,* 31**,** 3285-3298.
FORTEA, J., SALA-LLONCH, R., BARTRES-FAZ, D., LLADO, A., SOLE-PADULLES, C., BOSCH, B., ANTONELL, A., OLIVES, J., SANCHEZ-VALLE, R., MOLINUEVO, J. L. & RAMI, L. 2011. Cognitively preserved subjects with transitional cerebrospinal fluid ss-amyloid 1-42 values have thicker cortex in Alzheimer's disease vulnerable areas. *Biol Psychiatry,* 70**,** 183-90.
FRANCIS, P. T. & PERRY, E. K. 2007. Cholinergic and other neurotransmitter mechanisms in Parkinson's disease, Parkinson's disease dementia, and dementia with Lewy bodies. *Mov Disord,* 22 Suppl 17**,** S351-7.
FRANK, M. J., SAMANTA, J., MOUSTAFA, A. A. & SHERMAN, S. J. 2007. Hold your horses: impulsivity, deep brain stimulation, and medication in parkinsonism. *Science,* 318**,** 1309-12.
FRANK, R. A. & GRANT, S. G. 2017. Supramolecular organization of NMDA receptors and the postsynaptic density. *Curr Opin Neurobiol,* 45**,** 139-147.
FREI, K. & TRUONG, D. D. 2017. Hallucinations and the spectrum of psychosis in Parkinson's disease. *J Neurol Sci,* 374**,** 56-62.
FRIEDMAN, J. H. 2018. Dementia with Lewy Bodies and Parkinson Disease Dementia: It is the Same Disease! *Parkinsonism Relat Disord,* 46 Suppl 1**,** S6-S9.
FRIM, D. M., UHLER, T. A., GALPERN, W. R., BEAL, M. F., BREAKEFIELD, X. O. & ISACSON, O. 1994. Implanted fibroblasts genetically engineered to produce brain-derived neurotrophic factor prevent 1-methyl-4-phenylpyridinium toxicity to dopaminergic neurons in the rat. *Proc Natl Acad Sci U S A,* 91**,** 5104-8.
FROEMKE, R. C. 2015. Plasticity of cortical excitatory-inhibitory balance. *Annu Rev Neurosci,* 38**,** 195-219.
FROULA, J. M., HENDERSON, B. W., GONZALEZ, J. C., VADEN, J. H., MCLEAN, J. W., WU, Y., BANUMURTHY, G., OVERSTREET-WADICHE, L., HERSKOWITZ, J. H. & VOLPICELLI-DALEY, L. A. 2018. alpha-Synuclein fibril-induced paradoxical structural and functional defects in hippocampal neurons. *Acta Neuropathol Commun,* 6**,** 35.
FU, W. M., LIOU, H. C. & CHEN, Y. H. 1998. Nerve terminal currents induced by autoreception of acetylcholine release. *J Neurosci,* 18**,** 9954-61.
FUMAGALLI, F., RACAGNI, G., COLOMBO, E. & RIVA, M. A. 2003. BDNF gene expression is reduced in the frontal cortex of dopamine transporter knockout mice. *Mol Psychiatry,* 8**,** 898-9.
GALVAN, A. & WICHMANN, T. 2008. Pathophysiology of parkinsonism. *Clin Neurophysiol,* 119**,** 1459-74.

GALVIN, J. E., DUDA, J. E., KAUFER, D. I., LIPPA, C. F., TAYLOR, A. & ZARIT, S. H. 2010. Lewy body dementia: the caregiver experience of clinical care. *Parkinsonism Relat Disord,* 16**,** 388-92.
GALVIN, J. E., POLLACK, J. & MORRIS, J. C. 2006. Clinical phenotype of Parkinson disease dementia. *Neurology,* 67**,** 1605-11.
GALVIN, J. E., URYU, K., LEE, V. M. & TROJANOWSKI, J. Q. 1999. Axon pathology in Parkinson's disease and Lewy body dementia hippocampus contains alpha-, beta-, and gamma-synuclein. *Proc Natl Acad Sci U S A,* 96**,** 13450-5.
GAN-OR, Z., DION, P. A. & ROULEAU, G. A. 2015. Genetic perspective on the role of the autophagy-lysosome pathway in Parkinson disease. *Autophagy,* 11**,** 1443-57.
GARCIA-ESPARCIA, P., LOPEZ-GONZALEZ, I., GRAU-RIVERA, O., GARCIA-GARRIDO, M. F., KONETTI, A., LLORENS, F., ZAFAR, S., CARMONA, M., DEL RIO, J. A., ZERR, I., GELPI, E. & FERRER, I. 2017. Dementia with Lewy Bodies: Molecular Pathology in the Frontal Cortex in Typical and Rapidly Progressive Forms. *Front Neurol,* 8**,** 89.
GARCIA-GOMEZ, F. J., GARCIA-SOLIS, D., LUIS-SIMON, F. J., MARIN-OYAGA, V. A., CARRILLO, F., MIR, P. & VAZQUEZ-ALBERTINO, R. J. 2013. [Elaboration of the SPM template for the standardization of SPECT images with 123I-Ioflupane]. *Rev Esp Med Nucl Imagen Mol,* 32**,** 350-6.
GARCIA-REITBOCK, P., ANICHTCHIK, O., BELLUCCI, A., IOVINO, M., BALLINI, C., FINEBERG, E., GHETTI, B., DELLA CORTE, L., SPANO, P., TOFARIS, G. K., GOEDERT, M. & SPILLANTINI, M. G. 2010. SNARE protein redistribution and synaptic failure in a transgenic mouse model of Parkinson's disease. *Brain,* 133**,** 2032-44.
GASPAR, P., DUYCKAERTS, C., ALVAREZ, C., JAVOY-AGID, F. & BERGER, B. 1991. Alterations of dopaminergic and noradrenergic innervations in motor cortex in Parkinson's disease. *Ann Neurol,* 30**,** 365-74.
GASPAR, P. & GRAY, F. 1984. Dementia in idiopathic Parkinson's disease. A neuropathological study of 32 cases. *Acta Neuropathol,* 64**,** 43-52.
GERMAN, D. C., MANAYE, K. F., WHITE, C. L., 3RD, WOODWARD, D. J., MCINTIRE, D. D., SMITH, W. K., KALARIA, R. N. & MANN, D. M. 1992. Disease-specific patterns of locus coeruleus cell loss. *Ann Neurol,* 32**,** 667-76.
GIBB, W. R. 1989. Dementia and Parkinson's disease. *Br J Psychiatry,* 154**,** 596-614.
GIBB, W. R. & LEES, A. J. 1988. The relevance of the Lewy body to the pathogenesis of idiopathic Parkinson's disease. *J Neurol Neurosurg Psychiatry,* 51**,** 745-52.
GIGUERE, N., BURKE NANNI, S. & TRUDEAU, L. E. 2018. On Cell Loss and Selective Vulnerability of Neuronal Populations in Parkinson's Disease. *Front Neurol,* 9**,** 455.
GILL, S. S., PATEL, N. K., HOTTON, G. R., O'SULLIVAN, K., MCCARTER, R., BUNNAGE, M., BROOKS, D. J., SVENDSEN, C. N. & HEYWOOD, P. 2003. Direct brain infusion of glial cell line-derived neurotrophic factor in Parkinson disease. *Nat Med,* 9**,** 589-95.
GILLARD, M., CHATELAIN, P. & FUKS, B. 2006. Binding characteristics of levetiracetam to synaptic vesicle protein 2A (SV2A) in human brain and in CHO cells expressing the human recombinant protein. *Eur J Pharmacol,* 536**,** 102-8.
GJEDDE, A., REITH, J., DYVE, S., LEGER, G., GUTTMAN, M., DIKSIC, M., EVANS, A. & KUWABARA, H. 1991. Dopa decarboxylase activity of the living human brain. *Proc Natl Acad Sci U S A,* 88**,** 2721-5.
GOEDERT, M. 2001. Alpha-synuclein and neurodegenerative diseases. *Nat Rev Neurosci,* 2**,** 492-501.
GOEDERT, M., JAKES, R. & SPILLANTINI, M. G. 2017. The Synucleinopathies: Twenty Years On. *J Parkinsons Dis,* 7**,** S51-S69.

GOELZ, S. E., NESTLER, E. J., CHEHRAZI, B. & GREENGARD, P. 1981. Distribution of protein I in mammalian brain as determined by a detergent-based radioimmunoassay. *Proc Natl Acad Sci U S A,* 78**,** 2130-4.
GOETZ, C. G., EMRE, M. & DUBOIS, B. 2008. Parkinson's disease dementia: definitions, guidelines, and research perspectives in diagnosis. *Ann Neurol,* 64 Suppl 2**,** S81-92.
GOLDBERG, J. A., GUZMAN, J. N., ESTEP, C. M., ILIJIC, E., KONDAPALLI, J., SANCHEZ-PADILLA, J. & SURMEIER, D. J. 2012. Calcium entry induces mitochondrial oxidant stress in vagal neurons at risk in Parkinson's disease. *Nat Neurosci,* 15**,** 1414-21.
GOLDBERG, M. S., PISANI, A., HABURCAK, M., VORTHERMS, T. A., KITADA, T., COSTA, C., TONG, Y., MARTELLA, G., TSCHERTER, A., MARTINS, A., BERNARDI, G., ROTH, B. L., POTHOS, E. N., CALABRESI, P. & SHEN, J. 2005. Nigrostriatal dopaminergic deficits and hypokinesia caused by inactivation of the familial Parkinsonism-linked gene DJ-1. *Neuron,* 45**,** 489-96.
GOLDMANN GROSS, R., SIDEROWF, A. & HURTIG, H. I. 2008. Cognitive impairment in Parkinson's disease and dementia with lewy bodies: a spectrum of disease. *Neurosignals,* 16**,** 24-34.
GOMEZ-ISLA, T., GROWDON, W. B., MCNAMARA, M., NEWELL, K., GOMEZ-TORTOSA, E., HEDLEY-WHYTE, E. T. & HYMAN, B. T. 1999. Clinicopathologic correlates in temporal cortex in dementia with Lewy bodies. *Neurology,* 53**,** 2003-9.
GOMEZ-TORTOSA, E., IRIZARRY, M. C., GOMEZ-ISLA, T. & HYMAN, B. T. 2000. Clinical and neuropathological correlates of dementia with Lewy bodies. *Ann N Y Acad Sci,* 920**,** 9-15.
GOMEZ-TORTOSA, E., NEWELL, K., IRIZARRY, M. C., ALBERT, M., GROWDON, J. H. & HYMAN, B. T. 1999. Clinical and quantitative pathologic correlates of dementia with Lewy bodies. *Neurology,* 53**,** 1284-91.
GOMPERTS, S. N., LOCASCIO, J. J., MAKARETZ, S. J., SCHULTZ, A., CASO, C., VASDEV, N., SPERLING, R., GROWDON, J. H., DICKERSON, B. C. & JOHNSON, K. 2016a. Tau Positron Emission Tomographic Imaging in the Lewy Body Diseases. *JAMA Neurol,* 73**,** 1334-1341.
GOMPERTS, S. N., MARQUIE, M., LOCASCIO, J. J., BAYER, S., JOHNSON, K. A. & GROWDON, J. H. 2016b. PET Radioligands Reveal the Basis of Dementia in Parkinson's Disease and Dementia with Lewy Bodies. *Neurodegener Dis,* 16**,** 118-24.
GOTTSCHALL, P. E., AJMO, J. M., EAKIN, A. K., HOWELL, M. D., MEHTA, H. & BAILEY, L. A. 2010. Panel of synaptic protein ELISAs for evaluating neurological phenotype. *Exp Brain Res,* 201**,** 885-93.
GOUTAL, S., GUILLERMIER, M., BECKER, G., GAUDIN, M., BRAMOULLE, Y., LUXEN, A., LEMAIRE, C., PLENEVAUX, A., SALMON, E., HANTRAYE, P., BARRET, O. & VAN CAMP, N. 2021. The pharmacokinetics of [(18)F]UCB-H revisited in the healthy non-human primate brain. *EJNMMI Res,* 11**,** 36.
GRADE, M., HERNANDEZ TAMAMES, J. A., PIZZINI, F. B., ACHTEN, E., GOLAY, X. & SMITS, M. 2015. A neuroradiologist's guide to arterial spin labeling MRI in clinical practice. *Neuroradiology,* 57**,** 1181-202.
GRADINARU, V., MOGRI, M., THOMPSON, K. R., HENDERSON, J. M. & DEISSEROTH, K. 2009. Optical deconstruction of parkinsonian neural circuitry. *Science,* 324**,** 354-9.
GRATWICKE, J., JAHANSHAHI, M. & FOLTYNIE, T. 2015. Parkinson's disease dementia: a neural networks perspective. *Brain,* 138**,** 1454-76.
GRATWICKE, J., KAHAN, J., ZRINZO, L., HARIZ, M., LIMOUSIN, P., FOLTYNIE, T. & JAHANSHAHI, M. 2013. The nucleus basalis of Meynert: a new target for deep brain stimulation in dementia? *Neurosci Biobehav Rev,* 37**,** 2676-88.

GRAY, M. T. & WOULFE, J. M. 2015. Striatal blood-brain barrier permeability in Parkinson's disease. *J Cereb Blood Flow Metab,* 35**,** 747-50.
GREENLAND, J. C., WILLIAMS-GRAY, C. H. & BARKER, R. A. 2019. The clinical heterogeneity of Parkinson's disease and its therapeutic implications. *Eur J Neurosci,* 49**,** 328-338.
GREFFARD, S., VERNY, M., BONNET, A. M., BEINIS, J. Y., GALLINARI, C., MEAUME, S., PIETTE, F., HAUW, J. J. & DUYCKAERTS, C. 2006. Motor score of the Unified Parkinson Disease Rating Scale as a good predictor of Lewy body-associated neuronal loss in the substantia nigra. *Arch Neurol,* 63**,** 584-8.
GRONBORG, M., PAVLOS, N. J., BRUNK, I., CHUA, J. J., MUNSTER-WANDOWSKI, A., RIEDEL, D., AHNERT-HILGER, G., URLAUB, H. & JAHN, R. 2010. Quantitative comparison of glutamatergic and GABAergic synaptic vesicles unveils selectivity for few proteins including MAL2, a novel synaptic vesicle protein. *J Neurosci,* 30**,** 2-12.
GROSS, O. P. & VON GERSDORFF, H. 2016. Recycling at synapses. *Elife,* 5.
GUAN, J., PAVLOVIC, D., DALKIE, N., WALDVOGEL, H. J., O'CARROLL, S. J., GREEN, C. R. & NICHOLSON, L. F. 2013. Vascular degeneration in Parkinson's disease. *Brain Pathol,* 23**,** 154-64.
GUILLIN, O., DIAZ, J., CARROLL, P., GRIFFON, N., SCHWARTZ, J. C. & SOKOLOFF, P. 2001. BDNF controls dopamine D3 receptor expression and triggers behavioural sensitization. *Nature,* 411**,** 86-9.
GUNN, R. N., GUNN, S. R. & CUNNINGHAM, V. J. 2001. Positron emission tomography compartmental models. *J Cereb Blood Flow Metab,* 21**,** 635-52.
GUO, H., TANG, Z., YU, Y., XU, L., JIN, G. & ZHOU, J. 2002. Apomorphine induces trophic factors that support fetal rat mesencephalic dopaminergic neurons in cultures. *Eur J Neurosci,* 16**,** 1861-70.
GUO, J. T., CHEN, A. Q., KONG, Q., ZHU, H., MA, C. M. & QIN, C. 2008. Inhibition of vesicular monoamine transporter-2 activity in alpha-synuclein stably transfected SH-SY5Y cells. *Cell Mol Neurobiol,* 28**,** 35-47.
GUTTMAN, M., BOILEAU, I., WARSH, J., SAINT-CYR, J. A., GINOVART, N., MCCLUSKEY, T., HOULE, S., WILSON, A., MUNDO, E., RUSJAN, P., MEYER, J. & KISH, S. J. 2007. Brain serotonin transporter binding in non-depressed patients with Parkinson's disease. *Eur J Neurol,* 14**,** 523-8.
HAACKE, E. M., MIAO, Y., LIU, M., HABIB, C. A., KATKURI, Y., LIU, T., YANG, Z., LANG, Z., HU, J. & WU, J. 2010. Correlation of putative iron content as represented by changes in R2* and phase with age in deep gray matter of healthy adults. *J Magn Reson Imaging,* 32**,** 561-76.
HALE, M. W. & LOWRY, C. A. 2011. Functional topography of midbrain and pontine serotonergic systems: implications for synaptic regulation of serotonergic circuits. *Psychopharmacology (Berl),* 213**,** 243-64.
HALL, H., REYES, S., LANDECK, N., BYE, C., LEANZA, G., DOUBLE, K., THOMPSON, L., HALLIDAY, G. & KIRIK, D. 2014. Hippocampal Lewy pathology and cholinergic dysfunction are associated with dementia in Parkinson's disease. *Brain,* 137**,** 2493-508.
HALLIDAY, G. M., BLUMBERGS, P. C., COTTON, R. G., BLESSING, W. W. & GEFFEN, L. B. 1990. Loss of brainstem serotonin- and substance P-containing neurons in Parkinson's disease. *Brain Res,* 510**,** 104-7.
HALLIDAY, G. M., DEL TREDICI, K. & BRAAK, H. 2006. Critical appraisal of brain pathology staging related to presymptomatic and symptomatic cases of sporadic Parkinson's disease. *J Neural Transm Suppl***,** 99-103.
HALLIDAY, G. M., LEVERENZ, J. B., SCHNEIDER, J. S. & ADLER, C. H. 2014. The neurobiological basis of cognitive impairment in Parkinson's disease. *Mov Disord,* 29**,** 634-50.

HALLIDAY, G. M., SONG, Y. J. & HARDING, A. J. 2011. Striatal beta-amyloid in dementia with Lewy bodies but not Parkinson's disease. *J Neural Transm (Vienna),* 118**,** 713-9.
HAN, K., MIN, J., LEE, M., KANG, B. M., PARK, T., HAHN, J., YEI, J., LEE, J., WOO, J., LEE, C. J., KIM, S. G. & SUH, M. 2019. Neurovascular Coupling under Chronic Stress Is Modified by Altered GABAergic Interneuron Activity. *J Neurosci,* 39**,** 10081-10095.
HAN, S. K., MYTILINEOU, C. & COHEN, G. 1996. L-DOPA up-regulates glutathione and protects mesencephalic cultures against oxidative stress. *J Neurochem,* 66**,** 501-10.
HANGANU, A., BEDETTI, C., DEGROOT, C., MEJIA-CONSTAIN, B., LAFONTAINE, A. L., SOLAND, V., CHOUINARD, S., BRUNEAU, M. A., MELLAH, S., BELLEVILLE, S. & MONCHI, O. 2014. Mild cognitive impairment is linked with faster rate of cortical thinning in patients with Parkinson's disease longitudinally. *Brain,* 137**,** 1120-9.
HANSEN, A. K., DAMHOLDT, M. F., FEDOROVA, T. D., KNUDSEN, K., PARBO, P., ISMAIL, R., OSTERGAARD, K., BROOKS, D. J. & BORGHAMMER, P. 2017. In Vivo cortical tau in Parkinson's disease using 18F-AV-1451 positron emission tomography. *Mov Disord,* 32**,** 922-927.
HANSEN, C., ANGOT, E., BERGSTROM, A. L., STEINER, J. A., PIERI, L., PAUL, G., OUTEIRO, T. F., MELKI, R., KALLUNKI, P., FOG, K., LI, J. Y. & BRUNDIN, P. 2011. alpha-Synuclein propagates from mouse brain to grafted dopaminergic neurons and seeds aggregation in cultured human cells. *J Clin Invest,* 121**,** 715-25.
HANSEN, J. Y., MARKELLO, R. D., VOGEL, J. W., SEIDLITZ, J., BZDOK, D. & MISIC, B. 2021. Mapping gene transcription and neurocognition across human neocortex. *Nat Hum Behav,* 5**,** 1240-1250.
HANSEN, L., SALMON, D., GALASKO, D., MASLIAH, E., KATZMAN, R., DETERESA, R., THAL, L., PAY, M. M., HOFSTETTER, R., KLAUBER, M. & ET AL. 1990. The Lewy body variant of Alzheimer's disease: a clinical and pathologic entity. *Neurology,* 40**,** 1-8.
HANSEN, L. A., DANIEL, S. E., WILCOCK, G. K. & LOVE, S. 1998. Frontal cortical synaptophysin in Lewy body diseases: relation to Alzheimer's disease and dementia. *J Neurol Neurosurg Psychiatry,* 64**,** 653-6.
HARLEY, C. W. 1987. A role for norepinephrine in arousal, emotion and learning?: limbic modulation by norepinephrine and the Kety hypothesis. *Prog Neuropsychopharmacol Biol Psychiatry,* 11**,** 419-58.
HARRIS, J. J., JOLIVET, R. & ATTWELL, D. 2012. Synaptic energy use and supply. *Neuron,* 75**,** 762-77.
HASSAN, M. N. & THAKAR, J. H. 1988. Dopamine receptors in Parkinson's disease. *Prog Neuropsychopharmacol Biol Psychiatry,* 12**,** 173-82.
HAWKES, C. H., DEL TREDICI, K. & BRAAK, H. 2010. A timeline for Parkinson's disease. *Parkinsonism Relat Disord,* 16**,** 79-84.
HAWRYLYCZ, M. J., LEIN, E. S., GUILLOZET-BONGAARTS, A. L., SHEN, E. H., NG, L., MILLER, J. A., VAN DE LAGEMAAT, L. N., SMITH, K. A., EBBERT, A., RILEY, Z. L., ABAJIAN, C., BECKMANN, C. F., BERNARD, A., BERTAGNOLLI, D., BOE, A. F., CARTAGENA, P. M., CHAKRAVARTY, M. M., CHAPIN, M., CHONG, J., DALLEY, R. A., DAVID DALY, B., DANG, C., DATTA, S., DEE, N., DOLBEARE, T. A., FABER, V., FENG, D., FOWLER, D. R., GOLDY, J., GREGOR, B. W., HARADON, Z., HAYNOR, D. R., HOHMANN, J. G., HORVATH, S., HOWARD, R. E., JEROMIN, A., JOCHIM, J. M., KINNUNEN, M., LAU, C., LAZARZ, E. T., LEE, C., LEMON, T. A., LI, L., LI, Y., MORRIS, J. A., OVERLY, C. C., PARKER, P. D., PARRY, S. E., REDING, M., ROYALL, J. J., SCHULKIN, J., SEQUEIRA, P. A., SLAUGHTERBECK, C. R., SMITH, S. C., SODT, A. J., SUNKIN, S. M., SWANSON, B. E., VAWTER, M. P., WILLIAMS, D., WOHNOUTKA, P.,

ZIELKE, H. R., GESCHWIND, D. H., HOF, P. R., SMITH, S. M., KOCH, C., GRANT, S. G. N. & JONES, A. R. 2012. An anatomically comprehensive atlas of the adult human brain transcriptome. *Nature,* 489**,** 391-399.
HECKERS, S., GEULA, C. & MESULAM, M. M. 1992. Cholinergic innervation of the human thalamus: dual origin and differential nuclear distribution. *J Comp Neurol,* 325**,** 68-82.
HECKMAN, C. J., MOTTRAM, C., QUINLAN, K., THEISS, R. & SCHUSTER, J. 2009. Motoneuron excitability: the importance of neuromodulatory inputs. *Clin Neurophysiol,* 120**,** 2040-2054.
HEFTI, F., MELAMED, E. & WURTMAN, R. J. 1981. The site of dopamine formation in rat striatum after L-dopa administration. *J Pharmacol Exp Ther,* 217**,** 189-97.
HELY, M. A., REID, W. G., ADENA, M. A., HALLIDAY, G. M. & MORRIS, J. G. 2008. The Sydney multicenter study of Parkinson's disease: the inevitability of dementia at 20 years. *Mov Disord,* 23**,** 837-44.
HENRICH, M. T., GEIBL, F. F., LAKSHMINARASIMHAN, H., STEGMANN, A., GIASSON, B. I., MAO, X., DAWSON, V. L., DAWSON, T. M., OERTEL, W. H. & SURMEIER, D. J. 2020. Determinants of seeding and spreading of alpha-synuclein pathology in the brain. *Sci Adv,* 6.
HENSTRIDGE, C. M., PICKETT, E. & SPIRES-JONES, T. L. 2016. Synaptic pathology: A shared mechanism in neurological disease. *Ageing Res Rev,* 28**,** 72-84.
HEPP, D. H., VERGOOSSEN, D. L., HUISMAN, E., LEMSTRA, A. W., NETHERLANDS BRAIN, B., BERENDSE, H. W., ROZEMULLER, A. J., FONCKE, E. M. & VAN DE BERG, W. D. 2016. Distribution and Load of Amyloid-beta Pathology in Parkinson Disease and Dementia with Lewy Bodies. *J Neuropathol Exp Neurol,* 75**,** 936-945.
HEURLING, K., ASHTON, N. J., LEUZY, A., ZIMMER, E. R., BLENNOW, K., ZETTERBERG, H., ERIKSSON, J., LUBBERINK, M. & SCHOLL, M. 2019. Synaptic vesicle protein 2A as a potential biomarker in synaptopathies. *Mol Cell Neurosci,* 97**,** 34-42.
HIGLEY, M. J. & SABATINI, B. L. 2010. Competitive regulation of synaptic Ca2+ influx by D2 dopamine and A2A adenosine receptors. *Nat Neurosci,* 13**,** 958-66.
HILKER, R., SCHWEITZER, K., COBURGER, S., GHAEMI, M., WEISENBACH, S., JACOBS, A. H., RUDOLF, J., HERHOLZ, K. & HEISS, W. D. 2005a. Nonlinear progression of Parkinson disease as determined by serial positron emission tomographic imaging of striatal fluorodopa F 18 activity. *Arch Neurol,* 62**,** 378-82.
HILKER, R., THOMAS, A. V., KLEIN, J. C., WEISENBACH, S., KALBE, E., BURGHAUS, L., JACOBS, A. H., HERHOLZ, K. & HEISS, W. D. 2005b. Dementia in Parkinson disease: functional imaging of cholinergic and dopaminergic pathways. *Neurology,* 65**,** 1716-22.
HILTON, J., YOKOI, F., DANNALS, R. F., RAVERT, H. T., SZABO, Z. & WONG, D. F. 2000. Column-switching HPLC for the analysis of plasma in PET imaging studies. *Nucl Med Biol,* 27**,** 627-30.
HIRSCH, E., GRAYBIEL, A. M. & AGID, Y. A. 1988. Melanized dopaminergic neurons are differentially susceptible to degeneration in Parkinson's disease. *Nature,* 334**,** 345-8.
HOGAN, D. B., FIEST, K. M., ROBERTS, J. I., MAXWELL, C. J., DYKEMAN, J., PRINGSHEIM, T., STEEVES, T., SMITH, E. E., PEARSON, D. & JETTE, N. 2016. The Prevalence and Incidence of Dementia with Lewy Bodies: a Systematic Review. *Can J Neurol Sci,* 43 Suppl 1**,** S83-95.
HOGLINGER, G. U., RIZK, P., MURIEL, M. P., DUYCKAERTS, C., OERTEL, W. H., CAILLE, I. & HIRSCH, E. C. 2004. Dopamine depletion impairs precursor cell proliferation in Parkinson disease. *Nat Neurosci,* 7**,** 726-35.
HOHL, U., TIRABOSCHI, P., HANSEN, L. A., THAL, L. J. & COREY-BLOOM, J. 2000. Diagnostic accuracy of dementia with Lewy bodies. *Arch Neurol,* 57**,** 347-51.

HOLLAND, N., JONES, P. S., SAVULICH, G., WIGGINS, J. K., HONG, Y. T., FRYER, T. D., MANAVAKI, R., SEPHTON, S. M., BOROS, I., MALPETTI, M., HEZEMANS, F. H., AIGBIRHIO, F. I., COLES, J. P., O'BRIEN, J. & ROWE, J. B. 2020. Synaptic Loss in Primary Tauopathies Revealed by [(11) C]UCB-J Positron Emission Tomography. *Mov Disord,* 35**,** 1834-1842.

HOLLAND, N., MALPETTI, M., RITTMAN, T., MAK, E. E., PASSAMONTI, L., KAALUND, S. S., HEZEMANS, F. H., JONES, P. S., SAVULICH, G., HONG, Y. T., FRYER, T. D., AIGBIRHIO, F. I., O'BRIEN, J. T. & ROWE, J. B. 2021. Molecular pathology and synaptic loss in primary tauopathies: an 18F-AV-1451 and 11C-UCB-J PET study. *Brain.*

HOLMES, S. E., SCHEINOST, D., FINNEMA, S. J., NAGANAWA, M., DAVIS, M. T., DELLAGIOIA, N., NABULSI, N., MATUSKEY, D., ANGARITA, G. A., PIETRZAK, R. H., DUMAN, R. S., SANACORA, G., KRYSTAL, J. H., CARSON, R. E. & ESTERLIS, I. 2019. Lower synaptic density is associated with depression severity and network alterations. *Nat Commun,* 10**,** 1529.

HORNYKIEWICZ, O. 1998. Biochemical aspects of Parkinson's disease. *Neurology,* 51**,** S2-9.

HORNYKIEWICZ, O. & KISH, S. J. 1984. Neurochemical basis of dementia in Parkinson's disease. *Can J Neurol Sci,* 11**,** 185-90.

HORVATH, J., HERRMANN, F. R., BURKHARD, P. R., BOURAS, C. & KOVARI, E. 2013. Neuropathology of dementia in a large cohort of patients with Parkinson's disease. *Parkinsonism Relat Disord,* 19**,** 864-8; discussion 864.

HOSOKAI, Y., NISHIO, Y., HIRAYAMA, K., TAKEDA, A., ISHIOKA, T., SAWADA, Y., SUZUKI, K., ITOYAMA, Y., TAKAHASHI, S., FUKUDA, H. & MORI, E. 2009. Distinct patterns of regional cerebral glucose metabolism in Parkinson's disease with and without mild cognitive impairment. *Mov Disord,* 24**,** 854-62.

HOWARTH, C., GLEESON, P. & ATTWELL, D. 2012. Updated energy budgets for neural computation in the neocortex and cerebellum. *J Cereb Blood Flow Metab,* 32**,** 1222-32.

HOWARTH, C., MISHRA, A. & HALL, C. N. 2021. More than just summed neuronal activity: how multiple cell types shape the BOLD response. *Philos Trans R Soc Lond B Biol Sci,* 376**,** 20190630.

HOWELLS, D. W., PORRITT, M. J., WONG, J. Y., BATCHELOR, P. E., KALNINS, R., HUGHES, A. J. & DONNAN, G. A. 2000. Reduced BDNF mRNA expression in the Parkinson's disease substantia nigra. *Exp Neurol,* 166**,** 127-35.

HOWLETT, D. R., WHITFIELD, D., JOHNSON, M., ATTEMS, J., O'BRIEN, J. T., AARSLAND, D., LAI, M. K., LEE, J. H., CHEN, C., BALLARD, C., HORTOBAGYI, T. & FRANCIS, P. T. 2015. Regional Multiple Pathology Scores Are Associated with Cognitive Decline in Lewy Body Dementias. *Brain Pathol,* 25**,** 401-8.

HSIAO, I. T., WENG, Y. H., HSIEH, C. J., LIN, W. Y., WEY, S. P., KUNG, M. P., YEN, T. C., LU, C. S. & LIN, K. J. 2014. Correlation of Parkinson disease severity and 18F-DTBZ positron emission tomography. *JAMA Neurol,* 71**,** 758-66.

HUANG, C., MATTIS, P., PERRINE, K., BROWN, N., DHAWAN, V. & EIDELBERG, D. 2008. Metabolic abnormalities associated with mild cognitive impairment in Parkinson disease. *Neurology,* 70**,** 1470-7.

HUANG, C., MATTIS, P., TANG, C., PERRINE, K., CARBON, M. & EIDELBERG, D. 2007. Metabolic brain networks associated with cognitive function in Parkinson's disease. *Neuroimage,* 34**,** 714-23.

HUANG, X., NG, S. Y., CHIA, N. S., ACHARYYA, S., SETIAWAN, F., LU, Z. H., NG, E., TAY, K. Y., AU, W. L., TAN, E. K. & TAN, L. C. 2018. Serum uric acid level and its association with motor subtypes and non-motor symptoms in early Parkinson's disease: PALS study. *Parkinsonism Relat Disord,* 55**,** 50-54.

HUGHES, P. E., ALEXI, T., WALTON, M., WILLIAMS, C. E., DRAGUNOW, M., CLARK, R. G. & GLUCKMAN, P. D. 1999. Activity and injury-dependent expression of inducible transcription factors, growth factors and apoptosis-related genes within the central nervous system. *Prog Neurobiol,* 57**,** 421-50.

HUNG, G. U., CHIU, P. Y. & MATSUDA, H. 2018. The difference of regional cerebral perfusion between dementia with Lewy bodies and Parkinson's disease dementia. *J Nucl Med,* 59**,** 1659.

HUNN, B. H., CRAGG, S. J., BOLAM, J. P., SPILLANTINI, M. G. & WADE-MARTINS, R. 2015. Impaired intracellular trafficking defines early Parkinson's disease. *Trends Neurosci,* 38**,** 178-88.

HUOT, P., JOHNSTON, T. H., DARR, T., HAZRATI, L. N., VISANJI, N. P., PIRES, D., BROTCHIE, J. M. & FOX, S. H. 2010. Increased 5-HT2A receptors in the temporal cortex of parkinsonian patients with visual hallucinations. *Mov Disord,* 25**,** 1399-408.

HUOT, P., JOHNSTON, T. H., WINKELMOLEN, L., FOX, S. H. & BROTCHIE, J. M. 2012. 5-HT2A receptor levels increase in MPTP-lesioned macaques treated chronically with L-DOPA. *Neurobiol Aging,* 33**,** 194 e5-15.

HUOT, P. & PARENT, A. 2007. Dopaminergic neurons intrinsic to the striatum. *J Neurochem,* 101**,** 1441-7.

IADECOLA, C. 2004. Neurovascular regulation in the normal brain and in Alzheimer's disease. *Nat Rev Neurosci,* 5**,** 347-60.

IADECOLA, C. 2017. The Neurovascular Unit Coming of Age: A Journey through Neurovascular Coupling in Health and Disease. *Neuron,* 96**,** 17-42.

INGELSSON, M. 2016. Alpha-Synuclein Oligomers-Neurotoxic Molecules in Parkinson's Disease and Other Lewy Body Disorders. *Front Neurosci,* 10**,** 408.

INGHAM, C. A., HOOD, S. H. & ARBUTHNOTT, G. W. 1989. Spine density on neostriatal neurones changes with 6-hydroxydopamine lesions and with age. *Brain Res,* 503**,** 334-8.

INNIS, R. B., CUNNINGHAM, V. J., DELFORGE, J., FUJITA, M., GJEDDE, A., GUNN, R. N., HOLDEN, J., HOULE, S., HUANG, S. C., ICHISE, M., IIDA, H., ITO, H., KIMURA, Y., KOEPPE, R. A., KNUDSEN, G. M., KNUUTI, J., LAMMERTSMA, A. A., LARUELLE, M., LOGAN, J., MAGUIRE, R. P., MINTUN, M. A., MORRIS, E. D., PARSEY, R., PRICE, J. C., SLIFSTEIN, M., SOSSI, V., SUHARA, T., VOTAW, J. R., WONG, D. F. & CARSON, R. E. 2007. Consensus nomenclature for in vivo imaging of reversibly binding radioligands. *J Cereb Blood Flow Metab,* 27**,** 1533-9.

IRANZO, A., SANTAMARIA, J. & TOLOSA, E. 2016. Idiopathic rapid eye movement sleep behaviour disorder: diagnosis, management, and the need for neuroprotective interventions. *Lancet Neurol,* 15**,** 405-19.

IRWIN, D. J., GROSSMAN, M., WEINTRAUB, D., HURTIG, H. I., DUDA, J. E., XIE, S. X., LEE, E. B., VAN DEERLIN, V. M., LOPEZ, O. L., KOFLER, J. K., NELSON, P. T., JICHA, G. A., WOLTJER, R., QUINN, J. F., KAYE, J., LEVERENZ, J. B., TSUANG, D., LONGFELLOW, K., YEAROUT, D., KUKULL, W., KEENE, C. D., MONTINE, T. J., ZABETIAN, C. P. & TROJANOWSKI, J. Q. 2017. Neuropathological and genetic correlates of survival and dementia onset in synucleinopathies: a retrospective analysis. *Lancet Neurol,* 16**,** 55-65.

IRWIN, D. J. & HURTIG, H. I. 2018. The Contribution of Tau, Amyloid-Beta and Alpha-Synuclein Pathology to Dementia in Lewy Body Disorders. *J Alzheimers Dis Parkinsonism,* 8.

IRWIN, D. J., WHITE, M. T., TOLEDO, J. B., XIE, S. X., ROBINSON, J. L., VAN DEERLIN, V., LEE, V. M., LEVERENZ, J. B., MONTINE, T. J., DUDA, J. E., HURTIG, H. I. & TROJANOWSKI, J. Q. 2012. Neuropathologic substrates of Parkinson disease dementia. *Ann Neurol,* 72**,** 587-98.

IWAI, A., MASLIAH, E., YOSHIMOTO, M., GE, N., FLANAGAN, L., DE SILVA, H. A., KITTEL, A. & SAITOH, T. 1995. The precursor protein of non-A beta component of Alzheimer's disease amyloid is a presynaptic protein of the central nervous system. *Neuron,* 14**,** 467-75.
JACKSON, J., JAMBRINA, E., LI, J., MARSTON, H., MENZIES, F., PHILLIPS, K. & GILMOUR, G. 2019. Targeting the Synapse in Alzheimer's Disease. *Front Neurosci,* 13**,** 735.
JAKES, R., SPILLANTINI, M. G. & GOEDERT, M. 1994. Identification of two distinct synucleins from human brain. *FEBS Lett,* 345**,** 27-32.
JAMIESON, J. 2004. Analysis of covariance (ANCOVA) with difference scores. *Int J Psychophysiol,* 52**,** 277-83.
JANELIDZE, S., HERTZE, J., NAGGA, K., NILSSON, K., NILSSON, C., SWEDISH BIO, F. S. G., WENNSTROM, M., VAN WESTEN, D., BLENNOW, K., ZETTERBERG, H. & HANSSON, O. 2017. Increased blood-brain barrier permeability is associated with dementia and diabetes but not amyloid pathology or APOE genotype. *Neurobiol Aging,* 51**,** 104-112.
JANKOVIC, J. & KAPADIA, A. S. 2001. Functional decline in Parkinson disease. *Arch Neurol,* 58**,** 1611-5.
JANKOVIC, J., MCDERMOTT, M., CARTER, J., GAUTHIER, S., GOETZ, C., GOLBE, L., HUBER, S., KOLLER, W., OLANOW, C., SHOULSON, I. & ET AL. 1990. Variable expression of Parkinson's disease: a base-line analysis of the DATATOP cohort. The Parkinson Study Group. *Neurology,* 40**,** 1529-34.
JANKOWSKI, M. M., RONNQVIST, K. C., TSANOV, M., VANN, S. D., WRIGHT, N. F., ERICHSEN, J. T., AGGLETON, J. P. & O'MARA, S. M. 2013. The anterior thalamus provides a subcortical circuit supporting memory and spatial navigation. *Front Syst Neurosci,* 7**,** 45.
JANUSONIS, S. 2017. A receptor-based analysis of local ecosystems in the human brain. *BMC Neurosci,* 18**,** 33.
JANZ, R., GODA, Y., GEPPERT, M., MISSLER, M. & SUDHOF, T. C. 1999. SV2A and SV2B function as redundant Ca2+ regulators in neurotransmitter release. *Neuron,* 24**,** 1003-16.
JANZ, R. & SUDHOF, T. C. 1999. SV2C is a synaptic vesicle protein with an unusually restricted localization: anatomy of a synaptic vesicle protein family. *Neuroscience,* 94**,** 1279-90.
JAVOY-AGID, F., HIRSCH, E. C., DUMAS, S., DUYCKAERTS, C., MALLET, J. & AGID, Y. 1990. Decreased tyrosine hydroxylase messenger RNA in the surviving dopamine neurons of the substantia nigra in Parkinson's disease: an in situ hybridization study. *Neuroscience,* 38**,** 245-53.
JELLINGER, K. 1988. The pedunculopontine nucleus in Parkinson's disease, progressive supranuclear palsy and Alzheimer's disease. *J Neurol Neurosurg Psychiatry,* 51**,** 540-3.
JELLINGER, K. A. 2004. Influence of Alzheimer pathology on clinical diagnostic accuracy in dementia with Lewy bodies. *Neurology,* 62**,** 160; author reply 160.
JELLINGER, K. A. 2008. Re: In dementia with Lewy bodies, Braak stage determines phenotype, not Lewy body distribution. *Neurology,* 70**,** 407-8.
JELLINGER, K. A. 2009a. A critical evaluation of current staging of alpha-synuclein pathology in Lewy body disorders. *Biochim Biophys Acta,* 1792**,** 730-40.
JELLINGER, K. A. 2009b. Significance of brain lesions in Parkinson disease dementia and Lewy body dementia. *Front Neurol Neurosci,* 24**,** 114-125.
JELLINGER, K. A. & KORCZYN, A. D. 2018. Are dementia with Lewy bodies and Parkinson's disease dementia the same disease? *BMC Med,* 16**,** 34.

JELLINGER, K. A., WENNING, G. K. & SEPPI, K. 2007. Predictors of survival in dementia with lewy bodies and Parkinson dementia. *Neurodegener Dis,* 4**,** 428-30.
JENKINSON, M., BANNISTER, P., BRADY, M. & SMITH, S. 2002. Improved optimization for the robust and accurate linear registration and motion correction of brain images. *Neuroimage,* 17**,** 825-41.
JENKINSON, N. & BROWN, P. 2011. New insights into the relationship between dopamine, beta oscillations and motor function. *Trends Neurosci,* 34**,** 611-8.
JENNER, P., SHEEHY, M. & MARSDEN, C. D. 1983. Noradrenaline and 5-hydroxytryptamine modulation of brain dopamine function: implications for the treatment of Parkinson's disease. *Br J Clin Pharmacol,* 15 Suppl 2**,** 277S-289S.
JENNINGS, D., SIDEROWF, A., STERN, M., SEIBYL, J., EBERLY, S., OAKES, D., MAREK, K. & INVESTIGATORS, P. 2017. Conversion to Parkinson Disease in the PARS Hyposmic and Dopamine Transporter-Deficit Prodromal Cohort. *JAMA Neurol,* 74**,** 933-940.
JEONG, H. K., JI, K. M., MIN, K. J., CHOI, I., CHOI, D. J., JOU, I. & JOE, E. H. 2014. Astrogliosis is a possible player in preventing delayed neuronal death. *Mol Cells,* 37**,** 345-55.
JEONG, Y. J., YOON, H. J. & KANG, D. Y. 2017. Assessment of change in glucose metabolism in white matter of amyloid-positive patients with Alzheimer disease using F-18 FDG PET. *Medicine (Baltimore),* 96**,** e9042.
JI, Y., ZHANG, X., WANG, Z., QIN, W., LIU, H., XUE, K., TANG, J., XU, Q., ZHU, D., LIU, F. & YU, C. 2021. Genes associated with gray matter volume alterations in schizophrenia. *Neuroimage,* 225**,** 117526.
JIA, X., LIANG, P., LI, Y., SHI, L., WANG, D. & LI, K. 2015. Longitudinal Study of Gray Matter Changes in Parkinson Disease. *AJNR Am J Neuroradiol,* 36**,** 2219-26.
JIANG, L., KIM, M., CHODKOWSKI, B., DONAHUE, M. J., PEKAR, J. J., VAN ZIJL, P. C. & ALBERT, M. 2010. Reliability and reproducibility of perfusion MRI in cognitively normal subjects. *Magn Reson Imaging,* 28**,** 1283-9.
JIMENEZ-MARIN, A., DIEZ, I., LABAYRU, G., SISTIAGA, A., CABALLERO, M. C., ANDRES-BENITO, P., SEPULCRE, J., FERRER, I., LOPEZ DE MUNAIN, A. & CORTES, J. M. 2021. Transcriptional signatures of synaptic vesicle genes define myotonic dystrophy type I neurodegeneration. *Neuropathol Appl Neurobiol.*
JOHNSON, A. R., BUCKS, R. S., KANE, R. T., THOMAS, M. G., GASSON, N. & LOFTUS, A. M. 2016. Motor Subtype as a Predictor of Future Working Memory Performance in Idiopathic Parkinson's Disease. *PLoS One,* 11**,** e0152534.
JONES, T., RABINER, E. A. & COMPANY, P. E. T. R. A. 2012. The development, past achievements, and future directions of brain PET. *J Cereb Blood Flow Metab,* 32**,** 1426-54.
JOUTSA, J., GARDBERG, M., ROYTTA, M. & KAASINEN, V. 2014. Diagnostic accuracy of parkinsonism syndromes by general neurologists. *Parkinsonism Relat Disord,* 20**,** 840-4.
JUBAULT, T., GAGNON, J. F., KARAMA, S., PITTO, A., LAFONTAINE, A. L., EVANS, A. C. & MONCHI, O. 2011. Patterns of cortical thickness and surface area in early Parkinson's disease. *Neuroimage,* 55**,** 462-7.
KAHLE, P. J., NEUMANN, M., OZMEN, L., MULLER, V., JACOBSEN, H., SCHINDZIELORZ, A., OKOCHI, M., LEIMER, U., VAN DER PUTTEN, H., PROBST, A., KREMMER, E., KRETZSCHMAR, H. A. & HAASS, C. 2000. Subcellular localization of wild-type and Parkinson's disease-associated mutant alpha -synuclein in human and transgenic mouse brain. *J Neurosci,* 20**,** 6365-73.
KALAITZAKIS, M. E. & PEARCE, R. K. 2009. The morbid anatomy of dementia in Parkinson's disease. *Acta Neuropathol,* 118**,** 587-98.
KALIA, L. V. & LANG, A. E. 2015. Parkinson's disease. *Lancet,* 386**,** 896-912.

KALLER, S., RULLMANN, M., PATT, M., BECKER, G. A., LUTHARDT, J., GIRBARDT, J., MEYER, P. M., WERNER, P., BARTHEL, H., BRESCH, A., FRITZ, T. H., HESSE, S. & SABRI, O. 2017. Test-retest measurements of dopamine D1-type receptors using simultaneous PET/MRI imaging. *Eur J Nucl Med Mol Imaging,* 44**,** 1025-1032.

KAMAGATA, K., MOTOI, Y., ABE, O., SHIMOJI, K., HORI, M., NAKANISHI, A., SANO, T., KUWATSURU, R., AOKI, S. & HATTORI, N. 2012. White matter alteration of the cingulum in Parkinson disease with and without dementia: evaluation by diffusion tensor tract-specific analysis. *AJNR Am J Neuroradiol,* 33**,** 890-5.

KAMAGATA, K., MOTOI, Y., HORI, M., SUZUKI, M., NAKANISHI, A., SHIMOJI, K., KYOUGOKU, S., KUWATSURU, R., SASAI, K., ABE, O., MIZUNO, Y., AOKI, S. & HATTORI, N. 2011. Posterior hypoperfusion in Parkinson's disease with and without dementia measured with arterial spin labeling MRI. *J Magn Reson Imaging,* 33**,** 803-7.

KANG, Y. & KITAI, S. T. 1990. Electrophysiological properties of pedunculopontine neurons and their postsynaptic responses following stimulation of substantia nigra reticulata. *Brain Res,* 535**,** 79-95.

KANG, Y., MOZLEY, P. D., VERMA, A., SCHLYER, D., HENCHCLIFFE, C., GAUTHIER, S. A., CHIAO, P. C., HE, B., NIKOLOPOULOU, A., LOGAN, J., SULLIVAN, J. M., PRYOR, K. O., HESTERMAN, J., KOTHARI, P. J. & VALLABHAJOSULA, S. 2018. Noninvasive PK11195-PET Image Analysis Techniques Can Detect Abnormal Cerebral Microglial Activation in Parkinson's Disease. *J Neuroimaging,* 28**,** 496-505.

KANO, M., OHNO-SHOSAKU, T., HASHIMOTODANI, Y., UCHIGASHIMA, M. & WATANABE, M. 2009. Endocannabinoid-mediated control of synaptic transmission. *Physiol Rev,* 89**,** 309-80.

KASAMA, S., TACHIBANA, H., KAWABATA, K. & YOSHIKAWA, H. 2005. Cerebral blood flow in Parkinson's disease, dementia with Lewy bodies, and Alzheimer's disease according to three-dimensional stereotactic surface projection imaging. *Dement Geriatr Cogn Disord,* 19**,** 266-75.

KAUFMAN, A. C., SALAZAR, S. V., HAAS, L. T., YANG, J., KOSTYLEV, M. A., JENG, A. T., ROBINSON, S. A., GUNTHER, E. C., VAN DYCK, C. H., NYGAARD, H. B. & STRITTMATTER, S. M. 2015. Fyn inhibition rescues established memory and synapse loss in Alzheimer mice. *Ann Neurol,* 77**,** 953-71.

KEANE, P. C., KURZAWA, M., BLAIN, P. G. & MORRIS, C. M. 2011. Mitochondrial dysfunction in Parkinson's disease. *Parkinsons Dis,* 2011**,** 716871.

KEHAGIA, A. A., BARKER, R. A. & ROBBINS, T. W. 2013. Cognitive impairment in Parkinson's disease: the dual syndrome hypothesis. *Neurodegener Dis,* 11**,** 79-92.

KEIFER, O. P., JR., HURT, R. C., GUTMAN, D. A., KEILHOLZ, S. D., GOURLEY, S. L. & RESSLER, K. J. 2015. Voxel-based morphometry predicts shifts in dendritic spine density and morphology with auditory fear conditioning. *Nat Commun,* 6**,** 7582.

KEMPADOO, K. A., MOSHAROV, E. V., CHOI, S. J., SULZER, D. & KANDEL, E. R. 2016. Dopamine release from the locus coeruleus to the dorsal hippocampus promotes spatial learning and memory. *Proc Natl Acad Sci U S A,* 113**,** 14835-14840.

KEO, A., MAHFOUZ, A., INGRASSIA, A. M. T., MENEBOO, J. P., VILLENET, C., MUTEZ, E., COMPTDAER, T., LELIEVELDT, B. P. F., FIGEAC, M., CHARTIER-HARLIN, M. C., VAN DE BERG, W. D. J., VAN HILTEN, J. J. & REINDERS, M. J. T. 2020. Transcriptomic signatures of brain regional vulnerability to Parkinson's disease. *Commun Biol,* 3**,** 101.

KERENYI, L., RICAURTE, G. A., SCHRETLEN, D. J., MCCANN, U., VARGA, J., MATHEWS, W. B., RAVERT, H. T., DANNALS, R. F., HILTON, J., WONG, D. F. & SZABO, Z. 2003. Positron emission tomography of striatal serotonin transporters in Parkinson disease. *Arch Neurol,* 60**,** 1223-9.

KHALIQ, Z. M. & BEAN, B. P. 2010. Pacemaking in dopaminergic ventral tegmental area neurons: depolarizing drive from background and voltage-dependent sodium conductances. *J Neurosci,* 30**,** 7401-13.
KILBOURN, M. R., SHERMAN, P. & ABBOTT, L. C. 1998. Reduced MPTP neurotoxicity in striatum of the mutant mouse tottering. *Synapse,* 30**,** 205-10.
KIM, K. J., RAMIRO DIAZ, J., IDDINGS, J. A. & FILOSA, J. A. 2016. Vasculo-Neuronal Coupling: Retrograde Vascular Communication to Brain Neurons. *J Neurosci,* 36**,** 12624-12639.
KIM, M. A., LEE, H. S., LEE, B. Y. & WATERHOUSE, B. D. 2004. Reciprocal connections between subdivisions of the dorsal raphe and the nuclear core of the locus coeruleus in the rat. *Brain Res,* 1026**,** 56-67.
KIM, W. S., KAGEDAL, K. & HALLIDAY, G. M. 2014. Alpha-synuclein biology in Lewy body diseases. *Alzheimers Res Ther,* 6**,** 73.
KING, J. M., MUTHIAN, G., MACKEY, V., SMITH, M. & CHARLTON, C. 2011. L-Dihydroxyphenylalanine modulates the steady-state expression of mouse striatal tyrosine hydroxylase, aromatic L-amino acid decarboxylase, dopamine and its metabolites in an MPTP mouse model of Parkinson's disease. *Life Sci,* 89**,** 638-43.
KINGSBURY, A. E., BANDOPADHYAY, R., SILVEIRA-MORIYAMA, L., AYLING, H., KALLIS, C., STERLACCI, W., MAEIR, H., POEWE, W. & LEES, A. J. 2010. Brain stem pathology in Parkinson's disease: an evaluation of the Braak staging model. *Mov Disord,* 25**,** 2508-15.
KIRIK, D., ROSENBLAD, C., BURGER, C., LUNDBERG, C., JOHANSEN, T. E., MUZYCZKA, N., MANDEL, R. J. & BJORKLUND, A. 2002. Parkinson-like neurodegeneration induced by targeted overexpression of alpha-synuclein in the nigrostriatal system. *J Neurosci,* 22**,** 2780-91.
KISH, S. J., SHANNAK, K. & HORNYKIEWICZ, O. 1988. Uneven pattern of dopamine loss in the striatum of patients with idiopathic Parkinson's disease. Pathophysiologic and clinical implications. *N Engl J Med,* 318**,** 876-80.
KISH, S. J., TONG, J., HORNYKIEWICZ, O., RAJPUT, A., CHANG, L. J., GUTTMAN, M. & FURUKAWA, Y. 2008. Preferential loss of serotonin markers in caudate versus putamen in Parkinson's disease. *Brain,* 131**,** 120-31.
KISLER, K., NELSON, A. R., MONTAGNE, A. & ZLOKOVIC, B. V. 2017. Cerebral blood flow regulation and neurovascular dysfunction in Alzheimer disease. *Nat Rev Neurosci,* 18**,** 419-434.
KITADA, T., PISANI, A., KAROUANI, M., HABURCAK, M., MARTELLA, G., TSCHERTER, A., PLATANIA, P., WU, B., POTHOS, E. N. & SHEN, J. 2009. Impaired dopamine release and synaptic plasticity in the striatum of parkin-/- mice. *J Neurochem,* 110**,** 613-21.
KLAIPS, C. L., JAYARAJ, G. G. & HARTL, F. U. 2018. Pathways of cellular proteostasis in aging and disease. *J Cell Biol,* 217**,** 51-63.
KLEIN, C. & WESTENBERGER, A. 2012. Genetics of Parkinson's disease. *Cold Spring Harb Perspect Med,* 2**,** a008888.
KNAUS, P., BETZ, H. & REHM, H. 1986. Expression of synaptophysin during postnatal development of the mouse brain. *J Neurochem,* 47**,** 1302-4.
KOESTER, H. J. & JOHNSTON, D. 2005. Target cell-dependent normalization of transmitter release at neocortical synapses. *Science,* 308**,** 863-6.
KOPITO, R. R. 2000. Aggresomes, inclusion bodies and protein aggregation. *Trends Cell Biol,* 10**,** 524-30.
KORDOWER, J. H., CHU, Y., HAUSER, R. A., FREEMAN, T. B. & OLANOW, C. W. 2008a. Lewy body-like pathology in long-term embryonic nigral transplants in Parkinson's disease. *Nat Med,* 14**,** 504-6.

KORDOWER, J. H., CHU, Y., HAUSER, R. A., OLANOW, C. W. & FREEMAN, T. B. 2008b. Transplanted dopaminergic neurons develop PD pathologic changes: a second case report. *Mov Disord,* 23**,** 2303-6.
KORDOWER, J. H., OLANOW, C. W., DODIYA, H. B., CHU, Y., BEACH, T. G., ADLER, C. H., HALLIDAY, G. M. & BARTUS, R. T. 2013. Disease duration and the integrity of the nigrostriatal system in Parkinson's disease. *Brain,* 136**,** 2419-31.
KORTEKAAS, R., LEENDERS, K. L., VAN OOSTROM, J. C., VAALBURG, W., BART, J., WILLEMSEN, A. T. & HENDRIKSE, N. H. 2005. Blood-brain barrier dysfunction in parkinsonian midbrain in vivo. *Ann Neurol,* 57**,** 176-9.
KOUROUPI, G., TAOUFIK, E., VLACHOS, I. S., TSIORAS, K., ANTONIOU, N., PAPASTEFANAKI, F., CHRONI-TZARTOU, D., WRASIDLO, W., BOHL, D., STELLAS, D., POLITIS, P. K., VEKRELLIS, K., PAPADIMITRIOU, D., STEFANIS, L., BREGESTOVSKI, P., HATZIGEORGIOU, A. G., MASLIAH, E. & MATSAS, R. 2017. Defective synaptic connectivity and axonal neuropathology in a human iPSC-based model of familial Parkinson's disease. *Proc Natl Acad Sci U S A,* 114**,** E3679-E3688.
KRABBE, K., KARLSBORG, M., HANSEN, A., WERDELIN, L., MEHLSEN, J., LARSSON, H. B. & PAULSON, O. B. 2005. Increased intracranial volume in Parkinson's disease. *J Neurol Sci,* 239**,** 45-52.
KRAMBERGER, M. G., AUESTAD, B., GARCIA-PTACEK, S., ABDELNOUR, C., OLMO, J. G., WALKER, Z., LEMSTRA, A. W., LONDOS, E., BLANC, F., BONANNI, L., MCKEITH, I., WINBLAD, B., DE JONG, F. J., NOBILI, F., STEFANOVA, E., PETROVA, M., FALUP-PECURARIU, C., REKTOROVA, I., BOSTANTJOPOULOU, S., BIUNDO, R., WEINTRAUB, D., AARSLAND, D. & E, D. L. B. 2017. Long-Term Cognitive Decline in Dementia with Lewy Bodies in a Large Multicenter, International Cohort. *J Alzheimers Dis,* 57**,** 787-795.
KRAMER, M. L. & SCHULZ-SCHAEFFER, W. J. 2007. Presynaptic alpha-synuclein aggregates, not Lewy bodies, cause neurodegeneration in dementia with Lewy bodies. *J Neurosci,* 27**,** 1405-10.
KRAYBILL, M. L., LARSON, E. B., TSUANG, D. W., TERI, L., MCCORMICK, W. C., BOWEN, J. D., KUKULL, W. A., LEVERENZ, J. B. & CHERRIER, M. M. 2005. Cognitive differences in dementia patients with autopsy-verified AD, Lewy body pathology, or both. *Neurology,* 64**,** 2069-73.
KUCINSKI, A. & SARTER, M. 2015. Modeling Parkinson's disease falls associated with brainstem cholinergic systems decline. *Behav Neurosci,* 129**,** 96-104.
KUFFLER, S. W., NICHOLLS, J. G. & ORKAND, R. K. 1966. Physiological properties of glial cells in the central nervous system of amphibia. *J Neurophysiol,* 29**,** 768-87.
KUHL, D. E., MINOSHIMA, S., FESSLER, J. A., FREY, K. A., FOSTER, N. L., FICARO, E. P., WIELAND, D. M. & KOEPPE, R. A. 1996. In vivo mapping of cholinergic terminals in normal aging, Alzheimer's disease, and Parkinson's disease. *Ann Neurol,* 40**,** 399-410.
KUROKI, T., MELTZER, H. Y. & ICHIKAWA, J. 1999. Effects of antipsychotic drugs on extracellular dopamine levels in rat medial prefrontal cortex and nucleus accumbens. *J Pharmacol Exp Ther,* 288**,** 774-81.
KUROWSKA, Z., KORDOWER, J. H., STOESSL, A. J., BURKE, R. E., BRUNDIN, P., YUE, Z., BRADY, S. T., MILBRANDT, J., TRAPP, B. D., SHERER, T. B. & MEDICETTY, S. 2016. Is Axonal Degeneration a Key Early Event in Parkinson's Disease? *J Parkinsons Dis,* 6**,** 703-707.
KUUSISTO, E., PARKKINEN, L. & ALAFUZOFF, I. 2003. Morphogenesis of Lewy bodies: dissimilar incorporation of alpha-synuclein, ubiquitin, and p62. *J Neuropathol Exp Neurol,* 62**,** 1241-53.

KUZUHARA, S., MORI, H., IZUMIYAMA, N., YOSHIMURA, M. & IHARA, Y. 1988. Lewy bodies are ubiquitinated. A light and electron microscopic immunocytochemical study. *Acta Neuropathol,* 75**,** 345-53.
LACOR, P. N., BUNIEL, M. C., FURLOW, P. W., CLEMENTE, A. S., VELASCO, P. T., WOOD, M., VIOLA, K. L. & KLEIN, W. L. 2007. Abeta oligomer-induced aberrations in synapse composition, shape, and density provide a molecular basis for loss of connectivity in Alzheimer's disease. *J Neurosci,* 27**,** 796-807.
LAGANA, M. M., PIRASTRU, A., PELIZZARI, L., ROSSETTO, F., DI TELLA, S., BERGSLAND, N., NEMNI, R., MELONI, M. & BAGLIO, F. 2020. Multimodal Evaluation of Neurovascular Functionality in Early Parkinson's Disease. *Front Neurol,* 11**,** 831.
LAI, Y., KIM, S., VARKEY, J., LOU, X., SONG, J. K., DIAO, J., LANGEN, R. & SHIN, Y. K. 2014. Nonaggregated alpha-synuclein influences SNARE-dependent vesicle docking via membrane binding. *Biochemistry,* 53**,** 3889-96.
LANG, A. E. & LOZANO, A. M. 1998. Parkinson's disease. First of two parts. *N Engl J Med,* 339**,** 1044-53.
LANGER, S. Z. 2008. Presynaptic autoreceptors regulating transmitter release. *Neurochem Int,* 52**,** 26-30.
LARSEN, K. E., SCHMITZ, Y., TROYER, M. D., MOSHAROV, E., DIETRICH, P., QUAZI, A. Z., SAVALLE, M., NEMANI, V., CHAUDHRY, F. A., EDWARDS, R. H., STEFANIS, L. & SULZER, D. 2006. Alpha-synuclein overexpression in PC12 and chromaffin cells impairs catecholamine release by interfering with a late step in exocytosis. *J Neurosci,* 26**,** 11915-22.
LARSSON, V., TORISSON, G. & LONDOS, E. 2018. Relative survival in patients with dementia with Lewy bodies and Parkinson's disease dementia. *PLoS One,* 13**,** e0202044.
LASHLEY, T., HOLTON, J. L., GRAY, E., KIRKHAM, K., O'SULLIVAN, S. S., HILBIG, A., WOOD, N. W., LEES, A. J. & REVESZ, T. 2008. Cortical alpha-synuclein load is associated with amyloid-beta plaque burden in a subset of Parkinson's disease patients. *Acta Neuropathol,* 115**,** 417-25.
LECRUX, C., TOUSSAY, X., KOCHARYAN, A., FERNANDES, P., NEUPANE, S., LEVESQUE, M., PLAISIER, F., SHMUEL, A., CAULI, B. & HAMEL, E. 2011. Pyramidal neurons are "neurogenic hubs" in the neurovascular coupling response to whisker stimulation. *J Neurosci,* 31**,** 9836-47.
LEE, C. S., SAMII, A., SOSSI, V., RUTH, T. J., SCHULZER, M., HOLDEN, J. E., WUDEL, J., PAL, P. K., DE LA FUENTE-FERNANDEZ, R., CALNE, D. B. & STOESSL, A. J. 2000. In vivo positron emission tomographic evidence for compensatory changes in presynaptic dopaminergic nerve terminals in Parkinson's disease. *Ann Neurol,* 47**,** 493-503.
LEE, C. Y., CHENG, S. J., LIN, H. C., LIAO, Y. L. & CHEN, P. H. 2018. Quality of Life in Patients with Dementia with Lewy Bodies. *Behav Neurol,* 2018**,** 8320901.
LEE, L., BOORMAN, L., GLENDENNING, E., CHRISTMAS, C., SHARP, P., REDGRAVE, P., SHABIR, O., BRACCI, E., BERWICK, J. & HOWARTH, C. 2020. Key Aspects of Neurovascular Control Mediated by Specific Populations of Inhibitory Cortical Interneurons. *Cereb Cortex,* 30**,** 2452-2464.
LEE, S. H., KIM, S. S., TAE, W. S., LEE, S. Y., CHOI, J. W., KOH, S. B. & KWON, D. Y. 2011. Regional volume analysis of the Parkinson disease brain in early disease stage: gray matter, white matter, striatum, and thalamus. *AJNR Am J Neuroradiol,* 32**,** 682-7.
LEE, S. J., JEON, H. & KANDROR, K. V. 2008. Alpha-synuclein is localized in a subpopulation of rat brain synaptic vesicles. *Acta Neurobiol Exp (Wars),* 68**,** 509-15.
LEHTO, J., JOHANSSON, J., VUORILEHTO, L., LUOTO, P., ARPONEN, E., SCHEININ, H., ROURU, J. & SCHEININ, M. 2015. Sensitivity of [(11)C]ORM-13070 to increased

extracellular noradrenaline in the CNS - a PET study in human subjects. *Psychopharmacology (Berl),* 232**,** 4169-78.
LEIBSON, C. L., LONG, K. H., MARAGANORE, D. M., BOWER, J. H., RANSOM, J. E., O'BRIEN, P. C. & ROCCA, W. A. 2006. Direct medical costs associated with Parkinson's disease: a population-based study. *Mov Disord,* 21**,** 1864-71.
LERCH, J. P., YIU, A. P., MARTINEZ-CANABAL, A., PEKAR, T., BOHBOT, V. D., FRANKLAND, P. W., HENKELMAN, R. M., JOSSELYN, S. A. & SLED, J. G. 2011. Maze training in mice induces MRI-detectable brain shape changes specific to the type of learning. *Neuroimage,* 54**,** 2086-95.
LEUBE, R. E., KAISER, P., SEITER, A., ZIMBELMANN, R., FRANKE, W. W., REHM, H., KNAUS, P., PRIOR, P., BETZ, H., REINKE, H. & ET AL. 1987. Synaptophysin: molecular organization and mRNA expression as determined from cloned cDNA. *EMBO J,* 6**,** 3261-8.
LEWIS, M. M., DU, G., LEE, E. Y., NASRALAH, Z., STERLING, N. W., ZHANG, L., WAGNER, D., KONG, L., TROSTER, A. I., STYNER, M., ESLINGER, P. J., MAILMAN, R. B. & HUANG, X. 2016. The pattern of gray matter atrophy in Parkinson's disease differs in cortical and subcortical regions. *J Neurol,* 263**,** 68-75.
LEWIS, S. J., FOLTYNIE, T., BLACKWELL, A. D., ROBBINS, T. W., OWEN, A. M. & BARKER, R. A. 2005. Heterogeneity of Parkinson's disease in the early clinical stages using a data driven approach. *J Neurol Neurosurg Psychiatry,* 76**,** 343-8.
LI, J., SEIDLITZ, J., SUCKLING, J., FAN, F., JI, G. J., MENG, Y., YANG, S., WANG, K., QIU, J., CHEN, H. & LIAO, W. 2021. Cortical structural differences in major depressive disorder correlate with cell type-specific transcriptional signatures. *Nat Commun,* 12**,** 1647.
LI, J. Y., ENGLUND, E., HOLTON, J. L., SOULET, D., HAGELL, P., LEES, A. J., LASHLEY, T., QUINN, N. P., REHNCRONA, S., BJORKLUND, A., WIDNER, H., REVESZ, T., LINDVALL, O. & BRUNDIN, P. 2008. Lewy bodies in grafted neurons in subjects with Parkinson's disease suggest host-to-graft disease propagation. *Nat Med,* 14**,** 501-3.
LI, Q., KE, Y., CHAN, D. C., QIAN, Z. M., YUNG, K. K., KO, H., ARBUTHNOTT, G. W. & YUNG, W. H. 2012. Therapeutic deep brain stimulation in Parkinsonian rats directly influences motor cortex. *Neuron,* 76**,** 1030-41.
LI, S., CAI, Z., WU, X., HOLDEN, D., PRACITTO, R., KAPINOS, M., GAO, H., LABAREE, D., NABULSI, N., CARSON, R. E. & HUANG, Y. 2019a. Synthesis and in Vivo Evaluation of a Novel PET Radiotracer for Imaging of Synaptic Vesicle Glycoprotein 2A (SV2A) in Nonhuman Primates. *ACS Chem Neurosci,* 10**,** 1544-1554.
LI, S., CAI, Z., ZHANG, W., HOLDEN, D., LIN, S. F., FINNEMA, S. J., SHIRALI, A., ROPCHAN, J., CARRE, S., MERCIER, J., CARSON, R. E., NABULSI, N. & HUANG, Y. 2019b. Synthesis and in vivo evaluation of [(18)F]UCB-J for PET imaging of synaptic vesicle glycoprotein 2A (SV2A). *Eur J Nucl Med Mol Imaging,* 46**,** 1952-1965.
LI, X., PATEL, J. C., WANG, J., AVSHALUMOV, M. V., NICHOLSON, C., BUXBAUM, J. D., ELDER, G. A., RICE, M. E. & YUE, Z. 2010a. Enhanced striatal dopamine transmission and motor performance with LRRK2 overexpression in mice is eliminated by familial Parkinson's disease mutation G2019S. *J Neurosci,* 30**,** 1788-97.
LI, X., XING, Y., SCHWARZ, S. T. & AUER, D. P. 2017. Limbic grey matter changes in early Parkinson's disease. *Hum Brain Mapp,* 38**,** 3566-3578.
LI, Y., HUANG, X. F., DENG, C., MEYER, B., WU, A., YU, Y., YING, W., YANG, G. Y., YENARI, M. A. & WANG, Q. 2010b. Alterations in 5-HT2A receptor binding in various brain regions among 6-hydroxydopamine-induced Parkinsonian rats. *Synapse,* 64**,** 224-30.

LI, Y., JIAO, Q., DU, X., BI, M., HAN, S., JIAO, L. & JIANG, H. 2018. Investigation of Behavioral Dysfunctions Induced by Monoamine Depletions in a Mouse Model of Parkinson's Disease. *Front Cell Neurosci,* 12**,** 241.

LIBOW, L. S., FRISINA, P. G., HAROUTUNIAN, V., PERL, D. P. & PUROHIT, D. P. 2009. Parkinson's disease dementia: a diminished role for the Lewy body. *Parkinsonism Relat Disord,* 15**,** 572-5.

LIEBERMAN, A., LOCKHART, T. E., OLSON, M. C., SMITH HUSSAIN, V. A., FRAMES, C. W., SADREDDIN, A., MCCAULEY, M. & LUDINGTON, E. 2019. Nicotine Bitartrate Reduces Falls and Freezing of Gait in Parkinson Disease: A Reanalysis. *Front Neurol,* 10**,** 424.

LIEPELT, I., REIMOLD, M., MAETZLER, W., GODAU, J., REISCHL, G., GAENSLEN, A., HERBST, H. & BERG, D. 2009. Cortical hypometabolism assessed by a metabolic ratio in Parkinson's disease primarily reflects cognitive deterioration-[18F]FDG-PET. *Mov Disord,* 24**,** 1504-11.

LIN, W. C., CHEN, P. C., HUANG, Y. C., TSAI, N. W., CHEN, H. L., WANG, H. C., LIN, T. K., CHOU, K. H., CHEN, M. H., CHEN, Y. W. & LU, C. H. 2016. Dopaminergic Therapy Modulates Cortical Perfusion in Parkinson Disease With and Without Dementia According to Arterial Spin Labeled Perfusion Magnetic Resonance Imaging. *Medicine (Baltimore),* 95**,** e2206.

LIPPA, C. F., DUDA, J. E., GROSSMAN, M., HURTIG, H. I., AARSLAND, D., BOEVE, B. F., BROOKS, D. J., DICKSON, D. W., DUBOIS, B., EMRE, M., FAHN, S., FARMER, J. M., GALASKO, D., GALVIN, J. E., GOETZ, C. G., GROWDON, J. H., GWINN-HARDY, K. A., HARDY, J., HEUTINK, P., IWATSUBO, T., KOSAKA, K., LEE, V. M., LEVERENZ, J. B., MASLIAH, E., MCKEITH, I. G., NUSSBAUM, R. L., OLANOW, C. W., RAVINA, B. M., SINGLETON, A. B., TANNER, C. M., TROJANOWSKI, J. Q., WSZOLEK, Z. K. & GROUP, D. P. W. 2007. DLB and PDD boundary issues: diagnosis, treatment, molecular pathology, and biomarkers. *Neurology,* 68**,** 812-9.

LIU, S., SEIDLITZ, J., BLUMENTHAL, J. D., CLASEN, L. S. & RAZNAHAN, A. 2020. Integrative structural, functional, and transcriptomic analyses of sex-biased brain organization in humans. *Proc Natl Acad Sci U S A,* 117**,** 18788-18798.

LIX, L. M., HOBSON, D. E., AZIMAEE, M., LESLIE, W. D., BURCHILL, C. & HOBSON, S. 2010. Socioeconomic variations in the prevalence and incidence of Parkinson's disease: a population-based analysis. *J Epidemiol Community Health,* 64**,** 335-40.

LLOYD, K. G., DAVIDSON, L. & HORNYKIEWICZ, O. 1975. The neurochemistry of Parkinson's disease: effect of L-dopa therapy. *J Pharmacol Exp Ther,* 195**,** 453-64.

LOCASCIO, J. J. & ATRI, A. 2011. An overview of longitudinal data analysis methods for neurological research. *Dement Geriatr Cogn Dis Extra,* 1**,** 330-57.

LOGSDON, S., JOHNSTONE, A. F., VIELE, K. & COOPER, R. L. 2006. Regulation of synaptic vesicles pools within motor nerve terminals during short-term facilitation and neuromodulation. *J Appl Physiol (1985),* 100**,** 662-71.

LORENZ, R., SAMNICK, S., DILLMANN, U., SCHILLER, M., ONG, M. F., FASSBENDER, K., BUCK, A. & SPIEGEL, J. 2014. Nicotinic alpha4beta2 acetylcholine receptors and cognitive function in Parkinson's disease. *Acta Neurol Scand,* 130**,** 164-71.

LOUGHLIN, S. E., FOOTE, S. L. & BLOOM, F. E. 1986. Efferent projections of nucleus locus coeruleus: topographic organization of cells of origin demonstrated by three-dimensional reconstruction. *Neuroscience,* 18**,** 291-306.

LOWE, J., BLANCHARD, A., MORRELL, K., LENNOX, G., REYNOLDS, L., BILLETT, M., LANDON, M. & MAYER, R. J. 1988. Ubiquitin is a common factor in intermediate filament inclusion bodies of diverse type in man, including those of Parkinson's disease,

Pick's disease, and Alzheimer's disease, as well as Rosenthal fibres in cerebellar astrocytomas, cytoplasmic bodies in muscle, and mallory bodies in alcoholic liver disease. *J Pathol,* 155**,** 9-15.
LU, Y., TOYONAGA, T., NAGANAWA, M., GALLEZOT, J. D., CHEN, M. K., MECCA, A. P., VAN DYCK, C. H. & CARSON, R. E. 2021. Partial volume correction analysis for (11)C-UCB-J PET studies of Alzheimer's disease. *Neuroimage,* 238**,** 118248.
LUK, K. C., KEHM, V., CARROLL, J., ZHANG, B., O'BRIEN, P., TROJANOWSKI, J. Q. & LEE, V. M. 2012. Pathological alpha-synuclein transmission initiates Parkinson-like neurodegeneration in nontransgenic mice. *Science,* 338**,** 949-53.
LUNDBLAD, M., DECRESSAC, M., MATTSSON, B. & BJORKLUND, A. 2012. Impaired neurotransmission caused by overexpression of alpha-synuclein in nigral dopamine neurons. *Proc Natl Acad Sci U S A,* 109**,** 3213-9.
LYNCH, B. A., LAMBENG, N., NOCKA, K., KENSEL-HAMMES, P., BAJJALIEH, S. M., MATAGNE, A. & FUKS, B. 2004. The synaptic vesicle protein SV2A is the binding site for the antiepileptic drug levetiracetam. *Proc Natl Acad Sci U S A,* 101**,** 9861-6.
LYNCH, B. A., MATAGNE, A., BRANNSTROM, A., VON EULER, A., JANSSON, M., HAUZENBERGER, E. & SODERHALL, J. A. 2008. Visualization of SV2A conformations in situ by the use of Protein Tomography. *Biochem Biophys Res Commun,* 375**,** 491-5.
MA, S. Y., ROYTTA, M., RINNE, J. O., COLLAN, Y. & RINNE, U. K. 1997. Correlation between neuromorphometry in the substantia nigra and clinical features in Parkinson's disease using disector counts. *J Neurol Sci,* 151**,** 83-7.
MA, Y., TANG, C., SPETSIERIS, P. G., DHAWAN, V. & EIDELBERG, D. 2007. Abnormal metabolic network activity in Parkinson's disease: test-retest reproducibility. *J Cereb Blood Flow Metab,* 27**,** 597-605.
MACKENZIE, I. R. 2000. Activated microglia in dementia with Lewy bodies. *Neurology,* 55**,** 132-4.
MACLAREN, D. A., SANTINI, J. A., RUSSELL, A. L., MARKOVIC, T. & CLARK, S. D. 2014. Deficits in motor performance after pedunculopontine lesions in rats--impairment depends on demands of task. *Eur J Neurosci,* 40**,** 3224-36.
MADHYASTHA, T. M., ASKREN, M. K., BOORD, P., ZHANG, J., LEVERENZ, J. B. & GRABOWSKI, T. J. 2015. Cerebral perfusion and cortical thickness indicate cortical involvement in mild Parkinson's disease. *Mov Disord,* 30**,** 1893-900.
MAETZLER, W., BERG, D., SYNOFZIK, M., BROCKMANN, K., GODAU, J., MELMS, A., GASSER, T., HORNIG, S. & LANGKAMP, M. 2011. Autoantibodies against amyloid and glial-derived antigens are increased in serum and cerebrospinal fluid of Lewy body-associated dementias. *J Alzheimers Dis,* 26**,** 171-9.
MAHLKNECHT, P., SEPPI, K. & POEWE, W. 2015. The Concept of Prodromal Parkinson's Disease. *J Parkinsons Dis,* 5**,** 681-97.
MAILLET, A., KRACK, P., LHOMMEE, E., METEREAU, E., KLINGER, H., FAVRE, E., LE BARS, D., SCHMITT, E., BICHON, A., PELISSIER, P., FRAIX, V., CASTRIOTO, A., SGAMBATO-FAURE, V., BROUSSOLLE, E., TREMBLAY, L. & THOBOIS, S. 2016. The prominent role of serotonergic degeneration in apathy, anxiety and depression in de novo Parkinson's disease. *Brain,* 139**,** 2486-502.
MAK, E., BERGSLAND, N., DWYER, M. G., ZIVADINOV, R. & KANDIAH, N. 2014. Subcortical atrophy is associated with cognitive impairment in mild Parkinson disease: a combined investigation of volumetric changes, cortical thickness, and vertex-based shape analysis. *AJNR Am J Neuroradiol,* 35**,** 2257-64.
MAK, E., HOLLAND, N., JONES, P. S., SAVULICH, G., LOW, A., MALPETTI, M., KAALUND, S. S., PASSAMONTI, L., RITTMAN, T., ROMERO-GARCIA, R., MANAVAKI, R., WILLIAMS, G. B., HONG, Y. T., FRYER, T. D., AIGBIRHIO, F.

I., O'BRIEN, J. T. & ROWE, J. B. 2021. In vivo coupling of dendritic complexity with presynaptic density in primary tauopathies. *Neurobiol Aging,* 101**,** 187-198.
MAK, E., SU, L., WILLIAMS, G. B., FIRBANK, M. J., LAWSON, R. A., YARNALL, A. J., DUNCAN, G. W., OWEN, A. M., KHOO, T. K., BROOKS, D. J., ROWE, J. B., BARKER, R. A., BURN, D. J. & O'BRIEN, J. T. 2015a. Baseline and longitudinal grey matter changes in newly diagnosed Parkinson's disease: ICICLE-PD study. *Brain,* 138**,** 2974-86.
MAK, E., SU, L., WILLIAMS, G. B., WATSON, R., FIRBANK, M., BLAMIRE, A. M. & O'BRIEN, J. T. 2015b. Longitudinal assessment of global and regional atrophy rates in Alzheimer's disease and dementia with Lewy bodies. *Neuroimage Clin,* 7**,** 456-62.
MALLET, N., LEBLOIS, A., MAURICE, N. & BEURRIER, C. 2019. Striatal Cholinergic Interneurons: How to Elucidate Their Function in Health and Disease. *Front Pharmacol,* 10**,** 1488.
MALOTEAUX, J. M., LATERRE, E. C., LADURON, P. M., JAVOY-AGID, F. & AGID, Y. 1988. Decrease of serotonin-S2 receptors in temporal cortex of patients with Parkinson's disease and progressive supranuclear palsy. *Mov Disord,* 3**,** 255-62.
MANSUR, A., RABINER, E. A., COMLEY, R. A., LEWIS, Y., MIDDLETON, L. T., HUIBAN, M., PASSCHIER, J., TSUKADA, H., GUNN, R. N. & CONSORTIUM, M.-M. 2020. Characterization of 3 PET Tracers for Quantification of Mitochondrial and Synaptic Function in Healthy Human Brain: (18)F-BCPP-EF, (11)C-SA-4503, and (11)C-UCB-J. *J Nucl Med,* 61**,** 96-103.
MARDER, K. S., TANG, M. X., MEJIA-SANTANA, H., ROSADO, L., LOUIS, E. D., COMELLA, C. L., COLCHER, A., SIDEROWF, A. D., JENNINGS, D., NANCE, M. A., BRESSMAN, S., SCOTT, W. K., TANNER, C. M., MICKEL, S. F., ANDREWS, H. F., WATERS, C., FAHN, S., ROSS, B. M., COTE, L. J., FRUCHT, S., FORD, B., ALCALAY, R. N., REZAK, M., NOVAK, K., FRIEDMAN, J. H., PFEIFFER, R. F., MARSH, L., HINER, B., NEILS, G. D., VERBITSKY, M., KISSELEV, S., CACCAPPOLO, E., OTTMAN, R. & CLARK, L. N. 2010. Predictors of parkin mutations in early-onset Parkinson disease: the consortium on risk for early-onset Parkinson disease study. *Arch Neurol,* 67**,** 731-8.
MARKELLO, R. D. & MISIC, B. 2021. Comparing spatial null models for brain maps. *Neuroimage,* 236**,** 118052.
MARQUES, O. & OUTEIRO, T. F. 2012. Alpha-synuclein: from secretion to dysfunction and death. *Cell Death Dis,* 3**,** e350.
MARQUIE, M., LOCASCIO, J. J., RENTZ, D. M., BECKER, J. A., HEDDEN, T., JOHNSON, K. A., GROWDON, J. H. & GOMPERTS, S. N. 2014. Striatal and extrastriatal dopamine transporter levels relate to cognition in Lewy body diseases: an (11)C altropane positron emission tomography study. *Alzheimers Res Ther,* 6**,** 52.
MARSDEN, C. D. 1982. Basal ganglia disease. *Lancet,* 2**,** 1141-7.
MARSDEN, C. D. 1990. Parkinson's disease. *Lancet,* 335**,** 948-52.
MARSILI, L., RIZZO, G. & COLOSIMO, C. 2018. Diagnostic Criteria for Parkinson's Disease: From James Parkinson to the Concept of Prodromal Disease. *Front Neurol,* 9**,** 156.
MARTEL, A. C. & APICELLA, P. 2021. Temporal processing in the striatum: Interplay between midbrain dopamine neurons and striatal cholinergic interneurons. *Eur J Neurosci,* 53**,** 2090-2099.
MARTIN, L. J., PAN, Y., PRICE, A. C., STERLING, W., COPELAND, N. G., JENKINS, N. A., PRICE, D. L. & LEE, M. K. 2006. Parkinson's disease alpha-synuclein transgenic mice develop neuronal mitochondrial degeneration and cell death. *J Neurosci,* 26**,** 41-50.
MARTINEZ-VICENTE, M., TALLOCZY, Z., KAUSHIK, S., MASSEY, A. C., MAZZULLI, J., MOSHAROV, E. V., HODARA, R., FREDENBURG, R., WU, D. C., FOLLENZI, A., DAUER, W., PRZEDBORSKI, S., ISCHIROPOULOS, H., LANSBURY, P. T.,

SULZER, D. & CUERVO, A. M. 2008. Dopamine-modified alpha-synuclein blocks chaperone-mediated autophagy. *J Clin Invest,* 118**,** 777-88.
MARTINO, M. E., DE VILLORIA, J. G., LACALLE-AURIOLES, M., OLAZARAN, J., CRUZ, I., NAVARRO, E., GARCIA-VAZQUEZ, V., CARRERAS, J. L. & DESCO, M. 2013. Comparison of different methods of spatial normalization of FDG-PET brain images in the voxel-wise analysis of MCI patients and controls. *Ann Nucl Med,* 27**,** 600-9.
MARTINS, D., GIACOMEL, A., WILLIAMS, S. C. R., TURKHEIMER, F., DIPASQUALE, O., VERONESE, M. & GROUP, P. E. T. T. W. 2021. Imaging transcriptomics: Convergent cellular, transcriptomic, and molecular neuroimaging signatures in the healthy adult human brain. *Cell Rep,* 37**,** 110173.
MARUI, W., ISEKI, E., NAKAI, T., MIURA, S., KATO, M., UEDA, K. & KOSAKA, K. 2002. Progression and staging of Lewy pathology in brains from patients with dementia with Lewy bodies. *J Neurol Sci,* 195**,** 153-9.
MASLIAH, E., TERRY, R. D., ALFORD, M. & DETERESA, R. 1990. Quantitative immunohistochemistry of synaptophysin in human neocortex: an alternative method to estimate density of presynaptic terminals in paraffin sections. *J Histochem Cytochem,* 38**,** 837-44.
MASON, S. T. & FIBIGER, H. C. 1979. Regional topography within noradrenergic locus coeruleus as revealed by retrograde transport of horseradish peroxidase. *J Comp Neurol,* 187**,** 703-24.
MASSA, S. M., YANG, T., XIE, Y., SHI, J., BILGEN, M., JOYCE, J. N., NEHAMA, D., RAJADAS, J. & LONGO, F. M. 2010. Small molecule BDNF mimetics activate TrkB signaling and prevent neuronal degeneration in rodents. *J Clin Invest,* 120**,** 1774-85.
MASSANO, J. & BHATIA, K. P. 2012. Clinical approach to Parkinson's disease: features, diagnosis, and principles of management. *Cold Spring Harb Perspect Med,* 2**,** a008870.
MASUDA-SUZUKAKE, M., NONAKA, T., HOSOKAWA, M., OIKAWA, T., ARAI, T., AKIYAMA, H., MANN, D. M. & HASEGAWA, M. 2013. Prion-like spreading of pathological alpha-synuclein in brain. *Brain,* 136**,** 1128-38.
MATHIISEN, T. M., LEHRE, K. P., DANBOLT, N. C. & OTTERSEN, O. P. 2010. The perivascular astroglial sheath provides a complete covering of the brain microvessels: an electron microscopic 3D reconstruction. *Glia,* 58**,** 1094-103.
MATSUDA, W., FURUTA, T., NAKAMURA, K. C., HIOKI, H., FUJIYAMA, F., ARAI, R. & KANEKO, T. 2009. Single nigrostriatal dopaminergic neurons form widely spread and highly dense axonal arborizations in the neostriatum. *J Neurosci,* 29**,** 444-53.
MATTA, S., VAN KOLEN, K., DA CUNHA, R., VAN DEN BOGAART, G., MANDEMAKERS, W., MISKIEWICZ, K., DE BOCK, P. J., MORAIS, V. A., VILAIN, S., HADDAD, D., DELBROEK, L., SWERTS, J., CHAVEZ-GUTIERREZ, L., ESPOSITO, G., DANEELS, G., KARRAN, E., HOLT, M., GEVAERT, K., MOECHARS, D. W., DE STROOPER, B. & VERSTREKEN, P. 2012. LRRK2 controls an EndoA phosphorylation cycle in synaptic endocytosis. *Neuron,* 75**,** 1008-21.
MATTILA, P. M., ROYTTA, M., LONNBERG, P., MARJAMAKI, P., HELENIUS, H. & RINNE, J. O. 2001. Choline acetytransferase activity and striatal dopamine receptors in Parkinson's disease in relation to cognitive impairment. *Acta Neuropathol,* 102**,** 160-6.
MATTILA, P. M., ROYTTA, M., TORIKKA, H., DICKSON, D. W. & RINNE, J. O. 1998. Cortical Lewy bodies and Alzheimer-type changes in patients with Parkinson's disease. *Acta Neuropathol,* 95**,** 576-82.
MATUSKEY, D., TINAZ, S., WILCOX, K. C., NAGANAWA, M., TOYONAGA, T., DIAS, M., HENRY, S., PITTMAN, B., ROPCHAN, J., NABULSI, N., SURIDJAN, I., COMLEY, R. A., HUANG, Y., FINNEMA, S. J. & CARSON, R. E. 2020. Synaptic Changes in Parkinson Disease Assessed with in vivo Imaging. *Ann Neurol,* 87**,** 329-338.

MAVRIDIS, M., DEGRYSE, A. D., LATEGAN, A. J., MARIEN, M. R. & COLPAERT, F. C. 1991. Effects of locus coeruleus lesions on parkinsonian signs, striatal dopamine and substantia nigra cell loss after 1-methyl-4-phenyl-1,2,3,6-tetrahydropyridine in monkeys: a possible role for the locus coeruleus in the progression of Parkinson's disease. *Neuroscience,* 41**,** 507-23.

MAWLAWI, O., MARTINEZ, D., SLIFSTEIN, M., BROFT, A., CHATTERJEE, R., HWANG, D. R., HUANG, Y., SIMPSON, N., NGO, K., VAN HEERTUM, R. & LARUELLE, M. 2001. Imaging human mesolimbic dopamine transmission with positron emission tomography: I. Accuracy and precision of D(2) receptor parameter measurements in ventral striatum. *J Cereb Blood Flow Metab,* 21**,** 1034-57.

MCALONAN, K., CAVANAUGH, J. & WURTZ, R. H. 2008. Guarding the gateway to cortex with attention in visual thalamus. *Nature,* 456**,** 391-4.

MCCALL, J. G., SIUDA, E. R., BHATTI, D. L., LAWSON, L. A., MCELLIGOTT, Z. A., STUBER, G. D. & BRUCHAS, M. R. 2017. Locus coeruleus to basolateral amygdala noradrenergic projections promote anxiety-like behavior. *Elife,* 6.

MCCANN, C. M., TAPIA, J. C., KIM, H., COGGAN, J. S. & LICHTMAN, J. W. 2008. Rapid and modifiable neurotransmitter receptor dynamics at a neuronal synapse in vivo. *Nat Neurosci,* 11**,** 807-15.

MCCANN, U. D., SZABO, Z., SECKIN, E., ROSENBLATT, P., MATHEWS, W. B., RAVERT, H. T., DANNALS, R. F. & RICAURTE, G. A. 2005. Quantitative PET studies of the serotonin transporter in MDMA users and controls using [11C]McN5652 and [11C]DASB. *Neuropsychopharmacology,* 30**,** 1741-50.

MCCULLUMSMITH, R. E., HAMMOND, J. H., SHAN, D. & MEADOR-WOODRUFF, J. H. 2014. Postmortem brain: an underutilized substrate for studying severe mental illness. *Neuropsychopharmacology,* 39**,** 65-87.

MCKAY, B. E., PLACZEK, A. N. & DANI, J. A. 2007. Regulation of synaptic transmission and plasticity by neuronal nicotinic acetylcholine receptors. *Biochem Pharmacol,* 74**,** 1120-33.

MCKEITH, I., FAIRBAIRN, A., PERRY, R., THOMPSON, P. & PERRY, E. 1992. Neuroleptic sensitivity in patients with senile dementia of Lewy body type. *BMJ,* 305**,** 673-8.

MCKEITH, I. G., BOEVE, B. F., DICKSON, D. W., HALLIDAY, G., TAYLOR, J. P., WEINTRAUB, D., AARSLAND, D., GALVIN, J., ATTEMS, J., BALLARD, C. G., BAYSTON, A., BEACH, T. G., BLANC, F., BOHNEN, N., BONANNI, L., BRAS, J., BRUNDIN, P., BURN, D., CHEN-PLOTKIN, A., DUDA, J. E., EL-AGNAF, O., FELDMAN, H., FERMAN, T. J., FFYTCHE, D., FUJISHIRO, H., GALASKO, D., GOLDMAN, J. G., GOMPERTS, S. N., GRAFF-RADFORD, N. R., HONIG, L. S., IRANZO, A., KANTARCI, K., KAUFER, D., KUKULL, W., LEE, V. M. Y., LEVERENZ, J. B., LEWIS, S., LIPPA, C., LUNDE, A., MASELLIS, M., MASLIAH, E., MCLEAN, P., MOLLENHAUER, B., MONTINE, T. J., MORENO, E., MORI, E., MURRAY, M., O'BRIEN, J. T., ORIMO, S., POSTUMA, R. B., RAMASWAMY, S., ROSS, O. A., SALMON, D. P., SINGLETON, A., TAYLOR, A., THOMAS, A., TIRABOSCHI, P., TOLEDO, J. B., TROJANOWSKI, J. Q., TSUANG, D., WALKER, Z., YAMADA, M. & KOSAKA, K. 2017. Diagnosis and management of dementia with Lewy bodies: Fourth consensus report of the DLB Consortium. *Neurology,* 89**,** 88-100.

MCKEITH, I. G., DICKSON, D. W., LOWE, J., EMRE, M., O'BRIEN, J. T., FELDMAN, H., CUMMINGS, J., DUDA, J. E., LIPPA, C., PERRY, E. K., AARSLAND, D., ARAI, H., BALLARD, C. G., BOEVE, B., BURN, D. J., COSTA, D., DEL SER, T., DUBOIS, B., GALASKO, D., GAUTHIER, S., GOETZ, C. G., GOMEZ-TORTOSA, E., HALLIDAY, G., HANSEN, L. A., HARDY, J., IWATSUBO, T., KALARIA, R. N., KAUFER, D., KENNY, R. A., KORCZYN, A., KOSAKA, K., LEE, V. M., LEES, A., LITVAN, I., LONDOS, E., LOPEZ, O. L., MINOSHIMA, S., MIZUNO, Y.,

MOLINA, J. A., MUKAETOVA-LADINSKA, E. B., PASQUIER, F., PERRY, R. H., SCHULZ, J. B., TROJANOWSKI, J. Q., YAMADA, M. & CONSORTIUM ON, D. L. B. 2005. Diagnosis and management of dementia with Lewy bodies: third report of the DLB Consortium. *Neurology,* 65**,** 1863-72.

MCKEITH, I. G., GALASKO, D., KOSAKA, K., PERRY, E. K., DICKSON, D. W., HANSEN, L. A., SALMON, D. P., LOWE, J., MIRRA, S. S., BYRNE, E. J., LENNOX, G., QUINN, N. P., EDWARDSON, J. A., INCE, P. G., BERGERON, C., BURNS, A., MILLER, B. L., LOVESTONE, S., COLLERTON, D., JANSEN, E. N., BALLARD, C., DE VOS, R. A., WILCOCK, G. K., JELLINGER, K. A. & PERRY, R. H. 1996. Consensus guidelines for the clinical and pathologic diagnosis of dementia with Lewy bodies (DLB): report of the consortium on DLB international workshop. *Neurology,* 47**,** 1113-24.

MCNAUGHT, K. S., SHASHIDHARAN, P., PERL, D. P., JENNER, P. & OLANOW, C. W. 2002. Aggresome-related biogenesis of Lewy bodies. *Eur J Neurosci,* 16**,** 2136-48.

MECCA, A. P., CHEN, M. K., O'DELL, R. S., NAGANAWA, M., TOYONAGA, T., GODEK, T. A., HARRIS, J. E., BARTLETT, H. H., ZHAO, W., NABULSI, N. B., WYK, B. C. V., VARMA, P., ARNSTEN, A. F. T., HUANG, Y., CARSON, R. E. & VAN DYCK, C. H. 2020. In vivo measurement of widespread synaptic loss in Alzheimer's disease with SV2A PET. *Alzheimers Dement,* 16**,** 974-982.

MEIRELES, J. & MASSANO, J. 2012. Cognitive impairment and dementia in Parkinson's disease: clinical features, diagnosis, and management. *Front Neurol,* 3**,** 88.

MELZER, T. R., WATTS, R., MACASKILL, M. R., PEARSON, J. F., RUEGER, S., PITCHER, T. L., LIVINGSTON, L., GRAHAM, C., KEENAN, R., SHANKARANARAYANAN, A., ALSOP, D. C., DALRYMPLE-ALFORD, J. C. & ANDERSON, T. J. 2011. Arterial spin labelling reveals an abnormal cerebral perfusion pattern in Parkinson's disease. *Brain,* 134**,** 845-55.

MENA, M. A., CASAREJOS, M. J., CARAZO, A., PAINO, C. L. & GARCIA DE YEBENES, J. 1997a. Glia protect fetal midbrain dopamine neurons in culture from L-DOPA toxicity through multiple mechanisms. *J Neural Transm (Vienna),* 104**,** 317-28.

MENA, M. A., DAVILA, V. & SULZER, D. 1997b. Neurotrophic effects of L-DOPA in postnatal midbrain dopamine neuron/cortical astrocyte cocultures. *J Neurochem,* 69**,** 1398-408.

MENDEZ, I., VINUELA, A., ASTRADSSON, A., MUKHIDA, K., HALLETT, P., ROBERTSON, H., TIERNEY, T., HOLNESS, R., DAGHER, A., TROJANOWSKI, J. Q. & ISACSON, O. 2008. Dopamine neurons implanted into people with Parkinson's disease survive without pathology for 14 years. *Nat Med,* 14**,** 507-9.

MENDOZA-TORREBLANCA, J. G., VANOYE-CARLO, A., PHILLIPS-FARFAN, B. V., CARMONA-APARICIO, L. & GOMEZ-LIRA, G. 2013. Synaptic vesicle protein 2A: basic facts and role in synaptic function. *Eur J Neurosci,* 38**,** 3529-39.

MERCURI, N. B. & BERNARDI, G. 2005. The 'magic' of L-dopa: why is it the gold standard Parkinson's disease therapy? *Trends Pharmacol Sci,* 26**,** 341-4.

MERDES, A. R., HANSEN, L. A., JESTE, D. V., GALASKO, D., HOFSTETTER, C. R., HO, G. J., THAL, L. J. & COREY-BLOOM, J. 2003. Influence of Alzheimer pathology on clinical diagnostic accuracy in dementia with Lewy bodies. *Neurology,* 60**,** 1586-90.

MESULAM, M. M. & GEULA, C. 1988. Nucleus basalis (Ch4) and cortical cholinergic innervation in the human brain: observations based on the distribution of acetylcholinesterase and choline acetyltransferase. *J Comp Neurol,* 275**,** 216-40.

MICHIELS, L., DELVA, A., VAN AALST, J., CECCARINI, J., VANDENBERGHE, W., VANDENBULCKE, M., KOOLE, M., LEMMENS, R. & LAERE, K. V. 2021. Synaptic density in healthy human aging is not influenced by age or sex: a (11)C-UCB-J PET study. *Neuroimage,* 232**,** 117877.

MILBER, J. M., NOORIGIAN, J. V., MORLEY, J. F., PETROVITCH, H., WHITE, L., ROSS, G. W. & DUDA, J. E. 2012. Lewy pathology is not the first sign of degeneration in vulnerable neurons in Parkinson disease. *Neurology,* 79**,** 2307-14.
MILLER, G. A. & CHAPMAN, J. P. 2001. Misunderstanding analysis of covariance. *J Abnorm Psychol,* 110**,** 40-8.
MILNERWOOD, A. J. & RAYMOND, L. A. 2010. Early synaptic pathophysiology in neurodegeneration: insights from Huntington's disease. *Trends Neurosci,* 33**,** 513-23.
MINERS, S., MOULDING, H., DE SILVA, R. & LOVE, S. 2014. Reduced vascular endothelial growth factor and capillary density in the occipital cortex in dementia with Lewy bodies. *Brain Pathol,* 24**,** 334-43.
MINK, J. W., BLUMENSCHINE, R. J. & ADAMS, D. B. 1981. Ratio of central nervous system to body metabolism in vertebrates: its constancy and functional basis. *Am J Physiol,* 241**,** R203-12.
MINOSHIMA, S., FOSTER, N. L., SIMA, A. A., FREY, K. A., ALBIN, R. L. & KUHL, D. E. 2001. Alzheimer's disease versus dementia with Lewy bodies: cerebral metabolic distinction with autopsy confirmation. *Ann Neurol,* 50**,** 358-65.
MISGELD, T. & SCHWARZ, T. L. 2017. Mitostasis in Neurons: Maintaining Mitochondria in an Extended Cellular Architecture. *Neuron,* 96**,** 651-666.
MISHRA, A. 2017. Binaural blood flow control by astrocytes: listening to synapses and the vasculature. *J Physiol,* 595**,** 1885-1902.
MISHRA, A., REYNOLDS, J. P., CHEN, Y., GOURINE, A. V., RUSAKOV, D. A. & ATTWELL, D. 2016. Astrocytes mediate neurovascular signaling to capillary pericytes but not to arterioles. *Nat Neurosci,* 19**,** 1619-1627.
MISHRA, A., SINGH, S., TIWARI, V., PARUL & SHUKLA, S. 2019. Dopamine D1 receptor activation improves adult hippocampal neurogenesis and exerts anxiolytic and antidepressant-like effect via activation of Wnt/beta-catenin pathways in rat model of Parkinson's disease. *Neurochem Int,* 122**,** 170-186.
MISSLER, M., SUDHOF, T. C. & BIEDERER, T. 2012. Synaptic cell adhesion. *Cold Spring Harb Perspect Biol,* 4**,** a005694.
MISU, Y., KITAHAMA, K. & GOSHIMA, Y. 2003. L-3,4-Dihydroxyphenylalanine as a neurotransmitter candidate in the central nervous system. *Pharmacol Ther,* 97**,** 117-37.
MOELLER, J. R., NAKAMURA, T., MENTIS, M. J., DHAWAN, V., SPETSIERES, P., ANTONINI, A., MISSIMER, J., LEENDERS, K. L. & EIDELBERG, D. 1999. Reproducibility of regional metabolic covariance patterns: comparison of four populations. *J Nucl Med,* 40**,** 1264-9.
MOGI, M., TOGARI, A., KONDO, T., MIZUNO, Y., KOMURE, O., KUNO, S., ICHINOSE, H. & NAGATSU, T. 1999. Brain-derived growth factor and nerve growth factor concentrations are decreased in the substantia nigra in Parkinson's disease. *Neurosci Lett,* 270**,** 45-8.
MOK, W., CHOW, T. W., ZHENG, L., MACK, W. J. & MILLER, C. 2004. Clinicopathological concordance of dementia diagnoses by community versus tertiary care clinicians. *Am J Alzheimers Dis Other Demen,* 19**,** 161-5.
MONCHI, O., HANGANU, A. & BELLEC, P. 2016. Markers of cognitive decline in PD: The case for heterogeneity. *Parkinsonism Relat Disord,* 24**,** 8-14.
MONCHI, O., PETRIDES, M., MEJIA-CONSTAIN, B. & STRAFELLA, A. P. 2007. Cortical activity in Parkinson's disease during executive processing depends on striatal involvement. *Brain,* 130**,** 233-44.
MONTEGGIA, L. M. 2011. Toward neurotrophin-based therapeutics. *Am J Psychiatry,* 168**,** 114-6.
MOR, D. E., TSIKA, E., MAZZULLI, J. R., GOULD, N. S., KIM, H., DANIELS, M. J., DOSHI, S., GUPTA, P., GROSSMAN, J. L., TAN, V. X., KALB, R. G., CALDWELL,

K. A., CALDWELL, G. A., WOLFE, J. H. & ISCHIROPOULOS, H. 2017. Dopamine induces soluble alpha-synuclein oligomers and nigrostriatal degeneration. *Nat Neurosci,* 20**,** 1560-1568.
MORAIS, V. A., VERSTREKEN, P., ROETHIG, A., SMET, J., SNELLINX, A., VANBRABANT, M., HADDAD, D., FREZZA, C., MANDEMAKERS, W., VOGT-WEISENHORN, D., VAN COSTER, R., WURST, W., SCORRANO, L. & DE STROOPER, B. 2009. Parkinson's disease mutations in PINK1 result in decreased Complex I activity and deficient synaptic function. *EMBO Mol Med,* 1**,** 99-111.
MORGAN, S. E., SEIDLITZ, J., WHITAKER, K. J., ROMERO-GARCIA, R., CLIFTON, N. E., SCARPAZZA, C., VAN AMELSVOORT, T., MARCELIS, M., VAN OS, J., DONOHOE, G., MOTHERSILL, D., CORVIN, A., POCKLINGTON, A., RAZNAHAN, A., MCGUIRE, P., VERTES, P. E. & BULLMORE, E. T. 2019. Cortical patterning of abnormal morphometric similarity in psychosis is associated with brain expression of schizophrenia-related genes. *Proc Natl Acad Sci U S A,* 116**,** 9604-9609.
MORRIS, R., MARTINI, D. N., MADHYASTHA, T., KELLY, V. E., GRABOWSKI, T. J., NUTT, J. & HORAK, F. 2019. Overview of the cholinergic contribution to gait, balance and falls in Parkinson's disease. *Parkinsonism Relat Disord,* 63**,** 20-30.
MORRISH, P. K. 2003. How valid is dopamine transporter imaging as a surrogate marker in research trials in Parkinson's disease? *Mov Disord,* 18 Suppl 7**,** S63-70.
MORRISH, P. K., SAWLE, G. V. & BROOKS, D. J. 1995. Clinical and [18F] dopa PET findings in early Parkinson's disease. *J Neurol Neurosurg Psychiatry,* 59**,** 597-600.
MOSHAROV, E. V., LARSEN, K. E., KANTER, E., PHILLIPS, K. A., WILSON, K., SCHMITZ, Y., KRANTZ, D. E., KOBAYASHI, K., EDWARDS, R. H. & SULZER, D. 2009. Interplay between cytosolic dopamine, calcium, and alpha-synuclein causes selective death of substantia nigra neurons. *Neuron,* 62**,** 218-29.
MOURADIAN, R. D., SESSLER, F. M. & WATERHOUSE, B. D. 1991. Noradrenergic potentiation of excitatory transmitter action in cerebrocortical slices: evidence for mediation by an alpha 1 receptor-linked second messenger pathway. *Brain Res,* 546**,** 83-95.
MUELLER, C., BALLARD, C., CORBETT, A. & AARSLAND, D. 2017. The prognosis of dementia with Lewy bodies. *Lancet Neurol,* 16**,** 390-398.
MUELLER, C., PERERA, G., RAJKUMAR, A. P., BHATTARAI, M., PRICE, A., O'BRIEN, J. T., BALLARD, C., STEWART, R. & AARSLAND, D. 2018. Hospitalization in people with dementia with Lewy bodies: Frequency, duration, and cost implications. *Alzheimers Dement (Amst),* 10**,** 143-152.
MUKAETOVA-LADINSKA, E. B., ANDRAS, A., MILNE, J., ABDEL-ALL, Z., BORR, I., JAROS, E., PERRY, R. H., HONER, W. G., CLEGHORN, A., DOHERTY, J., MCINTOSH, G., PERRY, E. K., KALARIA, R. N. & MCKEITH, I. G. 2013. Synaptic proteins and choline acetyltransferase loss in visual cortex in dementia with Lewy bodies. *J Neuropathol Exp Neurol,* 72**,** 53-60.
MULLER-GARTNER, H. W., LINKS, J. M., PRINCE, J. L., BRYAN, R. N., MCVEIGH, E., LEAL, J. P., DAVATZIKOS, C. & FROST, J. J. 1992. Measurement of radiotracer concentration in brain gray matter using positron emission tomography: MRI-based correction for partial volume effects. *J Cereb Blood Flow Metab,* 12**,** 571-83.
MURER, M. G., DZIEWCZAPOLSKI, G., MENALLED, L. B., GARCIA, M. C., AGID, Y., GERSHANIK, O. & RAISMAN-VOZARI, R. 1998. Chronic levodopa is not toxic for remaining dopamine neurons, but instead promotes their recovery, in rats with moderate nigrostriatal lesions. *Ann Neurol,* 43**,** 561-75.
MURPHY, D. D., RUETER, S. M., TROJANOWSKI, J. Q. & LEE, V. M. 2000. Synucleins are developmentally expressed, and alpha-synuclein regulates the size of the presynaptic vesicular pool in primary hippocampal neurons. *J Neurosci,* 20**,** 3214-20.

MURRAY, K. C., STEPHENS, M. J., BALLOU, E. W., HECKMAN, C. J. & BENNETT, D. J. 2011. Motoneuron excitability and muscle spasms are regulated by 5-HT2B and 5-HT2C receptor activity. *J Neurophysiol,* 105**,** 731-48.

MUTCH, S. A., KENSEL-HAMMES, P., GADD, J. C., FUJIMOTO, B. S., ALLEN, R. W., SCHIRO, P. G., LORENZ, R. M., KUYPER, C. L., KUO, J. S., BAJJALIEH, S. M. & CHIU, D. T. 2011. Protein quantification at the single vesicle level reveals that a subset of synaptic vesicle proteins are trafficked with high precision. *J Neurosci,* 31**,** 1461-70.

MYTILINEOU, C., HAN, S. K. & COHEN, G. 1993. Toxic and protective effects of L-dopa on mesencephalic cell cultures. *J Neurochem,* 61**,** 1470-8.

NABULSI, N. B., MERCIER, J., HOLDEN, D., CARRE, S., NAJAFZADEH, S., VANDERGETEN, M. C., LIN, S. F., DEO, A., PRICE, N., WOOD, M., LARA-JAIME, T., MONTEL, F., LARUELLE, M., CARSON, R. E., HANNESTAD, J. & HUANG, Y. 2016. Synthesis and Preclinical Evaluation of 11C-UCB-J as a PET Tracer for Imaging the Synaptic Vesicle Glycoprotein 2A in the Brain. *J Nucl Med,* 57**,** 777-84.

NAGANAWA, M., LI, S., NABULSI, N., HENRY, S., ZHENG, M. Q., PRACITTO, R., CAI, Z., GAO, H., KAPINOS, M., LABAREE, D., MATUSKEY, D., HUANG, Y. & CARSON, R. E. 2021. First-in-Human Evaluation of (18)F-SynVesT-1, a Radioligand for PET Imaging of Synaptic Vesicle Glycoprotein 2A. *J Nucl Med,* 62**,** 561-567.

NAGANO-SAITO, A., WASHIMI, Y., ARAHATA, Y., KACHI, T., LERCH, J. P., EVANS, A. C., DAGHER, A. & ITO, K. 2005. Cerebral atrophy and its relation to cognitive impairment in Parkinson disease. *Neurology,* 64**,** 224-9.

NAGATSU, T., MOGI, M., ICHINOSE, H. & TOGARI, A. 2000. Changes in cytokines and neurotrophins in Parkinson's disease. *J Neural Transm Suppl***,** 277-90.

NAHIMI, A., SOMMERAUER, M., KINNERUP, M. B., OSTERGAARD, K., WINTERDAHL, M., JACOBSEN, J., SCHACHT, A., JOHNSEN, B., DAMHOLDT, M. F., BORGHAMMER, P. & GJEDDE, A. 2018. Noradrenergic Deficits in Parkinson Disease Imaged with (11)C-MeNER. *J Nucl Med,* 59**,** 659-664.

NAKANO, I. & HIRANO, A. 1984. Parkinson's disease: neuron loss in the nucleus basalis without concomitant Alzheimer's disease. *Ann Neurol,* 15**,** 415-8.

NAKANO, K., KAYAHARA, T., TSUTSUMI, T. & USHIRO, H. 2000. Neural circuits and functional organization of the striatum. *J Neurol,* 247 Suppl 5**,** V1-15.

NAMBU, A., TOKUNO, H., HAMADA, I., KITA, H., IMANISHI, M., AKAZAWA, T., IKEUCHI, Y. & HASEGAWA, N. 2000. Excitatory cortical inputs to pallidal neurons via the subthalamic nucleus in the monkey. *J Neurophysiol,* 84**,** 289-300.

NANDHAGOPAL, R., KURAMOTO, L., SCHULZER, M., MAK, E., CRAGG, J., MCKENZIE, J., MCCORMICK, S., RUTH, T. J., SOSSI, V., DE LA FUENTE-FERNANDEZ, R. & STOESSL, A. J. 2011. Longitudinal evolution of compensatory changes in striatal dopamine processing in Parkinson's disease. *Brain,* 134**,** 3290-8.

NAVAILLES, S., LAGIERE, M., CONTINI, A. & DE DEURWAERDERE, P. 2013. Multisite intracerebral microdialysis to study the mechanism of L-DOPA induced dopamine and serotonin release in the parkinsonian brain. *ACS Chem Neurosci,* 4**,** 680-92.

NAVONE, F., JAHN, R., DI GIOIA, G., STUKENBROK, H., GREENGARD, P. & DE CAMILLI, P. 1986. Protein p38: an integral membrane protein specific for small vesicles of neurons and neuroendocrine cells. *J Cell Biol,* 103**,** 2511-27.

NEDELSKA, Z., SENJEM, M. L., PRZYBELSKI, S. A., LESNICK, T. G., LOWE, V. J., BOEVE, B. F., ARANI, A., VEMURI, P., GRAFF-RADFORD, J., FERMAN, T. J., JONES, D. T., SAVICA, R., KNOPMAN, D. S., PETERSEN, R. C., JACK, C. R. & KANTARCI, K. 2018. Regional cortical perfusion on arterial spin labeling MRI in dementia with Lewy bodies: Associations with clinical severity, glucose metabolism and tau PET. *Neuroimage Clin,* 19**,** 939-947.

NELSON, P. T., JICHA, G. A., KRYSCIO, R. J., ABNER, E. L., SCHMITT, F. A., COOPER, G., XU, L. O., SMITH, C. D. & MARKESBERY, W. R. 2010. Low sensitivity in clinical diagnoses of dementia with Lewy bodies. *J Neurol,* 257**,** 359-66.
NEMANI, V. M., LU, W., BERGE, V., NAKAMURA, K., ONOA, B., LEE, M. K., CHAUDHRY, F. A., NICOLL, R. A. & EDWARDS, R. H. 2010. Increased expression of alpha-synuclein reduces neurotransmitter release by inhibiting synaptic vesicle reclustering after endocytosis. *Neuron,* 65**,** 66-79.
NG, K. Y., CHASE, T. N., COLBURN, R. W. & KOPIN, I. J. 1970. L-Dopa-induced release of cerebral monoamines. *Science,* 170**,** 76-7.
NICASTRO, N., HOLLAND, N., SAVULICH, G., CARTER, S. F., MAK, E., HONG, Y. T., MILICEVIC SEPHTON, S., FRYER, T. D., AIGBIRHIO, F. I., ROWE, J. B. & O'BRIEN, J. T. 2020. (11)C-UCB-J synaptic PET and multimodal imaging in dementia with Lewy bodies. *Eur J Hybrid Imaging,* 4**,** 25.
NIENS, J., REH, F., COBAN, B., CICHEWICZ, K., ECKARDT, J., LIU, Y. T., HIRSH, J. & RIEMENSPERGER, T. D. 2017. Dopamine Modulates Serotonin Innervation in the Drosophila Brain. *Front Syst Neurosci,* 11**,** 76.
NIKOLAUS, S., ANTKE, C. & MULLER, H. W. 2009. In vivo imaging of synaptic function in the central nervous system: I. Movement disorders and dementia. *Behav Brain Res,* 204**,** 1-31.
NIKOLAUS, S., BEU, M., HAUTZEL, H., SILVA, A. M., ANTKE, C., WIRRWAR, A., HUSTON, J. P. & MULLER, H. W. 2013. Effects of L-DOPA on striatal iodine-123-FP-CIT binding and behavioral parameters in the rat. *Nucl Med Commun,* 34**,** 1223-32.
NISHIJIMA, H., SUZUKI, S., KON, T., FUNAMIZU, Y., UENO, T., HAGA, R., SUZUKI, C., ARAI, A., KIMURA, T., SUZUKI, C., MEGURO, R., MIKI, Y., YAMADA, J., MIGITA, K., ICHINOHE, N., UENO, S., BABA, M. & TOMIYAMA, M. 2014. Morphologic changes of dendritic spines of striatal neurons in the levodopa-induced dyskinesia model. *Mov Disord,* 29**,** 336-43.
NISHIJIMA, H., UENO, T., FUNAMIZU, Y., UENO, S. & TOMIYAMA, M. 2018. Levodopa treatment and dendritic spine pathology. *Mov Disord,* 33**,** 877-888.
NIWA, K., ARAKI, E., MORHAM, S. G., ROSS, M. E. & IADECOLA, C. 2000. Cyclooxygenase-2 contributes to functional hyperemia in whisker-barrel cortex. *J Neurosci,* 20**,** 763-70.
NOBILI, F., ARNALDI, D., CAMPUS, C., FERRARA, M., DE CARLI, F., BRUGNOLO, A., DESSI, B., GIRTLER, N., MORBELLI, S., ABRUZZESE, G., SAMBUCETI, G. & RODRIGUEZ, G. 2011. Brain perfusion correlates of cognitive and nigrostriatal functions in de novo Parkinson's disease. *Eur J Nucl Med Mol Imaging,* 38**,** 2209-18.
NOMBELA, C., ROWE, J. B., WINDER-RHODES, S. E., HAMPSHIRE, A., OWEN, A. M., BREEN, D. P., DUNCAN, G. W., KHOO, T. K., YARNALL, A. J., FIRBANK, M. J., CHINNERY, P. F., ROBBINS, T. W., O'BRIEN, J. T., BROOKS, D. J., BURN, D. J., GROUP, I.-P. S. & BARKER, R. A. 2014. Genetic impact on cognition and brain function in newly diagnosed Parkinson's disease: ICICLE-PD study. *Brain,* 137**,** 2743-58.
NORTLEY, R. & ATTWELL, D. 2017. Control of brain energy supply by astrocytes. *Curr Opin Neurobiol,* 47**,** 80-85.
NOWACK, A., YAO, J., CUSTER, K. L. & BAJJALIEH, S. M. 2010. SV2 regulates neurotransmitter release via multiple mechanisms. *Am J Physiol Cell Physiol,* 299**,** C960-7.
O'BRIEN, J. T., COLLOBY, S., FENWICK, J., WILLIAMS, E. D., FIRBANK, M., BURN, D., AARSLAND, D. & MCKEITH, I. G. 2004. Dopamine transporter loss visualized with FP-CIT SPECT in the differential diagnosis of dementia with Lewy bodies. *Arch Neurol,* 61**,** 919-25.
O'CALLAGHAN, C., HEZEMANS, F. H., YE, R., RUA, C., JONES, P. S., MURLEY, A. G., HOLLAND, N., REGENTHAL, R., TSVETANOV, K. A., WOLPE, N., BARKER, R.

A., WILLIAMS-GRAY, C. H., ROBBINS, T. W., PASSAMONTI, L. & ROWE, J. B. 2021. Locus coeruleus integrity and the effect of atomoxetine on response inhibition in Parkinson's disease. *Brain,* 144**,** 2513-2526.
O'CONNOR, D. H., FUKUI, M. M., PINSK, M. A. & KASTNER, S. 2002. Attention modulates responses in the human lateral geniculate nucleus. *Nat Neurosci,* 5**,** 1203-9.
OBESO, J. A., MARIN, C., RODRIGUEZ-OROZ, C., BLESA, J., BENITEZ-TEMINO, B., MENA-SEGOVIA, J., RODRIGUEZ, M. & OLANOW, C. W. 2008. The basal ganglia in Parkinson's disease: current concepts and unexplained observations. *Ann Neurol,* 64 Suppl 2**,** S30-46.
OEPPEN, J. & VAUPEL, J. W. 2002. Demography. Broken limits to life expectancy. *Science,* 296**,** 1029-31.
OHTA, K., FUJINAMI, A., KUNO, S., SAKAKIMOTO, A., MATSUI, H., KAWAHARA, Y. & OHTA, M. 2004. Cabergoline stimulates synthesis and secretion of nerve growth factor, brain-derived neurotrophic factor and glial cell line-derived neurotrophic factor by mouse astrocytes in primary culture. *Pharmacology,* 71**,** 162-8.
OHTA, K., KUNO, S., MIZUTA, I., FUJINAMI, A., MATSUI, H. & OHTA, M. 2003. Effects of dopamine agonists bromocriptine, pergolide, cabergoline, and SKF-38393 on GDNF, NGF, and BDNF synthesis in cultured mouse astrocytes. *Life Sci,* 73**,** 617-26.
OHTA, M., MIZUTA, I., OHTA, K., NISHIMURA, M., MIZUTA, E., HAYASHI, K. & KUNO, S. 2000. Apomorphine up-regulates NGF and GDNF synthesis in cultured mouse astrocytes. *Biochem Biophys Res Commun,* 272**,** 18-22.
OKAZAWA, H., MURATA, M., WATANABE, M., KAMEI, M. & KANAZAWA, I. 1992. Dopaminergic stimulation up-regulates the in vivo expression of brain-derived neurotrophic factor (BDNF) in the striatum. *FEBS Lett,* 313**,** 138-42.
OLANOW, C. W. 2019. Levodopa is the best symptomatic therapy for PD: Nothing more, nothing less. *Mov Disord,* 34**,** 812-815.
OLANOW, C. W., PERL, D. P., DEMARTINO, G. N. & MCNAUGHT, K. S. 2004. Lewy-body formation is an aggresome-related process: a hypothesis. *Lancet Neurol,* 3**,** 496-503.
OLIVERO, P., LOZANO, C., SOTOMAYOR-ZARATE, R., MEZA-CONCHA, N., ARANCIBIA, M., CORDOVA, C., GONZALEZ-ARRIAGADA, W., RAMIREZ-BARRANTES, R. & MARCHANT, I. 2018. Proteostasis and Mitochondrial Role on Psychiatric and Neurodegenerative Disorders: Current Perspectives. *Neural Plast,* 2018**,** 6798712.
OLSEN, M. L. & SONTHEIMER, H. 2008. Functional implications for Kir4.1 channels in glial biology: from K+ buffering to cell differentiation. *J Neurochem,* 107**,** 589-601.
OMIATEK, D. M., BRESSLER, A. J., CANS, A. S., ANDREWS, A. M., HEIEN, M. L. & EWING, A. G. 2013. The real catecholamine content of secretory vesicles in the CNS revealed by electrochemical cytometry. *Sci Rep,* 3**,** 1447.
ONOFRJ, M., VARANESE, S., BONANNI, L., TAYLOR, J. P., ANTONINI, A., VALENTE, E. M., PETRUCCI, S., STOCCHI, F., THOMAS, A. & PERFETTI, B. 2013. Cohort study of prevalence and phenomenology of tremor in dementia with Lewy bodies. *J Neurol,* 260**,** 1731-42.
ONWORDI, E. C., HALFF, E. F., WHITEHURST, T., MANSUR, A., COTEL, M. C., WELLS, L., CREENEY, H., BONSALL, D., ROGDAKI, M., SHATALINA, E., REIS MARQUES, T., RABINER, E. A., GUNN, R. N., NATESAN, S., VERNON, A. C. & HOWES, O. D. 2020. Synaptic density marker SV2A is reduced in schizophrenia patients and unaffected by antipsychotics in rats. *Nat Commun,* 11**,** 246.
ORIMO, S., UCHIHARA, T., NAKAMURA, A., MORI, F., KAKITA, A., WAKABAYASHI, K. & TAKAHASHI, H. 2008. Axonal alpha-synuclein aggregates herald centripetal degeneration of cardiac sympathetic nerve in Parkinson's disease. *Brain,* 131**,** 642-50.

OSADA, O. & IWASAKI, A. 2017. A case of successful treatment with donepezil of olfactory hallucination in parkinson disease. *Rinsho Shinkeigaku,* 57**,** 29-32.
OUCHI, Y., YOSHIKAWA, E., SEKINE, Y., FUTATSUBASHI, M., KANNO, T., OGUSU, T. & TORIZUKA, T. 2005. Microglial activation and dopamine terminal loss in early Parkinson's disease. *Ann Neurol,* 57**,** 168-75.
PACELLI, C., GIGUERE, N., BOURQUE, M. J., LEVESQUE, M., SLACK, R. S. & TRUDEAU, L. E. 2015. Elevated Mitochondrial Bioenergetics and Axonal Arborization Size Are Key Contributors to the Vulnerability of Dopamine Neurons. *Curr Biol,* 25**,** 2349-60.
PAGANO, G., NICCOLINI, F. & POLITIS, M. 2018. The serotonergic system in Parkinson's patients with dyskinesia: evidence from imaging studies. *J Neural Transm (Vienna),* 125**,** 1217-1223.
PAGANO, G. & POLITIS, M. 2018. Molecular Imaging of the Serotonergic System in Parkinson's Disease. *Int Rev Neurobiol,* 141**,** 173-210.
PAGONABARRAGA, J., SORIANO-MAS, C., LLEBARIA, G., LOPEZ-SOLA, M., PUJOL, J. & KULISEVSKY, J. 2014. Neural correlates of minor hallucinations in non-demented patients with Parkinson's disease. *Parkinsonism Relat Disord,* 20**,** 290-6.
PAILLE, V., PICCONI, B., BAGETTA, V., GHIGLIERI, V., SGOBIO, C., DI FILIPPO, M., VISCOMI, M. T., GIAMPA, C., FUSCO, F. R., GARDONI, F., BERNARDI, G., GREENGARD, P., DI LUCA, M. & CALABRESI, P. 2010. Distinct levels of dopamine denervation differentially alter striatal synaptic plasticity and NMDA receptor subunit composition. *J Neurosci,* 30**,** 14182-93.
PAKKENBERG, B., PELVIG, D., MARNER, L., BUNDGAARD, M. J., GUNDERSEN, H. J., NYENGAARD, J. R. & REGEUR, L. 2003. Aging and the human neocortex. *Exp Gerontol,* 38**,** 95-9.
PALMER, S. J., NG, B., ABUGHARBIEH, R., EIGENRAAM, L. & MCKEOWN, M. J. 2009. Motor reserve and novel area recruitment: amplitude and spatial characteristics of compensation in Parkinson's disease. *Eur J Neurosci,* 29**,** 2187-96.
PAN, T., KONDO, S., LE, W. & JANKOVIC, J. 2008. The role of autophagy-lysosome pathway in neurodegeneration associated with Parkinson's disease. *Brain,* 131**,** 1969-78.
PAPAGNO, C. & TROJANO, L. 2018. Cognitive and behavioral disorders in Parkinson's disease: an update. I: cognitive impairments. *Neurol Sci,* 39**,** 215-223.
PARAIN, K., MURER, M. G., YAN, Q., FAUCHEUX, B., AGID, Y., HIRSCH, E. & RAISMAN-VOZARI, R. 1999. Reduced expression of brain-derived neurotrophic factor protein in Parkinson's disease substantia nigra. *Neuroreport,* 10**,** 557-61.
PARENT, M., WALLMAN, M. J., GAGNON, D. & PARENT, A. 2011. Serotonin innervation of basal ganglia in monkeys and humans. *J Chem Neuroanat,* 41**,** 256-65.
PARKINSON, J. 2002. An essay on the shaking palsy. 1817. *J Neuropsychiatry Clin Neurosci,* 14**,** 223-36; discussion 222.
PARKINSON STUDY, G. 2002. Dopamine transporter brain imaging to assess the effects of pramipexole vs levodopa on Parkinson disease progression. *JAMA,* 287**,** 1653-61.
PARKKINEN, L., PIRTTILA, T. & ALAFUZOFF, I. 2008. Applicability of current staging/categorization of alpha-synuclein pathology and their clinical relevance. *Acta Neuropathol,* 115**,** 399-407.
PATANIA, A., SELVAGGI, P., VERONESE, M., DIPASQUALE, O., EXPERT, P. & PETRI, G. 2019. Topological gene expression networks recapitulate brain anatomy and function. *Netw Neurosci,* 3**,** 744-762.
PATEL, Y., SHIN, J., DRAKESMITH, M., EVANS, J., PAUSOVA, Z. & PAUS, T. 2020. Virtual histology of multi-modal magnetic resonance imaging of cerebral cortex in young men. *Neuroimage,* 218**,** 116968.

PATT, S. & GERHARD, L. 1993. A Golgi study of human locus coeruleus in normal brains and in Parkinson's disease. *Neuropathol Appl Neurobiol,* 19**,** 519-23.
PATT, S., GERTZ, H. J., GERHARD, L. & CERVOS-NAVARRO, J. 1991. Pathological changes in dendrites of substantia nigra neurons in Parkinson's disease: a Golgi study. *Histol Histopathol,* 6**,** 373-80.
PAULUS, W. & JELLINGER, K. 1991. The neuropathologic basis of different clinical subgroups of Parkinson's disease. *J Neuropathol Exp Neurol,* 50**,** 743-55.
PAVESE, N., METTA, V., BOSE, S. K., CHAUDHURI, K. R. & BROOKS, D. J. 2010. Fatigue in Parkinson's disease is linked to striatal and limbic serotonergic dysfunction. *Brain,* 133**,** 3434-43.
PAVESE, N., RIVERO-BOSCH, M., LEWIS, S. J., WHONE, A. L. & BROOKS, D. J. 2011. Progression of monoaminergic dysfunction in Parkinson's disease: a longitudinal 18F-dopa PET study. *Neuroimage,* 56**,** 1463-8.
PELIZZARI, L., DI TELLA, S., ROSSETTO, F., LAGANA, M. M., BERGSLAND, N., PIRASTRU, A., MELONI, M., NEMNI, R. & BAGLIO, F. 2020. Parietal Perfusion Alterations in Parkinson's Disease Patients Without Dementia. *Front Neurol,* 11**,** 562.
PENCEA, V., BINGAMAN, K. D., WIEGAND, S. J. & LUSKIN, M. B. 2001. Infusion of brain-derived neurotrophic factor into the lateral ventricle of the adult rat leads to new neurons in the parenchyma of the striatum, septum, thalamus, and hypothalamus. *J Neurosci,* 21**,** 6706-17.
PERDAHL, E., ADOLFSSON, R., ALAFUZOFF, I., ALBERT, K. A., NESTLER, E. J., GREENGARD, P. & WINBLAD, B. 1984. Synapsin I (protein I) in different brain regions in senile dementia of Alzheimer type and in multi-infarct dementia. *J Neural Transm,* 60**,** 133-41.
PEREIRA, J. B., JANELIDZE, S., OSSENKOPPELE, R., KVARTSBERG, H., BRINKMALM, A., MATTSSON-CARLGREN, N., STOMRUD, E., SMITH, R., ZETTERBERG, H., BLENNOW, K. & HANSSON, O. 2021. Untangling the association of amyloid-beta and tau with synaptic and axonal loss in Alzheimer's disease. *Brain,* 144**,** 310-324.
PEREIRA, J. B., JUNQUE, C., MARTI, M. J., RAMIREZ-RUIZ, B., BARGALLO, N. & TOLOSA, E. 2009. Neuroanatomical substrate of visuospatial and visuoperceptual impairment in Parkinson's disease. *Mov Disord,* 24**,** 1193-9.
PEREZ, F., HELMER, C., DARTIGUES, J. F., AURIACOMBE, S. & TISON, F. 2010. A 15-year population-based cohort study of the incidence of Parkinson's disease and dementia with Lewy bodies in an elderly French cohort. *J Neurol Neurosurg Psychiatry,* 81**,** 742-6.
PEREZ, R. G., WAYMIRE, J. C., LIN, E., LIU, J. J., GUO, F. & ZIGMOND, M. J. 2002. A role for alpha-synuclein in the regulation of dopamine biosynthesis. *J Neurosci,* 22**,** 3090-9.
PEREZ-LLORET, S. & BARRANTES, F. J. 2016. Deficits in cholinergic neurotransmission and their clinical correlates in Parkinson's disease. *NPJ Parkinsons Dis,* 2**,** 16001.
PERRY, E. K., CURTIS, M., DICK, D. J., CANDY, J. M., ATACK, J. R., BLOXHAM, C. A., BLESSED, G., FAIRBAIRN, A., TOMLINSON, B. E. & PERRY, R. H. 1985. Cholinergic correlates of cognitive impairment in Parkinson's disease: comparisons with Alzheimer's disease. *J Neurol Neurosurg Psychiatry,* 48**,** 413-21.
PETROVA, M., MEHRABIAN-SPASOVA, S., AARSLAND, D., RAYCHEVA, M. & TRAYKOV, L. 2015. Clinical and Neuropsychological Differences between Mild Parkinson's Disease Dementia and Dementia with Lewy Bodies. *Dement Geriatr Cogn Dis Extra,* 5**,** 212-20.
PHAN, J. A., STOKHOLM, K., ZAREBA-PASLAWSKA, J., JAKOBSEN, S., VANG, K., GJEDDE, A., LANDAU, A. M. & ROMERO-RAMOS, M. 2017. Early synaptic

dysfunction induced by alpha-synuclein in a rat model of Parkinson's disease. *Sci Rep,* 7**,** 6363.
PHILIPPART, F., DESTREEL, G., MERINO-SEPULVEDA, P., HENNY, P., ENGEL, D. & SEUTIN, V. 2016. Differential Somatic Ca2+ Channel Profile in Midbrain Dopaminergic Neurons. *J Neurosci,* 36**,** 7234-45.
PICCONI, B., CENTONZE, D., ROSSI, S., BERNARDI, G. & CALABRESI, P. 2004. Therapeutic doses of L-dopa reverse hypersensitivity of corticostriatal D2-dopamine receptors and glutamatergic overactivity in experimental parkinsonism. *Brain,* 127**,** 1661-9.
PICCONI, B., GHIGLIERI, V. & CALABRESI, P. 2010. L-3,4-dihydroxyphenylalanine-induced sprouting of serotonin axon terminals: A useful biomarker for dyskinesias? *Ann Neurol,* 68**,** 578-80.
PICCONI, B., PAILLE, V., GHIGLIERI, V., BAGETTA, V., BARONE, I., LINDGREN, H. S., BERNARDI, G., ANGELA CENCI, M. & CALABRESI, P. 2008. l-DOPA dosage is critically involved in dyskinesia via loss of synaptic depotentiation. *Neurobiol Dis,* 29**,** 327-35.
PICCONI, B., PICCOLI, G. & CALABRESI, P. 2012. Synaptic dysfunction in Parkinson's disease. *Adv Exp Med Biol,* 970**,** 553-72.
PICCONI, B., PISANI, A., BARONE, I., BONSI, P., CENTONZE, D., BERNARDI, G. & CALABRESI, P. 2005. Pathological synaptic plasticity in the striatum: implications for Parkinson's disease. *Neurotoxicology,* 26**,** 779-83.
PICKRELL, A. M. & YOULE, R. J. 2015. The roles of PINK1, parkin, and mitochondrial fidelity in Parkinson's disease. *Neuron,* 85**,** 257-73.
PIFL, C., KISH, S. J. & HORNYKIEWICZ, O. 2012. Thalamic noradrenaline in Parkinson's disease: deficits suggest role in motor and non-motor symptoms. *Mov Disord,* 27**,** 1618-24.
PIMLOTT, S. L., PIGGOTT, M., BALLARD, C., MCKEITH, I., PERRY, R., KOMETA, S., OWENS, J., WYPER, D. & PERRY, E. 2006. Thalamic nicotinic receptors implicated in disturbed consciousness in dementia with Lewy bodies. *Neurobiol Dis,* 21**,** 50-6.
PINARD, A. & ROBITAILLE, R. 2008. Nitric oxide dependence of glutamate-mediated modulation at a vertebrate neuromuscular junction. *Eur J Neurosci,* 28**,** 577-87.
PINTO, M. J. & ALMEIDA, R. D. 2016. Puzzling out presynaptic differentiation. *J Neurochem,* 139**,** 921-942.
PISANI, V., STEFANI, A., PIERANTOZZI, M., NATOLI, S., STANZIONE, P., FRANCIOTTA, D. & PISANI, A. 2012. Increased blood-cerebrospinal fluid transfer of albumin in advanced Parkinson's disease. *J Neuroinflammation,* 9**,** 188.
PISSADAKI, E. K. & BOLAM, J. P. 2013. The energy cost of action potential propagation in dopamine neurons: clues to susceptibility in Parkinson's disease. *Front Comput Neurosci,* 7**,** 13.
PITCHER, T. L., MELZER, T. R., MACASKILL, M. R., GRAHAM, C. F., LIVINGSTON, L., KEENAN, R. J., WATTS, R., DALRYMPLE-ALFORD, J. C. & ANDERSON, T. J. 2012. Reduced striatal volumes in Parkinson's disease: a magnetic resonance imaging study. *Transl Neurodegener,* 1**,** 17.
POEWE, W., SEPPI, K., TANNER, C. M., HALLIDAY, G. M., BRUNDIN, P., VOLKMANN, J., SCHRAG, A. E. & LANG, A. E. 2017. Parkinson disease. *Nat Rev Dis Primers,* 3**,** 17013.
POLITIS, M. & NICCOLINI, F. 2015. Serotonin in Parkinson's disease. *Behav Brain Res,* 277**,** 136-45.
POLITIS, M., WU, K., LOANE, C., BROOKS, D. J., KIFERLE, L., TURKHEIMER, F. E., BAIN, P., MOLLOY, S. & PICCINI, P. 2014. Serotonergic mechanisms responsible for levodopa-induced dyskinesias in Parkinson's disease patients. *J Clin Invest,* 124**,** 1340-9.

POLITIS, M., WU, K., LOANE, C., KIFERLE, L., MOLLOY, S., BROOKS, D. J. & PICCINI, P. 2010a. Staging of serotonergic dysfunction in Parkinson's disease: an in vivo 11C-DASB PET study. *Neurobiol Dis,* 40**,** 216-21.
POLITIS, M., WU, K., LOANE, C., TURKHEIMER, F. E., MOLLOY, S., BROOKS, D. J. & PICCINI, P. 2010b. Depressive symptoms in PD correlate with higher 5-HTT binding in raphe and limbic structures. *Neurology,* 75**,** 1920-7.
POSTUMA, R. B., BERG, D., STERN, M., POEWE, W., OLANOW, C. W., OERTEL, W., MAREK, K., LITVAN, I., LANG, A. E., HALLIDAY, G., GOETZ, C. G., GASSER, T., DUBOIS, B., CHAN, P., BLOEM, B. R., ADLER, C. H. & DEUSCHL, G. 2016. Abolishing the 1-year rule: How much evidence will be enough? *Mov Disord,* 31**,** 1623-1627.
POSTUMA, R. B., BERG, D., STERN, M., POEWE, W., OLANOW, C. W., OERTEL, W., OBESO, J., MAREK, K., LITVAN, I., LANG, A. E., HALLIDAY, G., GOETZ, C. G., GASSER, T., DUBOIS, B., CHAN, P., BLOEM, B. R., ADLER, C. H. & DEUSCHL, G. 2015. MDS clinical diagnostic criteria for Parkinson's disease. *Mov Disord,* 30**,** 1591-601.
POSTUMA, R. B., IRANZO, A., HU, M., HOGL, B., BOEVE, B. F., MANNI, R., OERTEL, W. H., ARNULF, I., FERINI-STRAMBI, L., PULIGHEDDU, M., ANTELMI, E., COCHEN DE COCK, V., ARNALDI, D., MOLLENHAUER, B., VIDENOVIC, A., SONKA, K., JUNG, K. Y., KUNZ, D., DAUVILLIERS, Y., PROVINI, F., LEWIS, S. J., BUSKOVA, J., PAVLOVA, M., HEIDBREDER, A., MONTPLAISIR, J. Y., SANTAMARIA, J., BARBER, T. R., STEFANI, A., ST LOUIS, E. K., TERZAGHI, M., JANZEN, A., LEU-SEMENESCU, S., PLAZZI, G., NOBILI, F., SIXEL-DOERING, F., DUSEK, P., BES, F., CORTELLI, P., EHGOETZ MARTENS, K., GAGNON, J. F., GAIG, C., ZUCCONI, M., TRENKWALDER, C., GAN-OR, Z., LO, C., ROLINSKI, M., MAHLKNECHT, P., HOLZKNECHT, E., BOEVE, A. R., TEIGEN, L. N., TOSCANO, G., MAYER, G., MORBELLI, S., DAWSON, B. & PELLETIER, A. 2019. Risk and predictors of dementia and parkinsonism in idiopathic REM sleep behaviour disorder: a multicentre study. *Brain,* 142**,** 744-759.
POSTUMA, R. B., POEWE, W., LITVAN, I., LEWIS, S., LANG, A. E., HALLIDAY, G., GOETZ, C. G., CHAN, P., SLOW, E., SEPPI, K., SCHAFFER, E., RIOS-ROMENETS, S., MI, T., MAETZLER, C., LI, Y., HEIM, B., BLEDSOE, I. O. & BERG, D. 2018. Validation of the MDS clinical diagnostic criteria for Parkinson's disease. *Mov Disord,* 33**,** 1601-1608.
PRESA, J. L., SARAVIA, F., BAGI, Z. & FILOSA, J. A. 2020. Vasculo-Neuronal Coupling and Neurovascular Coupling at the Neurovascular Unit: Impact of Hypertension. *Front Physiol,* 11**,** 584135.
PRESCOTT, I. A., DOSTROVSKY, J. O., MORO, E., HODAIE, M., LOZANO, A. M. & HUTCHISON, W. D. 2009. Levodopa enhances synaptic plasticity in the substantia nigra pars reticulata of Parkinson's disease patients. *Brain,* 132**,** 309-18.
PRICE, C. J. & FRISTON, K. J. 1997. Cognitive conjunction: a new approach to brain activation experiments. *Neuroimage,* 5**,** 261-70.
PRINGSHEIM, T., JETTE, N., FROLKIS, A. & STEEVES, T. D. 2014. The prevalence of Parkinson's disease: a systematic review and meta-analysis. *Mov Disord,* 29**,** 1583-90.
PURUSHOTHAMAN, G., MARION, R., LI, K. & CASAGRANDE, V. A. 2012. Gating and control of primary visual cortex by pulvinar. *Nat Neurosci,* 15**,** 905-12.
RABINER, E. A. 2018. Imaging Synaptic Density: A Different Look at Neurologic Diseases. *J Nucl Med,* 59**,** 380-381.
RADHAKRISHNAN, R., SKOSNIK, P. D., RANGANATHAN, M., NAGANAWA, M., TOYONAGA, T., FINNEMA, S., HILLMER, A. T., ESTERLIS, I., HUANG, Y.,

NABULSI, N., CARSON, R. E. & D'SOUZA, D. C. 2021. In vivo evidence of lower synaptic vesicle density in schizophrenia. *Mol Psychiatry*.
RAFF, M. C., WHITMORE, A. V. & FINN, J. T. 2002. Axonal self-destruction and neurodegeneration. *Science,* 296**,** 868-71.
RAHKONEN, T., ELONIEMI-SULKAVA, U., RISSANEN, S., VATANEN, A., VIRAMO, P. & SULKAVA, R. 2003. Dementia with Lewy bodies according to the consensus criteria in a general population aged 75 years or older. *J Neurol Neurosurg Psychiatry,* 74**,** 720-4.
RAICHLE, M. E. 1998. Behind the scenes of functional brain imaging: a historical and physiological perspective. *Proc Natl Acad Sci U S A,* 95**,** 765-72.
RAICHLE, M. E., HARTMAN, B. K., EICHLING, J. O. & SHARPE, L. G. 1975. Central noradrenergic regulation of cerebral blood flow and vascular permeability. *Proc Natl Acad Sci U S A,* 72**,** 3726-30.
RAMIREZ-RUIZ, B., JUNQUE, C., MARTI, M. J., VALLDEORIOLA, F. & TOLOSA, E. 2007. Cognitive changes in Parkinson's disease patients with visual hallucinations. *Dement Geriatr Cogn Disord,* 23**,** 281-8.
RANJBAR-SLAMLOO, Y. & FAZLALI, Z. 2019. Dopamine and Noradrenaline in the Brain; Overlapping or Dissociate Functions? *Front Mol Neurosci,* 12**,** 334.
RANK, M. M., MURRAY, K. C., STEPHENS, M. J., D'AMICO, J., GORASSINI, M. A. & BENNETT, D. J. 2011. Adrenergic receptors modulate motoneuron excitability, sensory synaptic transmission and muscle spasms after chronic spinal cord injury. *J Neurophysiol,* 105**,** 410-22.
RAVAL, N. R., JOHANSEN, A., DONOVAN, L. L., ROS, N. F., OZENNE, B., HANSEN, H. D. & KNUDSEN, G. M. 2021. A Single Dose of Psilocybin Increases Synaptic Density and Decreases 5-HT2A Receptor Density in the Pig Brain. *Int J Mol Sci,* 22.
RAVINA, B., EIDELBERG, D., AHLSKOG, J. E., ALBIN, R. L., BROOKS, D. J., CARBON, M., DHAWAN, V., FEIGIN, A., FAHN, S., GUTTMAN, M., GWINN-HARDY, K., MCFARLAND, H., INNIS, R., KATZ, R. G., KIEBURTZ, K., KISH, S. J., LANGE, N., LANGSTON, J. W., MAREK, K., MORIN, L., MOY, C., MURPHY, D., OERTEL, W. H., OLIVER, G., PALESCH, Y., POWERS, W., SEIBYL, J., SETHI, K. D., SHULTS, C. W., SHEEHY, P., STOESSL, A. J. & HOLLOWAY, R. 2005. The role of radiotracer imaging in Parkinson disease. *Neurology,* 64**,** 208-15.
RAY CHAUDHURI, K., POEWE, W. & BROOKS, D. 2018. Motor and Nonmotor Complications of Levodopa: Phenomenology, Risk Factors, and Imaging Features. *Mov Disord,* 33**,** 909-919.
RAZ, L., KNOEFEL, J. & BHASKAR, K. 2016. The neuropathology and cerebrovascular mechanisms of dementia. *J Cereb Blood Flow Metab,* 36**,** 172-86.
REGEHR, W. G., CAREY, M. R. & BEST, A. R. 2009. Activity-dependent regulation of synapses by retrograde messengers. *Neuron,* 63**,** 154-70.
REICHMANN, H. 2000. Long-term treatment with dopamine agonists in idiopathic Parkinson's disease. *J Neurol,* 247 Suppl 4**,** IV/17-9.
REIJNDERS, J. S., EHRT, U., LOUSBERG, R., AARSLAND, D. & LEENTJENS, A. F. 2009. The association between motor subtypes and psychopathology in Parkinson's disease. *Parkinsonism Relat Disord,* 15**,** 379-82.
REKTOROVA, I., BIUNDO, R., MARECEK, R., WEIS, L., AARSLAND, D. & ANTONINI, A. 2014. Grey matter changes in cognitively impaired Parkinson's disease patients. *PLoS One,* 9**,** e85595.
REN, Y., LIU, W., JIANG, H., JIANG, Q. & FENG, J. 2005. Selective vulnerability of dopaminergic neurons to microtubule depolymerization. *J Biol Chem,* 280**,** 34105-12.
REVUELTA, G. J., ROSSO, A. & LIPPA, C. F. 2008. Neuritic pathology as a correlate of synaptic loss in dementia with lewy bodies. *Am J Alzheimers Dis Other Demen,* 23**,** 97-102.

RIBEIRO, J. A. & SEBASTIAO, A. M. 2010. Modulation and metamodulation of synapses by adenosine. *Acta Physiol (Oxf),* 199**,** 161-9.
RIEDERER, P. & WUKETICH, S. 1976. Time course of nigrostriatal degeneration in parkinson's disease. A detailed study of influential factors in human brain amine analysis. *J Neural Transm,* 38**,** 277-301.
RIZZO, G., ARCUTI, S., COPETTI, M., ALESSANDRIA, M., SAVICA, R., FONTANA, A., LIGUORI, R. & LOGROSCINO, G. 2018. Accuracy of clinical diagnosis of dementia with Lewy bodies: a systematic review and meta-analysis. *J Neurol Neurosurg Psychiatry,* 89**,** 358-366.
RIZZO, G., COPETTI, M., ARCUTI, S., MARTINO, D., FONTANA, A. & LOGROSCINO, G. 2016. Accuracy of clinical diagnosis of Parkinson disease: A systematic review and meta-analysis. *Neurology,* 86**,** 566-76.
RIZZO, G., VERONESE, M., HECKEMANN, R. A., SELVARAJ, S., HOWES, O. D., HAMMERS, A., TURKHEIMER, F. E. & BERTOLDO, A. 2014. The predictive power of brain mRNA mappings for in vivo protein density: a positron emission tomography correlation study. *J Cereb Blood Flow Metab,* 34**,** 827-35.
ROBERTS, J. A., PERRY, A., LORD, A. R., ROBERTS, G., MITCHELL, P. B., SMITH, R. E., CALAMANTE, F. & BREAKSPEAR, M. 2016. The contribution of geometry to the human connectome. *Neuroimage,* 124**,** 379-393.
ROMERO-GARCIA, R., WHITAKER, K. J., VASA, F., SEIDLITZ, J., SHINN, M., FONAGY, P., DOLAN, R. J., JONES, P. B., GOODYER, I. M., CONSORTIUM, N., BULLMORE, E. T. & VERTES, P. E. 2018. Structural covariance networks are coupled to expression of genes enriched in supragranular layers of the human cortex. *Neuroimage,* 171**,** 256-267.
ROMMELFANGER, K. S. & WEINSHENKER, D. 2007. Norepinephrine: The redheaded stepchild of Parkinson's disease. *Biochem Pharmacol,* 74**,** 177-90.
ROMMELFANGER, K. S., WEINSHENKER, D. & MILLER, G. W. 2004. Reduced MPTP toxicity in noradrenaline transporter knockout mice. *J Neurochem,* 91**,** 1116-24.
ROSEN, S. C., SUSSWEIN, A. J., CROPPER, E. C., WEISS, K. R. & KUPFERMANN, I. 1989. Selective modulation of spike duration by serotonin and the neuropeptides, FMRFamide, SCPB, buccalin and myomodulin in different classes of mechanoafferent neurons in the cerebral ganglion of Aplysia. *J Neurosci,* 9**,** 390-402.
ROSENBERG-KATZ, K., HERMAN, T., JACOB, Y., GILADI, N., HENDLER, T. & HAUSDORFF, J. M. 2013. Gray matter atrophy distinguishes between Parkinson disease motor subtypes. *Neurology,* 80**,** 1476-84.
ROSENGARTEN, B., DANNHARDT, V., BURR, O., POHLER, M., ROSENGARTEN, S., OECHSNER, M. & REUTER, I. 2010. Neurovascular coupling in Parkinson's disease patients: effects of dementia and acetylcholinesterase inhibitor treatment. *J Alzheimers Dis,* 22**,** 415-21.
ROSS, G. W., PETROVITCH, H., ABBOTT, R. D., NELSON, J., MARKESBERY, W., DAVIS, D., HARDMAN, J., LAUNER, L., MASAKI, K., TANNER, C. M. & WHITE, L. R. 2004. Parkinsonian signs and substantia nigra neuron density in decendents elders without PD. *Ann Neurol,* 56**,** 532-9.
ROSSANO, S., TOYONAGA, T., FINNEMA, S. J., NAGANAWA, M., LU, Y., NABULSI, N., ROPCHAN, J., DE BRUYN, S., OTOUL, C., STOCKIS, A., NICOLAS, J. M., MARTIN, P., MERCIER, J., HUANG, Y., MAGUIRE, R. P. & CARSON, R. E. 2020. Assessment of a white matter reference region for (11)C-UCB-J PET quantification. *J Cereb Blood Flow Metab,* 40**,** 1890-1901.
ROSSI, C., VOLTERRANI, D., NICOLETTI, V., MANCA, G., FROSINI, D., KIFERLE, L., UNTI, E., DE FEO, P., BONUCCELLI, U. & CERAVOLO, R. 2009. "Parkinson-

dementia" diseases: a comparison by double tracer SPECT studies. *Parkinsonism Relat Disord,* 15**,** 762-6.
ROUACH, N., AVIGNONE, E., MEME, W., KOULAKOFF, A., VENANCE, L., BLOMSTRAND, F. & GIAUME, C. 2002. Gap junctions and connexin expression in the normal and pathological central nervous system. *Biol Cell,* 94**,** 457-75.
ROY, S. 2017. Synuclein and dopamine: the Bonnie and Clyde of Parkinson's disease. *Nat Neurosci,* 20**,** 1514-1515.
RUBERG, M., PLOSKA, A., JAVOY-AGID, F. & AGID, Y. 1982. Muscarinic binding and choline acetyltransferase activity in Parkinsonian subjects with reference to dementia. *Brain Res,* 232**,** 129-39.
RUBERG, M., RIEGER, F., VILLAGEOIS, A., BONNET, A. M. & AGID, Y. 1986. Acetylcholinesterase and butyrylcholinesterase in frontal cortex and cerebrospinal fluid of demented and non-demented patients with Parkinson's disease. *Brain Res,* 362**,** 83-91.
RUFFMANN, C., CALBOLI, F. C., BRAVI, I., GVERIC, D., CURRY, L. K., DE SMITH, A., PAVLOU, S., BUXTON, J. L., BLAKEMORE, A. I., TAKOUSIS, P., MOLLOY, S., PICCINI, P., DEXTER, D. T., RONCAROLI, F., GENTLEMAN, S. M. & MIDDLETON, L. T. 2016. Cortical Lewy bodies and Abeta burden are associated with prevalence and timing of dementia in Lewy body diseases. *Neuropathol Appl Neurobiol,* 42**,** 436-50.
RUSSO, M., CARRARINI, C., DONO, F., RISPOLI, M. G., DI PIETRO, M., DI STEFANO, V., FERRI, L., BONANNI, L., SENSI, S. L. & ONOFRJ, M. 2019. The Pharmacology of Visual Hallucinations in Synucleinopathies. *Front Pharmacol,* 10**,** 1379.
RYLANDER, D., PARENT, M., O'SULLIVAN, S. S., DOVERO, S., LEES, A. J., BEZARD, E., DESCARRIES, L. & CENCI, M. A. 2010. Maladaptive plasticity of serotonin axon terminals in levodopa-induced dyskinesia. *Ann Neurol,* 68**,** 619-28.
SAALMANN, Y. B. & KASTNER, S. 2011. Cognitive and perceptual functions of the visual thalamus. *Neuron,* 71**,** 209-23.
SAALMANN, Y. B., PINSK, M. A., WANG, L., LI, X. & KASTNER, S. 2012. The pulvinar regulates information transmission between cortical areas based on attention demands. *Science,* 337**,** 753-6.
SAAVEDRA, A., BALTAZAR, G., CARVALHO, C. M. & DUARTE, E. P. 2005. GDNF modulates HO-1 expression in substantia nigra postnatal cell cultures. *Free Radic Biol Med,* 39**,** 1611-9.
SAAVEDRA, A., BALTAZAR, G., SANTOS, P., CARVALHO, C. M. & DUARTE, E. P. 2006. Selective injury to dopaminergic neurons up-regulates GDNF in substantia nigra postnatal cell cultures: role of neuron-glia crosstalk. *Neurobiol Dis,* 23**,** 533-42.
SABBAGH, M. N., ADLER, C. H., LAHTI, T. J., CONNOR, D. J., VEDDERS, L., PETERSON, L. K., CAVINESS, J. N., SHILL, H. A., SUE, L. I., ZIABREVA, I., PERRY, E., BALLARD, C. G., AARSLAND, D., WALKER, D. G. & BEACH, T. G. 2009. Parkinson disease with dementia: comparing patients with and without Alzheimer pathology. *Alzheimer Dis Assoc Disord,* 23**,** 295-7.
SADIQ, D., WHITFIELD, T., LEE, L., STEVENS, T., COSTAFREDA, S. & WALKER, Z. 2017. Prodromal Dementia with Lewy Bodies and Prodromal Alzheimer's Disease: A Comparison of the Cognitive and Clinical Profiles. *J Alzheimers Dis,* 58**,** 463-470.
SAEED, U., COMPAGNONE, J., AVIV, R. I., STRAFELLA, A. P., BLACK, S. E., LANG, A. E. & MASELLIS, M. 2017. Imaging biomarkers in Parkinson's disease and Parkinsonian syndromes: current and emerging concepts. *Transl Neurodegener,* 6**,** 8.
SAKURAI, A., DARGHOUTH, N. R., BUTERA, R. J. & KATZ, P. S. 2006. Serotonergic enhancement of a 4-AP-sensitive current mediates the synaptic depression phase of spike timing-dependent neuromodulation. *J Neurosci,* 26**,** 2010-21.

SALA-LLONCH, R., LLADO, A., FORTEA, J., BOSCH, B., ANTONELL, A., BALASA, M., BARGALLO, N., BARTRES-FAZ, D., MOLINUEVO, J. L. & SANCHEZ-VALLE, R. 2015. Evolving brain structural changes in PSEN1 mutation carriers. *Neurobiol Aging,* 36**,** 1261-70.

SAMPATHKUMAR, V., MILLER-HANSEN, A., SHERMAN, S. M. & KASTHURI, N. 2021. Integration of signals from different cortical areas in higher order thalamic neurons. *Proc Natl Acad Sci U S A,* 118.

SANCHEZ-PADILLA, J., GUZMAN, J. N., ILIJIC, E., KONDAPALLI, J., GALTIERI, D. J., YANG, B., SCHIEBER, S., OERTEL, W., WOKOSIN, D., SCHUMACKER, P. T. & SURMEIER, D. J. 2014. Mitochondrial oxidant stress in locus coeruleus is regulated by activity and nitric oxide synthase. *Nat Neurosci,* 17**,** 832-40.

SANTANGELO, G., TROJANO, L., VITALE, C., IANNICIELLO, M., AMBONI, M., GROSSI, D. & BARONE, P. 2007. A neuropsychological longitudinal study in Parkinson's patients with and without hallucinations. *Mov Disord,* 22**,** 2418-25.

SARA, S. J. 2009. The locus coeruleus and noradrenergic modulation of cognition. *Nat Rev Neurosci,* 10**,** 211-23.

SARASSO, E., AGOSTA, F., PIRAMIDE, N., STOJKOVIC, T., STANKOVIC, I., BASAIA, S., TOMIC, A., MARKOVIC, V., STEFANOVA, E., VLADIMIR, K. & FILIPPI, M. 2021. Longitudinal Structural Brain Alterations in Parkinson's Disease Patients with Freezing of Gait (2708). *Neurology,* 86**,** 2708.

SASAKI, M., SHIBATA, E., TOHYAMA, K., TAKAHASHI, J., OTSUKA, K., TSUCHIYA, K., TAKAHASHI, S., EHARA, S., TERAYAMA, Y. & SAKAI, A. 2006. Neuromelanin magnetic resonance imaging of locus ceruleus and substantia nigra in Parkinson's disease. *Neuroreport,* 17**,** 1215-8.

SASAKI, T., MATSUKI, N. & IKEGAYA, Y. 2011. Action-potential modulation during axonal conduction. *Science,* 331**,** 599-601.

SATAKE, W., NAKABAYASHI, Y., MIZUTA, I., HIROTA, Y., ITO, C., KUBO, M., KAWAGUCHI, T., TSUNODA, T., WATANABE, M., TAKEDA, A., TOMIYAMA, H., NAKASHIMA, K., HASEGAWA, K., OBATA, F., YOSHIKAWA, T., KAWAKAMI, H., SAKODA, S., YAMAMOTO, M., HATTORI, N., MURATA, M., NAKAMURA, Y. & TODA, T. 2009. Genome-wide association study identifies common variants at four loci as genetic risk factors for Parkinson's disease. *Nat Genet,* 41**,** 1303-7.

SATO, A., SATO, Y. & UCHIDA, S. 2001. Regulation of regional cerebral blood flow by cholinergic fibers originating in the basal forebrain. *Int J Dev Neurosci,* 19**,** 327-37.

SATO, K., HATANO, T., YAMASHIRO, K., KAGOHASHI, M., NISHIOKA, K., IZAWA, N., MOCHIZUKI, H., HATTORI, N., MORI, H., MIZUNO, Y. & JUNTENDO PARKINSON STUDY, G. 2006. Prognosis of Parkinson's disease: time to stage III, IV, V, and to motor fluctuations. *Mov Disord,* 21**,** 1384-95.

SAVICA, R., GROSSARDT, B. R., BOWER, J. H., AHLSKOG, J. E. & ROCCA, W. A. 2013a. Incidence and pathology of synucleinopathies and tauopathies related to parkinsonism. *JAMA Neurol,* 70**,** 859-66.

SAVICA, R., GROSSARDT, B. R., BOWER, J. H., BOEVE, B. F., AHLSKOG, J. E. & ROCCA, W. A. 2013b. Incidence of dementia with Lewy bodies and Parkinson disease dementia. *JAMA Neurol,* 70**,** 1396-402.

SAVLI, M., BAUER, A., MITTERHAUSER, M., DING, Y. S., HAHN, A., KROLL, T., NEUMEISTER, A., HAEUSLER, D., UNGERSBOECK, J., HENRY, S., ISFAHANI, S. A., RATTAY, F., WADSAK, W., KASPER, S. & LANZENBERGER, R. 2012. Normative database of the serotonergic system in healthy subjects using multi-tracer PET. *Neuroimage,* 63**,** 447-59.

SAWADA, H., UDAKA, F., KAMEYAMA, M., SERIU, N., NISHINAKA, K., SHINDOU, K., KODAMA, M., NISHITANI, N. & OKUMIYA, K. 1992. SPECT findings in Parkinson's disease associated with dementia. *J Neurol Neurosurg Psychiatry,* 55**,** 960-3.
SAWCZAK, C. M., BARNETT, A. J. & COHN, M. 2019. Increased Cortical Thickness in Attentional Networks in Parkinson's Disease with Minor Hallucinations. *Parkinsons Dis,* 2019**,** 5351749.
SCALZO, P., KUMMER, A., BRETAS, T. L., CARDOSO, F. & TEIXEIRA, A. L. 2010. Serum levels of brain-derived neurotrophic factor correlate with motor impairment in Parkinson's disease. *J Neurol,* 257**,** 540-5.
SCHAIN, M., BENJAMINSSON, S., VARNAS, K., FORSBERG, A., HALLDIN, C., LANSNER, A., FARDE, L. & VARRONE, A. 2013. Arterial input function derived from pairwise correlations between PET-image voxels. *J Cereb Blood Flow Metab,* 33**,** 1058-65.
SCHERMAN, D., DESNOS, C., DARCHEN, F., POLLAK, P., JAVOY-AGID, F. & AGID, Y. 1989. Striatal dopamine deficiency in Parkinson's disease: role of aging. *Ann Neurol,* 26**,** 551-7.
SCHIRINZI, T., MADEO, G., MARTELLA, G., MALTESE, M., PICCONI, B., CALABRESI, P. & PISANI, A. 2016. Early synaptic dysfunction in Parkinson's disease: Insights from animal models. *Mov Disord,* 31**,** 802-13.
SCHRAG, A., HORSFALL, L., WALTERS, K., NOYCE, A. & PETERSEN, I. 2015. Prediagnostic presentations of Parkinson's disease in primary care: a case-control study. *Lancet Neurol,* 14**,** 57-64.
SCHULZ-SCHAEFFER, W. J. 2010. The synaptic pathology of alpha-synuclein aggregation in dementia with Lewy bodies, Parkinson's disease and Parkinson's disease dementia. *Acta Neuropathol,* 120**,** 131-43.
SCHULZ-SCHAEFFER, W. J. 2015. Is Cell Death Primary or Secondary in the Pathophysiology of Idiopathic Parkinson's Disease? *Biomolecules,* 5**,** 1467-79.
SCHUMACHER, J., PERAZA, L. R., FIRBANK, M., THOMAS, A. J., KAISER, M., GALLAGHER, P., O'BRIEN, J. T., BLAMIRE, A. M. & TAYLOR, J. P. 2019. Dysfunctional brain dynamics and their origin in Lewy body dementia. *Brain,* 142**,** 1767-1782.
SCHWARTZ, M., GROSHAR, D., INZELBERG, R. & HOCHERMAN, S. 2004. Dopamine-transporter imaging and visuo-motor testing in essential tremor, practical possibilities for detection of early stage Parkinson's disease. *Parkinsonism Relat Disord,* 10**,** 385-9.
SCHWARZ, S. T., XING, Y., TOMAR, P., BAJAJ, N. & AUER, D. P. 2017. In Vivo Assessment of Brainstem Depigmentation in Parkinson Disease: Potential as a Severity Marker for Multicenter Studies. *Radiology,* 283**,** 789-798.
SCOTT, D. & ROY, S. 2012. alpha-Synuclein inhibits intersynaptic vesicle mobility and maintains recycling-pool homeostasis. *J Neurosci,* 32**,** 10129-35.
SCOTT, D. A., TABAREAN, I., TANG, Y., CARTIER, A., MASLIAH, E. & ROY, S. 2010. A pathologic cascade leading to synaptic dysfunction in alpha-synuclein-induced neurodegeneration. *J Neurosci,* 30**,** 8083-95.
SEAMANS, J. K. & YANG, C. R. 2004. The principal features and mechanisms of dopamine modulation in the prefrontal cortex. *Prog Neurobiol,* 74**,** 1-58.
SEGURA-AGUILAR, J., PARIS, I., MUNOZ, P., FERRARI, E., ZECCA, L. & ZUCCA, F. A. 2014. Protective and toxic roles of dopamine in Parkinson's disease. *J Neurochem,* 129**,** 898-915.
SEIDEL, K., MAHLKE, J., SISWANTO, S., KRUGER, R., HEINSEN, H., AUBURGER, G., BOUZROU, M., GRINBERG, L. T., WICHT, H., KORF, H. W., DEN DUNNEN, W. & RUB, U. 2015. The brainstem pathologies of Parkinson's disease and dementia with Lewy bodies. *Brain Pathol,* 25**,** 121-35.

SEIDLITZ, J., NADIG, A., LIU, S., BETHLEHEM, R. A. I., VERTES, P. E., MORGAN, S. E., VASA, F., ROMERO-GARCIA, R., LALONDE, F. M., CLASEN, L. S., BLUMENTHAL, J. D., PAQUOLA, C., BERNHARDT, B., WAGSTYL, K., POLIOUDAKIS, D., DE LA TORRE-UBIETA, L., GESCHWIND, D. H., HAN, J. C., LEE, N. R., MURPHY, D. G., BULLMORE, E. T. & RAZNAHAN, A. 2020. Transcriptomic and cellular decoding of regional brain vulnerability to neurogenetic disorders. *Nat Commun,* 11**,** 3358.

SEIDLITZ, J., VASA, F., SHINN, M., ROMERO-GARCIA, R., WHITAKER, K. J., VERTES, P. E., WAGSTYL, K., KIRKPATRICK REARDON, P., CLASEN, L., LIU, S., MESSINGER, A., LEOPOLD, D. A., FONAGY, P., DOLAN, R. J., JONES, P. B., GOODYER, I. M., CONSORTIUM, N., RAZNAHAN, A. & BULLMORE, E. T. 2018. Morphometric Similarity Networks Detect Microscale Cortical Organization and Predict Inter-Individual Cognitive Variation. *Neuron,* 97**,** 231-247 e7.

SELVAGGI, P., HAWKINS, P. C. T., DIPASQUALE, O., RIZZO, G., BERTOLINO, A., DUKART, J., SAMBATARO, F., PERGOLA, G., WILLIAMS, S. C. R., TURKHEIMER, F., ZELAYA, F., VERONESE, M. & MEHTA, M. A. 2019. Increased cerebral blood flow after single dose of antipsychotics in healthy volunteers depends on dopamine D2 receptor density profiles. *Neuroimage,* 188**,** 774-784.

SELVAGGI, P., RIZZO, G., MEHTA, M. A., TURKHEIMER, F. E. & VERONESE, M. 2021. Integration of human whole-brain transcriptome and neuroimaging data: Practical considerations of current available methods. *J Neurosci Methods,* 355**,** 109128.

SERBY, M., BRICKMAN, A. M., HAROUTUNIAN, V., PUROHIT, D. P., MARIN, D., LANTZ, M., MOHS, R. C. & DAVIS, K. L. 2003. Cognitive burden and excess Lewy-body pathology in the Lewy-body variant of Alzheimer disease. *Am J Geriatr Psychiatry,* 11**,** 371-4.

SERPELL, L. C., BERRIMAN, J., JAKES, R., GOEDERT, M. & CROWTHER, R. A. 2000. Fiber diffraction of synthetic alpha-synuclein filaments shows amyloid-like cross-beta conformation. *Proc Natl Acad Sci U S A,* 97**,** 4897-902.

SHANKAR, G. M., LI, S., MEHTA, T. H., GARCIA-MUNOZ, A., SHEPARDSON, N. E., SMITH, I., BRETT, F. M., FARRELL, M. A., ROWAN, M. J., LEMERE, C. A., REGAN, C. M., WALSH, D. M., SABATINI, B. L. & SELKOE, D. J. 2008. Amyloid-beta protein dimers isolated directly from Alzheimer's brains impair synaptic plasticity and memory. *Nat Med,* 14**,** 837-42.

SHANNAK, K., RAJPUT, A., ROZDILSKY, B., KISH, S., GILBERT, J. & HORNYKIEWICZ, O. 1994. Noradrenaline, dopamine and serotonin levels and metabolism in the human hypothalamus: observations in Parkinson's disease and normal subjects. *Brain Res,* 639**,** 33-41.

SHARP, S. I., BALLARD, C. G., ZIABREVA, I., PIGGOTT, M. A., PERRY, R. H., PERRY, E. K., AARSLAND, D., EHRT, U., LARSEN, J. P. & FRANCIS, P. T. 2008. Cortical serotonin 1A receptor levels are associated with depression in patients with dementia with Lewy bodies and Parkinson's disease dementia. *Dement Geriatr Cogn Disord,* 26**,** 330-8.

SHEN, E. H., OVERLY, C. C. & JONES, A. R. 2012. The Allen Human Brain Atlas: comprehensive gene expression mapping of the human brain. *Trends Neurosci,* 35**,** 711-4.

SHEN, J., YANG, B., XIE, Z., WU, H., ZHENG, Z., WANG, J., WANG, P., ZHANG, P., LI, W., YE, Z. & YU, C. 2021. Cell-Type-Specific Gene Modules Related to the Regional Homogeneity of Spontaneous Brain Activity and Their Associations With Common Brain Disorders. *Front Neurosci,* 15**,** 639527.

SHENG, M. & KIM, E. 2011. The postsynaptic organization of synapses. *Cold Spring Harb Perspect Biol,* 3.

SHENG, Z. H. 2014. Mitochondrial trafficking and anchoring in neurons: New insight and implications. *J Cell Biol,* 204**,** 1087-98.

SHI, J., ANDERSON, D., LYNCH, B. A., CASTAIGNE, J. G., FOERCH, P. & LEBON, F. 2011. Combining modelling and mutagenesis studies of synaptic vesicle protein 2A to identify a series of residues involved in racetam binding. *Biochem Soc Trans,* 39**,** 1341-7.
SHIMADA, H., HIRANO, S., SHINOTOH, H., AOTSUKA, A., SATO, K., TANAKA, N., OTA, T., ASAHINA, M., FUKUSHI, K., KUWABARA, S., HATTORI, T., SUHARA, T. & IRIE, T. 2009. Mapping of brain acetylcholinesterase alterations in Lewy body disease by PET. *Neurology,* 73**,** 273-8.
SHIN, J., FRENCH, L., XU, T., LEONARD, G., PERRON, M., PIKE, G. B., RICHER, L., VEILLETTE, S., PAUSOVA, Z. & PAUS, T. 2018. Cell-Specific Gene-Expression Profiles and Cortical Thickness in the Human Brain. *Cereb Cortex,* 28**,** 3267-3277.
SHINOHARA, M., FUJIOKA, S., MURRAY, M. E., WOJTAS, A., BAKER, M., ROVELET-LECRUX, A., RADEMAKERS, R., DAS, P., PARISI, J. E., GRAFF-RADFORD, N. R., PETERSEN, R. C., DICKSON, D. W. & BU, G. 2014. Regional distribution of synaptic markers and APP correlate with distinct clinicopathological features in sporadic and familial Alzheimer's disease. *Brain,* 137**,** 1533-49.
SHINOHARA, M., PETERSEN, R. C., DICKSON, D. W. & BU, G. 2013. Brain regional correlation of amyloid-beta with synapses and apolipoprotein E in non-demented individuals: potential mechanisms underlying regional vulnerability to amyloid-beta accumulation. *Acta Neuropathol,* 125**,** 535-47.
SHINOTOH, H., NAMBA, H., YAMAGUCHI, M., FUKUSHI, K., NAGATSUKA, S., IYO, M., ASAHINA, M., HATTORI, T., TANADA, S. & IRIE, T. 1999. Positron emission tomographic measurement of acetylcholinesterase activity reveals differential loss of ascending cholinergic systems in Parkinson's disease and progressive supranuclear palsy. *Ann Neurol,* 46**,** 62-9.
SHIYAM SUNDAR, L. K., MUZIK, O., RISCHKA, L., HAHN, A., LANZENBERGER, R., HIENERT, M., KLEBERMASS, E. M., BAUER, M., RAUSCH, I., PATARAIA, E., TRAUB-WEIDINGER, T. & BEYER, T. 2020. Promise of Fully Integrated PET/MRI: Noninvasive Clinical Quantification of Cerebral Glucose Metabolism. *J Nucl Med,* 61**,** 276-284.
SIERRA, M., SANCHEZ-JUAN, P., MARTINEZ-RODRIGUEZ, M. I., GONZALEZ-ARAMBURU, I., GARCIA-GOROSTIAGA, I., QUIRCE, M. R., PALACIO, E., CARRIL, J. M., BERCIANO, J., COMBARROS, O. & INFANTE, J. 2013. Olfaction and imaging biomarkers in premotor LRRK2 G2019S-associated Parkinson disease. *Neurology,* 80**,** 621-6.
SIGURDSSON, S., FORSBERG, L., ASPELUND, T., VAN DER GEEST, R. J., VAN BUCHEM, M. A., LAUNER, L. J., GUDNASON, V. & VAN OSCH, M. J. 2015. Feasibility of Using Pseudo-Continuous Arterial Spin Labeling Perfusion in a Geriatric Population at 1.5 Tesla. *PLoS One,* 10**,** e0144743.
SIMON-SANCHEZ, J., SCHULTE, C., BRAS, J. M., SHARMA, M., GIBBS, J. R., BERG, D., PAISAN-RUIZ, C., LICHTNER, P., SCHOLZ, S. W., HERNANDEZ, D. G., KRUGER, R., FEDEROFF, M., KLEIN, C., GOATE, A., PERLMUTTER, J., BONIN, M., NALLS, M. A., ILLIG, T., GIEGER, C., HOULDEN, H., STEFFENS, M., OKUN, M. S., RACETTE, B. A., COOKSON, M. R., FOOTE, K. D., FERNANDEZ, H. H., TRAYNOR, B. J., SCHREIBER, S., AREPALLI, S., ZONOZI, R., GWINN, K., VAN DER BRUG, M., LOPEZ, G., CHANOCK, S. J., SCHATZKIN, A., PARK, Y., HOLLENBECK, A., GAO, J., HUANG, X., WOOD, N. W., LORENZ, D., DEUSCHL, G., CHEN, H., RIESS, O., HARDY, J. A., SINGLETON, A. B. & GASSER, T. 2009. Genome-wide association study reveals genetic risk underlying Parkinson's disease. *Nat Genet,* 41**,** 1308-12.
SINGLETON, A. B., FARRER, M., JOHNSON, J., SINGLETON, A., HAGUE, S., KACHERGUS, J., HULIHAN, M., PEURALINNA, T., DUTRA, A., NUSSBAUM, R.,

LINCOLN, S., CRAWLEY, A., HANSON, M., MARAGANORE, D., ADLER, C., COOKSON, M. R., MUENTER, M., BAPTISTA, M., MILLER, D., BLANCATO, J., HARDY, J. & GWINN-HARDY, K. 2003. alpha-Synuclein locus triplication causes Parkinson's disease. *Science,* 302**,** 841.

SLEVIN, J. T., GASH, D. M., SMITH, C. D., GERHARDT, G. A., KRYSCIO, R., CHEBROLU, H., WALTON, A., WAGNER, R. & YOUNG, A. B. 2007. Unilateral intraputamenal glial cell line-derived neurotrophic factor in patients with Parkinson disease: response to 1 year of treatment and 1 year of withdrawal. *J Neurosurg,* 106**,** 614-20.

SLEVIN, J. T., GERHARDT, G. A., SMITH, C. D., GASH, D. M., KRYSCIO, R. & YOUNG, B. 2005. Improvement of bilateral motor functions in patients with Parkinson disease through the unilateral intraputaminal infusion of glial cell line-derived neurotrophic factor. *J Neurosurg,* 102**,** 216-22.

SMART, K., LIU, H., MATUSKEY, D., CHEN, M. K., TORRES, K., NABULSI, N., LABAREE, D., ROPCHAN, J., HILLMER, A. T., HUANG, Y. & CARSON, R. E. 2021. Binding of the synaptic vesicle radiotracer [(11)C]UCB-J is unchanged during functional brain activation using a visual stimulation task. *J Cereb Blood Flow Metab,* 41**,** 1067-1079.

SMITH, S. M. 2002. Fast robust automated brain extraction. *Hum Brain Mapp,* 17**,** 143-55.

SODERSTROM, K., O'MALLEY, J., STEECE-COLLIER, K. & KORDOWER, J. H. 2006. Neural repair strategies for Parkinson's disease: insights from primate models. *Cell Transplant,* 15**,** 251-65.

SOLIS, O., LIMON, D. I., FLORES-HERNANDEZ, J. & FLORES, G. 2007. Alterations in dendritic morphology of the prefrontal cortical and striatum neurons in the unilateral 6-OHDA-rat model of Parkinson's disease. *Synapse,* 61**,** 450-8.

SOMMERAUER, M., FEDOROVA, T. D., HANSEN, A. K., KNUDSEN, K., OTTO, M., JEPPESEN, J., FREDERIKSEN, Y., BLICHER, J. U., GEDAY, J., NAHIMI, A., DAMHOLDT, M. F., BROOKS, D. J. & BORGHAMMER, P. 2018a. Evaluation of the noradrenergic system in Parkinson's disease: an 11C-MeNER PET and neuromelanin MRI study. *Brain,* 141**,** 496-504.

SOMMERAUER, M., HANSEN, A. K., PARBO, P., FEDOROVA, T. D., KNUDSEN, K., FREDERIKSEN, Y., NAHIMI, A., BARBE, M. T., BROOKS, D. J. & BORGHAMMER, P. 2018b. Decreased noradrenaline transporter density in the motor cortex of Parkinson's disease patients. *Mov Disord,* 33**,** 1006-1010.

SOMOZA, R., JURI, C., BAES, M., WYNEKEN, U. & RUBIO, F. J. 2010. Intranigral transplantation of epigenetically induced BDNF-secreting human mesenchymal stem cells: implications for cell-based therapies in Parkinson's disease. *Biol Blood Marrow Transplant,* 16**,** 1530-40.

SONG, H. F., KENNEDY, H. & WANG, X. J. 2014. Spatial embedding of structural similarity in the cerebral cortex. *Proc Natl Acad Sci U S A,* 111**,** 16580-5.

SONG, S. K., LEE, J. E., PARK, H. J., SOHN, Y. H., LEE, J. D. & LEE, P. H. 2011. The pattern of cortical atrophy in patients with Parkinson's disease according to cognitive status. *Mov Disord,* 26**,** 289-96.

SONNINEN, T. M., HAMALAINEN, R. H., KOSKUVI, M., OKSANEN, M., SHAKIRZYANOVA, A., WOJCIECHOWSKI, S., PUTTONEN, K., NAUMENKO, N., GOLDSTEINS, G., LAHAM-KARAM, N., LEHTONEN, M., TAVI, P., KOISTINAHO, J. & LEHTONEN, S. 2020. Metabolic alterations in Parkinson's disease astrocytes. *Sci Rep,* 10**,** 14474.

SOTIRIOU, E., VASSILATIS, D. K., VILA, M. & STEFANIS, L. 2010. Selective noradrenergic vulnerability in alpha-synuclein transgenic mice. *Neurobiol Aging,* 31**,** 2103-14.

SPILLANTINI, M. G. & GOEDERT, M. 2013. Tau pathology and neurodegeneration. *Lancet Neurol,* 12**,** 609-22.
SPILLANTINI, M. G., SCHMIDT, M. L., LEE, V. M., TROJANOWSKI, J. Q., JAKES, R. & GOEDERT, M. 1997. Alpha-synuclein in Lewy bodies. *Nature,* 388**,** 839-40.
STEVENS, T., LIVINGSTON, G., KITCHEN, G., MANELA, M., WALKER, Z. & KATONA, C. 2002. Islington study of dementia subtypes in the community. *Br J Psychiatry,* 180**,** 270-6.
STRAUB, V. A., GRANT, J., O'SHEA, M. & BENJAMIN, P. R. 2007. Modulation of serotonergic neurotransmission by nitric oxide. *J Neurophysiol,* 97**,** 1088-99.
SUAREZ, L. M., SOLIS, O., SANZ-MAGRO, A., ALBERQUILLA, S. & MORATALLA, R. 2020. Dopamine D1 Receptors Regulate Spines in Striatal Direct-Pathway and Indirect-Pathway Neurons. *Mov Disord,* 35**,** 1810-1821.
SUDHOF, T. C. 2012. The presynaptic active zone. *Neuron,* 75**,** 11-25.
SUDHOF, T. C. 2013. A molecular machine for neurotransmitter release: synaptotagmin and beyond. *Nat Med,* 19**,** 1227-31.
SUDHOF, T. C. 2018. Towards an Understanding of Synapse Formation. *Neuron,* 100**,** 276-293.
SULZER, D. & SURMEIER, D. J. 2013. Neuronal vulnerability, pathogenesis, and Parkinson's disease. *Mov Disord,* 28**,** 41-50.
SUMMERFIELD, C., JUNQUE, C., TOLOSA, E., SALGADO-PINEDA, P., GOMEZ-ANSON, B., MARTI, M. J., PASTOR, P., RAMIREZ-RUIZ, B. & MERCADER, J. 2005. Structural brain changes in Parkinson disease with dementia: a voxel-based morphometry study. *Arch Neurol,* 62**,** 281-5.
SUN, X., ZHAO, Y. & WOLF, M. E. 2005. Dopamine receptor stimulation modulates AMPA receptor synaptic insertion in prefrontal cortex neurons. *J Neurosci,* 25**,** 7342-51.
SURMEIER, D. J., DING, J., DAY, M., WANG, Z. & SHEN, W. 2007. D1 and D2 dopamine-receptor modulation of striatal glutamatergic signaling in striatal medium spiny neurons. *Trends Neurosci,* 30**,** 228-35.
SURMEIER, D. J., GUZMAN, J. N., SANCHEZ, J. & SCHUMACKER, P. T. 2012. Physiological phenotype and vulnerability in Parkinson's disease. *Cold Spring Harb Perspect Med,* 2**,** a009290.
SURMEIER, D. J., OBESO, J. A. & HALLIDAY, G. M. 2017. Selective neuronal vulnerability in Parkinson disease. *Nat Rev Neurosci,* 18**,** 101-113.
SWEENEY, M. D., KISLER, K., MONTAGNE, A., TOGA, A. W. & ZLOKOVIC, B. V. 2018. The role of brain vasculature in neurodegenerative disorders. *Nat Neurosci,* 21**,** 1318-1331.
SYRIMI, Z. J., VOJTISEK, L., ELIASOVA, I., VISKOVA, J., SVATKOVA, A., VANICEK, J. & REKTOROVA, I. 2017. Arterial spin labelling detects posterior cortical hypoperfusion in non-demented patients with Parkinson's disease. *J Neural Transm (Vienna),* 124**,** 551-557.
TACHIBANA, H., TOMINO, Y., KAWABATA, K., SUGITA, M. & FUKUCHI, M. 1995. Twelve-month follow-up study of regional cerebral blood flow in Parkinson's disease. *Dementia,* 6**,** 89-93.
TAGLIAVINI, F., PILLERI, G., BOURAS, C. & CONSTANTINIDIS, J. 1984. The basal nucleus of Meynert in idiopathic Parkinson's disease. *Acta Neurol Scand,* 70**,** 20-8.
TAKAMORI, S., HOLT, M., STENIUS, K., LEMKE, E. A., GRONBORG, M., RIEDEL, D., URLAUB, H., SCHENCK, S., BRUGGER, B., RINGLER, P., MULLER, S. A., RAMMNER, B., GRATER, F., HUB, J. S., DE GROOT, B. L., MIESKES, G., MORIYAMA, Y., KLINGAUF, J., GRUBMULLER, H., HEUSER, J., WIELAND, F. & JAHN, R. 2006. Molecular anatomy of a trafficking organelle. *Cell,* 127**,** 831-46.
TAKAMURA, N., NAKAGAWA, S., MASUDA, T., BOKU, S., KATO, A., SONG, N., AN, Y., KITAICHI, Y., INOUE, T., KOYAMA, T. & KUSUMI, I. 2014. The effect of

dopamine on adult hippocampal neurogenesis. *Prog Neuropsychopharmacol Biol Psychiatry,* 50**,** 116-24.
TANAKA, H., KANNARI, K., MAEDA, T., TOMIYAMA, M., SUDA, T. & MATSUNAGA, M. 1999. Role of serotonergic neurons in L-DOPA-derived extracellular dopamine in the striatum of 6-OHDA-lesioned rats. *Neuroreport,* 10**,** 631-4.
TANAKA, M., KIM, Y. M., LEE, G., JUNN, E., IWATSUBO, T. & MOURADIAN, M. M. 2004. Aggresomes formed by alpha-synuclein and synphilin-1 are cytoprotective. *J Biol Chem,* 279**,** 4625-31.
TANG, C. C., POSTON, K. L., ECKERT, T., FEIGIN, A., FRUCHT, S., GUDESBLATT, M., DHAWAN, V., LESSER, M., VONSATTEL, J. P., FAHN, S. & EIDELBERG, D. 2010. Differential diagnosis of parkinsonism: a metabolic imaging study using pattern analysis. *Lancet Neurol,* 9**,** 149-58.
TANG, J., SU, Q., ZHANG, X., QIN, W., LIU, H., LIANG, M. & YU, C. 2021. Brain Gene Expression Pattern Correlated with the Differential Brain Activation by Pain and Touch in Humans. *Cereb Cortex,* 31**,** 3506-3521.
TANG, Y., NYENGAARD, J. R., DE GROOT, D. M. & GUNDERSEN, H. J. 2001. Total regional and global number of synapses in the human brain neocortex. *Synapse,* 41**,** 258-73.
TAO, J., BULGARI, D., DEITCHER, D. L. & LEVITAN, E. S. 2017. Limited distal organelles and synaptic function in extensive monoaminergic innervation. *J Cell Sci,* 130**,** 2520-2529.
TAQUET, H., JAVOY-AGID, F., CESSELIN, F., HAMON, M., LEGRAND, J. C. & AGID, Y. 1982. Microtopography of methionine-enkephalin, dopamine and noradrenaline in the ventral mesencephalon of human control and Parkinsonian brains. *Brain Res,* 235**,** 303-14.
TAYLOR, J. P., FIRBANK, M. J., HE, J., BARNETT, N., PEARCE, S., LIVINGSTONE, A., VUONG, Q., MCKEITH, I. G. & O'BRIEN, J. T. 2012. Visual cortex in dementia with Lewy bodies: magnetic resonance imaging study. *Br J Psychiatry,* 200**,** 491-8.
TEHRANIAN, R., MONTOYA, S. E., VAN LAAR, A. D., HASTINGS, T. G. & PEREZ, R. G. 2006. Alpha-synuclein inhibits aromatic amino acid decarboxylase activity in dopaminergic cells. *J Neurochem,* 99**,** 1188-96.
TEUNE, L. K., RENKEN, R. J., DE JONG, B. M., WILLEMSEN, A. T., VAN OSCH, M. J., ROERDINK, J. B., DIERCKX, R. A. & LEENDERS, K. L. 2014. Parkinson's disease-related perfusion and glucose metabolic brain patterns identified with PCASL-MRI and FDG-PET imaging. *Neuroimage Clin,* 5**,** 240-4.
THEYEL, B. B., LLANO, D. A. & SHERMAN, S. M. 2010. The corticothalamocortical circuit drives higher-order cortex in the mouse. *Nat Neurosci,* 13**,** 84-8.
THOBOIS, S., VINGERHOETS, F., FRAIX, V., XIE-BRUSTOLIN, J., MOLLION, H., COSTES, N., MERTENS, P., BENABID, A. L., POLLAK, P. & BROUSSOLLE, E. 2004. Role of dopaminergic treatment in dopamine receptor down-regulation in advanced Parkinson disease: a positron emission tomographic study. *Arch Neurol,* 61**,** 1705-9.
THOMAS, B. A., CUPLOV, V., BOUSSE, A., MENDES, A., THIELEMANS, K., HUTTON, B. F. & ERLANDSSON, K. 2016. PETPVC: a toolbox for performing partial volume correction techniques in positron emission tomography. *Phys Med Biol,* 61**,** 7975-7993.
TIRABOSCHI, P., ATTEMS, J., THOMAS, A., BROWN, A., JAROS, E., LETT, D. J., OSSOLA, M., PERRY, R. H., RAMSAY, L., WALKER, L. & MCKEITH, I. G. 2015. Clinicians' ability to diagnose dementia with Lewy bodies is not affected by beta-amyloid load. *Neurology,* 84**,** 496-9.
TISON, F., MONS, N., GEFFARD, M. & HENRY, P. 1991. The metabolism of exogenous L-dopa in the brain: an immunohistochemical study of its conversion to dopamine in non-catecholaminergic cells of the rat brain. *J Neural Transm Park Dis Dement Sect,* 3**,** 27-39.

TISSINGH, G., BOOIJ, J., BERGMANS, P., WINOGRODZKA, A., JANSSEN, A. G., VAN ROYEN, E. A., STOOF, J. C. & WOLTERS, E. C. 1998. Iodine-123-N-omega-fluoropropyl-2beta-carbomethoxy-3beta-(4-iod ophenyl)tropane SPECT in healthy controls and early-stage, drug-naive Parkinson's disease. *J Nucl Med,* 39**,** 1143-8.
TOFARIS, G. K. & SPILLANTINI, M. G. 2005. Alpha-synuclein dysfunction in Lewy body diseases. *Mov Disord,* 20 Suppl 12**,** S37-44.
TOLA-ARRIBAS, M. A., YUGUEROS, M. I., GAREA, M. J., ORTEGA-VALIN, F., CERON-FERNANDEZ, A., FERNANDEZ-MALVIDO, B., SAN JOSE-GALLEGOS, A., GONZALEZ-TOUYA, M., BOTRAN-VELICIA, A., IGLESIAS-RODRIGUEZ, V. & DIAZ-GOMEZ, B. 2013. Prevalence of dementia and subtypes in Valladolid, northwestern Spain: the DEMINVALL study. *PLoS One,* 8**,** e77688.
TOLEDO, J. B., CAIRNS, N. J., DA, X., CHEN, K., CARTER, D., FLEISHER, A., HOUSEHOLDER, E., AYUTYANONT, N., ROONTIVA, A., BAUER, R. J., EISEN, P., SHAW, L. M., DAVATZIKOS, C., WEINER, M. W., REIMAN, E. M., MORRIS, J. C., TROJANOWSKI, J. Q. & ALZHEIMER'S DISEASE NEUROIMAGING, I. 2013. Clinical and multimodal biomarker correlates of ADNI neuropathological findings. *Acta Neuropathol Commun,* 1**,** 65.
TOMIYAMA, M., MORI, F., KIMURA, T., ICHINOHE, N., WAKABAYASHI, K., MATSUNAGA, M. & BABA, M. 2004. Hypertrophy of medial globus pallidus and substantia nigra reticulata in 6-hydroxydopamine-lesioned rats treated with L-DOPA: implication for L-DOPA-induced dyskinesia in Parkinson's disease. *Neuropathology,* 24**,** 290-5.
TOMPKINS, M. M. & HILL, W. D. 1997. Contribution of somal Lewy bodies to neuronal death. *Brain Res,* 775**,** 24-9.
TONG, J., FITZMAURICE, P. S., ANG, L. C., FURUKAWA, Y., GUTTMAN, M. & KISH, S. J. 2004. Brain dopamine-stimulated adenylyl cyclase activity in Parkinson's disease, multiple system atrophy, and progressive supranuclear palsy. *Ann Neurol,* 55**,** 125-9.
TOTH, P., TARANTINI, S., CSISZAR, A. & UNGVARI, Z. 2017. Functional vascular contributions to cognitive impairment and dementia: mechanisms and consequences of cerebral autoregulatory dysfunction, endothelial impairment, and neurovascular uncoupling in aging. *Am J Physiol Heart Circ Physiol,* 312**,** H1-H20.
TOUSSAY, X., BASU, K., LACOSTE, B. & HAMEL, E. 2013. Locus coeruleus stimulation recruits a broad cortical neuronal network and increases cortical perfusion. *J Neurosci,* 33**,** 3390-401.
TREMBLAY, C., RAHAYEL, S., VO, A., MORYS, F., SHAFIEI, G., ABBASI, N., MARKELLO, R. D., GAN-OR, Z., MISIC, B. & DAGHER, A. 2021. Brain atrophy progression in Parkinson's disease is shaped by connectivity and local vulnerability. *Brain Commun,* 3**,** fcab269.
TRIMMER, P. A., SCHWARTZ, K. M., BORLAND, M. K., DE TABOADA, L., STREETER, J. & ORON, U. 2009. Reduced axonal transport in Parkinson's disease cybrid neurites is restored by light therapy. *Mol Neurodegener,* 4**,** 26.
TRIPATHI, M., TANG, C. C., FEIGIN, A., DE LUCIA, I., NAZEM, A., DHAWAN, V. & EIDELBERG, D. 2016. Automated Differential Diagnosis of Early Parkinsonism Using Metabolic Brain Networks: A Validation Study. *J Nucl Med,* 57**,** 60-6.
TRITSCH, N. X. & SABATINI, B. L. 2012. Dopaminergic modulation of synaptic transmission in cortex and striatum. *Neuron,* 76**,** 33-50.
TSUBOI, Y., UCHIKADO, H. & DICKSON, D. W. 2007. Neuropathology of Parkinson's disease dementia and dementia with Lewy bodies with reference to striatal pathology. *Parkinsonism Relat Disord,* 13 Suppl 3**,** S221-4.
TUNCEL, H., BOELLAARD, R., COOMANS, E. M., DE VRIES, E. F., GLAUDEMANS, A. W., FELTES, P. K., GARCIA, D. V., VERFAILLIE, S. C., WOLTERS, E. E.,

SWEENEY, S. P., RYAN, J. M., IVARSSON, M., LYNCH, B. A., SCHOBER, P., SCHELTENS, P., SCHUIT, R. C., WINDHORST, A. D., DE DEYN, P. P., VAN BERCKEL, B. N. & GOLLA, S. S. 2021. Kinetics and 28-day test-retest repeatability and reproducibility of [(11)C]UCB-J PET brain imaging. *J Cereb Blood Flow Metab,* 41**,** 1338-1350.

TWELVES, D., PERKINS, K. S. & COUNSELL, C. 2003. Systematic review of incidence studies of Parkinson's disease. *Mov Disord,* 18**,** 19-31.

TZIORTZI, A. C., SEARLE, G. E., TZIMOPOULOU, S., SALINAS, C., BEAVER, J. D., JENKINSON, M., LARUELLE, M., RABINER, E. A. & GUNN, R. N. 2011. Imaging dopamine receptors in humans with [11C]-(+)-PHNO: dissection of D3 signal and anatomy. *Neuroimage,* 54**,** 264-77.

UCHIHARA, T. 2017. An order in Lewy body disorders: Retrograde degeneration in hyperbranching axons as a fundamental structural template accounting for focal/multifocal Lewy body disease. *Neuropathology,* 37**,** 129-149.

UCHIHARA, T. & GIASSON, B. I. 2016. Propagation of alpha-synuclein pathology: hypotheses, discoveries, and yet unresolved questions from experimental and human brain studies. *Acta Neuropathol,* 131**,** 49-73.

ULUSOY, A., RUSCONI, R., PEREZ-REVUELTA, B. I., MUSGROVE, R. E., HELWIG, M., WINZEN-REICHERT, B. & DI MONTE, D. A. 2013. Caudo-rostral brain spreading of alpha-synuclein through vagal connections. *EMBO Mol Med,* 5**,** 1119-27.

UNAL, B., SHAH, F., KOTHARI, J. & TEPPER, J. M. 2015. Anatomical and electrophysiological changes in striatal TH interneurons after loss of the nigrostriatal dopaminergic pathway. *Brain Struct Funct,* 220**,** 331-49.

UNDERWOOD, M. D., BAKALIAN, M. J., ARANGO, V. & MANN, J. J. 1995. Effect of chemical stimulation of the dorsal raphe nucleus on cerebral blood flow in rat. *Neurosci Lett,* 199**,** 228-30.

UNTERHOLZNER, J., GRYGLEWSKI, G., PHILIPPE, C., SEIGER, R., PICHLER, V., GODBERSEN, G. M., BERROTERAN-INFANTE, N., MURGAS, M., HAHN, A., WADSAK, W., MITTERHAUSER, M., KASPER, S. & LANZENBERGER, R. 2020. Topologically Guided Prioritization of Candidate Gene Transcripts Coexpressed with the 5-HT1A Receptor by Combining In Vivo PET and Allen Human Brain Atlas Data. *Cereb Cortex,* 30**,** 3771-3780.

VALASTRO, B., DEKUNDY, A., KROGH, M., LUNDBLAD, M., JAMES, P., DANYSZ, W., QUACK, G. & CENCI, M. A. 2007. Proteomic analysis of striatal proteins in the rat model of L-DOPA-induced dyskinesia. *J Neurochem,* 102**,** 1395-409.

VALLORTIGARA, J., RANGARAJAN, S., WHITFIELD, D., ALGHAMDI, A., HOWLETT, D., HORTOBAGYI, T., JOHNSON, M., ATTEMS, J., BALLARD, C., THOMAS, A., O'BRIEN, J., AARSLAND, D. & FRANCIS, P. 2014. Dynamin1 concentration in the prefrontal cortex is associated with cognitive impairment in Lewy body dementia. *F1000Res,* 3**,** 108.

VAN AALST, J., CECCARINI, J., SUNAERT, S., DUPONT, P., KOOLE, M. & VAN LAERE, K. 2021. In vivo synaptic density relates to glucose metabolism at rest in healthy subjects, but is strongly modulated by regional differences. *J Cereb Blood Flow Metab,* 41**,** 1978-1987.

VAN DEN EEDEN, S. K., TANNER, C. M., BERNSTEIN, A. L., FROSS, R. D., LEIMPETER, A., BLOCH, D. A. & NELSON, L. M. 2003. Incidence of Parkinson's disease: variation by age, gender, and race/ethnicity. *Am J Epidemiol,* 157**,** 1015-22.

VAN DER FLIER, W. M. & SCHELTENS, P. 2005. Epidemiology and risk factors of dementia. *J Neurol Neurosurg Psychiatry,* 76 Suppl 5**,** v2-7.

VAN KAMPEN, J. M. & ECKMAN, C. B. 2006. Dopamine D3 receptor agonist delivery to a model of Parkinson's disease restores the nigrostriatal pathway and improves locomotor behavior. *J Neurosci,* 26**,** 7272-80.
VAN KAMPEN, J. M. & ROBERTSON, H. A. 2005. A possible role for dopamine D3 receptor stimulation in the induction of neurogenesis in the adult rat substantia nigra. *Neuroscience,* 136**,** 381-6.
VAN LAAR, V. S., MISHIZEN, A. J., CASCIO, M. & HASTINGS, T. G. 2009. Proteomic identification of dopamine-conjugated proteins from isolated rat brain mitochondria and SH-SY5Y cells. *Neurobiol Dis,* 34**,** 487-500.
VANN JONES, S. A. & O'BRIEN, J. T. 2014. The prevalence and incidence of dementia with Lewy bodies: a systematic review of population and clinical studies. *Psychol Med,* 44**,** 673-83.
VARANESE, S., PERFETTI, B., MONACO, D., THOMAS, A., BONANNI, L., TIRABOSCHI, P. & ONOFRJ, M. 2010. Fluctuating cognition and different cognitive and behavioural profiles in Parkinson's disease with dementia: comparison of dementia with Lewy bodies and Alzheimer's disease. *J Neurol,* 257**,** 1004-11.
VARGAS, K. J., MAKANI, S., DAVIS, T., WESTPHAL, C. H., CASTILLO, P. E. & CHANDRA, S. S. 2014. Synucleins regulate the kinetics of synaptic vesicle endocytosis. *J Neurosci,* 34**,** 9364-76.
VARGAS, K. J., SCHROD, N., DAVIS, T., FERNANDEZ-BUSNADIEGO, R., TAGUCHI, Y. V., LAUGKS, U., LUCIC, V. & CHANDRA, S. S. 2017. Synucleins Have Multiple Effects on Presynaptic Architecture. *Cell Rep,* 18**,** 161-173.
VASA, F., SEIDLITZ, J., ROMERO-GARCIA, R., WHITAKER, K. J., ROSENTHAL, G., VERTES, P. E., SHINN, M., ALEXANDER-BLOCH, A., FONAGY, P., DOLAN, R. J., JONES, P. B., GOODYER, I. M., CONSORTIUM, N., SPORNS, O. & BULLMORE, E. T. 2018. Adolescent Tuning of Association Cortex in Human Structural Brain Networks. *Cereb Cortex,* 28**,** 281-294.
VAUCHER, E., BORREDON, J., SEYLAZ, J. & LACOMBE, P. 1995. Autoradiographic distribution of cerebral blood flow increases elicited by stimulation of the nucleus basalis magnocellularis in the unanesthetized rat. *Brain Res,* 691**,** 57-68.
VENDA, L. L., CRAGG, S. J., BUCHMAN, V. L. & WADE-MARTINS, R. 2010. alpha-Synuclein and dopamine at the crossroads of Parkinson's disease. *Trends Neurosci,* 33**,** 559-68.
VENTON, B. J., ZHANG, H., GARRIS, P. A., PHILLIPS, P. E., SULZER, D. & WIGHTMAN, R. M. 2003. Real-time decoding of dopamine concentration changes in the caudate-putamen during tonic and phasic firing. *J Neurochem,* 87**,** 1284-95.
VETTERMANN, F. J., RULLMANN, M., BECKER, G. A., LUTHARDT, J., ZIENTEK, F., PATT, M., MEYER, P. M., MCLEOD, A., BRENDEL, M., BLUHER, M., STUMVOLL, M., HILBERT, A., DING, Y. S., SABRI, O. & HESSE, S. 2018. Noradrenaline transporter availability on [(11)C]MRB PET predicts weight loss success in highly obese adults. *Eur J Nucl Med Mol Imaging,* 45**,** 1618-1625.
VIVIANI, R., SIM, E. J., LO, H., RICHTER, S., HAFFER, S., OSTERFELD, N., THONE, J. & BESCHONER, P. 2009. Components of variance in brain perfusion and the design of studies of individual differences: the baseline study. *Neuroimage,* 46**,** 12-22.
VLAGSMA, T. T., KOERTS, J., TUCHA, O., DIJKSTRA, H. T., DUITS, A. A., VAN LAAR, T. & SPIKMAN, J. M. 2016. Mental slowness in patients with Parkinson's disease: Associations with cognitive functions? *J Clin Exp Neuropsychol,* 38**,** 844-52.
VOLLES, M. J. & LANSBURY, P. T., JR. 2003. Zeroing in on the pathogenic form of alpha-synuclein and its mechanism of neurotoxicity in Parkinson's disease. *Biochemistry,* 42**,** 7871-8.

VOLPICELLI-DALEY, L. A. 2017. Effects of alpha-synuclein on axonal transport. *Neurobiol Dis,* 105**,** 321-327.
WALKER, L., MCALEESE, K. E., THOMAS, A. J., JOHNSON, M., MARTIN-RUIZ, C., PARKER, C., COLLOBY, S. J., JELLINGER, K. & ATTEMS, J. 2015a. Neuropathologically mixed Alzheimer's and Lewy body disease: burden of pathological protein aggregates differs between clinical phenotypes. *Acta Neuropathol,* 129**,** 729-48.
WALKER, Z., POSSIN, K. L., BOEVE, B. F. & AARSLAND, D. 2015b. Lewy body dementias. *Lancet,* 386**,** 1683-97.
WALLMAN, M. J., GAGNON, D. & PARENT, M. 2011. Serotonin innervation of human basal ganglia. *Eur J Neurosci,* 33**,** 1519-32.
WANG, J., LI, Y., HUANG, Z., WAN, W., ZHANG, Y., WANG, C., CHENG, X., YE, F., LIU, K., FEI, G., ZENG, M. & JIN, L. 2018. Neuromelanin-sensitive magnetic resonance imaging features of the substantia nigra and locus coeruleus in de novo Parkinson's disease and its phenotypes. *Eur J Neurol,* 25**,** 949-e73.
WANG, Y. F. & PARPURA, V. 2018. Astroglial Modulation of Hydromineral Balance and Cerebral Edema. *Front Mol Neurosci,* 11**,** 204.
WANG, Z., JACKSON, R. J., HONG, W., TAYLOR, W. M., CORBETT, G. T., MORENO, A., LIU, W., LI, S., FROSCH, M. P., SLUTSKY, I., YOUNG-PEARSE, T. L., SPIRES-JONES, T. L. & WALSH, D. M. 2017. Human Brain-Derived Abeta Oligomers Bind to Synapses and Disrupt Synaptic Activity in a Manner That Requires APP. *J Neurosci,* 37**,** 11947-11966.
WATABE-UCHIDA, M., ZHU, L., OGAWA, S. K., VAMANRAO, A. & UCHIDA, N. 2012. Whole-brain mapping of direct inputs to midbrain dopamine neurons. *Neuron,* 74**,** 858-73.
WATSON, R., COLLOBY, S. J., BLAMIRE, A. M., WESNES, K. A., WOOD, J. & O'BRIEN, J. T. 2017. Does attentional dysfunction and thalamic atrophy predict decline in dementia with Lewy bodies? *Parkinsonism Relat Disord,* 45**,** 69-74.
WEINGARTEN, J., LASSEK, M., MUELLER, B. F., ROHMER, M., LUNGER, I., BAEUMLISBERGER, D., DUDEK, S., GOGESCH, P., KARAS, M. & VOLKNANDT, W. 2014. The proteome of the presynaptic active zone from mouse brain. *Mol Cell Neurosci,* 59**,** 106-18.
WEINTRAUB, D., SIMUNI, T., CASPELL-GARCIA, C., COFFEY, C., LASCH, S., SIDEROWF, A., AARSLAND, D., BARONE, P., BURN, D., CHAHINE, L. M., EBERLING, J., ESPAY, A. J., FOSTER, E. D., LEVERENZ, J. B., LITVAN, I., RICHARD, I., TROYER, M. D., HAWKINS, K. A. & PARKINSON'S PROGRESSION MARKERS, I. 2015. Cognitive performance and neuropsychiatric symptoms in early, untreated Parkinson's disease. *Mov Disord,* 30**,** 919-27.
WEISMAN, D., CHO, M., TAYLOR, C., ADAME, A., THAL, L. J. & HANSEN, L. A. 2007. In dementia with Lewy bodies, Braak stage determines phenotype, not Lewy body distribution. *Neurology,* 69**,** 356-9.
WEN, J., GOYAL, M. S., ASTAFIEV, S. V., RAICHLE, M. E. & YABLONSKIY, D. A. 2018. Genetically defined cellular correlates of the baseline brain MRI signal. *Proc Natl Acad Sci U S A,* 115**,** E9727-E9736.
WERSINGER, C., PROU, D., VERNIER, P., NIZNIK, H. B. & SIDHU, A. 2003. Mutations in the lipid-binding domain of alpha-synuclein confer overlapping, yet distinct, functional properties in the regulation of dopamine transporter activity. *Mol Cell Neurosci,* 24**,** 91-105.
WERSINGER, C. & SIDHU, A. 2003. Attenuation of dopamine transporter activity by alpha-synuclein. *Neurosci Lett,* 340**,** 189-92.

WHITEHEAD, R. E., FERRER, J. V., JAVITCH, J. A. & JUSTICE, J. B. 2001. Reaction of oxidized dopamine with endogenous cysteine residues in the human dopamine transporter. *J Neurochem,* 76**,** 1242-51.
WHITEHOUSE, P. J., HEDREEN, J. C., WHITE, C. L., 3RD & PRICE, D. L. 1983. Basal forebrain neurons in the dementia of Parkinson disease. *Ann Neurol,* 13**,** 243-8.
WHITFIELD, D. R., VALLORTIGARA, J., ALGHAMDI, A., HOWLETT, D., HORTOBAGYI, T., JOHNSON, M., ATTEMS, J., NEWHOUSE, S., BALLARD, C., THOMAS, A. J., O'BRIEN, J. T., AARSLAND, D. & FRANCIS, P. T. 2014. Assessment of ZnT3 and PSD95 protein levels in Lewy body dementias and Alzheimer's disease: association with cognitive impairment. *Neurobiol Aging,* 35**,** 2836-2844.
WHONE, A. L., WATTS, R. L., STOESSL, A. J., DAVIS, M., RESKE, S., NAHMIAS, C., LANG, A. E., RASCOL, O., RIBEIRO, M. J., REMY, P., POEWE, W. H., HAUSER, R. A., BROOKS, D. J. & GROUP, R.-P. S. 2003. Slower progression of Parkinson's disease with ropinirole versus levodopa: The REAL-PET study. *Ann Neurol,* 54**,** 93-101.
WICHMANN, T. & DELONG, M. R. 1996. Functional and pathophysiological models of the basal ganglia. *Curr Opin Neurobiol,* 6**,** 751-8.
WIEDENMANN, B. & FRANKE, W. W. 1985. Identification and localization of synaptophysin, an integral membrane glycoprotein of Mr 38,000 characteristic of presynaptic vesicles. *Cell,* 41**,** 1017-28.
WIEDERMANN, M., DONGES, J. F., KURTHS, J. & DONNER, R. V. 2016. Spatial network surrogates for disentangling complex system structure from spatial embedding of nodes. *Phys Rev E,* 93**,** 042308.
WILHELM, B. G., MANDAD, S., TRUCKENBRODT, S., KROHNERT, K., SCHAFER, C., RAMMNER, B., KOO, S. J., CLASSEN, G. A., KRAUSS, M., HAUCKE, V., URLAUB, H. & RIZZOLI, S. O. 2014. Composition of isolated synaptic boutons reveals the amounts of vesicle trafficking proteins. *Science,* 344**,** 1023-8.
WILLIAMS, S. N. & UNDIEH, A. S. 2009. Dopamine D1-like receptor activation induces brain-derived neurotrophic factor protein expression. *Neuroreport,* 20**,** 606-10.
WILLIAMS-GRAY, C. H., EVANS, J. R., GORIS, A., FOLTYNIE, T., BAN, M., ROBBINS, T. W., BRAYNE, C., KOLACHANA, B. S., WEINBERGER, D. R., SAWCER, S. J. & BARKER, R. A. 2009. The distinct cognitive syndromes of Parkinson's disease: 5 year follow-up of the CamPaIGN cohort. *Brain,* 132**,** 2958-69.
WILLIAMS-GRAY, C. H., HAMPSHIRE, A., BARKER, R. A. & OWEN, A. M. 2008. Attentional control in Parkinson's disease is dependent on COMT val 158 met genotype. *Brain,* 131**,** 397-408.
WILSON, H., PAGANO, G., DE NATALE, E. R., MANSUR, A., CAMINITI, S. P., POLYCHRONIS, S., MIDDLETON, L. T., PRICE, G., SCHMIDT, K. F., GUNN, R. N., RABINER, E. A. & POLITIS, M. 2020. Mitochondrial Complex 1, Sigma 1, and Synaptic Vesicle 2A in Early Drug-Naive Parkinson's Disease. *Mov Disord.*
WINNER, B., DESPLATS, P., HAGL, C., KLUCKEN, J., AIGNER, R., PLOETZ, S., LAEMKE, J., KARL, A., AIGNER, L., MASLIAH, E., BUERGER, E. & WINKLER, J. 2009. Dopamine receptor activation promotes adult neurogenesis in an acute Parkinson model. *Exp Neurol,* 219**,** 543-52.
WINSHIP, I. R., PLAA, N. & MURPHY, T. H. 2007. Rapid astrocyte calcium signals correlate with neuronal activity and onset of the hemodynamic response in vivo. *J Neurosci,* 27**,** 6268-72.
WITHERS, G. S., GEORGE, J. M., BANKER, G. A. & CLAYTON, D. F. 1997. Delayed localization of synelfin (synuclein, NACP) to presynaptic terminals in cultured rat hippocampal neurons. *Brain Res Dev Brain Res,* 99**,** 87-94.
WOLF, R. L. & DETRE, J. A. 2007. Clinical neuroimaging using arterial spin-labeled perfusion magnetic resonance imaging. *Neurotherapeutics,* 4**,** 346-59.

WOLK, D. A. & DETRE, J. A. 2012. Arterial spin labeling MRI: an emerging biomarker for Alzheimer's disease and other neurodegenerative conditions. *Curr Opin Neurol,* 25**,** 421-8.
WU, H., WILLIAMS, J. & NATHANS, J. 2014. Complete morphologies of basal forebrain cholinergic neurons in the mouse. *Elife,* 3**,** e02444.
WU, Q., TAKANO, H., RIDDLE, D. M., TROJANOWSKI, J. Q., COULTER, D. A. & LEE, V. M. 2019. alpha-Synuclein (alphaSyn) Preformed Fibrils Induce Endogenous alphaSyn Aggregation, Compromise Synaptic Activity and Enhance Synapse Loss in Cultured Excitatory Hippocampal Neurons. *J Neurosci,* 39**,** 5080-5094.
XENIAS, H. S., IBANEZ-SANDOVAL, O., KOOS, T. & TEPPER, J. M. 2015. Are striatal tyrosine hydroxylase interneurons dopaminergic? *J Neurosci,* 35**,** 6584-99.
XIA, J., MIU, J., DING, H., WANG, X., CHEN, H., WANG, J., WU, J., ZHAO, J., HUANG, H. & TIAN, W. 2013. Changes of brain gray matter structure in Parkinson's disease patients with dementia. *Neural Regen Res,* 8**,** 1276-85.
XU, C., ZHUANG, P., HALLETT, M., ZHANG, Y., LI, J. & LI, Y. 2018. Parkinson's Disease Motor Subtypes Show Different Responses to Long-Term Subthalamic Nucleus Stimulation. *Front Hum Neurosci,* 12**,** 365.
XU, J., WU, X. S., SHENG, J., ZHANG, Z., YUE, H. Y., SUN, L., SGOBIO, C., LIN, X., PENG, S., JIN, Y., GAN, L., CAI, H. & WU, L. G. 2016. alpha-Synuclein Mutation Inhibits Endocytosis at Mammalian Central Nerve Terminals. *J Neurosci,* 36**,** 4408-14.
XU, Y., STOKES, A. H., ROSKOSKI, R., JR. & VRANA, K. E. 1998. Dopamine, in the presence of tyrosinase, covalently modifies and inactivates tyrosine hydroxylase. *J Neurosci Res,* 54**,** 691-7.
YAMADA, H., AIMI, Y., NAGATSU, I., TAKI, K., KUDO, M. & ARAI, R. 2007. Immunohistochemical detection of L-DOPA-derived dopamine within serotonergic fibers in the striatum and the substantia nigra pars reticulata in Parkinsonian model rats. *Neurosci Res,* 59**,** 1-7.
YAO, J., NOWACK, A., KENSEL-HAMMES, P., GARDNER, R. G. & BAJJALIEH, S. M. 2010. Cotrafficking of SV2 and synaptotagmin at the synapse. *J Neurosci,* 30**,** 5569-78.
YAO, N., WU, Y., ZHOU, Y., JU, L., LIU, Y., JU, R., DUAN, D. & XU, Q. 2015. Lesion of the locus coeruleus aggravates dopaminergic neuron degeneration by modulating microglial function in mouse models of Parkinsons disease. *Brain Res,* 1625**,** 255-74.
YETERIAN, E. H., PANDYA, D. N., TOMAIUOLO, F. & PETRIDES, M. 2012. The cortical connectivity of the prefrontal cortex in the monkey brain. *Cortex,* 48**,** 58-81.
YONG, S. W., YOON, J. K., AN, Y. S. & LEE, P. H. 2007. A comparison of cerebral glucose metabolism in Parkinson's disease, Parkinson's disease dementia and dementia with Lewy bodies. *Eur J Neurol,* 14**,** 1357-62.
YOUSAF, T., PAGANO, G., WILSON, H. & POLITIS, M. 2018. Neuroimaging of Sleep Disturbances in Movement Disorders. *Front Neurol,* 9**,** 767.
ZACCAI, J., BRAYNE, C., MCKEITH, I., MATTHEWS, F., INCE, P. G. & MRC COGNITIVE FUNCTION, A. N. S. 2008. Patterns and stages of alpha-synucleinopathy: Relevance in a population-based cohort. *Neurology,* 70**,** 1042-8.
ZALTIERI, M., GRIGOLETTO, J., LONGHENA, F., NAVARRIA, L., FAVERO, G., CASTREZZATI, S., COLIVICCHI, M. A., DELLA CORTE, L., REZZANI, R., PIZZI, M., BENFENATI, F., SPILLANTINI, M. G., MISSALE, C., SPANO, P. & BELLUCCI, A. 2015. alpha-synuclein and synapsin III cooperatively regulate synaptic function in dopamine neurons. *J Cell Sci,* 128**,** 2231-43.
ZANOTTI-FREGONARA, P., FADAILI EL, M., MAROY, R., COMTAT, C., SOULOUMIAC, A., JAN, S., RIBEIRO, M. J., GAURA, V., BAR-HEN, A. & TREBOSSEN, R. 2009. Comparison of eight methods for the estimation of the image-derived input function in dynamic [(18)F]-FDG PET human brain studies. *J Cereb Blood Flow Metab,* 29**,** 1825-35.

ZARKALI, A., MCCOLGAN, P., LEYLAND, L. A., LEES, A. J. & WEIL, R. S. 2021. Longitudinal thalamic white and grey matter changes associated with visual hallucinations in Parkinson's disease. *J Neurol Neurosurg Psychiatry*.
ZAROW, C., LYNESS, S. A., MORTIMER, J. A. & CHUI, H. C. 2003. Neuronal loss is greater in the locus coeruleus than nucleus basalis and substantia nigra in Alzheimer and Parkinson diseases. *Arch Neurol,* 60**,** 337-41.
ZENG, B. Y., IRAVANI, M. M., JACKSON, M. J., ROSE, S., PARENT, A. & JENNER, P. 2010. Morphological changes in serotoninergic neurites in the striatum and globus pallidus in levodopa primed MPTP treated common marmosets with dyskinesia. *Neurobiol Dis,* 40**,** 599-607.
ZETTERSTROM, T., HERRERA-MARSCHITZ, M. & UNGERSTEDT, U. 1986. Simultaneous measurement of dopamine release and rotational behaviour in 6-hydroxydopamine denervated rats using intracerebral dialysis. *Brain Res,* 376**,** 1-7.
ZETUSKY, W. J., JANKOVIC, J. & PIROZZOLO, F. J. 1985. The heterogeneity of Parkinson's disease: clinical and prognostic implications. *Neurology,* 35**,** 522-6.
ZHANG, K., HERZOG, H., MAULER, J., FILSS, C., OKELL, T. W., KOPS, E. R., TELLMANN, L., FISCHER, T., BROCKE, B., STURM, W., COENEN, H. H. & SHAH, N. J. 2014. Comparison of cerebral blood flow acquired by simultaneous [15O]water positron emission tomography and arterial spin labeling magnetic resonance imaging. *J Cereb Blood Flow Metab,* 34**,** 1373-80.
ZHANG, L., ZHANG, C., ZHU, Y., CAI, Q., CHAN, P., UEDA, K., YU, S. & YANG, H. 2008. Semi-quantitative analysis of alpha-synuclein in subcellular pools of rat brain neurons: an immunogold electron microscopic study using a C-terminal specific monoclonal antibody. *Brain Res,* 1244**,** 40-52.
ZHANG, X., ANDREN, P. E. & SVENNINGSSON, P. 2007. Changes on 5-HT2 receptor mRNAs in striatum and subthalamic nucleus in Parkinson's disease model. *Physiol Behav,* 92**,** 29-33.
ZHANG, Y., MEREDITH, G. E., MENDOZA-ELIAS, N., RADEMACHER, D. J., TSENG, K. Y. & STEECE-COLLIER, K. 2013. Aberrant restoration of spines and their synapses in L-DOPA-induced dyskinesia: involvement of corticostriatal but not thalamostriatal synapses. *J Neurosci,* 33**,** 11655-67.
ZHU, D., YUAN, T., GAO, J., XU, Q., XUE, K., ZHU, W., TANG, J., LIU, F., WANG, J. & YU, C. 2021. Correlation between cortical gene expression and resting-state functional network centrality in healthy young adults. *Hum Brain Mapp,* 42**,** 2236-2249.
ZIEGLER, G., DAHNKE, R., JANCKE, L., YOTTER, R. A., MAY, A. & GASER, C. 2012. Brain structural trajectories over the adult lifespan. *Hum Brain Mapp,* 33**,** 2377-89.
ZIGMOND, M. J. 1997. Do compensatory processes underlie the preclinical phase of neurodegenerative disease? Insights from an animal model of parkinsonism. *Neurobiol Dis,* 4**,** 247-53.
ZLOKOVIC, B. V. 2011. Neurovascular pathways to neurodegeneration in Alzheimer's disease and other disorders. *Nat Rev Neurosci,* 12**,** 723-38.

8 Appendix A

8.1 Partial volume correction

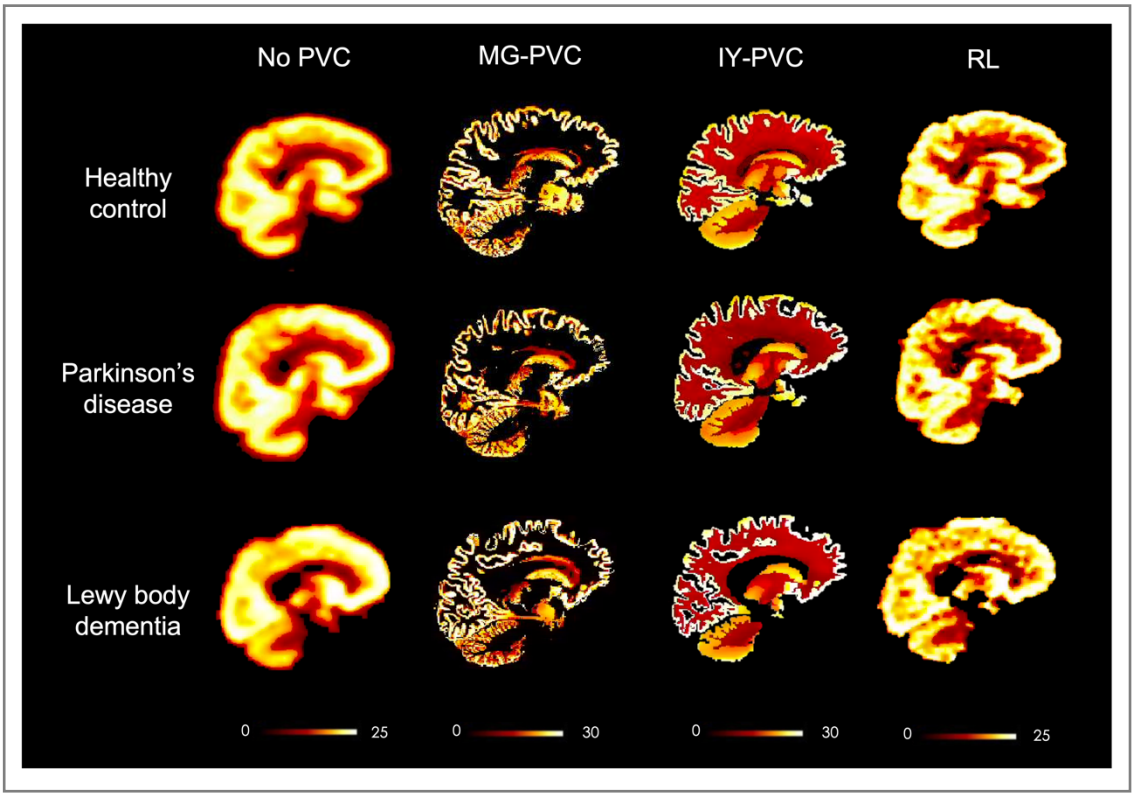

Figure 8.1. For illustrative purposes. Axial [^{11}C]UCB-J V_T parametric maps coregistered to T1-weighted MRI for a 68 year-old healthy male, a 67 year-old male Parkinson's disease patients and a 68 year-old male dementia with Lewy bodies patients. Only grey matter values are demonstrated for MG-PVC image. MG: Müller-Gärtner; IY: iterative Yang; RL: Richardson-Lucy

Table 8.1. [^{11}C]UCB-J V_T percentage change before and after PVC for all diagnostic groups

Method	% change: No-PVC vs MG-PVC					% change: No-PVC vs IY-PVC					% change: No-PVC vs RL-PVC				
Region-of-interest	**HC**	**Drug-naïve PD**	**Treated PD**	**PDD**	**DLB**	**HC**	**Drug-naïve PD**	**Treated PD**	**PDD**	**DLB**	**HC**	**Drug-naïve PD**	**Treated PD**	**PDD**	**DLB**
Frontal	51.3	51.4	49.3	51.1	62.8	50.6	51.4	49.2	51.3	62.5	12.6	11.6	13.6	11.3	13.1
Temporal	47.0	44.9	46.6	47.7	61.4	45.7	44.2	45.0	48.4	60.2	9.9	9.1	10.1	8.9	10.2
Parietal	37.2	36.5	35.8	38.3	43.5	38.6	38.2	36.6	40.5	45.0	11.6	11.1	12.3	11.2	11.9
Occipital	36.4	35.1	36.5	33.8	42.2	38.5	38.4	38.1	38.0	44.7	10.4	9.9	10.4	9.6	9.9
Caudate	59.9	61.4	57.2	51.6	68.9	54.5	51.9	52.9	43.4	48.7	29.0	26.4	27.7	21.3	21.9
Putamen	14.9	14.7	16.8	13.0	15.5	34.6	32.2	34.9	28.6	32.2	12.8	11.2	13.0	10.0	12.7
Thalamus	21.3	22.1	20.2	15.8	27.4	20.3	18.4	18.6	19.6	23.0	17.6	17.0	17.1	16.9	19.6
Substantia nigra	202.0	195.8	164.6	157.9	169.6	12.4	10.6	11.6	14.2	11.8	22.9	18.2	15.0	18.8	21.2

MG: Müller-Gärtner; IY: iterative Yang; RL: Richardson-Lucy

Table 8.2. Linear regression model: regional [^{11}C]UCB-J V_T vs regional volume for all subjects pooled together

Method	No-PVC			MG-PVC			IY-PVC			RL-PVC		
Region-of-interest	**R_{Linear}**	**R^2**	**P_{Linear}**	**R_{Linear}**	**R^2**	**P_{Linear}**	**R_{Linear}**	**R^2**	**P_{Linear}**	**R_{Linear}**	**R^2**	**P_{Linear}**
Frontal	+0.42	0.18	**<0.001**	+0.30	0.09	**0.018**	+0.33	0.11	**0.006**	+0.42	0.18	**<0.001**
Temporal	+0.42	0.18	**<0.001**	+0.25	0.06	**0.05**	+0.28	0.08	**0.023**	+0.39	0.15	**0.001**
Parietal	+0.40	0.16	**0.001**	+0.31	0.10	**0.016**	+0.34	0.11	**0.007**	+0.40	0.16	**0.001**
Occipital	+0.42	0.18	**<0.001**	+0.36	0.13	**0.001**	+0.39	0.15	**<0.001**	+0.41	0.17	**<0.001**
Caudate	+0.59	0.34	**<0.001**	+0.48	0.23	**<0.001**	+0.53	0.29	**<0.001**	+0.57	0.33	**<0.001**
Putamen	+0.13	0.02	0.274	+0.07	0.01	0.486	+0.14	0.02	0.221	+0.13	0.02	0.249
Thalamus	+0.43	0.18	**<0.001**	+0.30	0.09	**0.008**	+0.38	0.15	**0.001**	+0.39	0.15	**0.001**
Substantia nigra	+0.05	0.00	0.596	-0.40	0.16	**0.001**	+0.15	0.02	0.158	+0.01	0.00	0.923

MG: Müller-Gärtner; IY: iterative Yang; RL: Richardson-Lucy

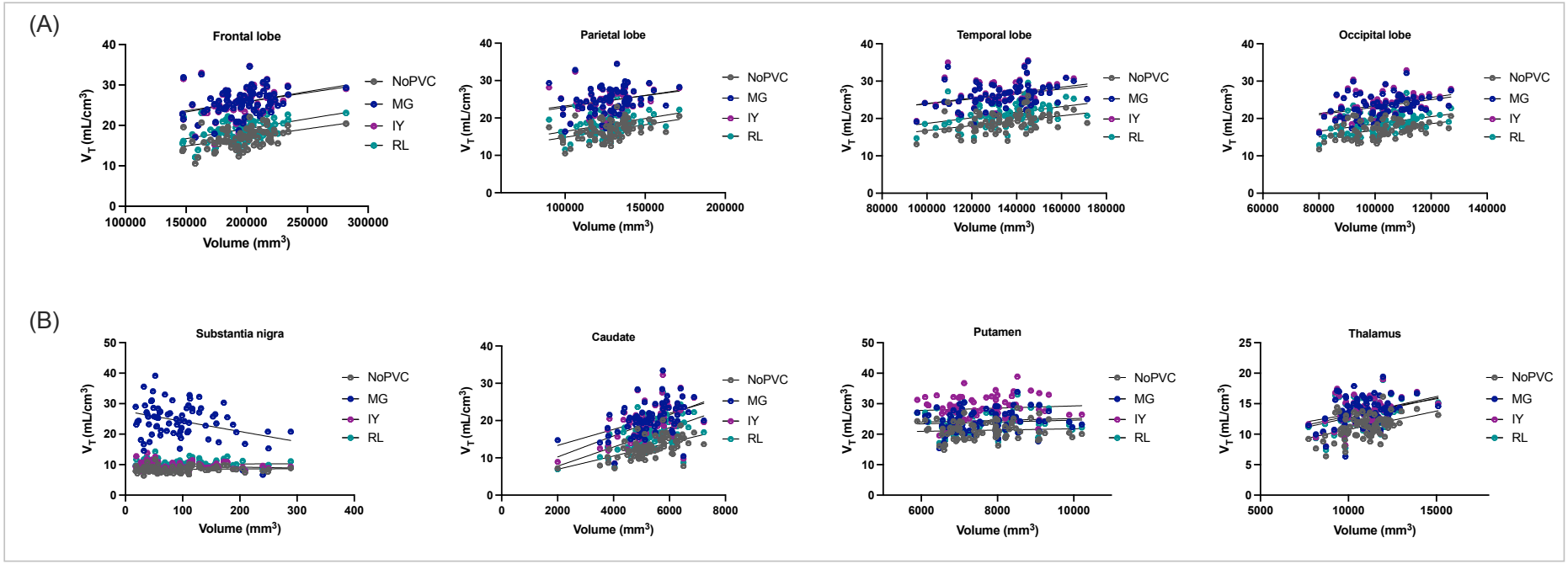

Figure 8.2. Volume vs [^{11}C]UCB-J V_T for all subjects in (A) cortical brain areas and (B) subcortical brain areas. In the substantia nigra, a negative association was observed for MG, but not for IT. For all other regions, positive or no associations were observed for all PVC techniques.

Table 8.3. Linear regression model: % change of [^{11}C]UCB-J V_T vs regional volume for all subjects pooled together

Method	**MG-PVC**			**IY-PVC**			**RL-PVC**		
Region-of-interest	**R_{Linear}**	**R^2**	**P_{Linear}**	**R_{Linear}**	**R^2**	**P_{Linear}**	**R_{Linear}**	**R^2**	**P_{Linear}**
Frontal	-0.42	0.17	**<0.001**	-0.56	0.32	0.378	-0.05	0.00	0.593
Temporal	-0.50	0.25	**<0.001**	-0.49	0.24	0.407	-0.25	0.06	**0.015**
Parietal	-0.55	0.30	**<0.001**	-0.59	0.35	0.383	-0.06	0.00	0.549
Occipital	-0.29	0.08	**0.009**	-0.66	0.44	0.359	-0.04	0.00	0.743
Caudate	-0.50	0.25	**0.002**	-0.53	0.28	0.301	-0.42	0.17	**0.016**
Putamen	-0.08	0.01	0.57	-0.61	0.37	0.382	-0.09	0.01	0.438
Thalamus	-0.30	0.09	**0.003**	-0.62	-0.38	0.375	-0.29	0.09	**0.004**
Substantia nigra	-0.48	0.23	**<0.001**	+0.05	0.00	0.758	+0.09	0.01	0.446

MG: Müller-Gärtner; IY: iterative Yang; RL: Richardson-Lucy

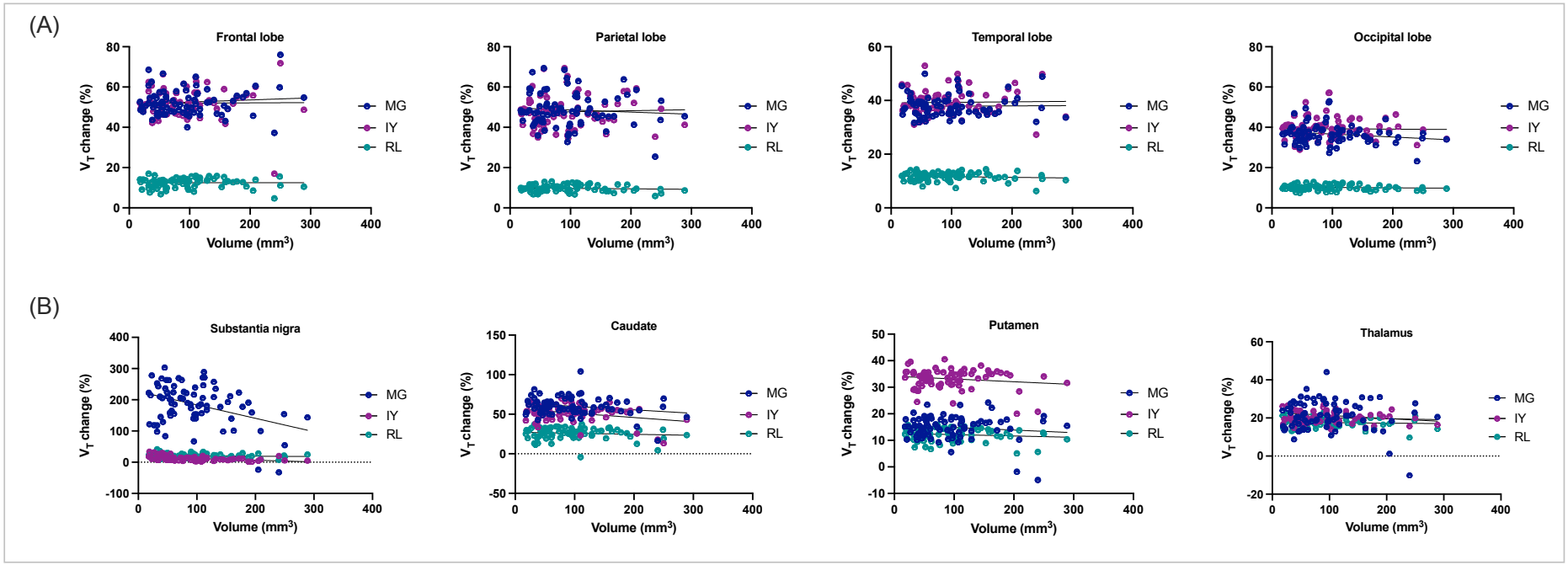

Figure 8.3. Volume vs percentage change of [^{11}C]UCB-J V_T for all subjects in (A) cortical brain areas and (B) subcortical brain areas. Significantly negative associations were observed for MG, but these were comparable to those associations observed for IY.

Table 8.4. Inter-subject [^{11}C]UCB-J V_T percent coefficient of variation.

Cohort	Healthy controls				Drug-naïve PD				Treated PD				PDD				DLB			
Region-of-interest	**No PVC**	**MG**	**IY**	**RL**	**No PVC**	**MG**	**IY**	**RL**	**No PVC**	**MG**	**IY**	**RL**	**No PVC**	**MG**	**IY**	**RL**	**No PVC**	**MG**	**IY**	**RL**
Frontal	12.70%	12.50%	12.80%	12.80%	11.90%	10.70%	11.10%	12.70%	9.00%	9.20%	9.50%	9.80%	20.60%	20.50%	22.60%	21.30%	13.90%	12.60%	12.90%	13.90%
Temporal	13.50%	13.00%	13.10%	13.80%	13.20%	11.70%	12.60%	13.10%	8.70%	9.10%	9.20%	8.80%	17.80%	17.60%	16.60%	17.80%	11.10%	12.40%	11.30%	11.30%
Parietal	13.10%	12.30%	12.70%	13.20%	10.00%	9.70%	10.00%	10.30%	8.60%	8.20%	8.40%	8.40%	18.60%	17.20%	17.80%	19.20%	13.10%	11.20%	11.70%	13.20%
Occipital	13.40%	12.50%	12.70%	13.70%	11.20%	11.20%	12.00%	11.00%	8.20%	8.40%	8.50%	8.40%	15.50%	15.30%	15.10%	15.50%	9.20%	10.20%	9.20%	9.50%
Caudate	18.30%	18.30%	19.80%	20.60%	19.80%	16.90%	19.90%	22.80%	10.90%	10.10%	12.10%	12.00%	30.70%	33.50%	35.80%	35.60%	17.10%	13.30%	24.30%	24.10%
Putamen	12.30%	13.10%	12.80%	12.80%	10.40%	11.10%	10.40%	10.90%	10.60%	9.60%	10.80%	11.10%	19.40%	23.70%	20.20%	20.90%	11.50%	10.90%	11.60%	11.30%
Thalamus	14.70%	14.20%	13.90%	14.50%	15.50%	15.30%	16.30%	15.40%	8.10%	9.70%	8.20%	8.70%	22.30%	27.30%	22.00%	23.90%	9.90%	12.00%	10.30%	10.50%
Substantia nigra	11.20%	19.90%	11.80%	11.50%	9.00%	14.40%	12.20%	8.80%	7.60%	18.90%	10.50%	10.50%	13.40%	39.80%	16.90%	12.10%	11.30%	21.70%	14.60%	17.30%

MG: Müller-Gärtner; IY: iterative Yang; RL: Richardson-Lucy

9 Appendix B

9.1 Parametric [^{11}C]UCB-J V_T maps: regions-of-interest

Table 9.1. Group comparison of parametric [^{11}C]UCB-J V_T in healthy controls, drug-naïve PD patients and treated PD patients

No PVC [^{11}C]UCB-J V_T, ml/cm^3 (mean ±SD)	HC	Drug naïve PD	Treated PD	P value HC vs drug-naïve PD	P value HC vs treated PD	P value Drug-naïve PD vs treated PD
Brainstem	8.5 ± 0.9	7.7 ± 0.8	8.1 ± 0.4	**0.004* (-9%)**	0.29 (-4%)	0.12 (+5%)
Substantia nigra	8.8 ± 1	8 ± 0.7	8.2 ± 0.6	**0.002* (-9%)**	0.037$ (-7%)	0.38 (+2%)
Caudate	13.8 ± 2.5	12.3 ± 2.4	13.1 ± 1.3	**0.007* (-11%)**	0.52 (-4%)	0.097 (+7%)
Precommissural putamen	23.3 ± 2.9	21.5 ± 2.3	22.6 ± 2.4	**0.037* (-8%)**	0.52 (-3%)	0.24 (+5%)
Postcommissural putamen	20.6 ± 2.6	19.2 ± 2	20.1 ± 2.1	**0.049* (-7%)**	0.56 (-2%)	0.26 (+5%)
Thalamus	11.9 ± 1.8	11 ± 1.7	11.9 ± 1	**0.024* (-8%)**	0.84 (0%)	**0.047$ (+9%)**
Precentral gyrus	15.7 ± 2	14.6 ± 1.7	15.6 ± 1.4	**0.028* (-7%)**	0.98 (0%)	0.080 (+7%)
Postcentral gyrus	15.2 ± 2.1	14.2 ± 1.9	15.4 ± 1.4	**0.042* (-7%)**	0.74 (+1%)	0.058 (+8%)
Supplementary motor area	17.4 ± 2.4	15.8 ± 2.3	17.1 ± 1.5	**0.013* (-9%)**	0.72 (-2%)	0.084 (+8%)
Dorsolateral prefrontal cortex	17.3 ± 2.3	16 ± 2	17.3 ± 1.6	**0.021* (-8%)**	0.95 (0%)	0.055 (+8%)
Superior parietal lobe	17.5 ± 2.4	16.2 ± 2.1	17.5 ± 1.5	**0.034* (-7%)**	0.88 (0%)	0.067 (+8%)
Temporal lobe	19.8 ± 2.6	18.5 ± 1.9	19.8 ± 1.8	**0.044* (-6%)**	1.00 (0%)	0.11 (+7%)
Occipital lobe	17.6 ± 2.4	16.6 ± 1.9	17.3 ± 1.4	0.074 (-6%)	0.77 (-2%)	0.23 (+5%)
Cerebellum	15.7 ± 1.9	14.5 ± 1.4	15.4 ± 1.4	**0.025* (-8%)**	0.61 (-2%)	0.16 (+6%)
Exploratory regions-of-interest						
Nucleus accumbens	21.4 ± 2.8	20.1 ± 2.2	21.2 ± 2.2	0.089 (-6%)	0.88 (-1%)	0.21 (+6%)
Parahippocampal gyrus	16.3 ± 2.2	15.3 ± 1.5	16.2 ± 1.2	0.071 (-6%)	0.92 (-1%)	0.17 (+5%)
Amygdala	17.2 ± 2.1	16.1 ± 1.4	16.8 ± 1.8	0.056 (-7%)	0.57 (-2%)	0.28 (+5%)
Insular cortex	20.9 ± 2.8	19.7 ± 2.1	21.2 ± 1.9	0.056	0.63	0.056

				(-6%)	(+2%)	(+8%)
Anterior cingulate	20.6 ± 2.7	19.3 ± 2.3	20.7 ± 1.8	0.058 (-6%)	0.87 (0%)	0.098 (+7%)
Posterior cingulate	19.7 ± 2.8	18.4 ± 2.3	19.4 ± 1.6	0.051 (-6%)	0.81 (-1%)	0.17 (+5%)

Table 9.2. Group comparison of partial volume corrected [^{11}C]UCB-J V_T in healthy controls, drug-naïve PD patients and treated PD patients

IY PVC [^{11}C]UCB-J V_T, ml/cm^3 (mean ±SD)	**HC**	**Drug naïve PD**	**Treated PD**	**P value HC vs drug-naïve PD**	**P value HC vs treated PD**	**P value Drug-naïve PD vs treated PD**
Brainstem	8.8 ± 1.1	8 ± 1	8.4 ± 0.5	**0.013* (-9%)**	0.097 (-5%)	0.24 (+4%)
Substantia nigra	9.9 ± 1.2	8.9 ± 1.1	9 ± 0.6	**0.003* (-11%)**	**0.014$ (-9%)**	0.64 (+1%)
Caudate	21.2 ± 4.2	18.6 ± 3.7	20.1 ± 2.5	**0.016* (-12%)**	0.47 (-5%)	0.15 (+8%)
Precommissural putamen	31.1 ± 4	28.3 ± 3	30.3 ± 3.3	**0.026* (-9%)**	0.57 (-3%)	0.17 (+7%)
Postcommissural putamen	28 ± 3.6	25.5 ± 2.6	27.5 ± 3	**0.02* (-9%)**	0.66 (-2%)	0.12 (+8%)
Thalamus	14.3 ± 2	13 ± 2.1	14.2 ± 1.3	**0.023* (-9%)**	0.89 (-1%)	0.08 (+9%)
Precentral gyrus	23.9 ± 3.1	22.3 ± 2.4	24 ± 2.3	0.059 (-7%)	0.86 (0%)	0.094 (+8%)
Postcentral gyrus	24.1 ± 3.3	22.5 ± 2.8	24.5 ± 2.4	0.09 (-7%)	0.64 (+2%)	0.082 (+9%)
Supplementary motor area	25 ± 3.4	23 ± 2.8	25.4 ± 3	**0.042* (-8%)**	0.73 (+1%)	0.054 (+10%)
Dorsolateral prefrontal cortex	26.2 ± 3.5	24.4 ± 3	26 ± 2.7	0.063 (-7%)	0.92 (-1%)	0.15 (+7%)
Superior parietal lobe	25.4 ± 3.3	23.4 ± 2.9	25.6 ± 2.3	**0.032* (-8%)**	0.83 (+1%)	0.056 (+9%)
Temporal lobe	28 ± 3.6	26.1 ± 2.6	27.6 ± 2.6	0.072 (-7%)	0.77 (-1%)	0.22 (+6%)
Occipital lobe	24.5 ± 3.1	23 ± 2.8	24.2 ± 2.2	0.095 (-6%)	0.84 (-1%)	0.23 (+5%)
Cerebellum	18 ± 2.2	16.8 ± 1.9	17.7 ± 1.7	0.073 (-7%)	0.71 (-2%)	0.24 (+5%)
Exploratory regions-of-interest						
Nucleus accumbens	29 ± 4	26.9 ± 3.2	29 ± 3.3	0.11 (-7%)	0.94 (0%)	0.18 (+8%)
Parahippocampal gyrus	20.1 ± 2.6	18.6 ± 2	19.8 ± 1.7	0.052 (-7%)	0.79 (-1%)	0.17 (+7%)
Amygdala	20.8 ± 2.5	19.8 ± 1.5	20.3 ± 2.3	0.20 (-5%)	0.56 (-2%)	0.56 (+3%)
Insular cortex	27.5 ± 3.3	25.8 ± 2.5	27.2 ± 3	0.084 (-6%)	0.74 (-1%)	0.25 (+5%)

Anterior cingulate	28.4 ± 3.5	27 ± 2.9	28.2 ± 3	0.16 (-5%)	0.83 (-1%)	0.33 (+4%)
Posterior cingulate	25.4 ± 3.6	24 ± 2.9	25.2 ± 2.3	0.11 (-6%)	0.89 (-1%)	0.23 (+5%)

10 Appendix C

10.1 Parametric [^{11}C]UCB-J V_T maps: regions-of-interest

10.1.1 Healthy controls vs non-demented PD vs PDD

Table 10.1. Group comparison of parametric [^{11}C]UCB-J V_T in healthy controls, non-demented PD patients and PDD patients

No PVC [^{11}C]UCB-J V_T, ml/cm^3 (mean ±SD)	HC	Non-demented PD	PDD	P value HC vs PDD	P value Non-demented PD vs PDD
Caudate	13.8 ± 2.5	13.1 ± 1.3	11.1 ± 3.4	**0.006* (-19%)**	0.068 (-16%)
Putamen	21.9 ± 2.7	21.4 ± 2.2	20.4 ± 3.9	0.25 (-7%)	0.59 (-5%)
Thalamus	11.9 ± 1.8	11.9 ± 1	10.1 ± 2.3	**0.016* (-15%)**	**0.042$ (-15%)**
Amygdala	17.2 ± 2.1	16.8 ± 1.8	17.1 ± 2.7	0.77 (-1%)	0.51 (+2%)
Hippocampus	14.2 ± 2	14.1 ± 1.2	13.2 ± 2.5	0.41 (-7%)	0.51 (-6%)
Precentral gyrus	15.7 ± 2	15.6 ± 1.4	14 ± 2.7	0.068 (-11%)	0.15 (-10%)
Supplementary motor area	17.4 ± 2.4	17.1 ± 1.5	15.3 ± 3	**0.04* (-12%)**	0.16 (-10%)
Dorsolateral prefrontal cortex	17.3 ± 2.3	17.3 ± 1.6	15.8 ± 3.5	0.19 (-8%)	0.29 (-8%)
Orbitofrontal prefrontal cortex	19.4 ± 2.4	19.5 ± 2	19.3 ± 3.8	0.78 (0%)	0.90 (-1%)
Postcentral gyrus	15.2 ± 2.1	15.4 ± 1.4	13.3 ± 2.6	**0.037* (-13%)**	0.06 (-13%)
Superior parietal lobule	16.6 ± 2.3	16.5 ± 1.8	13.8 ± 2.6	**0.003* (-17%)**	**0.019$ (-16%)**
Precuneus	19.2 ± 2.6	19.2 ± 1.6	16.9 ± 3	**0.049$ (-12%)**	0.11 (-12%)
Inferior Parietal lobe	17.9 ± 2.4	17.9 ± 1.5	15.5 ± 2.8	**0.018* (-14%)**	**0.024$ (-14%)**
Insular cortex	20.9 ± 2.8	21.2 ± 1.9	19.8 ± 4.1	0.55 (-5%)	0.43 (-7%)
Occipital lobe	17.6 ± 2.4	17.3 ± 1.4	16 ± 2.5	0.17 (-9%)	0.38 (-8%)
Exploratory regions-of-interest					
Brainstem	8.5 ± 0.9	8.1 ± 0.4	7.9 ± 1.2	0.25 (-7%)	0.88 (-3%)

Nucleus accumbens	21.4 ± 2.8	21.2 ± 2.2	19.7 ± 4.4	0.23 (-8%)	0.39 (-7%)
Parahippocampal gyrus	16.3 ± 2.2	16.2 ± 1.2	16 ± 2.8	0.81 (-1%)	0.76 (-1%)
Anterior cingulate	20.6 ± 2.7	20.7 ± 1.8	19.2 ± 4.2	0.32 (-7%)	0.32 (-7%)
Posterior cingulate	19.7 ± 2.8	19.4 ± 1.6	17.8 ± 3.2	0.14 (-10%)	0.36 (-8%)
Temporal lobe	19.8 ± 2.6	19.8 ± 1.8	18.6 ± 3.6	0.43 (-6%)	0.54 (-6%)
Cerebellum	15.7 ± 1.9	15.4 ± 1.4	14.6 ± 1.9	0.19 (-7%)	0.49 (-5%)

*p<0.05, FDR-corrected; $^{\$}p$<0.05, uncorrected

Table 10.2. Group comparison of partial volume corrected parametric [^{11}C]UCB-J V_T in healthy controls, non-demented PD patients and PDD patients

IY PVC [^{11}C]UCB-J V_T, ml/cm^3 (mean ±SD)	**HC**	**Non-demented PD**	**PDD**	**P value HC vs PDD**	**P value Non-demented PD vs PDD**
Caudate	21.2 ± 4.2	20.1 ± 2.5	15.9 ± 5.7	**0.001* (-25%)**	**0.017$^{\$}$ (-21%)**
Putamen	29.5 ± 3.8	28.9 ± 3.2	26.2 ± 5.3	0.055 (-11%)	0.21 (-9%%)
Thalamus	14.3 ± 2	14.2 ± 1.3	12.1 ± 2.7	**0.009* (-16%)**	**0.043$^{\$}$ (-15%)**
Amygdala	20.8 ± 2.5	20.3 ± 2.3	21.1 ± 3.3	0.53 (+2%)	0.35 (+4%)
Hippocampus	15.9 ± 2.5	15.7 ± 1.7	14.1 ± 3.2	0.10 (-11%)	0.23 (-10%)
Precentral gyrus	23.9 ± 3.1	24 ± 2.3	22 ± 4.1	0.23 (-8%)	0.28 (-8%)
Supplementary motor area	25 ± 3.4	25.4 ± 3	22.6 ± 4.9	0.13 (-10%)	0.16 (-11%)
Dorsolateral prefrontal cortex	26.2 ± 3.5	26 ± 2.7	24.1 ± 5.8	0.23 (-8%)	0.37 (-7%)
Orbitofrontal prefrontal cortex	28.5 ± 3.4	28.3 ± 2.8	28 ± 6.6	0.79 (-2%)	0.93 (-1%)
Postcentral gyrus	24.1 ± 3.3	24.5 ± 2.4	21.8 ± 4.1	0.12 (-10%)	0.12 (-11%)
Superior parietal lobule	26 ± 3.5	26.4 ± 2.6	22 ± 3.9	**0.005* (-16%)**	**0.009$^{\$}$ (-17%)**
Precuneus	25.5 ± 3.5	25.8 ± 2.4	22.3 ± 3.7	**0.037$^{\$}$ (-12%)**	**0.048$^{\$}$ (-14%)**
Inferior parietal lobe	26.1 ± 3.4	25.8 ± 2.2	23.2 ± 3.7	**0.042$^{\$}$ (-11%)**	0.14 (-10%)
Insular cortex	27.5 ± 3.3	27.2 ± 3	27.1 ± 4.6	0.98 (-2%)	0.81 (0%)

Occipital lobe	24.5 ± 3.1	24.2 ± 2.2	22.1 ± 3.4	0.1 (-7%)	0.24 (-11%)
Exploratory regions-of-interest					
Brainstem	8.8 ± 1.1	8.4 ± 0.5	8.3 ± 1.2	0.56 (-5%)	0.69 (-1%)
Nucleus accumbens	29 ± 4	29 ± 3.3	25.8 ± 5.8	0.085 (-11%)	0.15 (-11%)
Parahippocampal gyrus	20.1 ± 2.6	19.8 ± 1.7	19.7 ± 3.3	0.99 (-2%)	0.82 (-1%)
Anterior cingulate	28.4 ± 3.5	28.2 ± 3	26.8 ± 5.5	0.38 (-5%)	0.59 (-5%)
Posterior cingulate	25.4 ± 3.6	25.2 ± 2.3	23.3 ± 3.7	0.22 (-8%)	0.39 (-7%)
Temporal lobe	28 ± 3.6	27.6 ± 2.6	26.8 ± 4.8	0.63 (-4%)	0.87 (-3%)
Cerebellum	18 ± 2.2	17.7 ± 1.7	17 ± 2.3	0.34 (-5%)	0.64 (-4%)

*p<0.05, FDR-corrected; ^{S}p<0.05, uncorrected

10.1.2 Healthy controls vs DLB

Table 10.3. Group comparison of parametric [^{11}C]UCB-J V_T in healthy controls and DLB patients

No PVC [^{11}C]UCB-J V_T, ml/cm^3 (mean ±SD)	**HC**	**DLB**	**P value HC vs DLB**
Nucleus accumbens	21.4 ± 2.8	19 ± 2.3	**0.026* (-12%)**
Caudate	13.8 ± 2.5	10.5 ± 1.8	**<0.001* (-24%)**
Thalamus	11.9 ± 1.8	9.5 ± 0.9	**<0.001* (-20%)**
Amygdala	17.2 ± 2.1	15.3 ± 1.3	**0.015* (-11%)**
Frontal lobe	17.4 ± 2.2	15.6 ± 2.2	**0.026* (-10%)**
Temporal lobe	19.8 ± 2.6	17.1 ± 2.3	**0.004* (-13%)**
Precuneus	19.2 ± 2.6	15.7 ± 1.8	**<0.001* (-19%)**
Inferior parietal lobe	17.9 ± 2.4	14.9 ± 1.7	**0.001* (-16%)**
Superior parietal lobule	16.6 ± 2.3	13.7 ± 1.5	**0.001* (-18%)**
Lingual gyrus	18.8 ± 2.6	15.9 ± 1.5	**0.002* (-15%)**
Cuneus	18.3 ± 2.6	15.5 ± 1.5	**0.007***

			(-15%)
Calcarine sulcus	19.4 ± 2.7	16 ± 1.3	**0.001*** **(-18%)**
Occipital pole	17 ± 2.3	14.7 ± 1.4	**0.005*** **(-14%)**
Insular cortex	20.9 ± 2.8	17.8 ± 2.2	**0.002*** **(-15%)**
Anterior cingulate	20.6 ± 2.7	17.5 ± 2.3	**0.002*** **(-15%)**
Posterior cingulate	19.7 ± 2.8	16 ± 1.9	**<0.001*** **(-19%)**
Exploratory regions-of-interest			
Brainstem	21.9 ± 2.7	20.1 ± 2.3	0.067 (-8%)
Putamen	8.8 ± 1	7.8 ± 0.9	**0.004$** **(-12%)**
Hippocampus	14.2 ± 2	11.5 ± 0.6	**<0.001$** **(-19%)**
Parahippocampal gyrus	16.3 ± 2.2	14 ± 1.7	**0.003$** **(-14%)**
Fusiform gyrus	20.1 ± 2.6	17.5 ± 2	**0.005$** **(-13%)**
Cerebellum	15.7 ± 1.9	13.9 ± 1.3	**0.007$** **(-12%)**

*p<0.05, FDR-corrected; $^{\$}p$<0.05, uncorrected

Table 10.4. Group comparison of partial volume corrected [^{11}C]UCB-J V_T in healthy controls and DLB patients

IY PVC [^{11}C]UCB-J V_T, ml/cm^3 (mean ±SD)	**HC**	**DLB**	**P value HC vs DLB**
Nucleus accumbens	29 ± 4	25.4 ± 3.3	**0.025*** **(-12%)**
Caudate	21.2 ± 4.2	15.6 ± 3.8	**<0.001*** **(-27%)**
Thalamus	14.3 ± 2	11.7 ± 1.2	**0.001*** **(-18%)**
Amygdala	20.8 ± 2.5	19.3 ± 1.8	0.11 (-7%)
Frontal lobe	26.1 ± 3.3	25.3 ± 3.2	0.48 (-3%)
Temporal lobe	28 ± 3.6	25.5 ± 3	0.061 (-9%)
Precuneus	25.5 ± 3.5	23.1 ± 2.9	0.066 (-9%)
Inferior parietal lobe	26.1 ± 3.4	23.3 ± 2.5	**0.024*** **(-11%)**

Superior parietal lobule	26 ± 3.5	23.6 ± 2.6	0.056 (-10%)
Lingual gyrus	24.1 ± 3	21.5 ± 2.2	**0.014* (-11%)**
Cuneus	24.9 ± 3	23 ± 2	0.12 (-8%)
Calcarine sulcus	24.1 ± 3.1	21.3 ± 1.7	**0.017* (-12%)**
Occipital pole	24.6 ± 3.2	22 ± 2.1	**0.028* (-11%)**
Insular cortex	27.5 ± 3.3	26 ± 2.5	0.20 (-5%)
Anterior cingulate	28.4 ± 3.5	26.5 ± 3.1	0.12 (-7%)
Posterior cingulate	25.4 ± 3.6	22.7 ± 3.3	**0.025* (-11%)**
Exploratory regions-of-interest			
Brainstem	8.8 ± 1.1	7.7 ± 0.7	**0.006$ (-12%)**
Putamen	29.5 ± 3.8	26.6 ± 3.1	**0.008$ (-10%)**
Hippocampus	15.9 ± 2.5	12.8 ± 1.3	**<0.001$ (-20%)**
Parahippocampal gyrus	20.1 ± 2.6	17.7 ± 2.5	**0.011$ (-12%)**
Fusiform gyrus	26.6 ± 3.4	23.9 ± 2.6	**0.027$ (-10%)**
Cerebellum	18 ± 2.2	16.3 ± 1.7	**0.03$ (-10%)**

*p<0.05, FDR-corrected; $^{\$}p$<0.05, uncorrected

10.1.3 PDD vs DLB

Table 10.5. Group comparison of parametric [^{11}C]UCB-J V_T in PDD and DLB patients

No PVC [^{11}C]UCB-J V_T, ml/cm^3 (mean ±SD)	**PDD**	**DLB**	**P value PDD vs DLB**
Postcentral gyrus	13.3 ± 2.6	13.5 ± 1.5	0.51 (+1)
Precuneus	16.9 ± 3	15.7 ± 1.8	0.21 (-7%)
Inferior parietal lobe	15.5 ± 2.8	14.9 ± 1.7	0.40 (-3%)
Inferior temporal lobe	19 ± 3.5	18.1 ± 2.7	0.80 (-5%)
Calcarine sulcus	17.6 ± 2.7	16 ± 1.3	0.26 (-9%)

Cuneus	16.8 ± 2.8	15.5 ± 1.5	0.28 (-8%)
Anterior cingulate	19.2 ± 4.2	17.5 ± 2.3	0.27 (-9%)
Posterior cingulate	17.8 ± 3.2	16 ± 1.9	0.09 (-10%)
Insular cortex	19.8 ± 4.1	17.8 ± 2.2	0.31 (-10%)
Fusiform gyrus	18.9 ± 3	17.5 ± 2	0.38 (-8%)
Nucleus accumbens	19.7 ± 4.4	19 ± 2.3	0.63 (-4%)
Caudate	11.1 ± 3.4	10.5 ± 1.8	1.00 (-5%)
Putamen	20.4 ± 3.9	20.1 ± 2.3	0.99 (-1%)
Amygdala	17.1 ± 2.7	15.3 ± 1.3	0.30 (-10%)
Hippocampus	13.2 ± 2.5	11.5 ± 0.6	0.21 (-13%)
Parahippocampal gyrus	16 ± 2.8	14 ± 1.7	0.37 (-13%)
Exploratory regions-of-interest			
Precentral gyrus	14 ± 2.7	13.8 ± 1.6	0.36 (-1%)
Supplementary motor area	15.3 ± 3	14.5 ± 1.8	0.15 (-5%)
Dorsolateral prefrontal cortex	15.8 ± 3.5	15.5 ± 2.3	0.61 (-2%)
Superior temporal lobe	19.3 ± 3.8	17.7 ± 2.4	0.39 (-8%)
Middle temporal lobe	19 ± 3.3	17.7 ± 2.2	0.45 (-7%)
Brainstem	7.9 ± 1.2	7.2 ± 0.5	0.49 (-9%)
Substantia nigra	8.7 ± 1.2	7.8 ± 0.9	0.082 (-11%)

*p<0.05, FDR-corrected; ^{S}p<0.05, uncorrected

Table 10.6. Group comparison of partial volume corrected [^{11}C]UCB-J V_T in PDD and DLB patients

No PVC [^{11}C]UCB-J V_T, ml/cm^3 (mean ±SD)	**PDD**	**DLB**	**P value PDD vs DLB**
Postcentral gyrus	22 ± 4.1	23.7 ± 3.2	0.94 (+7%)
Precuneus	22.3 ± 3.7	23.1 ± 2.9	0.85 (+3%)

Inferior parietal lobe	23.2 ± 3.7	23.3 ± 2.5	0.60 (+1%)
Inferior temporal lobe	26.7 ± 4.5	25.4 ± 3	0.99 (-3%)
Calcarine sulcus	21.9 ± 2.7	21.3 ± 1.7	0.66 (-3%)
Cuneus	22.8 ± 4	23 ± 2	0.80 (+1%)
Anterior cingulate	26.8 ± 5.5	26.5 ± 3.1	0.74 (-1%)
Posterior cingulate	23.3 ± 3.7	22.7 ± 3.3	0.28 (-3%)
Insular cortex	27.1 ± 4.6	26 ± 2.5	0.70 (-4%)
Fusiform gyrus	25 ± 4.3	23.9 ± 2.6	0.66 (-5%)
Nucleus accumbens	25.8 ± 5.8	25.4 ± 3.3	0.93 (-2%)
Caudate	15.9 ± 5.7	15.6 ± 3.8	0.79 (-2%)
Putamen	26.2 ± 5.3	26.6 ± 3.1	0.67 (+2%)
Amygdala	21.1 ± 3.3	19.3 ± 1.8	0.42 (-9%)
Hippocampus	14.1 ± 3.2	12.8 ± 1.3	0.32 (-9%)
Parahippocampal gyrus	19.7 ± 3.3	17.7 ± 2.5	0.61 (-10%)
Exploratory regions-of-interest			
Precentral gyrus	22 ± 4.1	23.7 ± 3.2	0.94 (+7%)
Supplementary motor area	22.6 ± 4.9	23.9 ± 3.6	0.87 (+6%)
Dorsolateral prefrontal cortex	24.1 ± 5.8	25.2 ± 3.3	0.71 (+5%)
Superior temporal lobe	17 ± 2.3	16.3 ± 1.7	0.97 (-4%)
Middle temporal lobe	26.8 ± 5.2	25.6 ± 3.2	0.63 (-5%)
Brainstem	8.3 ± 1.2	7.7 ± 0.7	0.43 (-8%)
Substantia nigra	10 ± 1.7	8.7 ± 1.3	0.22 (-13%)

*p<0.05, FDR-corrected; $^{\S}p$<0.05, uncorrected

11 Appendix D

11.1 Results: Desikan-Killiany atlas

11.1.1 HC vs drug-naïve PD: Δ[^{11}C]UCB-J V_T

Given that the spatial permutation approach available incorporated only the Desikan-Killiany atlas, I firstly assessed the relationship between [^{11}C]UCB-J V_T contrast maps and PET templates following parcellation with the Desikan-Killiany atlas, particularly given the disparity between the two atlases in terms of the number of regions-of-interest per atlas (85 in the Desikan-Killiany vs 125 in the CIC atlas). Δ[^{11}C]UCB-J V_T in drug-naïve PD patients compared to healthy controls was only found to be significantly associated with ΔGM volume (r=+0.26) and ΔCBF (r=+0.23) profiles, with an association observed between Δ[^{11}C]UCB-J V_T and D_2 receptor density profile (r=-0.25), although this was not formally significant (Table S1). No other associations were observed. After accounting for the inherent spatial autocorrelation of the imaging data, Δ[^{11}C]UCB-J V_T correlated with ΔGM volume (r=+0.26, p=0.04).

Within subcortical regions only, Δ[^{11}C]UCB-J V_T in drug-naïve PD patients compared to healthy controls was found to be associated with the D_1 (r=-0.52; p=0.032) and D_2 (r=-0.53; p=0.018) receptor density profiles. After accounting for the inherent spatial autocorrelation of the subcortical imaging data, Δ[^{11}C]UCB-J V_T appeared to be associated with D_1R, although this did not reach the threshold for significance (r=-0.44, p=0.06).

Table 11.1. Variables that were predictive of the regional distribution of Δ[^{11}C]UCB-J V_T in drug-naïve PD patients compared to healthy controls following simple linear regressions.

Drug-naïve vs HC	**Δ[^{11}C]UCB-J V_T**		
	r	**R^2**	***p* value**
ΔGM volume	**+0.26**	**0.069**	**0.044**
ΔCBF	**+0.23**	**0.052**	**0.03**

$5HT_{1A}$	-0.009	0.00	0.95
$5HT_{1B}$	+0.032	0.001	0.79
$5HT_{2A}$	-0.069	0.005	0.68
SERT	+0.20	0.039	0.20
D_1	-0.19	0.036	0.17
D_2	-0.25	0.065	0.074
DAT	-0.068	0.005	0.72
NAT	+0.10	0.010	0.41
VaChT	-0.042	0.002	0.78